SMOKE CONTROL IN ATRIUM BUILDINGS: A STUDY OF THE THERMAL SPILL PLUME

by

Roger Harrison

Supervised by

Michael Spearpoint

Fire Engineering Research Thesis

July 2004

A research thesis presented as partial fulfilment of the requirements for the degree of Master of Engineering in Fire Engineering

Department of Civil Engineering
University of Canterbury
Private Bag 4800
Christchurch
New Zealand

ABSTRACT

In the event of a fire, atrium buildings often require the use of smoke control systems to provide conditions for safe means of escape. Hot smoky gases entering an atrium from a fire within an adjacent compartment will rise as a thermal spill plume into a buoyant layer of gases formed beneath the atrium ceiling. This spill plume will entrain large amounts of air, which must be calculated to determine the quantity of gases entering the smoke layer.

There are a number of calculation methods available to designers of smoke control systems involving the thermal spill plume. These methods are important to the designer in order to calculate the required fan capacity or vent area for a smoke exhaust ventilation system. This work describes research examining various uncertainties and limitations in the available calculation methods. A combination of both physical scale modelling and computational fluid dynamics modelling has been used in the analysis.

This work has demonstrated that the presence of a downstand at the spill edge of a compartment opening appears to have little effect on the entrainment of air into the subsequent spill plume.

A simplified spill plume formula has been developed to predict the mass flow rate of gases produced by a free spill plume, which inherently includes entrainment of air into the ends of the plume.

An empirical correlation has also been developed to predict the entrainment of air from a compartment opening to a higher projecting balcony, and hence, the subsequent mass flow rate of gases at the spill edge.

This work has addressed various uncertainties in spill plume calculations, providing robust and relevant simplified design formulae. This work has generally improved the guidance available to fire safety engineers for the spill plume in smoke control design.

ACKNOWLEDGEMENTS

I would like to thank the following people who have contributed to this research in various ways:

Mike Spearpoint, my supervisor, without whom, this research would simply not have happened. Mike seeded the idea of coming to Canterbury over two years ago. It has proved to be an invaluable experience. Thanks to Mike (and Fiona McCartin) for providing me with a place to live and making the transition to life in New Zealand so seamless.

The Society of Fire Protection Engineers Educational and Scientific Foundation, for providing funding for this research.

The University of Canterbury, for providing funding in the form of a Masters Scholarship.

Russell Peoples and Grant Dunlop, for their invaluable help with the design and construction of the experimental apparatus.

Dr Howard Morgan and Norman Marshall, for the benefit of their experience over the years and their contagious enthusiasm for research on spill plumes.

Dr Charley Fleischmann and Professor Andy Buchanan, for their contribution to the Fire Engineering program. Their input has significantly broadened my knowledge and fuelled my enthusiasm to carry out further research.

The New Zealand Fire Service Commission for their continued support of the Fire Engineering program at the University of Canterbury.

NV IFSET SA, for permission to reproduce selected figures within this report.

TABLE OF CONTENTS

1. INTRODUCTION 1

1.1 BACKGROUND 1

1.2 ATRIUM TYPE 2

1.2.1 Type of atrium by construction 2

1.2.2 Type of atrium by use 5

1.3 ATRIUM SMOKE CONTROL 5

1.3.1 Design objectives 5

1.3.2 Smoke control strategies 6

1.3.3 Smoke and Heat Exhaust Ventilation Systems (SHEVS) 8

1.3.3.1 Clear layer height 10

1.4 SMOKE PRODUCTION IN ATRIUM BUILDINGS 12

1.4.1 The Spill Plume 13

1.4.2 Entrainment of air into a flow from a compartment opening to a higher projecting balcony 17

1.5 RESEARCH OBJECTIVE 19

2. LITERATURE REVIEW 21

2.1 EXISTING CALCULATION METHODS FOR THE SPILL PLUME 21

2.1.1 General 21

2.1.2 The BRE spill plume method 22

2.1.2.1 The effective layer depth correction 26

2.1.3 Simplified spill plume formulae 29

2.1.3.1 Method by Law (1986) 30

2.1.3.2 Method by Thomas (1987) 32

2.1.3.3 Method by Law (1995) 33

2.1.3.4 Method in NFPA 92B 34

2.1.3.5 Method by Poreh et al 35

2.1.3.6 Method by Thomas et al (1998) 37

2.1.4 Selection of an appropriate spill plume formula 39

2.1.5 Entrainment of air into a thermal line plume 40

2.2 EXPERIMENTAL STUDIES OF THE SPILL PLUME 42

2.2.1 Morgan and Marshall (1975) 42

2.2.2 Morgan and Marshall (1979) 43

2.2.3 Hansell, Morgan and Marshall 44

2.2.3.1 Horizontal flow of gases toward a compartment opening 44

2.2.3.2 Comparison between visually and buoyancy derived layer depths 44

2.2.3.3 Effect of balcony breadth 45

2.2.3.4 Entrainment and temperature limitation 46

2.2.4 Marshall, Harrison and Morgan *47*
2.2.5 Marshall and Harrison *48*
2.2.5.1 Geometry of smoke reservoir 48
2.2.5.2 Counter flow at the compartment opening 48
2.2.5.3 Air entrainment into the ends of the spill plume 49
2.2.5.4 Helium as an alternative method 49
2.2.6 Yii *50*
2.3 COMPUTER MODELLING STUDIES OF THE SPILL PLUME 50
2.3.1 Miles, Kumar and Cox *50*
2.3.2 Chow (1998) *51*
2.3.3 Chow (1999) *51*
2.3.4 Chow and Li *52*
2.3.5 Li and Chow *52*
2.4 ENTRAINMENT OF AIR INTO A FLOW FROM A COMPARTMENT OPENING TO A HIGHER PROJECTING BALCONY 53
2.4.1 Hansell *54*
2.4.2 Garrad *56*
3. APPROACH 57
3.1 PHYSICAL SCALE MODELLING 57
3.1.1 The scaling laws for turbulent flow *57*
3.2 COMPUTATIONAL FLUID DYNAMICS MODELLING 61
3.2.1 Fire Dynamics Simulator (FDS) *62*
4. SCALE MODEL EXPERIMENTS: APPARATUS AND METHODOLOGY 63
4.1 EXPERIMENTS EXAMINING ENTRAINMENT OF AIR INTO A SPILL PLUME 63
4.1.1 The physical scale model *63*
4.1.1.1 Reynolds number of typical flows 66
4.1.1.2 The fire compartment 67
4.1.1.3 The smoke exhaust hood 68
4.1.1.4 Fire source 71
4.1.2 Instrumentation *73*
4.1.2.1 Gas temperatures 73
4.1.2.2 Gas concentrations 74
4.1.2.3 Gas velocities 74
4.1.2.4 Data recording 75
4.1.2.5 Visual records 76
4.1.3 Experimental method *76*
4.1.3.1 Parameters of interest 76
4.1.3.2 Parameter variation 76
4.1.3.3 The series of test fires 77
4.1.3.4 Experimental procedure 79
4.1.4 Analysis procedures and data reduction *80*

4.1.4.1 Heat output of IMS fuel source 80
4.1.4.2 Smoke layer depth 80
4.1.4.3 Calculation of the mass flow rate of gases at the spill edge 81
4.1.4.4 Calculation of the convective heat output of the gases at the spill edge 81
4.1.4.5 Calculation of the mass flow rate of gases due to a spill plume 82
4.1.4.6 Error analysis 84
4.2 EXPERIMENTS EXAMINING ENTRAINMENT OF AIR INTO A FLOW FROM A COMPARTMENT OPENING TO A HIGHER PROJECTING BALCONY 85
4.2.1 The physical scale model 85
4.2.1.1 The fire compartment 85
4.2.2 Instrumentation 88
4.2.2.1 Gas temperatures 88
4.2.2.2 Gas velocities 89
4.2.2.3 Visual records 90
4.2.3 Experimental method 91
4.2.3.1 Parameters of interest 91
4.2.3.2 Parameter variation 91
4.2.3.3 The series of fire tests 92
4.2.3.4 Experimental procedure 92
4.2.4 Analysis procedures and data reduction 93
4.2.4.1 Heat output of the IMS fire source 93
4.2.4.2 Smoke layer depth 93
4.2.4.3 Mass flow rate of gases at the compartment opening and at the spill edge 93
4.2.4.4 Error Analysis 93
5. CFD MODELLING: PROCEDURE AND SCENARIOS 95
5.1 FDS MODELLING PROCEDURE 95
5.1.1 Modelled geometry 95
5.1.2 Computational domain and grid size 96
5.1.3 Fire source 97
5.1.4 Predictions 98
5.2 MODELLED SIMULATIONS 98
5.2.1 Parameters of interest 98
5.2.2 Parameter variation 99
5.2.3 The series of FDS simulations 99
5.3 ANALYSIS PROCEDURES AND DATA REDUCTION 100
5.3.1 Smoke layer depth 100
5.3.2 Mass flow rate of gases at the compartment opening and at the spill edge 100
5.3.3 Error Analysis 101
6. RESULTS 103
6.1 ENTRAINMENT OF AIR INTO A SPILL PLUME 103
6.1.1 Approach flow at the spill edge (Tests 1 to 9) 103

6.1.1.1 Homogeneity of flow across the spill edge 103
6.1.1.2 Gas temperature and velocity profiles 105
6.1.1.3 Summary of results 106
6.1.2 Mass flow rate of gases produced by a spill plume (Tests 10-64) 107
6.1.2.1 Temperature profiles in the smoke exhaust hood 107
6.1.2.2 Summary of results 108
6.2 ENTRAINMENT OF AIR INTO A FLOW FROM A COMPARTMENT OPENING TO A HIGHER PROJECTING BALCONY 109
6.2.1 FDS simulation results 109
6.2.1.1 Onset of steady state conditions 109
6.2.1.2 Homogeneity of flow across the compartment opening and the spill edge 110
6.2.1.3 Temperature profiles at the compartment opening and at the spill edge 113
6.2.1.4 Velocity profiles at the compartment opening and at the spill edge 114
6.2.1.5 Summary of results 116
6.2.2 Physical scale modelling results (Tests 65 to 68) 117
6.2.2.1 Temperature profiles at the compartment opening and at the spill edge 117
6.2.2.2 Velocity profiles at the compartment opening and at the spill edge 118
6.2.2.3 Summary of results 120

7. DISCUSSION 125

7.1 ENTRAINMENT OF AIR INTO A SPILL PLUME 125
7.1.1 Plume behaviour 125
7.1.1.1 Flat ceiling at the spill edge 125
7.1.1.2 0.1 m downstand at the spill edge 127
7.1.1.3 0.2 m downstand at the spill edge 127
7.1.1.4 Smoke layer in exhaust hood 129
7.1.2 Mass flow rate of gases with entrainment of air into the ends (Tests 10 to 63) 132
7.1.2.1 Initial analysis of results 132
7.1.2.2 Effect of a downstand at the spill edge 134
7.1.2.3 A simplified spill plume formula for design purposes 135
7.1.3 Mass flow rate of gases without entrainment into the ends (Test 64) 138
7.1.4 Comparison of the experiment with the BRE method 138
7.1.4.1 Flat ceiling at the spill edge 139
7.1.4.2 0.1 m downstand at the spill edge 142
7.1.4.3 0.2 m downstand at the spill edge 144
7.1.5 Comparison of the experiment with simplified spill plume formulae 146
7.2 ENTRAINMENT OF AIR INTO A FLOW FROM A COMPARTMENT OPENING TO A HIGHER PROJECTING BALCONY 149
7.2.1 Flow behaviour 149
7.2.1.1 Wide compartment opening 149
7.2.1.2 Narrow compartment opening 153
7.2.1.3 Effect of balcony breadth 155
7.2.2 Comparison of FDS predictions with the experiment 156

7.2.2.1 Temperature profiles at the compartment opening 156
7.2.2.2 Temperature profiles at the spill edge 158
7.2.2.3 Velocity profiles at the compartment opening 160
7.2.2.4 Velocity profiles at the spill edge 161
7.2.2.5 General 162
7.2.3 Mass flow rate of gases at the spill edge 163
7.2.3.1 Analysis 163
7.2.3.2 Effect of balcony length 165
7.2.3.3 Empirical correlation for design purposes 166
7.2.3.4 Comparison with the Hansell method 168
7.2.3.5 General 169

8. CONCLUSIONS 171

8.1 ENTRAINMENT OF AIR INTO A SPILL PLUME 171
8.2 ENTRAINMENT OF AIR INTO A FLOW FROM A COMPARTMENT OPENING TO A HIGHER PROJECTING BALCONY 173
8.3 GENERAL 173

9. FURTHER WORK 175

9.1 ENTRAINMENT OF AIR INTO A SPILL PLUME 175
9.2 ENTRAINMENT OF AIR INTO A FLOW FROM A COMPARTMENT OPENING TO A HIGHER PROJECTING BALCONY 175

10. REFERENCES 177

APPENDIX A FUEL FLOWMETER CALIBRATION 183

APPENDIX B THERMOCOUPLE LOCATIONS 185

APPENDIX C IMS SAFETY DATA SHEET 189

APPENDIX D EXAMPLE FDS SOURCE CODE 191

APPENDIX E EXPERIMENTAL TEMPERATURE AND VELOCITY PROFILES AT THE SPILL EDGE (TESTS 1 TO 9) 195

APPENDIX F EXPERIMENTAL TEMPERATURE PROFILES IN THE SMOKE EXHAUST HOOD (TESTS 10 TO 64) 205

APPENDIX G FDS TEMPERATURE PROFILES (SIMULATIONS 1 TO 25) 233

APPENDIX H FDS VELOCITY PROFILES (SIMULATIONS 1 TO 25) 259

APPENDIX I EXPERIMENTAL TEMPERATURE PROFILES (TESTS 65 TO 68) 285

APPENDIX J EXPERIMENTAL VELOCITY PROFILES (TESTS 65 TO 68) 289

APPENDIX K COMPARISON OF EXPERIMENTAL AND FDS TEMPERATURE PROFILES (TESTS 65 TO 68, SIMULATIONS 1, 4, 5 AND 9) 293

APPENDIX L COMPARISON OF EXPERIMENTAL AND FDS VELOCITY PROFILES (TESTS 65 TO 68, SIMULATIONS 1, 4, 5 AND 9)..... 297

LIST OF FIGURES

Figure 1.1: Sterile tube atrium [courtesy of NV IFSET SA] 3
Figure 1.2: Closed atrium (non fire-resisting façade) [courtesy of NV IFSET SA] 3
Figure 1.3: Partially open atrium [courtesy of NV IFSET SA] 4
Figure 1.4: Fully open atrium [courtesy of NV IFSET SA] 4
Figure 1.5: Principle of a SHEVS [courtesy of NV IFSET SA] 9
Figure 1.6: Schematic drawing of clear layer height above highest walking level 10
Figure 1.7: A SHEVS with a spill plume [courtesy of NV IFSET SA] 14
Figure 1.8: Adhered (or single sided) spill plume [courtesy of NV IFSET SA] 15
Figure 1.9: Free (or double sided) spill plume [courtesy of NV IFSET SA] 15
Figure 1.10: Comparison of smoke production for an axisymmetric and a free spill plume [19] 17
Figure 1.11: Smoke flow from a compartment opening with a higher projecting balcony [courtesy of NV IFSET SA] 18
Figure 2.1: Typical temperature profile for a broad reservoir smoke layer [3] 27
Figure 2.2: Free spill plume based on a virtual line source 29
Figure 2.3: Typical smoke flow for balconies broader than 2 m [courtesy of NV IFSET SA] 45
Figure 2.4: Typical smoke flow for balconies narrower than 2 m [courtesy of NV IFSET SA] 46
Figure 4.1: Schematic drawing of the $1/10^{th}$ physical scale model 64
Figure 4.2: The physical scale model 65
Figure 4.3: The fire compartment 68
Figure 4.4: Locking mechanism for the walls of the smoke exhaust hood 69
Figure 4.5: The smoke exhaust hood for a deep layer 69
Figure 4.6: The bifurcated smoke exhaust fan 70
Figure 4.7: 'Butterfly' damper in exhaust vent 71
Figure 4.8: The IMS fire source 72
Figure 4.9: The fuel supply system 72
Figure 4.10: Thermocouple locations 74
Figure 4.11: The pitot tube arrangement 75
Figure 4.12: Schematic drawing of the fire compartment 86
Figure 4.13: The fire compartment for a wide geometry 87
Figure 4.14: The fire compartment for a narrow geometry 87
Figure 4.15: Thermocouple locations 89
Figure 4.16: The pitot tube arrangement 90
Figure 5.1: The computational domain in Smokeview 3.1 96
Figure 6.1: Typical temperature profile across gas layer (0.01 m below the spill edge) 104
Figure 6.2: Typical velocity profile across gas layer (0.01 m below the spill edge) 104
Figure 6.3: Temperature profile at the spill edge for Test 1 105
Figure 6.4: Velocity profile at the spill edge for Test 1 106

Figure 6.5: Temperature profile in the smoke exhaust hood (Test 34) 107
Figure 6.6: Temperature at the compartment opening with respect to time (Simulation 1) 109
Figure 6.7: Typical temperature profile across the gas layer at the compartment opening 110
Figure 6.8: Typical temperature profile across the gas layer at the spill edge 111
Figure 6.9: Typical velocity profile across the gas layer at the compartment opening 112
Figure 6.10: Typical velocity profile across the gas layer at the spill edge 112
Figure 6.11: Temperature profile at the compartment opening for Simulation 1 113
Figure 6.12: Temperature profile at the spill edge for Simulation 1 114
Figure 6.13: Velocity profile at the compartment opening for Simulation 1 115
Figure 6.14: Velocity profile at the spill edge for Simulation 1 115
Figure 6.15: Temperature profile at the compartment opening for Test 65 117
Figure 6.16: Temperature profile at the spill edge for Test 65 118
Figure 6.17: Velocity profile at the compartment opening for Test 65 119
Figure 6.18: Velocity profile at the spill edge for Test 65 119
Figure 6.19: Graph showing comparison of the experimental mass flow rates at the spill edge with those calculated using Equation (6-1) 121
Figure 7.1: Spill plume behaviour from a compartment with a flat ceiling 125
Figure 7.2: Lateral extent of the spill plume 126
Figure 7.3: Spill plume behaviour from a compartment with a 0.1 m downstand 127
Figure 7.4: Spill plume behaviour from a compartment with a 0.2 m downstand 128
Figure 7.5: Typical behaviour of the layer in the smoke exhaust hood 129
Figure 7.6: The smoke layer in the exhaust hood 130
Figure 7.7: Behaviour of the layer in the smoke exhaust hood for Tests 10 to 21 131
Figure 7.8: (M_p-M_b) with respect to $Q^{1/3}W^{2/3}(z+d_b)$ for Tests 10 to 63 133
Figure 7.9: (M_p-M_b) with respect to $Q^{1/3}W^{2/3}(z+d_b)$ for different spill edge geometries 135
Figure 7.10: (M_p-M_b) with respect to $Q^{1/3}W^{2/3}(z+d_b)$ for Tests 22 to 63 inclusive 136
Figure 7.11: Comparison between experiment and the BRE method (6kW, flat ceiling) 139
Figure 7.12: Comparison between experiment and the BRE method (9kW, flat ceiling) 141
Figure 7.13: Comparison between experiment and the BRE method (12kW, flat ceiling) 141
Figure 7.14: Comparison between experiment and the BRE method (6kW, 0.1 m downstand) 142
Figure 7.15: Comparison between experiment and the BRE method (9kW, 0.1 m downstand) 143
Figure 7.16: Comparison between experiment and the BRE method (12kW, 0.1 m downstand) 144
Figure 7.17: Comparison between experiment and the BRE method (6kW, 0.2 m downstand) 145
Figure 7.18: Comparison between experiment and the BRE method (9kW, 0.2 m downstand) 145
Figure 7.19: Comparison between experiment and the BRE method (12kW, 0.2 m downstand) 146
Figure 7.20: Comparison between experiment and simplified spill plume formulae (6kW) 147
Figure 7.21: Comparison between experiment and simplified spill plume formulae (9kW) 147
Figure 7.22: Comparison between experiment and simplified spill plume formulae (12kW) 148
Figure 7.23: Flow behaviour for a wide opening (Simulation 9) 149
Figure 7.24: Velocity vectors for a wide opening (Simulation 9) 150

Figure 7.25: Velocity map of the flow at the centre of the compartment (Simulation 9) 151
Figure 7.26: Temperature map of the flow at the centre of the compartment (Simulation 9) 151
Figure 7.27: Flow behaviour for a wide opening with a deep downstand (Simulation 17) 152
Figure 7.28: Velocity vectors for a wide opening with a deep downstand (Simulation 17) 152
Figure 7.29: Flow behaviour for a narrow opening (Simulation 13) 153
Figure 7.30: Velocity vectors for a narrow opening (Simulation 13) 153
Figure 7.31: Velocity map of the flow at the centre of the compartment (Simulation 13) 154
Figure 7.32: Temperature map of the flow at the centre of the compartment (Simulation 13) 154
Figure 7.33: Velocity vectors for a 0.5 m broad balcony (Simulation 19) 155
Figure 7.34: Velocity vectors for a 0.2 m broad balcony (Simulation 25) 156
Figure 7.35: Comparison of temperature at the compartment opening (1.0 m wide opening, 0.1 m deep downstand) 157
Figure 7.36: Comparison of temperature at the compartment opening (0.2 m wide opening, 0.1 m deep downstand) 157
Figure 7.37: Comparison of temperature at the spill edge (1.0 m wide opening, 0.1 m deep downstand) 159
Figure 7.38: Comparison of temperature at the spill edge (0.2 m wide opening, 0.1 m deep downstand) 159
Figure 7.39: Comparison of velocity at the compartment opening (1.0 m wide opening, 0.1 m deep downstand) 160
Figure 7.40: Comparison of velocity at the spill edge (1.0 m wide opening, 0.1 m deep downstand) 161
Figure 7.41: Comparison of velocity at the spill edge (0.2 m wide opening, 0.1 m deep downstand) 162
Figure 7.42: Correlated FDS predictions in the form of a power law 164
Figure 7.43: Comparison of correlated FDS predictions and experimental results 164
Figure 7.44: Comparison of FDS prediction for Simulation 25 with the other predictions 165

LIST OF TABLES

Table 1.1: Classification of atrium type by use [3] 5

Table 1.2: Recommended clear layer heights in the UK [8] 11

Table 2.1: Proposed values for dimensionless entrainment coefficient C_m 41

Table 2.2: Proposed values for entrainment coefficient α 41

Table 2.3: Limiting temperature criteria for the BRE spill plume method 46

Table 4.1: The series of test fires (Tests 1 to 64) 78

Table 4.2: The series of test fires (Tests 65 to 68) 92

Table 5.1: The series of FDS simulations 100

Table 6.1: Summary of results for the approach flow at the spill edge 106

Table 6.2: Summary of results for the mass flow rate due to a spill plume 108

Table 6.3: Summary of the FDS predictions for mass flow rate at the compartment opening and at the spill edge 116

Table 6.4: Summary of the experimental mass flow rate at the compartment opening and at the spill edge (Tests 65 to 68) 120

Table 6.5: Comparison of experimental mass flow rates at the spill edge with those calculated using Equation (6-1) 122

Table 6.6: Calculated mass flow rate at the compartment opening using Equation (2-1) 122

Table 6.7: Revised experimental mass flow rates at the compartment opening 123

Table 7.1: Assumed geometries and calculated values of M_w for Scenarios 1 and 2 168

Table 7.2: Calculated values of M_b using the Hansell method and Equation (7-6) 168

NOMENCLATURE

Symbol	Description
A	Area (m^2)
b	Balcony breadth (m)
B	A constant given in Equation (2-27) ($kgm^{1/3}s^{-1}kW^{-1/3}$)
c	Heat of combustion value ($kJkg^{-1}$)
C	A constant given in Equation (2-23) ($kgms^{-1}kW^{-1/3}$)
C_m	Dimensionless entrainment coefficient
c_p	Specific heat ($Jkg^{-1}K^{-1}$)
C_d	Coefficient of discharge
d	Depth (m)
D	Characteristic distance (m)
g	Acceleration due to gravity (ms^{-2})
h	Height above floor (m)
k	Thermal conductivity ($Wm^{-1}K^{-1}$)
L	Characteristic linear height of the model
M	Mass flow rate of gases (kgs^{-1})
δM	Mass flow rate of air entrained into the free ends of the plume (kgs^{-1})
δm	Mass flow rate of air entrained on rotation (kgs^{-1})
n'	Number of gas molecules in the volume V
N	Avogadro's number
P	Gas pressure (Pa)
ΔP	Pressure differential (Pa)
Re	Reynolds number
Q	Convective heat flux at the spill edge (kW)
Q_{TOTAL}	Total heat generated by the fire (kW)
R	Universal gas constant
T	Absolute gas temperature (K)

u	Velocity (ms^{-1})
v	Volume (m^3)
V	Volume flow rate (m^3s^{-1})
W	Lateral extent of gas flow spill edge (m)
w	Width (m)
X_u	A height parameter (m)
z	Height of rise of plume from the spill edge to the smoke layer base in the reservoir (m)
z_0	Height of virtual line source below the spill edge (m)

Greek symbol	**Description**
α	Entrainment constant for plume
α'	Entrainment constant for air mixing into gases rotating round a horizontal edge
α''	Effective rotational entrainment constant
χ	An angle (^{o})
θ	Excess temperature of gases above ambient temperature (^oC)
ρ	Density (kgm^{-3})
κ_M	Profile correction factor for mass flow (approx 1.3)
κ_Q	Profile correction factor for heat flux (approx 0.95)
τ	Carbon dioxide concentration by volume above ambient
ω	The time scale
μ	A velocity ratio
ν	Kinematic viscosity of air (m^2s^{-1})
λ	An empirical thermal plume constant ($\lambda = 0.9$)

List of subscripts	Description
1	An ambient property
a	Variable evaluated in atrium or smoke reservoir
air	A property of air
b	Variable evaluated in the horizontal layer flow at the spill edge
buoy	Variable evaluated from a buoyancy profile
c	Variable evaluated at highest point in a flow
CFI	A property of ceramic fibre insulation board
co_2	A property of CO_2 gas
comp	A property of the fire compartment
crit	A critical value prior to the onset of "plug-holing"
d	A property of the downstand
e	An effective property of the smoke layer
IMS	A property of Industrial Methylated Spirits
layer	A property of the layer in smoke exhaust hood
max	A maximum value
o	A property of the compartment opening
p	Variable evaluated in the plume at an arbitrary height of rise
v	A visual property of the smoke layer
ven	A property of the vent in the smoke exhaust hood
w	Variable evaluated in the horizontal layer flow at the compartment opening
y	Variable evaluated in a vertical flow past the top of the opening

CHAPTER 1

1. INTRODUCTION

1.1 Background

Over the last few decades, large undivided volume buildings such as atrium buildings, covered shopping malls, airport terminals and sports arenas have become increasingly popular. These buildings typically contain large spaces or voids which can occupy many storeys in height. The generic term 'atrium' can be applied to the large spaces within these types of buildings.

The concept of an atrium dates back to Roman times, when used as an entrance hall in a typical house. Developments in architectural techniques now allow an atrium to be an integral part of large buildings (e.g. covered shopping malls). Modern atria are designed with the intention to provide a visually and spatially external environment indoors [1].

In terms of fire protection, floors, ceilings and partitions are traditionally used to provide compartmentation to limit the spread of fire and smoke within a building. However, atrium buildings violate this fundamental approach in terms of horizontal compartmentation and vertical separation. In the event of a fire, the lack of physical separations can allow extensive smoke spread to occur throughout the entire space to areas remote from the fire source. Atrium buildings can contain large quantities of combustible materials and can also contain significant numbers of people which could be exposed to smoke, toxic gases and flames from a fire. The spread of fire and smoke can also cause a significant amount of property damage.

Atrium buildings are commonly designed such that the atrium space is connected to adjacent rooms or spaces. The boundary between the atrium and the adjacent room can either be glazed or fully open. Unprotected openings between the atrium and the

adjacent rooms are known as communicating spaces. Smoke and hot gases flowing from a communicating space can move unimpeded into an atrium space, possibly affecting other areas of the building. Therefore, the use of smoke control systems in atrium buildings is particularly important.

A smoke control system can provide conditions to allow safe means of escape from a building by ensuring adequate separation between the escaping occupants and the hot smoky gases from a fire. Property protection can primarily be achieved by providing improved conditions for effective Fire Service operations in addition to limiting the spread of smoke.

1.2 Atrium type

Atrium buildings can be classified by their construction or by their use. A brief description of different types of atrium building is described below.

1.2.1 Type of atrium by construction

In order for a suitable smoke control design to be identified, Morgan et al [2] categorised atria into the following groups depending upon the type of enclosure:

- Sterile tube atrium
- Closed atrium
- Partially open atrium, and
- Fully open atrium

The sterile tube atrium (see Figure 1.1) is where the atrium space is separated from the remainder of the building by a façade which is both fire and smoke resisting. This façade will act as a barrier to fire and smoke spread between the atrium and the adjacent spaces. The ideal sterile tube atrium would contain no flammable material on the atrium floor. The atrium space would generally have no functional use apart from as a circulation area for the occupants of the building.

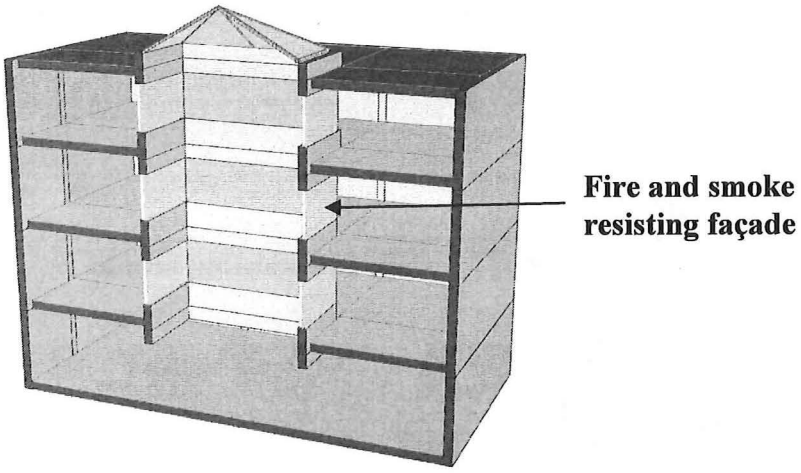

Figure 1.1: Sterile tube atrium [courtesy of NV IFSET SA]

Figure 1.2 shows a closed atrium in which the atrium is separated from the remainder of the building by a non fire resisting façade. This façade may not necessarily be smoke resisting (i.e. leaky). The atrium space may possibly have a functional use (e.g. cafés, restaurants, etc).

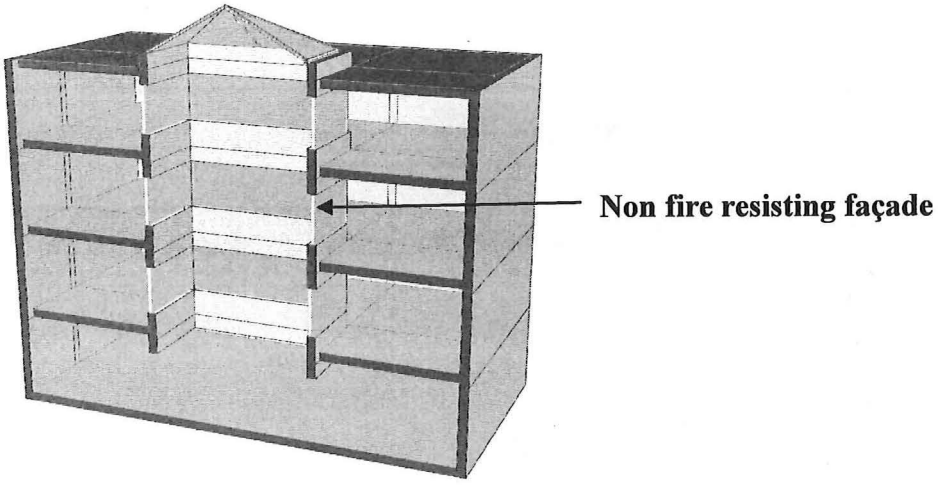

Figure 1.2: Closed atrium (non fire-resisting façade) [courtesy of NV IFSET SA]

A partially open atrium (see Figure 1.3) is when there are communicating spaces between the atrium space and the adjacent areas on some of the lower storeys. A non fire resisting façade provides separation between the atrium and adjacent areas on the upper storeys.

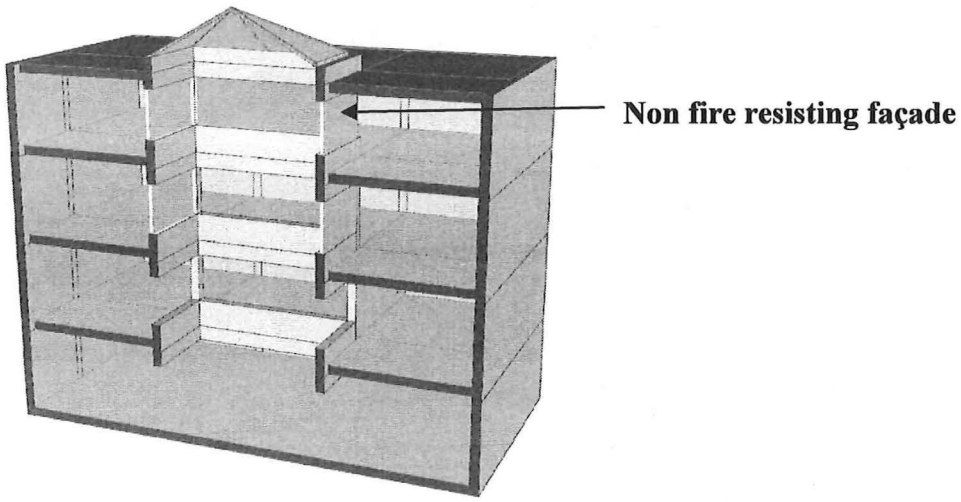

Figure 1.3: Partially open atrium [courtesy of NV IFSET SA]

A fully open atrium is when large openings exist between the atrium and adjacent areas on all storeys (see Figure 1.4).

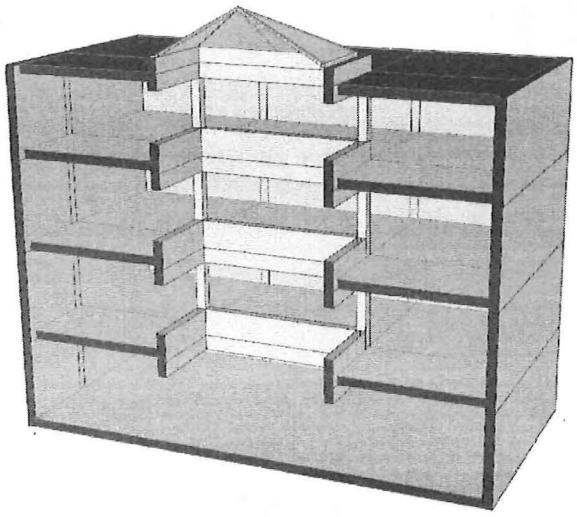

Figure 1.4: Fully open atrium [courtesy of NV IFSET SA]

1.2.2 Type of atrium by use

An atrium can also be classified by the way in which the occupants use the building [3]. These types of atrium building are described in Table 1.1.

Category	Atrium type
A	Occupants who are awake and predominantly familiar with the building. This includes office buildings.
B	Occupants who are awake but unfamiliar with the building. This includes shopping malls and most public assembly buildings.
C	Occupants who are likely to be asleep. There are three subdivsions. This broad category includes flats, halls of residence and hotels.
D	Occupants requiring nursing or medical care. This includes hospitals.

Table 1.1: Classification of atrium type by use [3]

1.3 Atrium smoke control

1.3.1 Design objectives

As described above, some form of smoke control (known as smoke management in the USA) is often required in atrium buildings primarily for life safety purposes. Milke [4] gives five design objectives for smoke control systems in atrium buildings:

1. Maintain a tenable environment in the means of egress in the atrium during the time required for evacuation.
2. Confine the smoke in the atrium to a limited region in that space.
3. Limit the migration of smoke into adjacent spaces from the atrium.
4. Provide conditions in the atrium that will assist emergency response personnel in conducting search-and-rescue operations and locating and controlling the fire.
5. Contribute to the overall protection of life and reduction in property loss.

Milke states that a design may be to achieve either one, or a combination of, these objectives. Milke also lists a number of 'hazard parameters' in which the design objectives can be evaluated in measurable terms, such as:

- Smoke layer depth
- Visibility through the smoke layer
- Carbon monoxide concentration
- Temperature rise in the smoke layer

Milke states that an acceptable smoke control system is one which maintains the hazard parameter(s) of concern to within acceptable levels. Performance criteria for smoke control systems are discussed further, with regard to a specific case, in section 1.3.3.1.

1.3.2 Smoke control strategies

There are a number of different smoke control strategies available for atrium buildings [2,5,6]. Morgan et al [2] describe various alternative approaches such as:

- **Smoke filling**
  This approach can be applied to atria which have large volumes, such that smoke ventilation may not be necessary. This strategy becomes viable when smoke can be contained in a roof void for the duration of the required safe egress time for the occupants of the building. In this case, the height of the smoke layer may not reach an unacceptable value before the fire consumes the available fuel. This approach assumes that the fire grows at a predictable rate. Klote and Milke [6] provide empirical relationships to determine the smoke layer height above the fire with respect to time for both steady and growing fires. This strategy should only be used if the smoke control designer can demonstrate by calculation that smoke ventilation is not necessary.

- **Smoke clearance**

  This approach provides sufficient ventilation to remove smoke from the atrium after the fire has been suppressed.

- **Smoke and heat exhaust ventilation from the atrium**

  This uses the buoyancy of the smoky gases from the fire to form a layer above the occupants of the building, providing a safe means of escape. This form of smoke control provides the main focus for this work and is described in detail in the following section.

- **Temperature control ventilation from the atrium**

  This strategy is used when the height of the smoke layer above the floor is not a critical design parameter. In this case, smoke exhaust can be used to achieve a maximum value of the temperature of the layer of smoky gases. This approach allows the use of materials which would otherwise be damaged by hot gases (e.g. atrium façade materials which are not fire-resisting).

- **Smoke and heat exhaust from each storey separately**

  In some cases it may be impractical to provide smoke exhaust ventilation from the atrium space if the height of rise of the smoke layer from the floor is too large. It may be beneficial to prevent smoke from entering the atrium altogether (particularly for fully open atria). This can be achieved by the use of strategically placed smoke curtains around the atrium space at each storey, and providing smoke exhaust ventilation from each storey separately.

- **Atrium depressurisation**

  Where the boundary between the atrium space and the adjacent areas is linked by small openings (e.g. doors gaps, leaky façade), it is possible to prevent smoke from travelling through these openings by reducing the pressure of the gases in the smoke layer. This approach is known as depressurisation. The purpose of this technique is to prevent smoke from travelling into the adjacent spaces and does not provide protection to the atrium space. This technique is

similar to that employed for natural environmental ventilation in atrium buildings [7].

- **Combination of above strategies (hybrid smoke control)**
  Various combinations of the above strategies can also be applied, such as atrium depressurisation with smoke and heat exhaust ventilation.

1.3.3 Smoke and Heat Exhaust Ventilation Systems (SHEVS)

The primary focus of this work concerns Smoke and Heat Exhaust Ventilation Systems (SHEVS) for atrium buildings. This approach provides smoke and heat exhaust from the upper regions of a building to create a clear layer beneath a buoyant stratified smoke layer, thus providing conditions for safe means of escape. For this approach to be effective, it is necessary for the temperature of the gas layer to be high enough to remain buoyant when at the design height. SHEVS may be naturally driven (due to buoyancy of the gases produced from the fire) or mechanically driven (mechanical exhaust fans).

Figure 1.5 shows the general principle of smoke and heat exhaust ventilation. When designing a SHEVS, an appropriate fire must be specified for the building and its contents. In general, it is necessary to ensure that the size of the fire does not become too large so that the SHEVS does not perform effectively. Therefore, as part of the design strategy, it is often necessary to include the use of sprinklers to control the size of the fire. Smoke from a fire will rise as a plume which will subsequently entrain air. This entrainment will significantly increase the volume of smoky gases produced. The hot gases rise and form a buoyant layer within the enclosure. Smoke and heat will exhaust from the ventilators in the roof of the enclosure either by natural or mechanical means. The hot gas layer will deepen until equilibrium is reached between the quantity of gases being ventilated and the quantity of gases entering the layer. For the smoke ventilation to be effective, it is necessary to provide an adequate amount of inlet air to replace the hot gases being removed.

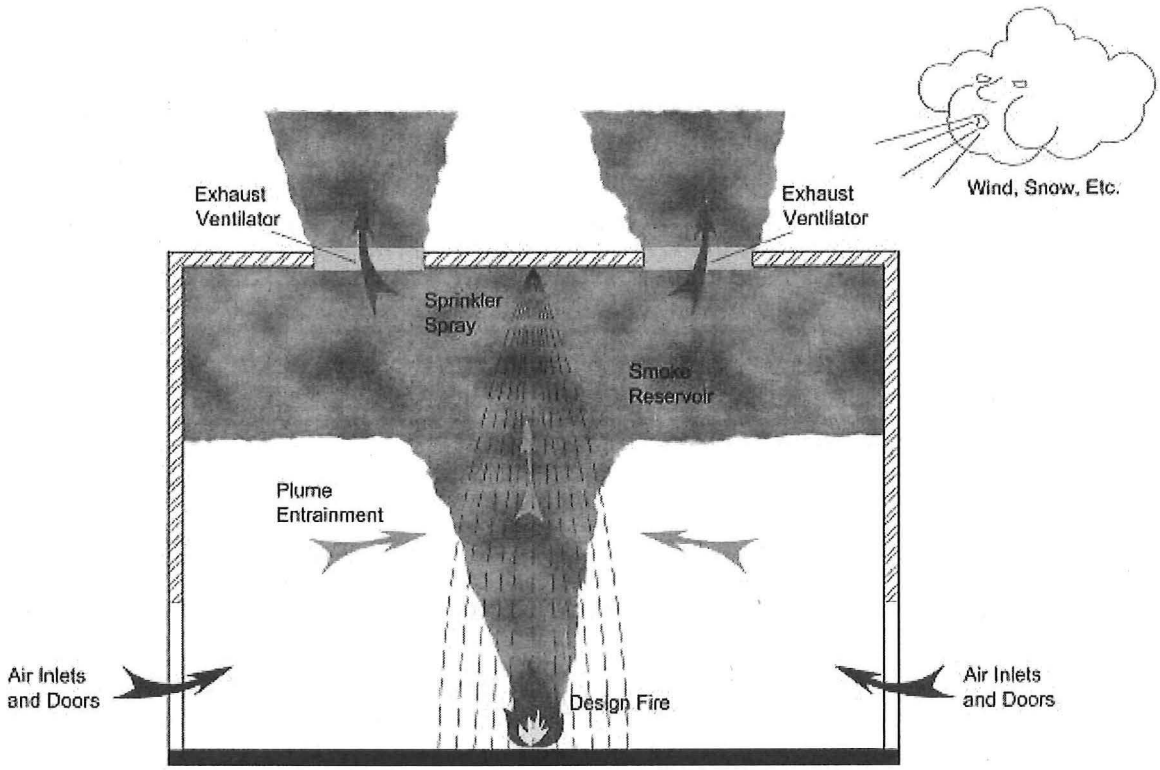

Figure 1.5: Principle of a SHEVS [courtesy of NV IFSET SA]

The performance of SHEVS can depend on various factors [8] such as:

- Temperature of the smoke layer
- Aerodynamic free area of natural ventilators/volume of smoke exhausted by mechanical fans
- Wind effects
- Geometry, size and location of inlet air openings
- Geometry, size and location of the smoke reservoir

SHEVS provides the safe use of escape routes which are in the same space as the fire. The amount of smoke exhaust must be calculated to ensure that the smoke layer is at a safe height above the occupants using these escape routes. In addition to providing conditions for safe means for escape, SHEVS also provide improved conditions for effective fire-fighting operations, which in turn can provide improved property protection.

1.3.3.1 Clear layer height

When considering life safety, a critical design parameter of SHEVS is the clear layer height. The clear layer height is the height between the level of the fire and the base of the buoyant smoke layer in the atrium. The design clear layer height will usually provide a layer with a safe height above the highest egress route. Figure 1.6 shows a schematic drawing of a design clear layer height for a multi-storey atrium. This clear layer height will provide a tenable environment for safe egress for the duration of the fire (provided the design fire is not exceeded).

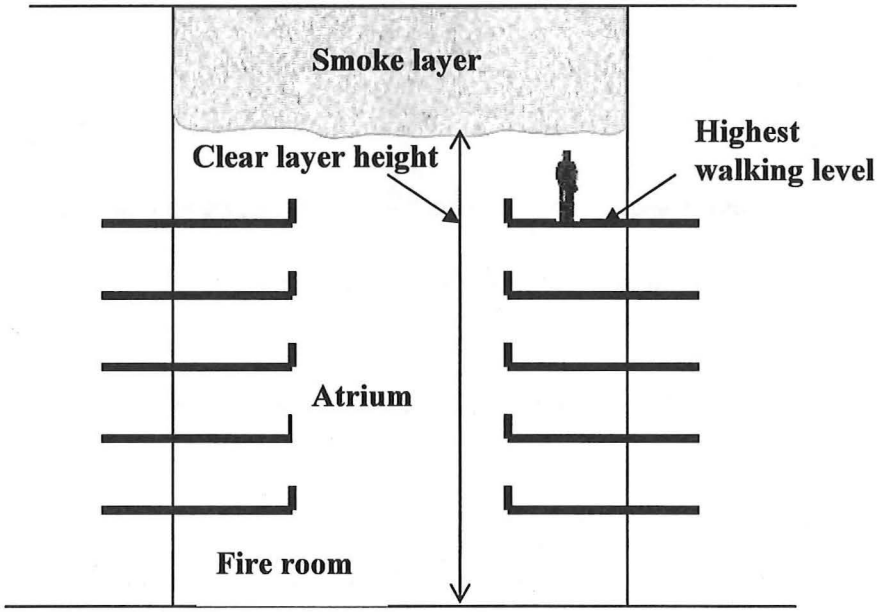

Figure 1.6: Schematic drawing of clear layer height above highest walking level

Milke [4] provides factors which must be taken into consideration (depending on the design objectives) when identifying a design clear layer height, such as:

- Location of means of egress within the open space
- Separation of adjacent spaces from the open space
- Environmental and geometric factors

Guidance on the recommended clear layer height for SHEVS varies worldwide.

NFPA 101 [9] (2000, section 8.2.5.6) states that "a clear layer height of 1.85 m must be achieved above the highest floor level of exit access open to the atrium for a period of 1.5 times the calculated egress time, or 20 minutes, whichever is the greater".

The history of guidance on acceptable clear layer heights in the UK has recently been discussed by Morgan [10]. Current guidance in the UK [8] recommends a minimum clear height depending on the type of building (see Table 1.2).

Type of building	Minimum clear height (m)
Public buildings (e.g. covered shopping malls)	3.0
Non public buildings (e.g. offices, apartments)	2.5

Table 1.2: Recommended clear layer heights in the UK [8]

Where the predicted smoke layer temperature is less than 50°C above ambient temperature, the minimum clear heights shown in Table 1.2 should be increased by 0.5 m [8], as the smoke layer interface may not be well defined. Morgan et al [2] also recommend that the smoke layer temperature should not exceed 200 °C due to downward radiation from the hot gas layer.

The current guidance within New Zealand [11] recommends a clear layer height of at least 2.0 m above the highest intermediate floor open to an atrium space.

1.4 Smoke production in atrium buildings

The volume of smoky gases generated from a fire within an atrium is highly governed by the amount of air entrained into the rising smoke plume. The volume of smoke must be calculated in order to determine the required fan capacity or vent area for a smoke ventilation system. The amount of air entrained into the plume will depend on the configuration of the plume produced. Milke [4] identified five configurations of smoke plume which may exist within atrium buildings, these are:

1. **Axisymmetric plume**

   An axisymmetric plume is generally expected from a fire located near the centre of an atrium floor. This type of plume is typically remote from any walls and air is entrained around all sides of the plume. Entrainment of air will occur over the full height of the plume until it reaches the interface with a smoke layer which may have formed above. A classical analysis of axisymmetric plumes has been carried out by Morton, Taylor and Turner [12]. This analysis has been extended for turbulent plumes due to fires in buildings [13,14]. Plume entrainment theories for axisymmetric plumes are reasonably well established and will not be addressed further in this report.

2. **Wall plume**

   A plume which is generated from a fire against a wall is known as a wall plume. Zukoski [15] developed a wall plume entrainment correlation based on "mirror symmetry". Work by Poreh and Garrad [16] has highlighted that further research on wall plume entrainment is desirable.

3. **Corner plume**

   A plume which is generated from a fire located in the corner of a room, where the walls form a 90^{o} angle, is known as a corner plume. Zukoski [15] treated corner plumes in a similar manner to a wall plume with the use of "mirror symmetry" for plume entrainment. Again, work by Poreh and Garrad [16] has demonstrated that further research is desirable for corner plume entrainment.

4. **Spill plume**

   A spill plume is a vertically rising plume resulting from an initially horizontally moving smoke layer which then subsequently rises at a spill edge (e.g. at an opening onto an atrium space). This type of plume is the major focus of this work as is described in detail in the following section.

5. **Window plume**

   A window plume is a plume which flows from a window (or doorway) into an atrium space [6]. Typically, window plumes are generated from post-flashover fires [17]. An entrainment correlation was developed by Heskestad, by comparing the air entrainment for a window plume with that of an axisymmetric plume. The window plume entrainment correlation is given by Klote and Milke [6].

1.4.1 The Spill Plume

If a fire were to occur in a communicating space within an atrium building (e.g. a shop or office unit), a horizontally moving buoyant layer of hot smoky gases will form within that space (see Figure 1.7). This layer will spread laterally and flow toward the opening connecting to the atrium space. If there are no smoke control measures to confine the smoke layer to the room of origin, this horizontally moving layer will flow out of the opening. If a balcony exists beyond the compartment opening, smoke will flow beneath the balcony. The smoke flow will then rotate around the free edge of the balcony (i.e. the 'spill edge'). This region is often known as the 'rotation' or 'turning' region of the plume. The smoke will then rise vertically as a plume into the atrium space and entrain large quantities of air (see Figure 1.7). Entrainment of air will also occur into the free ends of the plume as it rises.

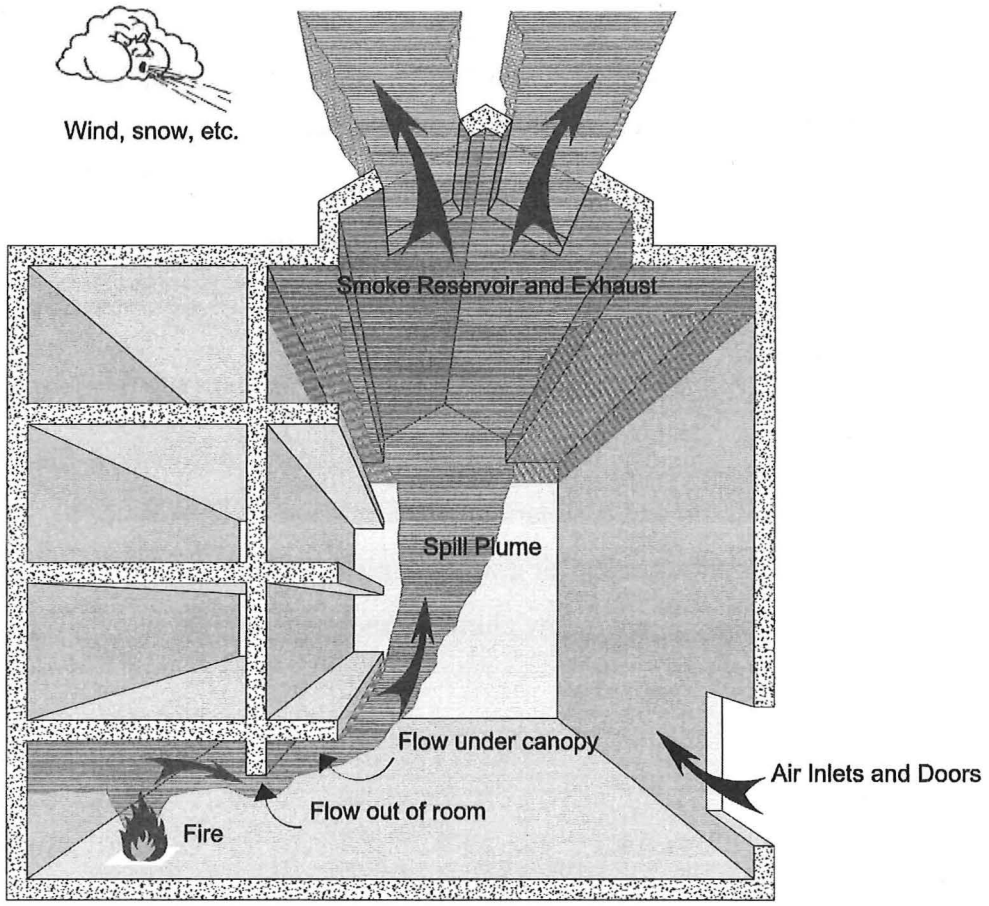

Figure 1.7: A SHEVS with a spill plume [courtesy of NV IFSET SA]

This type of plume is commonly known as a 'spill' or 'line' plume. The term 'line' is used, as immediately after the turning region, the plume is relatively long and narrow.

Spill plumes can be categorised into two groups: adhered and free spill plumes. Figure 1.8 shows a schematic drawing of an adhered spill plume. In this case, the smoke layer within the compartment flows out of the opening and rotates at the spill edge. The subsequent plume then adheres to the vertical surface above the opening as it rises. Entrainment of air will occur into one side of the plume, across its lateral extent, as it rises vertically. This type of plume is also known as a single-sided spill plume.

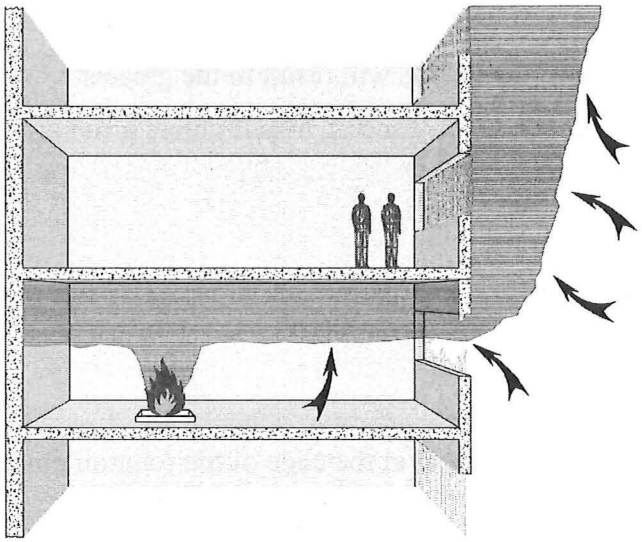

Figure 1.8: Adhered (or single sided) spill plume [courtesy of NV IFSET SA]

Figure 1.9 shows a schematic drawing of a free spill plume. In this case, the smoke layer flows from the compartment opening and under a horizontal projection (e.g. a balcony). The smoke layer then rotates at the spill edge (e.g. at the edge of the balcony) and rises vertically as a plume. Entrainment of air occurs into both sides of the plume across its lateral extent, as it rises (see Figure 1.9). This type of plume is also known as a double-sided spill plume.

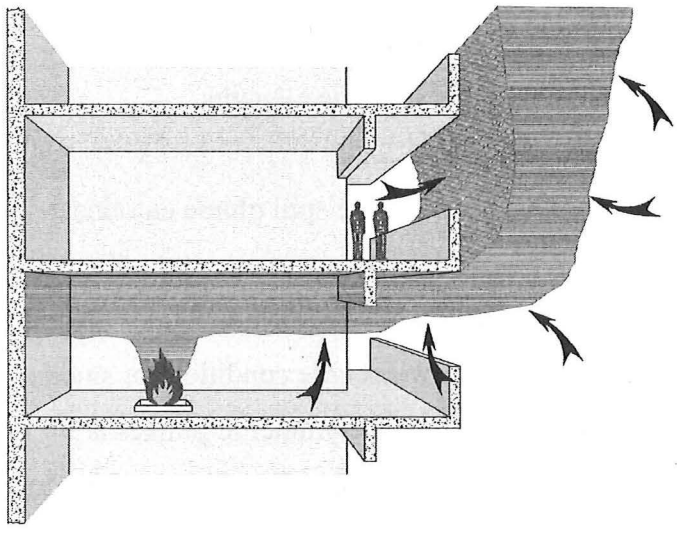

Figure 1.9: Free (or double sided) spill plume [courtesy of NV IFSET SA]

A fire in a communicating space on the lowest level of the building will maximise the amount of air entrainment into a rising spill plume, this will result in the greatest quantity of smoky gases entering the layer above. In general, a spill plume provides the worst case condition for this scenario [2].

The governing factors which affect the amount of air entrainment into a spill plume are given by Morgan and Marshall [18], these are:

- The mass flow rate or temperature of the gases at the edge of the rotation point into the atrium
- The convective heat flux of the gases
- The lateral extent of the spill plume entering the atrium, measured along the free edge past which the smoke spills
- The height over which the plume must rise

Milke [19] carried out a comparison between the smoke production rate of an axisymmetric plume with that of a free spill plume. The smoke production rate for the spill plume was determined using a formula developed by Law [20]. Milke states that this formula provides an approximation of the mass flow rate generated by a spill plume. Comparison between each type of plume was made for a fire with a convective heat output of 5000 kW. The smoke production rate for the spill plume was determined for a variety of balcony heights and spill edge lengths.

Milke [19] demonstrated that for the conditions studied, the spill plume entrains a greater amount of air than an axisymmetric plume for a height of rise up to 40 m (see Figure 1.10). This height of rise will cater for the majority of atrium heights and confirms that the spill plume generally provides the worst case condition for smoke production rate. Beyond a height of 40 m, the spill and axisymmetric plumes are likely to behave similarly in terms of smoke production rate. This is likely to be due to entrainment into the ends of the spill plume as it rises, causing it to become three dimensional in nature, and similar to an axisymmetric plume.

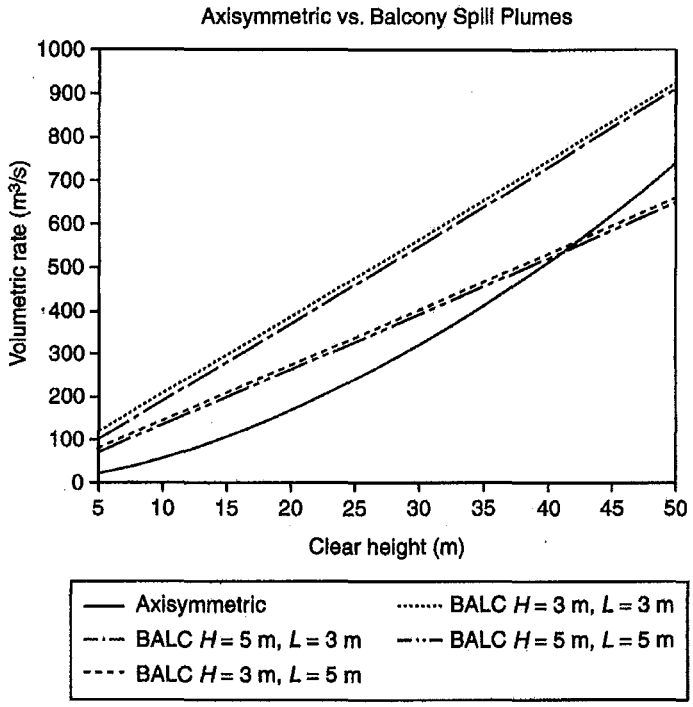

Figure 1.10: Comparison of smoke production for an axisymmetric and a free spill plume [19]

There are a number of calculation methods available to designers of SHEVS involving a thermal spill plume [e.g. 2,5,20-23]. These calculation methods will be discussed in detail in the following chapter.

1.4.2 Entrainment of air into a flow from a compartment opening to a higher projecting balcony

A key input parameter for spill plume calculations is the mass flow rate of gases at the spill edge. A common scenario is the presence of a downstand at a compartment opening from which a higher projecting balcony extends (see Figure 1.11). As smoke flows from beneath the compartment opening and rises to form a layer beneath the balcony, entrainment of air will occur into the smoke flow. This entrainment needs to be determined to accurately predict the mass flow rate of gases at the spill edge for design purposes.

A calculation method developed by Hansell [24] to determine the mass flow rate of gases at the spill edge had originally been thought to work well. However, more recent work by Garrad [25] has shown that this method only works well if applied to similar geometries from which the method was derived.

Current calculations make the crude assumption the mass flow rate of gases at the spill edge is twice that at the compartment opening [2]. Further research is required improve the available guidance to designers of SHEVS.

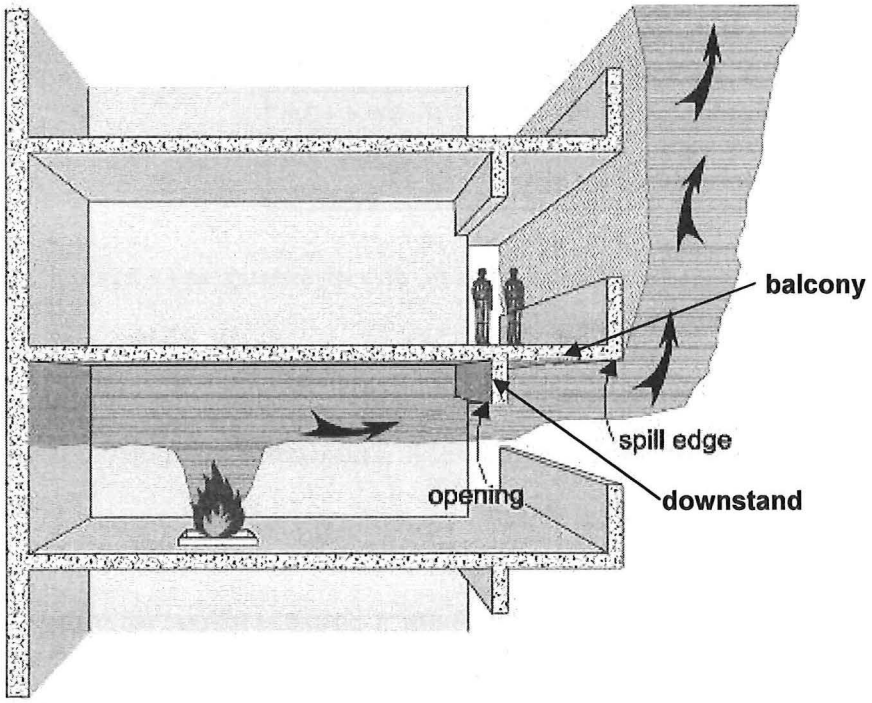

Figure 1.11: Smoke flow from a compartment opening with a higher projecting balcony [courtesy of NV IFSET SA]

1.5 Research objective

Currently, there are a number of calculation methods available to designers of SHEVS for atrium buildings involving the thermal spill plume. These include various simplified spill plume formulae and the BRE spill plume method. These methods are important to the designer in order to calculate the required fan capacity or vent area. However, there is some controversy over the accuracy and robustness of some of these design formulae for spill plumes. There are limitations to the available calculation methods and there are also areas of uncertainty which require further research. There are three specific objectives which this work aims to address, these objectives are described below:

- **A simplified spill plume formula to include entrainment of air into the free ends**
  Simplified spill plume formulae were initially developed by Law [20] and Thomas [21] in order to ease the task of the designers of SHEVS. However, more recent studies by Poreh et al [22] and Thomas et al [23] have developed simplified formulae with a more robust basis. These formulae were developed using data which did not allow for the common scenario of entrainment of air into the free ends of the spill plume. This work aims to provide a simplified formula to include entrainment into the free ends of the spill plume using existing correlation methods. It should be noted that the BRE spill plume method provides the option to include entrainment of air into the free ends of the plume.

- **A simplified spill plume formula when a downstand exists at the spill edge**
  The majority of spill plume calculation methods are based on experimental or theoretical studies in which the approach flow is from a compartment with a flat ceiling. A common scenario at the spill edge of a compartment opening is the presence of a downstand. The current simplified spill plume formulae [20-23] do not apply to flows with a downstand at the spill edge. There is also a lack of relevant experimental data for this scenario. This work aims to

develop a robust simplified spill plume formula when a downstand exists at the spill edge, using existing correlation methods. It should be noted that the BRE spill plume method includes the option of a downstand at the spill edge in the calculation. However, this scenario has never been validated experimentally.

- **Entrainment of air into a flow from a compartment opening to a higher projecting balcony**
  Spill plume calculation methods require the mass flow rate of gases at the spill edge as an input parameter. This requires the entrainment of air into a flow from a compartment opening to a higher projecting balcony/canopy to be accurately determined.

  These smoke flows are not well understood and the current guidance available to the designers of SHEVS is crude. Therefore, there is a need to provide empirical correlations to characterise these flows for a variety of compartment openings. This work aims to develop a simple empirical correlation in an attempt to improve the prediction of the mass flow rate of gases at the spill edge.

In general, the objective of this work is to address various uncertainties in spill plume calculations in order to improve the available guidance. The work aims to provide robust and relevant simplified formulae to enable accurate calculations involving the spill plume in smoke control design.

CHAPTER 2

2. LITERATURE REVIEW

This chapter presents a summary of the calculation methods available to predict entrainment of air into a spill plume, and hence, the subsequent mass flow rate of gases produced. The basis behind the derivation of these existing methods is presented and discussed. Experimental and computer modelling research on spill plumes is also presented.

Previous work addressing the issue of entrainment of air into a flow from a compartment opening to a higher projecting balcony is also presented.

2.1 Existing calculation methods for the spill plume

2.1.1 General

The behaviour of line plumes was first studied both experimentally and theoretically by Lee and Emmons [26]. Morgan and Marshall [18,27] drew upon this work in the mid 1970's in the development of a theory to predict entrainment of air into a thermal spill plume.

Simplified spill plume formulae (the form of a single equation) were subsequently developed by Law [20] and Thomas [21] using the experimental data obtained by Morgan and Marshall. Heskestad also developed a correlation based on the work by Law for guidance in the USA [28]. More recent studies by Poreh et al [22] and Thomas et al [23] have led to more robust simplified spill plume formulae.

2.1.2 The BRE spill plume method

The BRE spill plume method was first developed for free plumes by Morgan and Marshall [18, 27] of the Building Research Establishment (BRE) in the UK.

Modifications have subsequently been made to extend the method to apply to adhered plumes, and to update aspects of the horizontal flow from a compartment opening [29,30].

The BRE spill plume method was first developed in a series of $1/10^{th}$ physical scale model experiments (see section 2.2.1).

The BRE spill plume method is complicated and the calculation procedure is not fully reproduced herein. For full details of the calculation procedure, reference should be made to the original paper by Morgan and Marshall [18] and the current design document detailing a user guide to this calculation method [2]. However, a summary of the key features of the calculation method and some of the fundamental assumptions are described below.

The calculation method deals with the spill plume in three discrete regions:

1. The horizontally flowing buoyant layer of smoky gases approaching the spill edge (i.e. the approach flow).
2. The 'rotation' or 'turning' region, as the horizontally moving layer rotates around the spill edge (i.e. as the gases change from a horizontally moving flow to a vertically moving flow).
3. The vertically moving smoke flow in the form of a two dimensional line plume.

There is a specific dependence on the approach flow of a horizontally flowing thermal buoyant layer toward an opening, through which the gases then rise. The following assumptions are made for the approach flow [2].

- The flow is from beneath a flat ceiling (or a downstand) at the edge of the opening
- The flow is channelled by walls or channelling screens
- The flow has flow-lines which are everywhere parallel and which approach the edge of the opening at a right angle
- The approach flow is assumed to be fully turbulent
- There is no immersed ceiling jet
- The velocity of the clear air below the smoke layer has a value smaller than that of the layer itself

Two key parameters of the approach flow must initially be determined, such as the following combinations:

- Mass flow rate/heat flux
- Mass flow rate/mean layer temperature
- Mass flow rate/ceiling temperature
- Heat flux/mean layer temperature
- Heat flux/ceiling temperature
- Heat flux/layer depth
- Layer depth/mean layer temperature
- Layer depth/ceiling temperature

The remaining approach flow parameters can then be calculated using a theory to describe the horizontal flow of buoyant gases toward an opening by Morgan [30]. The mass flow rate of gases at the opening can be determined using Equation (2-1).

$$M_w = \frac{2}{3} C_d^{3/2} \left(2g\theta_{c,w} T_1\right)^{1/2} \frac{W\rho_1}{T_{c,w}} d_w^{3/2} \kappa_M \qquad (2\text{-}1)$$

For a flat ceiling at the compartment opening, Morgan [30] recommends a coefficient of discharge of 1.0 (i.e. $C_d = 1.0$). For a deep downstand the coefficient of discharge is 0.6 (i.e. $C_d = 0.6$).

The mass-weighted average layer temperature ($\overline{\theta}_w$) can be determined from Equation (2-2).

$$\overline{\theta}_w = \frac{\kappa_M}{\kappa_Q}\theta_{c,w} \tag{2-2}$$

Where κ_M and κ_Q are profile correction factors, taken to be 1.3 and 0.95 respectively for most typical flowing layers. These correction factors are weakly temperature dependent [30].

Morgan also gives expressions to determine the under balcony horizontal velocity for a layer under a flat ceiling or a deep downstand.

The amount of air entrainment into the gases which rotate around the spill edge can then be determined using Equation (2-3).

$$\delta m = \frac{2}{3}\rho_1 W \alpha' \left(\frac{2g\theta_{c,w}}{T_1}\right) d_w^{3/2} \tag{2-3}$$

Morgan and Hansell [29] empirically derived the entrainment constant (α') in the rotation region to be 1.1, updating the original value of 0.9 found by Morgan and Marshall [18]. Morgan and Hansell recognised that this high value for α' infers an anomalously large amount of entrainment into the rotating flow of gases at the spill edge. This large value of α' is a result of treating all anomalous entrainment above the spill edge as if it occurred in the entrainment region [2].

This aspect of the BRE spill plume method has led to some controversy and debate. Subsequent work by Miles et al [31] and Yii [32] indicate only a small degree of entrainment into the rotation region. However, the BRE spill plume method is recognised to be empirical in nature, and the overall calculation package provides good agreement with experimental results [29]. The BRE method has also provided

good agreement with the results from large scale fire tests [33,34] which suggest that it can be successfully used for design purposes.

Combining equations (2-1) and (2-3) provides the mass flow rate of gases rising in a vertical flow past the spill edge (M_y) [Equation (2-4)]. This is used in the subsequent analysis of entrainment of air into the vertically rising plume.

$$M_y = \delta m + M_w \tag{2-4}$$

Morgan and Marshall utilised the theory of Lee and Emmons [26] in the calculation of a virtual 'Equivalent Gaussian Source' (EGS) in the horizontal plane. The EGS provides the source of the vertically rising thermal plume at the spill edge. This plume is a two dimensional line plume rising from a 'retarded source' [18, 26]. Morgan and Marshall modified the Lee and Emmons approach to determine the source parameters of the EGS from the approach flow.

Morgan and Marshall also used the Lee and Emmons approach in the subsequent analysis of entrainment into the rising plume. This incorporated the use of an entrainment constant, α, empirically determined by Lee and Emmons to have a value of 0.16. For a particular height of rise above the spill edge, this method then allows the mass flow rate of gases to be determined ignoring any entrainment of air into the ends of the plume. This method makes the fundamental assumption that the entrainment coefficient is constant, and profiles of velocity and temperature across the plume are Gaussian throughout. Morgan and Marshall also provide an expression to determine entrainment of air into the ends of the plume, which updated the method given in their original work [27].

The methods for calculating the EGS, the entrainment of air into the rising plume and into the ends of the plume are given in the user guide [2]. The total mass flow rate of gases of the spill plume, at a particular height of rise, is the sum of the entrainment into the plume and the entrainment into the ends.

The user guide [2] also provides details of a calculation procedure for adhered spill plumes, which requires an entrainment constant, α, of 0.077 [35, 36]. The value of α for adhered plumes was experimentally determined in previous work by Grella and Faeth [36]. They found that adhered plumes are not truly Gaussian in nature, resulting in a value of α of approximately 0.068. This is close to the value of 0.077 found when a half Gaussian profile is assumed.

An experimental study [35] has demonstrated that the BRE spill plume method should not be used for approach flow temperatures in excess of approximately 350 °C. At present, accurate calculation methods for high temperature flows do not exist.

2.1.2.1 The effective layer depth correction

One of the fundamental assumptions of the Lee and Emmons line plume theory is that the surrounding ambient air, through which the plume rises, remains at a uniform ambient temperature. In reality, this fundamental assumption can be violated depending on the aspect ratio of the smoke reservoir and the design smoke layer depth. Experimental studies have demonstrated that when the width of the smoke reservoir or atrium (defined as the square root of the plan area) is small compared the smoke layer depth, then the air below the smoke layer usually has a uniform temperature. However, when the width of the smoke reservoir is large compared to the layer depth, the clear air beneath the visible layer can have an increased temperature with respect to the normal ambient temperature. This increased temperature beneath the visible smoke layer gives rise to an effective layer base beneath the visible layer (see Figure 2.1).

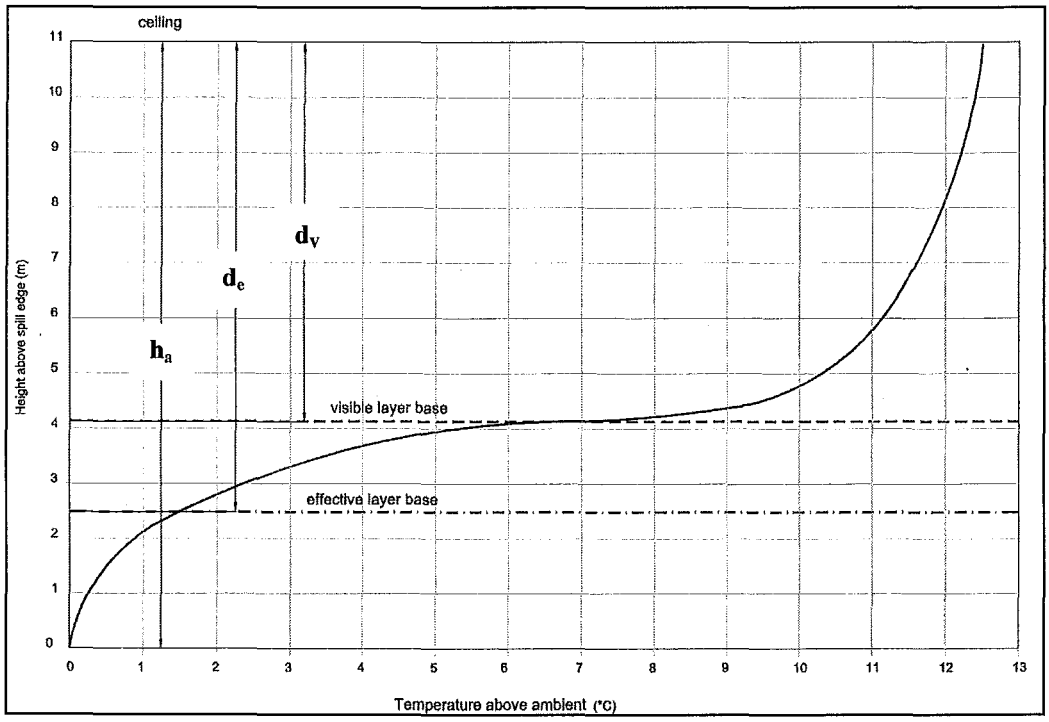

Figure 2.1: Typical temperature profile for a broad reservoir smoke layer [2]

Experimental studies have shown that there is a difference in entrainment between these two scenarios [27,35]. When the size of the reservoir is large compared to the size of the plume, the amount of entrainment is less than for smoke reservoirs which are comparable in size to the plume.

This difference in entrainment between the two scenarios may be taken into account by assigning a different entrainment coefficient for each case, whilst taking the height of rise of the plume to be at the visible smoke layer base. Alternatively, for the large area reservoir, the height of rise of the plume can be adjusted, whilst keeping the plume entrainment coefficient constant.

Morgan et al [2] present a method to take this effect into account based on an analysis of empirical data [27,35]. This method is known as the 'effective layer depth correction', which adjusts the height of rise of the plume to take into account the geometry of the smoke reservoir and subsequent differences in spill plume entrainment. This method is outlined below:

- **Large area reservoirs - smoke reservoirs where visible smoke layer depth is less than** $0.67A_a^{0.5}$

  When the visible smoke layer depth is less than $0.67A_a^{0.5}$ a correction factor needs to be applied to the smoke layer depth in the reservoir. Analysis of experimental data [27] has shown that the effective layer depth (d_e) is 1.26 times the visible layer depth (d_v) (see Figure 2.1). The effective height of rise of the plume is then described by Equation (2-5).

$$z = h_a - 1.26d_v \tag{2-5}$$

If $z < 0.75$ m after applying Equation (2-5) then z should then be defined by:

$$z = h_a - d_v \tag{2-6}$$

- **Small area reservoirs - smoke reservoirs where visible smoke layer depth is greater than** $0.67A_a^{0.5}$

  When the visible smoke layer depth is less than $0.67A_a^{0.5}$, no correction factor applies [see Equation (2-7)].

$$z = h_a - d_v \tag{2-7}$$

When using the BRE spill plume method, it is crucial that the designer identifies whether the effective layer depth correction applies to the particular design in question.

2.1.3 Simplified spill plume formulae

Simplified spill plume formulae typically consist of a single line equation to predict the mass flow rate of gases produced by a spill plume. This type of formula is desirable to ease the task of designing a SHEVS involving a spill plume.

The available simplified spill plume formulae are generally based on the assumption that the spill plume is generated from a virtual line source of zero width from below the spill edge (see Figure 2.2). The location of this virtual line source varies with respect to the fire size, the heat output per unit area of the fire and the compartment geometry.

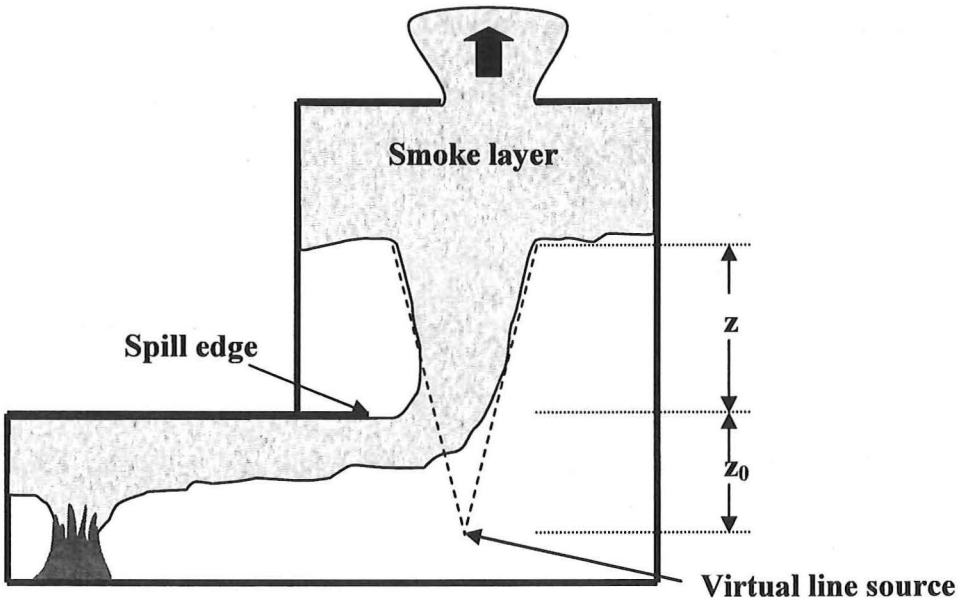

Figure 2.2: Free spill plume based on a virtual line source

These simplified formulae are generally based on empirical approaches, and therefore have specific limitations depending on the way in which the correlation was derived. They have all been derived from approach flows beneath a flat ceiling.

Most of the available methods make the fundamental assumption of similarity between cross sectional distributions of velocity and temperature across the plume. These distributions are assumed to be Gaussian in nature throughout the full height of the plume. A summary of each of these simplified formulae and their limitations are described below.

2.1.3.1 Method by Law (1986)

Law [20] developed a simplified spill plume formula by correlating the experimental data produced by Morgan and Marshall [18,27]. Law modified a relationship developed by Yokoi [37] between temperature rise and heat output of the fire, for flows from a window [see Equation (2-8)].

$$\theta_{p,\max} = \frac{6.89}{(z+z_0)}\left(\frac{Q}{W}\right)^{2/3} \tag{2-8}$$

Law used the data from Morgan and Marshall [18] to correlate the maximum temperature rise in the plume $\theta_{p,\max}$ versus Q/W and the maximum temperature rise at the spill edge $\theta_{b,\max}$ versus Q/W. These data provided relationships which obeyed a 2/3 power as proposed by Yokoi.

Law used these correlations to estimate the location of the virtual source below the spill edge (z_0). When correlating $\theta_{p,\max}$, the virtual source was estimated to be located at a distance of $0.67h_{comp}$ below the spill edge. However, when $\theta_{b,\max}$ was correlated, the virtual source was estimated to be at a distance of $0.5h_{comp}$ below the spill edge.

Law used $\theta_{b,\max}$ and the conservation of heat at the spill edge to develop the following relationship for the mass flow rate of gases at the spill edge (i.e. under the balcony), as given by Equation (2-9).

$$M_b = 0.025\left(QW^2\right)^{1/3} \tag{2-9}$$

By analogy, Law proposed the following relationship for the mass flow rate of gases with respect to height above a virtual source, as given by Equation (2-10) .

$$M_p \propto \left(QW^2\right)^{1/3}(z+z_o) \tag{2-10}$$

Law then utilised further experimental data from Morgan and Marshall [27] to plot $\frac{M_p}{(QW^2)^{1/3}}$ with respect to z. Law also used Equation (2-9), to determine the value of M_p when $z = 0$ (which was included with the experimental data in the correlation). From this analysis, Law developed the following formula to determine the mass flow rate of gases produced by a free spill plume as given in Equation (2-11).

$$M_p = 0.34(QW^2)^{1/3}(z + 0.075) \tag{2-11}$$

Law commented that the intercept value of 0.075 was equivalent to $0.15h_{comp}$ which suggested that the virtual source of the plume was only a small distance below the spill edge. Equation (2-11) was therefore generalised, giving Equation (2-12).

$$M_p = 0.34(QW^2)^{1/3}(z + 0.15h_{comp}) \tag{2-12}$$

Law proposed that Equation (2-12) could be used as an alternative to the BRE spill plume method for interim use until further analysis had been carried out. Equation (2-12) only applies to free spill plumes and to approach flows which are channelled by vertical screens. Equation (2-12) also includes entrainment into the free ends of the plume.

Morgan [38] questioned the use of $\theta_{b,\max}$ in the development of this correlation, due to its dependence on the flow behaviour upstream of the measuring region. Morgan commented that this result may not necessarily apply to other geometries.

Morgan also stated that the use of Equation (2-9) to determine M_p when $z = 0$ appeared to be unjustified, and that this particular data point was given much greater weight than the experimental data in deriving Equation (2-12).

Morgan proposed a modified form of the Law correlation [see Equation (2-13)] by only using the experimental data points and applying the effective layer depth correction to adjust the height of rise (see section 2.1.2.1).

$$\frac{M_p}{\left(QW^2\right)^{1/3}} = 0.40(h_a - d_e) + 0.061 \qquad (2\text{-}13)$$

Morgan stated that Equation (2-13) implies that the virtual line source appears to be located at a distance $0.3h_{comp}$ below the spill edge.

Morgan suggested that Equation (2-13) could possibly be used for design purposes, however, due to the inconsistencies in the location of the virtual line source, the BRE spill plume method was recommended if greater accuracy was required.

In response to these comments by Morgan, Law [39] agreed that the correlation given by Equation (2-12) need not necessarily pass through the data point generated from Equation (2-9). However, as the correlation was developed using an empirical approach, Law stated that Equation (2-12) could reasonably be used for design purposes. Law also questioned whether the BRE spill plume method gave greater accuracy due to reservations on the application of the effective layer depth correction.

2.1.3.2 Method by Thomas (1987)

Thomas [21] also used the experimental data from Morgan and Marshall [18, 27] to develop an alternative simplified spill plume formula.

Thomas used a relationship developed by Lee and Emmons [26] to determine the location of the virtual source beneath the spill edge (z_0). This relationship reduced to a form similar to that of Yokoi, as used by Law, which relates θ to Q/W. Analysis of the data showed that the location of the virtual source varied between $0.32\,h_{comp}$ and $0.66\,h_{comp}$ depending on the region in which θ was measured (i.e. the approach flow or the plume).

Thomas also noted that the location of the virtual source was dependent on the experimental geometry. Thomas presented a number of possible virtual source locations from the analysis.

Thomas also used a relationship by Lee and Emmons (see Equation (2-14)) to describe the mass flow rate per unit width of a line plume above a virtual line source.

$$\frac{M_p}{W} = 2^{5/6}\rho\alpha^{2/3}\left(1+\lambda^2\right)^{1/6}\left(\frac{gQ}{\rho c_{p,air}WT_1}\right)^{1/3}\left(z+z_o\right) \tag{2-14}$$

Equation (2-14) was reduced to give Equation (2-15).

$$M_p = 0.58\rho\left(\frac{gQW^2}{\rho c_{p,air}T_1}\right)^{1/3}\left(z+z_o\right) \tag{2-15}$$

Thomas also developed an explicit relationship to determine the entrainment of air into the free ends of the plume by modifying a previous analysis by Morgan and Marshall [18]. This term was included into Equation (2-15) to give the final form of the spill plume formula for free plumes as shown in Equation (2-16).

$$M_p = 0.58\rho\left(\frac{gQW^2}{\rho c_{p,air}T_1}\right)^{1/3}\left(z+z_o\right)\left(1+\frac{0.22\left(z+2z_o\right)}{W}\right)^{2/3} \tag{2-16}$$

2.1.3.3 Method by Law (1995)

Law [40] used a similar analysis to that described in section 2.1.3.1 using further experimental data from Hansell et al [35]. This analysis led to a revised correlation as given by Equation (2-17).

$$M_p = 0.31\left(QW^2\right)^{1/3}\left(z+0.25h_{comp}\right) \tag{2-17}$$

Equation (2-17) applies to approach flows which are channelled by vertical screens, it also includes entrainment into the ends of the plume.

Law also noted that if no channelling screens were present at the approach flow beneath the balcony, the layer can become diffuse and ill defined. For this condition, Law proposed an effective width of the plume as given by Equation (2-18).

$$W_e = W + b \tag{2-18}$$

A modified version of Equation (2-17) is included within guidance given by the Chartered Institution of Building Service Engineers (CIBSE) in the UK [41] where,

$$M_p = 0.36\left(QW^2\right)^{1/3}\left(z + 0.25h_{comp}\right) \tag{2-19}$$

2.1.3.4 Method in NFPA 92B

Current guidance on spill plume entrainment in the USA [5] uses a correlation which is described as being 'based on Law's interpretation of small-scale experiments by Morgan and Marshall' [see Equation (2-20)]. This applies to free spill plumes only.

$$M_p = 0.41\left(QW^2\right)^{1/3}\left(z + 0.25h_{comp}\right) \tag{2-20}$$

Equation (2-20) provides alternative advice to a previous edition of the guidance [28] which was developed by Heskestad. This correlation is described as being 'based on Law's interpretation of data given by Morgan and Marshall, a subsequent reanalysis by Morgan, and modifications of a kind suggested by Thomas to make the calculated entrainment rate approach that for an axisymmetric plume at large heights'. This correlation is given by Equation (2-21).

$$M_p = 0.41\left(QW^2\right)^{1/3}\left(z + 0.25h_{comp}\right)\left(1 + \frac{0.063\left(z + 0.6h_{comp}\right)}{W}\right) \tag{2-21}$$

Comparison between Equations (2-20) and (2-21) suggest that the current correlation ignores the explicit term for entrainment into the ends of the plume. However, it is unclear why this explicit term was required, as Law's original correlation included air entrainment into the ends.

2.1.3.5 Method by Poreh et al

Using dimensional analysis, Poreh et al [22] deduced a relationship between the mass flow rate for a line plume and the convective heat output of the gases. This assumed that the volumetric flux of the ambient air into a unit length of the plume in the far field is a function of the buoyant flux per unit length and the distance from the virtual source. The following correlation was developed [Equation (2-22)] which was not dependent on ρ, the density of the gases in the plume [as required by Equation (2-14)].

$$M_p = CQ^{1/3}(z + z_0) \tag{2-22}$$

Where

$$C = 0.3C_m\rho_1 W^{2/3} \tag{2-23}$$

C_m is a dimensionless entrainment coefficient which depends on the entrainment constants α and λ (as given by Lee and Emmons [26]). This entrainment coefficient was deduced empirically and will be discussed in relation to more fundamental line plume studies in section 2.1.5. Poreh et al deduced the location of the virtual source of the plume, by examining the condition when the height of the layer in the smoke reservoir was the same as the base of the approach flow. In this case, there is no additional entrainment as the smoke flows from the spill edge and, $M_p = M_b$. For this condition, the height of the smoke layer above the spill edge, $z = -d_b$. Therefore, Poreh et al deduced from Equation (2-22) that,

$$M_b = CQ^{1/3}(-d_b + z_0) \tag{2-24}$$

Hence,

$$z_0 = d_b + \frac{M_b}{CQ^{1/3}} \tag{2-25}$$

By substituting Equation (2-25) into Equation (2-22), Poreh et al deduced the following simplified formula to determine the mass flow rate of gases due to a spill plume [see Equation (2-26)].

$$M_p = Q^{1/3} C\left(z + d_b + \frac{M_b}{CQ^{1/3}}\right) \tag{2-26}$$

To determine the value of the constant C, Poreh et al used the data produced from five experimental studies of spill plumes described by Marshall and Harrison [42]. The experimental data was used to correlate $\frac{M_p}{Q^{1/3}}$ against $(z + z_0)$ for those studies which used a large area smoke reservoir (Series II to V).

The results of this correlation determined the constant, $C = 0.15$. Poreh et al deduced the dimensionless entrainment coefficient, $C_m = 0.44$, using Equation (2-23). This entrainment coefficient was slightly smaller than values of C_m proposed from more fundamental line plume studies. Poreh et al deduced that for $C_m = 0.44$, the entrainment coefficient, $\alpha = 0.11$, which was lower than the value of 0.16 proposed by Lee and Emmons [26]. This will be discussed further in section 2.1.5.

Equation (2-26) can be rearranged to express the amount of air entrained into the rising plume [i.e.$(M_p - M_b)$], which is described by Equation (2-27). In this case, the virtual source is conveniently located at the base of the smoke layer at the spill edge.

$$(M_p - M_b) = BQ^{1/3} W^{2/3} (z + d_b) \tag{2-27}$$

where,

$$B = 0.3 C_m \rho_1 \tag{2-28}$$

The correlated data determined the constant, $B = 0.16$, for a free spill plume with no entrainment into the ends. This form of the Poreh et al method is given within guidance on spill plumes in the UK [43].

Poreh et al state that this calculation method only applies to free spill plumes and does not include entrainment of air into the ends of the plume. It also applies to large area reservoirs from which the empirical constants were derived. This method should not be used for small area reservoirs. The criterion defining the differential between large and small area reservoirs can be considered to be that given by Morgan et al [2], which is described in section 2.1.2.1.

Poreh et al also carried out a similar correlation using data produced from small area smoke reservoirs. Experimental data from Marshall and Harrison (Series I) [42], and from Hansell et al [35] were used. Poreh et al highlighted a distinct increase in entrainment between these data ($C = 0.25$) and that produced from studies from large area reservoirs. Possible reasons for the difference in entrainment were discussed (e.g. the relative size and shape of the smoke reservoir, tendency for the plume to become three dimensional), however, Poreh et al stated that further work on the effect of entrainment due the geometry of the smoke reservoir is highly desirable.

2.1.3.6 Method by Thomas et al (1998)

Thomas et al used a rigorous dimensional analysis in the development of a simplified spill plume model. This method does not require an explicit term to specify the location of the virtual line source, nor does it make the assumption of self-similar flow profiles (e.g. Gaussian profiles) in terms of temperature and velocity throughout the plume.

Thomas et al used the data given by Marshall and Harrison [42] and Poreh et al [22] in the development of the calculation method. This method requires the prior calculation of the mass flow rate and convective heat release of the gases at the spill edge.

Thomas et al provided the following simplified spill plume formula [Equation (2-29)], which applies to free spill plumes in large area smoke reservoirs.

$$M_p = 0.16zQ^{1/3}W^{2/3} + 0.0027Q + 1.2M_b \tag{2-29}$$

Thomas et al also provided an alternative version of the spill plume formula provided by Poreh et al, so that it was in the same form as Equation (2-29). To achieve this, the following empirical relationship was derived from the data used by Poreh et al [see Equation (2-30)].

$$\frac{d_b\left(\frac{Q}{W}\right)^{1/3}}{\left(\frac{M_b}{W}\right)} = 2.50\left(1+\frac{Q}{c_{p,air}T_1M_b}\right) \tag{2-30}$$

Thomas et al then substituted Equation (2-30) into Equation (2-27) to remove an element of redundancy requiring the calculation of both M_b and d_b. This then gave Equation (2-31) which Thomas stated as being an acceptable alternative to Equation (2-29) . This form of the Thomas et al method is given within guidance on spill plumes in the UK [43].

$$M_p = 0.16zQ^{1/3}W^{2/3} + 0.0014Q + 1.4M_b \tag{2-31}$$

Thomas et al also proposed another term to quantify the entrainment of air into the free ends of the spill plume given by Equation (2-32). Thomas et al state that this term should be treated with caution, it applies when values of z/W are 'not too large' and the limit of this criterion remains unknown until further data is available.

$$\delta M = 0.09z\left(\frac{Q}{W}\right)^{1/3} \tag{2-32}$$

2.1.4 Selection of an appropriate spill plume formula

Morgan et al [2] presented a summary of some of the calculation methods described above, and provided recommendations for the appropriate selection of a spill plume formula.

Morgan et al state that whilst the BRE spill plume method is complicated to use, it covers both free and adhered plumes. It can also be used for spill plumes within large and small area smoke reservoirs, with or without air entrainment into the free ends. Morgan et al state that the BRE spill plume method is the most versatile of all of those methods available.

The method by Poreh et al (see section 2.1.3.5) is recognised by Morgan et al as being much simpler. However, this method only applies to the scenario for a spill plume bounded by walls, which prevents entrainment of air into the ends of the plume. This is likely to severely limit the range of scenarios in which this method can be applied. Although this method was derived using data from a free spill plume, work by Marshall [44] indicates that this method can also be applied to adhered spill plumes if the value of the entrainment coefficient, C_m, is reduced from 0.44 to 0.21. The Poreh et al method only applies to large area reservoirs.

Morgan et al state that the Thomas (1987) method (see section 2.1.3.2) only applies to free plumes and cannot be used for adhered plumes. However, entrainment into the free ends can be explicitly calculated. This method can only be applied with confidence for large area reservoirs, not small area reservoirs. They also highlighted the difficulty in selecting an appropriate location for the virtual line source, z_o, which is required as an input parameter for this method. They state that this method should only be used when the location of the virtual source can be calculated directly. Morgan et al suggest that the location of the virtual source as defined by Poreh et al [Equation (2-25)] could be used in the Thomas method as a reasonable approximation of the location of the virtual source.

Morgan et al state that the Thomas et al (1998) method (see section 2.1.3.6) can be expected to only apply to free plumes within large area reservoirs. The term which explicitly calculates the entrainment of air into the free ends of the plume is a speculative correction and should be treated with caution.

Morgan et al also made a comparison between these calculation methods for a particular design scenario. There was reasonably close agreement between all of the calculation methods for a height of rise of plume up to 5 m above the spill edge. The methods diverged for greater heights of rise. Morgan et al recommended the following for an appropriate choice of a spill plume formula:

- For free plumes rising less than 3 m above the spill edge, into a large reservoir, use the Thomas et al (1998) method (see section 2.1.3.6)
- For free plumes rising more than 3 m above the spill edge use either the BRE spill plume method (see section 2.1.2) for large or small area reservoirs, or the Thomas method (1987) (see section 2.1.3.2) for large reservoirs only
- For all other spill plume scenarios, use the BRE spill plume method

2.1.5 Entrainment of air into a thermal line plume

As described earlier, Poreh et al [22] determined the value of the dimensionless entrainment coefficient, $C_m = 0.44$. From this, the entrainment coefficient, $\alpha = 0.11$. This was lower than the value of $\alpha = 0.16$ proposed by Lee and Emmons [26].

Yuan and Cox [45] have presented a number of proposed values for C_m and α, based on the results from various studies of thermal line plumes. These data, in addition to the results from more recent work, are presented in Tables 2.1 and 2.2.

Author	C_m
Yuan and Cox [45]	0.51
Rouse et al [46]	0.58
Chen and Rodi [47] (from Rouse data)	0.48
Lee and Emmons [26]	0.58
Zukoski (Yokoi's data) [48]	0.52
Kotsovinos [49]	0.66
Ramparian and Chanrasekara [50]	0.50
Grove and Quintiere [51]	0.65

Table 2.1: Proposed values for dimensionless entrainment coefficient C_m

Author	α
Yuan and Cox [45]	0.126
Rouse et al [46]	0.162
Yokoi [37]	0.125
Chen and Rodi [47] (from Rouse data)	0.126
Lee and Emmons [26]	0.160
Kotsovinos [49]	0.200
Ramparian and Chanrasekara [50]	0.117
Grove and Quintiere [51]	0.189

Table 2.2: Proposed values for entrainment coefficient α

Poreh et al [22] noted that differences in the proposed values depended on whether estimates were based on direct measurements of the mass flow rate, or calculated from velocity and temperature distributions.

In general, there is increasing evidence to suggest a reduced value of entrainment from that originally proposed by Lee and Emmons.

2.2 Experimental studies of the spill plume

There have been a number of experimental studies of the thermal spill plume. This section describes gives a brief overview of some relevant studies and their findings.

2.2.1 Morgan and Marshall (1975)

Morgan and Marshall conducted a series of $1/10^{th}$ scale model experiments according to the scaling principles set out by Thomas et al [52]. The physical scale model simulated smoke flow from a single shop unit in the form of a free spill plume. Two shop compartments were examined, one compartment had a width of 0.7 m and the other was 1.4 m wide. Both compartments were 0.5 m deep. A removable downstand at the shop opening was also used for selected tests. A 0.4 m broad balcony extended across the full width of the compartment. Channelling screens were attached to each side of the opening to prevent lateral spread, and to achieve a more uniform temperature and velocity distribution across the spill edge.

The hot gases were produced by burning Industrial Methylated Spirits (IMS) at a controlled rate into a 0.2 m by 0.2 m tray. The emerging free spill plume was allowed to freely flow into the laboratory.

Measurements of gas temperature were made at 10 mm below the spill edge to determine θ_b. An array of thermocouples was also located above the spill edge to determine the maximum axial plume temperature. For the majority of the experiments, this array was located 0.31 m above the spill edge, however, for some tests, the array was located at a height of 0.40 m.

The temperature data obtained was used in the development of the BRE spill plume method (see section 2.1.2). Morgan and Marshall empirically determined the entrainment coefficient α' to be 0.90.

Good agreement was obtained between the experimental results and the theoretical prediction using the BRE spill plume method.

Morgan and Marshall noted that much larger smoke exhaust rates were required for safe means of escape than had previously been thought. To reduce the required smoke exhaust capacity, Morgan and Marshall recommended the use of channelling screens to prevent the lateral spread of smoke.

2.2.2 Morgan and Marshall (1979)

Morgan and Marshall [27] conducted another series of $1/10^{th}$ physical scale model experiments which simulated smoke flow from a shop unit into a two storey mall.

The majority of the experiments examined a shop with a width of 0.7 m. Four circular vents were located in the ceiling of the mall. These outlets were connected to an axial fan which provided mechanical exhaust. The model had an array of inlet vents which could be individually closed.

In this work, the hot gases were produced from convector heaters providing a heat output between 1 to 4 kW. This produced a free spill plume from the shop unit.

The mass flow rate of gases in the mall was measured directly using a carbon dioxide tracer gas technique. Columns of thermocouples were located in strategic positions to determine the smoke layer depth.

The fire size, compartment width, clear layer height and number of inlet vents were varied. The BRE spill plume method was used to compare the theoretical mass flow rates with those produced from the experiment.

The results of this study gave rise to the development of the effective layer depth correction (see section 2.1.2.1) to allow for the variation of temperature of the air beneath the smoke layer. The use of channelling screens was also shown to be effective in reducing the required quantity of smoke to be exhausted to achieve a given height of rise of plume.

2.2.3 Hansell, Morgan and Marshall

This work, by Hansell et al [35] describes a series of experiments within a $1/10^{th}$ scale model atrium building. The geometry of the model atrium was relatively tall and narrow compared to model used by Morgan and Marshall [27]. The hot gases were produced from a spatially distributed electrical heater within a compartment. Mechanical smoke exhaust was provided from the top of the atrium space to maintain the required clear layer height. Measurements of temperature and the mass flow rate of the gases were made at strategic locations.

This work aimed to address various uncertainties relating to smoke control calculation methods. Issues such as the horizontal flow of gases toward an opening, air entrainment into free and adhered plumes, limitations to the BRE spill plume method and the effect of balcony breadth were studied. A brief summary of the findings of this work is described below.

2.2.3.1 Horizontal flow of gases toward a compartment opening

A study of the approach flow of gases beneath the spill edge confirmed the assumption made by Morgan [30], that a horizontal flow approaching a flush ceiling free edge experiences an effective discharge coefficient of 1.0.

2.2.3.2 Comparison between visually and buoyancy derived layer depths

This work demonstrated that the relationship between visually and buoyancy (from thermocouple measurements) derived smoke layer depths was different to that observed in earlier work. This relationship appeared to be dependent on the smoke layer geometry (i.e. relationship between the layer depth to its width). This difference was linked to the aspect ratio of the smoke reservoir and has implications for the effective height of rise of the plume used for design.

A tentative proposal for reconciling these differences with respect to the aspect ratio of the smoke reservoir was presented. This has been taken into account when defining the criteria for applying the effective layer depth correction (see section 2.1.2.1). Hansell et al [35] stress that further work in this area is highly desirable.

2.2.3.3 Effect of balcony breadth

Hansell et al [35] examined the effect of changing the breadth of the balcony at the compartment opening. Three balcony breadths were examined, 1.25 m, 2.5 m and 5 m (full-scale equivalent).

For flows without channelling screens, lateral smoke spread beneath a projecting balcony was minimal for balconies not more than 1.5 m in breadth for large design fires (e.g. 5 MW), or not more than 1.0 m in breadth for smaller fires (e.g. 1 MW). It was recommended that channelling screens should be used with broader balconies.

It was found that balconies broader than 2 m will allow the plume to rise through the atrium space as a free plume (see Figure 2.3). Balconies narrower than 2 m will cause smoke logging between the plume and the wall behind (see Figure 2.4).

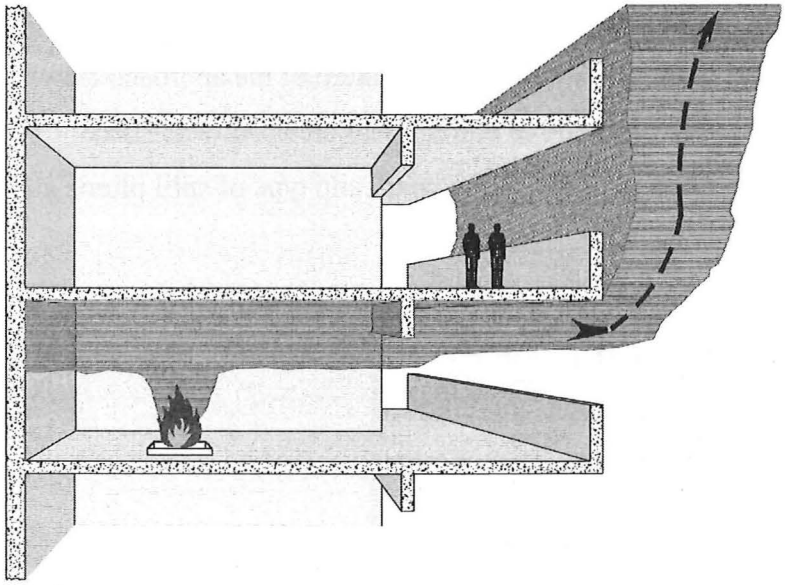

Figure 2.3: Typical smoke flow for balconies broader than 2 m [courtesy of NV IFSET SA]

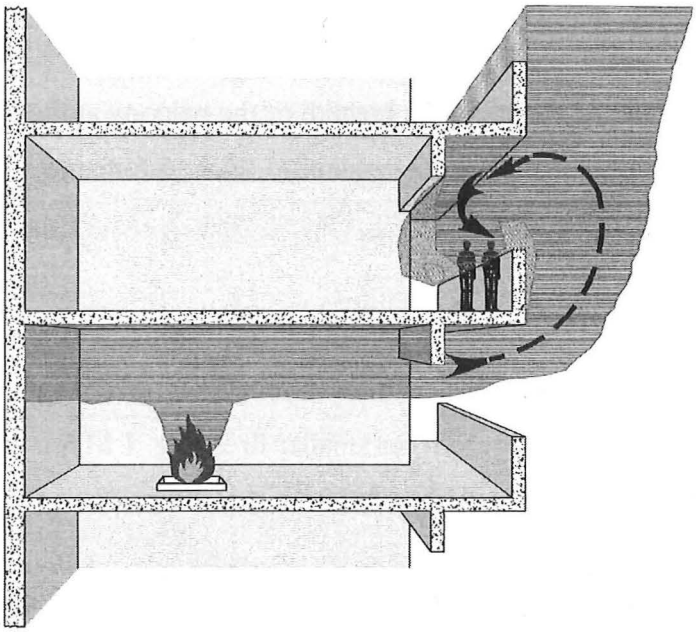

Figure 2.4: Typical smoke flow for balconies narrower than 2 m [courtesy of NV IFSET SA]

2.2.3.4 Entrainment and temperature limitation

Hansell et al [35] found that there was a critical temperature of the approach flow, above which, the BRE spill plume method of entrainment breaks down. These limiting temperature criteria are dependent on the width and type of spill plume and are given in Table 2.3.

Plume type	Opening width (m)	Limiting temperature (^{o}C)
Free	4 to 5	250
Free	7	330
Adhered	4	280

Table 2.3: Limiting temperature criteria for the BRE spill plume method

Hansell et al [35] also found that the BRE spill plume method for adhered plumes should be used with an effective entrainment constant, $\alpha = 0.077$. This is approximately half that for a free plume and should only be used with 'Gaussian profile' plume models.

2.2.4 Marshall, Harrison and Morgan

Marshall et al [53] again used the approach of physical scale modelling to examine air entrainment into a thermal spill plume. In this work, comparison was made between various calculation methods and the experiment for spill plumes with a low height of rise (up to approximately 5 m, full scale).

Marshall et al showed that for a free spill plume with entrainment of air into the ends of the plume, the BRE method was reliable above a minimum height of rise of 3 m (full scale). For free plumes without entrainment of air into the ends, the BRE method was reliable above a minimum height of rise between 4 to 5 m.

In general, this work highlighted a discrepancy between the experiment and the theoretical predictions below these limiting heights of rise of the plume. This discrepancy was suggested to be due to the violation of one of the fundamental assumptions in the theory. In general, the calculation methods make the assumption that the vertically rising spill plume has temperature and velocity profiles which are Gaussian in nature across the plume over its full height. However, Marshall et al recognised that for the spill plume, this condition will not occur immediately after the rotation region, as the temperature and velocity profiles are skewed. The gases need to pass through a "transition region" immediately after rotating around the spill edge, prior to the development of a flow which is Gaussian in nature. In general, it appears that for free plumes the height of this transition region is approximately 3 m (full scale).

This work also demonstrated that the method given in NFPA 92B [9] gave an extremely poor match with the experiment for all heights of rise examined.

2.2.5 Marshall and Harrison

Marshall and Harrison [42] summarised the results of five separate series of experiments on spill plumes using physical scale modelling. These experiments examined various uncertainties in spill plume calculations. The data produced from these studies was used in the development of the calculation method described by Poreh et al [22]. A summary of the general findings of these studies is given below.

2.2.5.1 Geometry of smoke reservoir

Each series of experiments contained a smoke reservoir with a different geometry. This work demonstrated that relatively small smoke reservoirs caused additional air entrainment compared to larger smoke reservoirs. This led to a larger mass flow rate of gases being measured in the smoke reservoir for identical fire conditions. Marshall and Harrison noted that the flows within the small reservoir were more turbulent compared to the larger reservoirs, with local deepening effects at the walls leading to an unstable fluctuating smoke layer.

The effect of smoke reservoir geometry on air entrainment has been taken in to consideration in guidance given by Morgan et al [2] which is described in section 2.1.2.1 . Further work is desirable to examine this effect in a systematic way.

2.2.5.2 Counter flow at the compartment opening

One of the fundamental assumptions of the BRE method is that the velocity of incoming air at the fire compartment opening is much smaller than the outward flowing hot gas layer. To ensure that this condition occurred, a sliding shutter was installed at the fire compartment opening (for two experimental series) to prevent the passage of free air to the fire, without significantly affecting the outward flowing gases. The height of this shutter was adjusted so that it was just beneath the observed smoke layer. The fire drew air in through ducts, at the rear and base of the compartment, allowing the inflow of air to be measured.

However, for the remaining experimental series, the shutter was removed and free air was allowed to pass into the compartment beneath the smoke layer. This created a counter flow to the outward flowing gas layer from the compartment opening.

Marshall and Harrison showed that a counter flow at a compartment opening produced a 30% increase in the layer depth and mass flow rate of gases at the opening. This led to a 15% increase in the mass flow rate of gases entering the layer in the smoke reservoir. Marshall and Harrison suggested that this increase was likely to be due to the inflow of air affecting the plume behaviour within the fire compartment. Visual observations showed that the inflow of air caused the fire plume to lean towards the rear wall of the compartment. Earlier work [24,54] has suggested that a leaning fire plume within a cellular room will entrain more air than an upright fire plume. Marshall and Harrison utilised an equation developed by Hansell [24] to demonstrate that the experimental measurements of the mass flow rate of gases at the compartment opening were comparable with the theoretical predictions for a leaning plume.

The results suggest that the BRE method could be used with confidence with counter flow air at a compartment opening.

2.2.5.3 Air entrainment into the ends of the spill plume

Marshall and Harrison demonstrated that entrainment of air into a rising spill plume increased by approximately 30% when air was allowed to enter into the free ends of the plume.

2.2.5.4 Helium as an alternative method

Marshall and Harrison also demonstrated the feasibility of using Helium gas as an alternative source to heated air for studying the flow of hot gases within physical scale models. This technique was originally suggested in unpublished work by Poreh. Helium has an advantage over thermal methods in that there is no heat transfer from the simulated fire source or from the resulting plume. Experiments could also be

carried out over a shorter time duration, since there is no need to wait for thermal equilibrium. The main disadvantage of Helium was its high cost.

2.2.6 Yii

Yii [32] carried out a study of the spill plume using salt water modelling and a Laser Induced Fluorescence (LIF) flow visualisation technique. The tests were carried out within a $1/20^{th}$ scale model. Salt water modelling can only simulate relatively small density differences, corresponding to relatively low temperatures above ambient (i.e. 30 to 50 ^{o}C above ambient)

Yii demonstrated that good flow visualisation of the spill plume could be achieved using the LIF technique.

Yii showed that there was a small degree of entrainment into the rotation region of the spill plume. It was also observed that the presence of a downstand at a compartment opening resulted in significant entrainment in the under balcony layer flow. Yii also showed that smoke logging on an upper balcony was found to be more severe for a short balcony compared to a long balcony.

This study only identified flow features of the spill plume as the LIF technique was the only method used for investigation. Measurements of the mass flow rate of the spill plume were not made.

2.3 Computer modelling studies of the spill plume

2.3.1 Miles, Kumar and Cox

Miles et al [31] used Computational Fluid Dynamics modelling (CFD) to examine entrainment of air into a spill plume. Numerical simulations were carried out of fires within the $1/10^{th}$ physical scale model described by Marshall and Harrison [42]. The CFD model, JASMINE, was used in the analysis. Comparisons were made between the CFD predictions and the experimental results.

The CFD study suggested that there was only a small degree of entrainment into the rotation region of the spill plume. The CFD predictions agreed well with the experimental data from Marshall and Harrison [42] for low heights of rise of the plume, but appeared to diverge at greater heights.

Miles et al suggested that this divergence could be due to the apparently unrealistic assumption of a horizontal layer within the smoke reservoir. Alternatively, this divergence could have been due to the application of an inappropriate turbulence model for this flow.

The simulations agreed well with the correlations developed by Poreh et al [22] and Thomas et al [23].

2.3.2 Chow (1998)

Chow [55] also used CFD to examine entrainment of air into a spill plume. The computer model CC-EXACT was used for the analysis. Chow also simulated fires within the $1/10^{th}$ physical scale model described by Marshall and Harrison [42]. Six simulations were carried out, varying the fire size and the smoke exhaust rate from the smoke reservoir.

A linear correlation was derived from the predicted results. This correlation provided a result which was similar to that described by Poreh et al [22].

Chow concluded that the results of this study suggest that the CC-EXACT model is a suitable tool to study smoke filling in atria from a spill plume.

2.3.3 Chow (1999)

Chow [56] again simulated the spill plume within the physical scale model described by Marshall and Harrison [42]. The CFD model PHOENICS 3.1 was used in this work.

A fixed fire size of 17 kW was examined with 6 different exhaust rates from the smoke reservoir. The location of the neutral plane in the smoke reservoir was examined with respect to each smoke exhaust rate.

2.3.4 Chow and Li

Chow and Li [57] developed a two-layer zone model named CL-Atrium to describe entrainment of air into a rising spill plume. The correlations given by Poreh et al [22], Thomas et al [23] and the correlation in NFPA-92B [28] were each used in the model and assessed.

Comparisons were made between the CL-Atrium model results and another zone model (CFAST). Both steady state and growing fires were used in the analysis.

The results from the model indicated that the layer temperature and interface height in the smoke reservoir were similar either when using the Poreh et al [22] or Thomas et al [23] methods.

The results based on the correlation in NFPA-92B [28] were similar to those predicted by CFAST.

2.3.5 Li and Chow

Li and Chow [58] again used the CFD model PHOENICS 3.1 to simulate a spill plume within an atrium building. However, in this study, the effect of smoke filling within a thermally stratified atrium space 30 m high, 20 m long and 10 m wide was examined.

This work demonstrated the effect of stratification of smoke from a spill plume prior to reaching the ceiling of the atrium space. Li and Chow provide an expression to determine the minimum fire size required such that stratification does not occur. The maximum height that the spill plume will reach can also be calculated.

2.4 Entrainment of air into a flow from a compartment opening to a higher projecting balcony

Unfortunately, there has been little work explicitly studying entrainment of air into a flow from a compartment opening to a higher projecting balcony. Morgan and Hansell [29] referenced unpublished work by Marshall, which had identified that this additional entrainment, when expressed as a percentage of the mass flow at the compartment, varied from 73% (+/- 19%) for a 7 m wide compartment opening to approximately 150% for a 14 m wide opening. This indicated that the amount of entrainment varied with the precise geometry involved. As there was insufficient data to accurately quantify the amount of entrainment for all likely geometries, an entrainment value of 100% was proposed as being representative for most cases. Therefore, for the purposes of engineering design, the mass flow rate of smoke at the spill edge was taken to be twice that at the compartment opening [see Equation (2-33)].

$$M_b = 2M_w \tag{2-33}$$

It was recognised that this assumption was crude and further work was necessary to quantify this entrainment. This advice is currently contained in guidance for the design of SHEVS in atrium buildings [2,8].

More recent work has been carried out in an attempt to better quantify this entrainment. A summary of this work is given below.

2.4.1 Hansell

A calculation method was developed by Hansell [24] to determine the entrainment of air into a flow from a compartment opening to a higher projecting balcony.

This method was derived from limited full scale experimental data obtained from fires within a relatively narrow compartment opening (a maximum of 5 m wide by 3 m high). In all cases, the compartment opening had a width which was equal to the spill edge. The Hansell method is given as follows:

- Assume a mass flow rate under the balcony at the spill edge (M_b). This will necessarily be greater than or equal to the mass flow rate of gases out of the room opening (M_w).

- Calculate the entrainment of air into the gases as they rise past the downstand to meet the balcony.

$$M_b - M_w \tag{2-34}$$

- Using the assumed value of M_b and the known convective heat output Q, calculate the depth of the flowing smoke layer at the spill edge (d_b) and the layer temperature at the spill edge (θ_b).

- Calculate a height parameter X_u

$$X_u = 0.5d_w + d_d - d_b \tag{2-35}$$

- Calculate a velocity ratio μ

$$\mu = \frac{(M_b - M_w)T_b}{Wd_b\rho_1(2g\theta_b T_1 X_u)} \tag{2-36}$$

- Calculate angle χ

$$\chi = 93.5 - 58.75\mu \tag{2-37}$$

- Calculate an effective rotational entrainment constant α"

$$\alpha" = \alpha Cos\chi \tag{2-38}$$

- Calculate the entrainment on rotation by whichever of the following is appropriate.

i) When $d_b \leq d_d$ and $(d_d - d_b) \leq 1$, then

$$\delta m = \frac{2}{3}\rho_1 W \alpha" \left[2g\frac{\theta}{T}\right]^{1/2} d_w^{3/2} \tag{2-39}$$

ii) When $d_b \rangle d_d$ entrainment during the partial rotation is smaller than in Equation (2-39) and can be calculated as follows. First calculate a function $Sin\psi$:

$$Sin\psi = \left[1 - \left(\frac{d_b - d_d}{d_w}\right)^2\right]^{1/2} \tag{2-40}$$

then calculate the entrainment on rotation.

$$\delta m = \frac{2}{3}\rho_1 W \alpha" \left[2g\frac{\theta}{T}\right]^{1/2} d_w^{3/2} Sin\psi \tag{2-41}$$

- Calculate a new value for the mass flow rate M_b

$$M_b = M_w + \delta m \tag{2-42}$$

- Compare the new value of M_b with the value assumed in Step 1 of this procedure.

Iterate the entire procedure from Step 1 until Equation (2-42) gives a result which has converged.

2.4.2 Garrad

Garrad [25] made an analysis of the Hansell method given in section 2.4.1. Fourteen calculations were carried out for compartment openings with different widths ranging from 1 to 20 m. The height of the compartment was assumed to be 4 m, and the compartment opening height was assumed to be 3 m, for all of the scenarios examined.

Garrad showed that the Hansell method was unstable for many different scenarios and convergence of a solution was often not achieved. The possibility of convergence was also sensitive to the chosen value for M_b at the start of the iteration process. In some cases the iterative result became chaotic.

Garrad found that convergence of a result was not possible for large openings, although a reasonable result was possible for narrow openings similar to those in which the method was derived.

For narrow openings, Garrad found that M_b was significantly smaller than $2M_w$ as given by Equation (2-33). However, Garrad recommended that until further research was carried out, the guidance given by Equation (2-33) should remain as a conservative estimate for design purposes.

CHAPTER 3

3. APPROACH

The technical approach for this study was a combination of physical scale modelling and CFD modelling. A brief description of each of these modelling techniques is described in this chapter.

3.1 Physical scale modelling

The approach of physical scale modelling is well established and has been used in many studies of smoke movement and control in buildings. The approach used in this work was primarily developed at the Fire Research Station in the UK [52,59] and typically takes the form of reduced scale fires within a physical model.

Measurements are generally made of temperature, velocity and gas concentrations, in addition to visual observations. Measurements can be extrapolated to full scale using the appropriate scaling laws.

3.1.1 The scaling laws for turbulent flow

To ensure that the results can be extrapolated to full scale, the physical scale model used in this study was designed to meet the scaling principles set out by Thomas et al [52]. This is effectively a modified Froude number scaling and requires that the equivalent flows are fully turbulent on both full and model scale, i.e. that the significant flows should have Reynolds numbers ≥ 4000 [60]. Based upon the work by Thomas et al [52], Morgan et al [61] derived dimensional relationships between fluid dynamic variables from first principles in a more explicit and simpler manner. The derivation is given as follows [61]:

Fully developed turbulent flows of incompressible fluids can be described by equations of the general form of D'Arcy's formula where the pressure difference driving the flow is approximately proportional to the flow-velocity squared.

$$\Delta P \propto u^2 \rho \tag{3-1}$$

The power of u can vary for different scenarios, and is a function of the Reynolds number [52]. However, for most cases, Equation (3-1) is a good approximation.

For the special case of fluid flows driven only by buoyancy, the pressure difference depends only on the buoyant head, i.e.

$$\Delta P = \Delta \rho g h = \rho_1 \frac{\theta}{T} g h \tag{3-2}$$

Equation (3-2) becomes

$$\Delta P \propto \theta h \tag{3-3}$$

Combining Equations (3-1) and (3-2), gives, in terms of the length scale,

$$\theta L \propto u^2 \tag{3-4}$$

The expression for the volume rate of flow across an area (A) normal to the flow is,

$$V = uA \tag{3-5}$$

In dimensional terms, this becomes,

$$V = uL^2 \tag{3-6}$$

The convected heat flow across this area due to the flow is given by,

$$Q = Mc_p\theta = \rho V c_p \theta = \rho_1 T_1 c_p V \frac{\theta}{T} \tag{3-7}$$

In dimensional terms, this is,

$$Q \propto \theta M \propto \frac{\theta V}{T} \tag{3-8}$$

Provided that each variable is assumed to refer to similar spatial locations in the fluid dynamic system (i.e. to similar points in both the full-scale system and in the small scale model), these dimensional relationships can be used to derive the scaling laws.

From Equations (3-4) and (3-5), and eliminating u,

$$V \propto L^{5/2}\,\theta^{1/2} \tag{3-9}$$

From Equations (3-8) and (3-9) , and eliminating V,

$$Q \propto \frac{L^{5/2}\,\theta^{3/2}}{T} \tag{3-10}$$

These relationships can be simplified by holding one of these variables constant. For experimental modelling, it is convenient to keep the temperature above ambient equal on both full and model scale. Hence, the same temperature must apply to the corresponding points in the flow system, irrespective of scale. Therefore, if the temperature above ambient is constant, the scaling laws become,

$$\begin{aligned} Q &\propto L^{5/2} \\ M &\propto L^{5/2} \\ V &\propto L^{5/2} \\ u &\propto L^{1/2} \end{aligned} \tag{3-11}$$

and the time scale ω, which is described for the flow system by,

$$\omega \propto \frac{L}{u} \propto L^{1/2} \tag{3-12}$$

Hence, if the linear scale is changed by a factor of 9, the time scale will change by a factor of 3, the mass flow rate by a factor of 243.

Alternatively, one can hold the length scale L constant. This is useful for extrapolating the results from a given size flow system for a particular heat input, to other values of heat input for the same size system. In this case, where $\theta \leq T$, Equation (3-10) becomes,

$$Q \propto \frac{\theta^{3/2}}{T} \tag{3-13}$$

The constant of proportionality can be found using experimental results and a new value of θ found for another value of the heat input. The scaling laws now become,

$$\begin{aligned} V &\propto \theta^{1/2} \\ M &\propto \frac{\theta^{1/2}}{T} \\ u &\propto \theta^{1/2} \\ \omega &\propto \theta^{-1/2} \end{aligned} \tag{3-14}$$

For 'cool' models, where $\theta \langle\langle T$, Equations (3-13) and (3-14) reduce to,

$$\begin{aligned} Q &\propto \theta^{3/2} \\ u &\propto \theta^{1/2} \\ V &\propto \theta^{1/2} \\ M &\propto \theta^{1/2} \\ \omega &\propto \theta^{-1/2} \end{aligned} \tag{3-15}$$

It should be noted that all of the above applies only to a flow that is fully turbulent, is driven by buoyancy forces alone and where there are large variations in density of the hot gases.

Similar scaling laws for laminar flow can be derived by replacing Equation (2-1) with an equation of the form of Poiseulle's formula,

i.e. $\Delta P \propto u$

and then proceeding by similar methods to those above.

It should be noted that the above scaling laws do not describe either conductive or radiative heat transfer processes. If either is present to a significant extent in the flow system, the scaling laws derived here cannot be applied.

For this particular study, the temperature above ambient has been assumed to be equal on both full and model scale. Therefore, those equations given by (3-11) will apply.

3.2 Computational Fluid Dynamics modelling

Computer models based on the techniques of CFD provide detailed predictions of the fluid flow and heat transfer processes associated with applications from across a wide range of science and engineering fields. These include smoke movement studies, which are being undertaken increasingly with CFD fire models in cases where the assumptions made in engineering calculations and zone models may no longer apply.

When using a CFD fire model the geometrical space is discretised with a three-dimensional numerical mesh containing somewhere between ten thousand and one million elements (known also as cells or control volumes). At each numerical mesh element, the model approximates the solution to the underlying set of coupled conservation equations for mass, momentum, energy and species concentrations. A summary of CFD modelling and its applications are provided by Versteeg and Malalasekera [62].

CFD has been used to investigate the entrainment of air into flows from a compartment opening to a higher projecting balcony. A detailed examination of this effect using physical scale modelling is potentially time consuming due to the nature of the measurement technique. Therefore, CFD modelling has enabled more scenarios to be examined in the time available. Selected tests have been carried out using physical scale modelling to assess the validity of the CFD predictions.

3.2.1 Fire Dynamics Simulator (FDS)

The CFD model used in this study was Fire Dynamics Simulator (FDS) which has been developed by McGrattan et al [63] of the National Institute of Standards and Technology.

This model numerically solves a form of the Navier-Stokes equations appropriate for low-speed, thermally driven flows typically generated by smoke and heat transport from fires. The fundamental equations and the numerical algorithm within the model are given by McGrattan et al [64] and are not repeated herein. In this study, FDS was set to treat turbulence by means of the Smagorinsky form of Large Eddy Simulation (LES).

The results of the model have been visualised using the post processing tool called Smokeview (version 3.1) developed by Forney and McGrattan [65]. Smokeview is a 3-dimensional imaging software tool which can show isosurfaces (e.g. temperature, mixture fraction) and 3D data files (e.g. temperature, velocity and pressure).

CHAPTER 4

4. SCALE MODEL EXPERIMENTS: APPARATUS AND METHODOLOGY

Physical scale modelling was used in a detailed examination of entrainment of air into a thermal spill plume. This approach was also used for selected tests to examine entrainment of air into a flow from a compartment opening to a higher projecting balcony for CFD validation purposes.

Details of each series of experiments are described below, including the experimental apparatus, instrumentation, method and data analysis techniques.

4.1 Experiments examining entrainment of air into a spill plume

4.1.1 The physical scale model

The apparatus used for this work was a $1/10^{th}$ physical scale model (see Figures 4.1 and 4.2). The model essentially consisted of a steel frame with 'Kaowool' ceramic fibre insulation (CFI) boards attached. The ceramic boards were protected on the external surfaces by a 2 mm thick steel substrate. The model simulated a fire within a communicating space in an atrium building, and consisted of two main units, the fire compartment and the smoke exhaust hood. The model was designed to meet the scaling principles set out by Thomas et al [52] (see section 4.1.1.1).

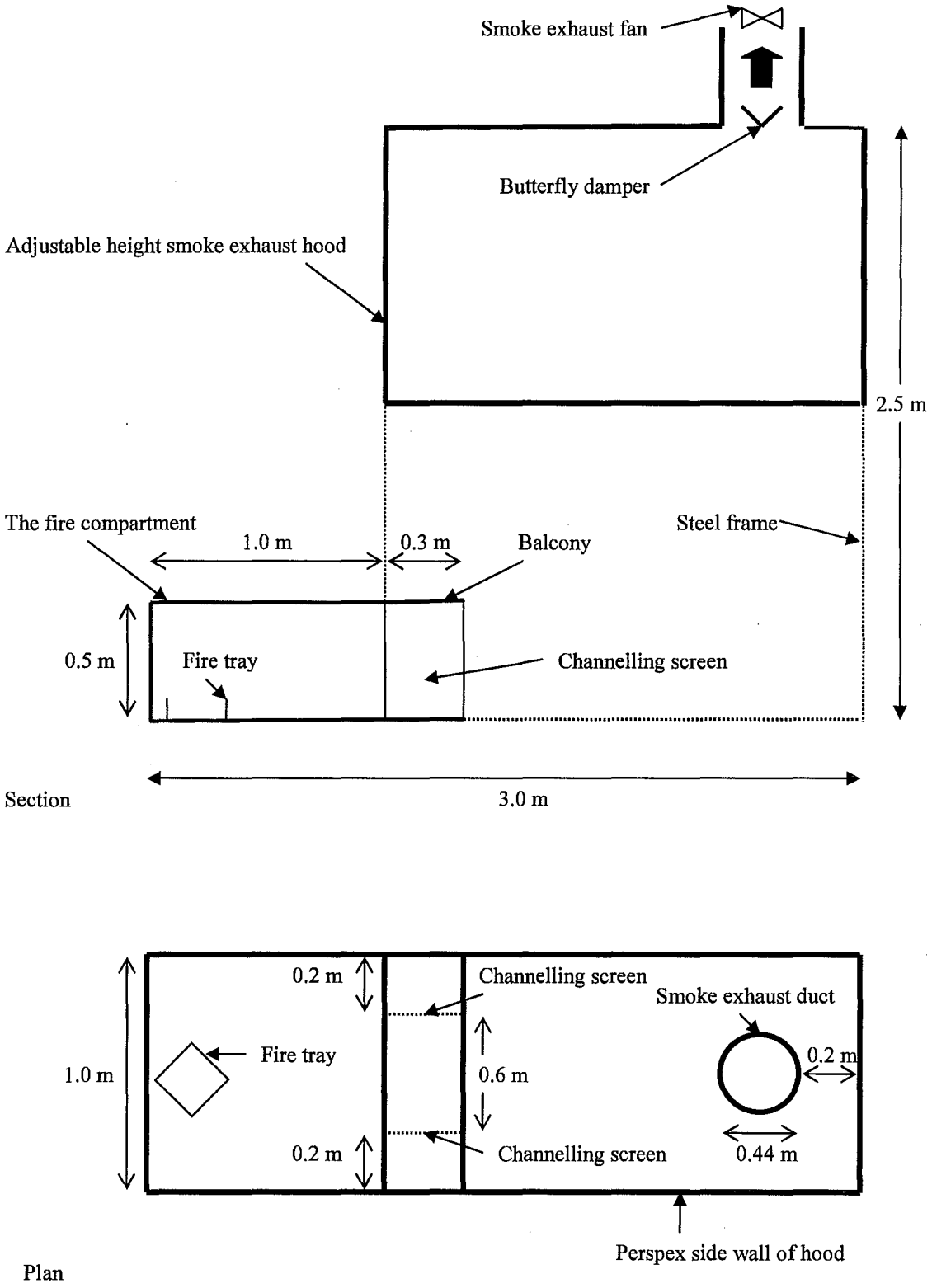

Figure 4.1: Schematic drawing of the 1/10th physical scale model

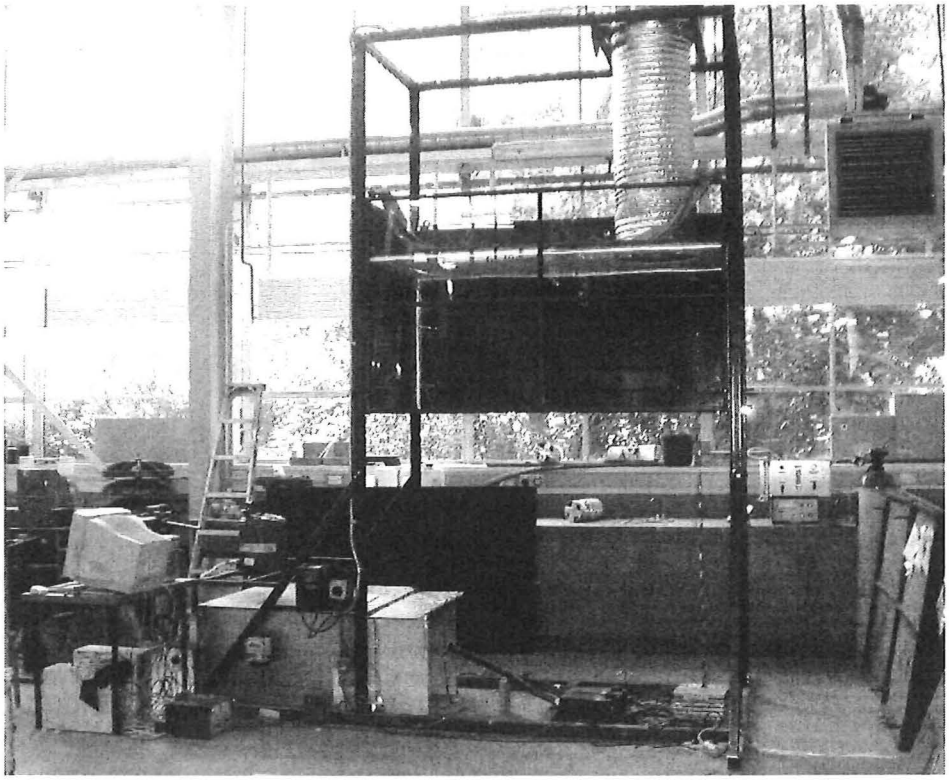

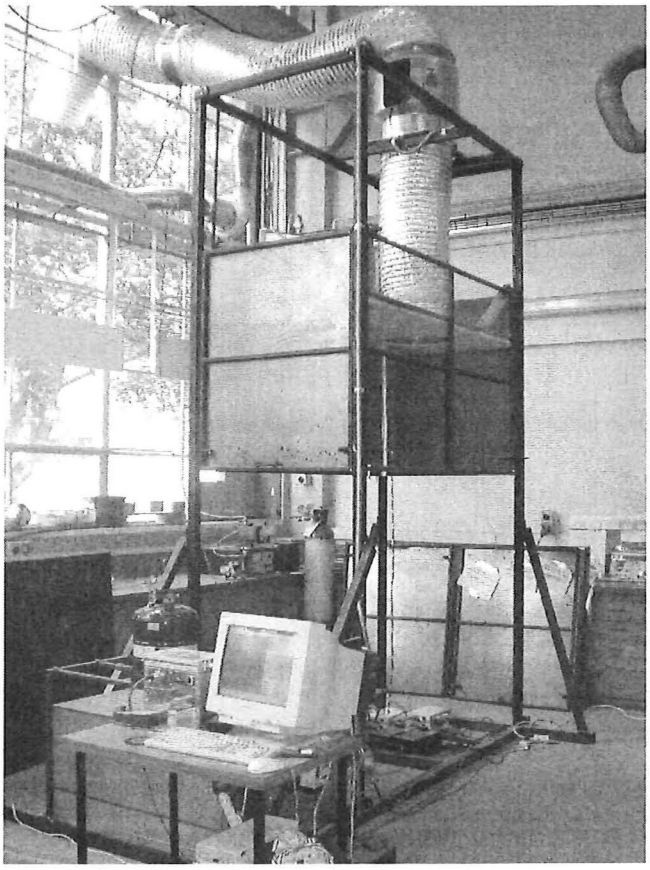

Figure 4.2: The physical scale model

4.1.1.1 Reynolds number of typical flows

As described in section 3.1.1, this particular form of scaling requires that the equivalent flows are turbulent on both full and model scale, i.e. that the significant flows should have Reynolds numbers > 4000 [60]. The Reynolds number can be calculated using the following equation.

$$\mathrm{Re} = \frac{uD}{\nu} \tag{4-1}$$

In this series of experiments the Reynolds number was calculated to range between 9,606 and 25,815 for the flows from the fire compartment opening (see Example 4.1 below). This demonstrated that the scaling laws could be applied with confidence for the physical scale model.

Example 4.1:

Calculation of Reynolds number for Test 1 (0.2 m downstand at spill edge, 6 kW fire):

u = 0.29 ms^{-1} (near base of gas layer)
ν = 17.91 x 10^{-6} (m^2s^{-1})
D = 0.6 m (lateral extent of spill plume)
Re = 9,606

Calculation of Reynolds number for Test 9 (flat ceiling at the spill edge, 12 kW fire)

u = 1.39 ms^{-1} (near top of gas layer)
ν = 32.39 x 10^{-6} (m^2s^{-1})
D = 0.6 m (lateral extent of spill plume)
Re = 25,815

4.1.1.2 The fire compartment

The fire compartment was constructed from 20 mm thick CFI board with a 2 mm thick steel substrate on each external face.

As the lateral extent of the spill plume will tend to broaden as the height of rise increases (with end entrainment), preliminary tests were carried out to determine an appropriate width of fire compartment opening so that plume would be contained within the 1.0 m wide smoke exhaust hood. An appropriate width of compartment opening was determined to be 0.6 m to contain smoke within the hood for all of the tests.

A 0.3 m broad balcony constructed from 10 mm thick CFI board with a 2 mm thick steel substrate was attached to the fire compartment opening and extended across its full width.

Channelling screens made from 10 mm thick CFI board were located at each side of the compartment opening beneath the balcony and occupied the full breadth of the balcony (see Figures 4.1 and 4.3). The channelling screens were used to provide reasonably homogeneous temperature and velocity profiles across the width of the opening. This enabled the mass flow rate of gases to be determined from a single velocity and temperature traverse through the smoke layer. The channelling screens occupied the full height of the fire compartment as in previous work [35,42]. In reality, these channelling screens would not occupy the full height of the compartment, but would be deep enough to contain the approach flow beneath the balcony. However, in the experiment, the channelling screens were made full height to contain all possible approach flows for the range of conditions studied. The flow conditions at the compartment opening are likely to be similar, either when using full height or short channelling screens, provided that the approach flow is contained within the screens.

The fire compartment was modified such that a downstand could be attached at the spill edge. There were 2 downstands used, 0.1 m and 0.2 m deep respectively. Each downstand was made from 10 mm thick CFI board.

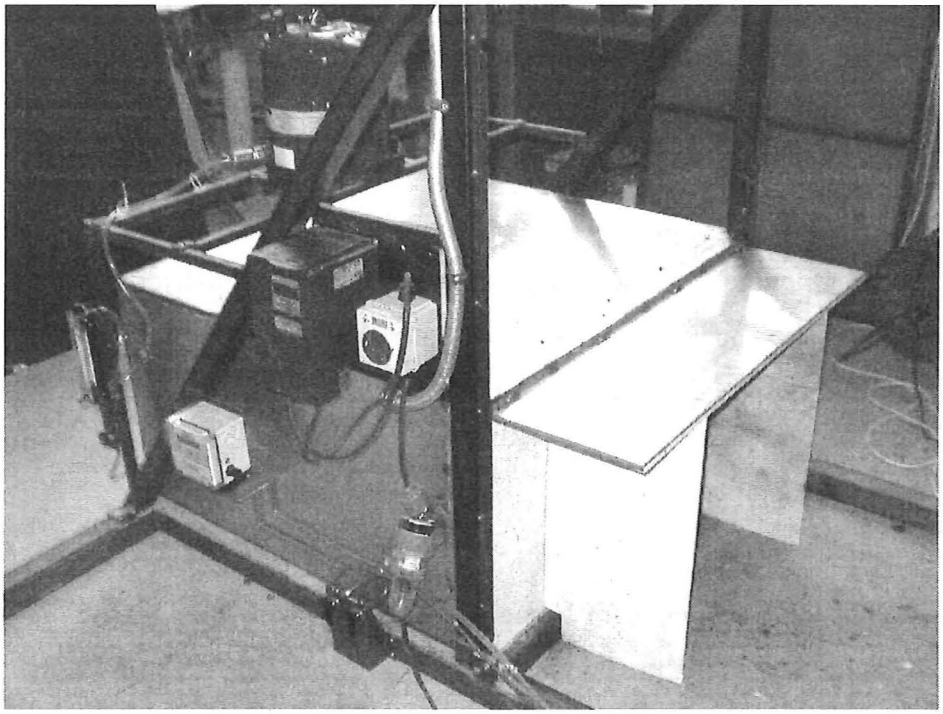

Figure 4.3: The fire compartment

4.1.1.3 The smoke exhaust hood

The side walls of the smoke exhaust hood (see Figure 4.1) were generally constructed from 10 mm thick CFI board with a 2 mm thick steel sheet substrate on each external face. However, one of the (long length) side walls was constructed from 12 mm thick Perspex sheet to enable visual observations to be made of the smoke layer within the collecting hood.

The model was designed such that the walls could freely move in a vertical direction within the supporting frame. However, each side wall contained locking bolts close to its base which could connect to the supporting frame at regular height intervals via holes in the frame (see Figure 4.4). This enabled each wall to be moved independently of each other to the base of the observed smoke layer in the hood. This prevented warming of the air nominally beneath the observed smoke layer through which the plume rises.

The interior walls of the hood (except the Perspex wall) were painted black to improve visual observations of the smoke behaviour.

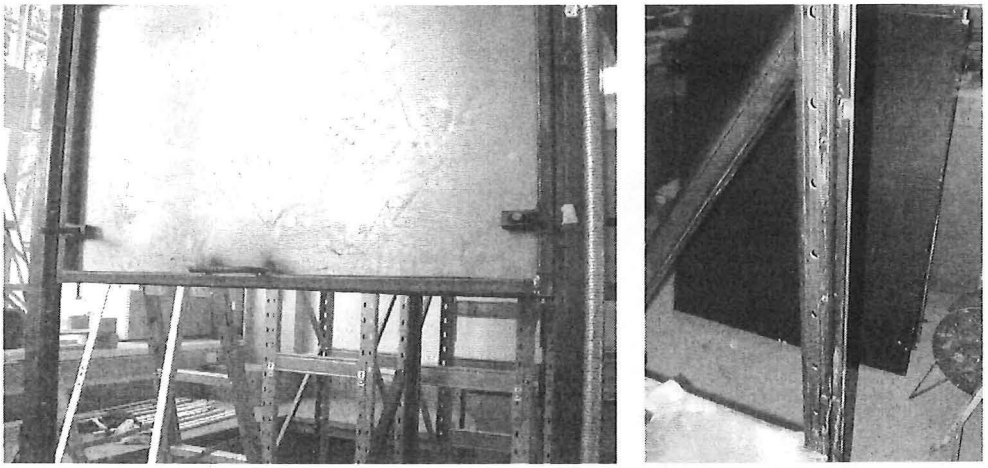

Figure 4.4: Locking mechanism for the walls of the smoke exhaust hood

The supporting steel frame was designed such that each side wall could contain up to two, smaller, modular walls which could be bolted together. This would then form a single wall on each face when examining deep smoke layers within the collecting hood (see Figure 4.5). The short length side walls consisted of modular panels each 1.0 m wide by 1.2 m high, the long length panels each were 2.0 m wide by 1.2 m high.

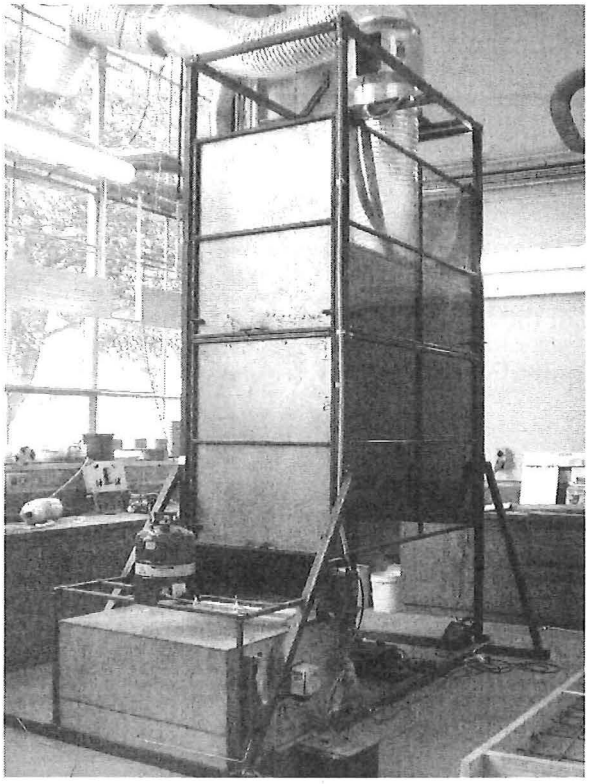

Figure 4.5: The smoke exhaust hood for a deep layer

The mechanical smoke exhaust system from the hood consisted of a 440 mm diameter bifurcated fan attached to the hood outlet using high temperature flexible ducting as shown in Figure 4.6.

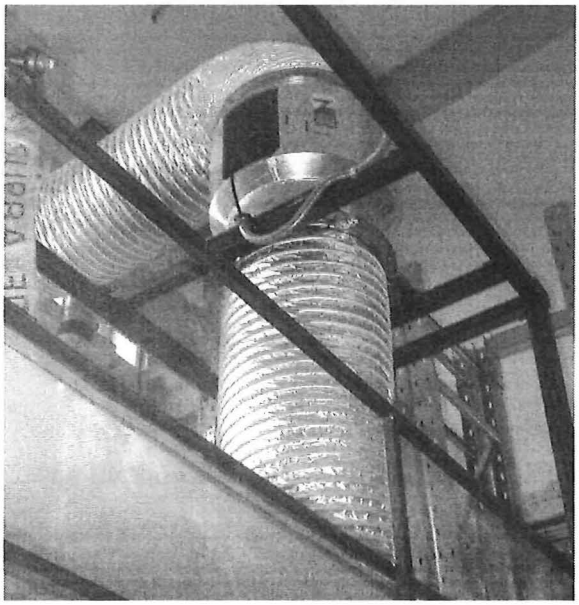

Figure 4.6: The bifurcated smoke exhaust fan

The gases were exhausted to the outside of the laboratory through flexible ducting which was connected to the exhaust end of the fan. The fan speed was controllable, which enabled different exhaust rates, and hence, variation in the height of rise of the plume to be examined.

The vent within the smoke exhaust hood contained a 'butterfly' damper which could be adjusted to alter the size of the vent from the hood (see Figure 4.7). This was necessary for those experiments which required very low smoke exhaust rates.

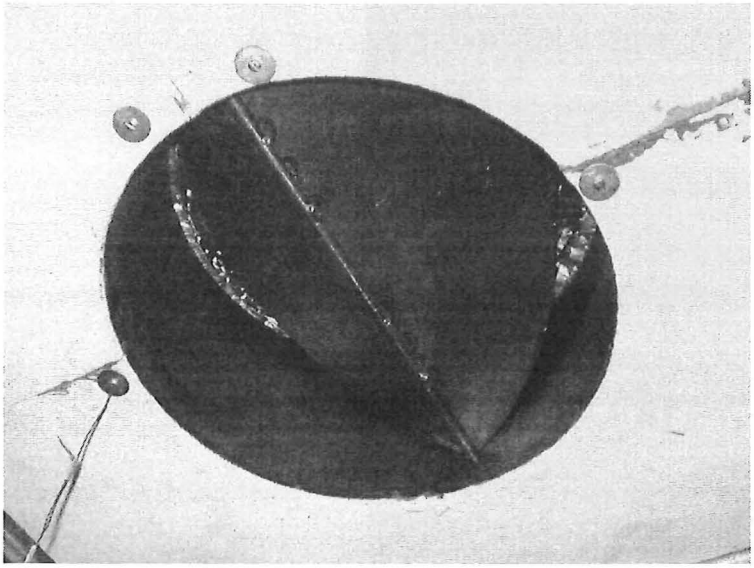

Figure 4.7: 'Butterfly' damper in exhaust vent

4.1.1.4 Fire source

The fire source was generated by supplying IMS into a metal tray within the fire compartment at a controlled and measured rate (see Figure 4.8). The fuel was supplied to the fire compartment continuously into a metal tray, via a fuel reservoir, flowmeter, tap and copper tubing (see Figure 4.9). The flow of fuel was controlled by a needle valve on the flowmeter. To maintain a constant flow, the fuel reservoir contained a constant pressure head device [18]. This incorporated a steel tube which passed into the fuel reservoir such that air was drawn in to replace the burning fuel. This caused fuel at the same height as the end of the steel tube (20 mm from the base of the reservoir) to be at atmospheric pressure.

The metal tray was located at the rear of the fire compartment. The tray was tilted toward the back of the compartment, so that the fuel surface remained reasonably uniform and automatically adjusted to match the burning rate to the inflow of fuel. The tray was 0.25 m by 0.25 m by 0.015 m high.

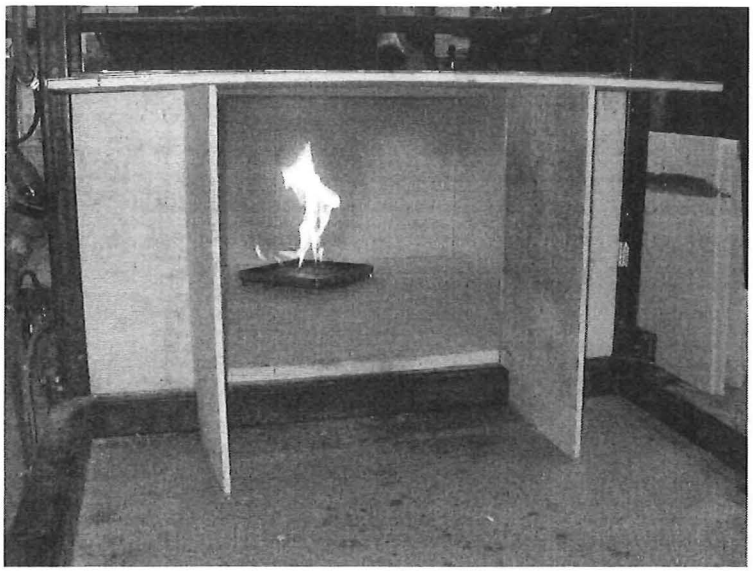

Figure 4.8: The IMS fire source

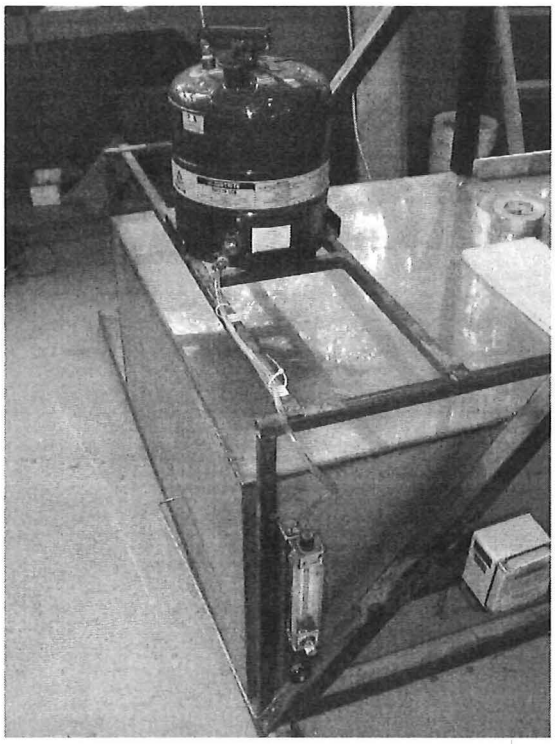

Figure 4.9: The fuel supply system

Since the heat of combustion and the volume flow rate of the fuel was known, the heat output of the fire could easily be determined (see section 4.1.4.1). The flowmeter was calibrated by collecting and measuring the quantity of fuel over known time intervals for a range of flow settings. Details of the flowmeter calibration are given in Appendix A.

The hot gases produced from the fire were visualised by injecting smoke from a commercial smoke generator (Fog Machine N6000) into the fire compartment. This highlighted the flowing gas layer from the compartment and the subsequent spill plume and smoke layer in the collecting hood.

4.1.2 Instrumentation

4.1.2.1 Gas temperatures

The gas temperatures in the model were measured using 0.5 mm diameter chromel/alumel (K-type) thermocouples. Thermocouples were positioned at various locations in the model, as follows:

- 1 column of 24 thermocouples (Column A) located within the smoke exhaust hood
- 1 column of 18 thermocouples (Column B) located centrally beneath the spill edge (under balcony)
- An array of 5 thermocouples (Array B) spaced equally across the width of the spill edge, projecting 10 mm below the edge
- 1 thermocouple located centrally within the smoke exhaust duct adjacent to the gas sampling tube
- 1 thermocouple located next to a pitot-static tube when carrying out velocity traverses of the smoke layer at the spill edge

Figure 4.10 and Appendix B detail the thermocouple locations and spacings.

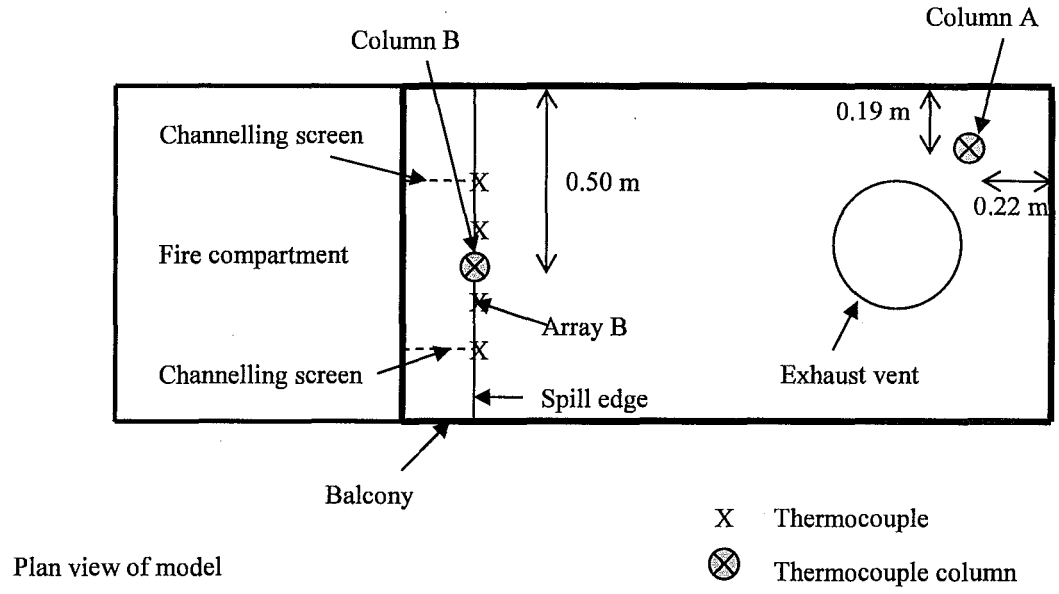

Figure 4.10: Thermocouple locations

4.1.2.2 Gas concentrations

A perforated gas sampling tube was located in the exhaust duct approximately 5.0 m downstream of the vent in the smoke exhaust hood. This enabled measurement of the CO_2 gas concentration in the duct to be made using an infra red gas analyser (Beckman, Model 864) which was calibrated on a daily basis. This measurement enabled the mass flow rate of gases in the smoke exhaust hood to be determined (see section 4.1.4.5).

4.1.2.3 Gas velocities

Vertical velocity profiles of the buoyant gas layer flow at the spill edge were made using a pitot-static tube and a thermocouple at each measurement location. The gas velocity was calculated from the measured pressure differential from the pitot tube and the gas temperature, as given by Equation (4-2).

$$u = \sqrt{\frac{2\Delta P T}{\rho_1 T_1}} \qquad (4\text{-}2)$$

The pitot-static tube was located in a central position beneath the balcony at the spill edge, and connected to a sensitive pressure transducer (Furness Controls FCO 352). The pitot tube was attached to a specially built steel stand which enabled a vertical traverses to easily be made (see Figure 4.11). Gas velocity measurements were made every 10 mm below the spill edge until the base of the smoke layer was reached. This measurement, in addition to the temperature profiles, enabled the mass flow rate and convective heat output of the layer flow at the spill edge to be determined (see sections 4.1.4.3 and 4.1.4.4).

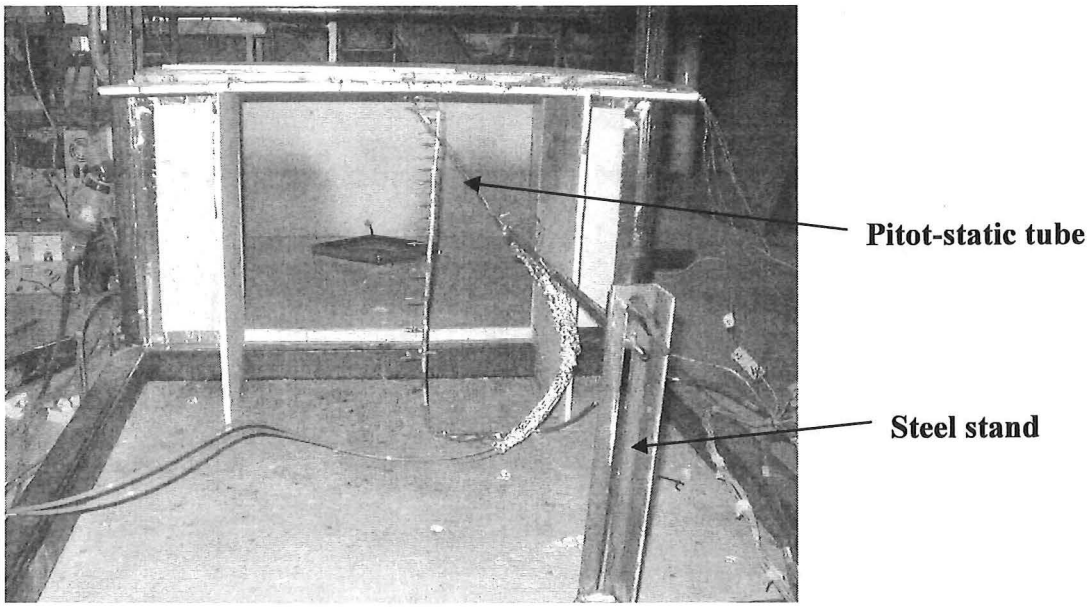

Figure 4.11: The pitot tube arrangement

Gas velocity measurements were also made across the opening, 10 mm below the spill edge, to measure the homogeneity of the gas flow. The gas velocity measurement was also used to determine the characteristic Reynolds number for the flows within the model.

4.1.2.4 Data recording

All the instrument readings were recorded using University of Canterbury data logging boxes associated with the Universal Data Logging (UDL) software package. The data were stored directly on to the hard disc of a PC in the form of an EXCEL spreadsheet, from which the data could be further processed and analysed.

4.1.2.5 Visual records

Visual observations of each test were carried out. These included smoke behaviour and layer depths. Artificial oil-mist smoke was used to mark the presence of the hot gas flows (as the IMS burns with no visible smoke). Photographic records were also made for selected tests.

4.1.3 Experimental method

4.1.3.1 Parameters of interest

The physical scale modelling study was used to examine various basic parameters which may affect entrainment of air into a rising spill plume. Some of the parameters of interest which may affect entrainment of air into a spill plume are listed below:

- Total heat output of the fire
- Mass flow rate of gases at the spill edge
- Convective heat output of the gases at the spill edge
- Depth of gas layer at the spill edge
- Type of spill plume (free or adhered)
- Height of rise of the spill plume
- Lateral extent of the plume at the spill edge (e.g. distance between channelling screens)
- Entrainment into the free ends of the vertically rising spill plume
- Presence of a downstand at the spill edge
- Smoke reservoir geometry

4.1.3.2 Parameter variation

For the vast majority of test fires, a free spill plume was examined allowing air entrainment into the free ends. The lateral extent of the plume at the spill edge was fixed at 0.6 m with the use of channelling screens at the compartment opening. The cross sectional area of the smoke exhaust hood also remained fixed (2.0 m long by 1.0 m wide) for the series of fire tests.

The total heat output of the fire was varied. Three fire sizes were examined with a nominal heat output of 6, 9 and 12 kW respectively. This equates to a fire size of 1.9, 2.8 and 3.8 MW respectively for a full scale equivalent. A maximum fire size of 12 kW was chosen so that the temperature at the spill edge did not exceed 300 °C for any of the test fires. Thus, not exceeding the maximum spill edge temperature at which the current theories can be applied.

Varying the total heat output will in turn vary the mass flow rate and convective heat output of the gases at the spill edge, in addition to varying the depth of the resulting smoke layer.

The effect of a downstand at the spill edge was examined. Two downstand depths were used, 0.1 m and 0.2 m deep respectively. The effect of no downstand at the spill edge (i.e. a flat ceiling) was also examined.

The height of rise of the plume was also varied. Six different heights of rise were examined for each spill edge geometry (i.e. presence of a downstand). The height of rise of the plume varied from a minimum of 0 m to a maximum of 1.2 m above the spill edge.

A single test was also carried out without entrainment of air into the ends of the plume. This was done as a check to confirm that the results from the model were consistent with earlier work.

4.1.3.3 The series of test fires

Table 4.1 shows the series of 64 test fires. This series included 9 tests to characterise the flow at the spill edge for each fire size and spill edge geometry examined.

A series of 55 test fires was carried out to examine the effect of varying selected parameters of interest on the entrainment of air into a spill plume.

Test	Fire size (kW)	Downtand depth (m)
1	6.0	0.2
2	9.0	0.2
3	12.0	0.2
4	6.0	0.1
5	9.0	0.1
6	12.0	0.1
7	6.0	0.0
8	9.0	0.0
9	12.0	0.0

Test	Fire size (kW)	Downtand depth (m)	Height of rise of plume above spill edge (m)
10	6.0	0.0	1.1
11	9.0	0.0	1.1
12	12.0	0.0	1.1
13	6.0	0.1	1.2
14	9.0	0.1	1.2
15	12.0	0.1	1.2
16	6.0	0.0	0.9
17	9.0	0.0	0.9
18	12.0	0.0	0.9
19	6.0	0.1	1.0
20	9.0	0.1	1.0
21	12.0	0.1	1.0
22	6.0	0.2	1.1
23	9.0	0.2	1.1
24	12.0	0.2	1.1
25	6.0	0.0	0.6
26	9.0	0.0	0.6
27	12.0	0.0	0.6
28	6.0	0.1	0.7
29	9.0	0.1	0.7
30	12.0	0.1	0.7
31	6.0	0.2	0.8
32	9.0	0.2	0.8
33	12.0	0.2	0.8
34	6.0	0.0	0.5
35	9.0	0.0	0.5
36	12.0	0.0	0.5
37	6.0	0.2	0.7
38	9.0	0.2	0.7
39	12.0	0.2	0.7
40	6.0	0.1	0.5
41	9.0	0.1	0.5
42	12.0	0.1	0.5
43	6.0	0.0	0.3
44	9.0	0.0	0.3
45	12.0	0.0	0.3
46	6.0	0.2	0.5
47	9.0	0.2	0.5
48	12.0	0.2	0.5
49	6.0	0.1	0.3
50	9.0	0.1	0.3
51	12.0	0.1	0.3
52	6.0	0.2	0.3
53	9.0	0.2	0.3
54	12.0	0.2	0.3
55	6.0	0.0	0.0
56	9.0	0.0	0.0
57	12.0	0.0	0.0
58	6.0	0.1	0.0
59	9.0	0.1	0.0
60	12.0	0.1	0.0
61	6.0	0.2	0.0
62	9.0	0.2	0.0
63	12.0	0.2	0.0
64*	6.0	0.0	0.3

* no entrainment into the ends, 1 m wide opening

Table 4.1: The series of test fires (Tests 1 to 64)

4.1.3.4 Experimental procedure

The experimental procedure for the series of 9 test fires to characterise the flow at the spill edge was as follows:

1. The required fire compartment geometry to be examined was set up.
2. The pitot tube arrangement was then set up.
3. IMS was then fed into the fire tray at a controlled and measured rate.
4. The fuel was ignited and the fire within the compartment was allowed to burn until the temperature of the gases had reached stability.
5. The smoke generator was switched on and smoke was injected just below the base of the layer in the compartment.
6. Visual observations were made of the smoke layer depth and behaviour
7. The smoke generator was switched off.
8. Gas velocity and temperature measurements were made every 10 mm below the spill edge until the base of the gas layer was reached. The data were stored directly onto a PC. Measurements were recorded for a period of 60 s for each scan carried out.

The experimental procedure for the series of 55 test fires to examine entrainment of air into a free spill plume was as follows:

1. The required fire compartment geometry and smoke exhaust hood height (i.e. height of rise of the spill plume) was set up.
2. The mechanical smoke exhaust fan was switched on to provide a nominal exhaust rate from the hood.
3. IMS was fed into the fire tray at a controlled and measured rate.
4. The fuel was ignited and the fire within the compartment was allowed to burn until the temperature of the gases had reached stability.
5. The smoke generator was switched on and smoke was injected just below the base of the layer in the compartment.
6. Visual observations were made of the smoke layer depth beneath the spill edge and the behaviour of the smoke as it flowed into the hood.

7. The speed of the mechanical exhaust fan was then adjusted until the lowest point of the smoke layer was just contained with smoke exhaust hood.
8. The smoke generator was switched off.
9. Measurements were made of the gas temperatures and the concentration of CO_2 in the duct. The data were stored directly onto a PC. Measurements were recorded for a period of 60 s.

4.1.4 Analysis procedures and data reduction

4.1.4.1 Heat output of IMS fuel source

The heat output of the IMS fuel source was determined from the measured flow rate of fuel through the flowmeter, the heat of combustion and the density of IMS [66] (see Appendix A). The total heat output of the fire was calculated using Equation (4-3).

$$Q_{TOTAL} = c_{IMS}\rho_{IMS}V_{IMS} \tag{4-3}$$

4.1.4.2 Smoke layer depth

The smoke layer depth was determined from visual observations.

However, the smoke layer depth was also determined from the measured gas temperature profiles. The thermocouple columns in the fire compartment and in the smoke exhaust hood enabled buoyancy $\left(\frac{\theta}{T}\right)$ profiles with respect to the depth below the ceiling to be determined. The smoke layer depth at each location was determined using a method which utilises the buoyancy profile from the thermocouple column. This method generally provides good agreement with visually observed layer depths for buoyancy profiles which exhibit a well defined 'S' shaped profile. The method essentially converts the area beneath the buoyancy profile into an equivalent "top hat" profile to determine the smoke layer depth. The smoke layer depth can be determined using Equation (4-4) given by Thomas et al [52].

$$d_{layer} = \frac{\int_0^{h_{comp}} \left(\frac{\theta}{T}\right)_h dh}{\left(\frac{\theta}{T}\right)_{max}} \tag{4-4}$$

To determine the layer depth, $\left(\frac{\theta}{T}\right)$ versus h was plotted. The area under the resulting curve, $\int_0^{h_{comp}} \left(\frac{\theta}{T}\right)_h dh$, was then found using the trapezoid rule in an EXCEL spreadsheet. This area was divided by the maximum value of $\left(\frac{\theta}{T}\right)$ to determine the layer depth.

4.1.4.3 Calculation of the mass flow rate of gases at the spill edge

The mass flow rate of gases at the spill edge was determined from the results of the vertical velocity profiles determined using the pitot tube traverses, in addition to the gas temperature profiles through the layer. The total mass flow rate of gases at the spill edge was then determined by performing an integration under the curve of $W\rho u$ with respect to the depth of the gas layer. This was done using the trapezoid rule in an EXCEL spreadsheet.

4.1.4.4 Calculation of the convective heat output of the gases at the spill edge

Similarly, the convective heat output of the gases at the spill edge was determined using the results of the vertical velocity and temperature profiles. The heat output was determined by performing an integration under the curve of $W\rho u c_p \theta$ with respect to the depth of the gas layer. This was done using the trapezoid rule in an EXCEL spreadsheet.

4.1.4.5 Calculation of the mass flow rate of gases due to a spill plume

The mass flow rate of gases entering the buoyant gas layer in the smoke exhaust hood (M_p), and therefore leaving the hood, was found by using a CO_2 tracer gas technique and calculation method. This method is detailed by Marshall [59] and is described here for completeness.

The gas layer can be considered to consist of hot air and tracer CO_2 produced by the combustion of IMS. Although CO_2 is present in air, it is only approximately 0.03% by volume. The ambient CO_2 concentration can be measured and taken into account. When CO_2 mixes with air it moves with the air and contributes to the overall gas pressure, which is given by Equation (4-5).

$$\left(P_{air} + P_{co_2}\right)v = \frac{n'_{air} + n'_{co_2}}{N} RT \tag{4-5}$$

This can also be written as,

$$\left(v_{air} + v_{co_2}\right)P = \frac{n'_{air} + n'_{co_2}}{N} RT \tag{4-6}$$

Considering the CO_2 tracer gas on its own,

$$Pv_{co_2} = \frac{n'_{co_2}}{N} RT \tag{4-7}$$

Therefore, the CO_2 gas concentration (τ) by volume is, from Equations (4-6) and (4-7),

$$\tau = \frac{n'_{co_2}}{n'_{air} + n'_{co_2}} = \frac{v_{co_2}}{v_{air} + v_{co_2}} \tag{4-8}$$

This result is not dependent on changes in temperature in a sample of gases removed from the scale model. From Equation (4-8), and replacing v_{air} with V_{air}, gives the volume flow rate of air through the model, such that,

$$V_{air} = \frac{(1-\tau)}{\tau} V_{co_2} \tag{4-9}$$

The mass flow rate of air is given by,

$$M_{air} = V_{air} \frac{\rho_{air} T}{T_1} \tag{4-10}$$

Which gives,

$$M_{air} = \frac{(1-\tau)\rho_{air} T V_{co_2}}{\tau T_1} \tag{4-11}$$

The mass flow rate of CO_2 is given by,

$$M_{co_2} = V_{co_2} \frac{\rho_{co_2} T}{T_1} \tag{4-12}$$

The total mass flow rate of gases is given by $M_{air} + M_{co_2}$, hence,

$$M = \frac{V_{co_2} T}{T_1} \left[\rho_{co_2} + \frac{(1-\tau)\rho_{air}}{\tau} \right] \tag{4-13}$$

Where, ρ_{air} and ρ_{co_2} are evaluated at $T = 273$ K and V_{co_2} is evaluated at T_1.

The calculation of V_{co_2} was determined using the following approach:

The amount of CO_2 produced by the fire was calculated from the mass of fuel burnt. IMS is essentially denatured ethanol, a material safety data sheet for this fuel is given in Appendix C. The chemical equation for the combustion of ethanol is given by Equation (4-14).

$$C_2H_5OH + 3O_2 \rightarrow 3H_2O + 2CO_2 \tag{4-14}$$

Therefore, one mole of ethanol produced two moles of CO_2.

One mole of CO_2 will occupy 22.4 x 10^{-3} m^3 at standard temperature and pressure. One mole of ethanol weighs 0.046 kg. Hence, burning 0.046 kg of IMS produces 44.8 x 10^{-3} m^3 of CO_2.

Therefore,

$$V_{co_2} = \frac{0.0448\, M_{IMS}}{0.046} \tag{4-15}$$

Where M_{IMS} was determined from the fuel flowmeter calibration.

4.1.4.6 Error analysis

Although the experimental measurements were made during nominally steady state conditions, fluctuations in various measurements (e.g. temperature, velocity, mass flow rate) occurred during the sampling period. Therefore, the experimental results were determined in terms of a time averaged mean value with an associated standard error. The standard error was determined by dividing the standard deviation of the sample by the square root of the number of samples. The standard deviation of the mean values were determined using the relevant function given in the EXCEL spreadsheet package.

4.2 Experiments examining entrainment of air into a flow from a compartment opening to a higher projecting balcony

4.2.1 The physical scale model

The physical scale model used for these experiments was the essentially the same as that described in section 4.1.1. These experiments only examined gas flows within the fire compartment and did not involve the smoke exhaust hood. The fire source was also identical to that described in section 4.1.1.4. Modifications were made to the geometry of the fire compartment between tests, as described below.

4.2.1.1 The fire compartment

The fire compartment was modified such that a downstand was present at the compartment opening prior to the spill edge. This created the presence of a projecting balcony above a compartment opening (see Figures 4.12 and 4.13).

There were 2 downstands used, 0.1 m and 0.2 m deep respectively. Each downstand was generally made from 10 mm thick CFI board, located 0.3 m prior to the spill edge (i.e. the balcony edge).

The width of the compartment opening (0.3 m prior to the spill edge) was also adjusted by inserting 10 mm thick CFI boards, of the desired width, beneath the downstand. Moveable channelling screens made from 10 mm thick CFI board, occupying the full breadth of the balcony, were located on either side of the compartment opening. The channelling screens were again used to provide reasonably constant temperature and velocity profiles across the width of the opening. This enabled the mass flow rate of gases to be determined from a single velocity and temperature traverse through the smoke layer. The channelling screens occupied the full height of the fire compartment.

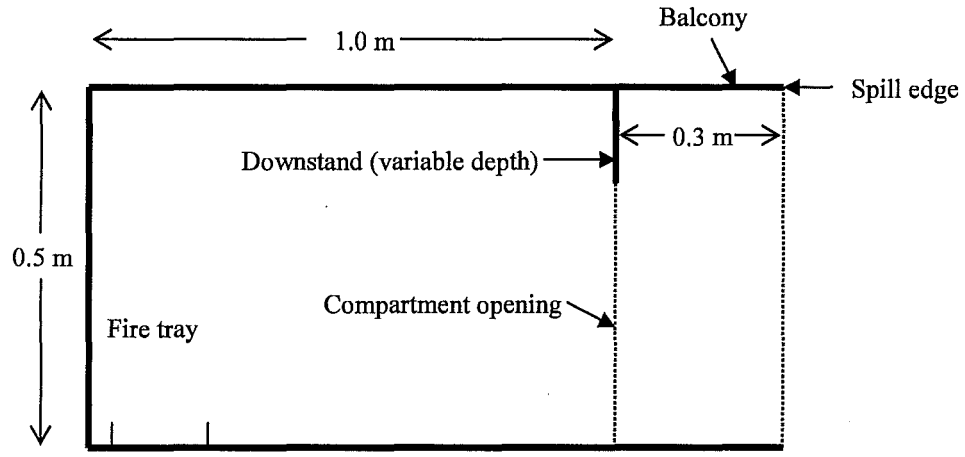

Section

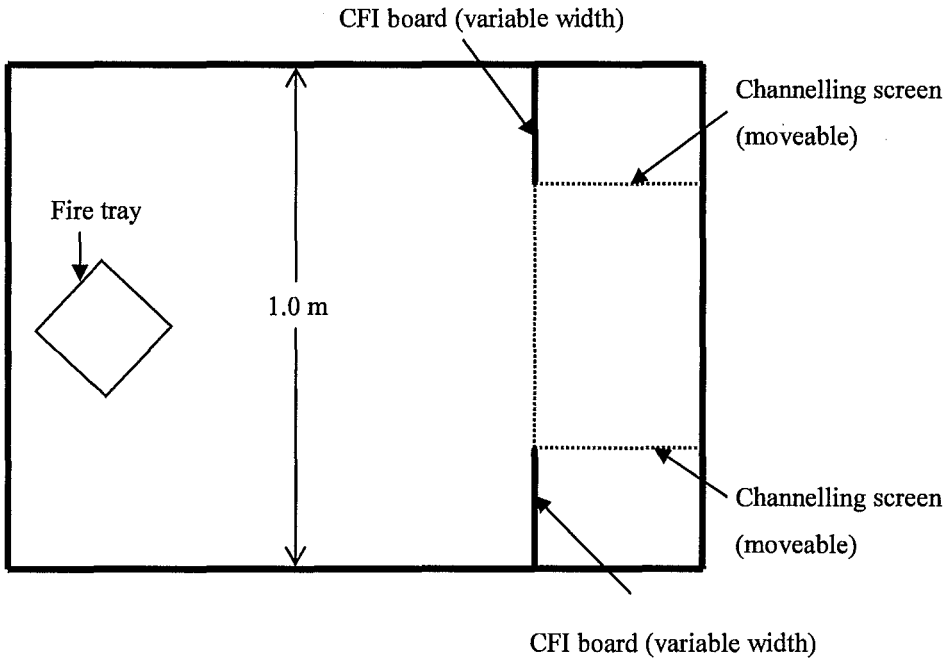

Plan

Figure 4.12: Schematic drawing of the fire compartment

Figures 4.13 and 4.14 show a photographs of the fire compartment for a wide and a narrow geometry respectively.

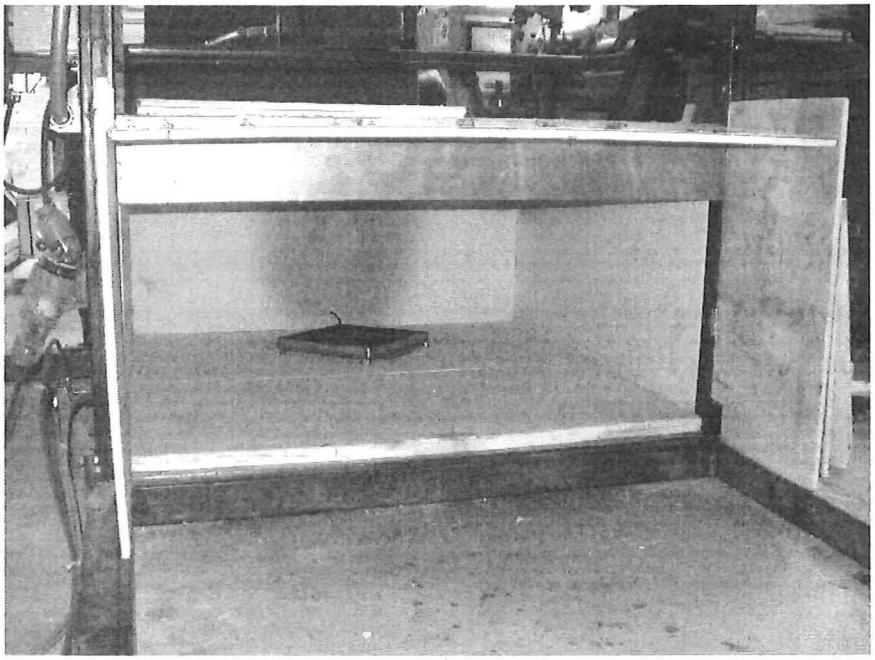

Figure 4.13: The fire compartment for a wide geometry

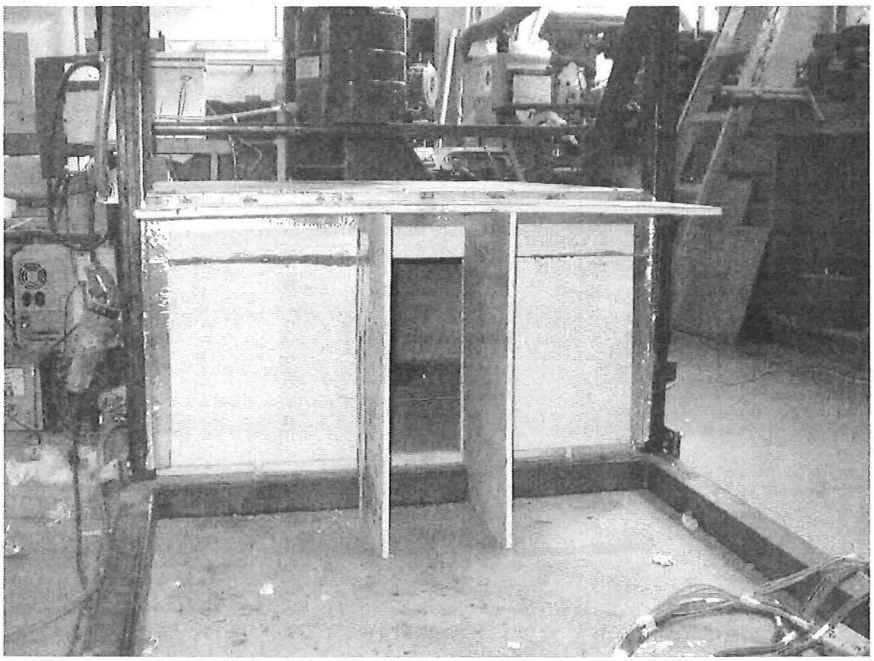

Figure 4.14: The fire compartment for a narrow geometry

4.2.2 Instrumentation

In these experiments, temperature and velocity measurements were made, in addition to visual observations. The data recording technique was the same as that described in section 4.1.2.4.

4.2.2.1 Gas temperatures

The gas temperatures in the model were again measured using 0.5 mm diameter chromel/alumel (K-type) thermocouples. In addition to those thermocouples in the fire compartment described in section 4.1.2.1, gas temperature measurements were also made at the following locations:

- 1 column of 16 thermocouples (Column C) located centrally beneath the downstand at the compartment opening.
- An array of 5 thermocouples (Array A) spaced equally across the width of the downstand at the compartment opening, projecting 10 mm below the edge.
- 1 thermocouple located next to an additional pitot-static tube when carrying out velocity traverses of the smoke layer beneath the downstand at the compartment opening.

Figure 4.15 and Appendix B detail the thermocouple locations and spacings.

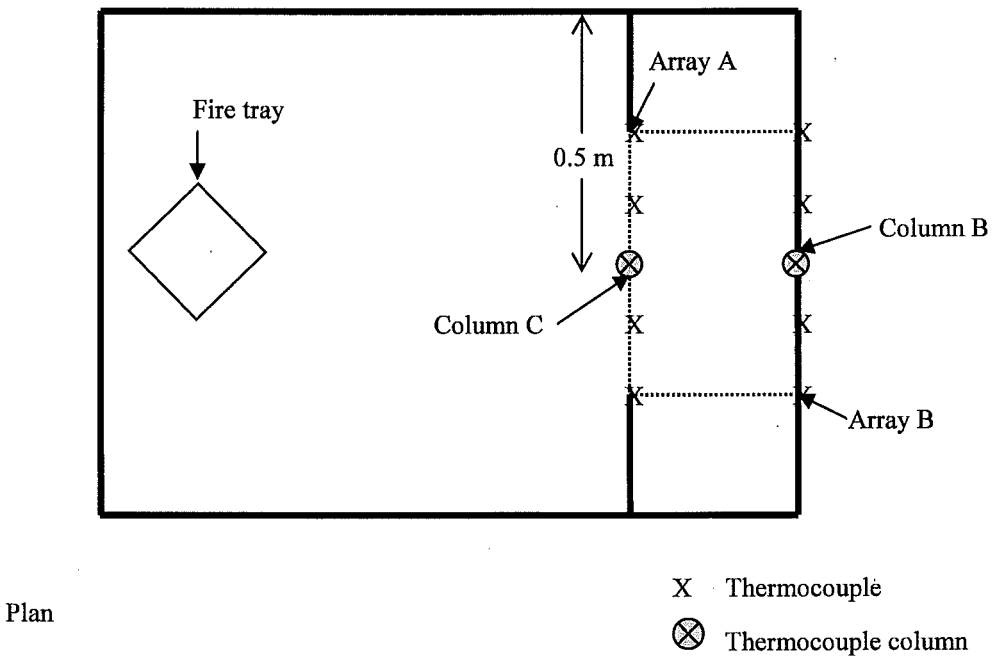

Figure 4.15: Thermocouple locations

4.2.2.2 Gas velocities

Gas velocities within the compartment were measured using the same technique described in section 4.1.2.3. However for these experiments, velocity and temperature traverses were carried out through the gas layer at the compartment opening and at the spill edge (see Figure 4.16).

Vertical velocity and temperature measurements were again made every 10 mm until the base of the smoke layer was reached in each location. This measurement allowed the mass flow rate of gases at the compartment opening (M_w) and at the spill edge (M_b) to be determined.

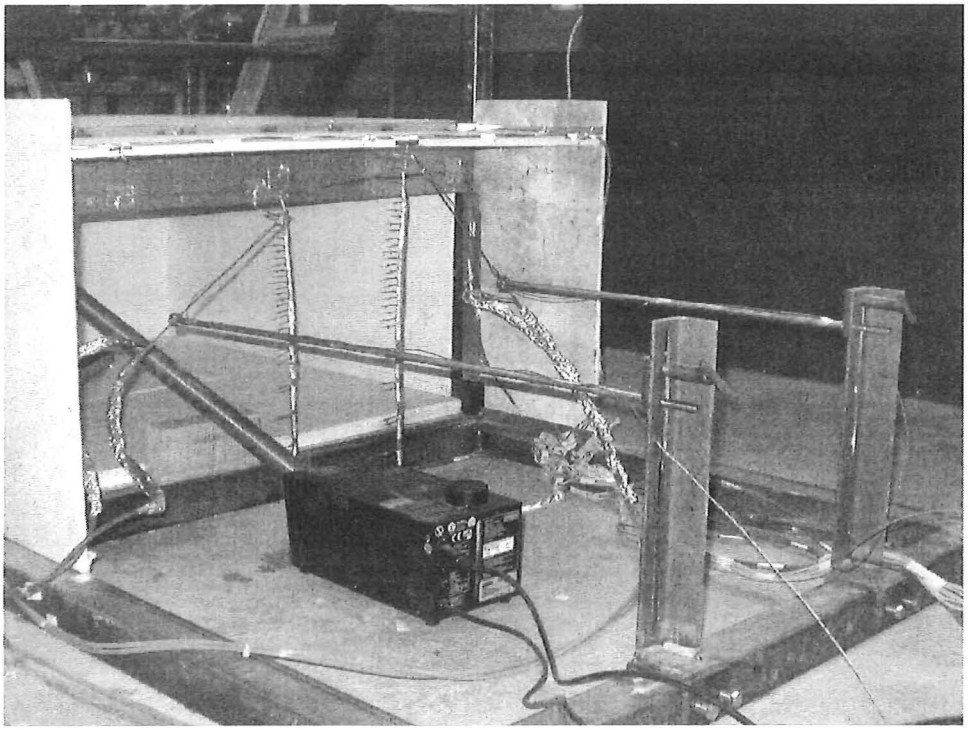

Figure 4.16: The pitot tube arrangement

Velocity measurements were also carried out across the gas flow at the compartment opening and at the spill edge (10 mm below the edge) to examine the homogeneity of the flow.

4.2.2.3 Visual records

Visual observations of each test were carried out. This included the smoke behaviour and the layer depth at the compartment opening and at the spill edge. Photographic records were also made for selected tests.

4.2.3 Experimental method

4.2.3.1 Parameters of interest

This study was used to examine various parameters which may affect entrainment of air into a flow from a compartment opening to a higher projecting balcony. Some of the various parameters of interest are listed below:

- Total heat output of the fire
- Mass flow rate of gases at the compartment opening
- Convective heat output of the gases at the compartment opening
- Mass flow rate of gases at the spill edge
- Convective heat output of the gases at the spill edge
- Depth of gas layer at the compartment opening
- Depth of gas layer beneath the spill edge
- Height of the fire compartment
- Height of the compartment opening
- Width of the compartment opening
- Breadth of the balcony
- Depth of the downstand

4.2.3.2 Parameter variation

As CFD modelling was primarily used to study this aspect of the work, only a selected number of experiments were carried out for CFD validation purposes only.

The height of the fire compartment, the breadth of the balcony and the size of the fire remained fixed for all of the experiments carried out.

The downstand depth was varied. Two downstand depths were used, 0.1 m and 0.2 m deep respectively. This in turn varied the height of the compartment opening.

The width of the compartment opening was also varied so that a range of aspect ratios of the opening (height/width) could be examined. The maximum width of opening

examined was 1.0 m, the minimum was 0.2 m. This gave a maximum aspect ratio of the compartment opening of 2.0, and a minimum of 0.3.

4.2.3.3 The series of fire tests

Table 4.2 shows the series of 4 test fires carried out.

Test	Fire size (kW)	Downtand depth (m)	Width of compartment opening (m)	Aspect ratio of compartment opening (Height/Width)
65	10.3	0.1	1.0	0.40
66	10.3	0.2	1.0	0.30
67	10.3	0.1	0.4	1.00
68	10.3	0.1	0.2	2.00

Table 4.2: The series of test fires (Tests 65 to 68)

4.2.3.4 Experimental procedure

The experimental procedure for the series of 4 test fires was as follows.

1. The required fire compartment geometry to be examined was set up.
2. The pitot-tube arrangement was then set up.
3. IMS was then fed into the fire tray at a controlled and measured rate.
4. The fuel was ignited and the fire within the compartment was allowed to burn until the temperature of the gases had reached stability.
5. The smoke generator was switched on and smoke was injected just below the base of the layer in the compartment.
6. Visual observations were made of the smoke layer depth and behaviour.
7. The smoke generator was switched off.
8. Gas velocity and temperature measurements were made every 10 mm below the spill edge until the base of the gas layer was reached. Gas temperature measurements at other locations in the model were also recorded. The data were stored directly onto a PC. Measurements were recorded for a period of 60 s.

4.2.4 Analysis procedures and data reduction

4.2.4.1 Heat output of the IMS fire source

The heat output of the IMS fire source was determined using the same technique described in section 4.1.4.1.

4.2.4.2 Smoke layer depth

The smoke layer depth was again determined using visual observations and the buoyancy profiles from the thermocouple columns. The technique used to determine the buoyancy derived layer depth is described in section 4.1.4.2 .

4.2.4.3 Mass flow rate of gases at the compartment opening and at the spill edge

The velocity traverses through the gas layer in the compartment enabled the mass flow rate of gases to be determined at each location. The technique used to determine these mass flow rates is described in section 4.1.4.3 .

4.2.4.4 Error Analysis

The experimental results were again determined in terms of a time averaged mean value with an associated standard error during the sampling period. The standard errors were determined using the method described in section 4.1.4.6.

CHAPTER 5

5. CFD MODELLING: PROCEDURE AND SCENARIOS

CFD modelling was only used to examine entrainment of air into a flow from a compartment opening to a higher projecting balcony. The CFD model, FDS, was used for all of the simulations carried out. This chapter describes the modelling procedure, the assumptions made, the scenarios modelled and the data analysis techniques used.

5.1 FDS modelling procedure

Details of the FDS modelling procedure and the assumptions made are described in this section. Appendix D gives an example of the FDS source code used for a particular simulation (Simulation 2).

5.1.1 Modelled geometry

FDS was used to model hot gas flows within the fire compartment of the $1/10^{th}$ physical scale model described in section 4.2.1.1 and shown in Figure 4.12. However, a greater range of fire compartment geometries were examined using FDS, than those carried out experimentally.

As in the experiment, the fire compartment was modelled such that a downstand was present at a compartment opening prior to a higher projecting balcony. A variety of downstand, balcony and fire compartment opening geometries were examined. Full height channelling screens were also modelled on either side of the compartment opening.

In general, the walls, ceiling and balcony of the fire compartment were assumed to be made of 20 mm thick CFI board. The channelling screens, downstands and walls to reduce the compartment opening width, were assumed to be made from 10 mm thick CFI board as in the experiment.

When constructing a chosen geometry, FDS calls upon a materials database containing thermal and physical properties of the materials modelled. The following thermal properties were assumed for CFI board [67] and added to the materials database.

k_{CFI} = 0.041 $Wm^{-1}K^{-1}$

ρ_{CFI} = 229 kgm^{-3}

$c_{p,CFI}$ = 2090 $Jkg^{-1}K^{-1}$

5.1.2 Computational domain and grid size

The computational domain contained a volume which was 1.8 m long by 1.0 m wide by 1.0 m high. The domain extended 0.5 m above and 0.5 m beyond the spill edge so that the initial gas flow beyond the fire compartment could be observed (see Figure 5.1).

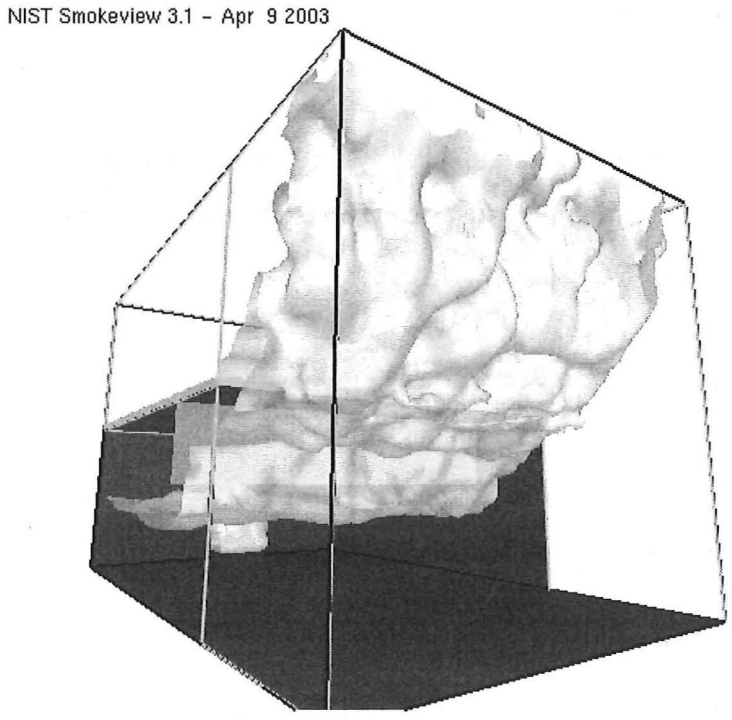

Figure 5.1: The computational domain in Smokeview 3.1

In an attempt to minimise any inaccuracies in the FDS prediction, preliminary simulations were carried out to determine the minimum grid size possible within the computational domain. It should be noted that a coarse grid size can give rise to misleading results. The grid size was systematically reduced (hence, increasing the total number of cells in the domain) until it was not possible to achieve a result due to limitations in the available computing power. The minimum grid size to achieve a result was found to be 20 mm. Thus, a grid size of 20 mm was used for all of the simulations which resulted in a total number of 225,000 grid cells within the computational domain.

Preliminary simulations were also carried out to determine the minimum simulation time within FDS such that reasonably steady state conditions were reached within the fire compartment. A simulation time of approximately 4 minutes produced steady state conditions in the fire compartment in terms of gas temperature (see section 6.2.1.1). The actual computing time required to complete a simulation was approximately 33 hours for all of the simulations carried out.

5.1.3 Fire source

The fire source assumed in FDS was an ethanol pool fire, as used in the experiment. The combustion properties of ethanol (e.g. heat of combustion) were within the materials database called upon within FDS. The fire source consisted of fuel within a tray which was 0.17 m long by 0.17 m wide by 0.015 m high for the majority of the simulations. FDS makes the assumption that the ethanol is contained over the full surface area of the tray. This particular tray size gave rise to a fire with a total heat output of 10.3 kW. When the fire size was varied, the size of the tray was altered to produce the desired total heat output.

5.1.4 Predictions

The FDS modelling predicted gas temperatures by assuming two arrays of five thermocouples equally spaced across the width of the compartment opening (under the downstand) and across the spill edge (under the balcony). These thermocouples were situated 10 mm below the edge and were used to determine if the temperature profile was reasonably homogeneous across the flow. Velocity measurements were also made at these locations.

Gas temperatures were also predicted by assuming a column of thermocouples being present in a central location at the compartment opening and at the spill edge. The thermocouples on each column were equally spaced at an interval of 10 mm from floor to ceiling level. Velocity measurements were also made at these locations.

Velocity and temperature slices were also generated within FDS in an x-z plane (long length) centrally through the compartment. These slices provided an overall velocity and temperature map throughout a plane.

The mixture fraction for ethanol was also calculated assuming stoichometric combustion, so that an isosurface highlighting the base of the gas layer and the subsequent plume could be viewed in Smokeview 3.1.

5.2 Modelled simulations

5.2.1 Parameters of interest

Those parameters of interest which may affect entrainment of air into a flow from a compartment opening to a higher projecting balcony are given in section 4.2.3.1 and are not repeated here.

5.2.2 Parameter variation

For all of the simulations modelled, the height of the fire compartment remained fixed at 0.5 m.

The total heat output of the fire was varied. For the majority of simulations, the fire size had a nominal total heat output of 10.3 kW. However, for selected tests, the fire size was varied to either 6 or 16 kW.

The width of the fire compartment opening was also varied. Five different opening widths were examined in total (0.2 m, 0.4 m, 0.6 m, 0.8 m and 1.0 m respectively).

The effect of balcony breadth was also examined. For the majority of the simulations, the balcony breadth was fixed at 0.3 m. However for selected tests, the balcony breadth was varied to either 0.2 m or 0.5 m.

The depth of the downstand was also varied. Five different downstand depths were examined, 0.1 m, 0.16 m, 0.2 m, 0.25 m and 0.3 m respectively. This in turn varied the height of the fire compartment opening.

The respective changes to the compartment opening geometry in turn varied the mass flow rate, convective heat output and the depth of the gas layer at the compartment opening and at the spill edge.

5.2.3 The series of FDS simulations

Table 5.1 shows the series of 25 FDS simulations carried out.

Simulation	Fire size Q_{TOTAL} (kW)	Downstand depth (m)	Height of opening h_o (m)	Width of opening w_o (m)	Height of compartment h_{comp} (m)	Balcony breadth b (m)
1	10.30	0.10	0.40	1.0	0.5	0.3
2	10.30	0.10	0.40	0.8	0.5	0.3
3	10.30	0.10	0.40	0.6	0.5	0.3
4	10.30	0.10	0.40	0.4	0.5	0.3
5	10.30	0.10	0.40	0.2	0.5	0.3
6	10.30	0.16	0.34	1.0	0.5	0.3
7	10.30	0.16	0.34	0.6	0.5	0.3
8	10.30	0.16	0.34	0.2	0.5	0.3
9	10.30	0.20	0.30	1.0	0.5	0.3
10	10.30	0.20	0.30	0.8	0.5	0.3
11	10.30	0.20	0.30	0.6	0.5	0.3
12	10.30	0.20	0.30	0.4	0.5	0.3
13	10.30	0.20	0.30	0.2	0.5	0.3
14	10.30	0.25	0.25	1.0	0.5	0.3
15	10.30	0.25	0.25	0.6	0.5	0.3
16	10.30	0.25	0.25	0.2	0.5	0.3
17	10.30	0.30	0.20	1.0	0.5	0.3
18	10.30	0.30	0.20	0.8	0.5	0.3
19	10.30	0.20	0.30	0.6	0.5	0.5
20	10.30	0.10	0.40	0.2	0.5	0.5
21	6.00	0.20	0.30	0.6	0.5	0.3
22	16.00	0.20	0.30	0.6	0.5	0.3
23	6.00	0.10	0.40	0.6	0.5	0.3
24	16.00	0.10	0.40	0.6	0.5	0.3
25	10.30	0.20	0.30	0.6	0.5	0.2

Table 5.1: The series of FDS simulations

5.3 Analysis procedures and data reduction

5.3.1 Smoke layer depth

The smoke layer depth was determined using the buoyancy profiles from the temperature predictions at the fire compartment opening and at the spill edge. The technique used to determine the buoyancy derived layer depth is described in section 4.1.4.2 .

5.3.2 Mass flow rate of gases at the compartment opening and at the spill edge

The velocity and temperature traverses through the gas layer enabled the mass flow rate of gases to be determined at each location. The technique used to determine these mass flow rates is described in section 4.1.4.3 .

5.3.3 Error Analysis

Once nominal steady state conditions of the flow were predicted within FDS (see section 6.2.1.1), the predictions were time averaged over the sampling period. The results of the FDS predictions were determined in terms of the time averaged mean value with an associated standard error. The standard errors were determined using the method described in section 4.1.4.6.

CHAPTER 6

6. RESULTS

6.1 Entrainment of air into a spill plume

The results from the physical scale modelling study to examine entrainment of air into a free spill plume are given below. The results are presented in two parts, the first part deals with those fires to characterise the horizontal approach flow at the spill edge (Tests 1-9), the second deals with the effect of varying selected parameters of interest on the mass flow rate of gases produced by a spill plume (Tests 10-64).

6.1.1 Approach flow at the spill edge (Tests 1 to 9)

6.1.1.1 Homogeneity of flow across the spill edge

As the mass flow rate and convective heat output of the gas layer at the spill edge were determined from a single velocity and temperature traverse through the centre of the smoke layer (with the results then being applied across the full width of the layer), it was first necessary to confirm if the gas temperature and velocity were reasonably homogeneous across the width of the gas layer.

Figure 6.1 shows the temperature profile across the gas layer 0.01 m below the spill edge for Tests 1 to 3 (6kW, 9 kW and 12 kW fires, 0.2 m downstand). Figure 6.1 shows that the temperature profile across the gas layer was reasonably constant across the full width of the spill edge for each fire size examined. A homogeneous flow was generally typical of all of the tests carried out, irrespective of the spill edge geometry (i.e. presence of a downstand).

Figure 6.2 shows the velocity profile across the gas layer 0.01 m below the spill edge for Tests 1 to 3 (6kW, 9 kW and 12 kW fires, 0.2 m downstand).

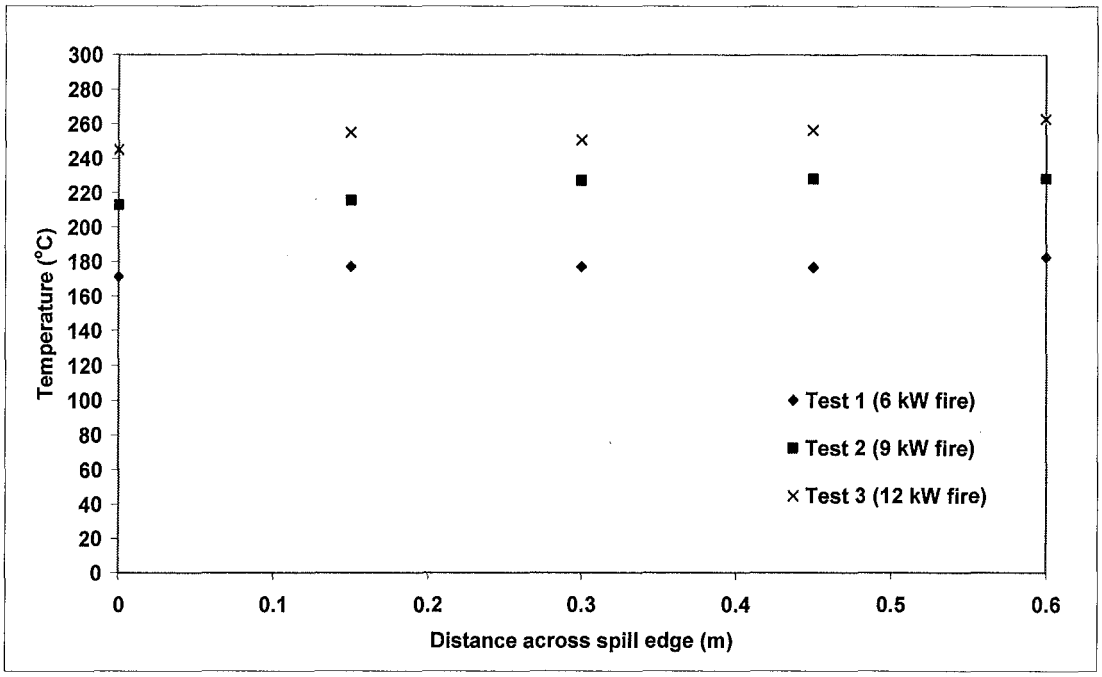

Figure 6.1: Typical temperature profile across gas layer (0.01 m below the spill edge)

Figure 6.2 shows that the velocity profile across the gas layer was also reasonably constant across the full width of the spill edge for each fire size examined. A homogeneous flow was generally typical of all of the tests carried out, irrespective of the spill edge geometry.

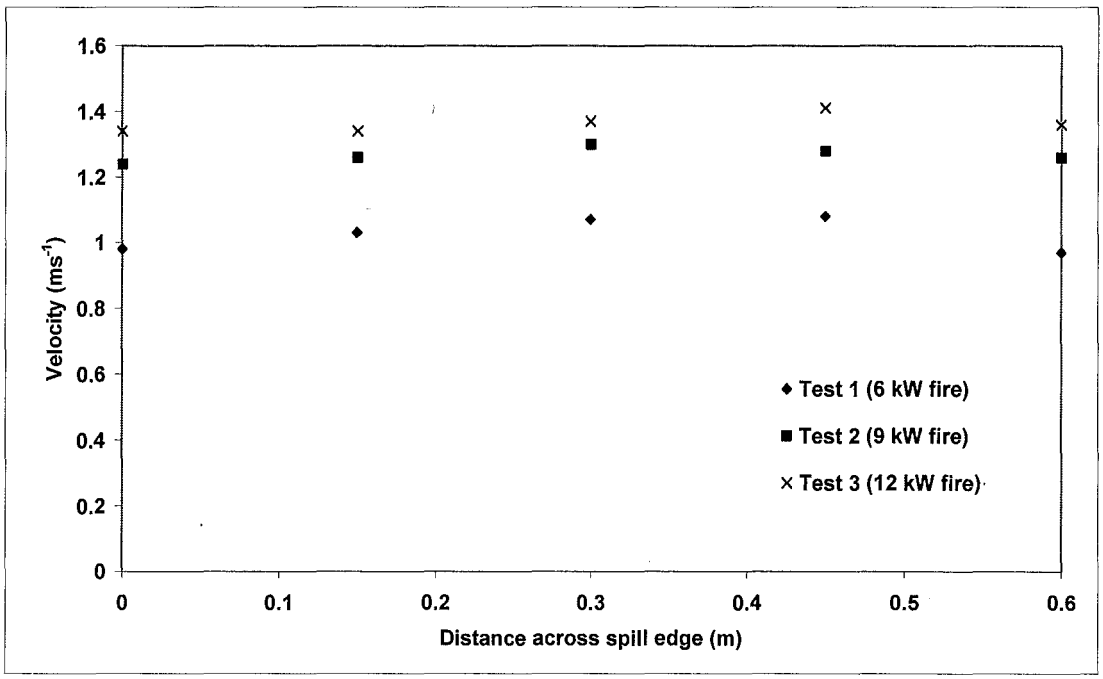

Figure 6.2: Typical velocity profile across gas layer (0.01 m below the spill edge)

The above result provided the confidence to enable an integration to be performed through the hot gas layer from a single velocity and temperature traverse, so that the mass flow rate and convective heat output of gases at the spill edge could be determined.

6.1.1.2 Gas temperature and velocity profiles

Figures 6.3 and 6.4 show the temperature and velocity profiles through the gas layer at the spill edge respectively for Test 1. The nature of these profiles is generally typical for all of the tests carried out.

Appendix E shows the temperature and velocity profiles at the spill edge for Tests 1 to 9 inclusive.

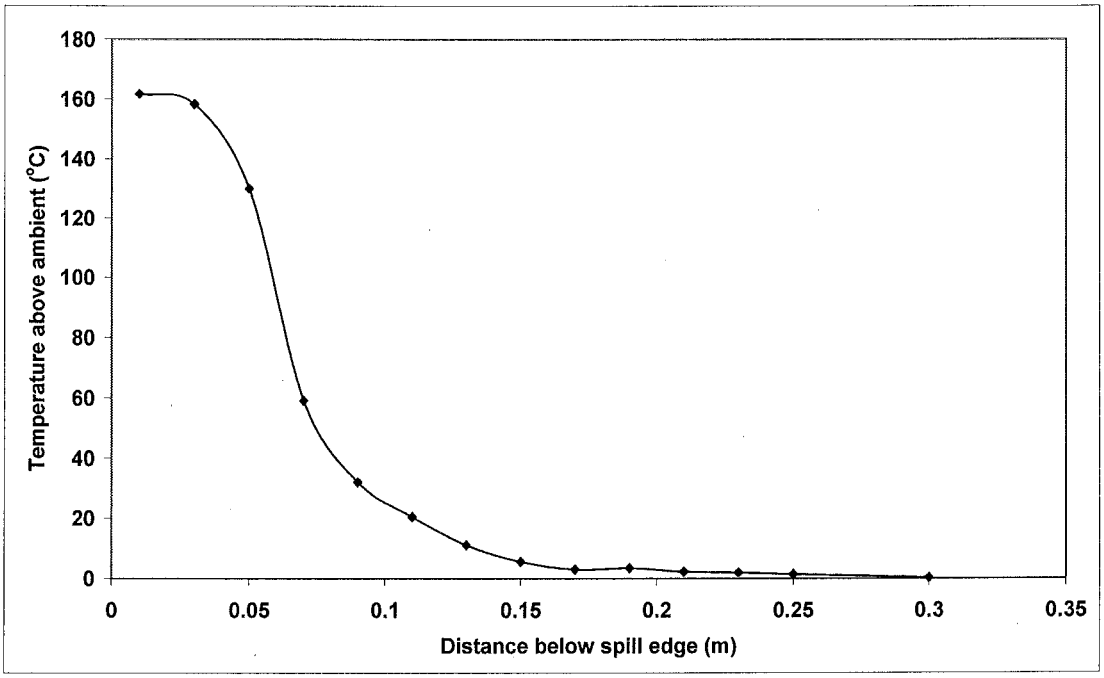

Figure 6.3: Temperature profile at the spill edge for Test 1

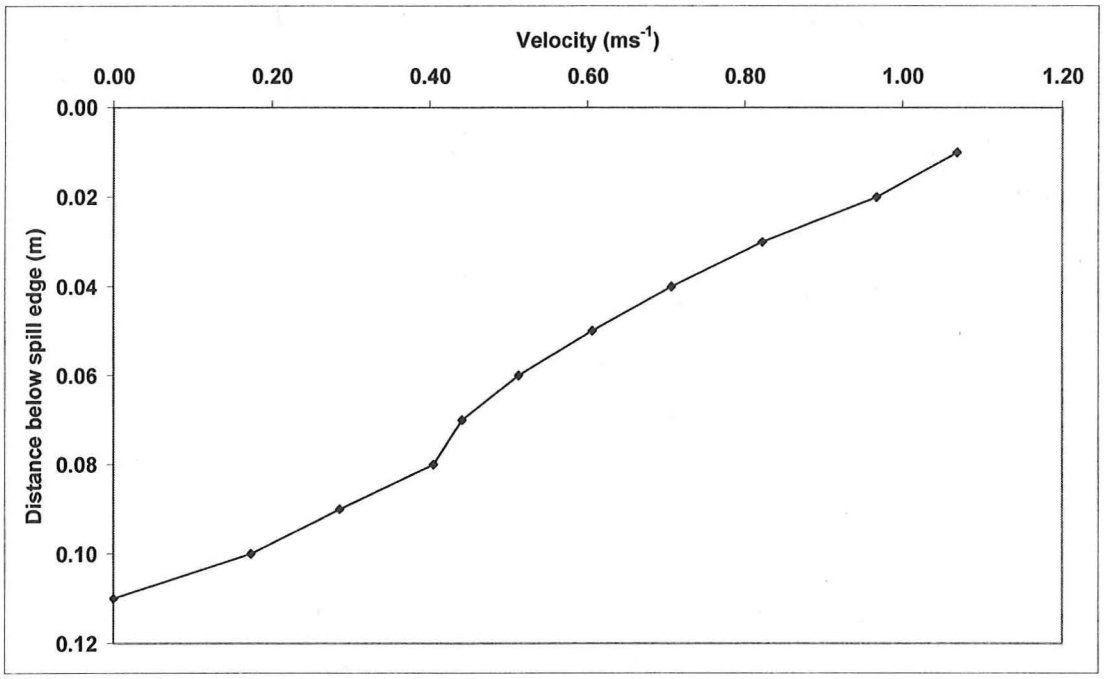

Figure 6.4: Velocity profile at the spill edge for Test 1

6.1.1.3 Summary of results

The temperature and velocity profiles at the spill edge were used to determine the mass flow rate and convective heat output of the gases at the spill edge. These results, in addition to the maximum temperature of the gas layer at the spill edge and the visual and buoyancy derived smoke layer depths are given in Table 6.1. The results are presented in terms of the time averaged mean value with associated standard errors. These results characterised the flow at the spill edge for each fire size and spill edge geometry examined, and have been used in the subsequent analysis of entrainment of air into a spill plume.

Test	Q_{TOTAL} (kW)	Q (kW)	$d_{b,v}$ (m)	$d_{b,buoy}$ (m)	$\theta_{b,max}$ (°C)	M_b (kgs^{-1})
1	6.0 +/- 0.2	4.11 +/- 0.59	0.105 +/- 0.01	0.090 +/- 0.002	161.70 +/- 3.15	0.0332 +/- 0.0058
2	9.0 +/- 0.2	6.34 +/- 1.36	0.110 +/- 0.01	0.096 +/- 0.002	210.20 +/- 6.58	0.0388 +/- 0.0130
3	12.0 +/- 0.2	8.74 +/- 1.38	0.115 +/- 0.01	0.117 +/- 0.002	258.60 +/- 5.97	0.0408 +/- 0.0076
4	6.0 +/- 0.2	4.33 +/- 0.46	0.125 +/- 0.01	0.119 +/- 0.002	121.80 +/- 2.02	0.0428 +/- 0.0049
5	9.0 +/- 0.2	6.33 +/- 0.77	0.130 +/- 0.01	0.126 +/- 0.002	158.50 +/- 4.32	0.0483 +/- 0.0064
6	12.0 +/- 0.2	9.10 +/- 1.03	0.140 +/- 0.01	0.140 +/- 0.002	200.60 +/- 2.15	0.0543 +/- 0.0067
7	6.0 +/- 0.2	4.89 +/- 0.53	0.130 +/- 0.01	0.107 +/- 0.002	104.20 +/- 2.91	0.0584 +/- 0.0073
8	9.0 +/- 0.2	7.40 +/- 0.78	0.140 +/- 0.01	0.120 +/- 0.002	132.60 +/- 5.13	0.0682 +/- 0.0083
9	12.0 +/- 0.2	10.37 +/- 1.25	0.150 +/- 0.01	0.138 +/- 0.002	166.60 +/- 7.03	0.0749 +/- 0.1080

Table 6.1: Summary of results for the approach flow at the spill edge

6.1.2 Mass flow rate of gases produced by a spill plume (Tests 10-64)

6.1.2.1 Temperature profiles in the smoke exhaust hood

The thermocouple column within the smoke exhaust hood (Column A) provided temperature profiles through the smoke layer for each height of rise of plume examined. Although visual observations were used to define the height the smoke layer above the spill edge in the experiment (i.e. the height of rise of the plume), the temperature (and hence, buoyancy) profiles also enabled the smoke layer depth in the hood to be calculated if required. Figure 6.5 shows the temperature profile in the exhaust hood for Test 34, where the height of rise of the plume was 0.5 m above the spill edge (1.5 m below the ceiling of the hood). This profile is generally typical of all the profiles measured in the hood.

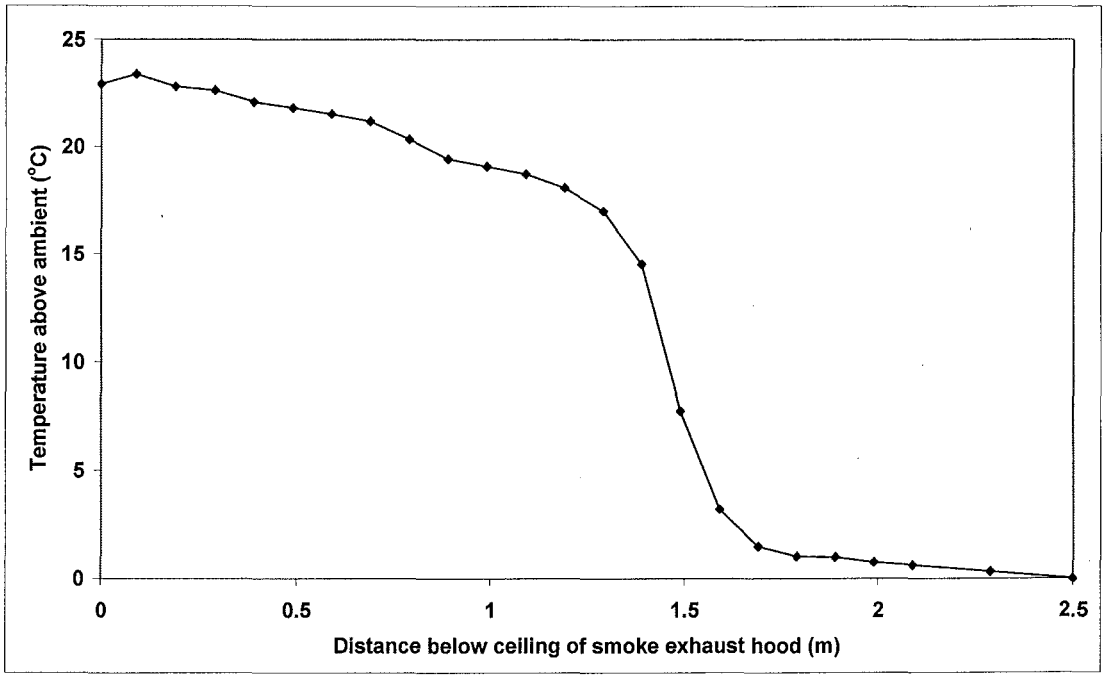

Figure 6.5: Temperature profile in the smoke exhaust hood (Test 34)

Appendix F shows the temperature profiles in the smoke exhaust hood for Tests 10 to 64 inclusive.

6.1.2.2 Summary of results

The mass flow rate of gases entering the layer in the smoke exhaust hood (i.e. M_p) for each test are given in Table 6.2 . The horizontal approach flow parameters are also included for completeness. The results are presented in terms of the time averaged mean value with associated standard errors.

Test	Q_{TOTAL} (kW)	Q (kW)	$d_{b,v}$ (m)	$d_{b,buoy}$ (m)	$\theta_{b,max}$ (°C)	M_b (kgs^{-1})	M_p (kgs^{-1})
10	6.0 +/- 0.2	4.89 +/- 0.53	0.130 +/- 0.01	0.107 +/- 0.002	104.20 +/- 2.91	0.0584 +/- 0.0073	0.7392 +/- 0.0010
11	9.0 +/- 0.2	7.40 +/- 0.78	0.140 +/- 0.01	0.120 +/- 0.002	132.60 +/- 5.13	0.0682 +/- 0.0083	0.8565 +/- 0.0010
12	12.0 +/- 0.2	10.37 +/- 1.25	0.150 +/- 0.01	0.138 +/- 0.002	166.60 +/- 7.03	0.0749 +/- 0.1080	0.9486 +/- 0.0010
13	6.0 +/- 0.2	4.33 +/- 0.46	0.125 +/- 0.01	0.119 +/- 0.002	121.80 +/- 2.02	0.0428 +/- 0.0049	0.9528 +/- 0.0010
14	9.0 +/- 0.2	6.33 +/- 0.77	0.130 +/- 0.01	0.126 +/- 0.002	158.50 +/- 4.32	0.0483 +/- 0.0064	1.1099 +/- 0.0010
15	12.0 +/- 0.2	9.10 +/- 1.03	0.140 +/- 0.01	0.140 +/- 0.002	200.60 +/- 2.15	0.0543 +/- 0.0067	1.2010 +/- 0.0010
16	6.0 +/- 0.2	4.89 +/- 0.53	0.130 +/- 0.01	0.107 +/- 0.002	104.20 +/- 2.91	0.0584 +/- 0.0073	0.6610 +/- 0.0010
17	9.0 +/- 0.2	7.40 +/- 0.78	0.140 +/- 0.01	0.120 +/- 0.002	132.60 +/- 5.13	0.0682 +/- 0.0083	0.7734 +/- 0.0010
18	12.0 +/- 0.2	10.37 +/- 1.25	0.150 +/- 0.01	0.138 +/- 0.002	166.60 +/- 7.03	0.0749 +/- 0.1080	0.8438 +/- 0.0010
19	6.0 +/- 0.2	4.33 +/- 0.46	0.125 +/- 0.01	0.119 +/- 0.002	121.80 +/- 2.02	0.0428 +/- 0.0049	0.6809 +/- 0.0010
20	9.0 +/- 0.2	6.33 +/- 0.77	0.130 +/- 0.01	0.126 +/- 0.002	158.50 +/- 4.32	0.0483 +/- 0.0064	0.8359 +/- 0.0010
21	12.0 +/- 0.2	9.10 +/- 1.03	0.140 +/- 0.01	0.140 +/- 0.002	200.60 +/- 2.15	0.0543 +/- 0.0067	0.8384 +/- 0.0010
22	6.0 +/- 0.2	4.11 +/- 0.59	0.105 +/- 0.01	0.090 +/- 0.002	161.70 +/- 3.15	0.0332 +/- 0.0058	0.3225 +/- 0.0010
23	9.0 +/- 0.2	6.34 +/- 1.36	0.110 +/- 0.01	0.096 +/- 0.002	210.20 +/- 6.58	0.0388 +/- 0.0130	0.3433 +/- 0.0010
24	12.0 +/- 0.2	8.74 +/- 1.38	0.115 +/- 0.01	0.117 +/- 0.002	258.60 +/- 5.97	0.0408 +/- 0.0076	0.3800 +/- 0.0010
25	6.0 +/- 0.2	4.89 +/- 0.53	0.130 +/- 0.01	0.107 +/- 0.002	104.20 +/- 2.91	0.0584 +/- 0.0073	0.2542 +/- 0.0010
26	9.0 +/- 0.2	7.40 +/- 0.78	0.140 +/- 0.01	0.120 +/- 0.002	132.60 +/- 5.13	0.0682 +/- 0.0083	0.2798 +/- 0.0010
27	12.0 +/- 0.2	10.37 +/- 1.25	0.150 +/- 0.01	0.138 +/- 0.002	166.60 +/- 7.03	0.0749 +/- 0.1080	0.2975 +/- 0.0010
28	6.0 +/- 0.2	4.33 +/- 0.46	0.125 +/- 0.01	0.119 +/- 0.002	121.80 +/- 2.02	0.0428 +/- 0.0049	0.2320 +/- 0.0010
29	9.0 +/- 0.2	6.33 +/- 0.77	0.130 +/- 0.01	0.126 +/- 0.002	158.50 +/- 4.32	0.0483 +/- 0.0064	0.2856 +/- 0.0010
30	12.0 +/- 0.2	9.10 +/- 1.03	0.140 +/- 0.01	0.140 +/- 0.002	200.60 +/- 2.15	0.0543 +/- 0.0067	0.2971 +/- 0.0010
31	6.0 +/- 0.2	4.11 +/- 0.59	0.105 +/- 0.01	0.090 +/- 0.002	161.70 +/- 3.15	0.0332 +/- 0.0058	0.2520 +/- 0.0010
32	9.0 +/- 0.2	6.34 +/- 1.36	0.110 +/- 0.01	0.096 +/- 0.002	210.20 +/- 6.58	0.0388 +/- 0.0130	0.2750 +/- 0.0010
33	12.0 +/- 0.2	8.74 +/- 1.38	0.115 +/- 0.01	0.117 +/- 0.002	258.60 +/- 5.97	0.0408 +/- 0.0076	0.2896 +/- 0.0010
34	6.0 +/- 0.2	4.89 +/- 0.53	0.130 +/- 0.01	0.107 +/- 0.002	104.20 +/- 2.91	0.0584 +/- 0.0073	0.2135 +/- 0.0010
35	9.0 +/- 0.2	7.40 +/- 0.78	0.140 +/- 0.01	0.120 +/- 0.002	132.60 +/- 5.13	0.0682 +/- 0.0083	0.2429 +/- 0.0010
36	12.0 +/- 0.2	10.37 +/- 1.25	0.150 +/- 0.01	0.138 +/- 0.002	166.60 +/- 7.03	0.0749 +/- 0.1080	0.2600 +/- 0.0010
37	6.0 +/- 0.2	4.11 +/- 0.59	0.105 +/- 0.01	0.090 +/- 0.002	161.70 +/- 3.15	0.0332 +/- 0.0058	0.2083 +/- 0.0010
38	9.0 +/- 0.2	6.34 +/- 1.36	0.110 +/- 0.01	0.096 +/- 0.002	210.20 +/- 6.58	0.0388 +/- 0.0130	0.2351 +/- 0.0010
39	12.0 +/- 0.2	8.74 +/- 1.38	0.115 +/- 0.01	0.117 +/- 0.002	258.60 +/- 5.97	0.0408 +/- 0.0076	0.2648 +/- 0.0010
40	6.0 +/- 0.2	4.33 +/- 0.46	0.125 +/- 0.01	0.119 +/- 0.002	121.80 +/- 2.02	0.0428 +/- 0.0049	0.2038 +/- 0.0010
41	9.0 +/- 0.2	6.33 +/- 0.77	0.130 +/- 0.01	0.126 +/- 0.002	158.50 +/- 4.32	0.0483 +/- 0.0064	0.2342 +/- 0.0010
42	12.0 +/- 0.2	9.10 +/- 1.03	0.140 +/- 0.01	0.140 +/- 0.002	200.60 +/- 2.15	0.0543 +/- 0.0067	0.2463 +/- 0.0010
43	6.0 +/- 0.2	4.89 +/- 0.53	0.130 +/- 0.01	0.107 +/- 0.002	104.20 +/- 2.91	0.0584 +/- 0.0073	0.1777 +/- 0.0010
44	9.0 +/- 0.2	7.40 +/- 0.78	0.140 +/- 0.01	0.120 +/- 0.002	132.60 +/- 5.13	0.0682 +/- 0.0083	0.1932 +/- 0.0010
45	12.0 +/- 0.2	10.37 +/- 1.25	0.150 +/- 0.01	0.138 +/- 0.002	166.60 +/- 7.03	0.0749 +/- 0.1080	0.2108 +/- 0.0010
46	6.0 +/- 0.2	4.11 +/- 0.59	0.105 +/- 0.01	0.090 +/- 0.002	161.70 +/- 3.15	0.0332 +/- 0.0058	0.1550 +/- 0.0010
47	9.0 +/- 0.2	6.34 +/- 1.36	0.110 +/- 0.01	0.096 +/- 0.002	210.20 +/- 6.58	0.0388 +/- 0.0130	0.1792 +/- 0.0010
48	12.0 +/- 0.2	8.74 +/- 1.38	0.115 +/- 0.01	0.117 +/- 0.002	258.60 +/- 5.97	0.0408 +/- 0.0076	0.1931 +/- 0.0010
49	6.0 +/- 0.2	4.33 +/- 0.46	0.125 +/- 0.01	0.119 +/- 0.002	121.80 +/- 2.02	0.0428 +/- 0.0049	0.1269 +/- 0.0010
50	9.0 +/- 0.2	6.33 +/- 0.77	0.130 +/- 0.01	0.126 +/- 0.002	158.50 +/- 4.32	0.0483 +/- 0.0064	0.1483 +/- 0.0010
51	12.0 +/- 0.2	9.10 +/- 1.03	0.140 +/- 0.01	0.140 +/- 0.002	200.60 +/- 2.15	0.0543 +/- 0.0067	0.1758 +/- 0.0010
52	6.0 +/- 0.2	4.11 +/- 0.59	0.105 +/- 0.01	0.090 +/- 0.002	161.70 +/- 3.15	0.0332 +/- 0.0058	0.1090 +/- 0.0010
53	9.0 +/- 0.2	6.34 +/- 1.36	0.110 +/- 0.01	0.096 +/- 0.002	210.20 +/- 6.58	0.0388 +/- 0.0130	0.1335 +/- 0.0010
54	12.0 +/- 0.2	8.74 +/- 1.38	0.115 +/- 0.01	0.117 +/- 0.002	258.60 +/- 5.97	0.0408 +/- 0.0076	0.1571 +/- 0.0010
55	6.0 +/- 0.2	4.89 +/- 0.53	0.130 +/- 0.01	0.107 +/- 0.002	104.20 +/- 2.91	0.0584 +/- 0.0073	0.0886 +/- 0.0010
56	9.0 +/- 0.2	7.40 +/- 0.78	0.140 +/- 0.01	0.120 +/- 0.002	132.60 +/- 5.13	0.0682 +/- 0.0083	0.0926 +/- 0.0010
57	12.0 +/- 0.2	10.37 +/- 1.25	0.150 +/- 0.01	0.138 +/- 0.002	166.60 +/- 7.03	0.0749 +/- 0.1080	0.1090 +/- 0.0010
58	6.0 +/- 0.2	4.33 +/- 0.46	0.125 +/- 0.01	0.119 +/- 0.002	121.80 +/- 2.02	0.0428 +/- 0.0049	0.0716 +/- 0.0010
59	9.0 +/- 0.2	6.33 +/- 0.77	0.130 +/- 0.01	0.126 +/- 0.002	158.50 +/- 4.32	0.0483 +/- 0.0064	0.0814 +/- 0.0010
60	12.0 +/- 0.2	9.10 +/- 1.03	0.140 +/- 0.01	0.140 +/- 0.002	200.60 +/- 2.15	0.0543 +/- 0.0067	0.0886 +/- 0.0010
61	6.0 +/- 0.2	4.11 +/- 0.59	0.105 +/- 0.01	0.090 +/- 0.002	161.70 +/- 3.15	0.0332 +/- 0.0058	0.0570 +/- 0.0010
62	9.0 +/- 0.2	6.34 +/- 1.36	0.110 +/- 0.01	0.096 +/- 0.002	210.20 +/- 6.58	0.0388 +/- 0.0130	0.0645 +/- 0.0010
63	12.0 +/- 0.2	8.74 +/- 1.38	0.115 +/- 0.01	0.117 +/- 0.002	258.60 +/- 5.97	0.0408 +/- 0.0076	0.0708 +/- 0.0010
64	6.0 +/- 0.2	4.62 +/- 0.50	0.110 +/- 0.01	0.099 +/- 0.002	89.10 +/- 1.60	0.0710 +/- 0.1000	0.1855 +/- 0.0010

Table 6.2: Summary of results for mass flow rate due to a spill plume

6.2 Entrainment of air into a flow from a compartment opening to a higher projecting balcony

The results from both the CFD and physical scale modelling studies to examine entrainment of air into a flow from a compartment opening to a higher projecting balcony are given below.

6.2.1 FDS simulation results

6.2.1.1 Onset of steady state conditions

Although the fire source was assumed to be steady state, it was first necessary to determine when reasonably steady state conditions had been reached in the compartment. Figure 6.6 shows a graph of the temperature close to the top of the compartment opening (0.01 m below the downstand) with respect to time for Simulation 1. Figure 6.6 show that the temperature within the compartment can be considered to be steady after approximately 180 s. This behaviour was typical for all of the simulations carried out. Therefore, the FDS results were averaged using the data measured between 180 and 240 s from ignition for all of the simulations.

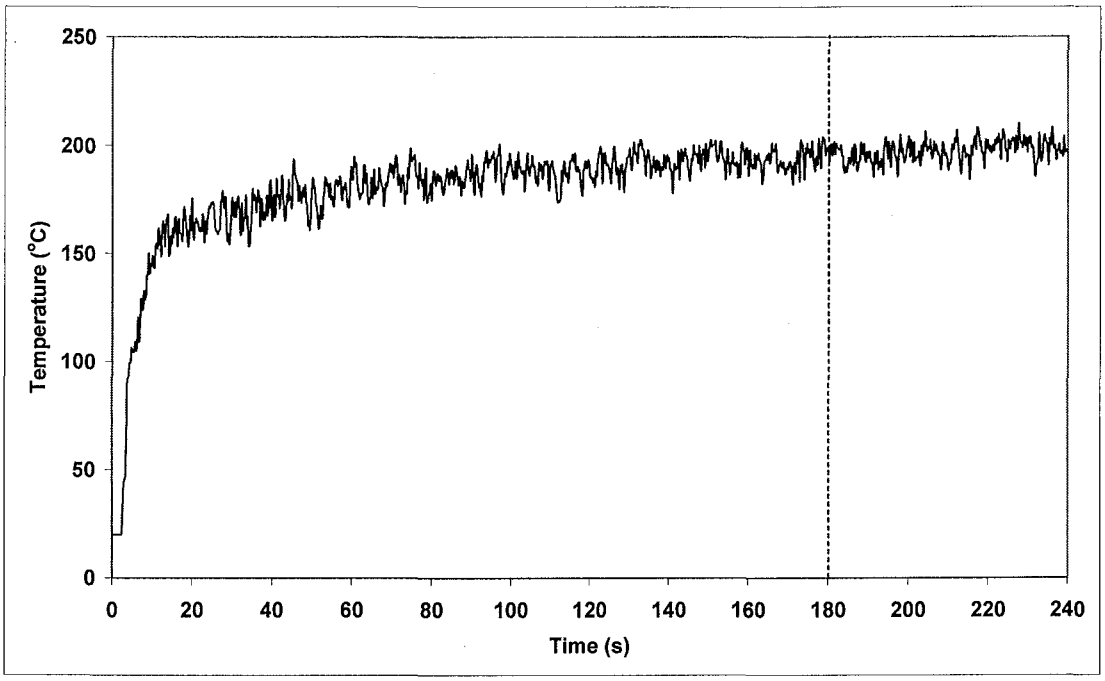

Figure 6.6: Temperature at the compartment opening with respect to time (Simulation 1)

6.2.1.2 Homogeneity of flow across the compartment opening and the spill edge

As the mass flow rate of gases at the compartment opening and at the spill edge were determined from a single velocity and temperature traverse through the centre of the layer, it was again necessary to confirm if the gas temperature and velocity profiles were reasonably homogeneous across the width of the gas layer at the compartment opening and at the spill edge.

Figures 6.7 and 6.8 show temperature profiles across the gas layer at the compartment opening and at the spill edge (0.01 m below the top of the opening) respectively for Simulations 1, 23 and 24. Figures 6.7 and 6.8 show that the temperature profiles across the gas layer were reasonably constant across the full width at each location (note that the width of the compartment opening was 0.6 m for Simulations 23 and 24). This behaviour was generally typical of all of the simulations carried out, irrespective of the width of the compartment opening or the downstand depth.

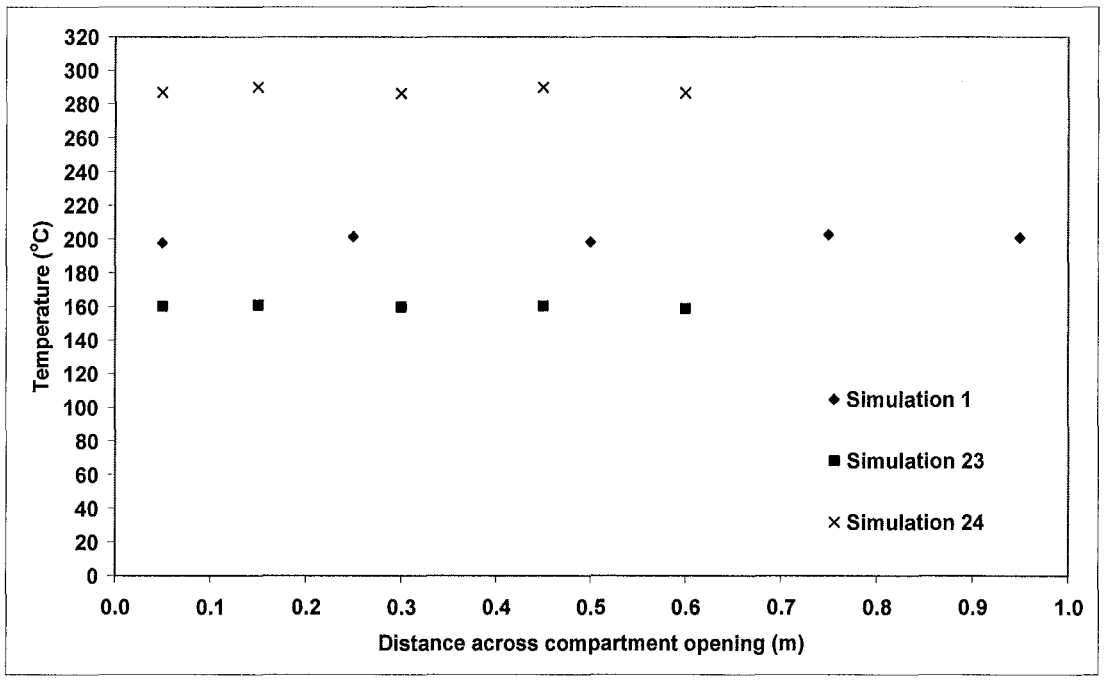

Figure 6.7: Typical temperature profile across the gas layer at the compartment opening

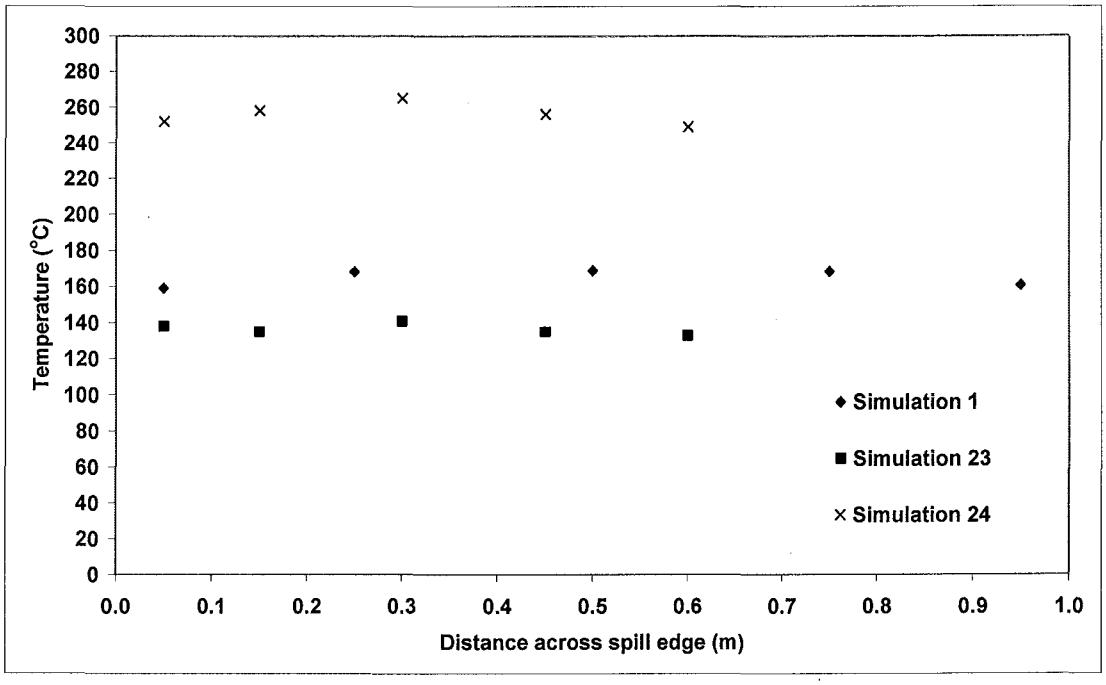

Figure 6.8: Typical temperature profile across the gas layer at the spill edge

Figures 6.9 and 6.10 show velocity profiles across the gas layer at the compartment opening and at the spill edge (0.01 m below the top of the opening) respectively for Simulations 1, 23 and 24. Figures 6.9 and 6.10 show that the velocity profiles across the gas layer were reasonably constant across the full width at each location. This behaviour was generally typical of all of the simulations carried out, irrespective of the width of the compartment opening or the downstand depth.

This analysis provided the confidence to enable an integration to be performed through the hot gas layer, from a single velocity and temperature traverse, so that the mass flow rate of the gas layer at the compartment opening and at the spill edge could be determined.

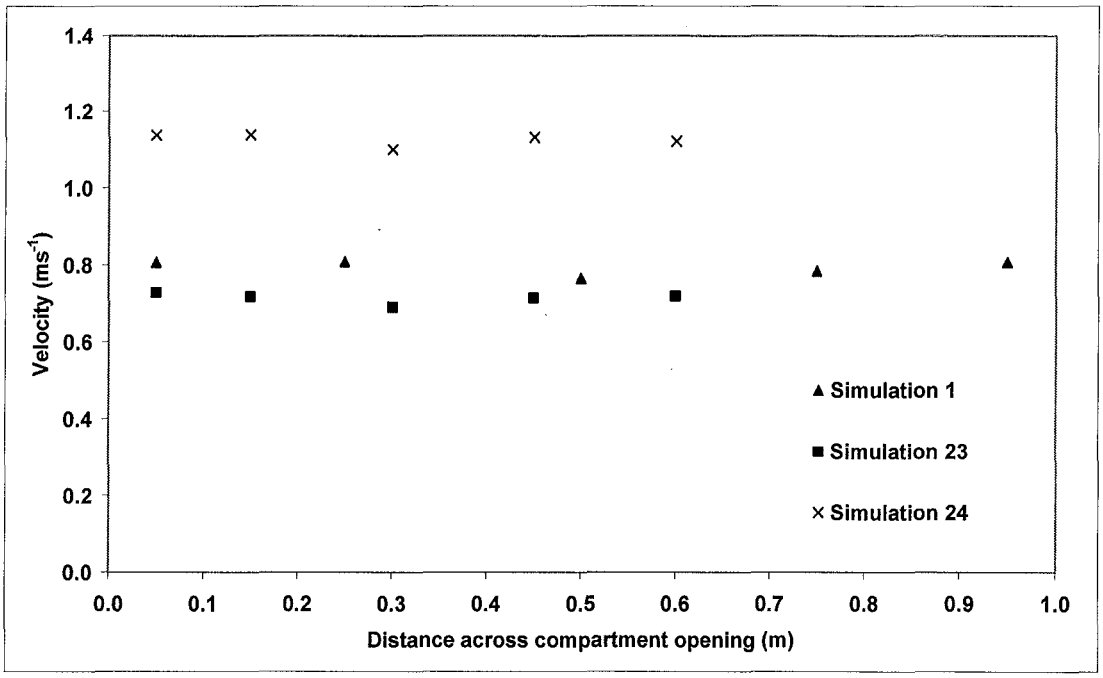

Figure 6.9: **Typical velocity profile across the gas layer at the compartment opening**

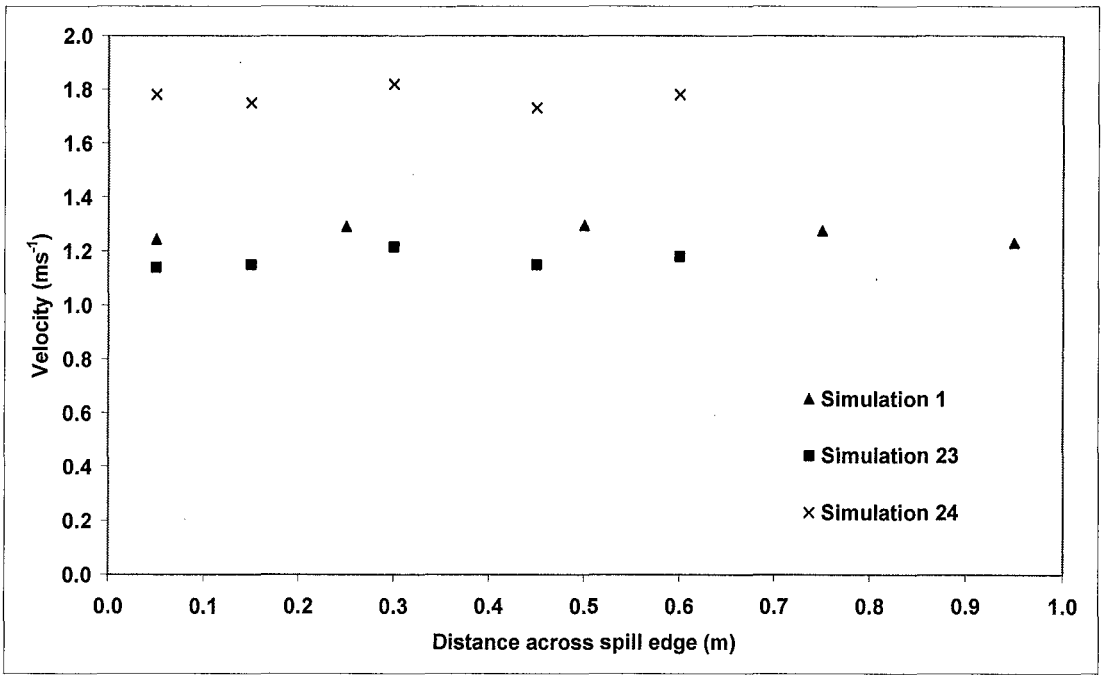

Figure 6.10: **Typical velocity profile across the gas layer at the spill edge**

6.2.1.3 Temperature profiles at the compartment opening and at the spill edge

Figures 6.11 and 6.12 show the temperature profiles through the gas layer at the compartment opening and at the spill edge respectively for Simulation 1. The nature of these profiles is generally typical of all of the simulations carried out.

Appendix G shows the temperature profiles at the compartment opening and at the spill edge for Simulations 1 to 25 inclusive.

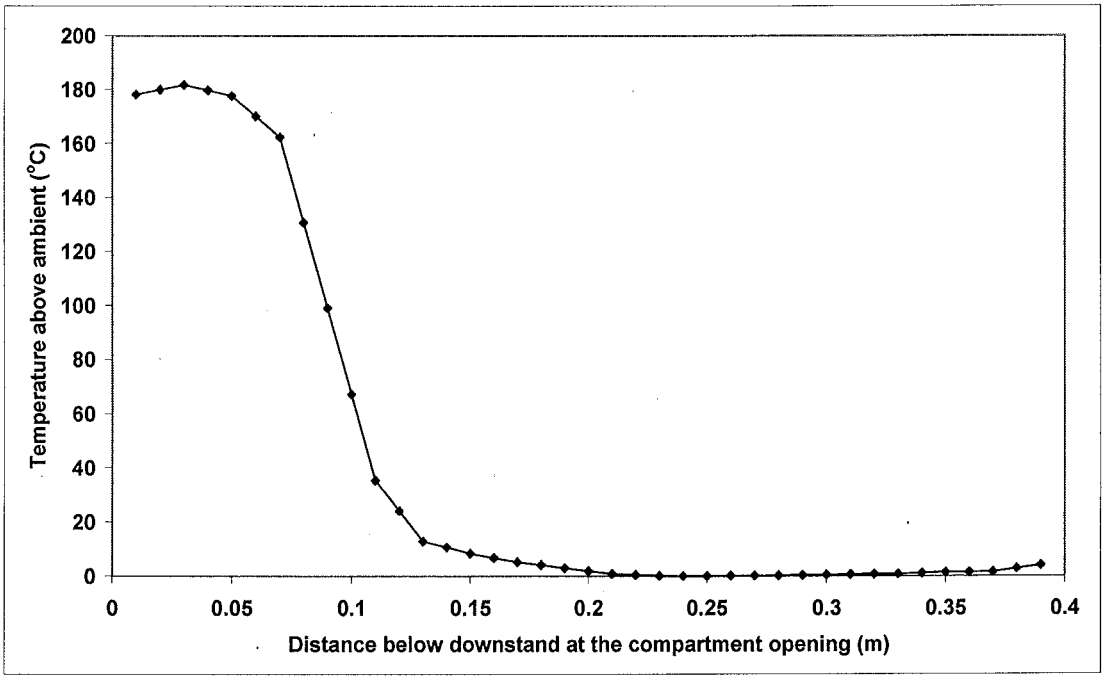

Figure 6.11: Temperature profile at the compartment opening for Simulation 1

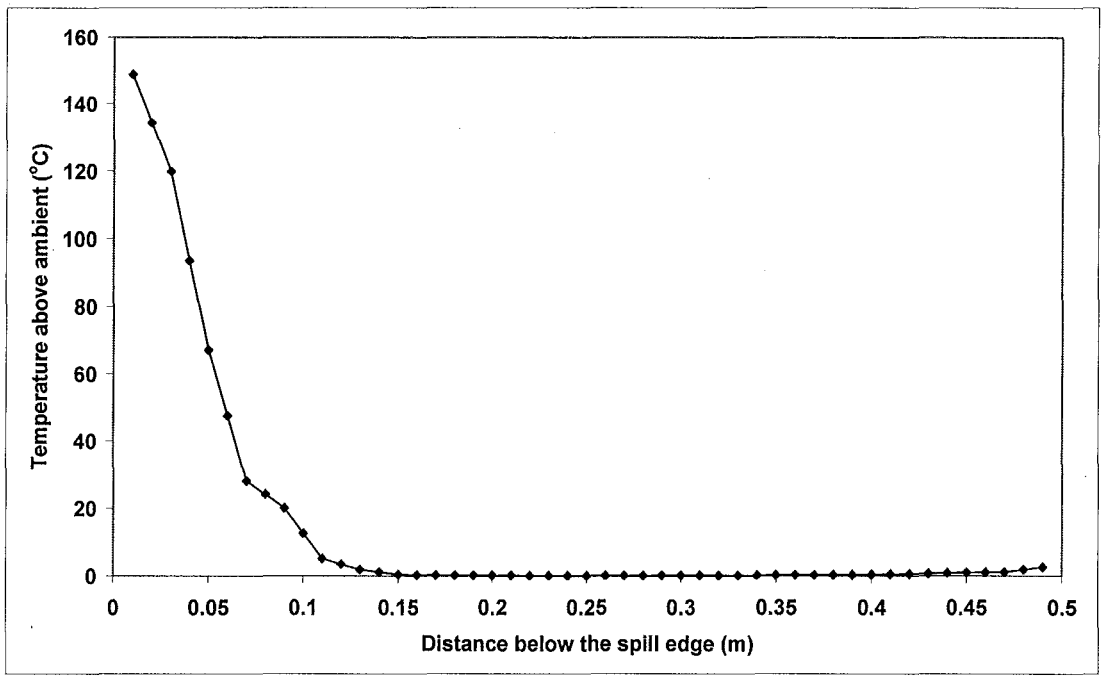

Figure 6.12: Temperature profile at the spill edge for Simulation 1

6.2.1.4 Velocity profiles at the compartment opening and at the spill edge

Figures 6.13 and 6.14 show the gas velocity profiles through the gas layer at the compartment opening and at the spill edge respectively for Simulation 1. The nature of these profiles is generally typical of all of the simulations carried out.

Appendix H shows the velocity profiles at the compartment opening and at the spill edge for Simulations 1 to 25 inclusive.

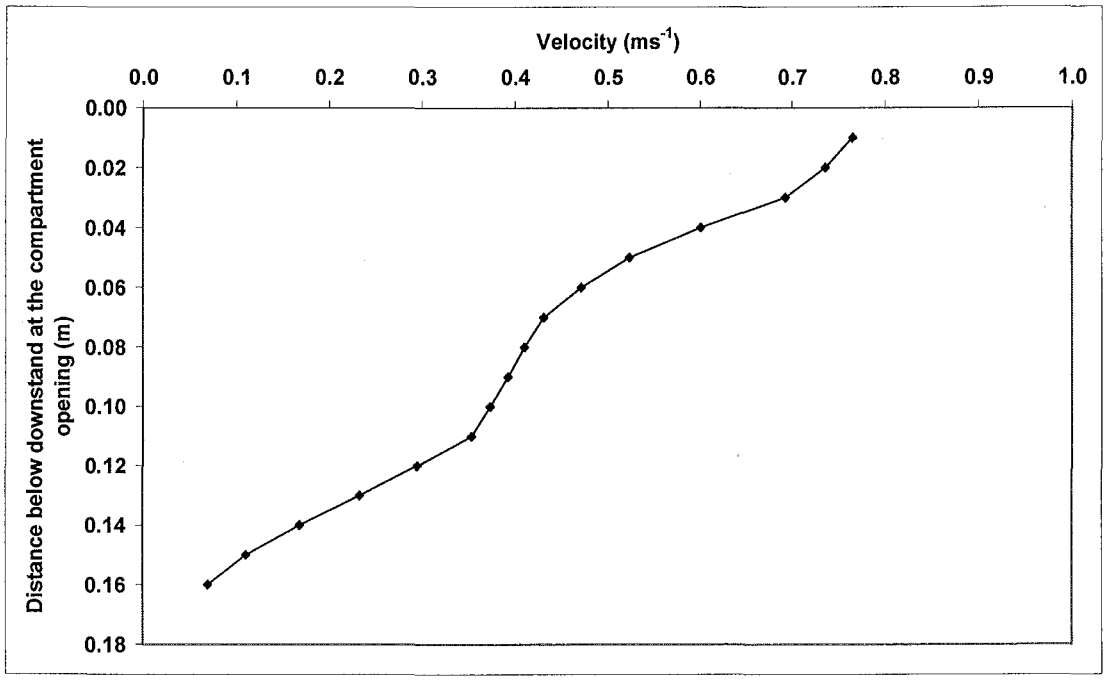

Figure 6.13: Velocity profile at the compartment opening for Simulation 1

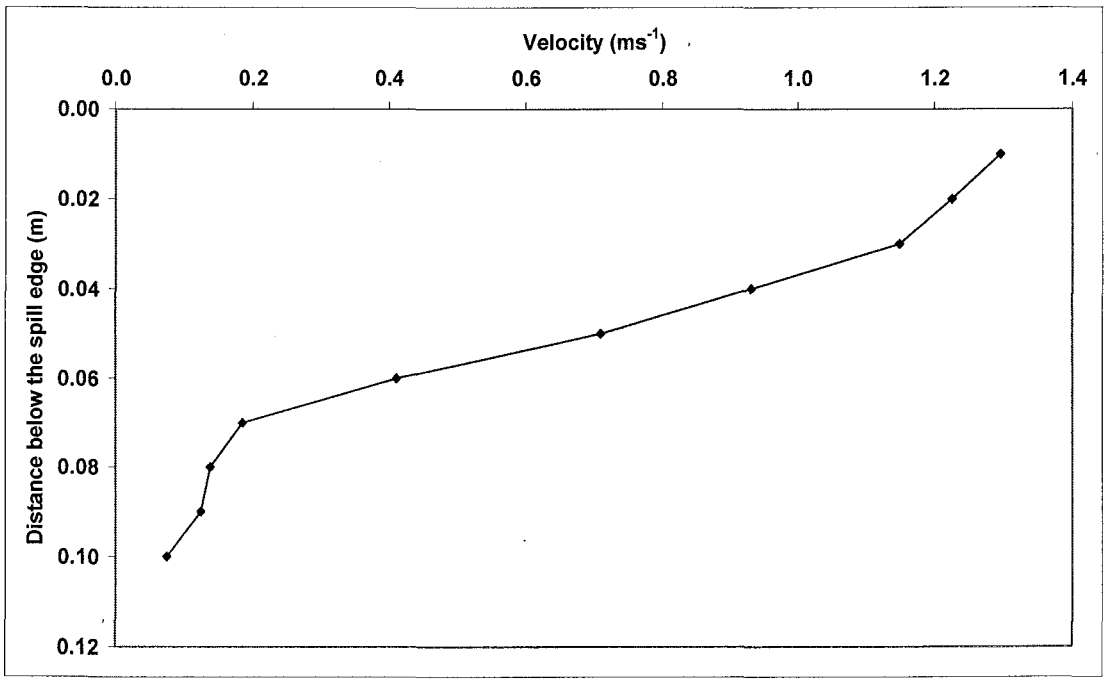

Figure 6.14: Velocity profile at the spill edge for Simulation 1

6.2.1.5 Summary of results

The calculated mass flow rate of gases at the compartment opening (M_w) and at the spill edge (M_b) from the FDS predictions are given in Table 6.3. The results are presented in terms of the time averaged mean value with associated standard errors. The ratio of (M_b / M_w) is also included for comparison with the current guidance on entrainment of air into these flows.

Simulation	M_w (kgs^{-1})	M_b (kgs^{-1})	M_b/M_w
1	0.0587 +/- 0.0004	0.0608 +/- 0.0006	1.0356
2	0.0563 +/- 0.0004	0.0582 +/- 0.0005	1.0344
3	0.0463 +/- 0.0004	0.0539 +/- 0.0005	1.1625
4	0.0361 +/- 0.0004	0.0430 +/- 0.0004	1.1905
5	0.0196 +/- 0.0003	0.0247 +/- 0.0003	1.2591
6	0.0517 +/- 0.0005	0.0619 +/- 0.0006	1.1968
7	0.0410 +/- 0.0004	0.0482 +/- 0.0004	1.1774
8	0.0158 +/- 0.0002	0.0231 +/- 0.0003	1.4603
9	0.0468 +/- 0.0004	0.0646 +/- 0.0006	1.3815
10	0.0422 +/- 0.0004	0.0553 +/- 0.0005	1.3101
11	0.0354 +/- 0.0003	0.0480 +/- 0.0004	1.3577
12	0.0255 +/- 0.0003	0.0348 +/- 0.0003	1.3675
13	0.0140 +/- 0.0002	0.0206 +/- 0.0002	1.4725
14	0.0335 +/- 0.0003	0.0592 +/- 0.0005	1.7685
15	0.0272 +/- 0.0003	0.0477 +/- 0.0004	1.7531
16	0.0109 +/- 0.0002	0.0168 +/- 0.0002	1.5327
17	0.0315 +/- 0.0003	0.0651 +/- 0.0006	2.0675
18	0.0269 +/- 0.0003	0.0493 +/- 0.0004	1.8299
19	0.0366 +/- 0.0003	0.0434 +/- 0.0004	1.1883
20	0.0191 +/- 0.0002	0.0218 +/- 0.0002	1.1417
21	0.0299 +/- 0.0003	0.0397 +/- 0.0003	1.3279
22	0.0401 +/- 0.0004	0.0548 +/- 0.0005	1.3645
23	0.0365 +/- 0.0003	0.0396 +/- 0.0004	1.0844
24	0.0525 +/- 0.0005	0.0650 +/- 0.0006	1.2379
25	0.0336 +/- 0.0003	0.0614 +/- 0.0006	1.8241

Table 6.3: Summary of the FDS predictions for mass flow rate at the compartment opening and at the spill edge

6.2.2 Physical scale modelling results (Tests 65 to 68)

6.2.2.1 Temperature profiles at the compartment opening and at the spill edge

Figures 6.15 and 6.16 show the temperature profiles through the gas layer at the compartment opening and at the spill edge respectively for Test 65. The nature of these profiles is generally typical of all of the simulations carried out.

Appendix I shows the temperature profiles at the compartment opening and at the spill edge for Tests 65 to 68 inclusive.

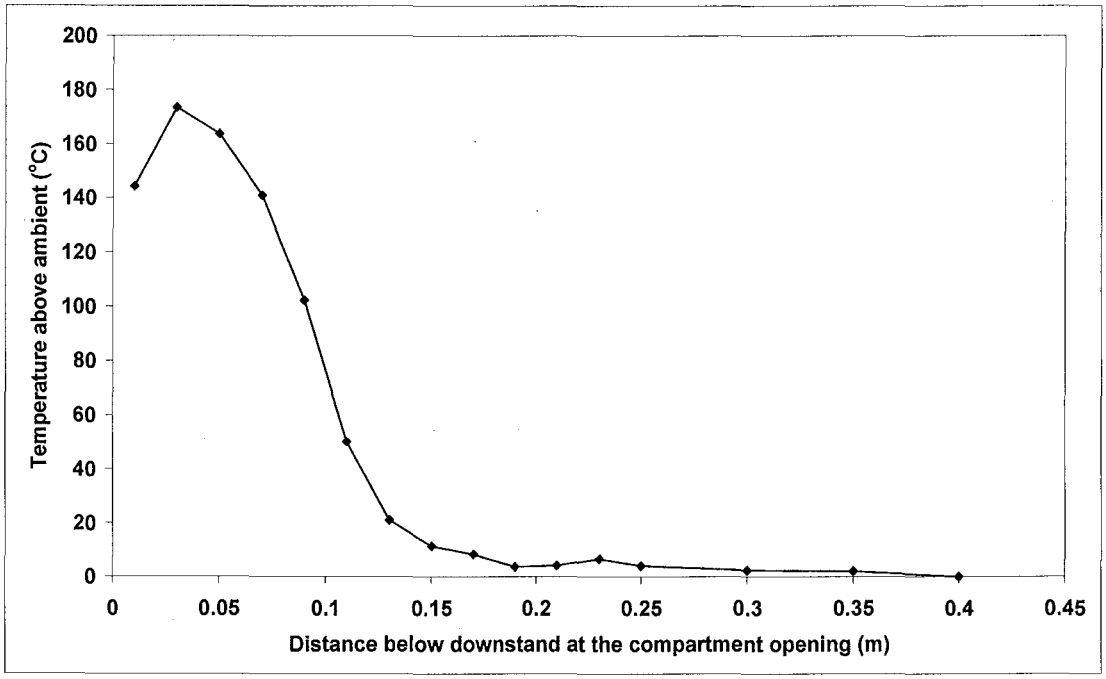

Figure 6.15: Temperature profile at the compartment opening for Test 65

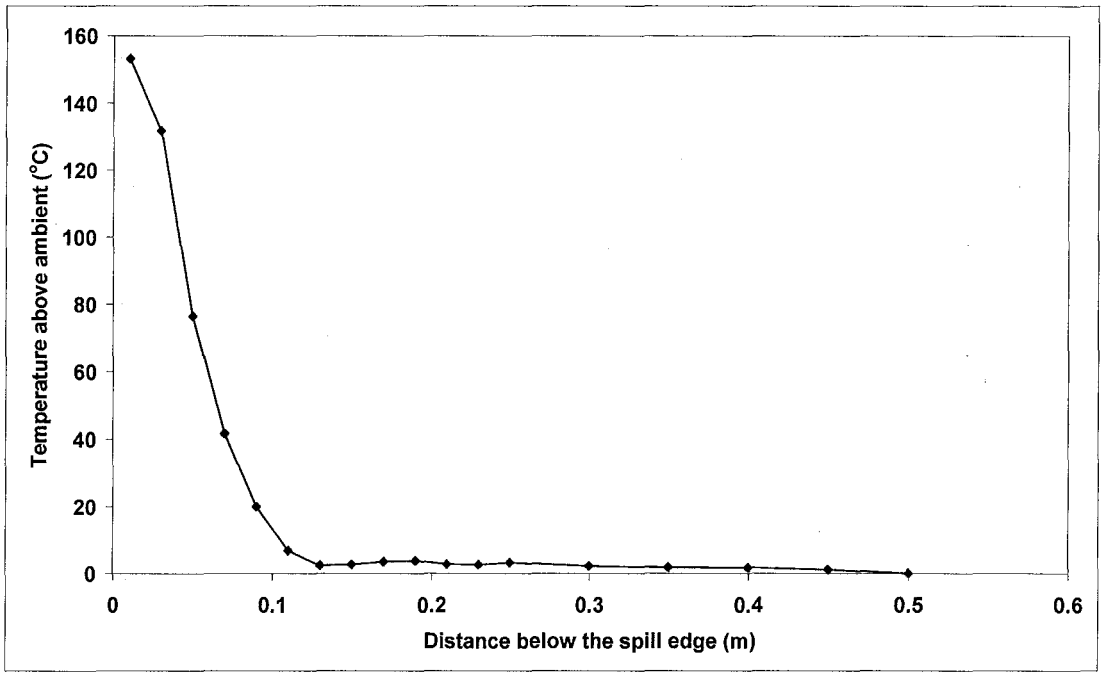

Figure 6.16: Temperature profile at the spill edge for Test 65

6.2.2.2 Velocity profiles at the compartment opening and at the spill edge

Figures 6.17 and 6.18 show the velocity profiles through the gas layer at the compartment opening and at the spill edge respectively for Test 65. The nature of these profiles is generally typical of all of the simulations carried out.

Appendix J shows the temperature profiles at the compartment opening and at the spill edge for Tests 65 to 68 inclusive.

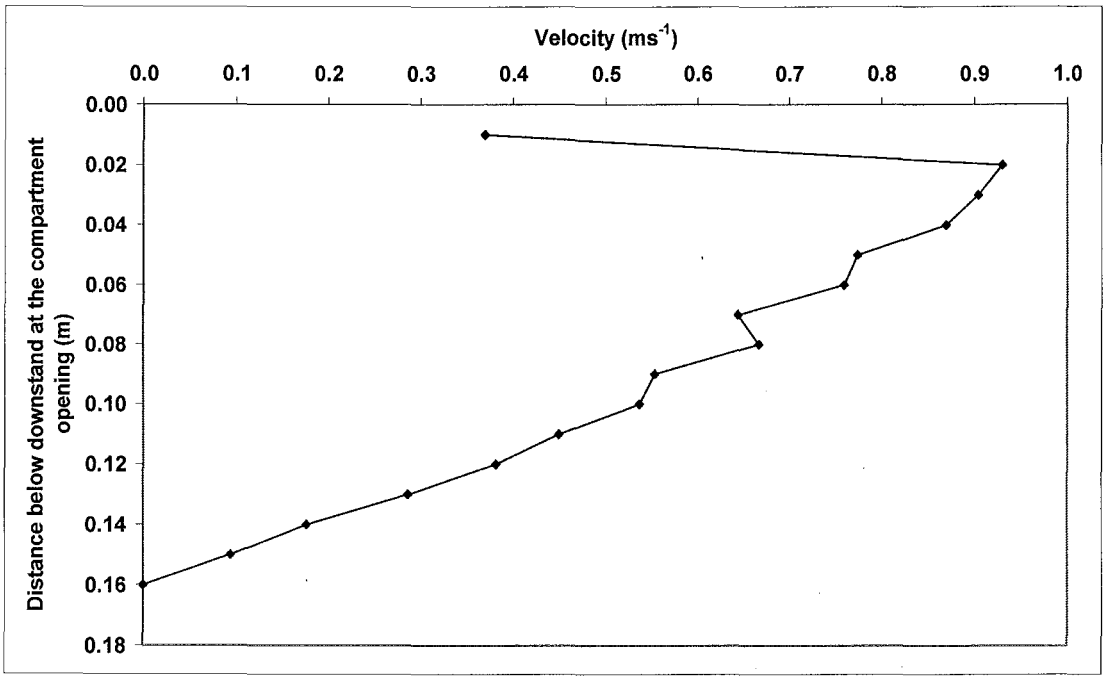

Figure 6.17: Velocity profile at the compartment opening for Test 65

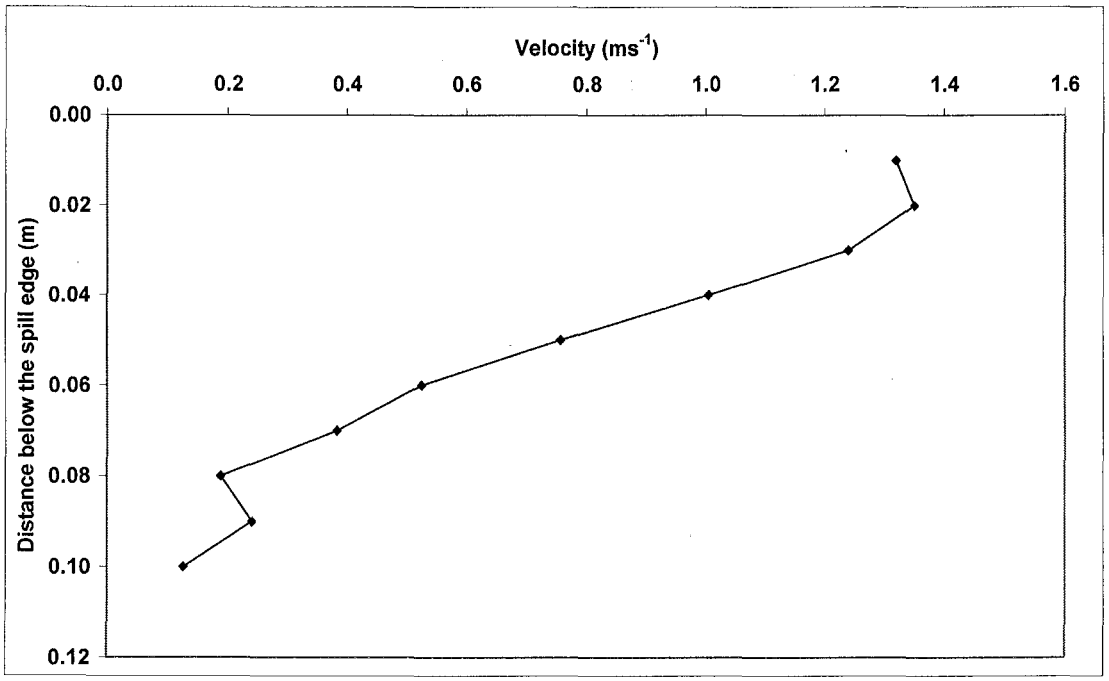

Figure 6.18: Velocity profile at the spill edge for Test 65

6.2.2.3 Summary of results

The calculated mass flow rate of gases at the compartment opening (M_w) and at the spill edge (M_b) from the velocity and temperature traverses are given in Table 6.4. Initial analysis of the experimental results showed that the mass flow rate at the compartment opening was greater than that at the spill edge for Tests 65, 67 and 68. This result is clearly implausible as the mass flow rate of gases cannot decrease between the compartment opening and the spill edge. This indicated a problem with the measurement technique in either, or both locations in which the velocity and temperature traverses were carried out.

Test	M_w (kgs^{-1})	M_b (kgs^{-1})	M_b/M_w
65	0.0707 +/- 0.0125	0.0680 +/- 0.0108	0.9618
66	0.0557 +/- 0.0151	0.0636 +/- 0.0118	1.1418
67	0.0447 +/- 0.0008	0.0411 +/- 0.0053	0.9195
68	0.0295 +/- 0.0008	0.0258 +/- 0.0035	0.8746

Table 6.4: Summary of the experimental mass flow rate at the compartment opening and at the spill edge (Tests 65 to 68)

If we first consider the flow of gases at the spill edge, previous work [42] has successfully used the technique of velocity traverses using pitot tubes to determine the mass flow rate of gases at this location. These measurements were typically made through a horizontally flowing hot gas layer at the spill edge. In this experiment, the flow conditions at the spill edge were similar to that in previous work. Therefore, there was greater confidence in these measurements compared to those made at the compartment opening.

In an attempt to validate the mass flow rate measurements at the spill edge (from the velocity traverses), a theory developed by Morgan [30] on the horizontal flow of gases toward a compartment opening was used. This theory has been validated from previous studies [35, 42] using a discharge coefficient (C_d) of 1.0 for a flat ceiling at a spill edge. The theory was used [using Equation (6-1)] to determine the mass flow rate of gases at the spill edge using the temperature and layer depth measurements from the experiment.

Morgan [30] states that the theory should be modified for flows from narrow openings (i.e. when the depth of the gas layer is much greater than the width of the opening). However, as the gas layer depth at the spill edge was generally much smaller than, or comparable to, the width of the compartment opening for Tests 65 to 68, Equation (6-1) was used for all compartment opening geometries studied.

$$M_b = \frac{2}{3} C_d^{3/2} \left(2 g \theta_{c,b} T_1\right)^{1/2} \frac{W \rho_1}{T_{c,b}} d_b^{3/2} \kappa_M \qquad (6\text{-}1)$$

Figure 6.19 and Table 6.5 shows a comparison between the experimental mass flow rates at the spill edge (from the velocity profiles) and those calculated using Equation (6-1) (using layer depth and temperature measurements). Figure 6.19 and Table 6.5 show that the experimental and calculated mass flow rates are equal (to within one standard error). This result indicates that the experimental mass flow rates at the spill edge (from the velocity profiles) were reliable.

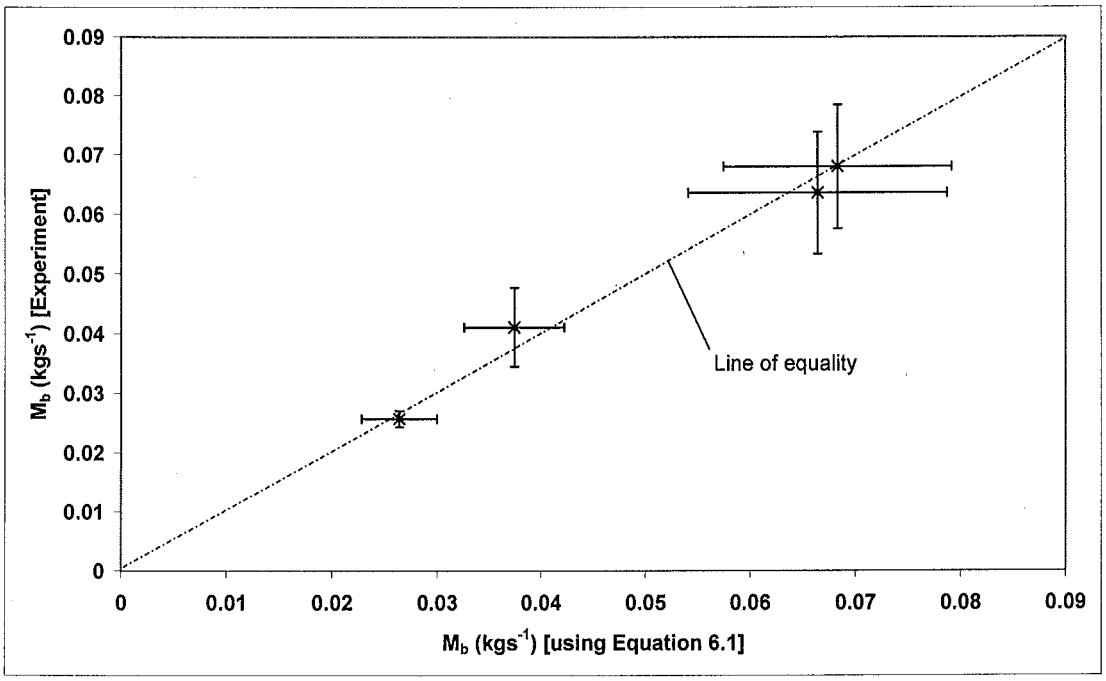

Figure 6.19 **Graph showing comparison of the experimental mass flow rates at the spill edge with those calculated using Equation (6-1)**

Test	$d_{b,v}$ (m)	$\theta_{c,b}$ (°C)	M_b [using Equation (6-1)] (kgs^{-1})	M_b (Experiment) (kgs^{-1})
65	0.10	153	0.0683 +/- 0.0105	0.0680 +/- 0.0108
66	0.10	132	0.0664 +/- 0.0107	0.0636 +/- 0.0118
67	0.12	216	0.0374 +/- 0.0060	0.0411 +/- 0.0053
68	0.15	289	0.0264 +/- 0.0014	0.0258 +/- 0.0035

Table 6.5: Comparison of experimental mass flow rates at the spill edge with those calculated using Equation (6-1)

The above result indicates that the measured mass flow rate of gases at the compartment opening must be anomalously high. It is likely that the directionality and velocity of the flow at the compartment opening were such that accurate velocity measurements using a pitot tube were not possible. An alternative type of velocity probe may be required to accurately measure this type of flow, such as the 5-hole probe described by Schulz [68].

In an attempt to quantify the mass flow rate of gases at the compartment opening from the experimental results, Morgan's horizontal flow theory was applied. Although this theory applies to a flow at a final exit, it has been used here as a best approximation. The experimental temperature and layer depth measurements at the compartment opening were used in this analysis [using Equation (2-1)].

Table 6.6 shows the calculated mass flow rates at the compartment opening for each test using in Equation (2-1).

Test	d_w (m)	$\theta_{c,w}$ (°C)	M_w [using Equation (2-1)] (kgs^{-1})
65	0.15	174	0.0594 +/- 0.0127
66	0.11	216	0.0383 +/- 0.0056
67	0.20	237	0.0374 +/- 0.0032
68	0.23	295	0.0229 +/- 0.0006

Table 6.6: Calculated mass flow rate at the compartment opening using Equation (2-1)

Table 6.7 shows a summary of the revised results for the mass flow rate of gases at the compartment opening and those measured at the spill edge (from the velocity profiles). These data, in addition to the relevant velocity and temperature profiles have been used in the subsequent analysis for comparison with the FDS predictions.

Test	M_w (kgs^{-1})	M_b (kgs^{-1})	M_b/M_w
65	0.0594 +/- 0.0127	0.0680 +/- 0.0108	1.1448
66	0.0383 +/- 0.0056	0.0636 +/- 0.0118	1.6606
67	0.0374 +/- 0.0032	0.0411 +/- 0.0053	1.0989
68	0.0229 +/- 0.0006	0.0258 +/- 0.0035	1.1266

Table 6.7: Revised experimental mass flow rates at the compartment opening

CHAPTER 7

7. DISCUSSION

7.1 Entrainment of air into a spill plume

7.1.1 Plume behaviour

7.1.1.1 Flat ceiling at the spill edge

The smoke layer within the fire compartment was observed to flow out from the opening, rotate at the spill edge, and rise as a spill plume which was approximately two-dimensional in nature. Figure 7.1 shows a photograph of the typical spill plume behaviour as it emerged from the fire compartment opening.

Figure 7.1: Spill plume behaviour from a compartment with a flat ceiling

Figure 7.1 shows that the resulting plume horizontally projects beyond the compartment opening before rising as a plume. This projection is due to the momentum of the horizontal approach flow with the compartment.

Visual observations identified entrainment of air occurring across the lateral extent of the spill plume by the generation of vortices being shed from the outer edges. These vortices are generally known as "vortex rolls". Larger vortices were observed on the front edge of the spill plume (furthest from the spill edge) as the gas temperature and velocity were lower in this region compared to the back edge of the plume.

Entrainment of air was also observed into the free ends of the plume as it entered into the smoke exhaust hood. The ends of the plume behaved in a "spiral" motion as the plume rose.

The lateral extent of the plume was observed to broaden as the height of rise increased (see Figure 7.2). However, the plume was contained within the smoke exhaust hood for all the tests carried out.

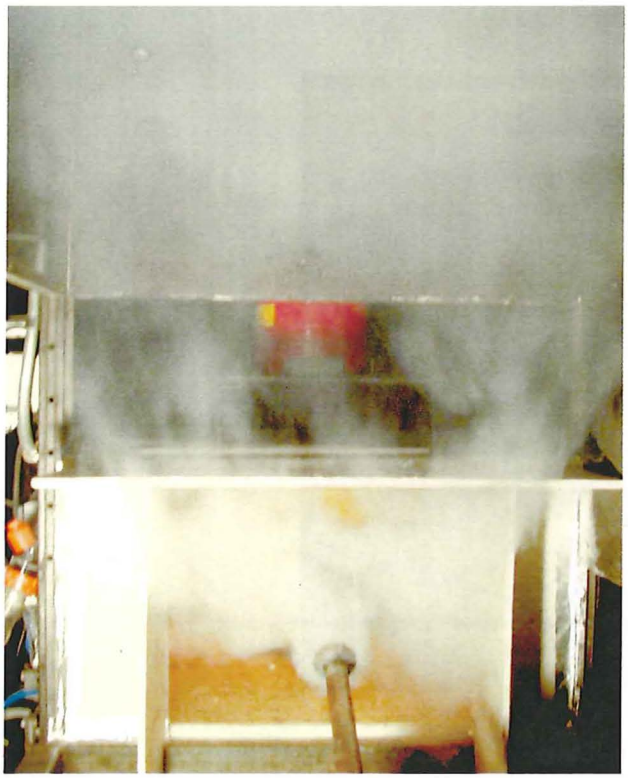

Figure 7.2: Lateral extent of the spill plume

7.1.1.2 0.1 m downstand at the spill edge

A similar plume behaviour was observed when a 0.1 m downstand was present at the spill edge. However, the presence of the downstand acted as a baffle, which caused the momentum of the horizontal flow from the opening to be reduced compared to the scenario with a flat ceiling. The spill plume was observed to be more vertical in nature (see Figure 7.3), possessing less horizontal projection when emerging from the opening.

Figure 7.3: Spill plume behaviour from a compartment with a 0.1 m downstand

The general entrainment processes across the lateral extent and into the free ends of the spill plume were similar to that described in section 7.1.1.1. The presence of the downstand limited the amount of entrainment into the back edge of the plume over the depth of the downstand, with the plume effectively being adhered in this region.

7.1.1.3 0.2 m downstand at the spill edge

Figure 7.4 shows a photograph of the emerging spill plume when a 0.2 m downstand was present at the spill edge. Figure 7.4 shows that the spill plume rises vertically when emerging from the compartment opening. This behaviour is likely to be due to the deep downstand acting as a baffle, which significantly reduced the momentum of the approach flow from the opening. The emerging plume has little horizontal

projection and rises vertically from the spill edge. The rising plume was also observed to migrate toward the rear wall of the exhaust hood for those tests with a high height of rise. This behaviour has significant implications for smoke logging on higher balconies, due to partial impingement of the rising plume with the balconies above. This could give rise to conditions similar to that shown in Figure 2.4.

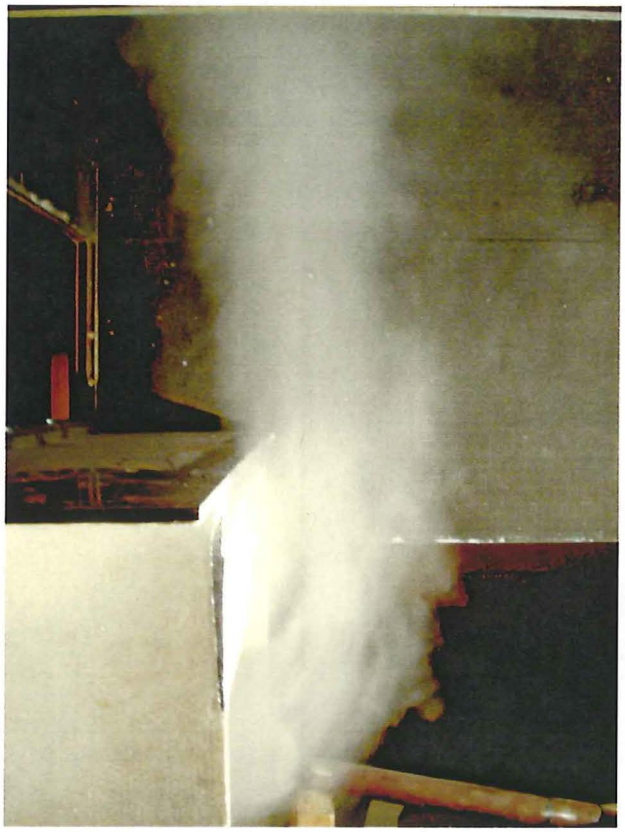

Figure 7.4: Spill plume behaviour from a compartment with a 0.2 m downstand

Entrainment of air was also observed to occur across the lateral extent of the spill plume, again via the generation of vortices on either edge of the plume. These vortices were observed to be similar in nature and size on both edges of the spill plume.

Entrainment of air also occurred into the free ends of the plume with a similar behaviour to that described in section 7.1.1.1.

The presence of the deep downstand effectively caused the plume to be adhered over the entire downstand depth, with little entrainment into the rear edge of the plume in this region.

7.1.1.4 Smoke layer in exhaust hood

In general, the rising spill plume subsequently gave rise to a layer with a reasonably uniform depth within the smoke exhaust hood. Figure 7.5 shows a schematic drawing of the typical smoke layer behaviour observed. Fresh air was allowed to be entrained into the rising plume directly beneath the smoke layer, such that there was no warming of the air nominally beneath the layer.

Figure 7.6 shows a photograph of a layer in the smoke exhaust hood for a plume with a flat ceiling at the spill edge. It should be noted that the rear wall (long length) of the hood had been lowered for photographic purposes only. In the experiment, the walls of the hood were at an identical height above the spill edge.

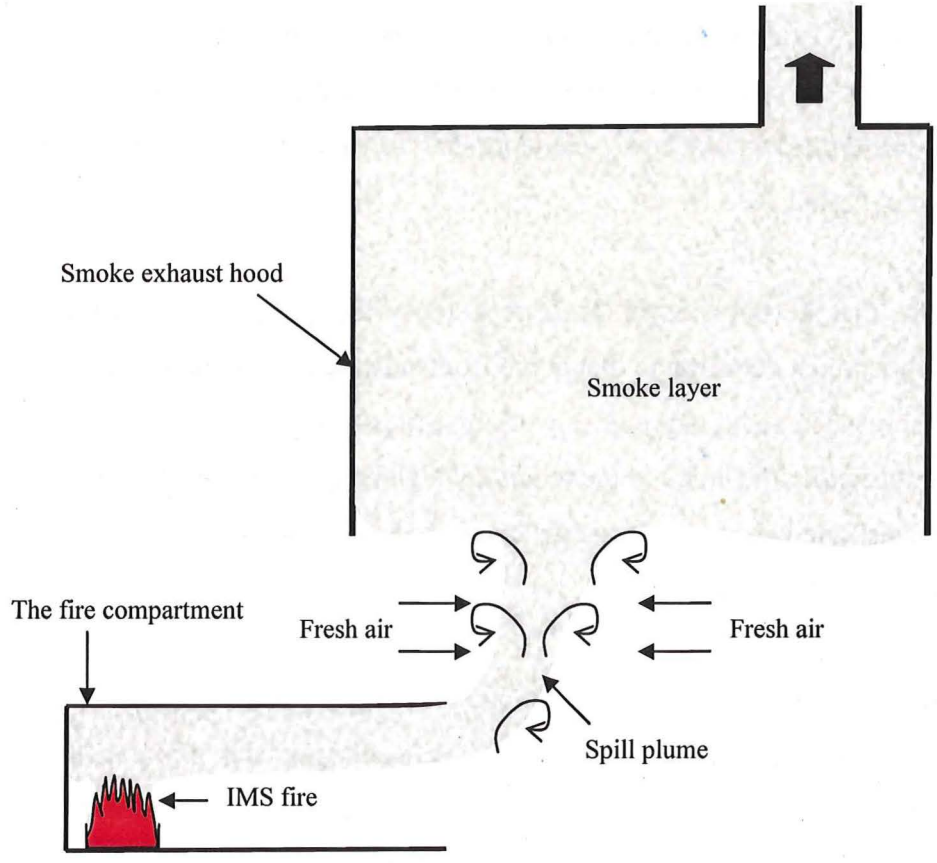

Figure 7.5: Typical behaviour of the layer in the smoke exhaust hood

Figure 7.6: The smoke layer in the exhaust hood

For some tests, which examined a spill plume with a relatively high height of rise (Tests 10-21), it was not possible to achieve a uniform layer depth within the smoke exhaust hood. The typical smoke layer behaviour and flow patterns observed for these tests are shown in Figure 7.7.

Figure 7.7 shows that the smoke layer on the rear side of the spill plume (near the fire compartment) was much deeper than that at the front side (near the exhaust vent). This behaviour was also noted in previous work by Miles et al [31], but was more pronounced in this experiment due to the relatively high height of rise of the plume. The smoke exhaust rate was set such that the layer on the rear side of the plume was just contained within the hood.

This layer behaviour appeared to be due to smoke being driven from the rear edge of the plume at ceiling level, with recirculation of smoke occurring back into the plume. As the rising plume was relatively fast moving, the plume acted as a "jet" which flowed directly into the smoke exhaust vent. This "jet" appeared to create an impedance to the recirculating smoke flow on the rear side of the plume, hence, generating a deeper layer.

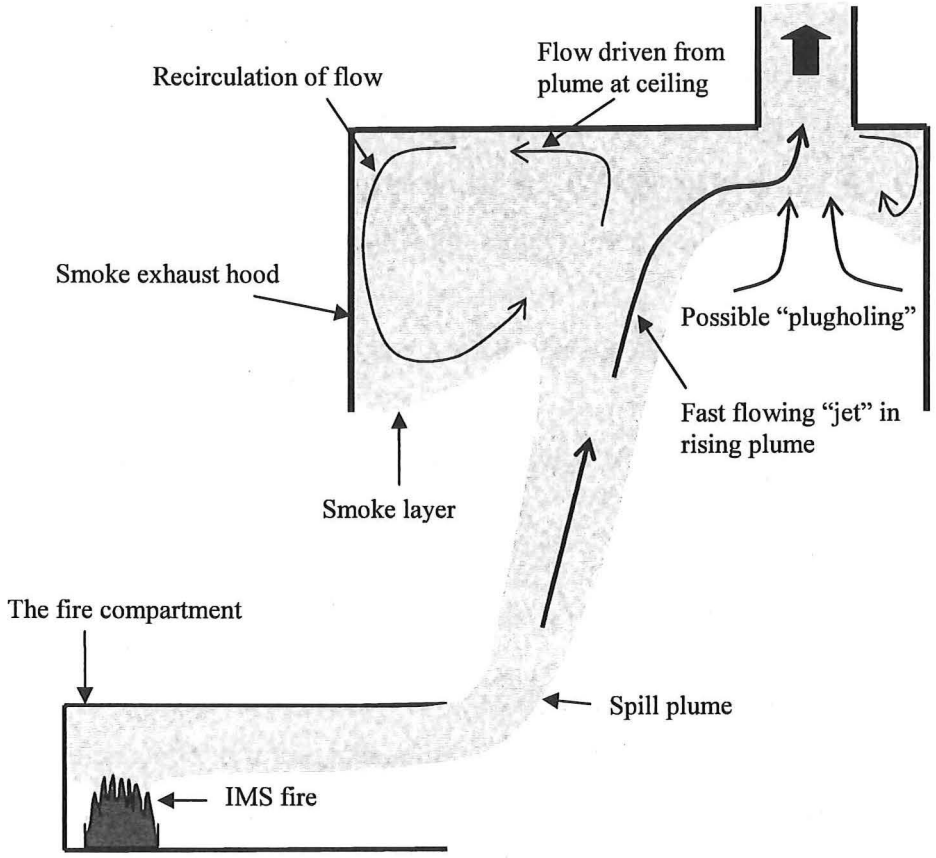

Figure 7.7: Behaviour of the layer in the smoke exhaust hood for Tests 10 to 21

The observed smoke behaviour was probably due to the experimental setup, with a number of contributing factors such as:

- a single large exhaust vent
- a relatively narrow smoke reservoir compared to the lateral extent of the plume
- a plume which entered the exhaust hood in a central location
- the velocity of the rising plume

This behaviour was not observed for any of the tests which examined a 0.2 m downstand at the spill edge. This appeared to be due to the plume rising with a reduced velocity into one end of the smoke exhaust hood (thus, eliminating the recirculation and impedance effects).

The smoke exhaust rate required to prevent spillage of smoke from beneath the rear wall of the hood, gave rise to a relatively cool and shallow layer on the front side of the spill plume. Visual observations suggested that fresh air was possibly being drawn up into the exhaust vent from beneath the layer. However, this was inconclusive due to the relatively thin nature of the smoke generator smoke. This effect is more commonly known as "plug-holing". A calculation to determine the critical exhaust rate for the onset of "plug-holing" in these tests, and the implications for the measured mass flow rate of gases in the smoke exhaust hood are described in section 7.1.2.1.

7.1.2 Mass flow rate of gases with entrainment of air into the ends (Tests 10 to 63)

7.1.2.1 Initial analysis of results

In an attempt to develop a simplified spill plume formula to predict the mass flow rate of gases due to a free spill plume, including the entrainment of air into the ends, the experimental results were initially correlated using the method by Poreh et al [22].

The data were correlated in a form described by Equation (2-27) to empirically determine the constant, B. This correlation utilises the mass of air entrained in the vertically rising plume (i.e. $M_p - M_b$) and assumes that the location of the virtual line source is at the base of the smoke layer at the spill edge (d_b).

Figure 7.8 shows the variation in $(M_p - M_b)$ with respect to $Q^{1/3}W^{2/3}(z + d_b)$ using the experimental data from Tests 10 to 63. Figure 7.8 shows that the results correlate into two distinct data sets, with the measured mass flow rate being anomalously high for Tests 10 to 21 compared to those from Tests 22 to 63.

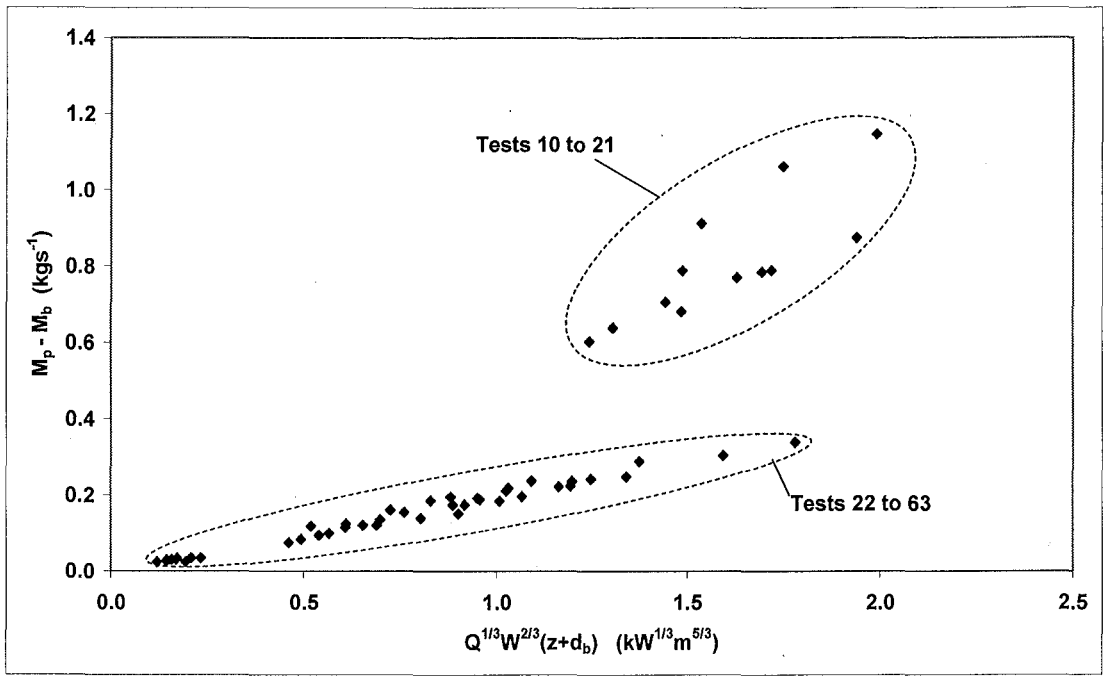

Figure 7.8: **(M_p-M_b) with respect to $Q^{1/3}W^{2/3}(z+d_b)$ for Tests 10 to 63**

The results from Tests 10 to 21 indicate that possible "plug-holing" was occurring in the experiment. The effect of "plug-holing" will tend to give an erroneously high mass flow rate, as the measurement technique is based on the dilution of CO_2 produced from the IMS fire source. The entrainment of clean air into the exhaust vent will give rise to an anomalous amount of dilution of CO_2 from the fire.

To determine if "plug- holing" was occurring during Tests 10 to 21, an empirically based calculation developed by Ghosh and given by Morgan [2] was used to predict the critical exhaust rate prior to the onset of "plug-holing" [see Equation (7-1)].

$$M_{crit} = \frac{2.05\rho_1 (gT_1\theta_l)^{1/2} d_l w_{ven}^{1/2}}{T} \qquad (7\text{-}1)$$

For the range of smoke layer temperatures and depths measured locally beneath the exhaust duct in the hood, the critical exhaust rate prior to the onset of "plug-holing" ranged between 0.07 to 0.12 kgs^{-1} (for Tests 10 to 21). The full area of the smoke exhaust vent was used in the calculation as a worst case.

To determine if "plug-holing" was occurring, the mass flow rate results for Tests 10 to 21 were compared with the critical exhaust rates for "plug-holing" calculated above. However, since there is uncertainty in the results for Tests 10 to 21, a comparison was made with the results from Tests 22 to 63, to determine the expected mass flow rates for these tests. If "plug-holing" were not occurring, we would expect the results from Tests 10 to 21 to be consistent with the results from Tests 22 to 63, which can be described by a linear relationship. With reference to Figure 7.8, the mass flow rates for Tests 10 to 21 are expected to be in excess of 0.2 kgs^{-1} to be consistent with the results from Tests 22 to 63. The expected mass flow rates for Tests 10 to 21 are higher than the range of critical exhaust rates for "plug-holing" calculated above. Therefore, the results indicate that "plug-holing" was occurring during these tests, and the mass flow rate results are in error. These results have therefore been neglected from the subsequent analysis described below.

7.1.2.2 Effect of a downstand at the spill edge

Figure 7.9 shows the correlated results from Tests 22 to 63 inclusive. The data is presented for those tests which had a flat ceiling, a 0.1 m deep downstand or a 0.2 m deep downstand at the spill edge respectively. For those tests with a downstand at the spill edge, the height of rise of the plume, z, was taken to be the height of the smoke layer above the bottom of the downstand. Figure 7.9 shows that the data can generally be described by a single linear relationship which is independent of the spill edge geometry. Figure 7.9 indicates that the presence of a downstand at the spill edge appears to have little effect on the subsequent entrainment of air into a rising spill plume compared to that with a flat ceiling at the spill edge.

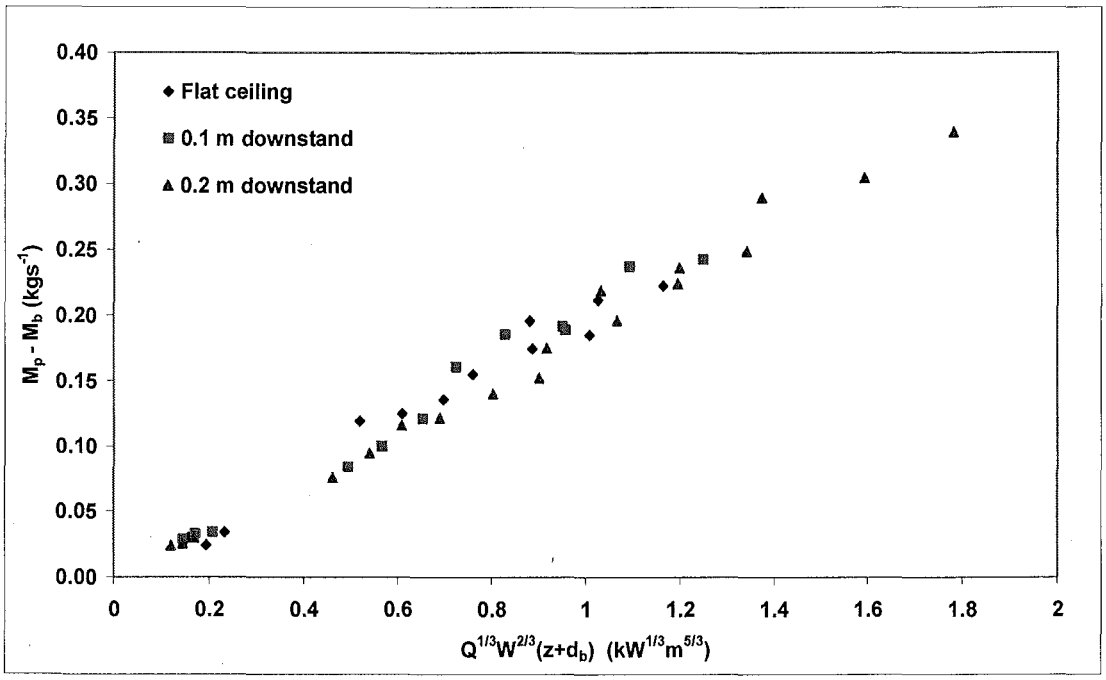

Figure 7.9: **$(M_p - M_b)$ with respect to $Q^{1/3}W^{2/3}(z+d_b)$ for different spill edge geometries**

7.1.2.3 A simplified spill plume formula for design purposes

Since the presence of a downstand at the spill edge appeared to have little effect on the entrainment of air into a spill plume compared to that from a flat ceiling, the results from Tests 22 to 63 were correlated as a single data series according to the method by Poreh et al [using Equation (2-27)] to determine the value of the constant, B.

Figure 7.10 shows that the variation in $(M_p - M_b)$ with respect to $Q^{1/3}W^{2/3}(z+d_b)$ can generally be described by a linear relationship.

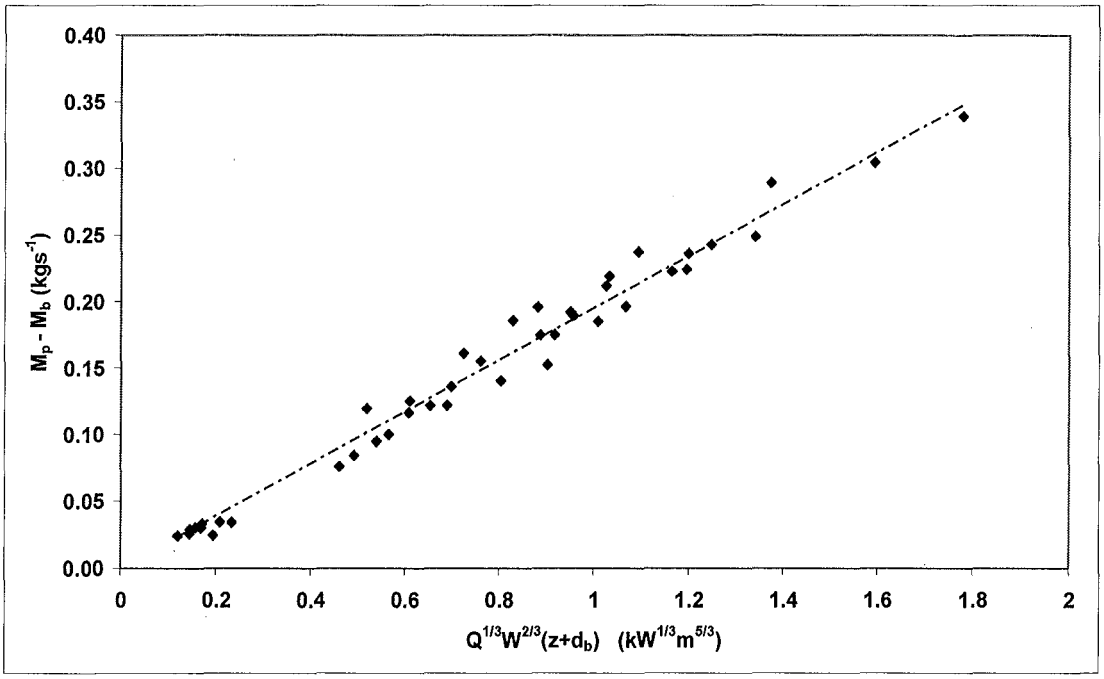

Figure 7.10: (M_p-M_b) with respect to $Q^{1/3}W^{2/3}(z+d_b)$ for Tests 22 to 63 inclusive

Figure 7.10 shows the line of best fit through the data set. This line of best fit is described by Equation (7-2).

$$M_p - M_b = 0.195 Q^{1/3} W^{2/3} (z + d_b) \tag{7-2}$$

Hence the constant, B, given in Equation (2-27) is equal to 0.195 in this case. It is therefore proposed, that for design purposes, the value of the constant, B, should be rounded to 0.20 to give the following simplified spill plume formula described by Equation (7-3).

$$M_p - M_b = 0.20 Q^{1/3} W^{2/3} (z + d_b) \tag{7-3}$$

Equation (7-3) can be rearranged to express the total mass flow rate of gases produced by a spill plume (M_p) given by Equation (7-4).

$$M_p = 0.20 Q^{1/3} W^{2/3} (z + d_b) + M_b \tag{7-4}$$

Equation (7-4) is therefore proposed as a simplified spill plume formula to predict the entrainment of air into a free spill plume, which inherently includes entrainment of air into the free ends of the plume.

A value of $B = 0.20$, results in a value of $C_m = 0.56$ [from Equation (2-28)]. However, this value inherently includes entrainment of air into the free ends. For a spill plume without entrainment into the free ends, Poreh et al gives $C_m = 0.44$.

Comparison with the work by Poreh et al [22] shows that the constant, B, has increased from 0.16 (for no entrainment of air into the ends) to 0.20 in this work. This indicates an increase of approximately 25% due to air entrainment into the ends of the plume. This compares well with the limited data from Marshall and Harrison [42] which indicated an increase in entrainment of approximately 30%. A reanalysis of this limited data (Series I), which included air entrainment into the ends of a free spill plume was carried out. The constant, B, was determined to be approximately 0.25 from this data. However, as this work was carried out within a small area smoke reservoir with additional entrainment occurring due to turbulence with the collecting hood, we would expect the constant, B, to be high in this case. Analysis of the data given by Hansell et al [35] gave rise to a value of $B = 0.34$. However, as this work was carried out within a relatively tall and narrow smoke reservoir, where the spill plume had a tendency to become three dimensional in nature, we would also expect this value of B to be high. It is encouraging that the value of B determined in this work is bounded by values which can be considered to be limiting.

Equation (7-4) can be expressed in an alternative form using a method developed by Thomas et al [23] (see section 2.1.3.6). This was done by substituting Equation (2-30) into Equation (7-4) to remove an element of redundancy requiring the calculation of both M_b and d_b. This then gave Equation (7-5) which is an acceptable alternative to Equation (7-4). It should be noted that M_b can be calculated using well established methods given either by Morgan [2], Thomas et al [52] or Quintiere et al [54].

$$M_p = 0.20Q^{1/3}W^{2/3}z + 0.0017Q + 1.5M_b \qquad (7\text{-}5)$$

7.1.3 Mass flow rate of gases without entrainment into the ends (Test 64)

In an attempt to confirm that the experimental results were consistent with previous work, a single test was carried out with a free spill plume without entrainment of air into the ends (Test 64). This test generated a free plume identical to that examined by Poreh et al [22].

The results from this test were used to determine the value of the constant, B, within Equation (2-27). The results gave rise to a value of $B = 0.167$, which was consistent with that determined by Poreh et al ($B = 0.16$).

7.1.4 Comparison of the experiment with the BRE method

The experimental results were compared with the prediction made by the BRE spill plume method [2] for the mass flow rate of gases produced by a free spill plume, with respect to the height of rise above the spill edge. The input parameters used in the BRE method were the mass flow rate and convective heat output of the gases at the spill edge for all of the tests. Comparisons were made for those tests which either had a flat ceiling or a downstand at the spill edge. The BRE method prediction is presented in the following forms:

- Using an entrainment constant, α, equal to 0.16, with no adjustment to the height of rise of the plume
- Applying the effective layer depth correction (see section 2.1.2.1) to adjust the height rise of the plume to take into account the smoke reservoir geometry
- Using an entrainment constant, α, equal to 0.11, with no adjustment to the height of rise of the plume. This value of α was demonstrated by Poreh et al [22] to give good agreement with experimental results for a free spill plume without entrainment of air into the ends

7.1.4.1 Flat ceiling at the spill edge

Figure 7.11 shows a comparison between the experimental results and the predictions for the mass flow rate of gases produced by a spill plume, with respect to the height of rise above the spill edge, for those tests with a fire size of 6 kW.

Figure 7.11 shows that when the BRE method is used with $\alpha = 0.16$, with no adjustment to the height of rise, the method over predicts the mass flow rate of gases due to a spill plume. This indicates that the smoke exhaust hood could be considered to be a large area reservoir, such that an adjustment to the height of rise, or the entrainment constant, is required for the prediction to match with the experiment.

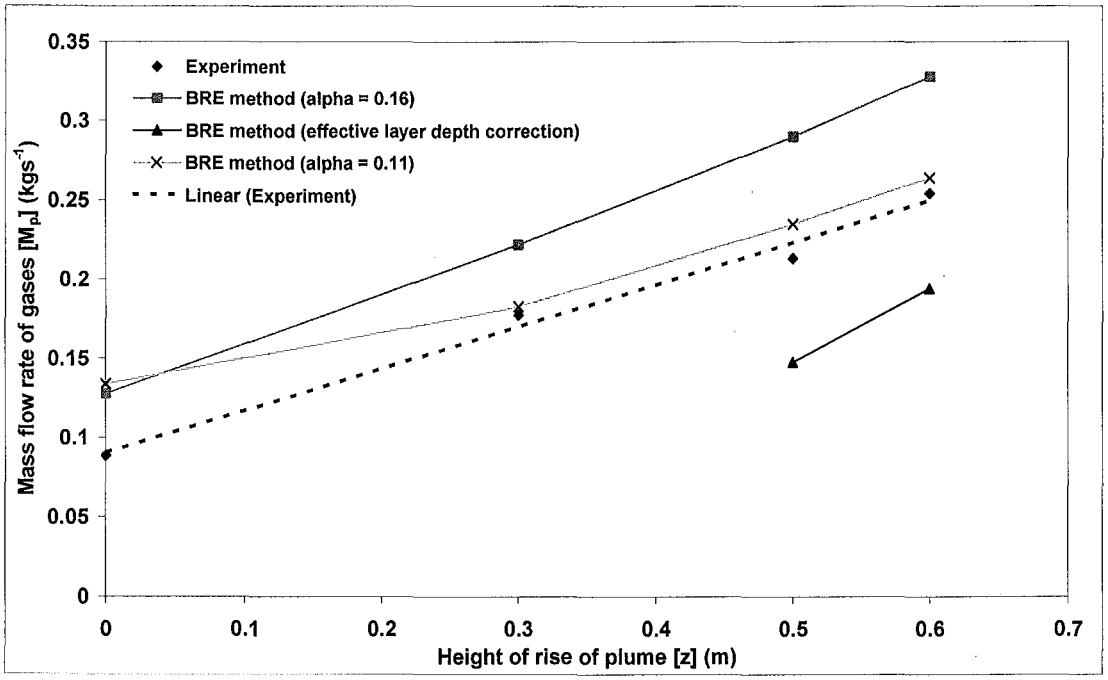

Figure 7.11: Comparison between experiment and the BRE method (6kW, flat ceiling)

However, this conclusion contradicts the criterion given in section 2.1.2.1 which suggests that the exhaust hood can be considered to be a small area reservoir for those tests shown in Figure 7.11. The results suggest that this criterion may not be reliable for all scenarios and should be used with caution. The results confirm that further work is necessary to examine the difference in entrainment between large and small area smoke reservoirs.

Figure 7.11 shows that when the effective layer depth correction is applied to the visual layer depth, the BRE method under predicts the experimental results. The prediction was only possible for two data points, since the correction resulted a negative height of rise in some cases. The effective layer depth correction was derived from empirical data to achieve a match between the BRE method and the experimental results for large area reservoirs. However, this correction was developed from experimental data [27] in which there was warming of the air beneath the visual layer base in the reservoir. In this experiment, there was no warming of the air nominally beneath the visible smoke layer. The results suggest that the effective layer depth correction may not be reliable when applied to conditions which are dissimilar to that in which the method was derived.

Figure 7.11 shows that when the BRE method is used with $\alpha = 0.11$, with no adjustment to the height of rise, the method gives a good match with the experimental results above a height of rise of 0.3 m above the spill edge. There is an expected discrepancy between the experiment and the prediction when the height of rise is zero, as one of the fundamental assumptions in the underpinning theory (e.g. Gaussian profiles across the plume) is violated in this region. It is encouraging to note that the slope of the line relating the mass flow rate gases with respect to the height of rise is similar between the prediction and the experimental results. This indicates that the BRE method accurately predicts the increase in entrainment with respect to the height of rise of the plume.

The above result indicates that, for large area reservoirs, it may be more reliable to apply the BRE method with a reduced entrainment constant of 0.11 rather than adjusting the height of rise of the plume.

Figures 7.12 and 7.13 also show a comparison between the experimental results and the prediction for those tests with a fire size of 9 kW and 12 kW respectively. These comparisons generally show a similar behaviour to that described above, however, the agreement between the experiment and the prediction using $\alpha = 0.11$ worsens with increasing fire size. This discrepancy may be due to inaccuracies in the term quantifying the entrainment of air into the ends of the plume for the larger fire sizes. However, the slope of the line relating the mass flow rate gases with respect to the

height of rise of the plume is again similar between the experimental results and the prediction when $\alpha = 0.11$.

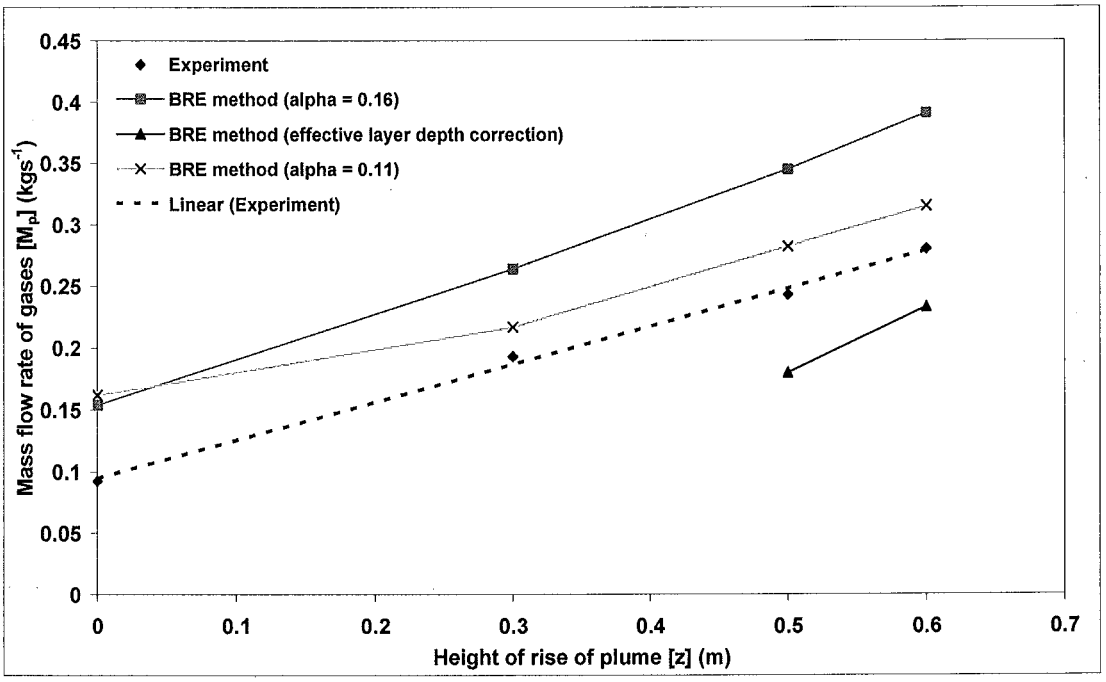

Figure 7.12: Comparison between experiment and the BRE method (9kW, flat ceiling)

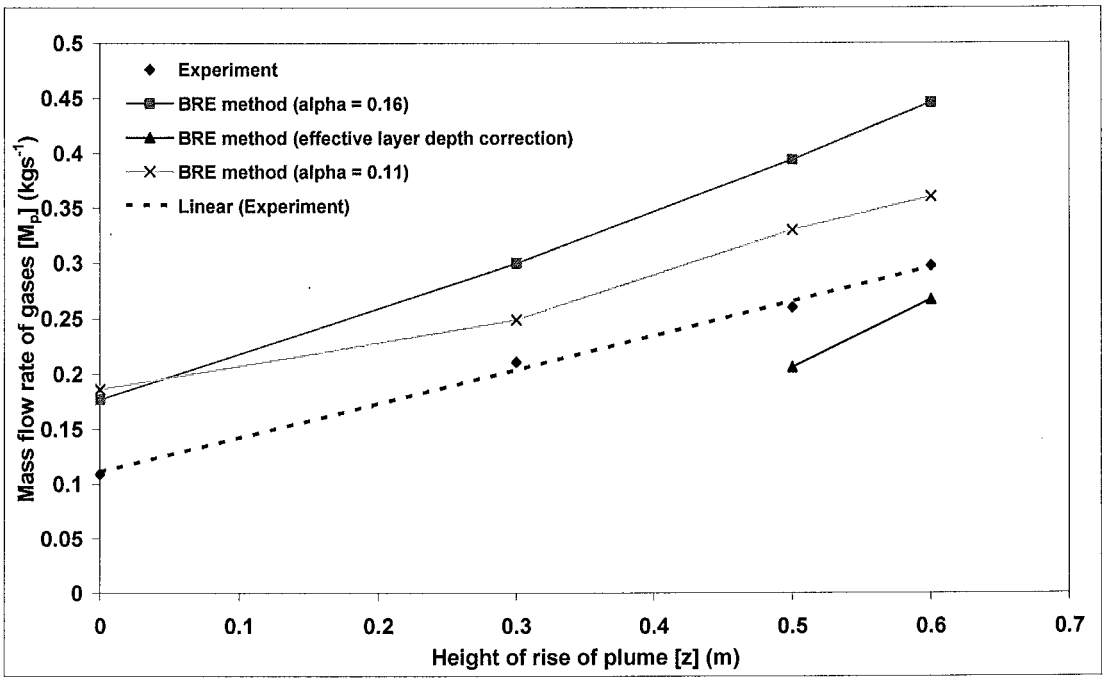

Figure 7.13: Comparison between experiment and the BRE method (12kW, flat ceiling)

7.1.4.2 0.1 m downstand at the spill edge

Figure 7.14 shows a comparison between the experimental results and the prediction for the mass flow rate of gases due to a spill plume, with respect to the height of rise plume, for those tests with a fire size of 6 kW.

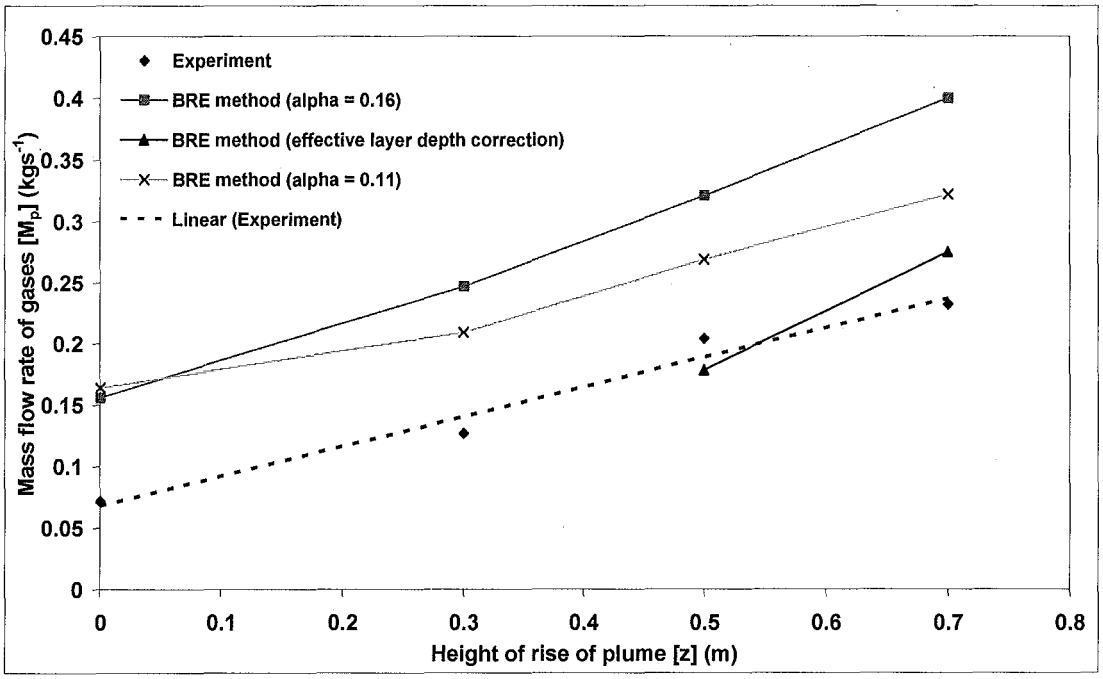

Figure 7.14: Comparison between experiment and the BRE method (6kW, 0.1 m downstand)

Figure 7.14 shows that when the BRE method is used with either $\alpha = 0.16$ or $\alpha = 0.11$, with no adjustment to the height of rise, the method over predicts the mass flow rate of gases due to a spill plume. It is unclear why the presence of downstand has worsened the agreement between the experiment and the prediction (with $\alpha = 0.11$) compared to those tests with a flat ceiling. This may be due to differences in the characteristics of the horizontal approach flow at the spill edge on the subsequent spill plume prediction. This discrepancy could also be due to the fact that a 0.1 m downstand may not be considered to be a "deep" downstand, as assumed in the BRE method.

The slope of the line relating the mass flow rate gases with respect to the height of rise of the plume is again similar between the experimental results and the prediction when $\alpha = 0.11$.

Figure 7.14 shows that when the effective layer depth correction is applied, the BRE method gives a reasonable match with the experimental results. Although it appears that there may be divergence between experiment and the prediction at higher heights of rise. Since there are only two data points for the prediction, the comparison is inconclusive.

Figures 7.15 and 7.16 also show a comparison between the experimental results and the prediction for those tests with a fire size of 9 kW and 12 kW respectively. These comparisons generally show a similar behaviour to that described above.

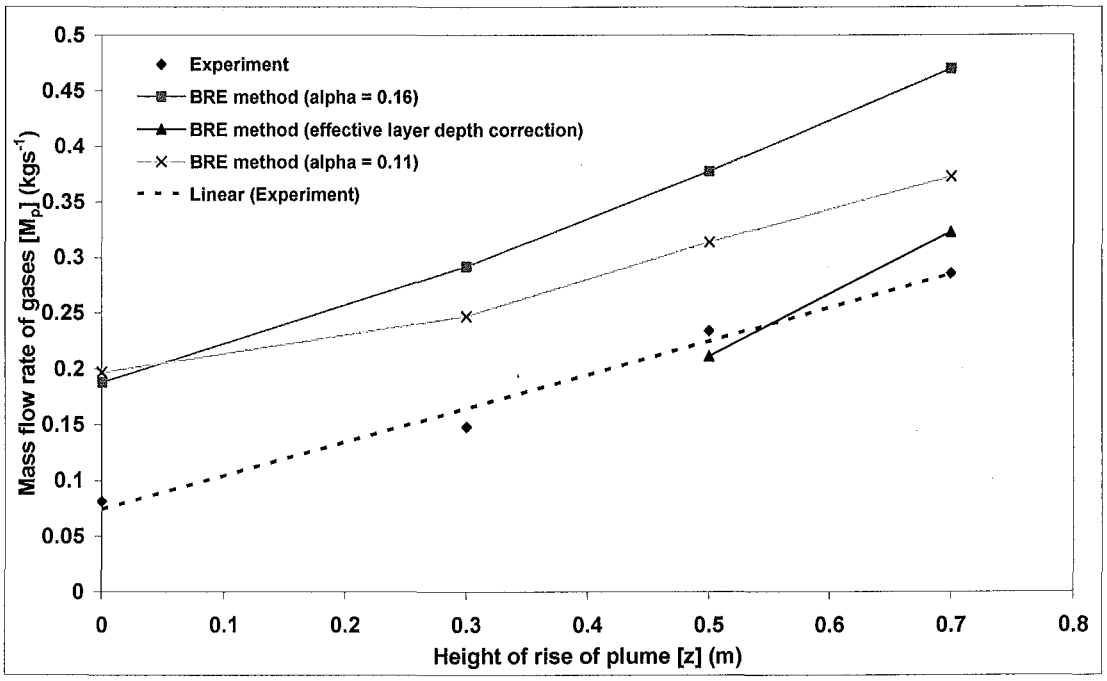

Figure 7.15: Comparison between experiment and the BRE method (9kW, 0.1 m downstand)

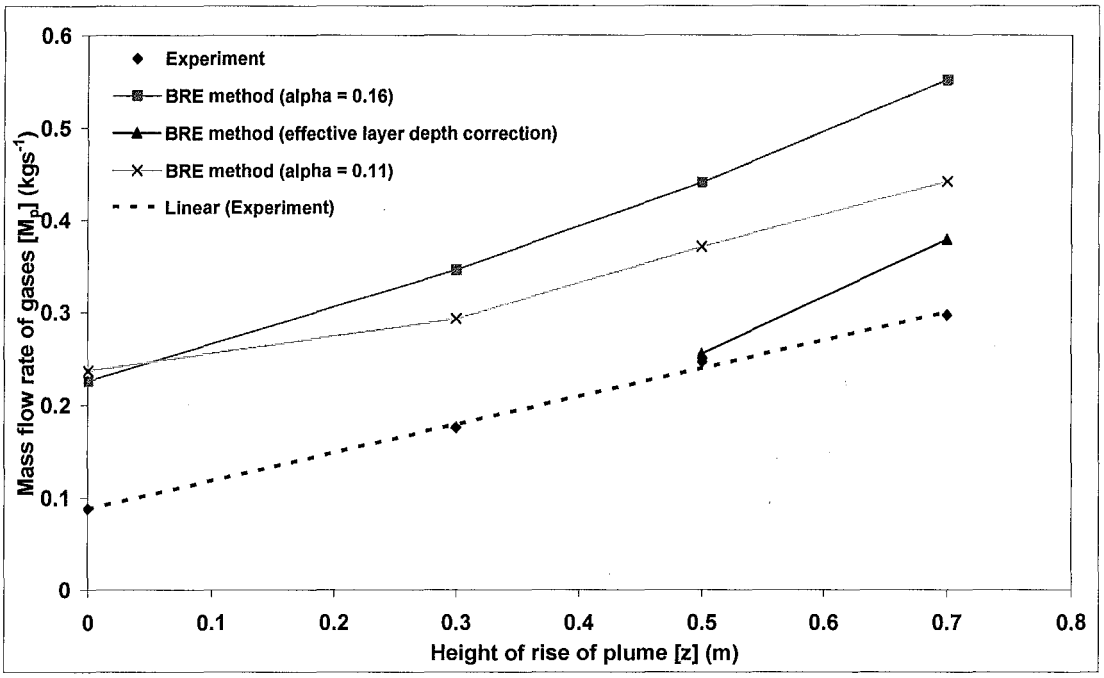

Figure 7.16: Comparison between experiment and the BRE method (12kW, 0.1 m downstand)

7.1.4.3 0.2 m downstand at the spill edge

Figure 7.17 shows a comparison between the experimental results and the prediction for the mass flow rate of gases due to a spill plume, with respect to the height of rise above the spill edge, for those tests with a fire size of 6 kW.

Figure 7.17 shows that when the BRE method is used with either $\alpha = 0.16$ or $\alpha = 0.11$, with no adjustment to the height of rise, the method again over predicts the mass flow rate of gases due to a spill plume. As noted above, the slope of the line relating the mass flow rate gases with respect to the height of rise of the plume is again similar between the experimental results and the prediction when $\alpha = 0.11$.

Figure 7.17 shows that when the effective layer depth correction is applied, there is divergence between experiment and the prediction which increases at higher heights of rise.

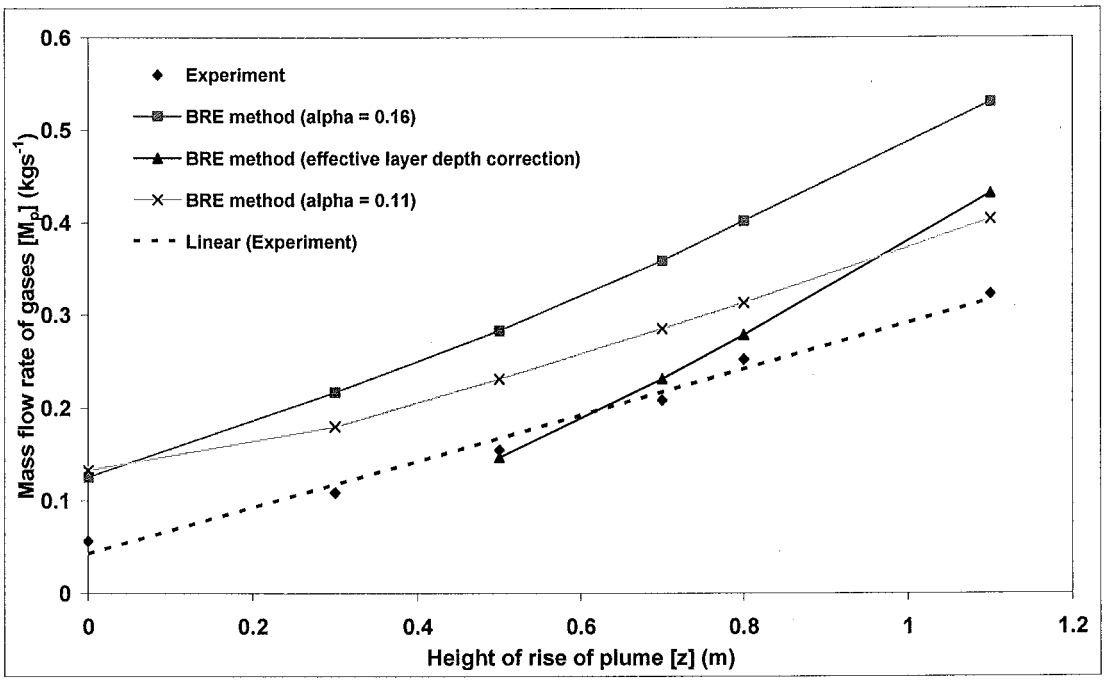

Figure 7.17: Comparison between experiment and the BRE method (6kW, 0.2 m downstand)

Figures 7.18 and 7.19 also show a comparison between the experimental results and the prediction for those tests with a fire size of 9 kW and 12 kW respectively. These comparisons generally show a similar behaviour to that described above.

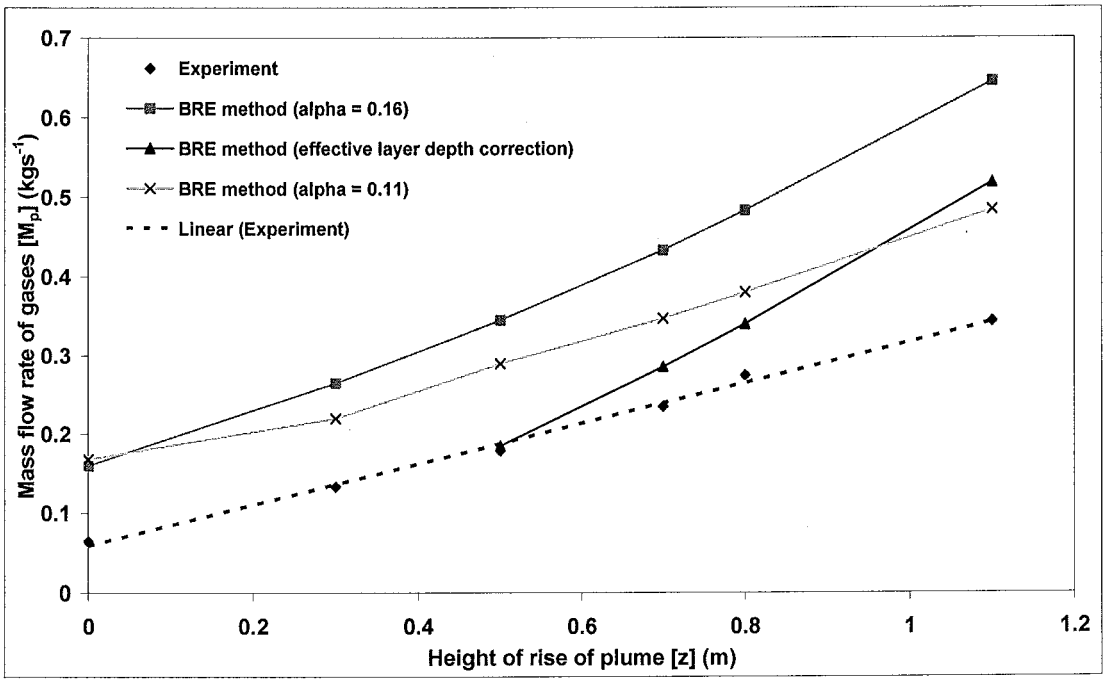

Figure 7.18: Comparison between experiment and the BRE method (9kW, 0.2 m downstand)

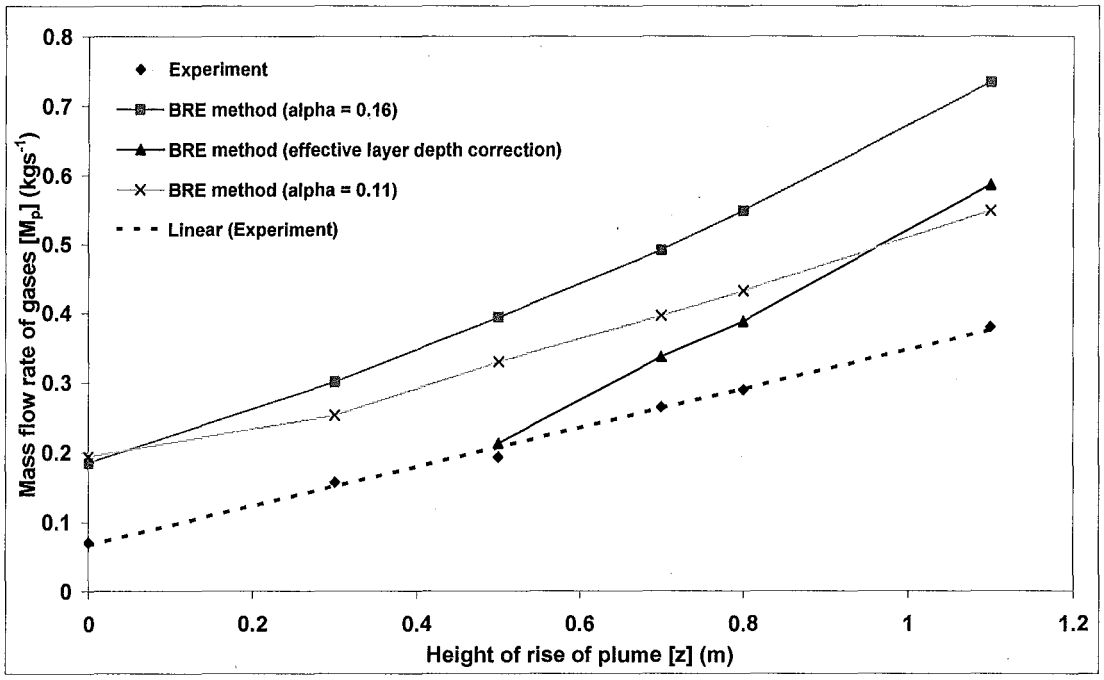

Figure 7.19: Comparison between experiment and the BRE method (12kW, 0.2 m downstand)

7.1.5 Comparison of the experiment with simplified spill plume formulae

Comparisons were also made between the experimental results and predictions made from various simplified spill plume formulae. Comparisons were only made for those tests which had a flat ceiling at the spill edge. These formulae do not apply to flows which have a downstand at the spill edge, as the location of the virtual source is based on experimental data with a flat ceiling at the spill edge. The following spill plume formulae, which include entrainment into the free ends, were examined for the comparison.

- Method by Law (1986) [Equation (2-12)].
- Method by Law (1995) [Equation (2-17)].
- Method by Thomas (1987), [Equation (2-16)]. The location of the virtual source was determined using Equation (2-25) from Poreh et al [22].
- Method given by CIBSE [Equation (2-19)].
- Method given in NFPA 92B [Equation (2-20)].

Figures 7.20 to 7.22 show comparisons between the experimental results and the predictions for the mass flow rate of gases due to a spill plume, with respect to the height of rise plume, for those tests with a fire size of 6 kW, 9 kW and 12 kW respectively.

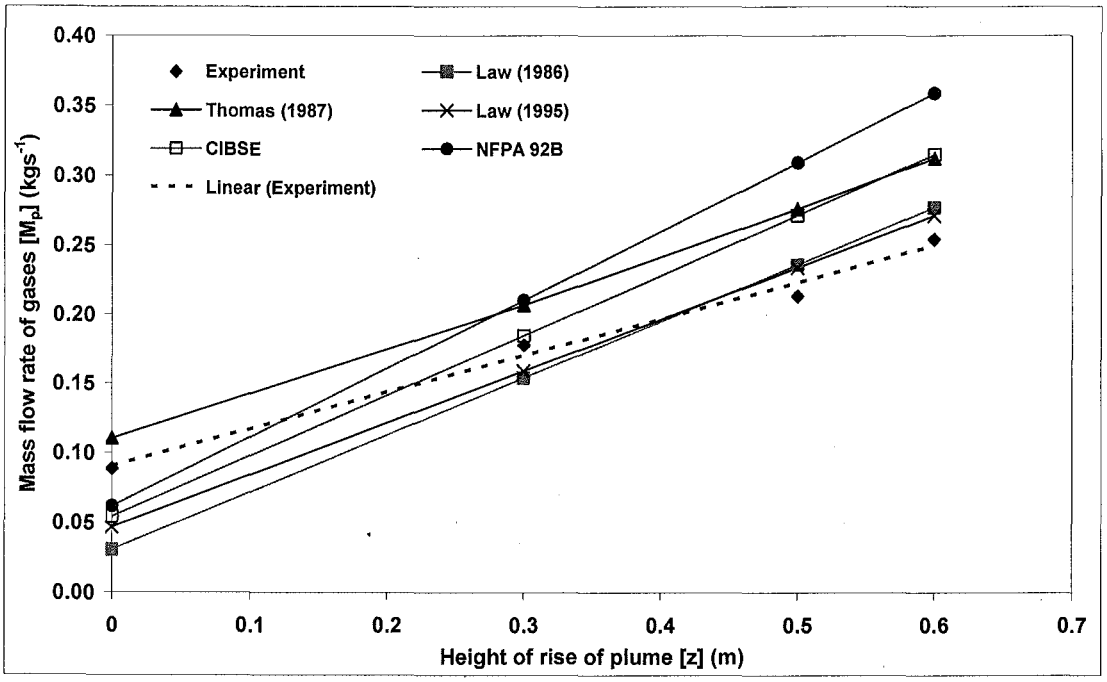

Figure 7.20: Comparison between experiment and simplified spill plume formulae (6 kW)

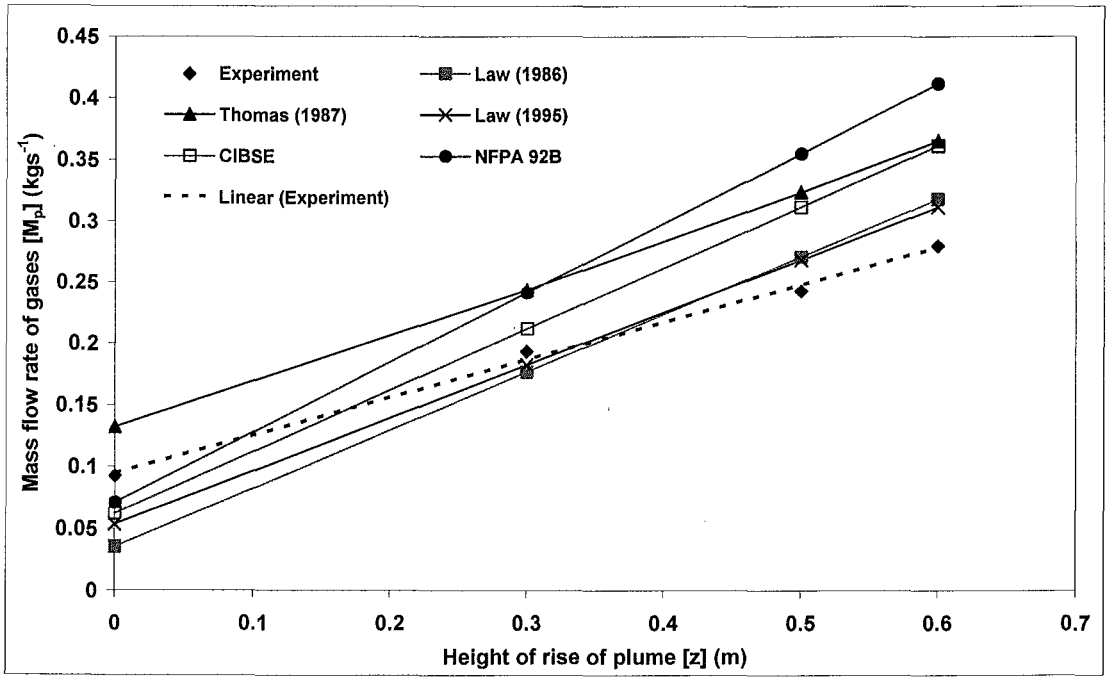

Figure 7.21: Comparison between experiment and simplified spill plume formulae (9 kW)

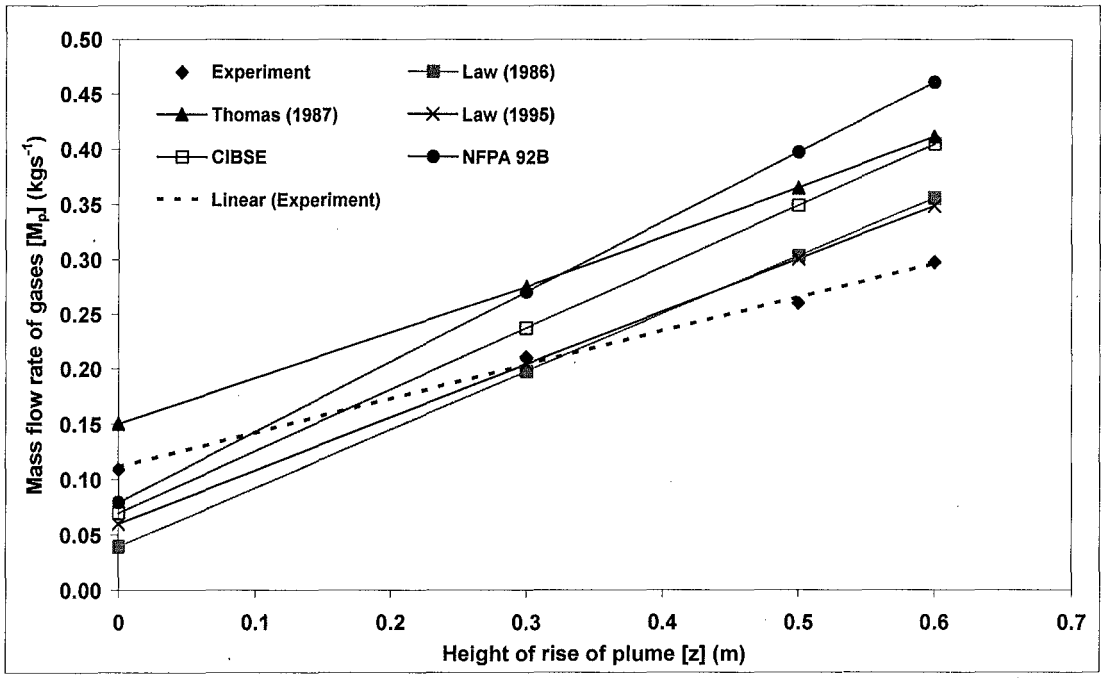

Figure 7.22: Comparison between experiment and simplified spill plume formulae (12 kW)

Figures 7.20 to 7.22 show that, with the exception of the method by Thomas [21], all of the simplified formulae under predict the mass flow rate due to a spill plume at a very low height of rise.

However, above a height of rise of approximately 0.3 m (3 m full scale), all of the methods generally tend to over predict the mass flow rate of gases due to a spill plume. The slope of the line relating the mass flow rate gases with respect to the height of rise of the plume, is generally greater for the various simplified formulae compared to the experiment. The comparison indicates that the discrepancy between the experiment and the predictions will increase as the height of rise increases.

The method given in NFPA 92B [28] significantly over predicts the mass flow rate of gases due to spill plume. The two methods by Law [20,40] give the best agreement with the experiment. The method by Thomas may give improved agreement with the experiment with if an alternative location of the virtual source is assumed.

7.2 Entrainment of air into a flow from a compartment opening to a higher projecting balcony

7.2.1 Flow behaviour

This section describes the behaviour of the flow from a compartment opening to a higher projecting balcony. This is primarily based on the FDS simulation results which were similar to that observed from the physical scale model experiments. The Smokeview 3.1 output from the FDS simulations have been used to show the flow behaviour.

7.2.1.1 Wide compartment opening

Figure 7.23 shows the typical behaviour of the flow from a wide compartment opening to a higher projecting balcony (Simulation 9).

Figure 7.23 shows the nominal base of the gas layer within the compartment and the subsequent spill plume. Figure 7.23 shows that the gas layer flows beneath the downstand at the compartment opening before rising to form a horizontally flowing layer beneath the balcony. This layer then rises as a plume as it flows beyond the spill edge.

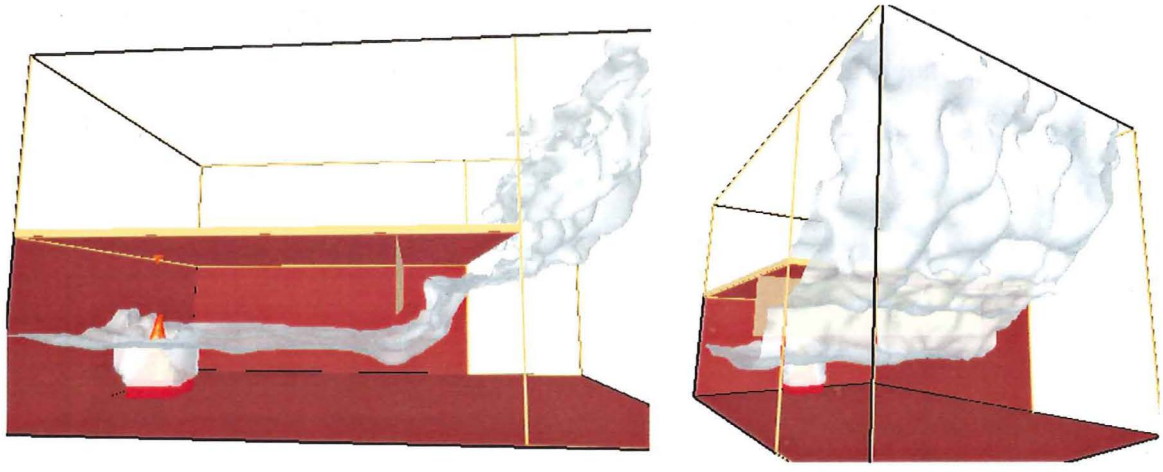

Figure 7.23: Flow behaviour for a wide opening (Simulation 9)

Figure 7.24 shows the detailed nature of the flow between the compartment opening and the spill edge in terms of velocity vectors. Figure 7.24 shows the flow rising from beneath the downstand as a discernable "jet" before flowing as a horizontally moving layer toward the spill edge. It also shows the recirculation of the flow behind this "jet" close to the downstand.

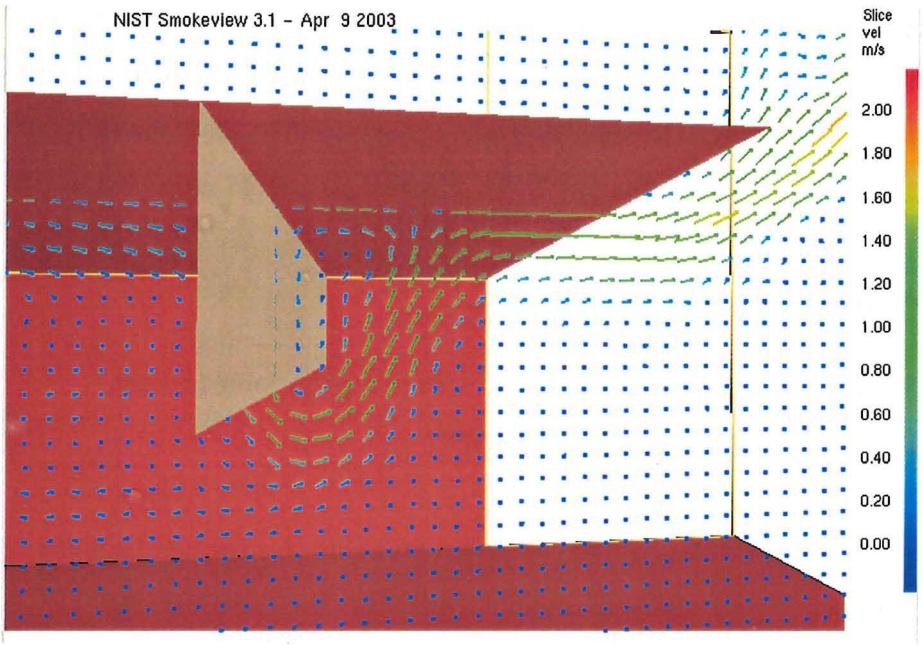

Figure 7.24: Velocity vectors for a wide opening (Simulation 9)

The presence of this "jet" is also highlighted in Figure 7.25 which shows a velocity map of a slice through the flow at the centre of the compartment in the x-z plane. Figure 7.25 shows the increased velocity of the flow between the compartment opening and the spill edge.

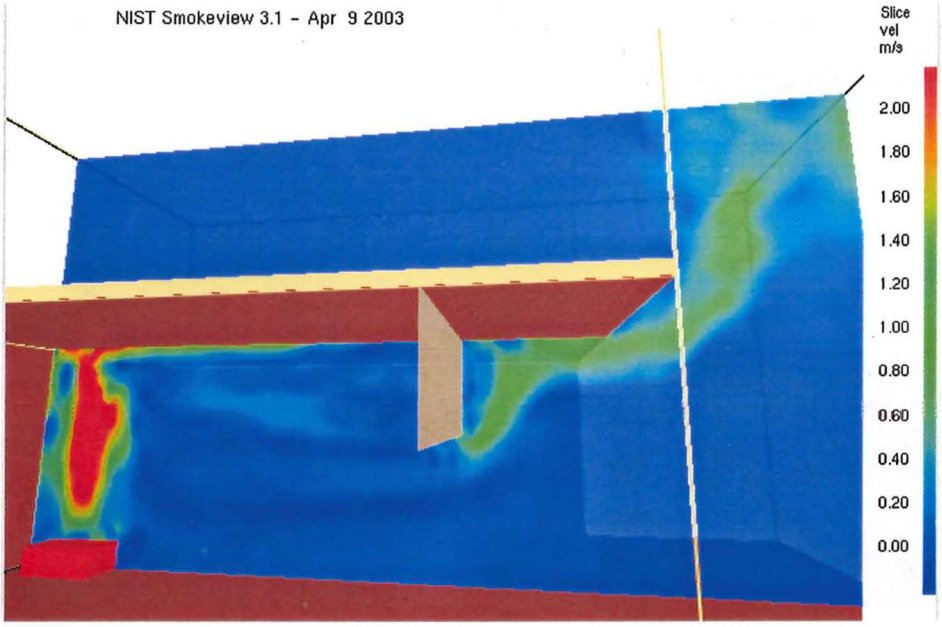

Figure 7.25: Velocity map of the flow at the centre of the compartment (Simulation 9)

Figure 7.26 shows a temperature map of a slice through the flow at the centre of the compartment in the x-z plane.

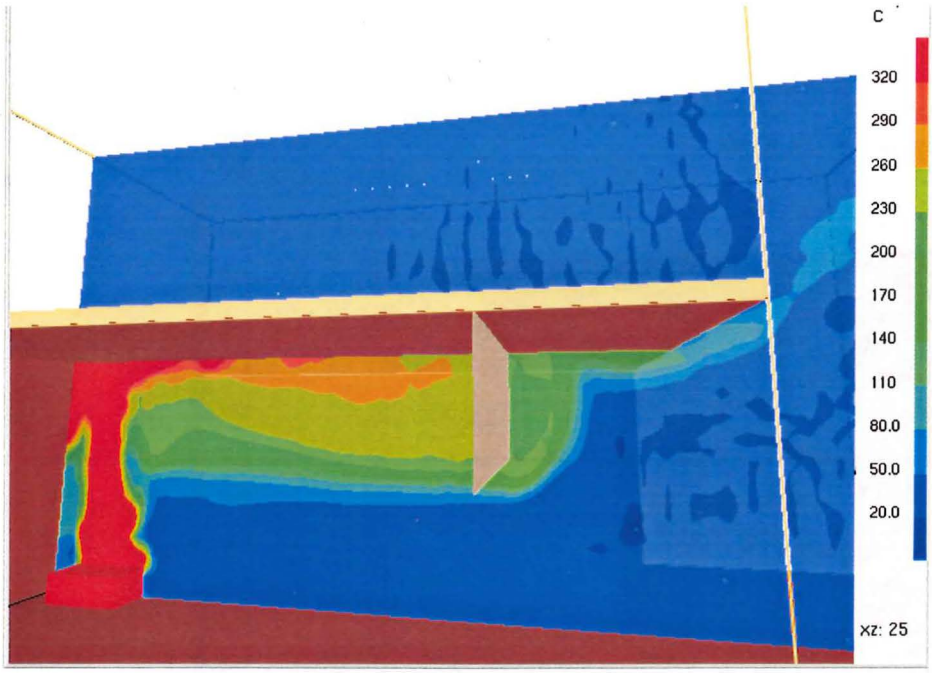

Figure 7.26: Temperature map of the flow at the centre of the compartment (Simulation 9)

For a deep downstand at the compartment opening, the flow is very similar to that described above (see Figure 7.27).

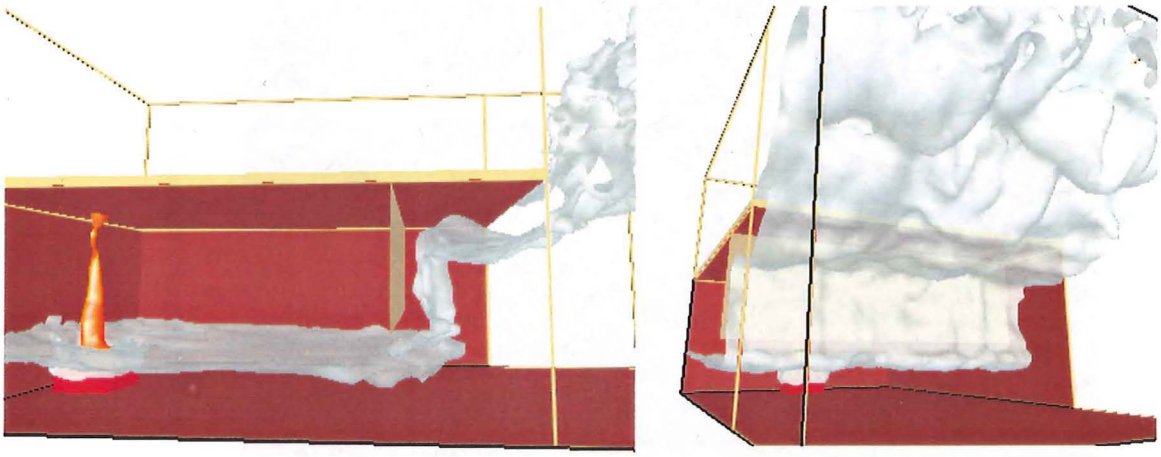

Figure 7.27: Flow behaviour for a wide opening with a deep downstand (Simulation 17)

However, Figure 7.28 shows that the flow rising from beneath the compartment opening, adheres to the downstand at it rises to form a horizontally flowing layer beneath the balcony. In this case, there is no recirculation of the flow close to the downstand.

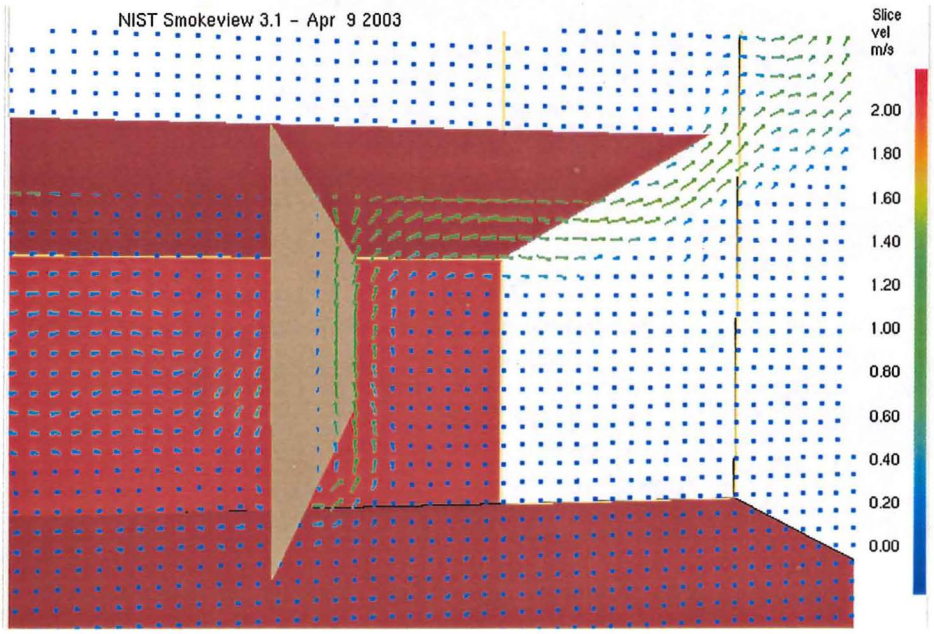

Figure 7.28: Velocity vectors for a wide opening with a deep downstand (Simulation 17)

7.2.1.2 Narrow compartment opening

The behaviour of the flow from a narrow compartment opening was generally similar to that described above (see Figure 7.29). However, the flow appeared to have and increased amount of horizontal projection from the opening compared to a wide opening.

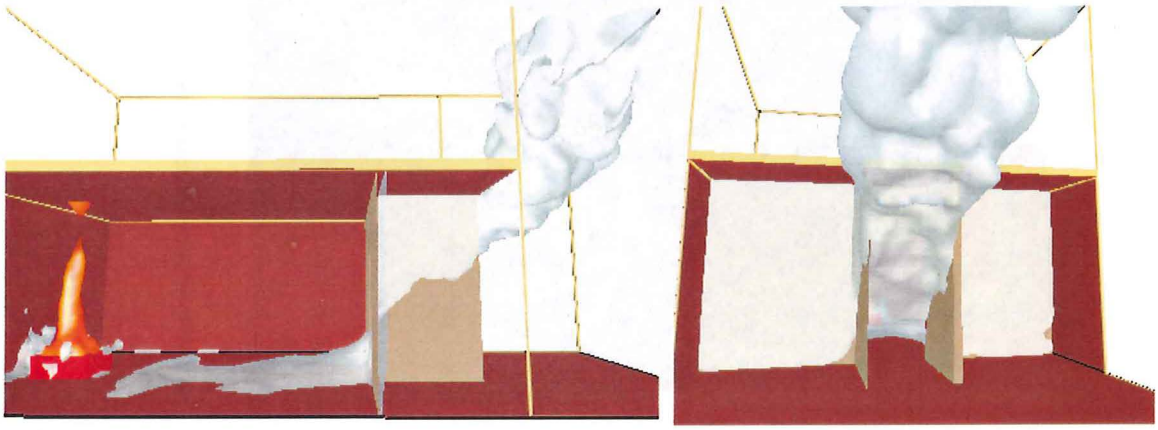

Figure 7.29: Flow behaviour for a narrow opening (Simulation 13)

Figure 7.30 shows that the "jet" projects beyond the compartment opening such that it just impinges beneath the projecting balcony prior to the spill edge. There is also recirculation of the flow behind this "jet" close to the downstand.

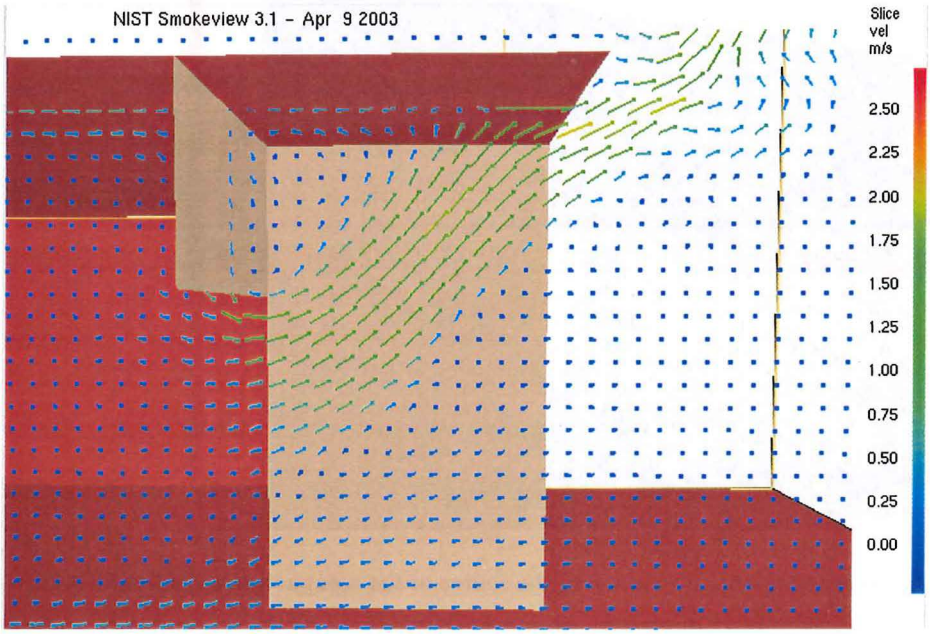

Figure 7.30: Velocity vectors for a narrow opening (Simulation 13)

Figure 7.31 shows that for the narrow opening, the "jet" is more enhanced, giving rise to a flow with a higher velocity compared to that from a wide opening.

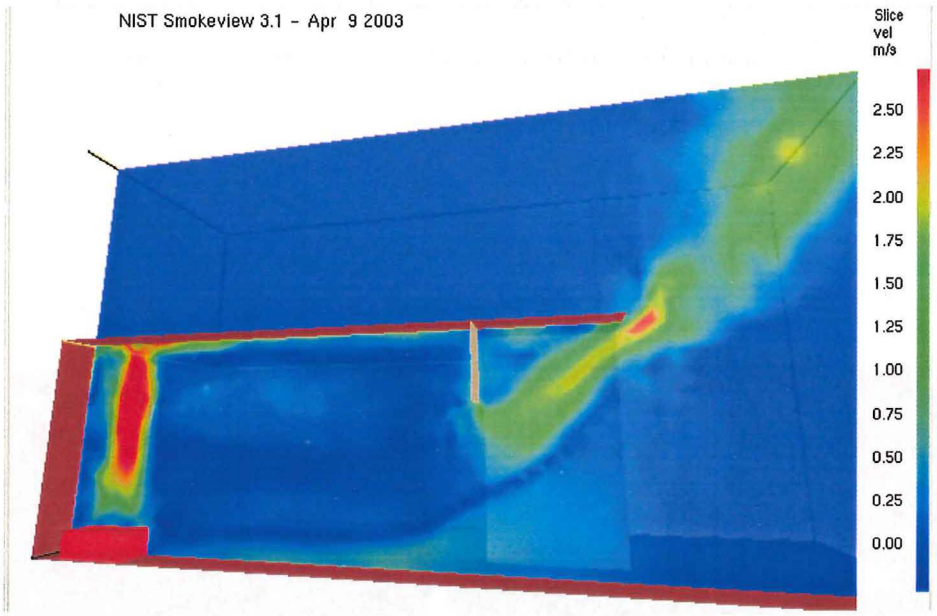

Figure 7.31: Velocity map of the flow at the centre of the compartment (Simulation 13)

Figure 7.32 shows that the narrow opening gives rise to a hotter and deeper gas layer within the compartment compared to that from a wide opening.

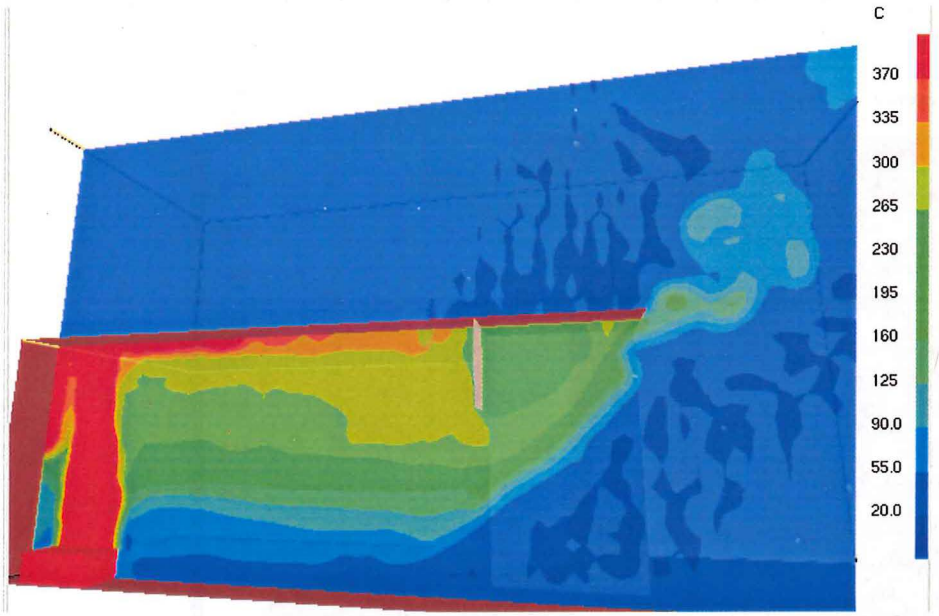

Figure 7.32: Temperature map of the flow at the centre of the compartment (Simulation 13)

7.2.1.3 Effect of balcony breadth

The flow behaviour for all of the simulations described above was for a balcony with a breadth of 0.3 m (3m full scale). For this breadth of balcony, the flow from the compartment opening generally transformed into a horizontally moving flow beneath the balcony before spilling at the free edge. This behaviour was also observed for those simulations which examined a balcony breadth of 0.5 m (see Figure 7.33).

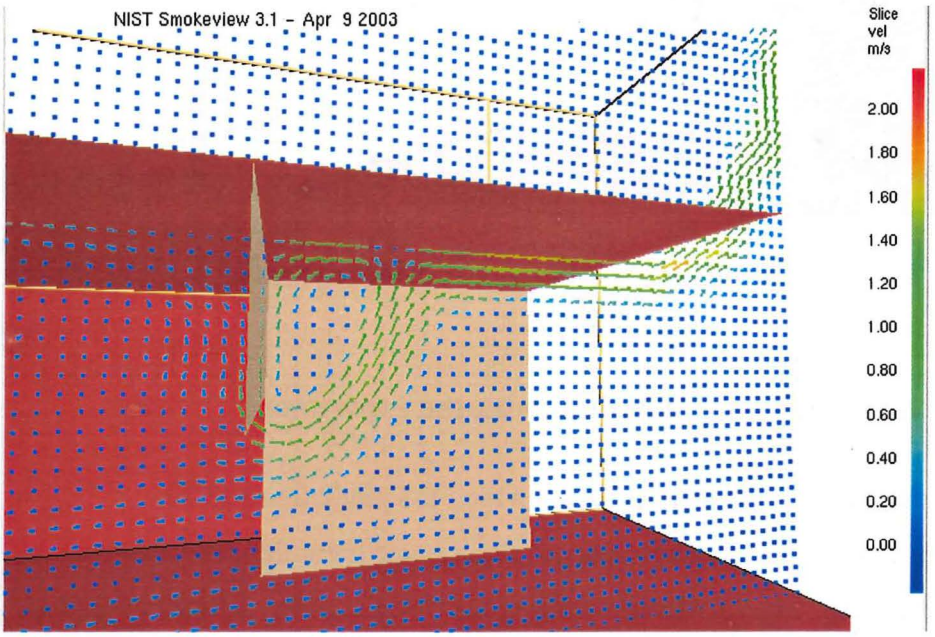

Figure 7.33: Velocity vectors for a 0.5 m broad balcony (Simulation 19)

However, the simulation which examined a balcony breadth of 0.2 m (Simulation 25) resulted in a flow which was different from the other simulations. Figure 7.34 shows that the rising "jet" from the compartment opening projected beyond the balcony, without a horizontally flowing layer forming at the balcony edge.

For this scenario, the effective spill edge will be at the top of the compartment opening, with the mass flow rate of gases at the compartment opening being an appropriate input parameter for spill plume calculations.

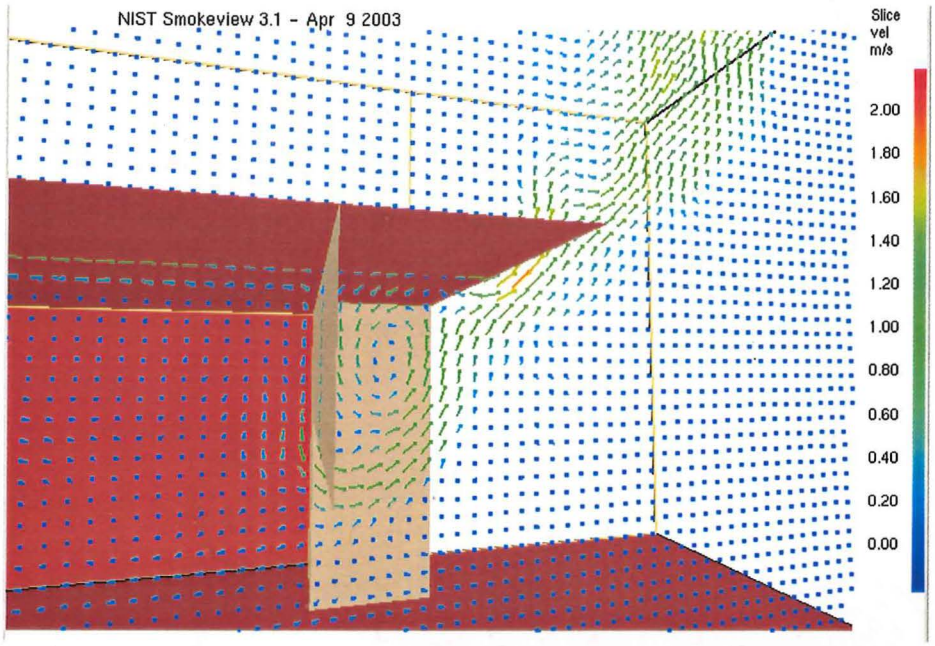

Figure 7.34: Velocity vectors for a 0.2 m broad balcony (Simulation 25)

7.2.2 Comparison of FDS predictions with the experiment

This section describes the comparison between the FDS prediction and the experimental results for the temperature and velocity profiles at the compartment opening and at the spill edge. Analysis of this comparison enabled an assessment to be made of the validity of the FDS predictions and the confidence in the application of the results.

7.2.2.1 Temperature profiles at the compartment opening

Figure 7.35 shows a comparison between the FDS prediction and the experiment for the gas layer temperature profile at the compartment opening (Test 65, Simulation 1). Figure 7.35 shows that there is good agreement between the FDS prediction and the experiment for this scenario. The temperature profiles each follow a similar shape, with the temperature above ambient being close to zero at approximately 0.15 m below the spill edge in each case. This indicates that FDS accurately predicts the gas layer depth at the compartment opening. In general, there was good to excellent agreement between the FDS prediction and the experiment for all comparisons of temperature at the compartment opening.

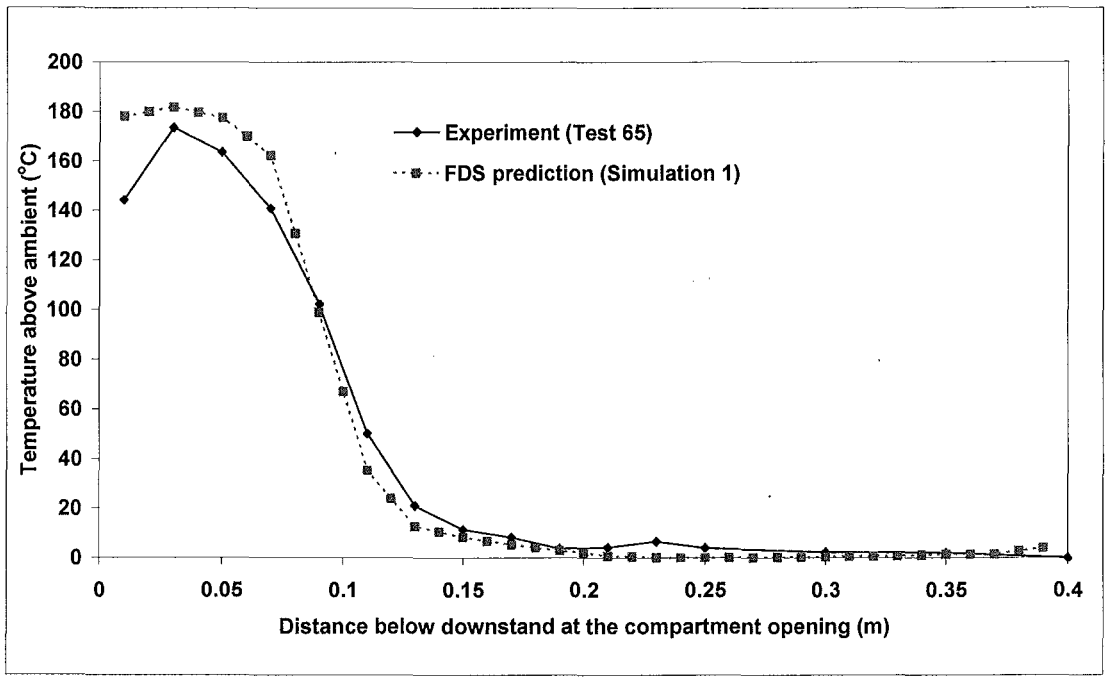

Figure 7.35: Comparison of temperature at the compartment opening (1.0 m wide opening, 0.1 m deep downstand)

The poorest agreement was observed for a compartment opening with a narrow geometry of 0.2 m (see Figure 7.36).

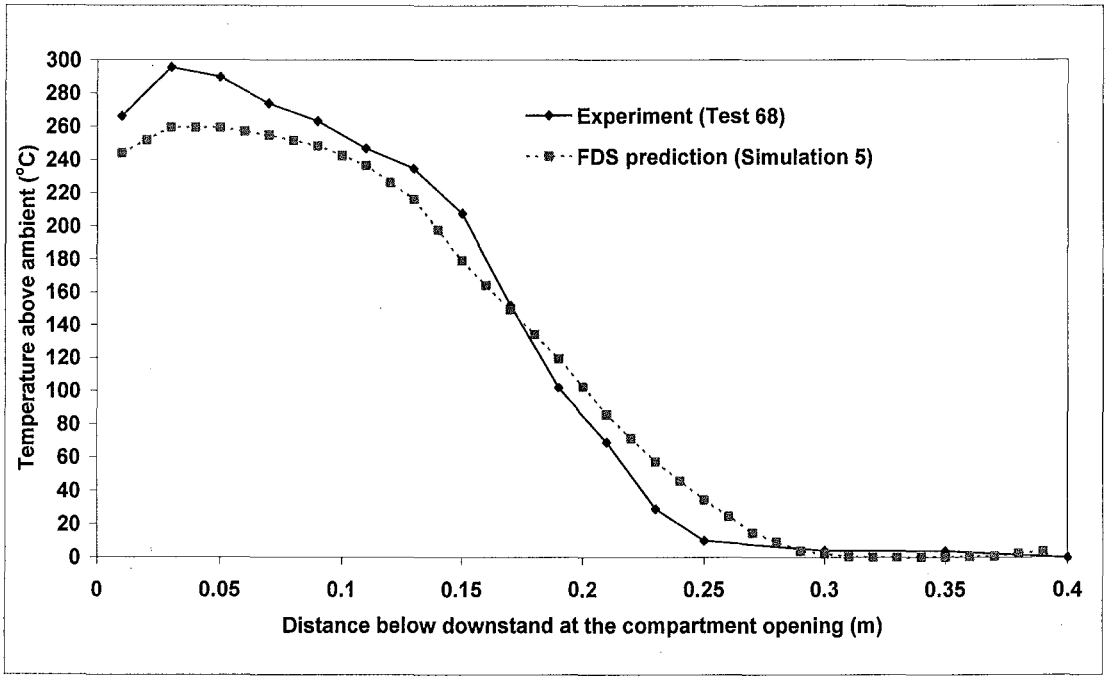

Figure 7.36: Comparison of temperature at the compartment opening (0.2 m wide opening, 0.1 m deep downstand)

Figure 7.36 shows that FDS slightly under predicts the temperature in the upper regions of the layer, whilst it over predicts the temperature in the lower regions of the layer. This behaviour may be due differences between FDS and the experiment with regard to heat losses from the compartment with a narrow opening. Since the gas temperatures in the compartment were much higher for the narrow opening, the thermal properties of the steel sheet substrate, on the exterior face of the compartment, may explain the higher temperatures measured in the experiment. FDS only modelled the fire compartment walls as 20 mm thick CFI board as a simplifying assumption and did not model the steel substrate. Any differences in heat losses from the compartment would be more pronounced for those tests with a narrow opening due to the increased temperatures.

Appendix K details all of the comparisons between the FDS predictions and the temperature profiles at the compartment opening.

7.2.2.2 Temperature profiles at the spill edge

Figure 7.37 shows a comparison between the FDS prediction and the experiment for the temperature profile of the gas layer at the spill edge (Test 65, Simulation 1). Figure 7.37 shows that there is excellent agreement between the FDS prediction and the experiment at this location. Again, the profiles follow a similar pattern, indicating that FDS also accurately predicts the depth of the gas layer at the spill edge.

The comparison between the FDS prediction and the experiment was generally excellent for all the comparisons carried out. However, the poorest agreement was again for the scenario which examined a narrow compartment opening geometry (see Figure 7.38). The possible reasons for this behaviour are described in section 7.2.2.1 above.

Appendix K details all of the comparisons between the FDS prediction and the experiment for the temperature profiles at the spill edge.

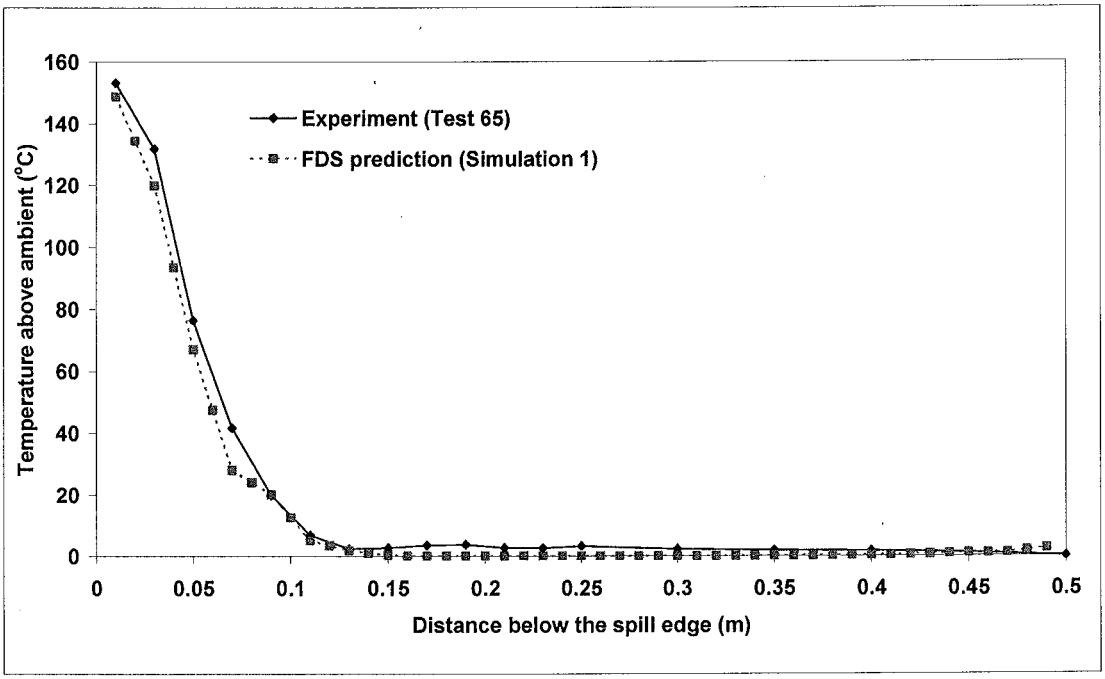

Figure 7.37: **Comparison of temperature at the spill edge (1.0 m wide opening, 0.1 m deep downstand)**

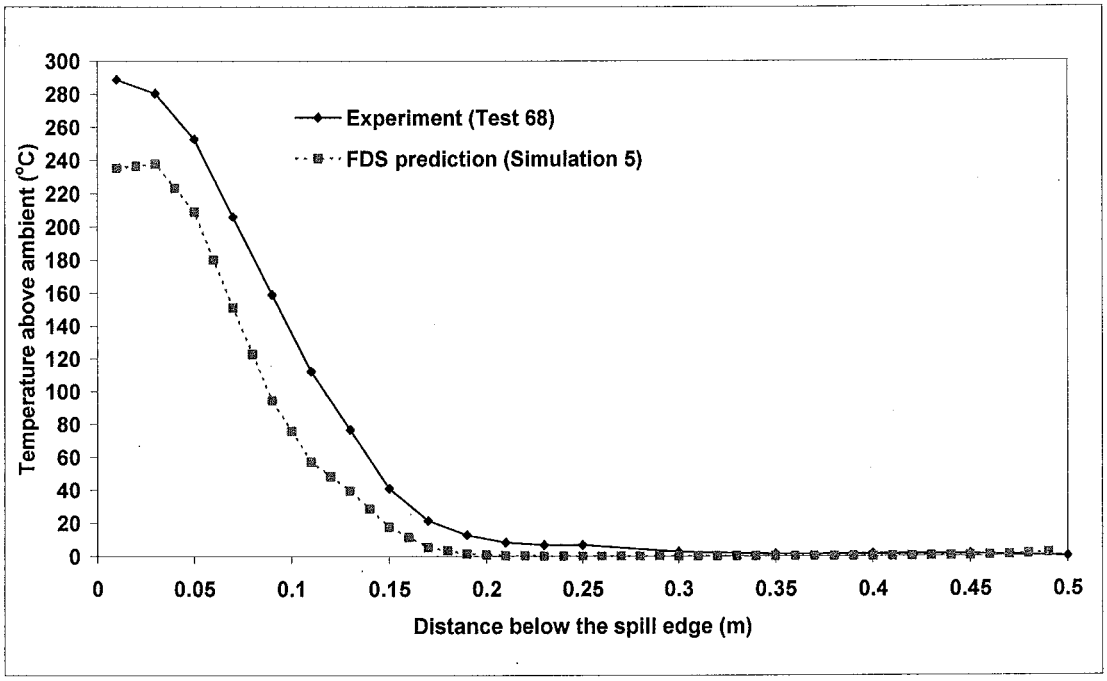

Figure 7.38: **Comparison of temperature at the spill edge (0.2 m wide opening, 0.1 m deep downstand)**

7.2.2.3 Velocity profiles at the compartment opening

Figure 7.39 shows a comparison between the FDS prediction and the experiment for the velocity profile of the gas layer at the compartment opening (Test 65, Simulation 1). Figure 7.39 shows that the experimental velocities are greater than those from the FDS predictions. However, with reference to section 6.2.2.3, the experimental velocities at the compartment opening are recognised to be erroneously high due to limitations in the instrumentation technique. Although it was not possible to validate the FDS prediction of velocity in this location, it is encouraging to note that FDS predicts a velocity which is lower than that measured in the experiment.

Appendix L details all of the comparisons between the FDS prediction and the experiment for the velocity profiles at the compartment opening.

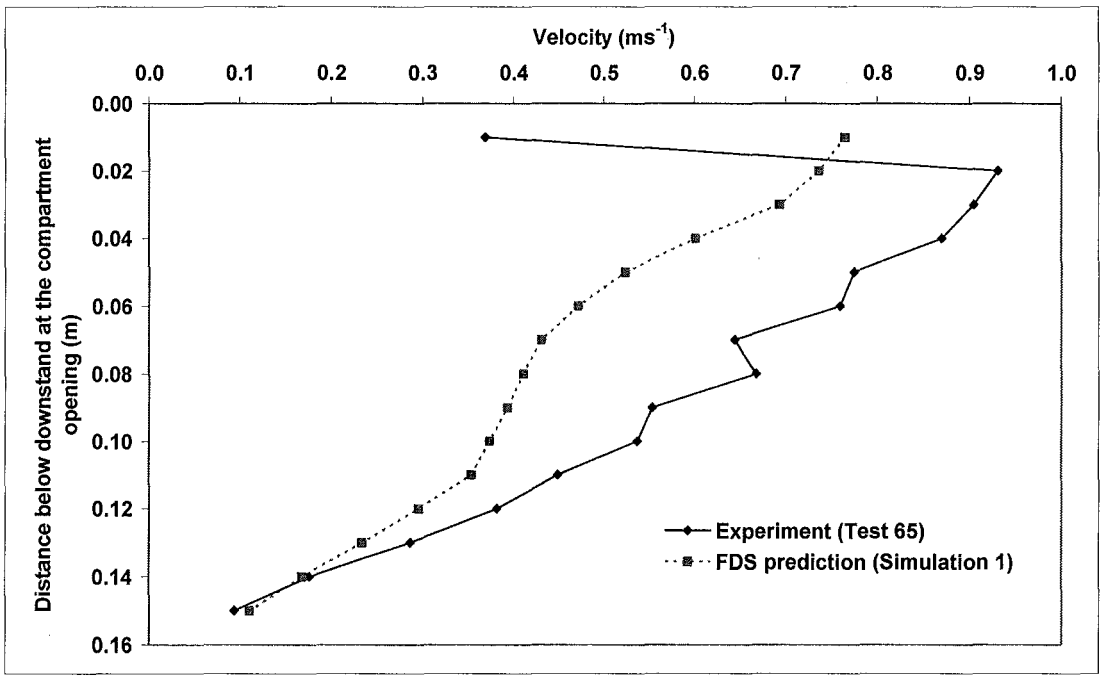

Figure 7.39: Comparison of velocity at the compartment opening (1.0 m wide opening, 0.1 m deep downstand)

7.2.2.4 Velocity profiles at the spill edge

Figure 7.40 shows a comparison between the FDS prediction and the experiment for the velocity profile of the gas layer at the spill edge (Test 65, Simulation 1).
Figure 7.40 shows that there is good agreement between the experiment and the FDS prediction in terms of velocity at this location. This agreement was generally typical of all of the tests carried out.

The poorest agreement was again observed for the scenario of a narrow compartment opening, where FDS tends to under predict the velocity (see Figure 7.41).

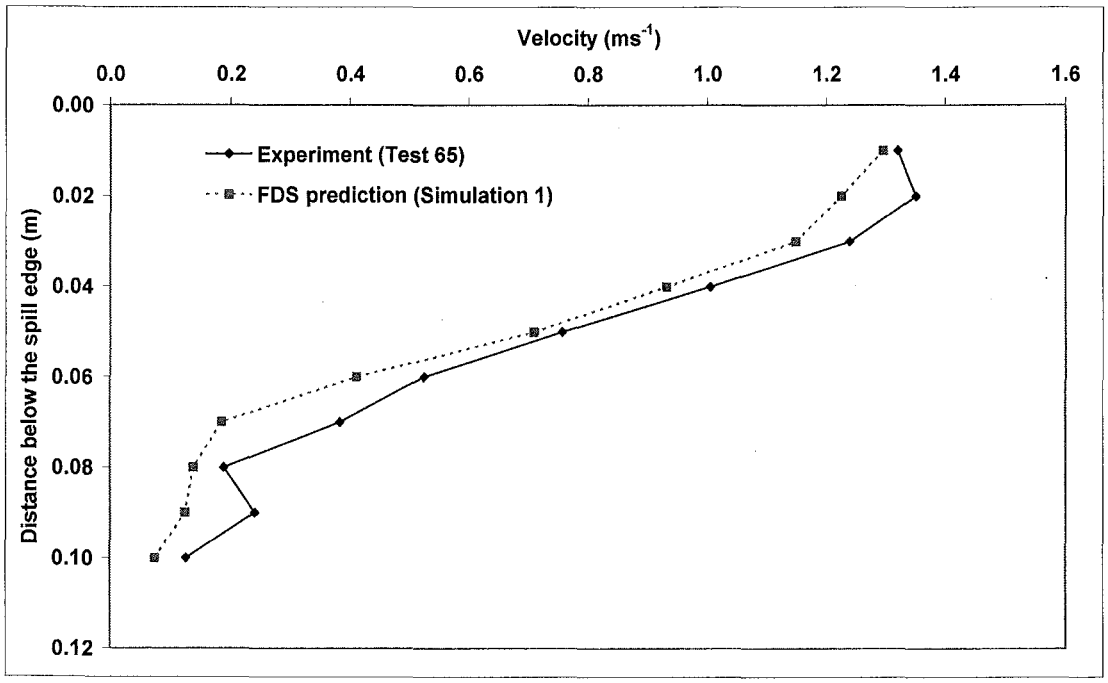

Figure 7.40: Comparison of velocity at the spill edge (1.0 m wide opening, 0.1 m deep downstand)

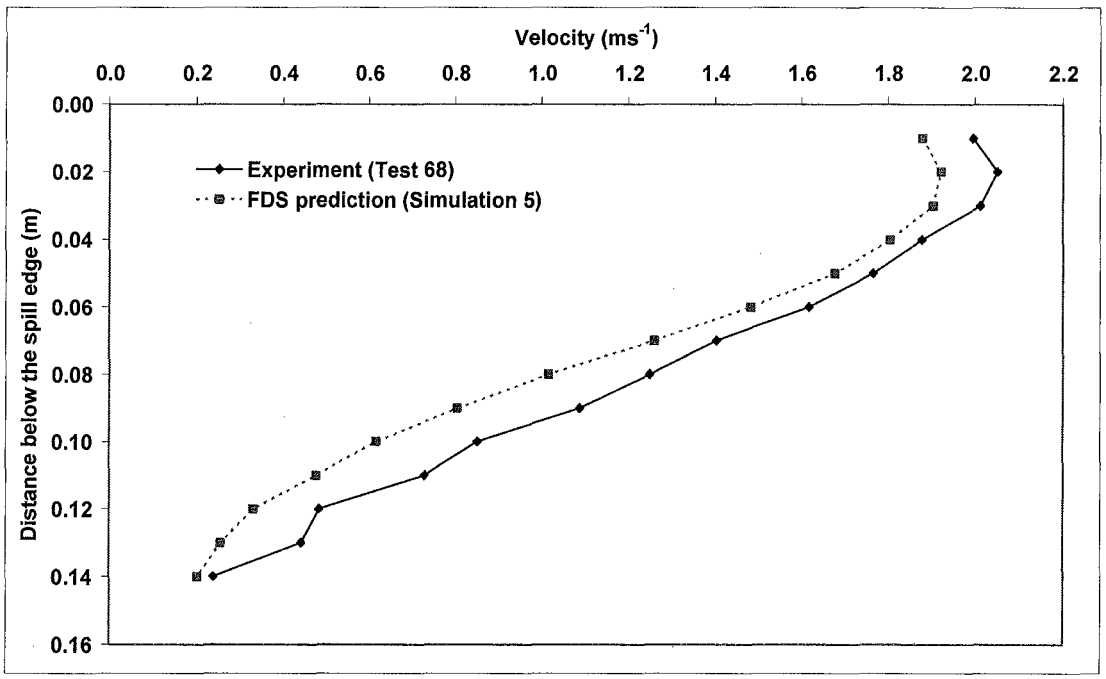

Figure 7.41: Comparison of velocity at the spill edge (0.2 m wide opening, 0.1 m deep downstand)

Appendix L details all of the comparisons between the FDS prediction and the experiment for the velocity profiles at the spill edge.

7.2.2.5 General

In general, the comparisons demonstrated good agreement between the experiment and the FDS predictions in terms of temperature and velocity. This provided the confidence in the FDS predictions to develop an empirical correlation to predict the entrainment of air into a flow from a compartment opening to a higher projecting balcony, and hence, the subsequent mass flow rate of gases at the spill edge.

7.2.3 Mass flow rate of gases at the spill edge

7.2.3.1 Analysis

In the absence of any underlying theory, the FDS results were correlated in various ways in an attempt to develop an empirical correlation to predict the mass flow rate of gases at the spill edge. Those parameters which were expected to influence the entrainment of air into these flows were included in the correlations. The following parameters were used:

- Mass flow rate of gases at the compartment opening (M_w)
- Mass flow rate of gases at the spill edge (M_b)
- Width of the compartment opening (w_o)
- Height of the compartment opening (h_o)
- Height of the compartment (h_{comp})

The results from Simulations 1 to 24 were used in the analysis. The results from Simulation 25, for a flow beneath a 0.2 m broad balcony, was not included since the nature of this flow was fundamentally different from all of the other simulations (see section 7.2.1.3). The effect of the breadth of the balcony on the mass flow rate at the spill edge is discussed further in section 7.2.3.2.

Figure 7.42 shows the correlated results from all of the simulations when $\left(\frac{M_b w_o}{M_w h_{comp}}\right)$ was plotted with respect to $\left(\frac{h_o}{w_o}\right)$. In this case, all of the predictions conveniently collapse down onto a single relationship described by a power law which is non-dimensional in nature. This relationship appears to be versatile, as it applies to a wide range of compartment opening geometries (i.e. aspect ratios) and downstand depths. It also appears to be independent of the heat output of the fire which was also varied in the simulations.

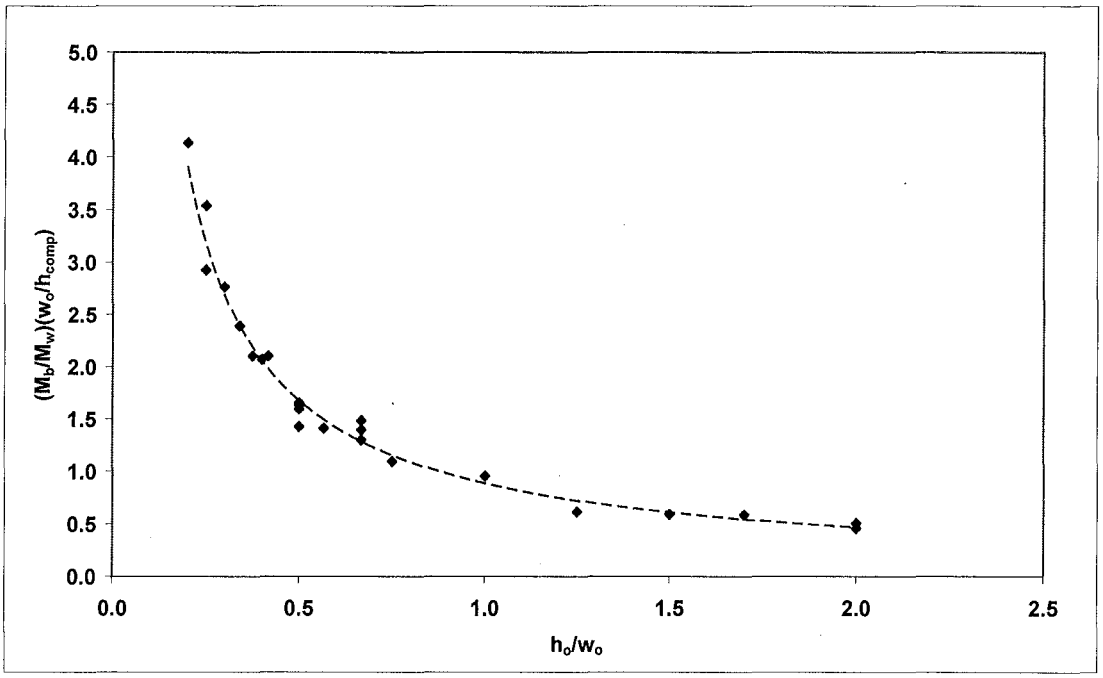

Figure 7.42: Correlated FDS predictions in the form of a power law

It appears that the line of best fit to describe this relationship could be used as an empirical correlation to predict the mass flow rate of gases at the spill edge. To assess the validity of this relationship, the experimental results were also plotted in a similar manner and compared with the FDS predictions (see Figure 7.43).

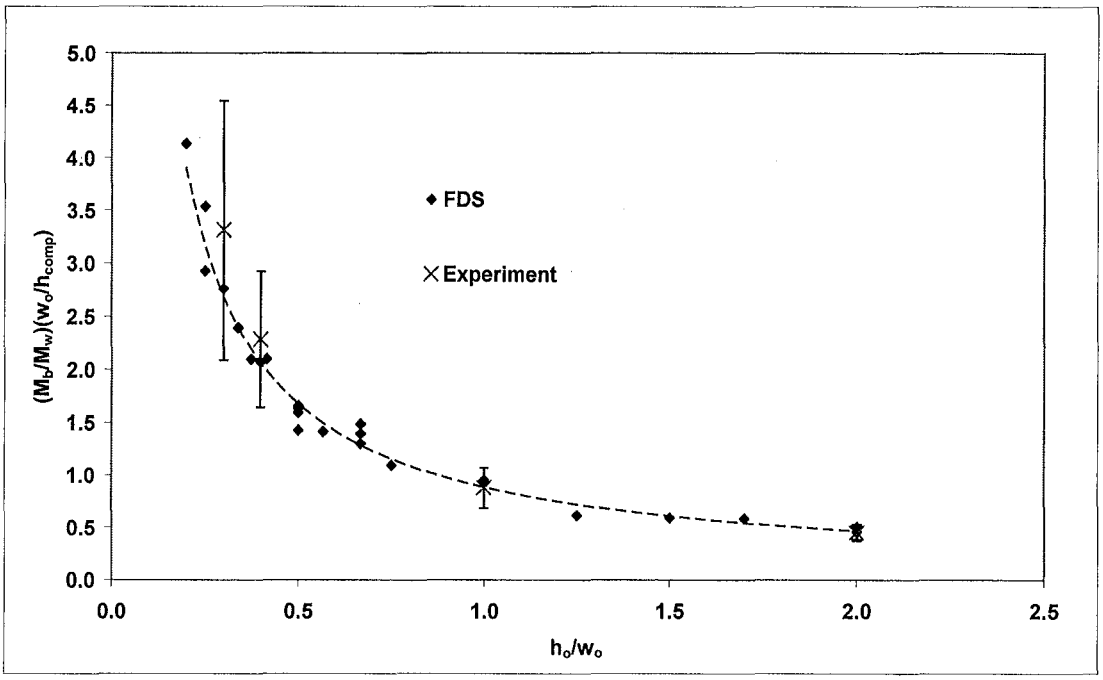

Figure 7.43: Comparison of correlated FDS predictions and experimental results

Figure 7.43 shows that the experimental measurements appear to obey the power law given by the FDS predictions. This provides further confidence for the use of this empirical relationship as a calculation method for design purposes.

7.2.3.2 Effect of balcony length

Since the nature of the flow for a relative short balcony (0.2 m broad) gave rise to a different flow from the other simulations, the FDS prediction for Simulation 25 was plotted separately and compared with the other correlated FDS predictions (see Figure 7.44).

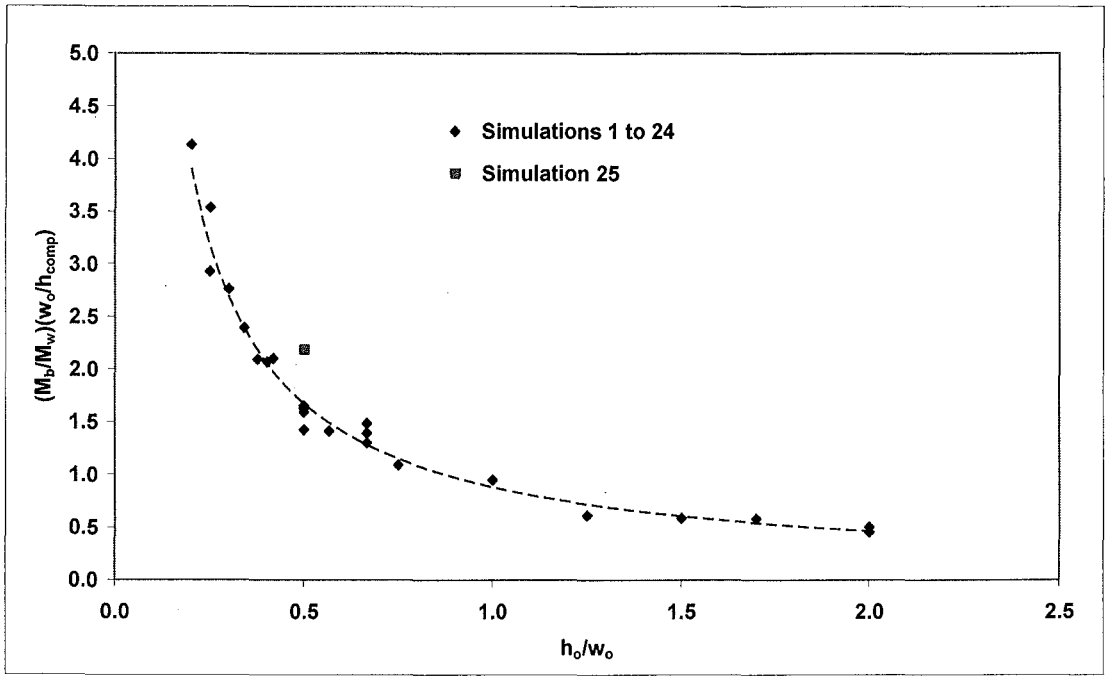

Figure 7.44: Comparison of FDS prediction for Simulation 25 with the other predictions

Figure 7.44 shows that the result from Simulation 25 does not agree with the power law relationship determined from the other FDS simulations. This resulted in a higher mass flow rate at the spill edge compared to the other FDS simulations with the same aspect ratio of compartment opening. This is not surprising, as for this simulation, the plume generally projected beyond the balcony edge, without a horizontally flowing layer forming beneath the balcony. Therefore, there was little impedance to the flow downstream of the compartment opening resulting in a higher velocity of the flow nominally beneath the balcony. This resulted in a greater mass flow rate being

measured beneath the balcony edge. This indicates that the power law relationship from the other simulations is only applicable for flows in which a horizontally flowing layer forms beneath the balcony, prior to rising as a plume at the spill edge.

7.2.3.3 Empirical correlation for design purposes

Equation (7-6) gives an empirical correlation to predict the entrainment of air from a compartment opening to a higher projecting balcony, and hence, the mass flow rate of gases at the spill edge. This was determined from the line of best fit of the power law relationship from the FDS predictions shown in Figure 7.42.

$$M_b = 0.89\left(\frac{h_o}{w_o}\right)^{-0.92}\left(\frac{h_{comp}M_w}{w_o}\right) \tag{7-6}$$

Since the empirical correlation is non-dimensional in nature, Equation (7-6) appears to be versatile and simple to use. It necessarily requires the calculation of the mass flow rate of gases at a compartment opening, which can be determined using simple well-established methods. The other parameters are physical, and are likely to be specified in the design. However, since Equation (7-6) is empirical in nature, there are constraints on its use which are dependent upon the range of conditions in which the correlation was derived. Therefore, the limits for the aspect ratio of the compartment opening in which Equation (7-6) applies are given by Equation (7-7) which is a non-dimensional criterion.

$$0.2 \le \frac{h_o}{w_o} \le 2.0 \tag{7-7}$$

Equation (7-6) only applies to a flow where a horizontally flowing layer forms beneath the higher projecting balcony. The criterion for the required breadth of balcony to achieve this flow, based on the on the conditions studied, is given by Equation (7-8) which is non-dimensional.

$$\left(\frac{h_{comp}}{h_o}\right)\left(\frac{b}{h_{comp}-h_o}\right) \geq 2.5 \tag{7-8}$$

It is interesting to note that Equation (7-6) contains a term which represents the aspect ratio of the compartment opening, $\left(\frac{h_o}{w_o}\right)$, which is raised to the power of -0.92. This indicates that entrainment of air into these flows is only loosely dependent on the width of the compartment opening. If the aspect ratio term in Equation (7-6) were to be simplified, and raised to the power of -1.0, this would give rise to an expression which is independent of the width of the compartment opening [69] [see Equation (7-9)].

$$M_b = 0.89\left(\frac{h_{comp} M_w}{h_o}\right) \tag{7-9}$$

It is proposed that Equation (7-9) could be considered to be an acceptable alternative to Equation (7-6) for a width of compartment opening which does not meet the criterion given in Equation (7-7).

The above empirical correlations only apply to a flow which is channelled, and where the width of the compartment opening is the same as that at the spill edge.

It should be noted that M_w can be calculated using well established methods given either by Morgan [2], Thomas et al [52] or Quintiere et al [54].

The above correlation applies to a wide range of typical compartment opening geometries such as a doorway opening (e.g. 2.0 m high by 1.0 m wide opening) to a wide shop unit (e.g. 10 m wide by 2 m high opening). It also applies for a compartment opening with a higher projecting balcony generally greater than 2 m in breadth.

7.2.3.4 Comparison with the Hansell method

In an attempt to provide further confidence in the empirical correlation given by Equation (7-6), a comparison was made with the results produced by the Hansell method [24] to predict the mass flow rate of gases at a spill edge. The analysis carried out by Garrad [25] was used to identify two scenarios in which the Hansell method converged to a solution. A comparison was then made between the results produced from the Hansell method and Equation (7-6) for each scenario. The two scenarios examined by Garrad were:

- Scenario 1 – A 1 MW fire within a small cellular office
- Scenario 2 – A 5 MW fire within a large area shop unit

Garrad used a calculation technique given by Morgan et al [2] to determine the mass flow rate of gases at the compartment opening for each scenario. Table 7.1 shows the assumed geometries and the calculated mass flow rate of gases at the compartment opening.

Scenario	h_{comp} (m)	h_o (m)	w_o (m)	M_w (kgs^{-1})
1	4.0	3.0	6.0	11.2
2	4.0	3.0	3.0	7.9

Table 7.1: Assumed geometries and calculated values of M_w for Scenarios 1 and 2

The subsequent mass flow rate of gases at the spill edge, determined using the Hansell method and Equation (7-6), are given in Table 7.2 for each scenario examined.

Scenario	Hansell method (M_b) (kgs^{-1})	Equation (7-6) (M_b) (kgs^{-1})
1	13.0	12.6
2	8.7	9.4

Table 7.2: Calculated values of M_b using the Hansell method and Equation (7-6)

Table 7.2 shows that for each scenario, there is good agreement between the Hansell method and Equation (7-6) in the prediction of the mass flow rate of gases at the spill edge. Since the Hansell method is recognised to give a reliable result for geometries similar to that in which the method was derived (as is the case for Scenarios 1 and 2), the good agreement gives further support for the use of Equation (7-6) as an empirical correlation for design purposes to predict the mass flow rate of gases at the spill edge.

7.2.3.5 General

Analysis of the results given in Table 6.3 shows that, in general, the current guidance on the entrainment of air into a flow from a compartment opening to a higher projecting balcony (i.e. $M_b = 2M_w$) is conservative. The majority of the simulations determined values of M_b which were much smaller than $2M_w$. However, for one particular simulation (Simulation 17), the value of M_b was equal to $2M_w$. This result suggests that entrainment of air into these flows is greatest for wide compartment openings with a deep downstand.

In general, it appears that the use of Equation (7-6) to predict the mass flow rate of gases at the spill edge, will give rise to a more cost effective smoke control design.

CHAPTER 8

8. CONCLUSIONS

This work has addressed various limitations and uncertainties in current calculation methods for the spill plume in smoke control design. The conclusions and findings from each aspect of this work are described below.

8.1 Entrainment of air into a spill plume

The physical scale modelling study provided the following conclusions:

- The presence of a downstand at the spill edge of a compartment appears to have little effect on the entrainment of air into the subsequent spill plume.

- The presence of a downstand at the spill edge caused the emerging plume to rise vertically from the opening. This behaviour has significant implications for smoke logging on higher storeys due to partial impingement of the plume with balconies above.

- A simplified spill plume formula has been determined to predict the mass flow rate of gases due to a free spill plume. This formula is given by:

$$M_p = 0.20 Q^{1/3} W^{2/3} (z + d_b) + M_b$$

This formula inherently includes entrainment of air into the free ends of the plume and applies to approach flows which have a flat ceiling or a deep downstand at the spill edge. This equation applies to large area smoke reservoirs. An acceptable alternative to this formula is given by,

$$M_p = 0.20 Q^{1/3} W^{2/3} z + 0.0017 Q + 1.5 M_b$$

- The results indicate that the value of C_m was approximately equal to 0.56. This value inherently includes entrainment of air into the free ends.

- The results indicate that for identical approach flow conditions at a spill edge, the entrainment of air into a spill plume is increased by approximately 25% due to entrainment of air into the free ends.

- For a flat ceiling at the spill edge, the BRE spill plume method gave a reasonably good agreement with the experimental results when used with an entrainment constant, $\alpha = 0.11$, with no adjustment to the height of rise of the plume. The agreement worsened with increasing fire size, which may be due to inaccuracies in the term to predict the entrainment of air into the free ends.

  The use of the effective layer depth correction (without adjusting α) did not provide good agreement with the experimental results. This suggests that the effective layer depth correction may not be reliable when applied to conditions which are dissimilar to that in which the method was derived.

  The above result indicates that, for large area reservoirs, it may be more reliable to apply the BRE method using an entrainment constant with $\alpha = 0.11$, rather than adjusting the height of rise of the plume.

  When a downstand was present at the spill edge, the BRE spill plume method did not generally give good agreement with the experimental results. However, the predicted results were conservative.

- The criteria for the classification of the geometry of a smoke reservoir may not be reliable for all scenarios and should be used with caution.

- Comparison of predictions from simplified spill plume formulae with the experimental results, indicated that these methods tended to under predict the mass flow rate of gases at low heights of rise, whilst over predicting at higher heights of rise above the spill edge (above 3 m full scale).

8.2 Entrainment of air into a flow from a compartment opening to a higher projecting balcony

The findings of the CFD and physical scale modelling studies provided the following conclusions:

- In general, the current guidance on the entrainment of air into a flow from a compartment opening to a higher projecting balcony is conservative.

- The results suggest that entrainment of air into these flows is greatest for wide openings with a deep downstand.

- An empirical correlation has been determined to predict the entrainment of air into a flow from a compartment opening to a higher projecting balcony, and hence, the subsequent mass flow rate of gases at the spill edge. This correlation is given by,

$$M_b = 0.89\left(\frac{h_o}{w_o}\right)^{-0.92}\left(\frac{h_{comp}M_w}{w_o}\right)$$

for

$$0.2 \le \frac{h_o}{w_o} \le 2.0 \quad \text{and} \quad \left(\frac{h_{comp}}{h_o}\right)\left(\frac{b}{h_{comp}-h_o}\right) \ge 2.5$$

This correlation only applies to a flow which is channelled, where the width of the compartment opening is the same as that at the spill edge.

8.3 General

This work has addressed various uncertainties in spill plume calculations, providing robust and relevant simplified design formulae to improve the guidance available to fire safety engineers. These formulae will generally give rise to a more cost-effective smoke control design.

CHAPTER 9

9. FURTHER WORK

9.1 Entrainment of air into a spill plume

Further work is required to determine a simplified spill plume formula to predict the entrainment of air into an adhered spill plume, inherently including entrainment of air into the free ends.

This work has also highlighted the need to examine the effect of the smoke reservoir geometry on the subsequent entrainment of air into a spill plume. This is required to be carried out in a systematic way for a range of smoke reservoir heights, widths and depths to characterise the entrainment behaviour of the spill plume.

Since there is a limiting temperature of the approach flow to which the current spill plume theories apply, further work is also required to examine the entrainment of air into high temperature spill plumes. This could also incorporate entrainment of air into a flame plume emerging from an opening, for which there are currently no design methods available.

9.2 Entrainment of air into a flow from a compartment opening to a higher projecting balcony

Further work is desirable to determine a robust theory to predict the entrainment of air into a flow from a compartment opening to a higher projecting balcony. The FDS predictions and experimental results from this work should be revisited in the development of a possible theory which does not have the constraints of an empirical correlation.

Further work is also required to characterise entrainment of air into flows which are not channelled between the compartment opening and the spill edge.

CHAPTER 10

10. REFERENCES

1. Saxon R. Atrium buildings, development and design. The Architectural Press. London, 1983.
2. Morgan H P, Ghosh B K, Garrad G, Pamlitschka R, De Smedt J-C and Schoonbaert L R. Design methodologies for smoke and heat exhaust ventilation. BRE Report 368, 1999.
3. British Standard Institution. BS5588: Fire precautions in the design, construction and use of buildings. Part 7: Code of practice for the incorporation of atria in buildings. London, BSI, 1997.
4. Milke J A. Smoke management for covered malls and atria. Fire Technology, vol 26 (3), pp 223-243, 1990.
5. National Fire Protection Association. Smoke management systems in malls, atria and large areas. 2000 edition. Publication No.92B. Quincy MA, USA, NFPA, 2000.
6. Klote J H and Milke J A. Design of smoke management systems. American Society of Heating, Refrigerating and Air-conditioning Engineers, Atlanta, GA, 1992.
7. Williams C, Perera E, Morgan H, Harrison R, Caplen B and Ferguson A. Natural ventilation in atria for environment and smoke control: an introductory guide. BRE Report 375, 1999.
8. British Standard Institution. BS7346 Part 4: Components for smoke and heat control systems. Functional recommendations and calculation methods for smoke and heat exhaust ventilation systems, employing steady-state design fires. Code of practice. London, BSI, 2003.
9. NFPA 101 (2000 Edition), Life Safety Code, NFPA, Quincy, MA, 2000.
10. Morgan H P. A brief note on the history of 'acceptable clear heights' for smoke and heat exhaust ventilation systems in the UK. International Journal on Engineering Performanced-Based Fire Codes, Volume 5, Number 2, p 43-44, 2003.

11. BIA: 2001. New Zealand Building Code Handbook and Approved Documents. Building Industry Authority, Wellington, New Zealand.
12. Morton B R, Taylor G I and Turner J S. Turbulent gravitational convection from maintained and instantaneous sources. Proc. Royal Society, A234, pp 1-23, 1956.
13. Cetegen B M, Zukoski E E and Kubota T. Entrainment in the near and far field of fire plumes. Combustion Science and Technology, vol 39, pp 305-331, 1984.
14. Heskestad G. Engineering relations for fire plumes. Fire Safety Journal, 7, No 1, pp 25-32, 1984.
15. Zukoski E E. Properties of fire plumes, in Combustion Fundamentals of Fire, Cox G, Editor. Academic Press, London, 1995.
16. Poreh M and Garrad G. A study of wall and corner fire plumes. Fire Safety Journal 34, pp 81-98, 2000.
17. Klote J H. An overview of atrium smoke management. Fire Protection Engineering, No 7, SFPE, pp 24-34, 2000.
18. Morgan H P and Marshall N R. Smoke hazards in covered multi-level shopping malls: an experimentally-based theory for smoke production. BRE Current Paper 48/75, BRE, 1975.
19. Milke J A. Smoke management in covered malls and atria. In: The SFPE Handbook of Fire Protection Engineering. Section 4/Chapter 13. DiNenno P J, Editor: 2002.
20. Law M. A note on smoke plumes from fires in multi-level shopping malls. Fire Safety Journal, 10, pp 197-202, 1986.
21. Thomas P H. On the upward movement of smoke and related shopping mall problems. Fire Safety Journal, 12, pp 191-203, 1987.
22. Poreh M, Morgan H P, Marshall N R and Harrison R, Entrainment by two dimensional spill plumes in malls and atria. Fire Safety Journal, 30, pp 1-19, 1998.
23. Thomas P H, Morgan H P and Marshall N R. The spill plume in smoke control design. Fire Safety Journal, 30, pp 21-46, 1998.
24. Hansell G O, Heat and mass transfer process affecting smoke control in atrium buildings. PhD thesis, South Bank University, London, 1993.

25. Garrad G, Calculations based on the Hansell method for calculating entrainment into hot gases flowing beneath a downstand and rising to a projecting canopy. Private communication, Building Research Establishment, 1996.
26. Shao-Lin Lee and Emmons H W. A study of natural convection above a line fire. Journal of Fluid Mechanics, 11(3), pp 353-368, 1961.
27. Morgan H P and Marshall N R. Smoke control measures in a covered two-storey shopping mall having balconies and pedestrian walk ways. BRE Current paper 11/79, BRE, 1979.
28. National Fire Protection Association. Smoke management systems in malls, atria and large areas. 1991 edition. Publication No.92B. Quincy MA, USA, NFPA, 1991.
29. Morgan H P and Hansell G O. Atrium buildings: calculating smoke flows in atria for smoke control design. Fire Safety Journal, 12, pp 9-35, 1987.
30. Morgan H P. The horizontal flow of buoyant gases toward an opening. Fire Safety Journal, 11, pp 193-200, 1986.
31. Miles S, Kumar S and Cox G. The balcony spill plume – Some CFD simulations. Fire Safety Science – Proceedings of the Fifth International Symposium, International Association of Fire Safety Science, pp 237-247, Melbourne, Australia.
32. Yii E H. Exploratory salt water experiments of balcony spill plume using laser induced fluorescence technique. Fire Engineering Research Report, University of Canterbury, 1998.
33. Morgan H P, Williams C, Harrison R, Shipp M P and De Smedt J-C. BATC: hot smoke ventilation test at Brussels Airport. 1st International Conference on Fire Safety of Large Enclosed Spaces, 25-27 September, Lille, France, 1995.
34. Williams C. In situ acceptance testing of smoke ventilation systems using real fires at the European Parliament Building. Proceedings Eurofire 98', Fire safety by design, engineering and management. Brussels, Belgium, 11-13 March 1998.
35. Hansell G O, Morgan H P and Marshall N R. Smoke flow experiments in a model atrium. BRE Occasional Paper OP55, BRE, 1993.
36. Grella J J and Faeth G M. Measurements in a two-dimensional thermal plume along a vertical adiabatic wall. Journal of Fluid Mechanics, 71 (4), pp 701-710, 1975.

37. Yokoi S. Study on the prevention of fire spread by hot upward current. Building Research Institute Report 34, Japan, 1960.
38. Morgan H P. Comments on "A note on smoke plumes from fires in multi-level shopping malls". Letters to the Editor, Fire Safety Journal, 12, pp 83-84, 1987.
39. Law M. Reply to Comments on "A note on smoke plumes from fires in multi-level shopping malls". Letters to the Editor, Fire Safety Journal, 12, p 85, 1987.
40. Law M. Measurements of balcony smoke flow. Fire Safety Journal, 24, pp 189-195, 1995.
41. Chartered Institution of Building Services Engineers. CIBSE Guide Volume E: Fire Engineering. London, CIBSE, 1997.
42. Marshall N R and Harrison R. Experimental studies of thermal spill plumes. Building Research Establishment Occasional Paper, OP1, 1996.
43. British Standards Institution. PD 7974: Application of fire safety engineering principles to the design of buildings. Part 2: Spread of smoke and toxic gases within and beyond the enclosure of origin. London, BSI, 2002.
44. Marshall N R. Adhered thermal line plume: a small scale study. Private Communication, Building Research Establishment, 1997.
45. Yuan L U and Cox G. An experimental study of some line fires. Fire Safety Journal, 27, pp 123-139, 1996.
46. Rouse H, Yih C S and Humphreys H W. Gravitational convection from a boundary source. Tellus, 4, pp 201-210, 1952.
47. Chen C and Rodi W. A review of experimental data of vertical turbulent buoyant jets. University of Karlsruhe Report No SFB 80/T/69, 1975.
48. Zukoski E E, Kubota T and Cetegen B. Entrainment in fire plumes. Fire Safety Journal, 3, pp 107-121, 1980.
49. Kotsovinos N E. A study of the entrainment and turbulence in a plane buoyant jet. W M Keck Laboratory of Hydraulics and Water Resources Report No KH-R-32, California Institute of Technology, Pasedena, CA, 1975.
50. Ramaprian B R and Chandrasekhara M S. Measurements in vertical plane turbulent plumes. Fluids Engineering, 111, pp 69-77, 1989.
51. Grove B S and Quintiere J G. Calculating entrainment and flame height in fire plumes of axisymmetric and infinite line geometries. Journal of Fire Protection Engineering, 12, pp 117- 137, 2002.

52. Thomas P H, Hinkley P L, Theobald C R and Simms D L. Investigations into the flow of hot gases in roof venting. Fire Research Technical Paper No 7, London, The Stationary Office, 1963.

53. Marshall N R. Harrison R and Morgan H P. A study of the mechanisms that govern the entrainment of air into a thermal line plume. Private communication, 1993.

54. Quintiere J G, Rinkinen W J and Jones W W. The effects of room openings on fire plume entrainment. Combustion Science and Technology, 26, pp 1983-201, 1981.

55. Chow W K. CFD simulations on balcony spill plume. Journal of Fire Sciences, 16, 6, pp 468-485, 1998.

56. Chow W K. Numerical simulations on balcony spill plume. Fire and Materials, 23, 6, pp 91-99, 1999.

57. Chow W K and Li J. Simulation on natural smoke filling in atrium with a balcony spill plume. Journal of Fire Sciences, 19, 4, pp 258-277, 2001.

58. Li J and Chow W K. Line plume approximation on atrium smoke filling with thermal stratified environment. Journal of Heat Transfer, 125, pp 289-300, 2003.

59. Marshall N R. The behaviour of hot gases flowing within a staircase. Fire Safety Journal, 9, pp 245-255, 1985.

60. Massey B S. Mechanics of fluids. Van Nostrand Reinhold Company, London, 1990.

61. Morgan H P, Marshall N R and Goldstone B M. Smoke hazards in covered multi-level shopping malls: some studies using a model 2-storey mall. Building Research Establishment Current Paper, CP45/76, BRE, 1976.

62. Versteeg H K and Malalasekera W. An introduction to Computational Fluid Dynamics - the finite volume method, Longman Scientific and Technical, 1995.

63. McGrattan K B, Forney G P, Floyd F E, Hostikka S and Prasad K. Fire Dynamics Simulator (Version 3) - User Guide. NISTIR 6784, National Institute of Technology and Standards, 2002.

64. McGrattan K B, Baum H R, Rehm R G, Hammins A, Forney G P and Prasad K: Fire Dynamics Simulator (Version 3) - Technical Reference Guide. NISTIR 6783, National Institute of Technology and Standards, 2002.

65. Forney G P and McGrattan K B. User's guide for Smokeview version 3.1 – a tool for visualizing fire dynamics simulation data. NISTIR 6980, National Institute of Technology and Standards, 2003.
66. B P Chemicals, Hull Research and Technology Centre, Saltend, Hull, UK.
67. Drysdale D. An Introduction to Fire Dynamics. Second Edition. Wiley Press.
68. Schulz J. Measurement of magnitude and direction of hot gas flow in a fire compartment with a five hole probe. Fire Engineering Research Report. University of Canterbury, New Zealand, 2002.
69. Nokes R. Private Communication. University of Canterbury, New Zealand, 2004.

APPENDIX A FUEL FLOWMETER CALIBRATION

The volume of IMS flowing through the flowmeter was measured over a fixed time period for each setting number examined. This was repeated five times, giving an average fuel flow rate. The heat of combustion (26.58 $MJkg^{-1}$) and density of ethanol (806.8 kgm^{-3}) were then used to determine a relationship between the total heat output of the fire and the flowmeter setting number. The results of the calibration were as follows:

Setting Number	Time interval (s)	Volume 2 (cc)	Volume 3 (cc)	Volume 4 (cc)	Volume 5 (cc)	Average volume (cc)
2	240.0	48.0	46.0	47.0	47.0	47.0
4	180.0	93.0	94.0	94.0	95.0	94.0
6	120.0	103.0	103.0	104.0	104.0	103.6
8	120.0	143.0	143.0	142.0	143.0	142.6
10	120.0	180.0	180.0	180.0	179.0	179.6

Table A1: Raw data from fuel flowmeter calibration

Setting Number	Vol flow rate ($cc\ s^{-1}$)	Mass flow rate (kgs^{-1})	Heat Output (kW)
2	0.196	0.00016	4.20
4	0.522	0.00042	11.20
6	0.863	0.00070	18.51
8	1.188	0.00096	25.48
10	1.497	0.00121	32.10

Table A2: Processed data from fuel flowmeter calibration

Appendix A

APPENDIX B THERMOCOUPLE LOCATIONS

Column A	
Thermocouple number	**Distance below ceiling of smoke exhaust hood (mm)**
1	0
2	80
3	180
4	280
5	380
6	480
7	580
8	680
9	780
10	880
11	980
12	1080
13	1180
14	1280
15	1380
16	1480
17	1580
18	1680
19	1780
20	1880
21	1980
22	2080
23	2280
24	2500

Table B1: Thermocouple spacings for Column A

Column B	
Thermocouple number	**Distance below spill edge (mm)**
25	10
26	30
27	50
28	70
29	90
30	110
31	130
32	150
33	170
34	190
35	210
36	230
37	250
38	300
39	350
40	400
41	450
42	500

Table B2: Thermocouple spacings for Column B

Column C (balcony entrainment tests only)	
Thermocouple number	**Distance below bottom of downstand (mm)**
43	10
44	30
45	50
46	70
47	90
48	110
49	130
50	150
51	170
52	190
53	210
54	230
55	250
56	300
57	350
58	400

Table B3: Thermocouple spacings for Column C

Array A, across base of downstand (balcony entrainment tests only)	
Thermocouple number	**Distance across downstand* (mm)**
59	0
60	150
61	300
62	450
63	600

Table B4: Thermocouple spacings for Array A

Array B, across spill edge	
Thermocouple number	**Distance across spill edge* (mm)**
64	0
65	150
66	300
67	450
68	600

Table B5: Thermocouple spacings for Array B

Thermocouple number	Location
69	CO_2 sampling tube
70	Pitot tube 1
71	Pitot tube 2

Table B6: Other thermocouple locations

* Movable for balcony entrainment tests such that thermocouples were evenly spaced

Appendix B

APPENDIX C IMS SAFETY DATA SHEET

Methylated Spirits Industrial

Infosafe No. ACPCT **Issue Date** June 2002 **Status** ISSUED by APSSC

Not classified as hazardous according to criteria of NOHSC

COMPANY DETAILS

Company Name	Asia Pacific Specialty Chemicals Limited (ABN 32000316138)
Address	15 Park Road SEVEN HILLS NSW 2147
Emergency Tel.	1800 022 037 (24H)
Tel/Fax	Tel: (02) 9839 4000 Fax: (02) 9674 6225
Other Information	New Zealand: Asia Pacific Specialty Chemicals (NZ) Limited 119 Carbine Road Mt Wellington, Auckland 6 Emergency Tel: 0800 243 622 (24H) Telephone: (09) 276 4019 Fax: (09) 276 7231

IDENTIFICATION

Product Name	Methylated Spirits Industrial
Proper Shipping Name	ETHANOL (ETHYL ALCOHOL)
UN Number	1170
DG Class	3
Packing Group	II
Hazchem Code	2[Y]E
Poisons Schedule	S5
Product Use	General industrial solvent

Physical Data

Appearance	Clear colourless liquid.
Melting Point	-117°C
Boiling Point	78°C
Vapour Pressure	44 mmHg @ 20°C
Specific Gravity	0.79-0.89 (H2O=1)
Flash Point	13°C (Abel closed cup)
Flamm. Limit LEL	3.5%
Flamm. Limit UEL	19.0%
Solubility in Water	Complete

Other Properties

Volatile Component	100%
Autoignition Temp.	392°C
Evaporation Rate	2.53 (n-Butyl Acetate = 1)
Vapour Density	1.59 (air=1)
Odour Threshold	Characteristic ethanol odour 5 ppm
Stability	Stable under normal conditions.
Haz. Polymerization	Will not occur.
Materials to Avoid	Strong oxidising agents.

Ingredients

Ingredients	**Name**	**CAS**	**Proportion**
	Ethanol	64-17-5	95.8-99.8 %
	Water	7732-18-5	0.2-4.2 %
	Denaturants		0-1 %

APPENDIX D EXAMPLE FDS SOURCE CODE

Simulation 2

```
&HEAD CHID='PLUME2(20mmgrid)',TITLE='ASPECT RATIO 2.0' /
&GRID IBAR=90,JBAR=50,KBAR=50 /
&PDIM XBAR=1.8,YBAR=1.0,ZBAR=1.0 /
&TIME DT=0.05,TWFIN=240. /
&MISC SURF_DEFAULT='CERAMIC BOARD',REACTION='ETHANOL',DTCORE=10.0,TMPA=20.0,
   DATABASE='c:\TEMP\fds3\database3\rhdatabase3.data'/
&VENT CB='XBAR',SURF_ID='OPEN' /
&VENT CB='ZBAR',SURF_ID='OPEN' /
&OBST XB=0.05,0.22,0.415,0.585,0.0,0.05
   SURF_IDS='ETHANOL','INERT','INERT',
   BLOCK_COLOR='RED'/ IMS Poolfire
&PL3D DTSAM=5.,TSTART=0.,TSTOP=240. /
&ISOF QUANTITY='MIXTURE_FRACTION',VALUE(1)=0.067,VALUE(2)=0.001,DTSAM=0.04 /
&SLCF PBY=0.5,QUANTITY='TEMPERATURE',DTSAM=0.08/
&SLCF PBY=0.5,QUANTITY='VELOCITY',VECTOR=.TRUE./
&VENT XB=0.0,1.3,0.0,0.0,0.5,1.0,SURF_ID='OPEN'/
&VENT XB=1.3,1.8,0.0,0.0,0.0,1.0,SURF_ID='OPEN'/
&VENT XB=0.0,1.3,1.0,1.0,0.5,1.0,SURF_ID='OPEN'/
&VENT XB=1.3,1.8,1.0,1.0,0.0,1.0,SURF_ID='OPEN'/
&VENT XB=0.0,0.0,0.0,1.0,0.5,1.0,SURF_ID='OPEN'/
&OBST XB=0.0,1.3,0.0,1.0,0.5,0.525,SURF_IDS='INERT','INERT','CERAMIC BOARD'/CEILING
&OBST XB=0.99,1.0,0.1,0.9,0.4,0.5,SURF_IDS='INERT','CERAMIC BOARD','CERAMIC BOARD',RGB=0.8,0.6,0.4/DOWNSTAND
&OBST XB=0.99,1.0,0.0,0.1,0.0,0.5,SURF_IDS='INERT','INERT','CERAMIC BOARD',RGB=0.8,0.6,0.4/SHOP SIDE 1
&OBST XB=0.99,1.0,0.9,1.0,0.0,0.5,SURF_IDS='INERT','INERT','CERAMIC BOARD',RGB=0.8,0.6,0.4/SHOP SIDE 1
&OBST XB=1.0,1.3,0.09,0.10,0.0,0.5,SURF_IDS='INERT','INERT','CERAMIC BOARD',RGB=0.8,0.6,0.4/CHANNEL SCREEN
&OBST XB=1.0,1.3,0.90,0.91,0.0,0.5,SURF_IDS='INERT','INERT','CERAMIC BOARD',RGB=0.8,0.6,0.4/CHANNEL SCREEN

&THCP XYZ=1.0,0.15,0.39,QUANTITY='TEMPERATURE',LABEL='Downstand TC 0.39(0.15) m' /tc along under downstand, 0.39 m from floor
&THCP XYZ=1.0,0.30,0.39,QUANTITY='TEMPERATURE',LABEL='Downstand TC 0.39(0.30) m' /tc along under downstand, 0.39 m from floor
&THCP XYZ=1.0,0.70,0.39,QUANTITY='TEMPERATURE',LABEL='Downstand TC 0.39(0.70) m' /tc along under downstand, 0.39 m from floor
&THCP XYZ=1.0,0.85,0.39,QUANTITY='TEMPERATURE',LABEL='Downstand TC 0.39(0.85) m' /tc along under downstand, 0.39 m from floor
&THCP XYZ=1.0,0.15,0.39,QUANTITY='VELOCITY',LABEL='Downstand vel 0.39(0.15)' /vel along under downstand, 0.39 m from floor
&THCP XYZ=1.0,0.30,0.39,QUANTITY='VELOCITY',LABEL='Downstand vel 0.39(0.30)' /vel along under downstand, 0.39 m from floor
&THCP XYZ=1.0,0.70,0.39,QUANTITY='VELOCITY',LABEL='Downstand vel 0.39(0.70)' /vel along under downstand, 0.39 m from floor
&THCP XYZ=1.0,0.85,0.39,QUANTITY='VELOCITY',LABEL='Downstand vel 0.39(0.85)' /vel along under downstand, 0.39 m from floor

&THCP XYZ=1.3,0.05,0.49,QUANTITY='TEMPERATURE',LABEL='Balcony TC 0.49(0.05) m' /tc along under balcony, 0.49 m from floor
&THCP XYZ=1.3,0.25,0.49,QUANTITY='TEMPERATURE',LABEL='Balcony TC 0.49(0.25) m' /tc along under balcony, 0.49 m from floor
&THCP XYZ=1.3,0.75,0.49,QUANTITY='TEMPERATURE',LABEL='Balcony TC 0.49(0.75) m' /tc along under balcony, 0.49 m from floor
&THCP XYZ=1.3,0.95,0.49,QUANTITY='TEMPERATURE',LABEL='Balcony TC 0.49(0.95) m' /tc along under balcony, 0.49 m from floor
&THCP XYZ=1.3,0.05,0.49,QUANTITY='VELOCITY',LABEL='Balcony TC 0.49(0.05) m' /Velocity along under balcony, 0.49 m from floor
&THCP XYZ=1.3,0.25,0.49,QUANTITY='VELOCITY',LABEL='Balcony TC 0.49(0.25) m' /Velocity along under balcony, 0.49 m from floor
&THCP XYZ=1.3,0.75,0.49,QUANTITY='VELOCITY',LABEL='Balcony TC 0.49(0.75) m' /Velocity along under balcony, 0.49 m from floor
&THCP XYZ=1.3,0.95,0.49,QUANTITY='VELOCITY',LABEL='Balcony TC 0.49(0.95) m' /Velocity along under balcony, 0.49 m from floor

&THCP XYZ=1.0,0.5,0.39,QUANTITY='TEMPERATURE',LABEL='Downstand TC 0.39 m' /tc centrally under downstand, 0.39 m from floor
&THCP XYZ=1.0,0.5,0.38,QUANTITY='TEMPERATURE',LABEL='Downstand TC 0.38 m' /tc centrally under downstand, 0.38 m from floor
&THCP XYZ=1.0,0.5,0.37,QUANTITY='TEMPERATURE',LABEL='Downstand TC 0.37 m' /tc centrally under downstand, 0.37 m from floor
&THCP XYZ=1.0,0.5,0.36,QUANTITY='TEMPERATURE',LABEL='Downstand TC 0.36 m' /tc centrally under downstand, 0.36 m from floor
&THCP XYZ=1.0,0.5,0.35,QUANTITY='TEMPERATURE',LABEL='Downstand TC 0.35 m' /tc centrally under downstand, 0.35 m from floor
&THCP XYZ=1.0,0.5,0.34,QUANTITY='TEMPERATURE',LABEL='Downstand TC 0.34 m' /tc centrally under downstand, 0.34 m from floor
&THCP XYZ=1.0,0.5,0.33,QUANTITY='TEMPERATURE',LABEL='Downstand TC 0.33 m' /tc centrally under downstand, 0.33 m from floor
```

&THCP XYZ=1.0,0.5,0.32,QUANTITY='TEMPERATURE',LABEL='Downstand TC 0.32 m' /tc centrally under downstand, 0.32 m from floor
&THCP XYZ=1.0,0.5,0.31,QUANTITY='TEMPERATURE',LABEL='Downstand TC 0.31 m' /tc centrally under downstand, 0.31 m from floor
&THCP XYZ=1.0,0.5,0.30,QUANTITY='TEMPERATURE',LABEL='Downstand TC 0.30 m' /tc centrally under downstand, 0.30 m from floor
&THCP XYZ=1.0,0.5,0.29,QUANTITY='TEMPERATURE',LABEL='Downstand TC 0.29 m' /tc centrally under downstand, 0.29 m from floor
&THCP XYZ=1.0,0.5,0.28,QUANTITY='TEMPERATURE',LABEL='Downstand TC 0.28 m' /tc centrally under downstand, 0.28 m from floor
&THCP XYZ=1.0,0.5,0.27,QUANTITY='TEMPERATURE',LABEL='Downstand TC 0.27 m' /tc centrally under downstand, 0.27 m from floor
&THCP XYZ=1.0,0.5,0.26,QUANTITY='TEMPERATURE',LABEL='Downstand TC 0.26 m' /tc centrally under downstand, 0.26 m from floor
&THCP XYZ=1.0,0.5,0.25,QUANTITY='TEMPERATURE',LABEL='Downstand TC 0.25 m' /tc centrally under downstand, 0.25 m from floor
&THCP XYZ=1.0,0.5,0.24,QUANTITY='TEMPERATURE',LABEL='Downstand TC 0.24 m' /tc centrally under downstand, 0.24 m from floor
&THCP XYZ=1.0,0.5,0.23,QUANTITY='TEMPERATURE',LABEL='Downstand TC 0.23 m' /tc centrally under downstand, 0.23 m from floor
&THCP XYZ=1.0,0.5,0.22,QUANTITY='TEMPERATURE',LABEL='Downstand TC 0.22 m' /tc centrally under downstand, 0.22 m from floor
&THCP XYZ=1.0,0.5,0.21,QUANTITY='TEMPERATURE',LABEL='Downstand TC 0.21 m' /tc centrally under downstand, 0.21 m from floor
&THCP XYZ=1.0,0.5,0.20,QUANTITY='TEMPERATURE',LABEL='Downstand TC 0.20 m' /tc centrally under downstand, 0.20 m from floor
&THCP XYZ=1.0,0.5,0.19,QUANTITY='TEMPERATURE',LABEL='Downstand TC 0.19 m' /tc centrally under downstand, 0.19 m from floor
&THCP XYZ=1.0,0.5,0.18,QUANTITY='TEMPERATURE',LABEL='Downstand TC 0.18 m' /tc centrally under downstand, 0.18 m from floor
&THCP XYZ=1.0,0.5,0.17,QUANTITY='TEMPERATURE',LABEL='Downstand TC 0.17 m' /tc centrally under downstand, 0.17 m from floor
&THCP XYZ=1.0,0.5,0.16,QUANTITY='TEMPERATURE',LABEL='Downstand TC 0.16 m' /tc centrally under downstand, 0.16 m from floor
&THCP XYZ=1.0,0.5,0.15,QUANTITY='TEMPERATURE',LABEL='Downstand TC 0.15 m' /tc centrally under downstand, 0.15 m from floor
&THCP XYZ=1.0,0.5,0.14,QUANTITY='TEMPERATURE',LABEL='Downstand TC 0.14 m' /tc centrally under downstand, 0.14 m from floor
&THCP XYZ=1.0,0.5,0.13,QUANTITY='TEMPERATURE',LABEL='Downstand TC 0.13 m' /tc centrally under downstand, 0.13 m from floor
&THCP XYZ=1.0,0.5,0.12,QUANTITY='TEMPERATURE',LABEL='Downstand TC 0.12 m' /tc centrally under downstand, 0.12 m from floor
&THCP XYZ=1.0,0.5,0.11,QUANTITY='TEMPERATURE',LABEL='Downstand TC 0.11 m' /tc centrally under downstand, 0.11 m from floor
&THCP XYZ=1.0,0.5,0.10,QUANTITY='TEMPERATURE',LABEL='Downstand TC 0.10 m' /tc centrally under downstand, 0.10 m from floor
&THCP XYZ=1.0,0.5,0.09,QUANTITY='TEMPERATURE',LABEL='Downstand TC 0.09 m' /tc centrally under downstand, 0.09 m from floor
&THCP XYZ=1.0,0.5,0.08,QUANTITY='TEMPERATURE',LABEL='Downstand TC 0.08 m' /tc centrally under downstand, 0.08 m from floor
&THCP XYZ=1.0,0.5,0.07,QUANTITY='TEMPERATURE',LABEL='Downstand TC 0.07 m' /tc centrally under downstand, 0.07 m from floor
&THCP XYZ=1.0,0.5,0.06,QUANTITY='TEMPERATURE',LABEL='Downstand TC 0.06 m' /tc centrally under downstand, 0.06 m from floor
&THCP XYZ=1.0,0.5,0.05,QUANTITY='TEMPERATURE',LABEL='Downstand TC 0.05 m' /tc centrally under downstand, 0.05 m from floor
&THCP XYZ=1.0,0.5,0.04,QUANTITY='TEMPERATURE',LABEL='Downstand TC 0.04 m' /tc centrally under downstand, 0.04 m from floor
&THCP XYZ=1.0,0.5,0.03,QUANTITY='TEMPERATURE',LABEL='Downstand TC 0.03 m' /tc centrally under downstand, 0.03 m from floor
&THCP XYZ=1.0,0.5,0.02,QUANTITY='TEMPERATURE',LABEL='Downstand TC 0.02 m' /tc centrally under downstand, 0.02 m from floor
&THCP XYZ=1.0,0.5,0.01,QUANTITY='TEMPERATURE',LABEL='Downstand TC 0.01 m' /tc centrally under downstand, 0.01 m from floor

&THCP XYZ=1.0,0.5,0.39,QUANTITY='VELOCITY',LABEL='Downstand Vel 0.39 m' /vel centrally under downstand, 0.39 m from floor
&THCP XYZ=1.0,0.5,0.38,QUANTITY='VELOCITY',LABEL='Downstand Vel 0.38 m' /vel centrally under downstand, 0.38 m from floor
&THCP XYZ=1.0,0.5,0.37,QUANTITY='VELOCITY',LABEL='Downstand Vel 0.37 m' /vel centrally under downstand, 0.37 m from floor
&THCP XYZ=1.0,0.5,0.36,QUANTITY='VELOCITY',LABEL='Downstand Vel 0.36 m' /vel centrally under downstand, 0.36 m from floor
&THCP XYZ=1.0,0.5,0.35,QUANTITY='VELOCITY',LABEL='Downstand Vel 0.35 m' /vel centrally under downstand, 0.35 m from floor
&THCP XYZ=1.0,0.5,0.34,QUANTITY='VELOCITY',LABEL='Downstand Vel 0.34 m' /vel centrally under downstand, 0.34 m from floor
&THCP XYZ=1.0,0.5,0.33,QUANTITY='VELOCITY',LABEL='Downstand Vel 0.33 m' /vel centrally under downstand, 0.33 m from floor
&THCP XYZ=1.0,0.5,0.32,QUANTITY='VELOCITY',LABEL='Downstand Vel 0.32 m' /vel centrally under downstand, 0.32 m from floor
&THCP XYZ=1.0,0.5,0.31,QUANTITY='VELOCITY',LABEL='Downstand Vel 0.31 m' /vel centrally under downstand, 0.31 m from floor
&THCP XYZ=1.0,0.5,0.30,QUANTITY='VELOCITY',LABEL='Downstand Vel 0.30 m' /vel centrally under downstand, 0.30 m from floor
&THCP XYZ=1.0,0.5,0.29,QUANTITY='VELOCITY',LABEL='Downstand Vel 0.29 m' /vel centrally under downstand, 0.29 m from floor
&THCP XYZ=1.0,0.5,0.28,QUANTITY='VELOCITY',LABEL='Downstand Vel 0.28 m' /vel centrally under downstand, 0.28 m from floor
&THCP XYZ=1.0,0.5,0.27,QUANTITY='VELOCITY',LABEL='Downstand Vel 0.27 m' /vel centrally under downstand, 0.27 m from floor
&THCP XYZ=1.0,0.5,0.26,QUANTITY='VELOCITY',LABEL='Downstand Vel 0.26 m' /vel centrally under downstand, 0.26 m from floor
&THCP XYZ=1.0,0.5,0.25,QUANTITY='VELOCITY',LABEL='Downstand Vel 0.25 m' /vel centrally under downstand, 0.25 m from floor
&THCP XYZ=1.0,0.5,0.24,QUANTITY='VELOCITY',LABEL='Downstand Vel 0.24 m' /vel centrally under downstand, 0.24 m from floor
&THCP XYZ=1.0,0.5,0.23,QUANTITY='VELOCITY',LABEL='Downstand Vel 0.23 m' /vel centrally under downstand, 0.23 m from floor
&THCP XYZ=1.0,0.5,0.22,QUANTITY='VELOCITY',LABEL='Downstand Vel 0.22 m' /vel centrally under downstand, 0.22 m from floor
&THCP XYZ=1.0,0.5,0.21,QUANTITY='VELOCITY',LABEL='Downstand Vel 0.21 m' /vel centrally under downstand, 0.21 m from floor
&THCP XYZ=1.0,0.5,0.20,QUANTITY='VELOCITY',LABEL='Downstand Vel 0.20 m' /vel centrally under downstand, 0.20 m from floor
&THCP XYZ=1.0,0.5,0.19,QUANTITY='VELOCITY',LABEL='Downstand Vel 0.19 m' /vel centrally under downstand, 0.19 m from floor
&THCP XYZ=1.0,0.5,0.18,QUANTITY='VELOCITY',LABEL='Downstand Vel 0.18 m' /vel centrally under downstand, 0.18 m from floor
&THCP XYZ=1.0,0.5,0.17,QUANTITY='VELOCITY',LABEL='Downstand Vel 0.17 m' /vel centrally under downstand, 0.17 m from floor
&THCP XYZ=1.0,0.5,0.16,QUANTITY='VELOCITY',LABEL='Downstand Vel 0.16 m' /vel centrally under downstand, 0.16 m from floor
&THCP XYZ=1.0,0.5,0.15,QUANTITY='VELOCITY',LABEL='Downstand Vel 0.15 m' /vel centrally under downstand, 0.15 m from floor

&THCP XYZ=1.0,0.5,0.14,QUANTITY='VELOCITY',LABEL='Downstand Vel 0.14 m' /vel centrally under downstand, 0.14 m from floor
&THCP XYZ=1.0,0.5,0.13,QUANTITY='VELOCITY',LABEL='Downstand Vel 0.13 m' /vel centrally under downstand, 0.13 m from floor
&THCP XYZ=1.0,0.5,0.12,QUANTITY='VELOCITY',LABEL='Downstand Vel 0.12 m' /vel centrally under downstand, 0.12 m from floor
&THCP XYZ=1.0,0.5,0.11,QUANTITY='VELOCITY',LABEL='Downstand Vel 0.11 m' /vel centrally under downstand, 0.11 m from floor
&THCP XYZ=1.0,0.5,0.10,QUANTITY='VELOCITY',LABEL='Downstand Vel 0.10 m' /vel centrally under downstand, 0.10 m from floor
&THCP XYZ=1.0,0.5,0.09,QUANTITY='VELOCITY',LABEL='Downstand Vel 0.09 m' /vel centrally under downstand, 0.09 m from floor
&THCP XYZ=1.0,0.5,0.08,QUANTITY='VELOCITY',LABEL='Downstand Vel 0.08 m' /vel centrally under downstand, 0.08 m from floor
&THCP XYZ=1.0,0.5,0.07,QUANTITY='VELOCITY',LABEL='Downstand Vel 0.07 m' /vel centrally under downstand, 0.07 m from floor
&THCP XYZ=1.0,0.5,0.06,QUANTITY='VELOCITY',LABEL='Downstand Vel 0.06 m' /vel centrally under downstand, 0.06 m from floor
&THCP XYZ=1.0,0.5,0.05,QUANTITY='VELOCITY',LABEL='Downstand Vel 0.05 m' /vel centrally under downstand, 0.05 m from floor
&THCP XYZ=1.0,0.5,0.04,QUANTITY='VELOCITY',LABEL='Downstand Vel 0.04 m' /vel centrally under downstand, 0.04 m from floor
&THCP XYZ=1.0,0.5,0.03,QUANTITY='VELOCITY',LABEL='Downstand Vel 0.03 m' /vel centrally under downstand, 0.03 m from floor
&THCP XYZ=1.0,0.5,0.02,QUANTITY='VELOCITY',LABEL='Downstand Vel 0.02 m' /vel centrally under downstand, 0.02 m from floor
&THCP XYZ=1.0,0.5,0.01,QUANTITY='VELOCITY',LABEL='Downstand Vel 0.01 m' /vel centrally under downstand, 0.01 m from floor

&THCP XYZ=1.3,0.5,0.49,QUANTITY='TEMPERATURE',LABEL='Balcony TC 0.49 m' /tc centrally under balcony, 0.49 m from floor
&THCP XYZ=1.3,0.5,0.48,QUANTITY='TEMPERATURE',LABEL='Balcony TC 0.48 m' /tc centrally under balcony, 0.48 m from floor
&THCP XYZ=1.3,0.5,0.47,QUANTITY='TEMPERATURE',LABEL='Balcony TC 0.47 m' /tc centrally under balcony, 0.47 m from floor
&THCP XYZ=1.3,0.5,0.46,QUANTITY='TEMPERATURE',LABEL='Balcony TC 0.46 m' /tc centrally under balcony, 0.46 m from floor
&THCP XYZ=1.3,0.5,0.45,QUANTITY='TEMPERATURE',LABEL='Balcony TC 0.45 m' /tc centrally under balcony, 0.45 m from floor
&THCP XYZ=1.3,0.5,0.44,QUANTITY='TEMPERATURE',LABEL='Balcony TC 0.44 m' /tc centrally under balcony, 0.44 m from floor
&THCP XYZ=1.3,0.5,0.43,QUANTITY='TEMPERATURE',LABEL='Balcony TC 0.43 m' /tc centrally under balcony, 0.43 m from floor
&THCP XYZ=1.3,0.5,0.42,QUANTITY='TEMPERATURE',LABEL='Balcony TC 0.42 m' /tc centrally under balcony, 0.42 m from floor
&THCP XYZ=1.3,0.5,0.41,QUANTITY='TEMPERATURE',LABEL='Balcony TC 0.41 m' /tc centrally under balcony, 0.41 m from floor
&THCP XYZ=1.3,0.5,0.40,QUANTITY='TEMPERATURE',LABEL='Balcony TC 0.40 m' /tc centrally under balcony, 0.40 m from floor
&THCP XYZ=1.3,0.5,0.39,QUANTITY='TEMPERATURE',LABEL='Balcony TC 0.39 m' /tc centrally under balcony, 0.39 m from floor
&THCP XYZ=1.3,0.5,0.38,QUANTITY='TEMPERATURE',LABEL='Balcony TC 0.38 m' /tc centrally under balcony, 0.38 m from floor
&THCP XYZ=1.3,0.5,0.37,QUANTITY='TEMPERATURE',LABEL='Balcony TC 0.37 m' /tc centrally under balcony, 0.37 m from floor
&THCP XYZ=1.3,0.5,0.36,QUANTITY='TEMPERATURE',LABEL='Balcony TC 0.36 m' /tc centrally under balcony, 0.36 m from floor
&THCP XYZ=1.3,0.5,0.35,QUANTITY='TEMPERATURE',LABEL='Balcony TC 0.35 m' /tc centrally under balcony, 0.35 m from floor
&THCP XYZ=1.3,0.5,0.34,QUANTITY='TEMPERATURE',LABEL='Balcony TC 0.34 m' /tc centrally under balcony, 0.34 m from floor
&THCP XYZ=1.3,0.5,0.33,QUANTITY='TEMPERATURE',LABEL='Balcony TC 0.33 m' /tc centrally under balcony, 0.33 m from floor
&THCP XYZ=1.3,0.5,0.32,QUANTITY='TEMPERATURE',LABEL='Balcony TC 0.32 m' /tc centrally under balcony, 0.32 m from floor
&THCP XYZ=1.3,0.5,0.31,QUANTITY='TEMPERATURE',LABEL='Balcony TC 0.31 m' /tc centrally under balcony, 0.31 m from floor
&THCP XYZ=1.3,0.5,0.30,QUANTITY='TEMPERATURE',LABEL='Balcony TC 0.30 m' /tc centrally under balcony, 0.30 m from floor
&THCP XYZ=1.3,0.5,0.29,QUANTITY='TEMPERATURE',LABEL='Balcony TC 0.29 m' /tc centrally under balcony, 0.29 m from floor
&THCP XYZ=1.3,0.5,0.28,QUANTITY='TEMPERATURE',LABEL='Balcony TC 0.28 m' /tc centrally under balcony, 0.28 m from floor
&THCP XYZ=1.3,0.5,0.27,QUANTITY='TEMPERATURE',LABEL='Balcony TC 0.27 m' /tc centrally under balcony, 0.27 m from floor
&THCP XYZ=1.3,0.5,0.26,QUANTITY='TEMPERATURE',LABEL='Balcony TC 0.26 m' /tc centrally under balcony, 0.26 m from floor
&THCP XYZ=1.3,0.5,0.25,QUANTITY='TEMPERATURE',LABEL='Balcony TC 0.25 m' /tc centrally under balcony, 0.25 m from floor
&THCP XYZ=1.3,0.5,0.24,QUANTITY='TEMPERATURE',LABEL='Balcony TC 0.24 m' /tc centrally under balcony, 0.24 m from floor
&THCP XYZ=1.3,0.5,0.23,QUANTITY='TEMPERATURE',LABEL='Balcony TC 0.23 m' /tc centrally under balcony, 0.23 m from floor
&THCP XYZ=1.3,0.5,0.22,QUANTITY='TEMPERATURE',LABEL='Balcony TC 0.22 m' /tc centrally under balcony, 0.22 m from floor
&THCP XYZ=1.3,0.5,0.21,QUANTITY='TEMPERATURE',LABEL='Balcony TC 0.21 m' /tc centrally under balcony, 0.21 m from floor
&THCP XYZ=1.3,0.5,0.20,QUANTITY='TEMPERATURE',LABEL='Balcony TC 0.20 m' /tc centrally under balcony, 0.20 m from floor
&THCP XYZ=1.3,0.5,0.19,QUANTITY='TEMPERATURE',LABEL='Balcony TC 0.19 m' /tc centrally under balcony, 0.19 m from floor
&THCP XYZ=1.3,0.5,0.18,QUANTITY='TEMPERATURE',LABEL='Balcony TC 0.18 m' /tc centrally under balcony, 0.18 m from floor
&THCP XYZ=1.3,0.5,0.17,QUANTITY='TEMPERATURE',LABEL='Balcony TC 0.17 m' /tc centrally under balcony, 0.17 m from floor
&THCP XYZ=1.3,0.5,0.16,QUANTITY='TEMPERATURE',LABEL='Balcony TC 0.16 m' /tc centrally under balcony, 0.16 m from floor
&THCP XYZ=1.3,0.5,0.15,QUANTITY='TEMPERATURE',LABEL='Balcony TC 0.15 m' /tc centrally under balcony, 0.15 m from floor
&THCP XYZ=1.3,0.5,0.14,QUANTITY='TEMPERATURE',LABEL='Balcony TC 0.14 m' /tc centrally under balcony, 0.14 m from floor
&THCP XYZ=1.3,0.5,0.13,QUANTITY='TEMPERATURE',LABEL='Balcony TC 0.13 m' /tc centrally under balcony, 0.13 m from floor
&THCP XYZ=1.3,0.5,0.12,QUANTITY='TEMPERATURE',LABEL='Balcony TC 0.12 m' /tc centrally under balcony, 0.12 m from floor
&THCP XYZ=1.3,0.5,0.11,QUANTITY='TEMPERATURE',LABEL='Balcony TC 0.11 m' /tc centrally under balcony, 0.11 m from floor
&THCP XYZ=1.3,0.5,0.10,QUANTITY='TEMPERATURE',LABEL='Balcony TC 0.10 m' /tc centrally under balcony, 0.10 m from floor
&THCP XYZ=1.3,0.5,0.09,QUANTITY='TEMPERATURE',LABEL='Balcony TC 0.09 m' /tc centrally under balcony, 0.09 m from floor
&THCP XYZ=1.3,0.5,0.08,QUANTITY='TEMPERATURE',LABEL='Balcony TC 0.08 m' /tc centrally under balcony, 0.08 m from floor
&THCP XYZ=1.3,0.5,0.07,QUANTITY='TEMPERATURE',LABEL='Balcony TC 0.07 m' /tc centrally under balcony, 0.07 m from floor

&THCP XYZ=1.3,0.5,0.06,QUANTITY='TEMPERATURE',LABEL='Balcony TC 0.06 m' /tc centrally under balcony, 0.06 m from floor
&THCP XYZ=1.3,0.5,0.05,QUANTITY='TEMPERATURE',LABEL='Balcony TC 0.05 m' /tc centrally under balcony, 0.05 m from floor
&THCP XYZ=1.3,0.5,0.04,QUANTITY='TEMPERATURE',LABEL='Balcony TC 0.04 m' /tc centrally under balcony, 0.04 m from floor
&THCP XYZ=1.3,0.5,0.03,QUANTITY='TEMPERATURE',LABEL='Balcony TC 0.03 m' /tc centrally under balcony, 0.03 m from floor
&THCP XYZ=1.3,0.5,0.02,QUANTITY='TEMPERATURE',LABEL='Balcony TC 0.02 m' /tc centrally under balcony, 0.02 m from floor
&THCP XYZ=1.3,0.5,0.01,QUANTITY='TEMPERATURE',LABEL='Balcony TC 0.01 m' /tc centrally under balcony, 0.01 m from floor

&THCP XYZ=1.3,0.5,0.49,QUANTITY='VELOCITY',LABEL='Balcony Vel 0.49 m' /Vel centrally under balcony, 0.49 m from floor
&THCP XYZ=1.3,0.5,0.48,QUANTITY='VELOCITY',LABEL='Balcony Vel 0.48 m' /Vel centrally under balcony, 0.48 m from floor
&THCP XYZ=1.3,0.5,0.47,QUANTITY='VELOCITY',LABEL='Balcony Vel 0.47 m' /Vel centrally under balcony, 0.47 m from floor
&THCP XYZ=1.3,0.5,0.46,QUANTITY='VELOCITY',LABEL='Balcony Vel 0.46 m' /Vel centrally under balcony, 0.46 m from floor
&THCP XYZ=1.3,0.5,0.45,QUANTITY='VELOCITY',LABEL='Balcony Vel 0.45 m' /Vel centrally under balcony, 0.45 m from floor
&THCP XYZ=1.3,0.5,0.44,QUANTITY='VELOCITY',LABEL='Balcony Vel 0.44 m' /Vel centrally under balcony, 0.44 m from floor
&THCP XYZ=1.3,0.5,0.43,QUANTITY='VELOCITY',LABEL='Balcony Vel 0.43 m' /Vel centrally under balcony, 0.43 m from floor
&THCP XYZ=1.3,0.5,0.42,QUANTITY='VELOCITY',LABEL='Balcony Vel 0.42 m' /Vel centrally under balcony, 0.42 m from floor
&THCP XYZ=1.3,0.5,0.41,QUANTITY='VELOCITY',LABEL='Balcony Vel 0.41 m' /Vel centrally under balcony, 0.41 m from floor
&THCP XYZ=1.3,0.5,0.40,QUANTITY='VELOCITY',LABEL='Balcony Vel 0.40 m' /Vel centrally under balcony, 0.40 m from floor
&THCP XYZ=1.3,0.5,0.39,QUANTITY='VELOCITY',LABEL='Balcony Vel 0.39 m' /Vel centrally under balcony, 0.39 m from floor
&THCP XYZ=1.3,0.5,0.38,QUANTITY='VELOCITY',LABEL='Balcony Vel 0.38 m' /Vel centrally under balcony, 0.38 m from floor
&THCP XYZ=1.3,0.5,0.37,QUANTITY='VELOCITY',LABEL='Balcony Vel 0.37 m' /Vel centrally under balcony, 0.37 m from floor
&THCP XYZ=1.3,0.5,0.36,QUANTITY='VELOCITY',LABEL='Balcony Vel 0.36 m' /Vel centrally under balcony, 0.36 m from floor
&THCP XYZ=1.3,0.5,0.35,QUANTITY='VELOCITY',LABEL='Balcony Vel 0.35 m' /Vel centrally under balcony, 0.35 m from floor
&THCP XYZ=1.3,0.5,0.34,QUANTITY='VELOCITY',LABEL='Balcony Vel 0.34 m' /Vel centrally under balcony, 0.34 m from floor
&THCP XYZ=1.3,0.5,0.33,QUANTITY='VELOCITY',LABEL='Balcony Vel 0.33 m' /Vel centrally under balcony, 0.33 m from floor
&THCP XYZ=1.3,0.5,0.32,QUANTITY='VELOCITY',LABEL='Balcony Vel 0.32 m' /Vel centrally under balcony, 0.32 m from floor
&THCP XYZ=1.3,0.5,0.31,QUANTITY='VELOCITY',LABEL='Balcony Vel 0.31 m' /Vel centrally under balcony, 0.31 m from floor
&THCP XYZ=1.3,0.5,0.30,QUANTITY='VELOCITY',LABEL='Balcony Vel 0.30 m' /Vel centrally under balcony, 0.30 m from floor
&THCP XYZ=1.3,0.5,0.29,QUANTITY='VELOCITY',LABEL='Balcony Vel 0.29 m' /Vel centrally under balcony, 0.29 m from floor
&THCP XYZ=1.3,0.5,0.28,QUANTITY='VELOCITY',LABEL='Balcony Vel 0.28 m' /Vel centrally under balcony, 0.28 m from floor
&THCP XYZ=1.3,0.5,0.27,QUANTITY='VELOCITY',LABEL='Balcony Vel 0.27 m' /Vel centrally under balcony, 0.27 m from floor
&THCP XYZ=1.3,0.5,0.26,QUANTITY='VELOCITY',LABEL='Balcony Vel 0.26 m' /Vel centrally under balcony, 0.26 m from floor
&THCP XYZ=1.3,0.5,0.25,QUANTITY='VELOCITY',LABEL='Balcony Vel 0.25 m' /Vel centrally under balcony, 0.25 m from floor
&THCP XYZ=1.3,0.5,0.24,QUANTITY='VELOCITY',LABEL='Balcony Vel 0.24 m' /Vel centrally under balcony, 0.24 m from floor
&THCP XYZ=1.3,0.5,0.23,QUANTITY='VELOCITY',LABEL='Balcony Vel 0.23 m' /Vel centrally under balcony, 0.23 m from floor
&THCP XYZ=1.3,0.5,0.22,QUANTITY='VELOCITY',LABEL='Balcony Vel 0.22 m' /Vel centrally under balcony, 0.22 m from floor
&THCP XYZ=1.3,0.5,0.21,QUANTITY='VELOCITY',LABEL='Balcony Vel 0.21 m' /Vel centrally under balcony, 0.21 m from floor
&THCP XYZ=1.3,0.5,0.20,QUANTITY='VELOCITY',LABEL='Balcony Vel 0.20 m' /Vel centrally under balcony, 0.20 m from floor
&THCP XYZ=1.3,0.5,0.19,QUANTITY='VELOCITY',LABEL='Balcony Vel 0.19 m' /Vel centrally under balcony, 0.19 m from floor
&THCP XYZ=1.3,0.5,0.18,QUANTITY='VELOCITY',LABEL='Balcony Vel 0.18 m' /Vel centrally under balcony, 0.18 m from floor
&THCP XYZ=1.3,0.5,0.17,QUANTITY='VELOCITY',LABEL='Balcony Vel 0.17 m' /Vel centrally under balcony, 0.17 m from floor
&THCP XYZ=1.3,0.5,0.16,QUANTITY='VELOCITY',LABEL='Balcony Vel 0.16 m' /Vel centrally under balcony, 0.16 m from floor
&THCP XYZ=1.3,0.5,0.15,QUANTITY='VELOCITY',LABEL='Balcony Vel 0.15 m' /Vel centrally under balcony, 0.15 m from floor
&THCP XYZ=1.3,0.5,0.14,QUANTITY='VELOCITY',LABEL='Balcony Vel 0.14 m' /Vel centrally under balcony, 0.14 m from floor
&THCP XYZ=1.3,0.5,0.13,QUANTITY='VELOCITY',LABEL='Balcony Vel 0.13 m' /Vel centrally under balcony, 0.13 m from floor
&THCP XYZ=1.3,0.5,0.12,QUANTITY='VELOCITY',LABEL='Balcony Vel 0.12 m' /Vel centrally under balcony, 0.12 m from floor
&THCP XYZ=1.3,0.5,0.11,QUANTITY='VELOCITY',LABEL='Balcony Vel 0.11 m' /Vel centrally under balcony, 0.11 m from floor
&THCP XYZ=1.3,0.5,0.10,QUANTITY='VELOCITY',LABEL='Balcony Vel 0.10 m' /Vel centrally under balcony, 0.10 m from floor
&THCP XYZ=1.3,0.5,0.09,QUANTITY='VELOCITY',LABEL='Balcony Vel 0.09 m' /Vel centrally under balcony, 0.09 m from floor
&THCP XYZ=1.3,0.5,0.08,QUANTITY='VELOCITY',LABEL='Balcony Vel 0.08 m' /Vel centrally under balcony, 0.08 m from floor
&THCP XYZ=1.3,0.5,0.07,QUANTITY='VELOCITY',LABEL='Balcony Vel 0.07 m' /Vel centrally under balcony, 0.07 m from floor
&THCP XYZ=1.3,0.5,0.06,QUANTITY='VELOCITY',LABEL='Balcony Vel 0.06 m' /Vel centrally under balcony, 0.06 m from floor
&THCP XYZ=1.3,0.5,0.05,QUANTITY='VELOCITY',LABEL='Balcony Vel 0.05 m' /Vel centrally under balcony, 0.05 m from floor
&THCP XYZ=1.3,0.5,0.04,QUANTITY='VELOCITY',LABEL='Balcony Vel 0.04 m' /Vel centrally under balcony, 0.04 m from floor
&THCP XYZ=1.3,0.5,0.03,QUANTITY='VELOCITY',LABEL='Balcony Vel 0.03 m' /Vel centrally under balcony, 0.03 m from floor
&THCP XYZ=1.3,0.5,0.02,QUANTITY='VELOCITY',LABEL='Balcony Vel 0.02 m' /Vel centrally under balcony, 0.02 m from floor
&THCP XYZ=1.3,0.5,0.01,QUANTITY='VELOCITY',LABEL='Balcony Vel 0.01 m' /Vel centrally under balcony, 0.01 m from floor

APPENDIX E EXPERIMENTAL TEMPERATURE AND VELOCITY PROFILES AT THE SPILL EDGE (TESTS 1 TO 9)

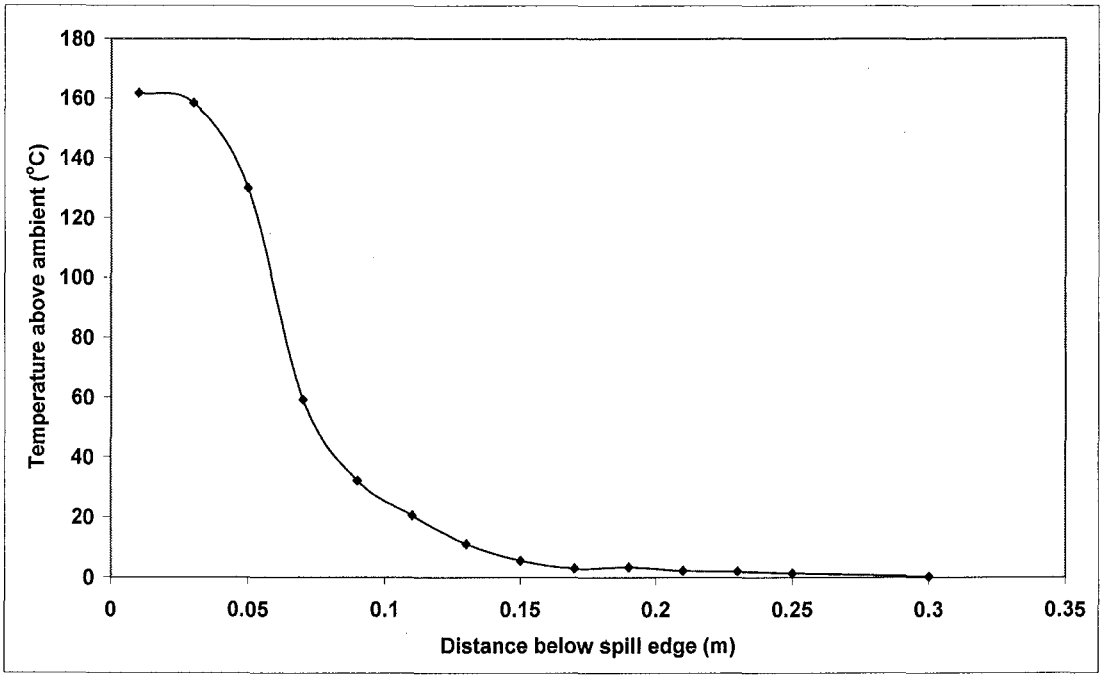

Figure E1: Temperature profile at spill edge for Test 1

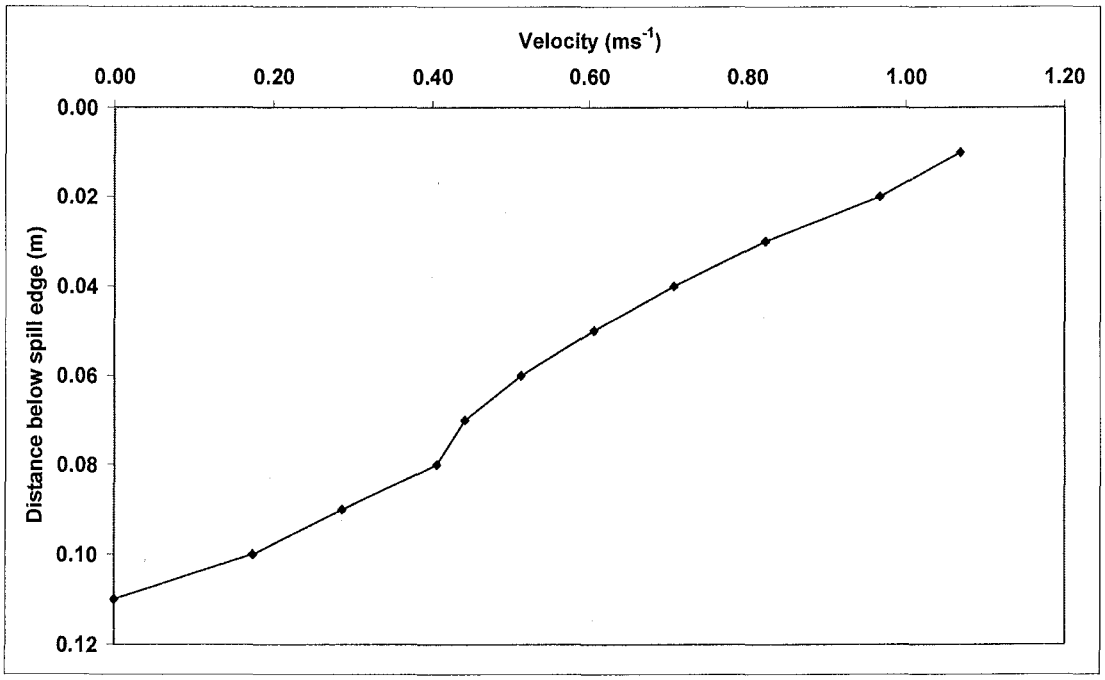

Figure E2: Velocity profile at spill edge for Test 1

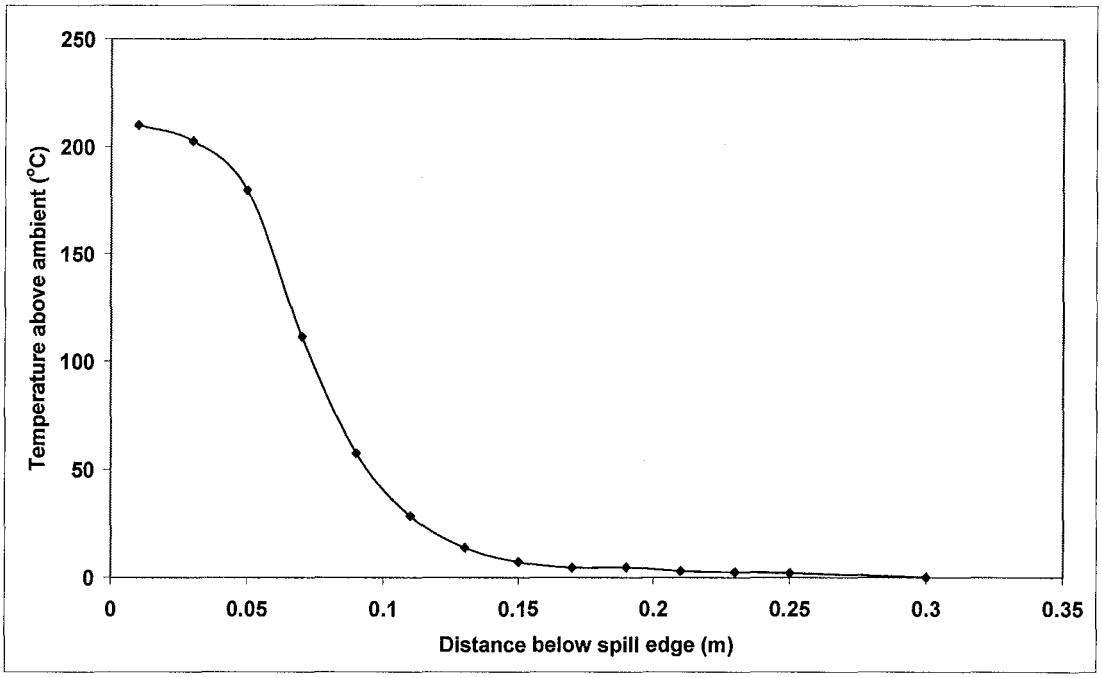

Figure E3: Temperature profile at spill edge for Test 2

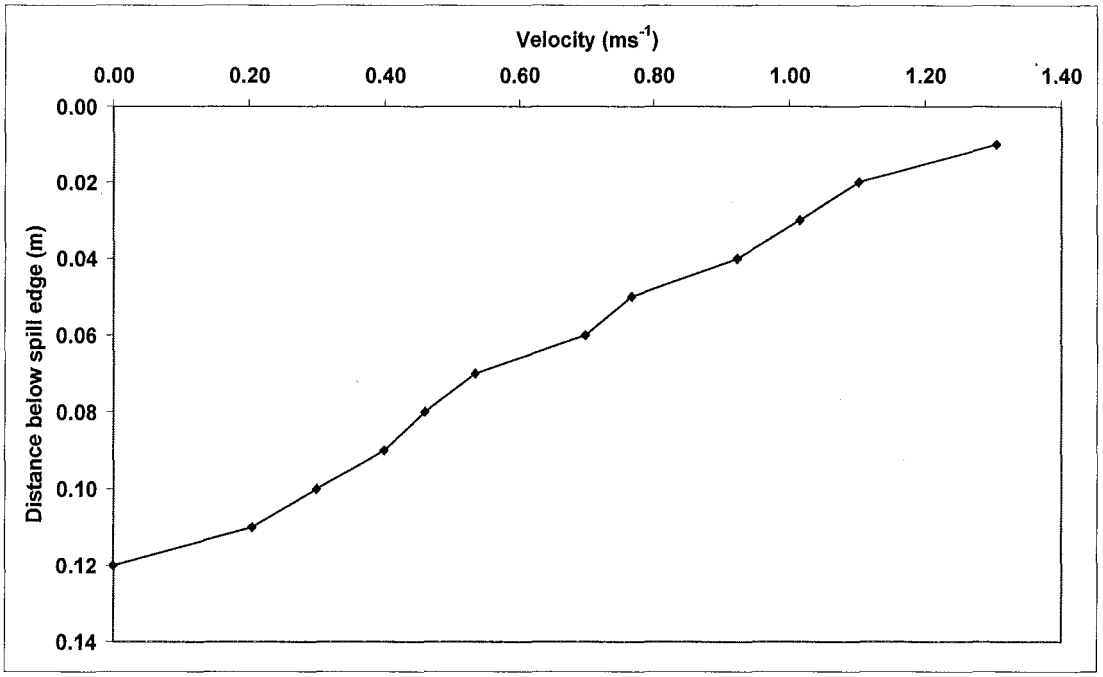

Figure E4: Velocity profile at spill edge for Test 2

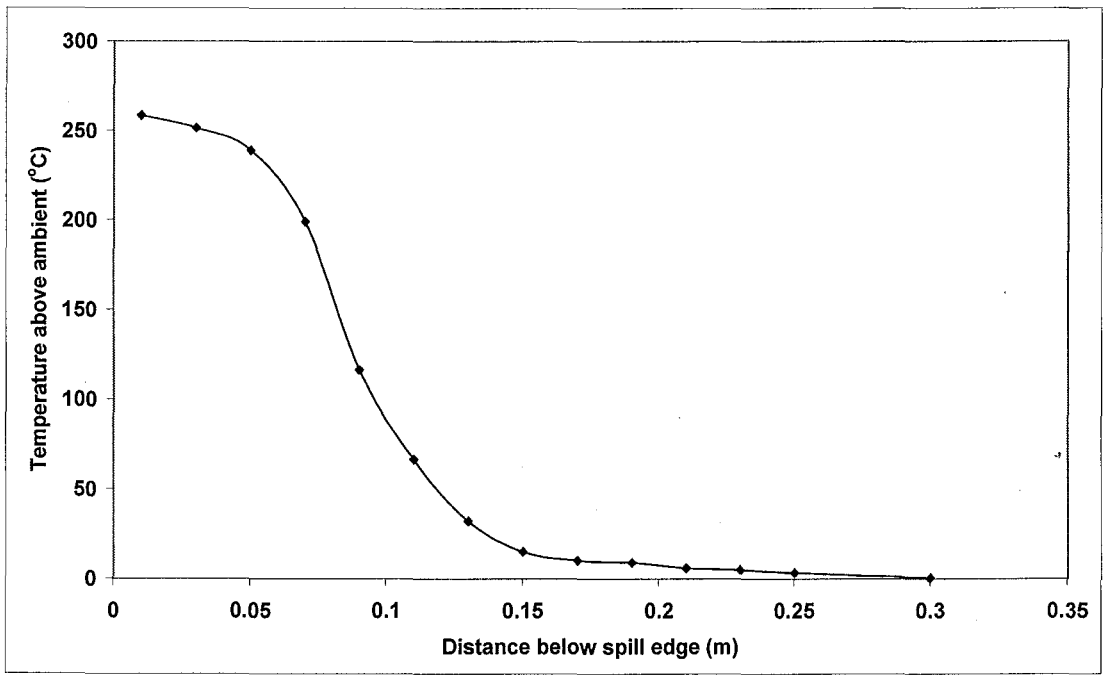

Figure E5: **Temperature profile at spill edge for Test 3**

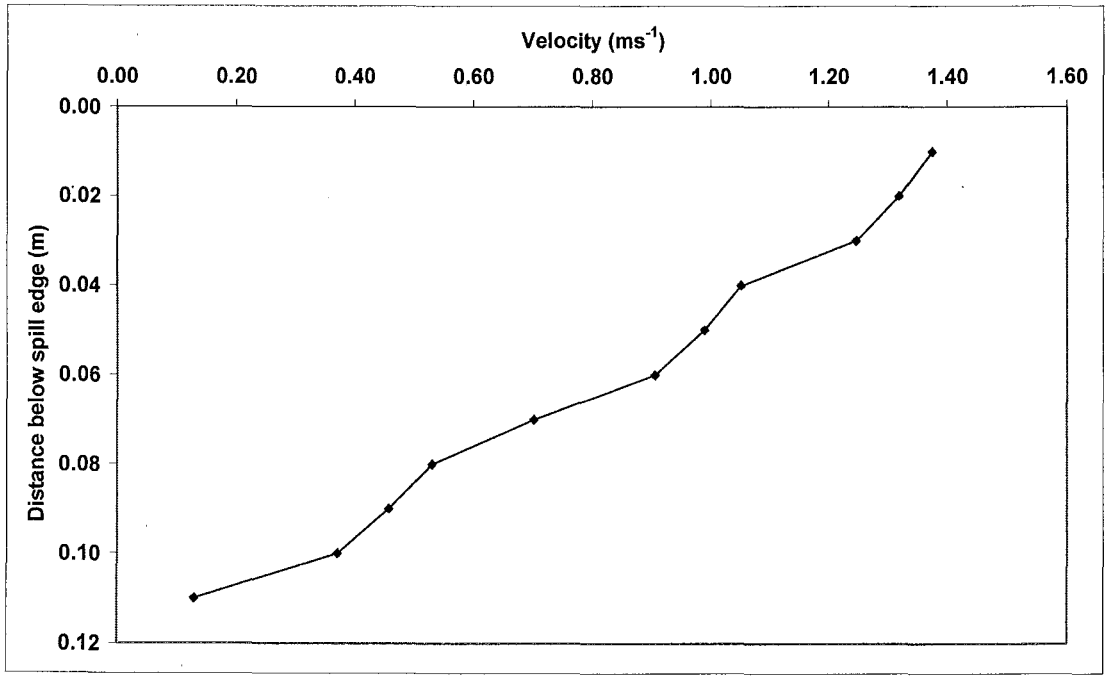

Figure E6: **Velocity profile at spill edge for Test 3**

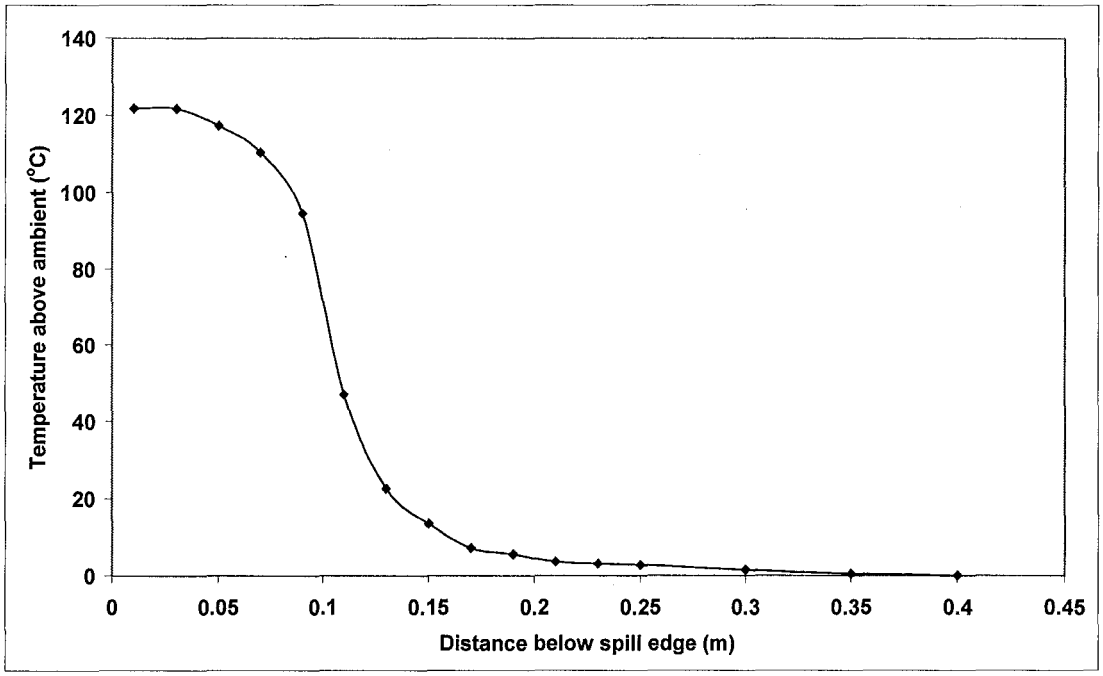

Figure E7: Temperature profile at spill edge for Test 4

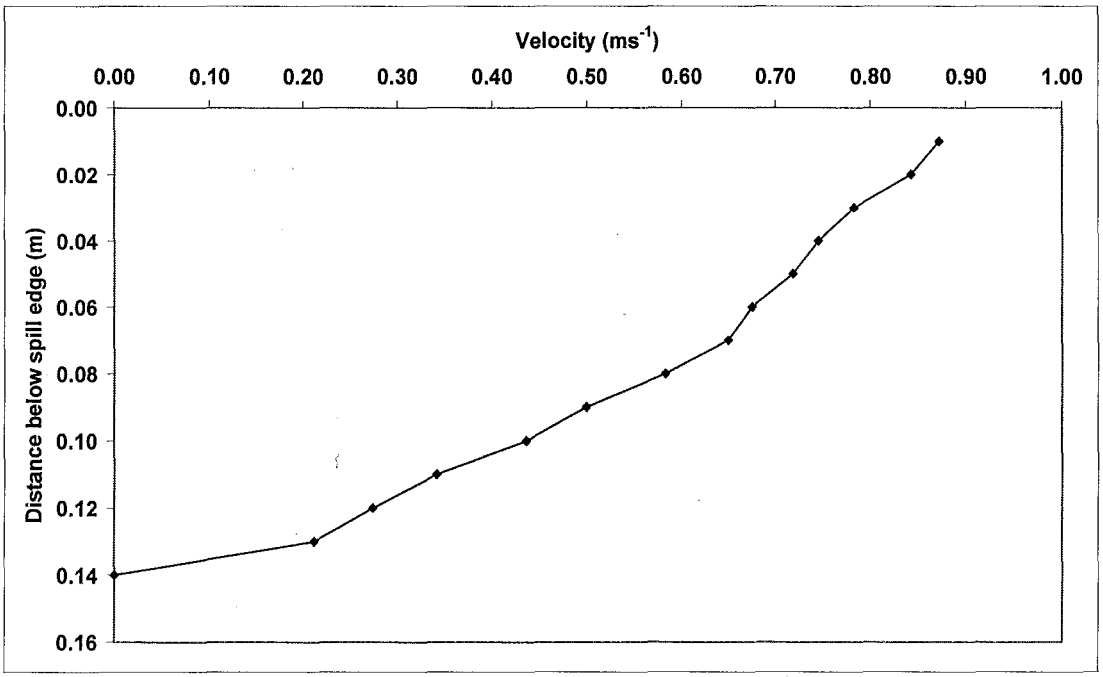

Figure E8: Velocity profile at spill edge for Test 4

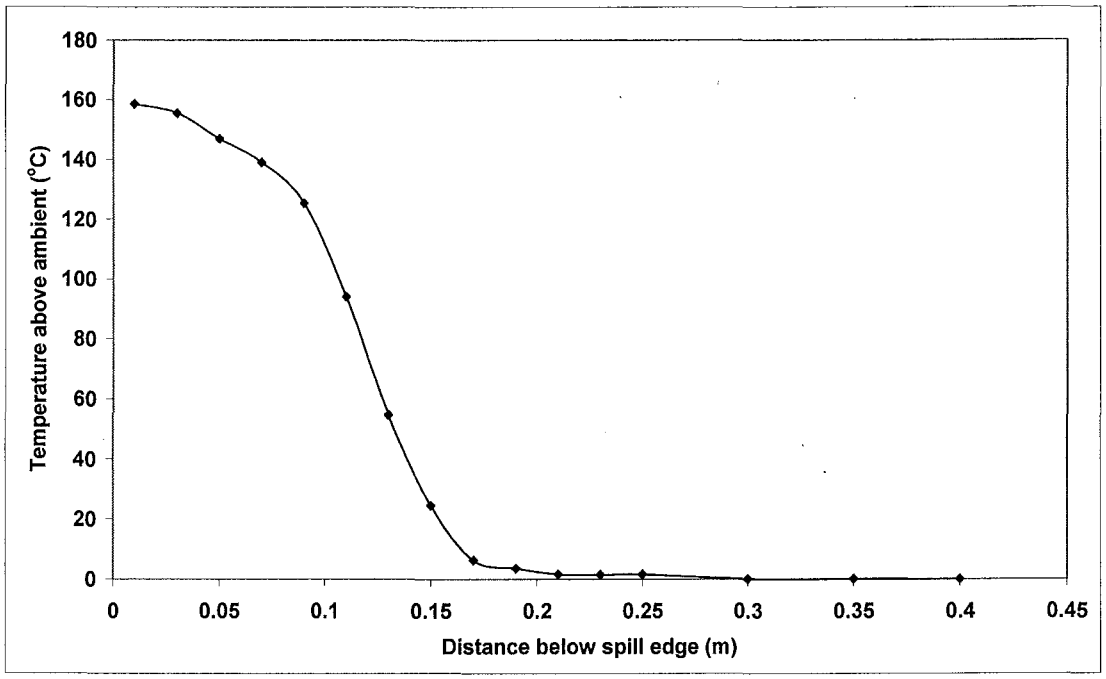

Figure E9: **Temperature profile at spill edge for Test 5**

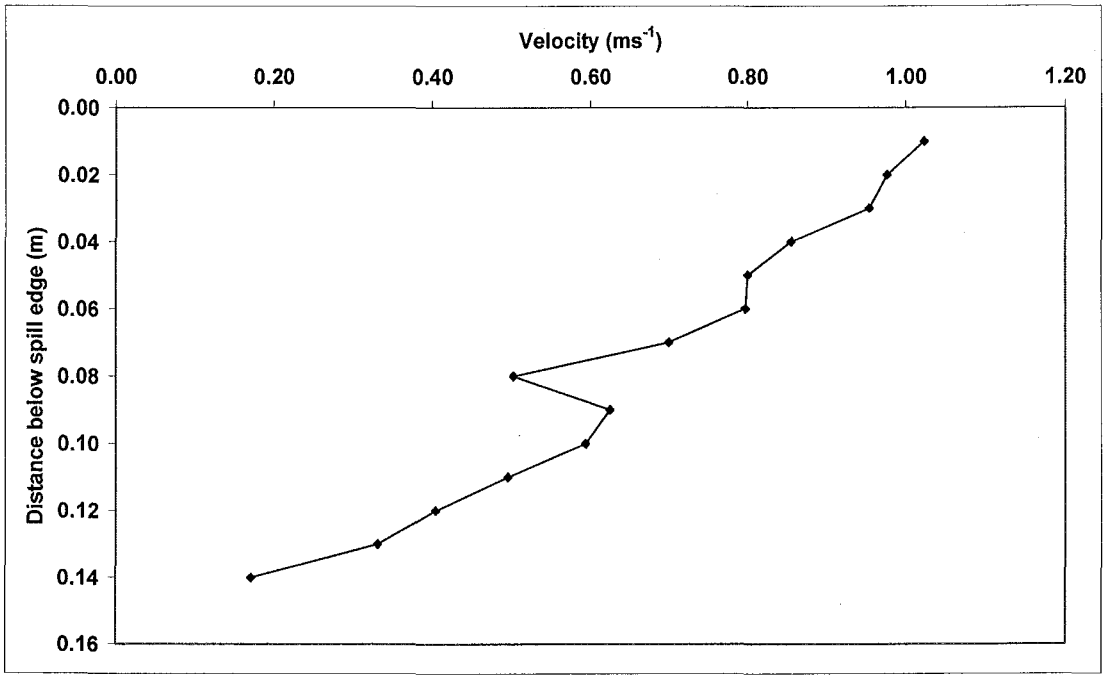

Figure E10: **Velocity profile at spill edge for Test 5**

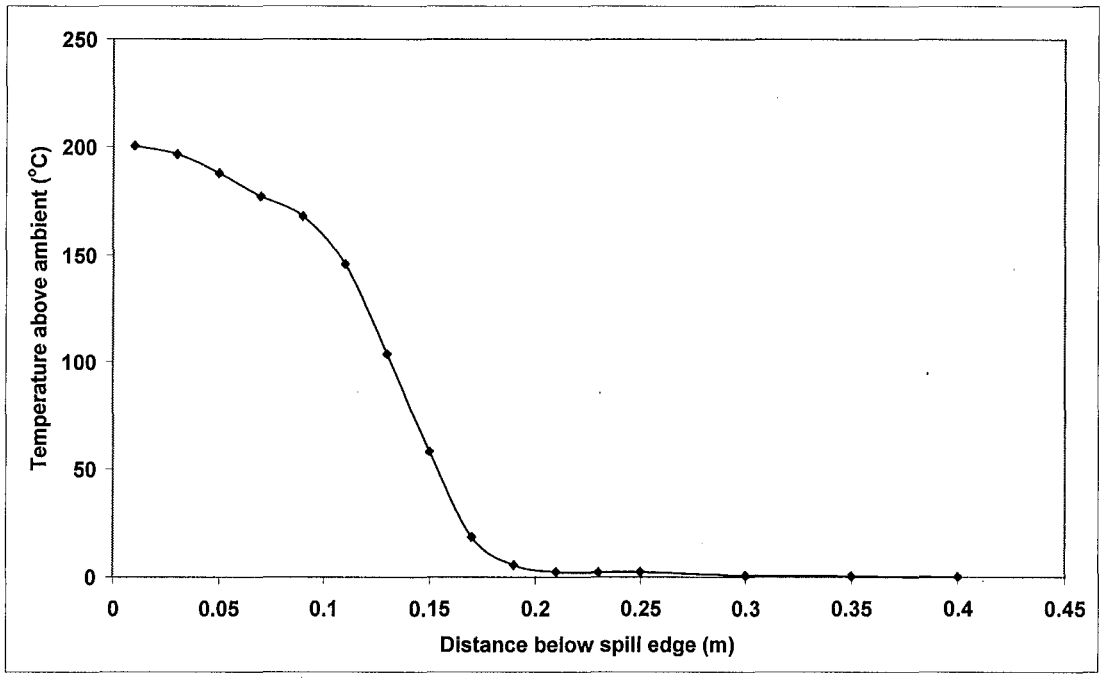

Figure E11: Temperature profile at spill edge for Test 6

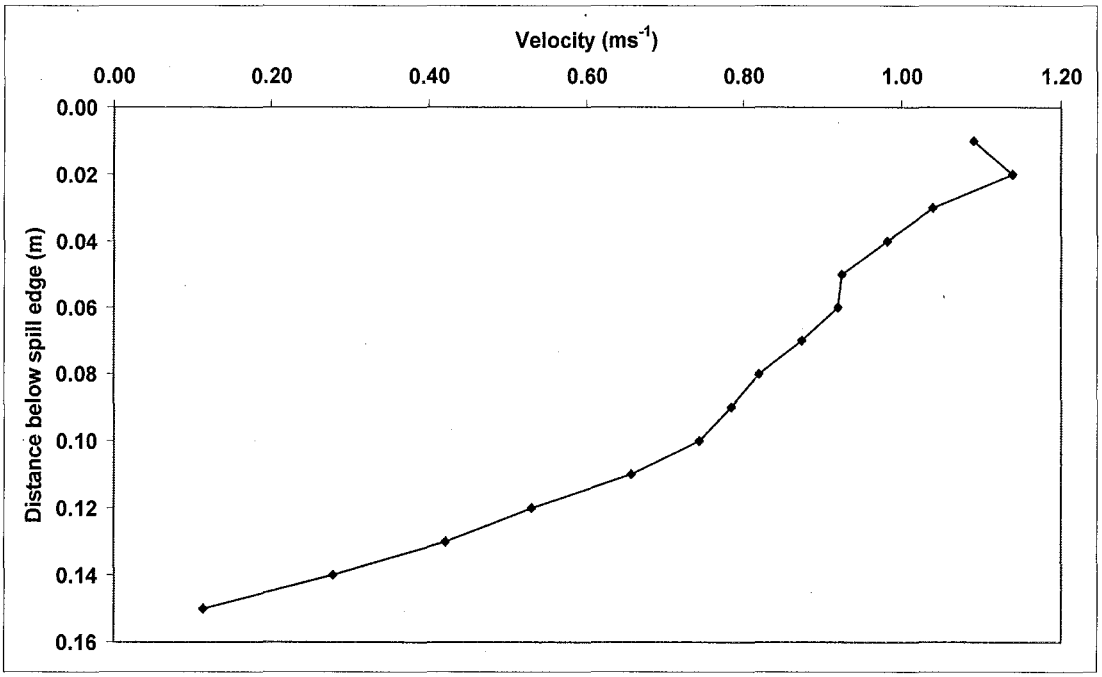

Figure E12: Velocity profile at spill edge for Test 6

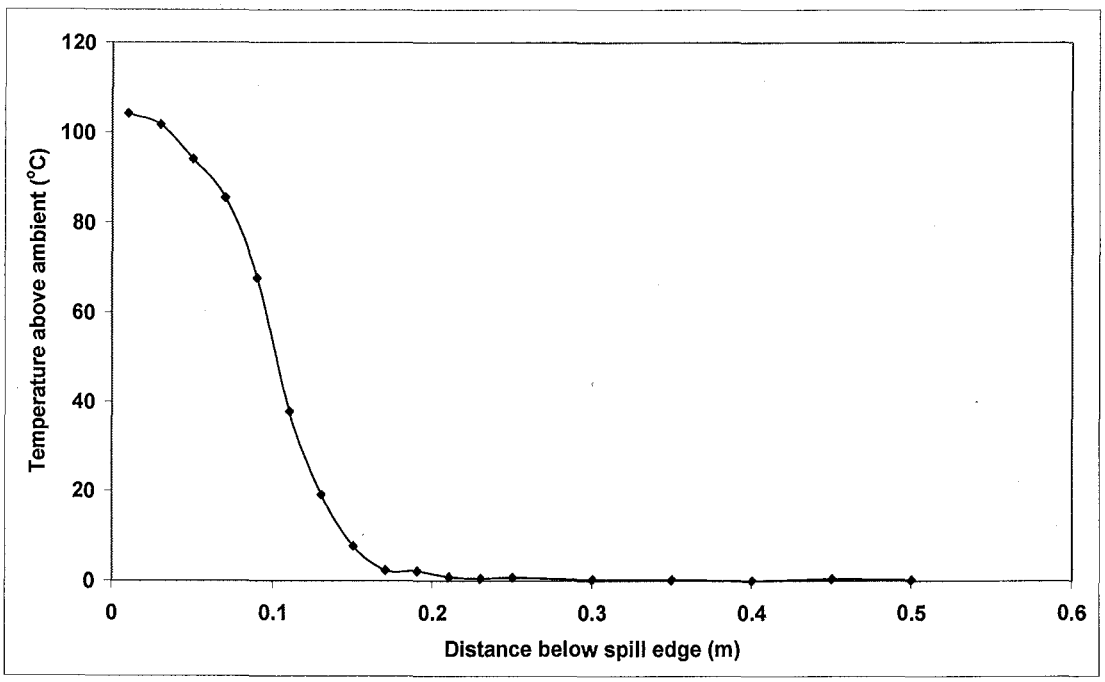

Figure E13: **Temperature profile at spill edge for Test 7**

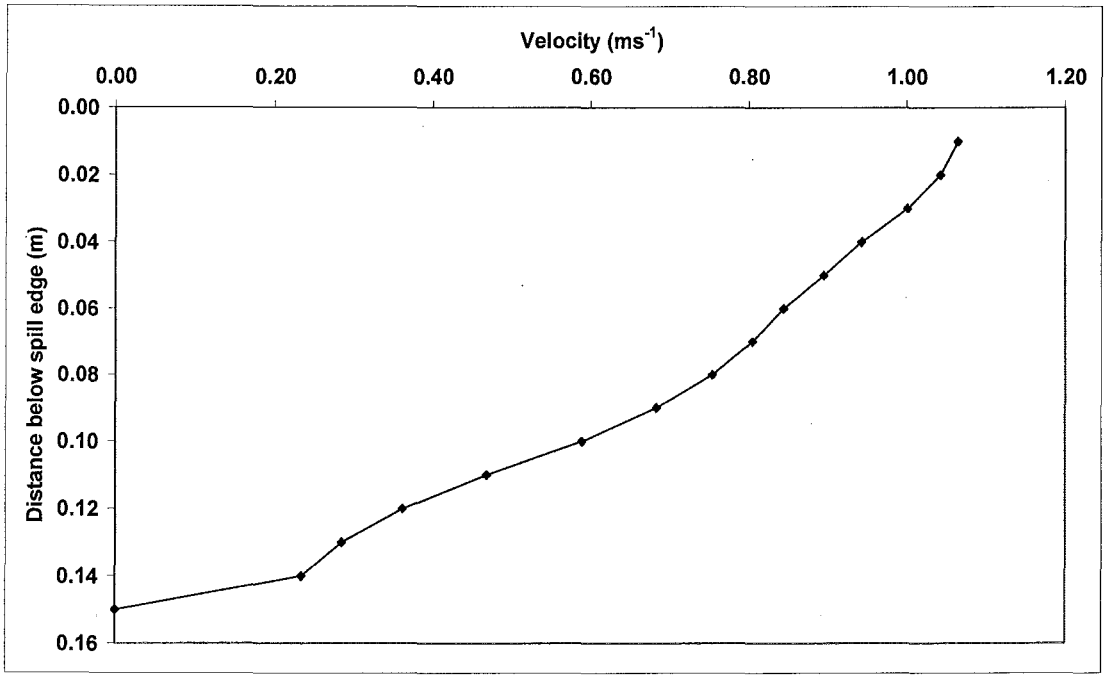

Figure E14: **Velocity profile at spill edge for Test 7**

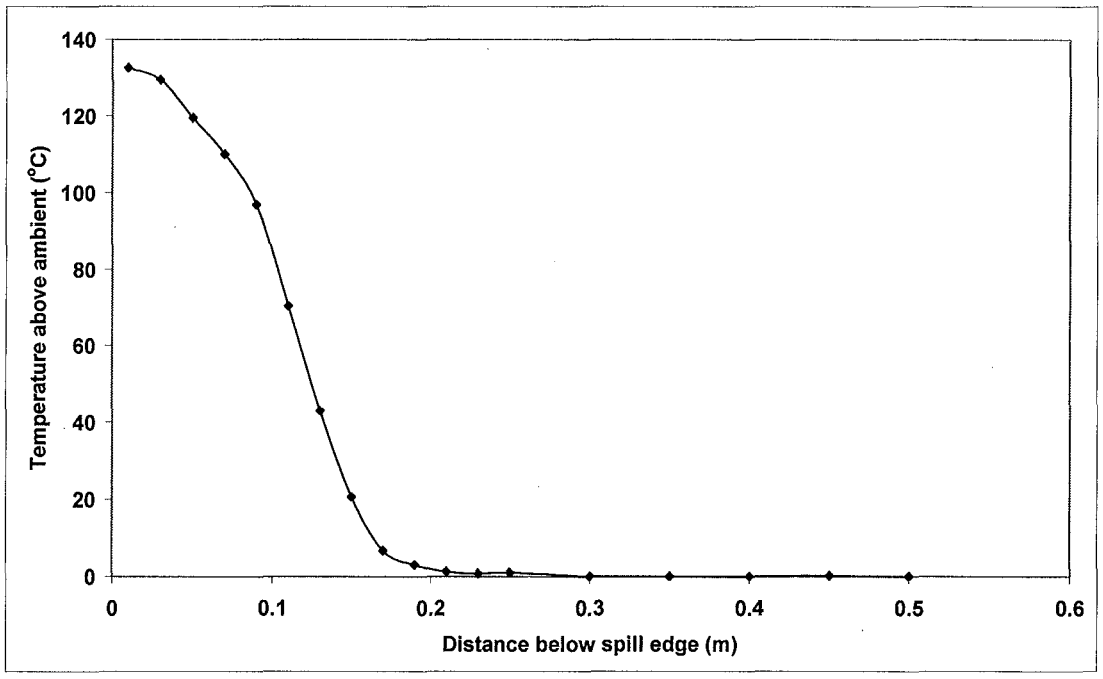

Figure E15: Temperature profile at spill edge for Test 8

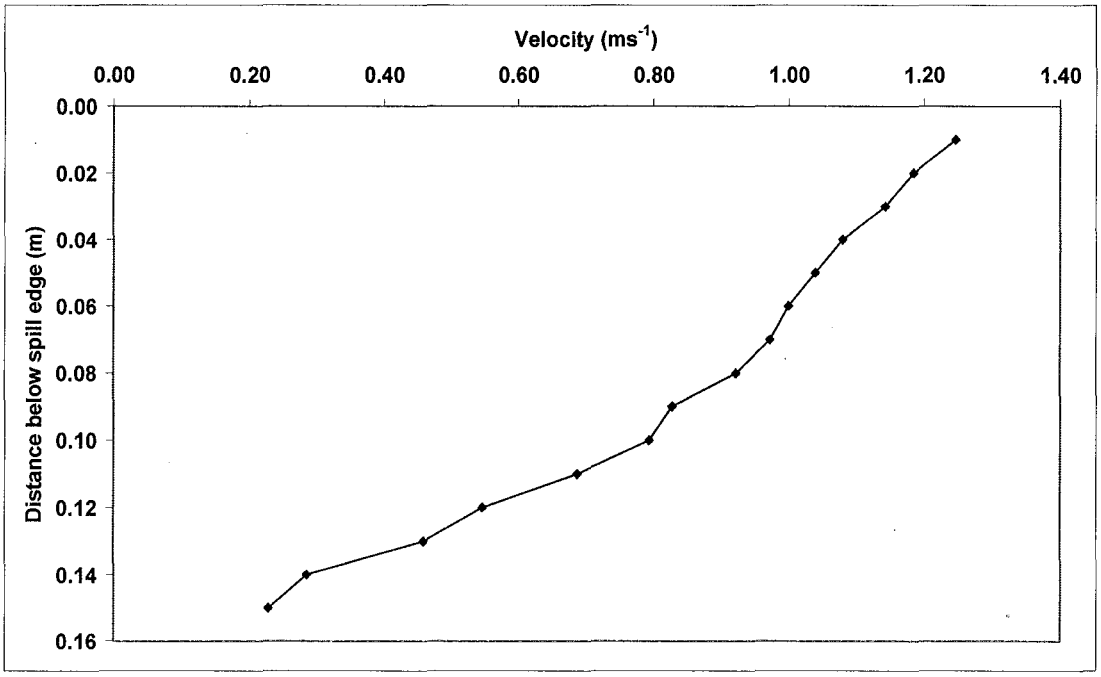

Figure E16: Velocity profile at spill edge for Test 8

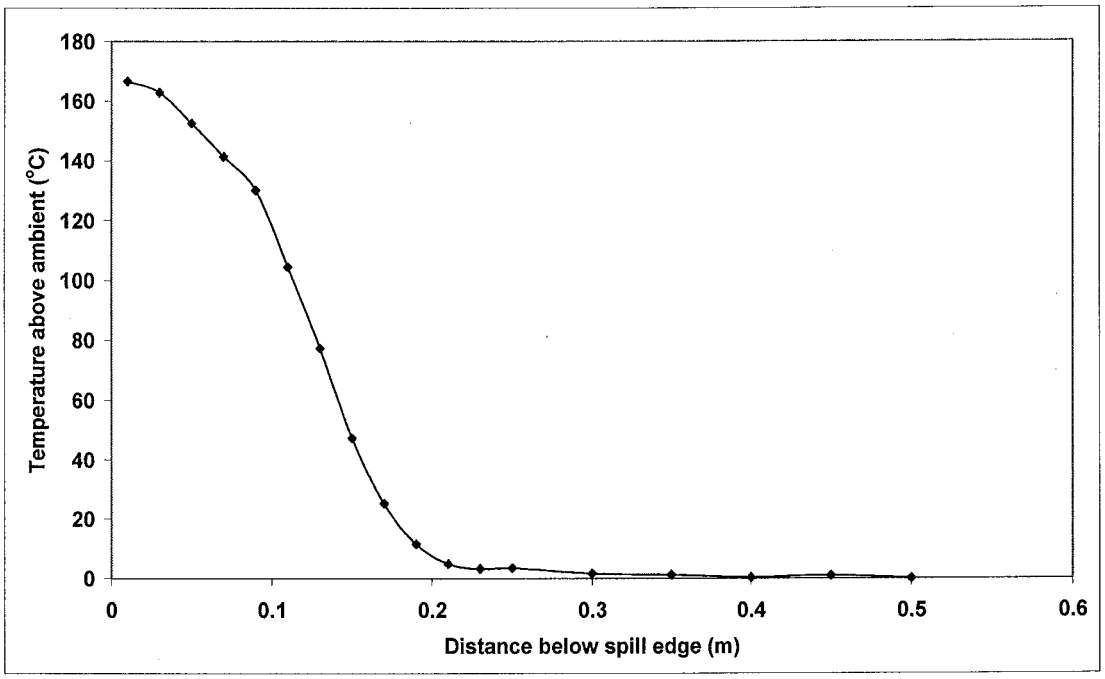

Figure E17: Temperature profile at spill edge for Test 9

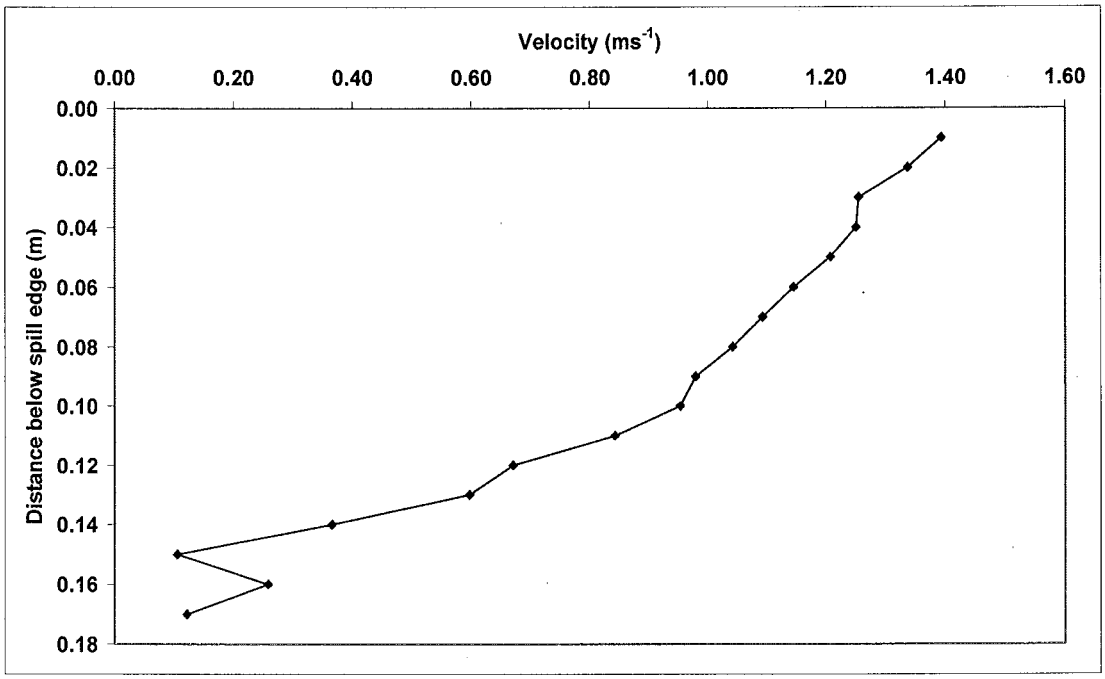

Figure E18: Velocity profile at spill edge for Test 9

Appendix E

APPENDIX F EXPERIMENTAL TEMPERATURE PROFILES IN THE SMOKE EXHAUST HOOD (TESTS 10 TO 64)

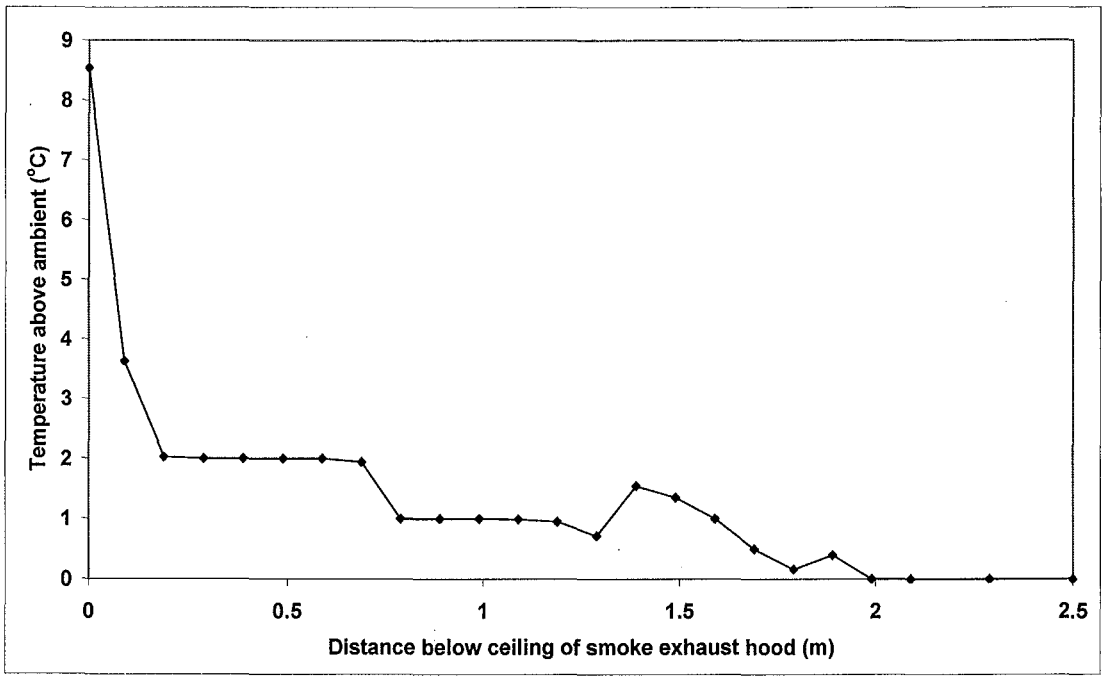

Figure F1: Temperature profile in smoke exhaust hood for Test 10

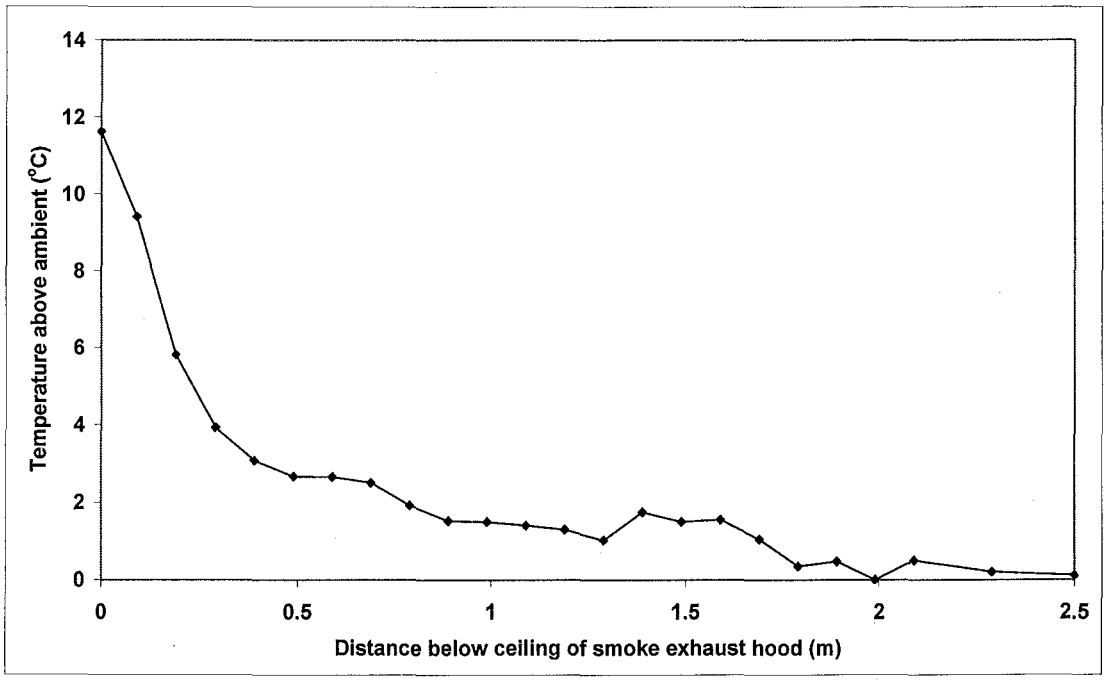

Figure F2: Temperature profile in smoke exhaust hood for Test 11

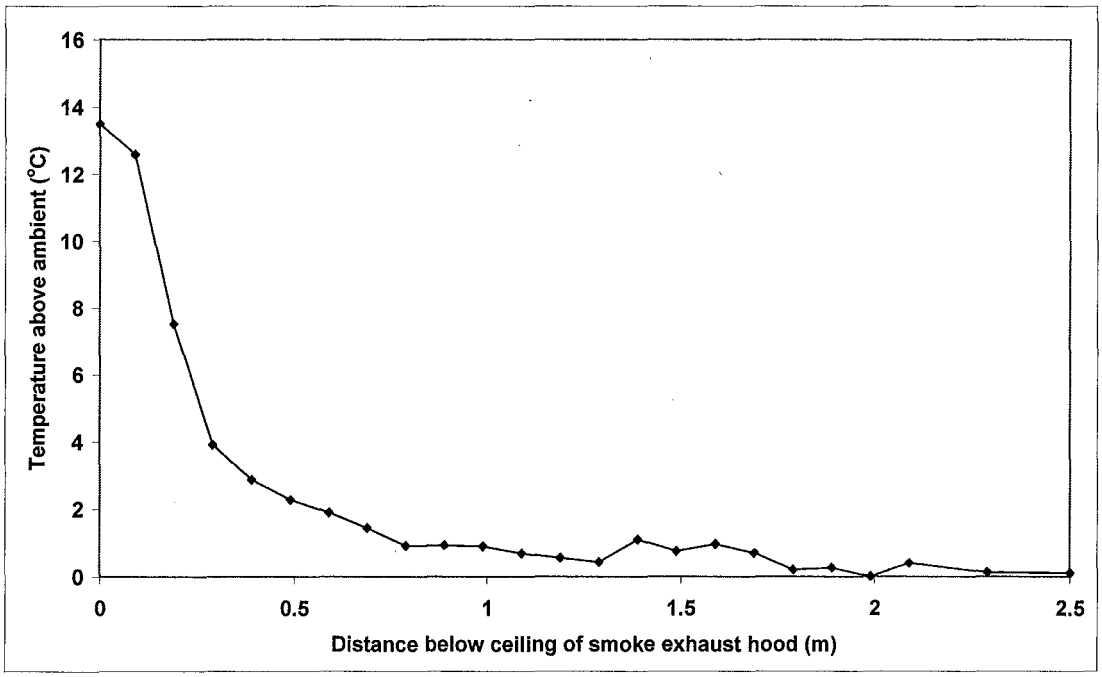

Figure F3: **Temperature profile in smoke exhaust hood for Test 12**

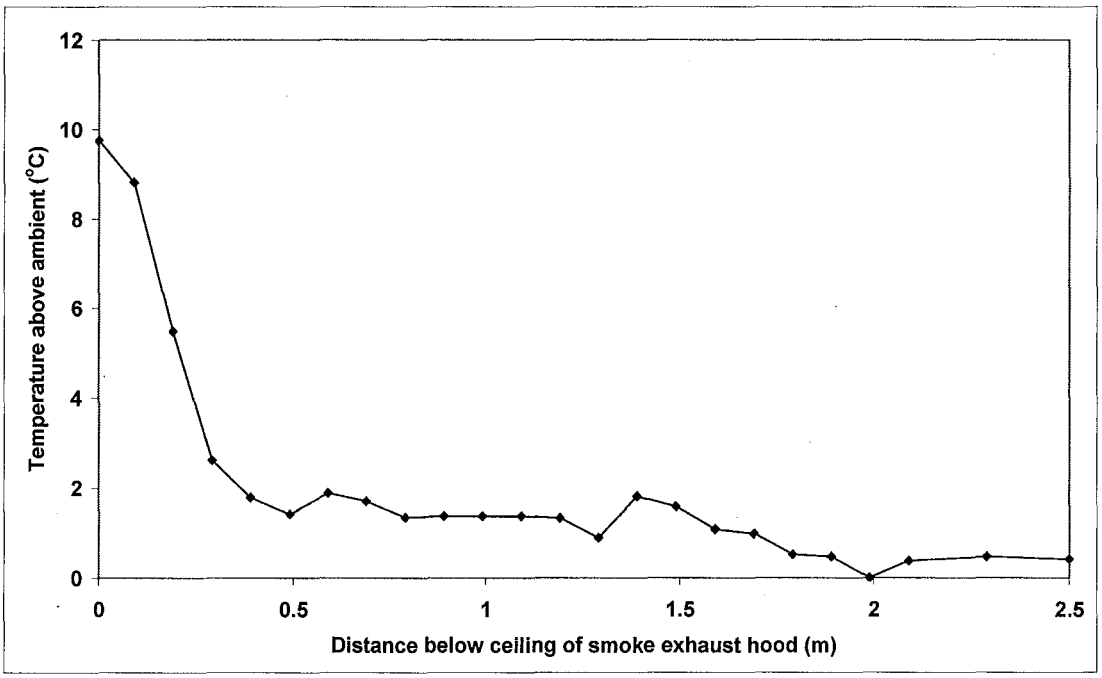

Figure F4: **Temperature profile in smoke exhaust hood for Test 13**

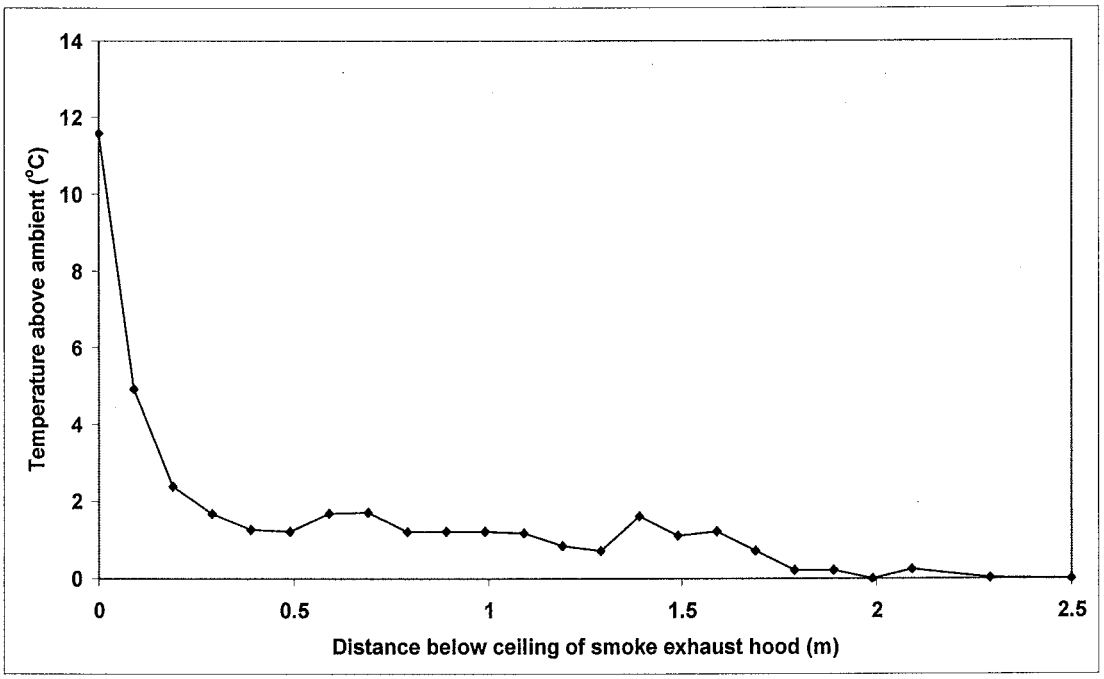

Figure F5: **Temperature profile in smoke exhaust hood for Test 14**

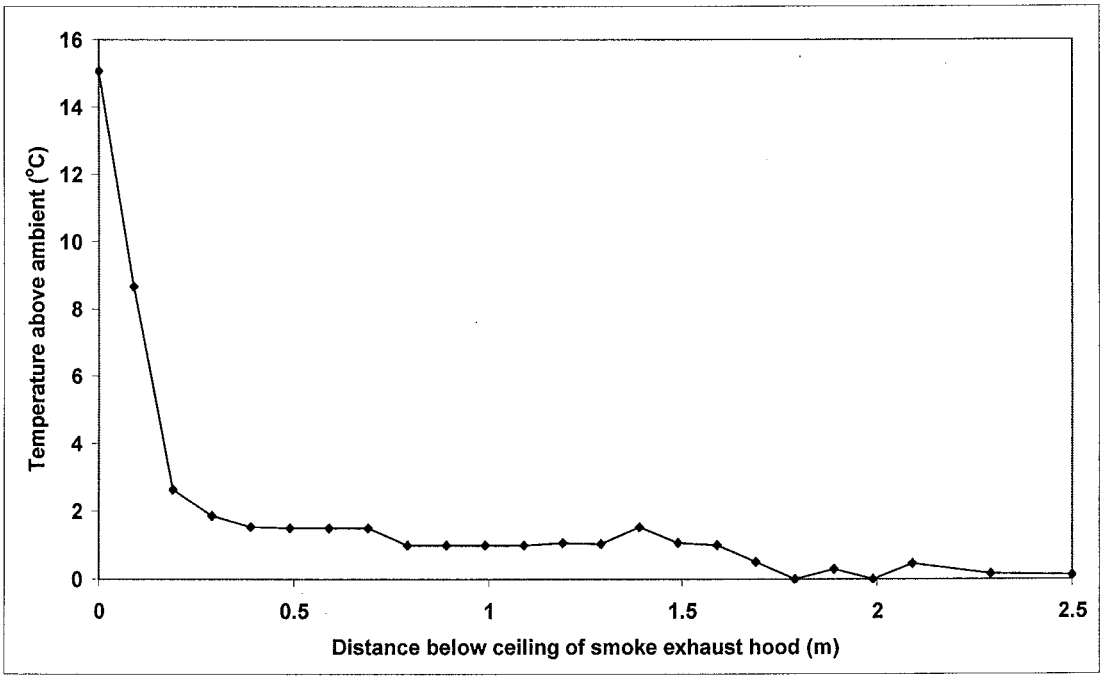

Figure F6: **Temperature profile in smoke exhaust hood for Test 15**

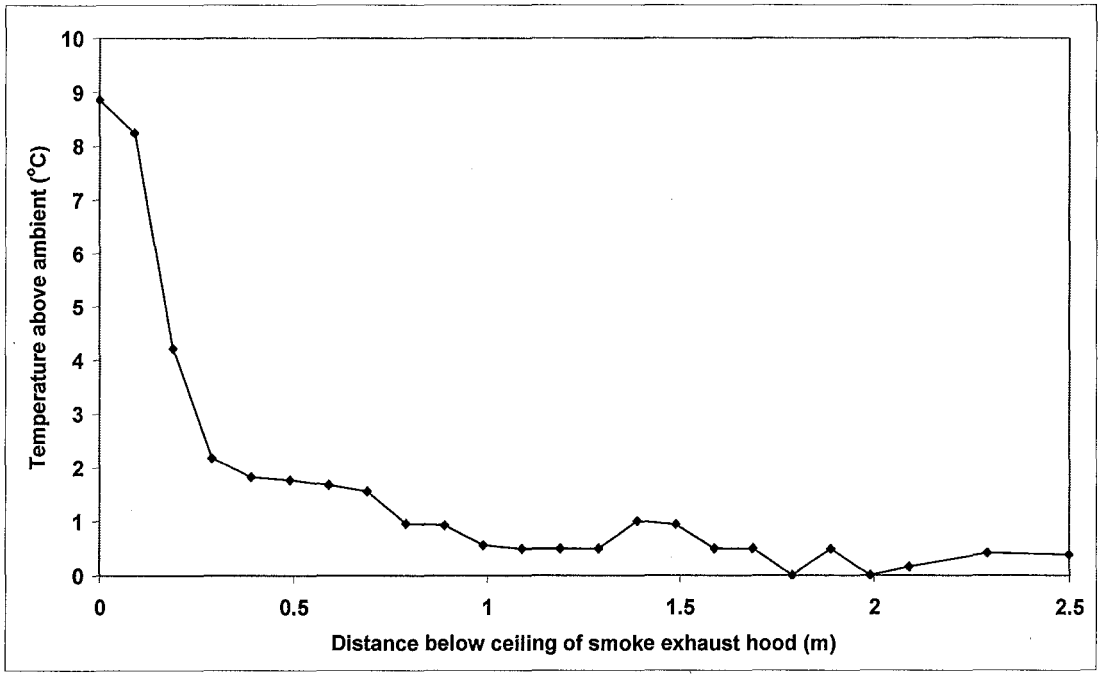

Figure F7: Temperature profile in smoke exhaust hood for Test 16

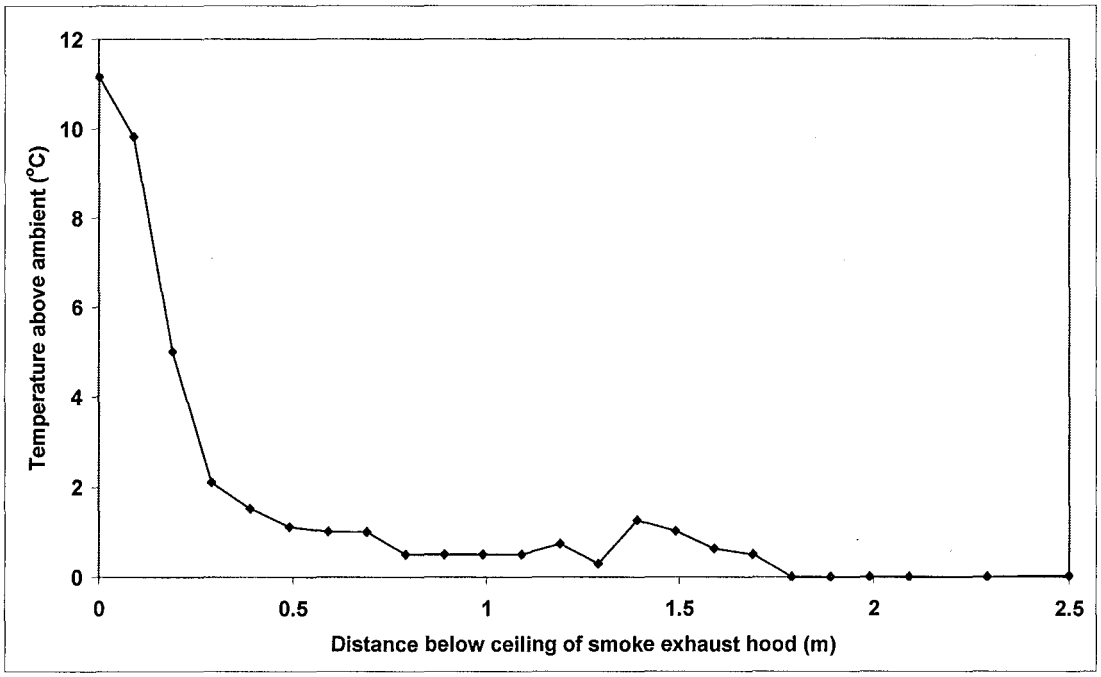

Figure F8: Temperature profile in smoke exhaust hood for Test 17

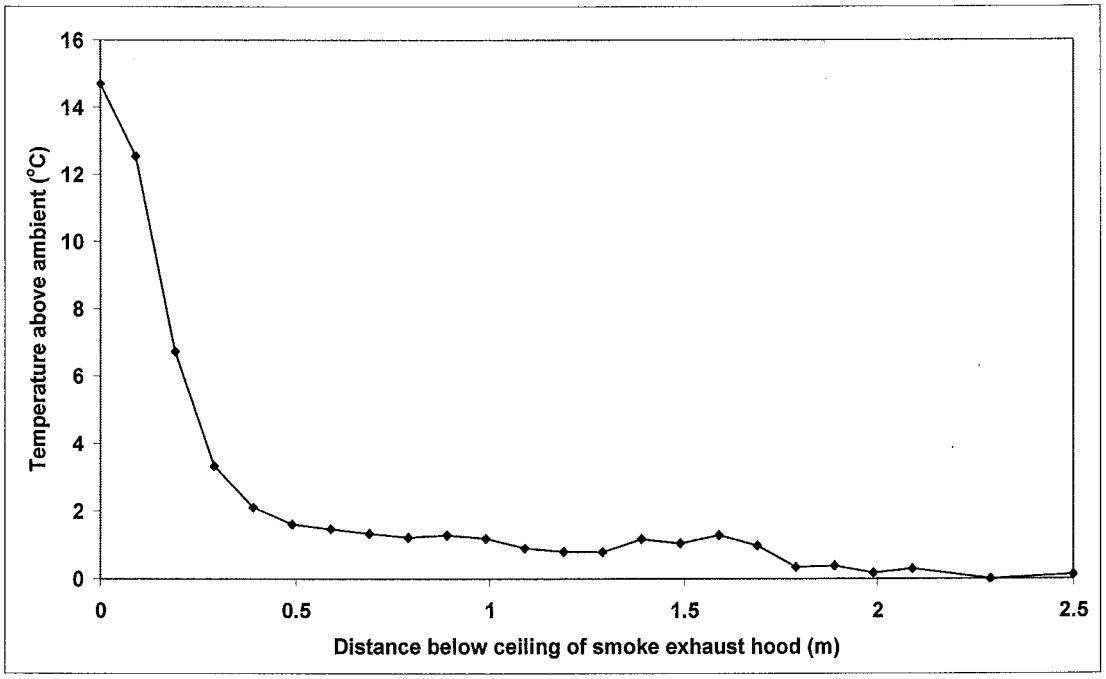

Figure F9: **Temperature profile in smoke exhaust hood for Test 18**

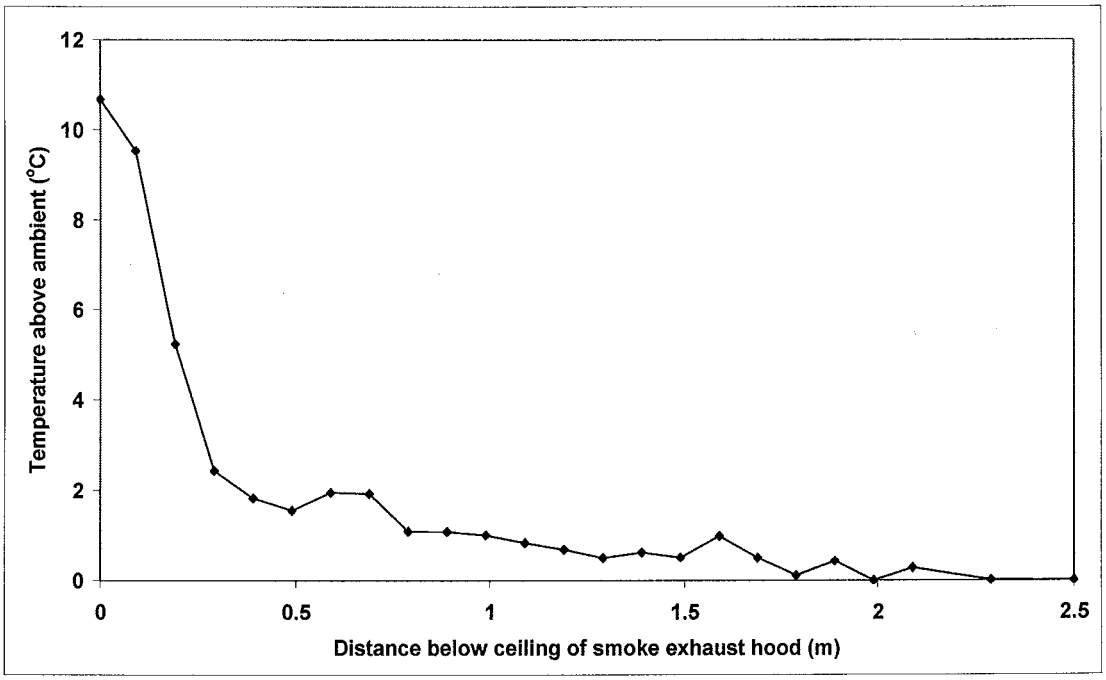

Figure F10: **Temperature profile in smoke exhaust hood for Test 19**

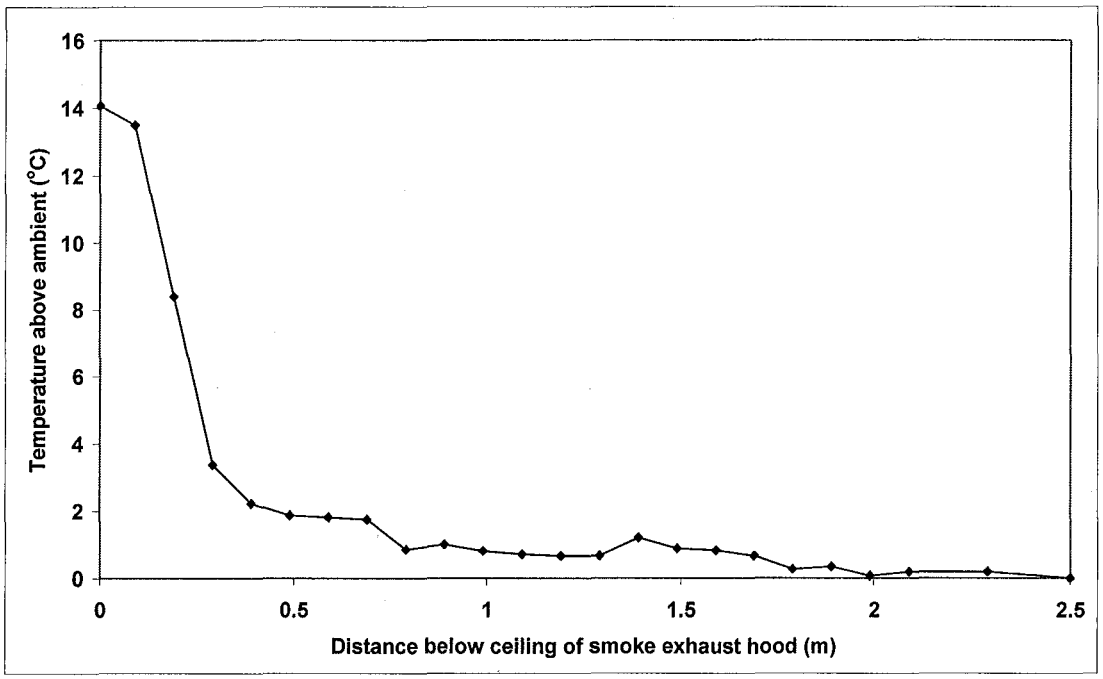

Figure F11: Temperature profile in smoke exhaust hood for Test 20

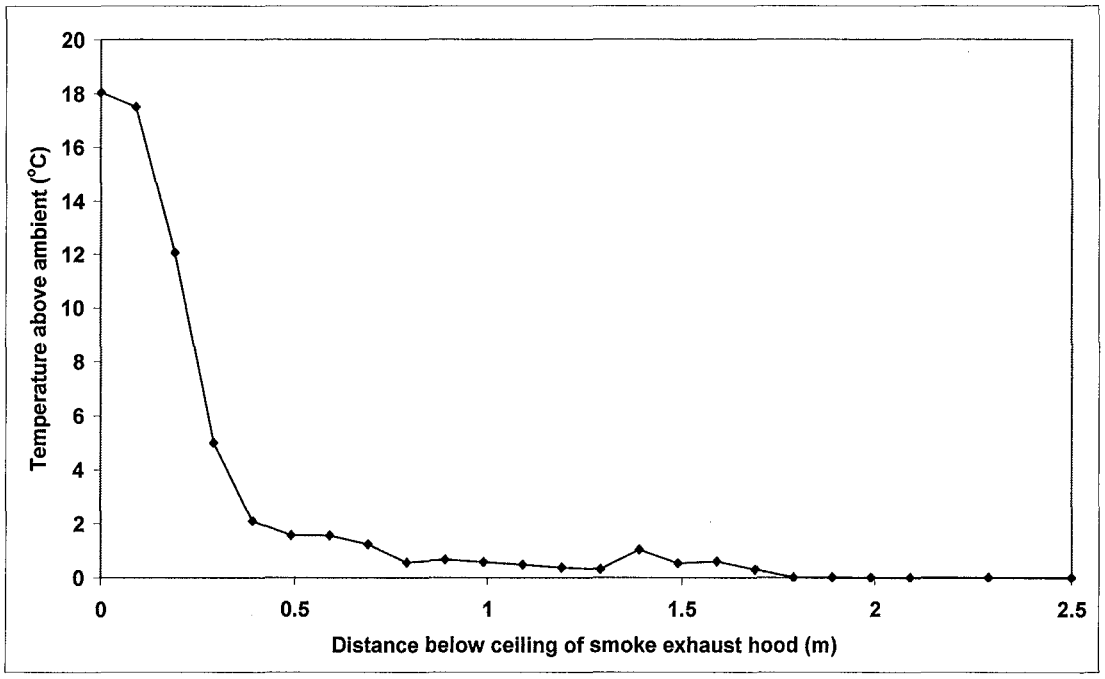

Figure F12: Temperature profile in smoke exhaust hood for Test 21

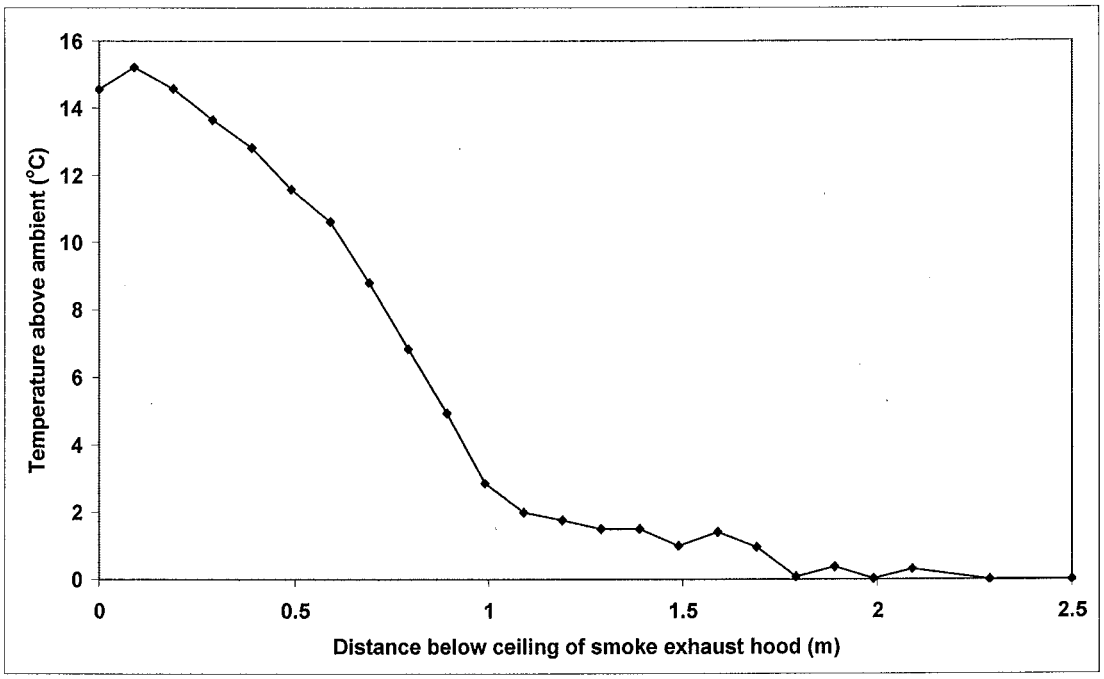

Figure F13: Temperature profile in smoke exhaust hood for Test 22

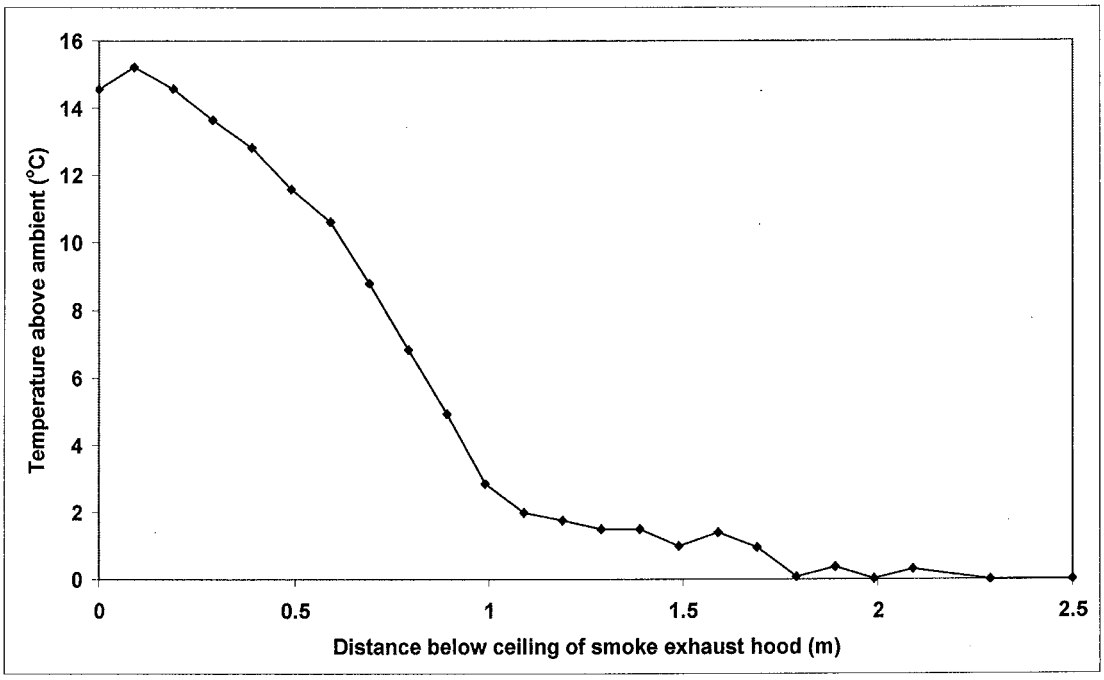

Figure F14: Temperature profile in smoke exhaust hood for Test 23

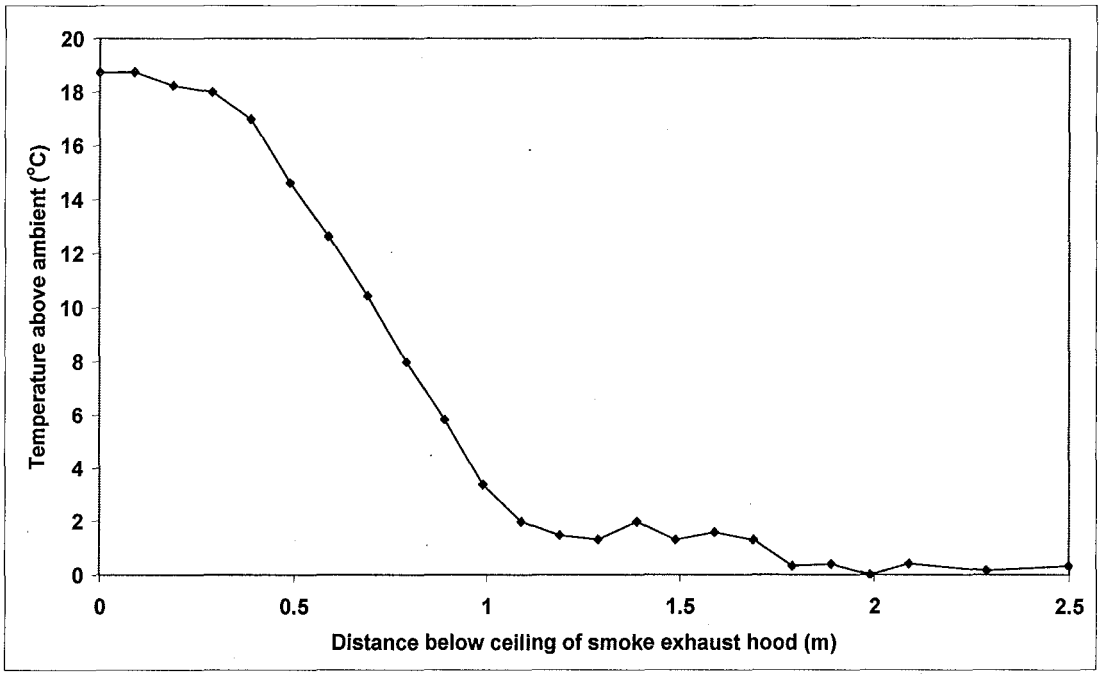

Figure F15: Temperature profile in smoke exhaust hood for Test 24

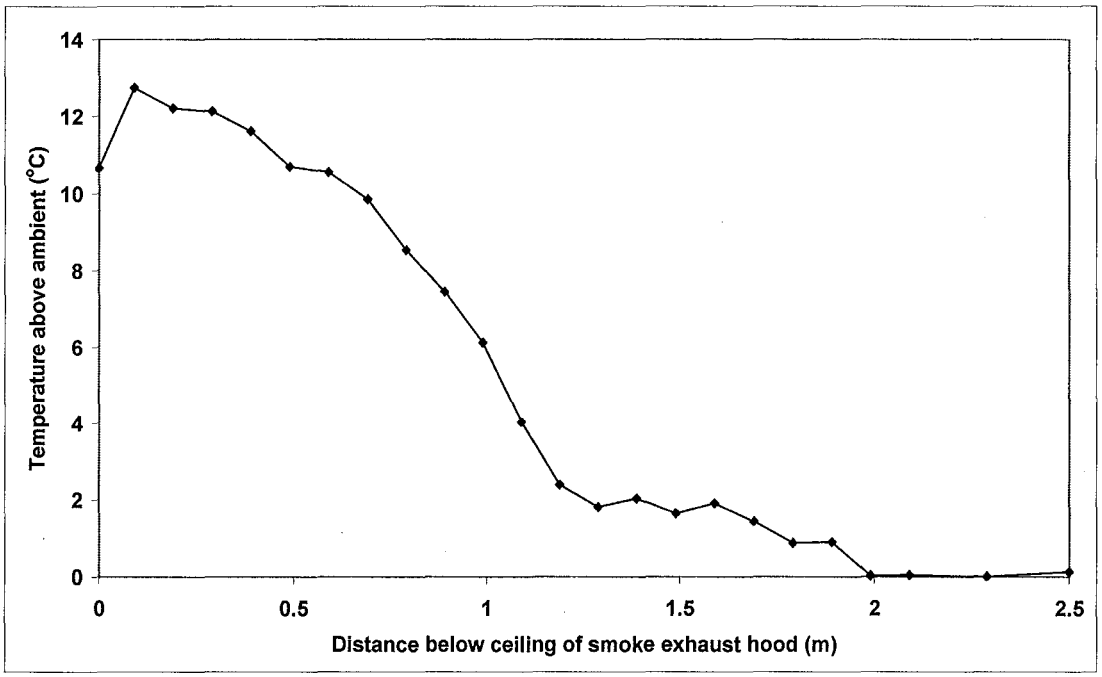

Figure F16: Temperature profile in smoke exhaust hood for Test 25

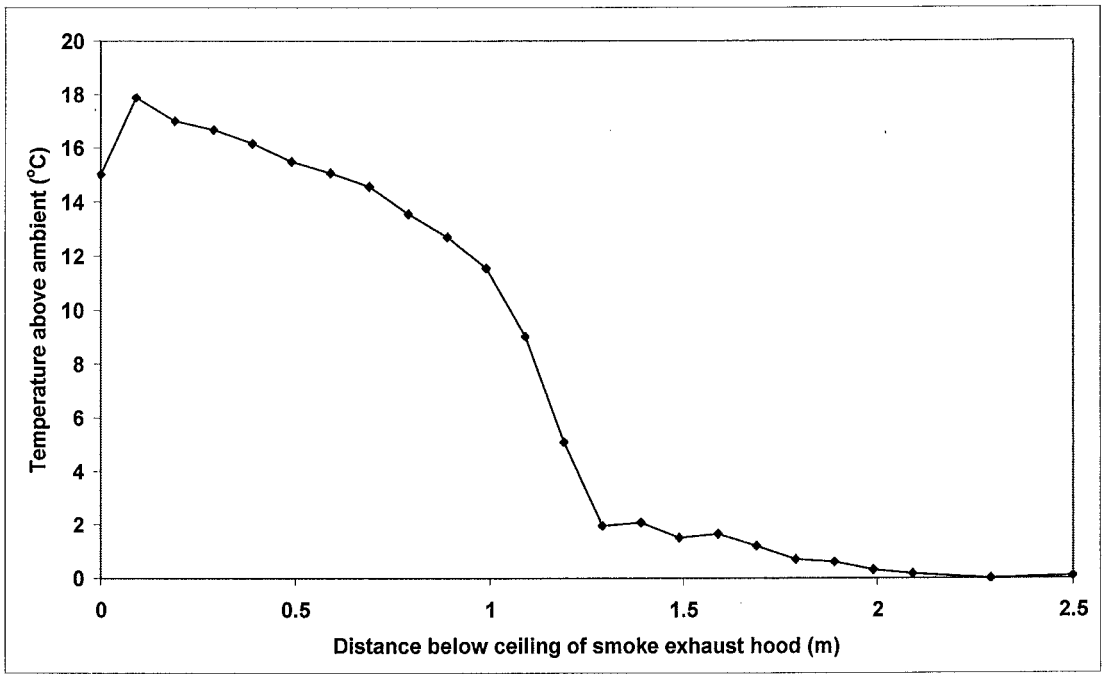

Figure F17: Temperature profile in smoke exhaust hood for Test 26

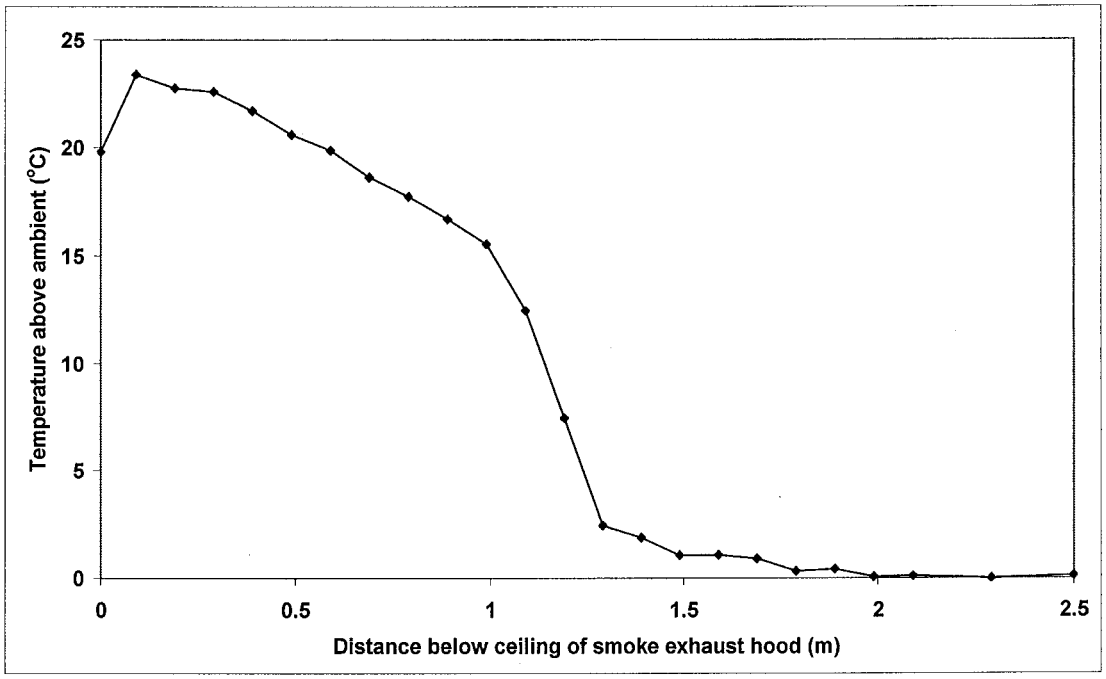

Figure F18: Temperature profile in smoke exhaust hood for Test 27

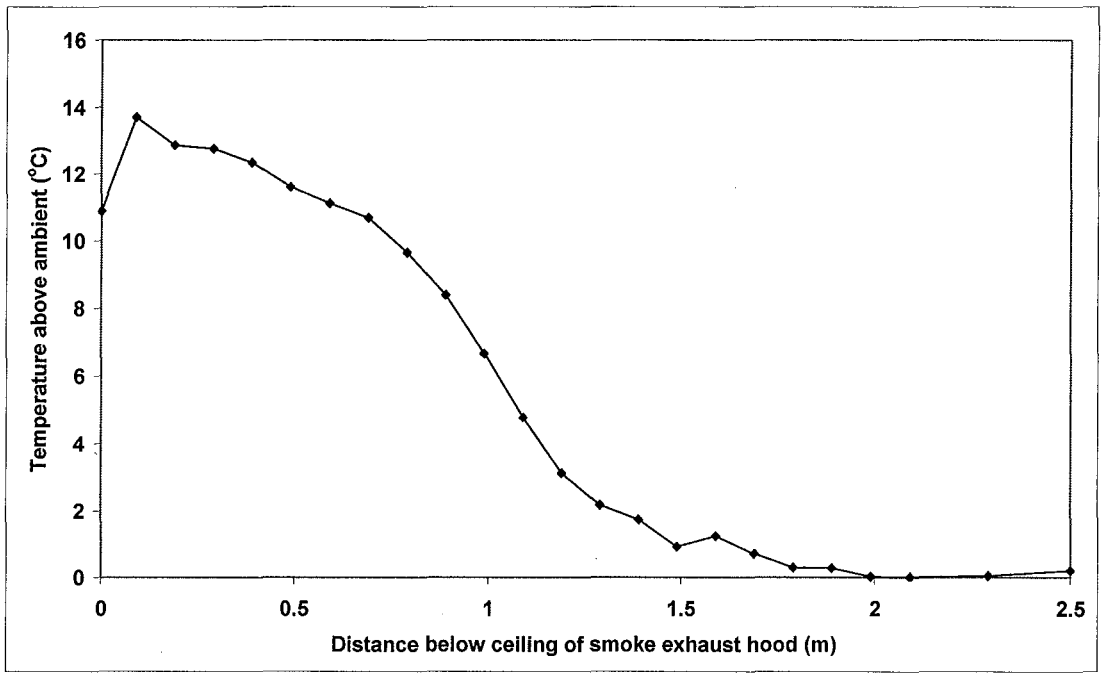

Figure F19: Temperature profile in smoke exhaust hood for Test 28

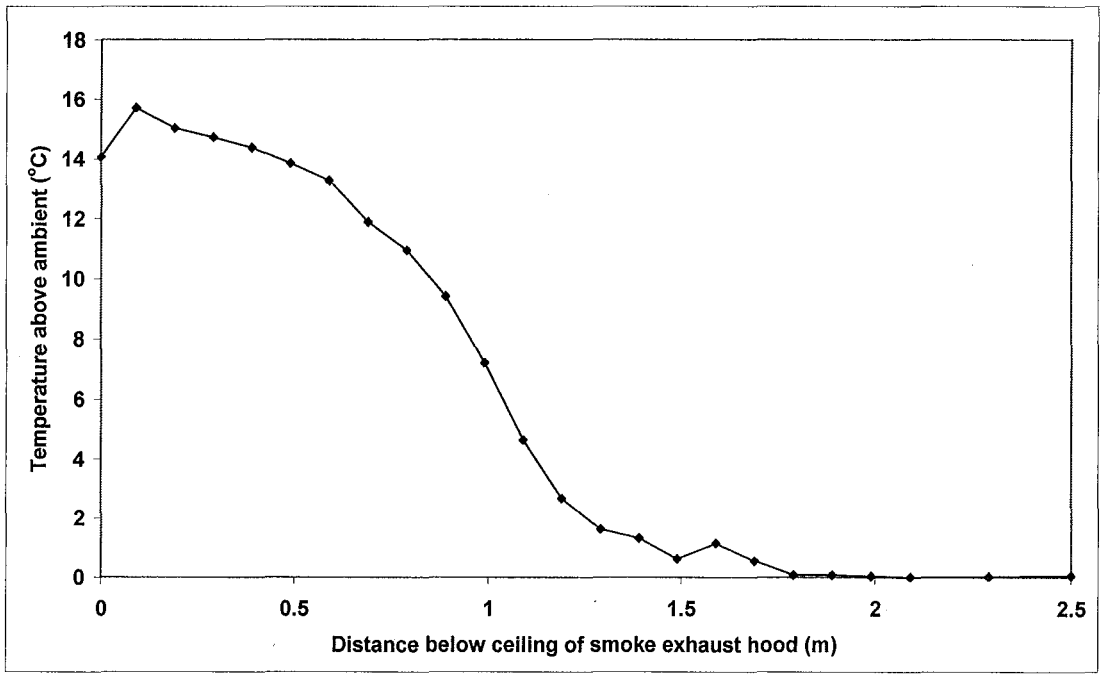

Figure F20: Temperature profile in smoke exhaust hood for Test 29

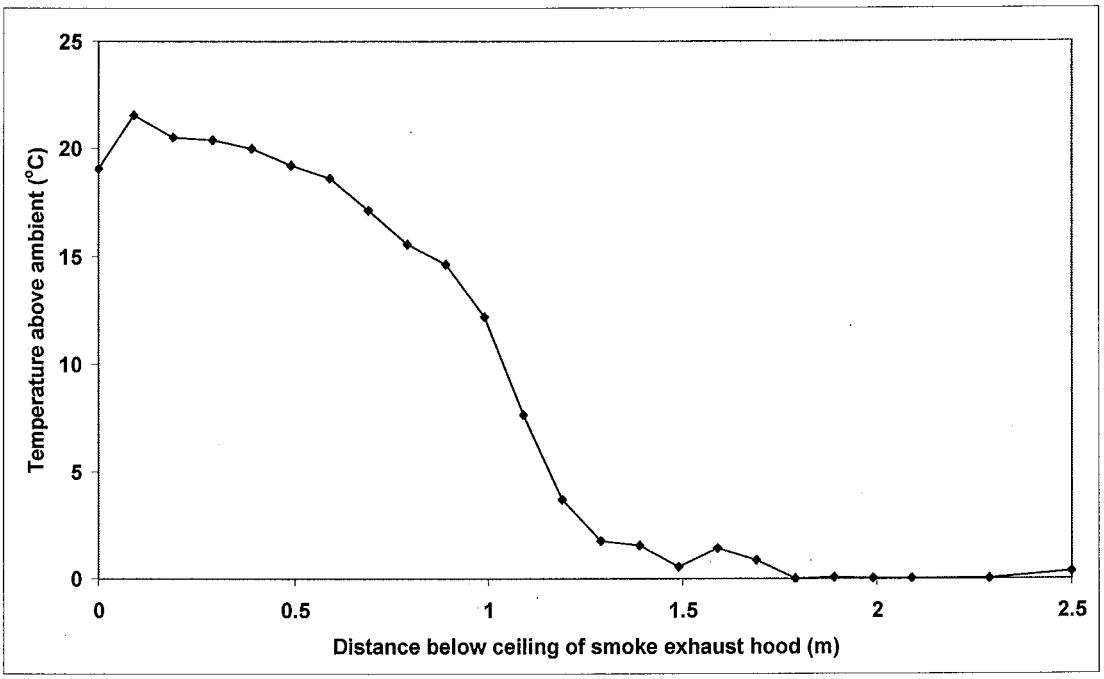

Figure F21: Temperature profile in smoke exhaust hood for Test 30

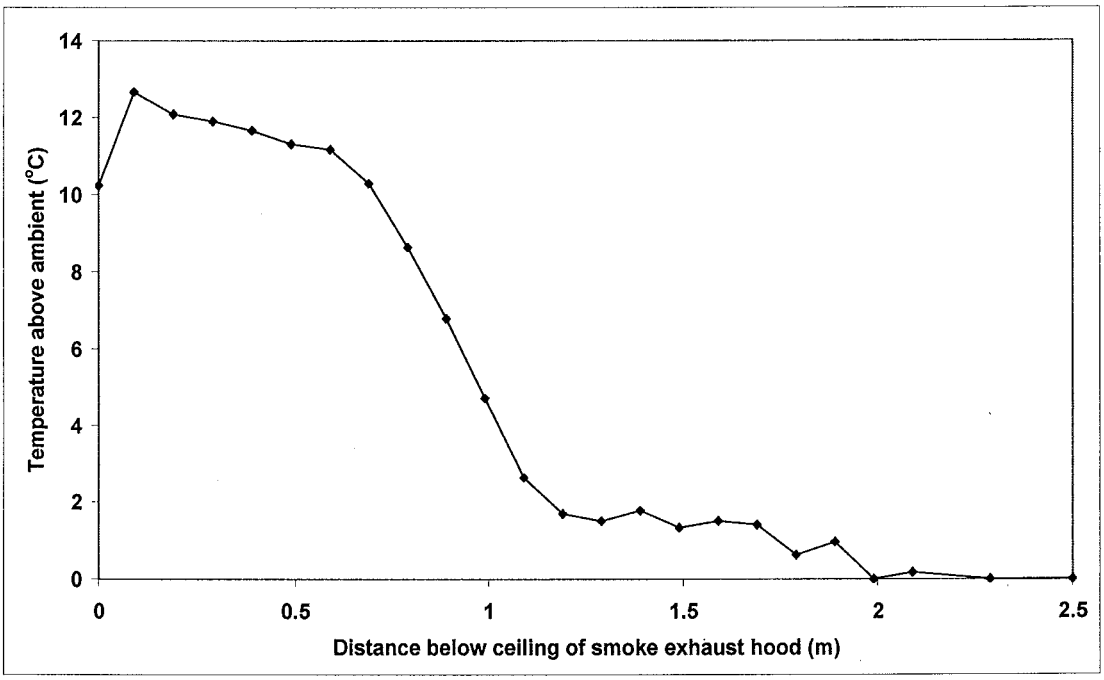

Figure F22: Temperature profile in smoke exhaust hood for Test 31

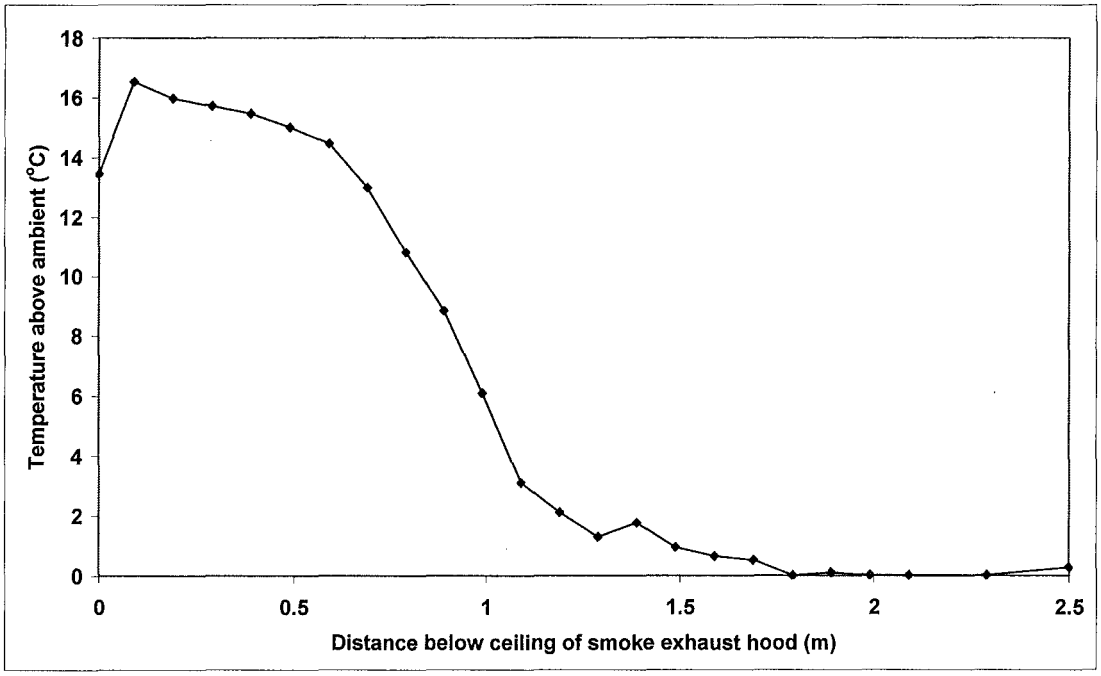

Figure F23: Temperature profile in smoke exhaust hood for Test 32

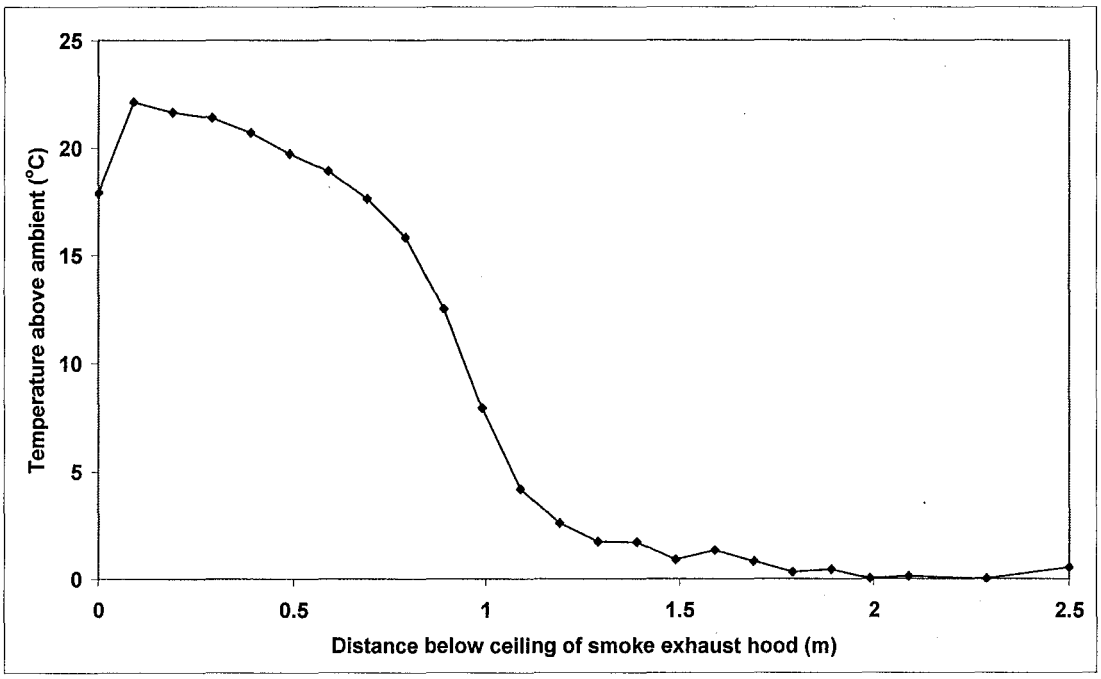

Figure F24: Temperature profile in smoke exhaust hood for Test 33

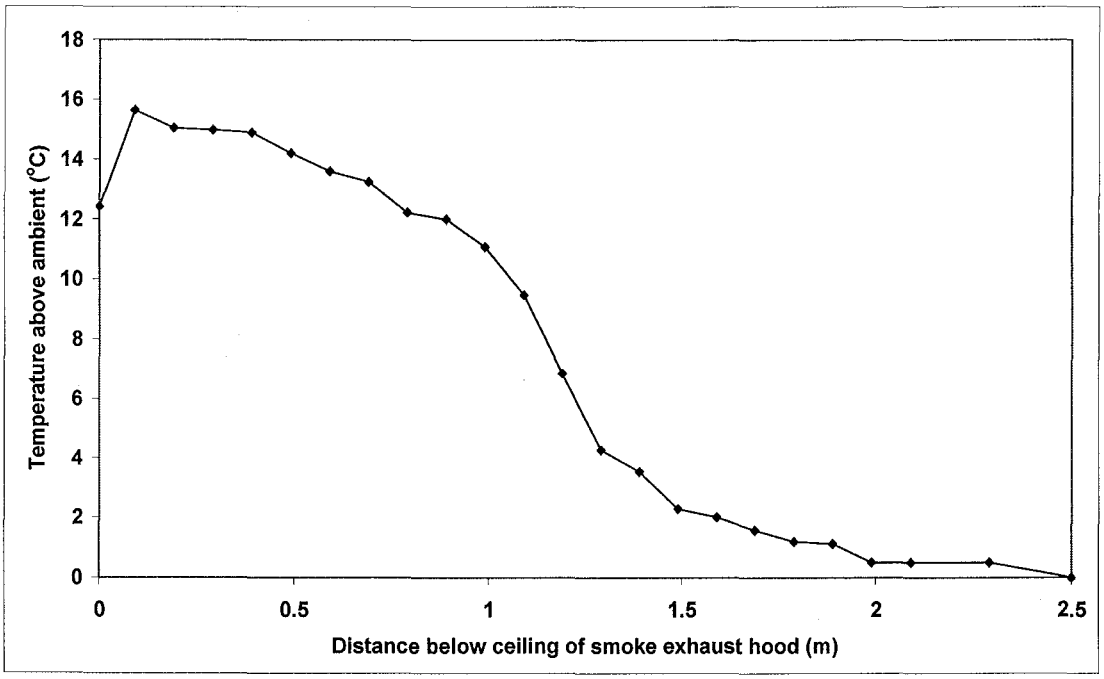

Figure F25: **Temperature profile in smoke exhaust hood for Test 34**

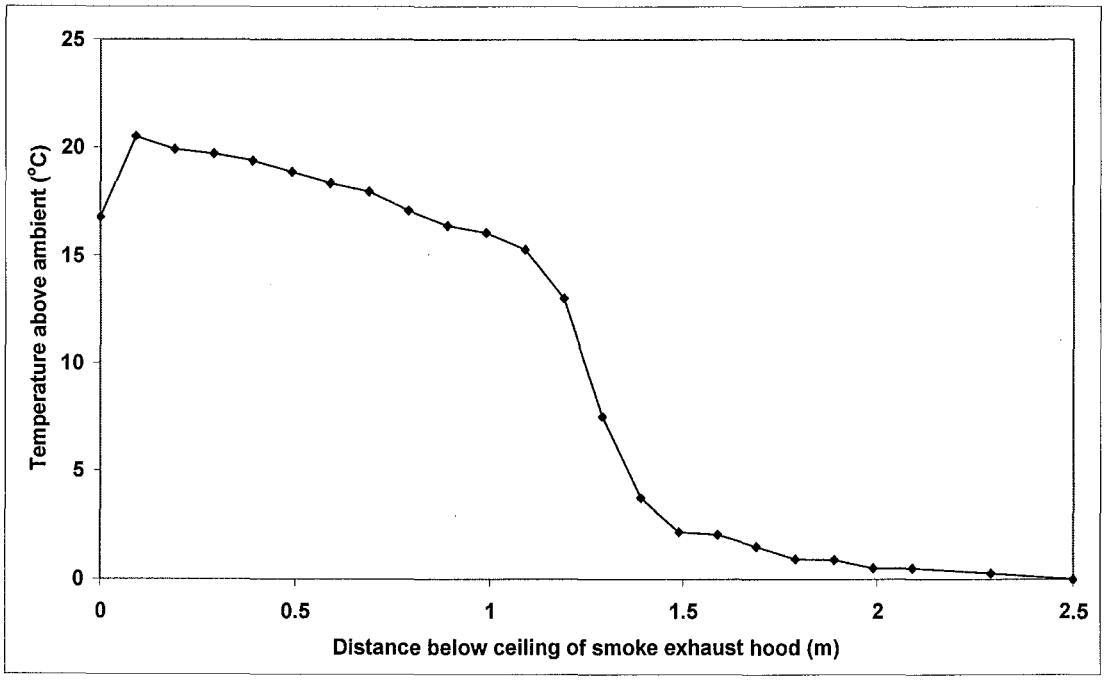

Figure F26: **Temperature profile in smoke exhaust hood for Test 35**

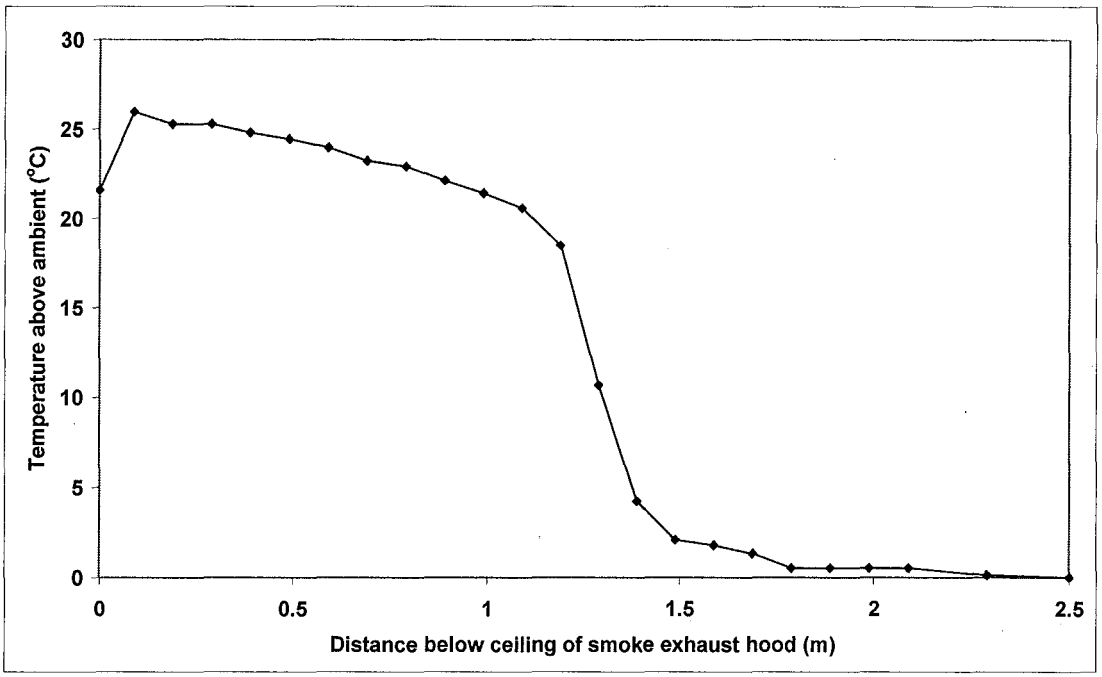

Figure F27: Temperature profile in smoke exhaust hood for Test 36

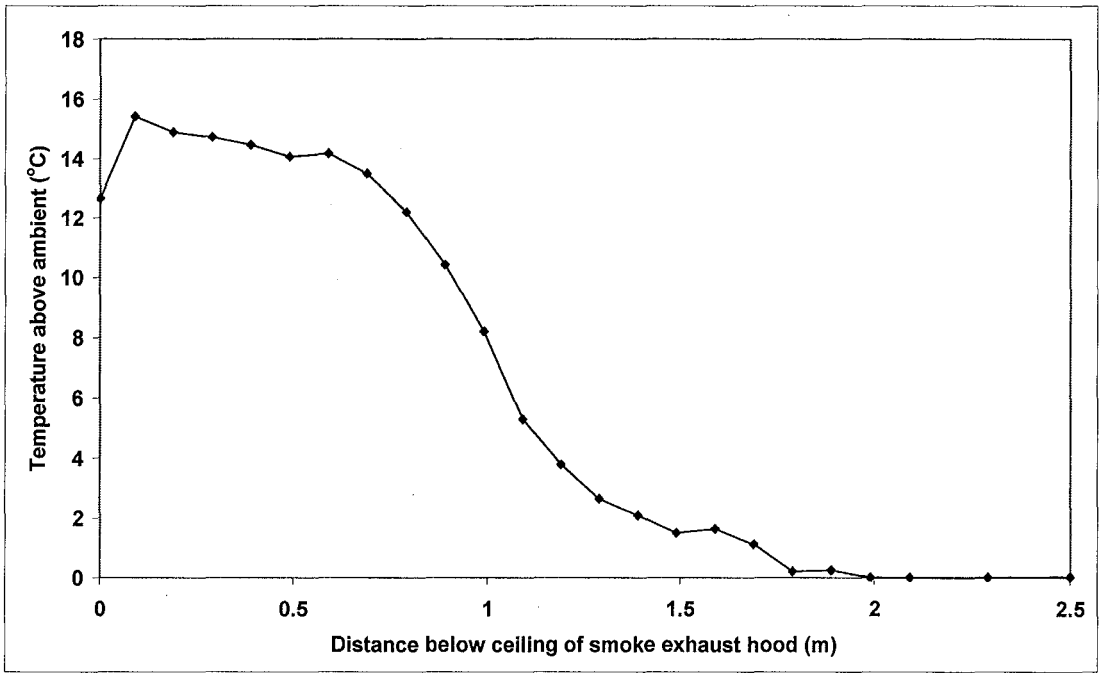

Figure F28: Temperature profile in smoke exhaust hood for Test 37

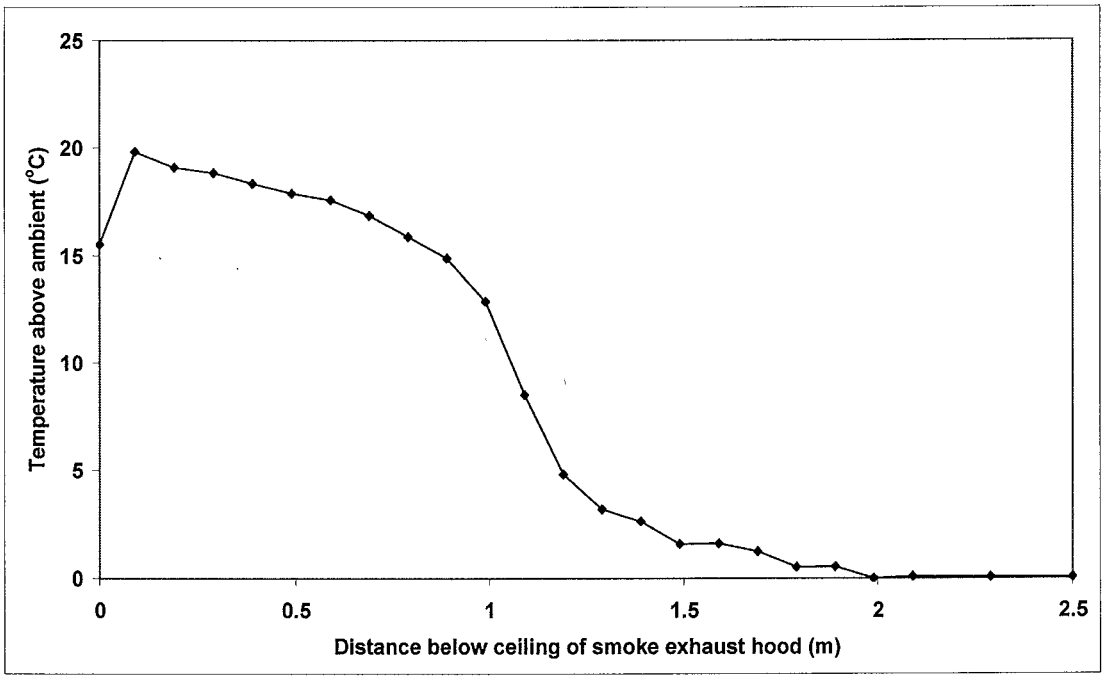

Figure F29: Temperature profile in smoke exhaust hood for Test 38

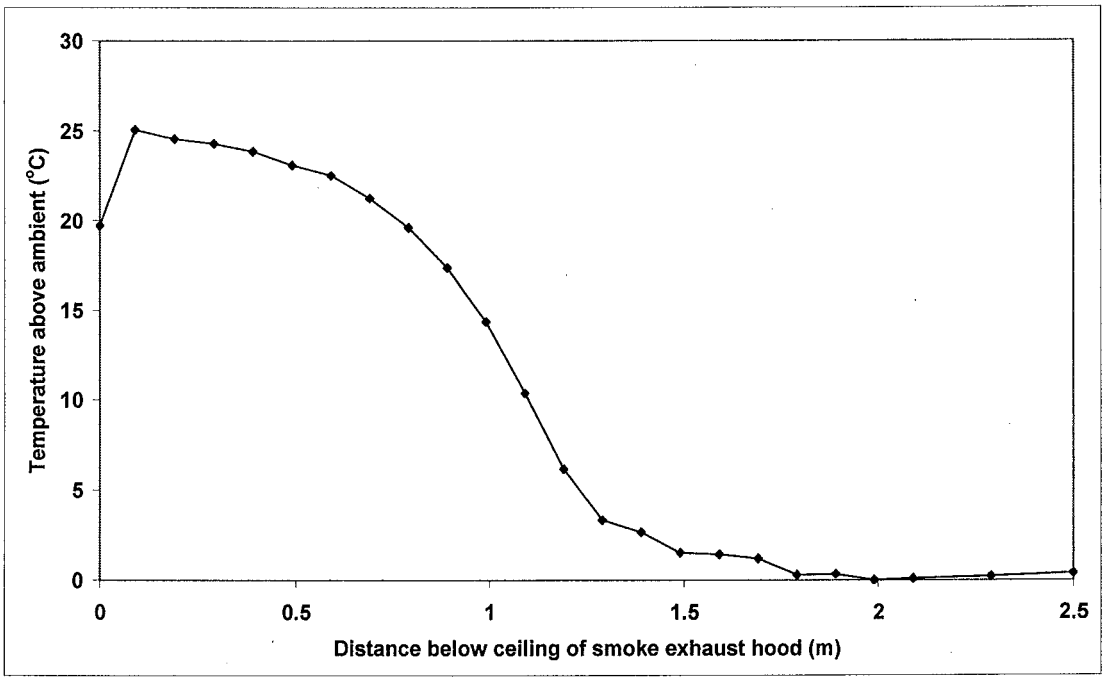

Figure F30: Temperature profile in smoke exhaust hood for Test 39

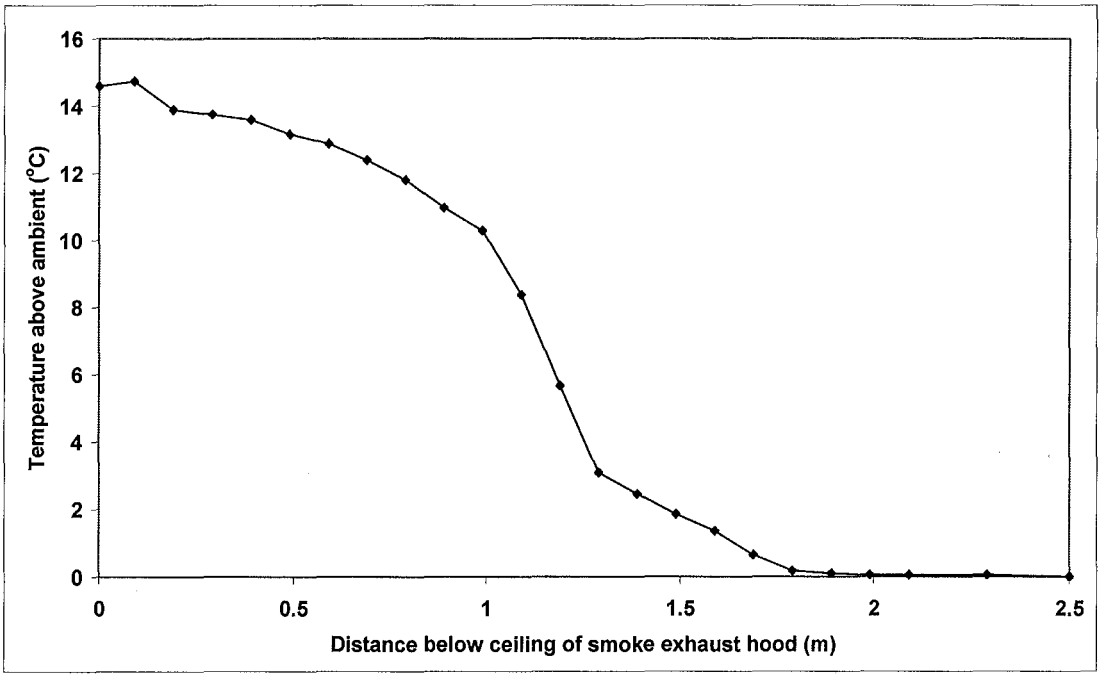

Figure F31: Temperature profile in smoke exhaust hood for Test 40

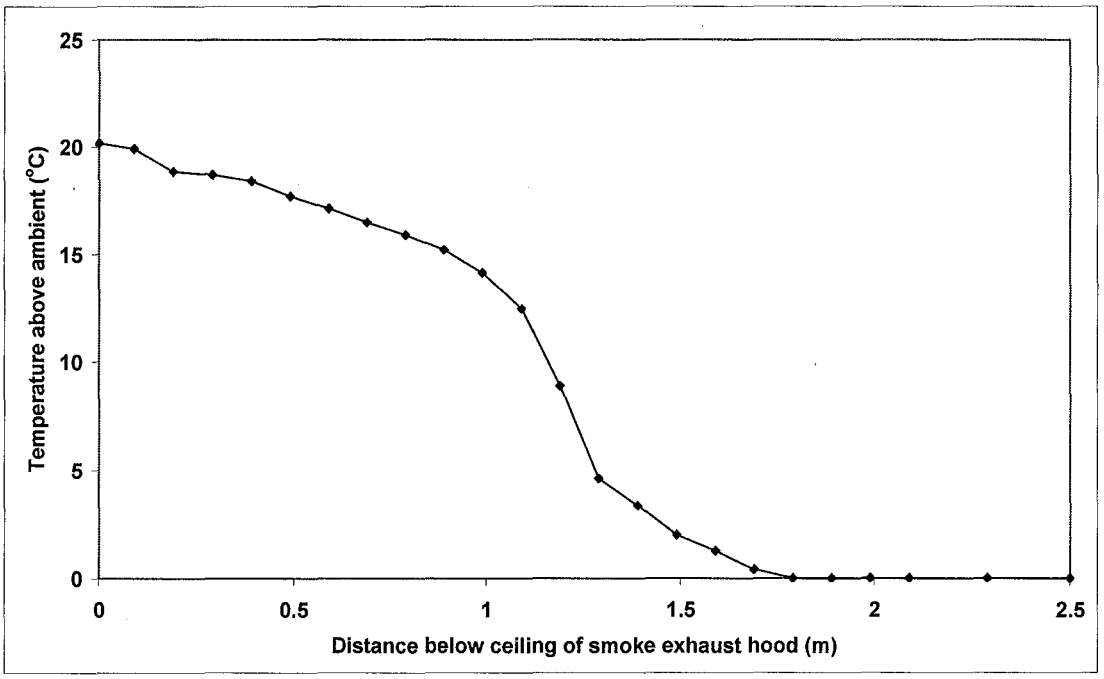

Figure F32: Temperature profile in smoke exhaust hood for Test 41

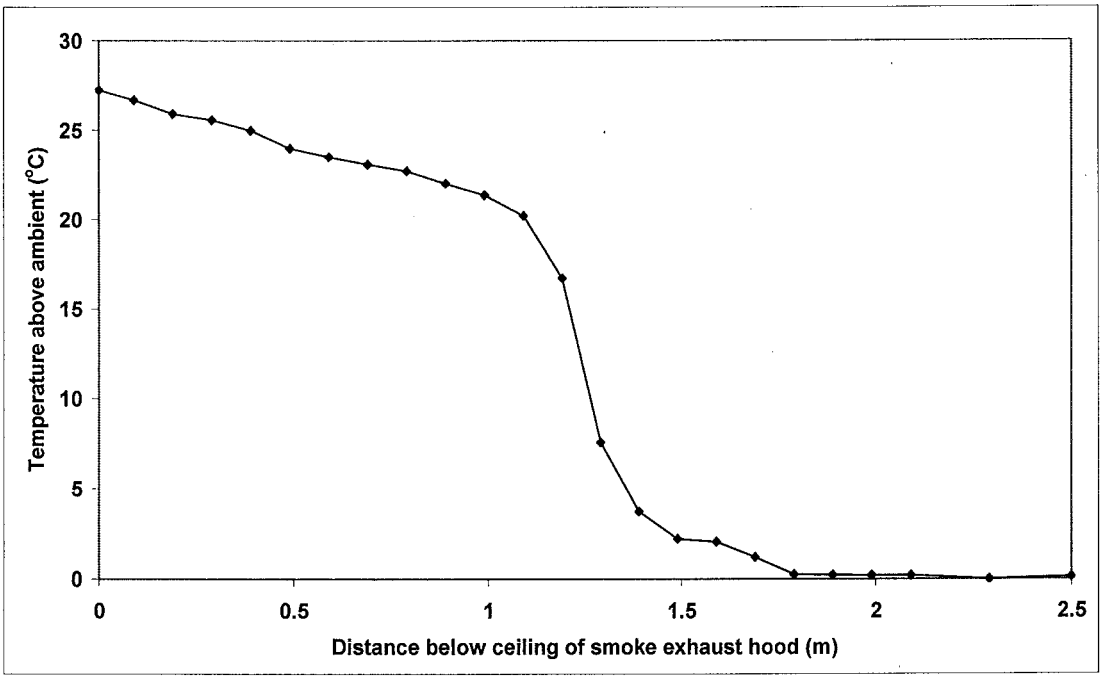

Figure F33: Temperature profile in smoke exhaust hood for Test 42

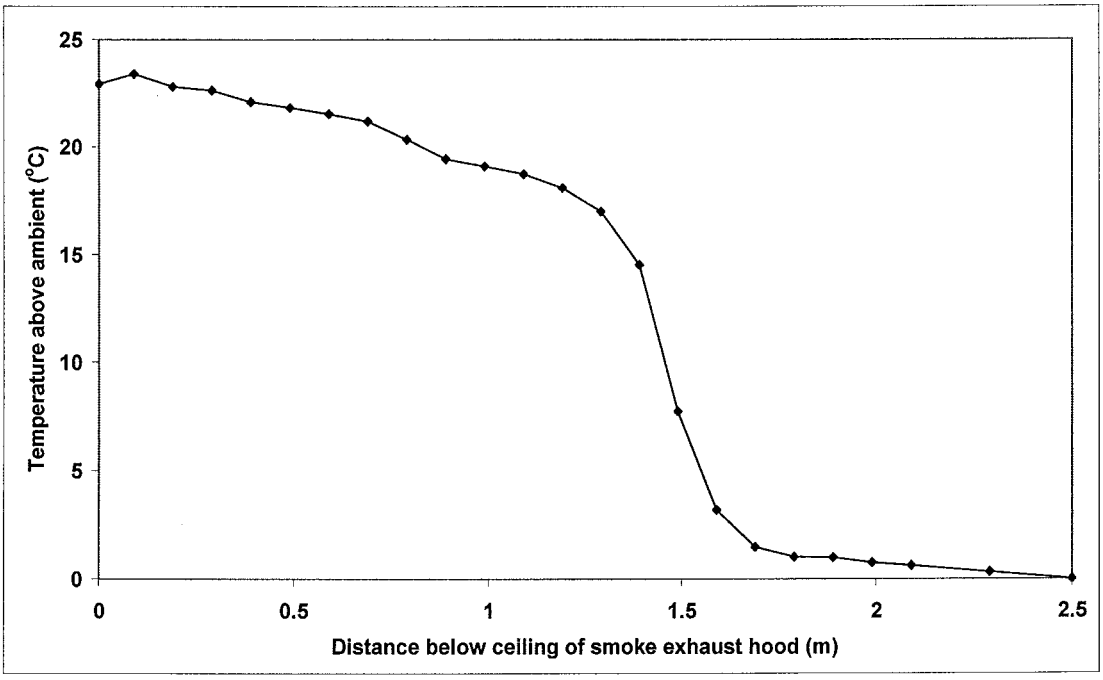

Figure F34: Temperature profile in smoke exhaust hood for Test 43

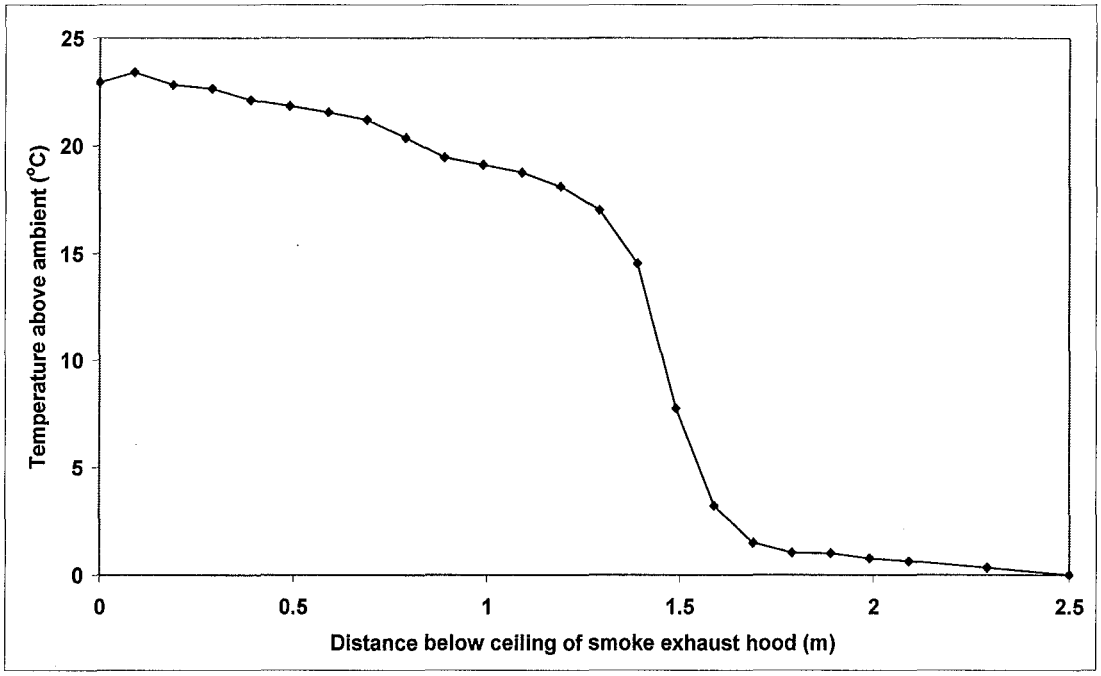

Figure F35: Temperature profile in smoke exhaust hood for Test 44

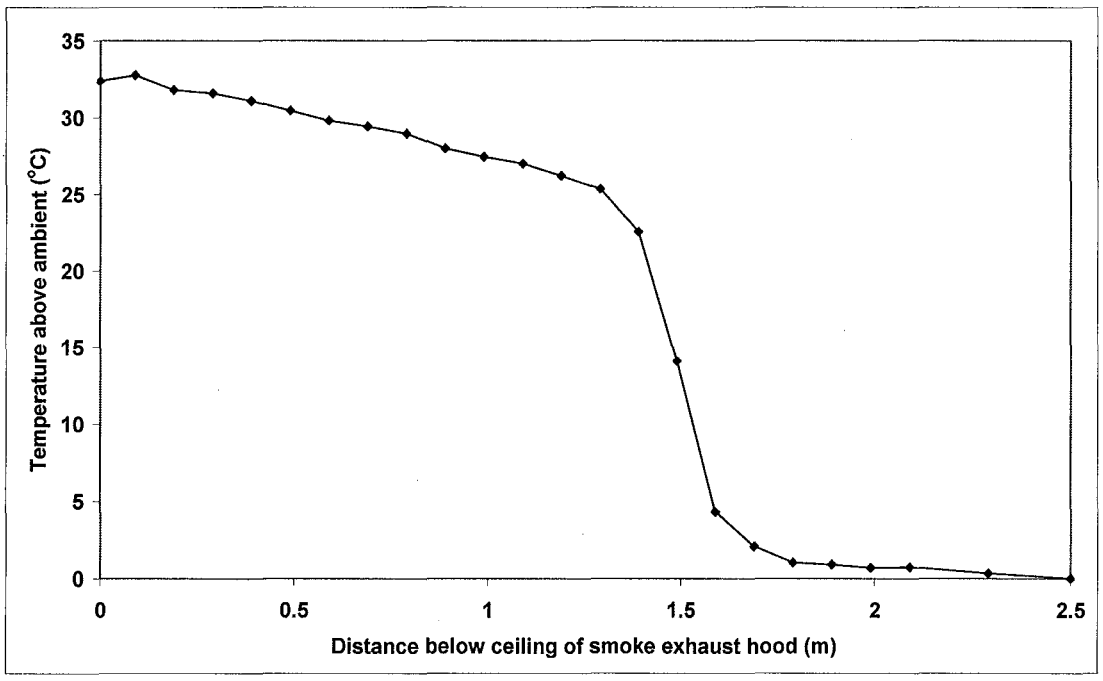

Figure F36: Temperature profile in smoke exhaust hood for Test 45

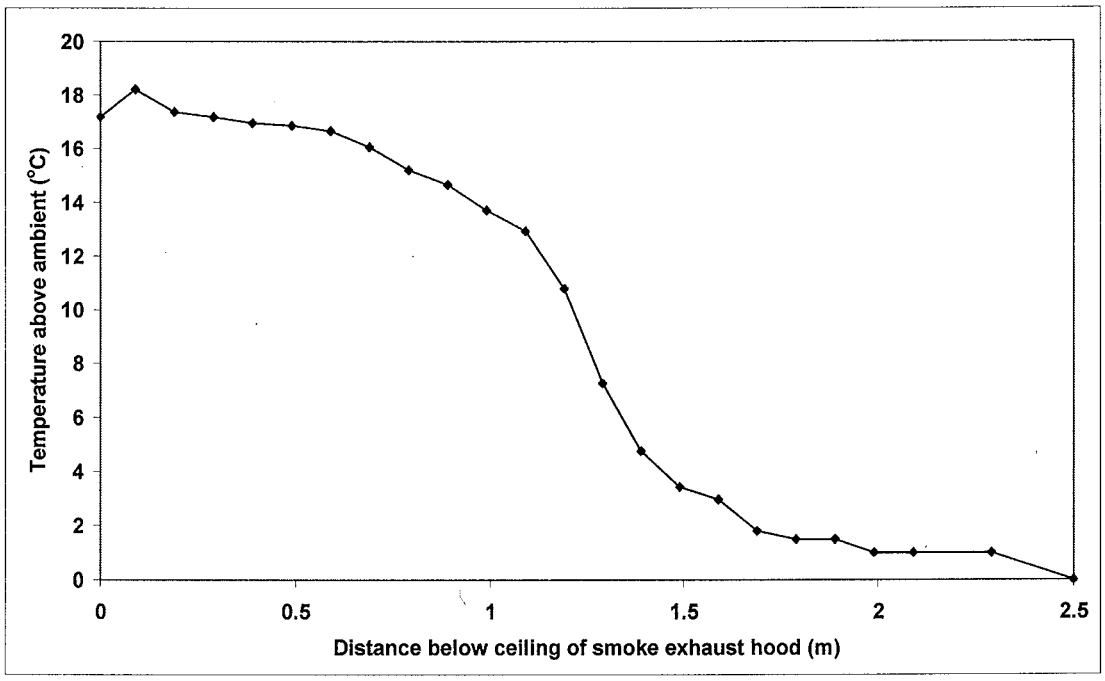

Figure F37: Temperature profile in smoke exhaust hood for Test 46

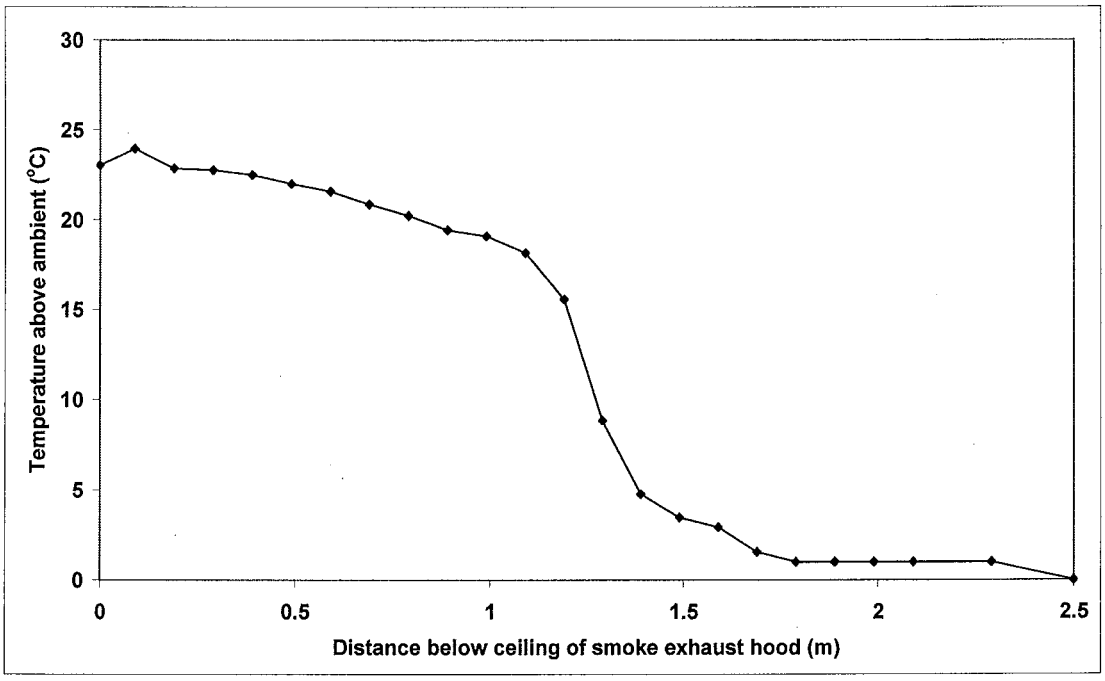

Figure F38: Temperature profile in smoke exhaust hood for Test 47

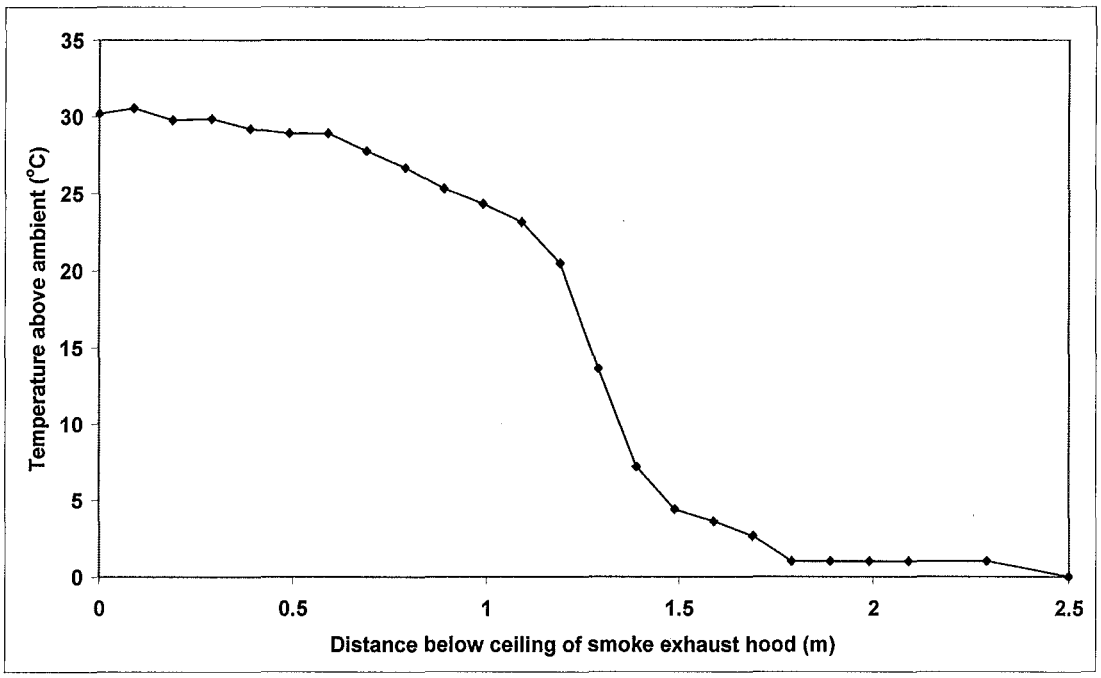

Figure F39: Temperature profile in smoke exhaust hood for Test 48

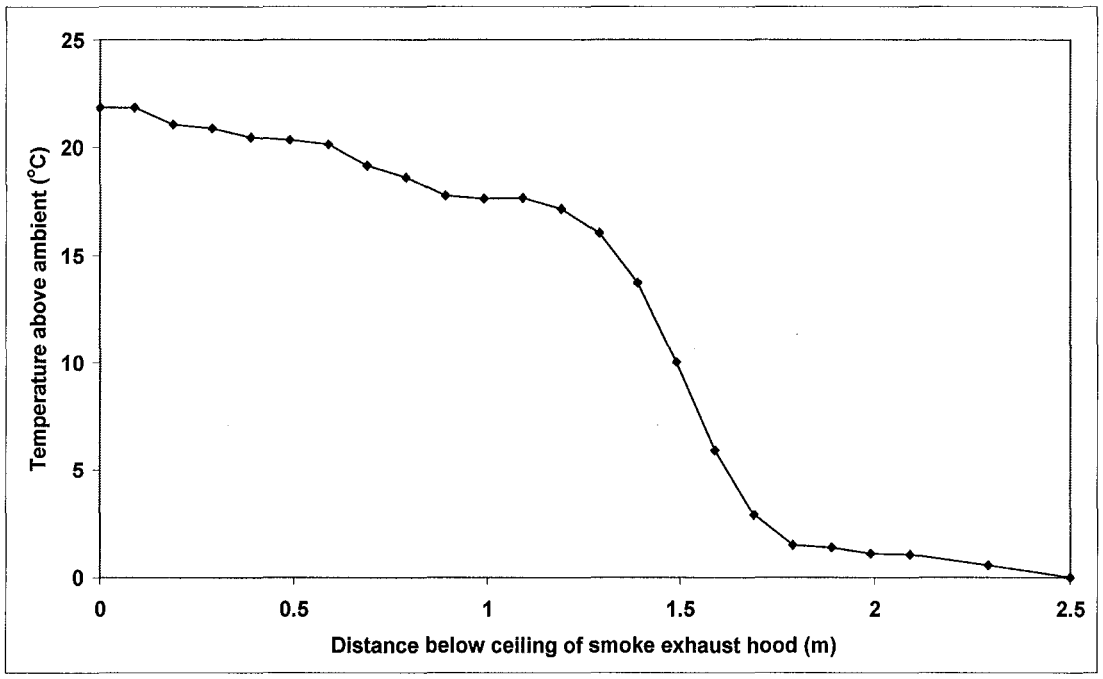

Figure F40: Temperature profile in smoke exhaust hood for Test 49

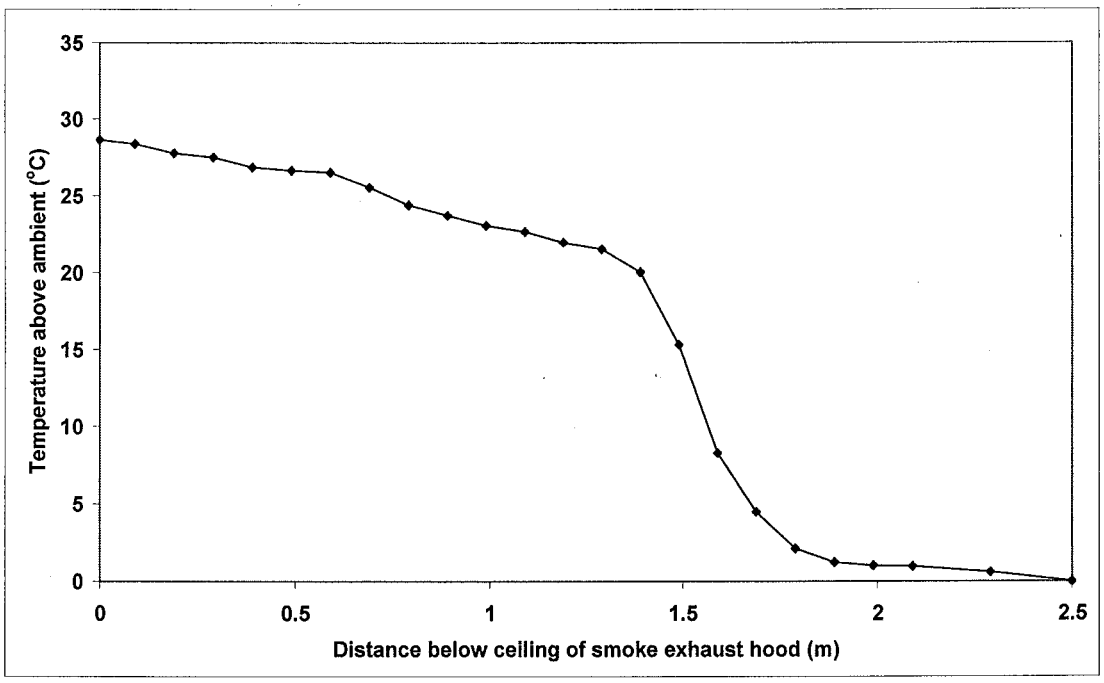

Figure F41: Temperature profile in smoke exhaust hood for Test 50

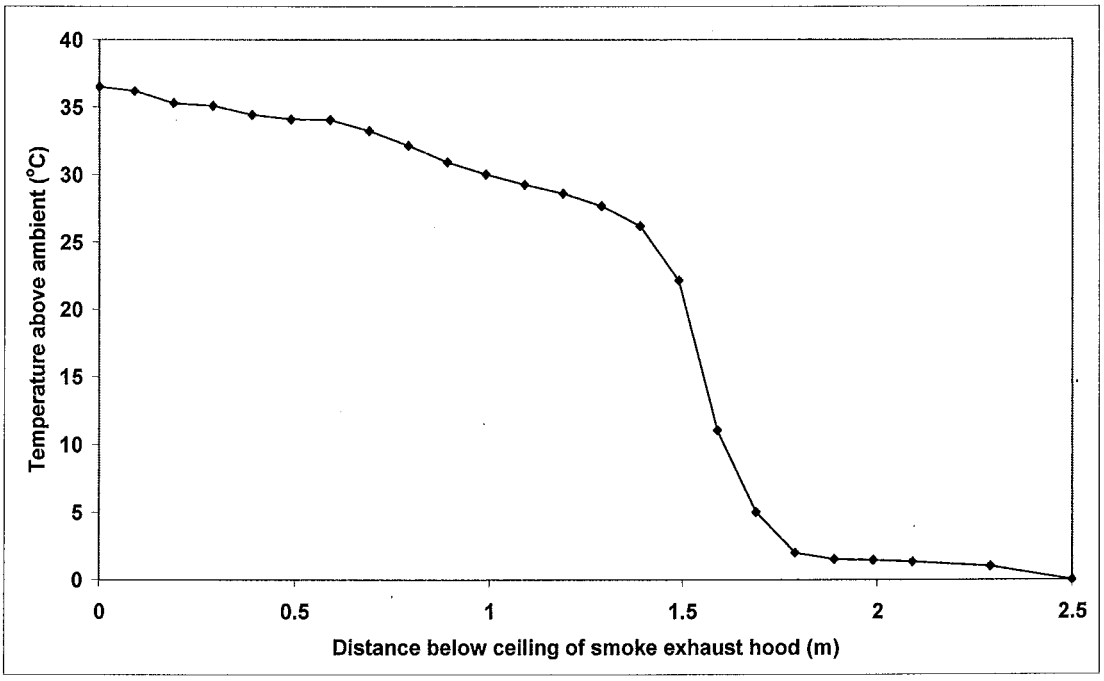

Figure F42: Temperature profile in smoke exhaust hood for Test 51

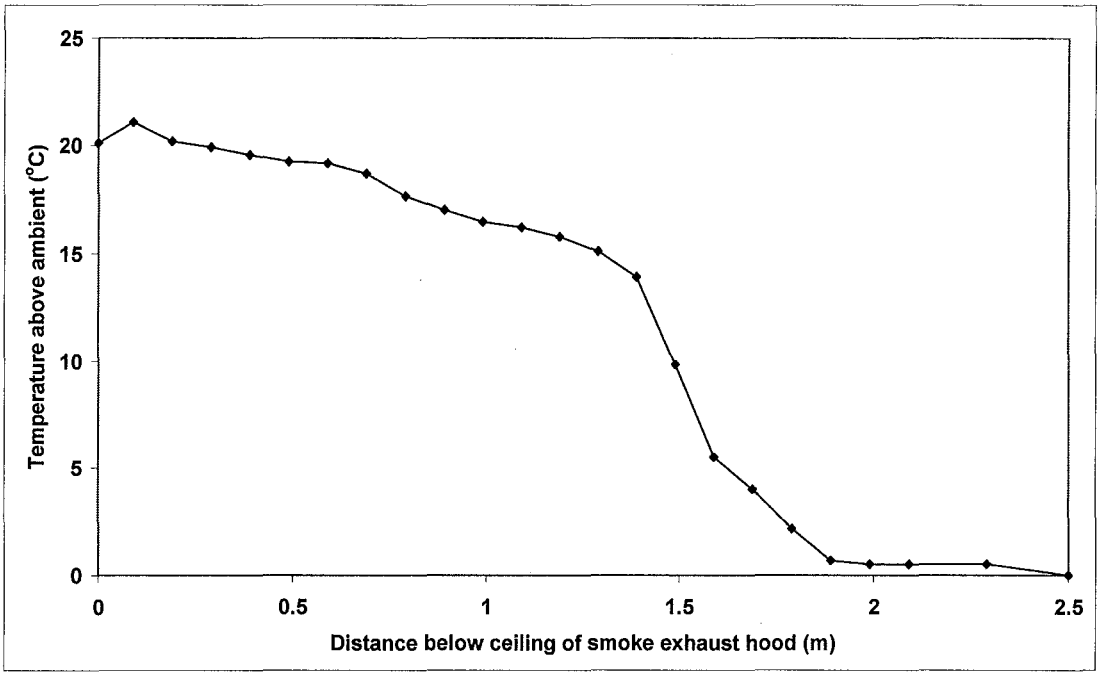

Figure F43: Temperature profile in smoke exhaust hood for Test 52

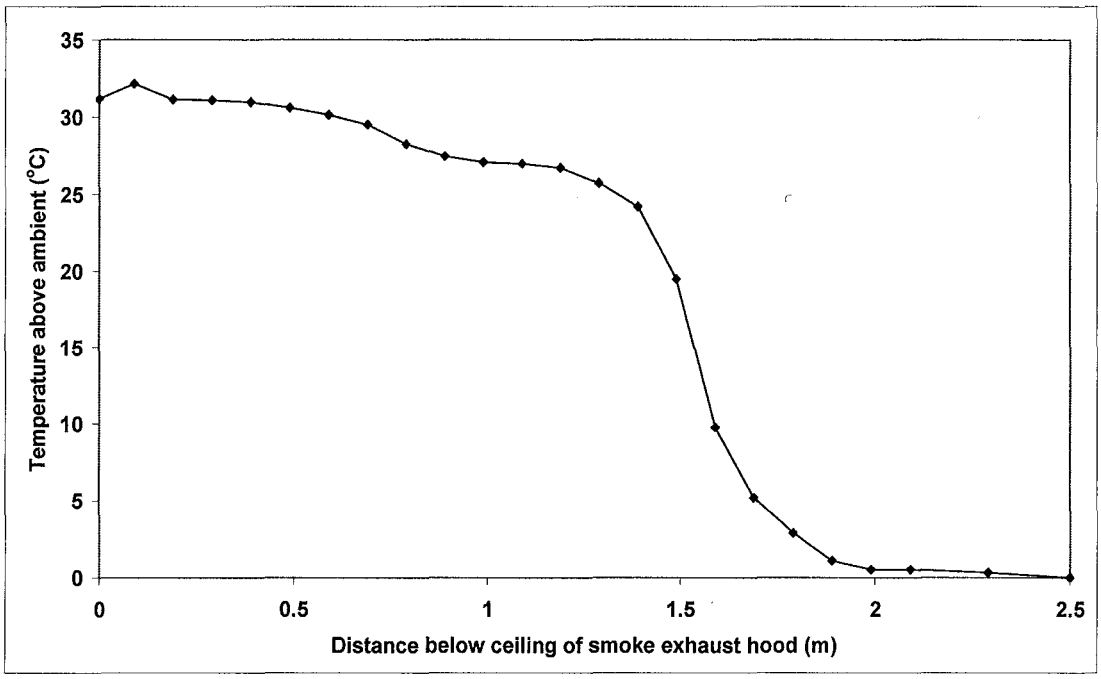

Figure F44: Temperature profile in smoke exhaust hood for Test 53

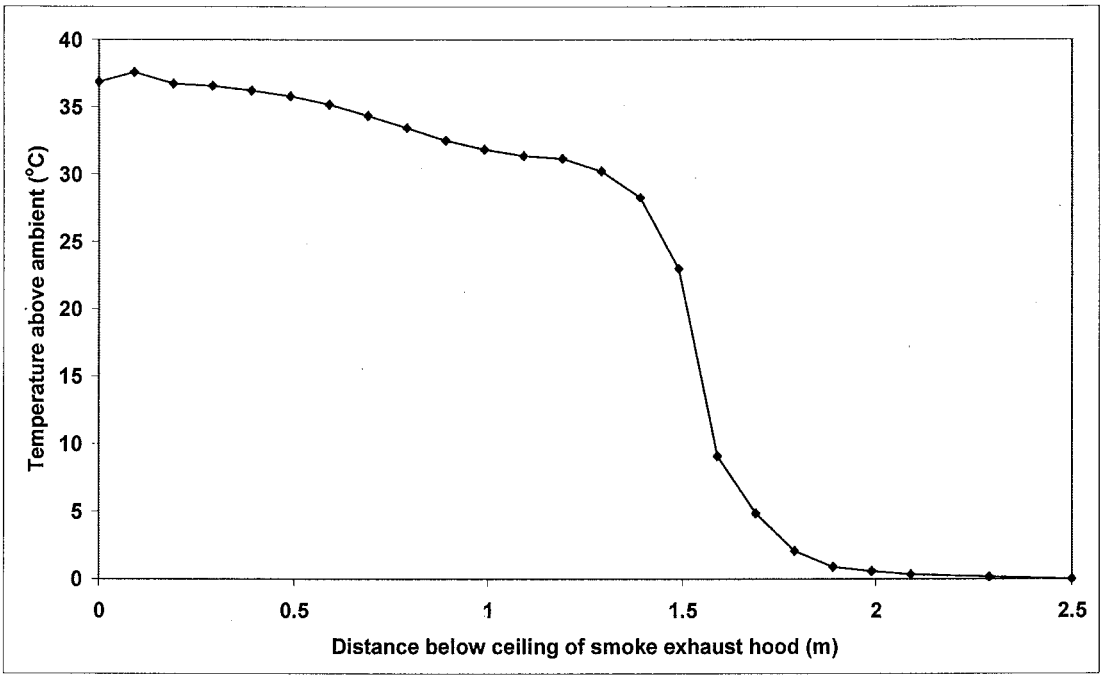

Figure F45: Temperature profile in smoke exhaust hood for Test 54

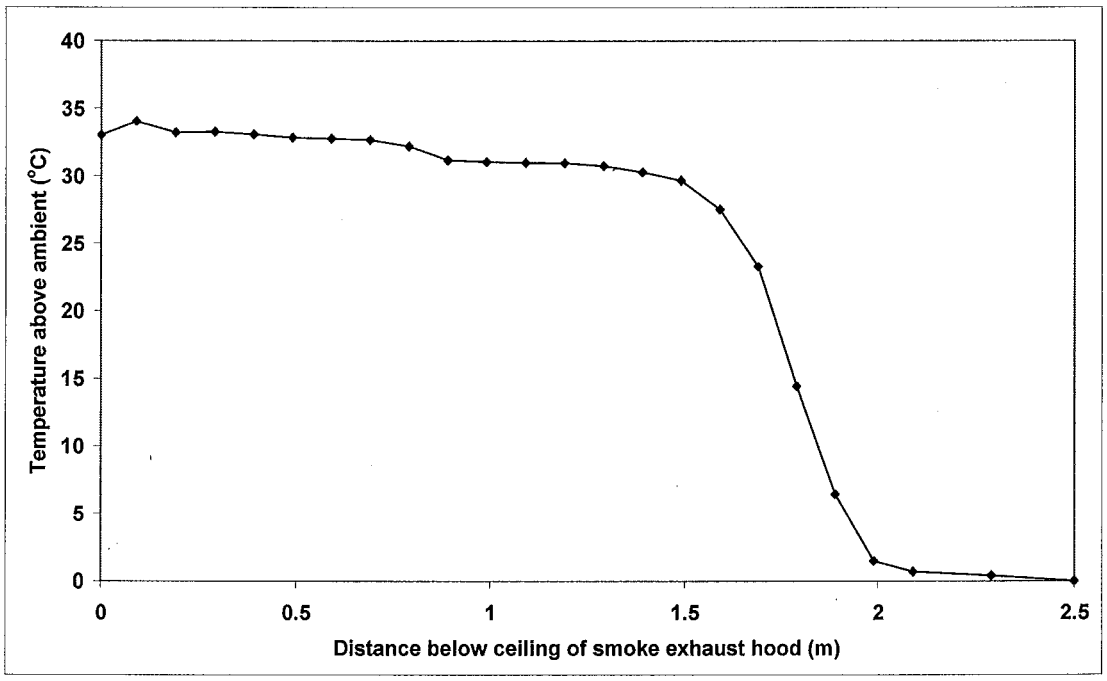

Figure F46: Temperature profile in smoke exhaust hood for Test 55

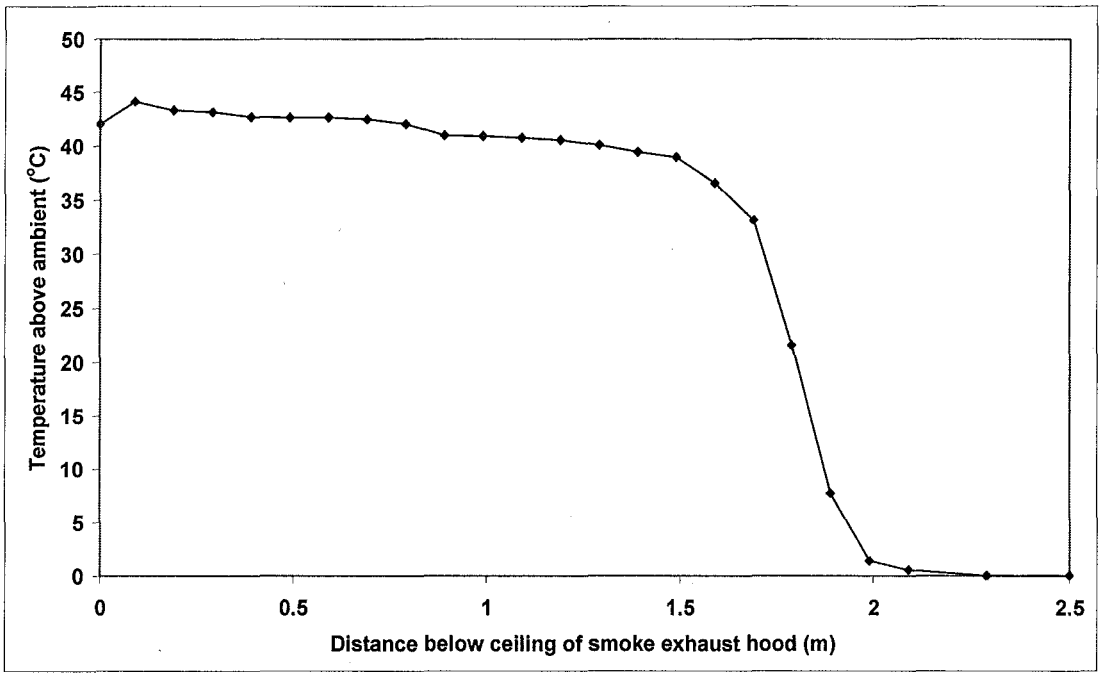

Figure F47: Temperature profile in smoke exhaust hood for Test 56

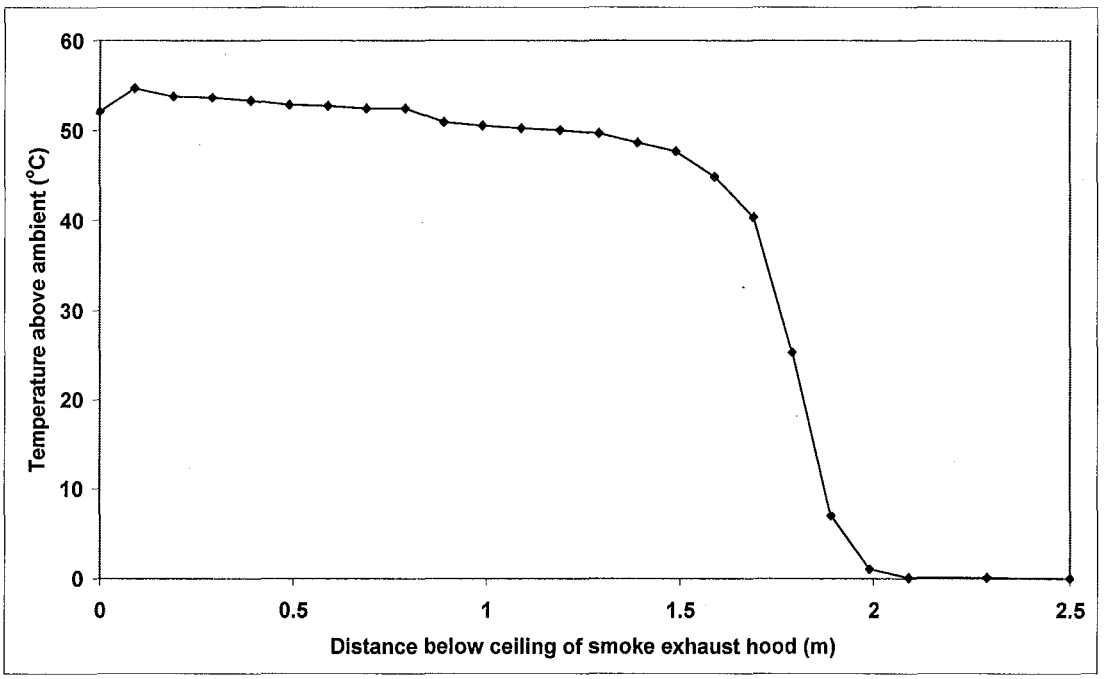

Figure F48: Temperature profile in smoke exhaust hood for Test 57

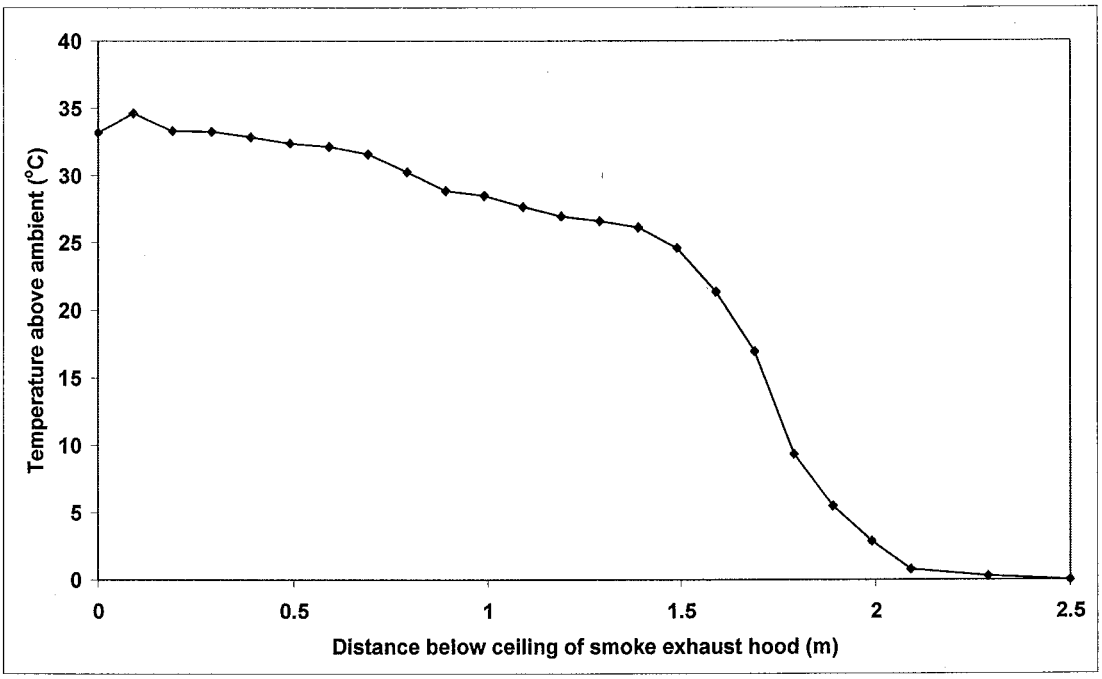

Figure F49: Temperature profile in smoke exhaust hood for Test 58

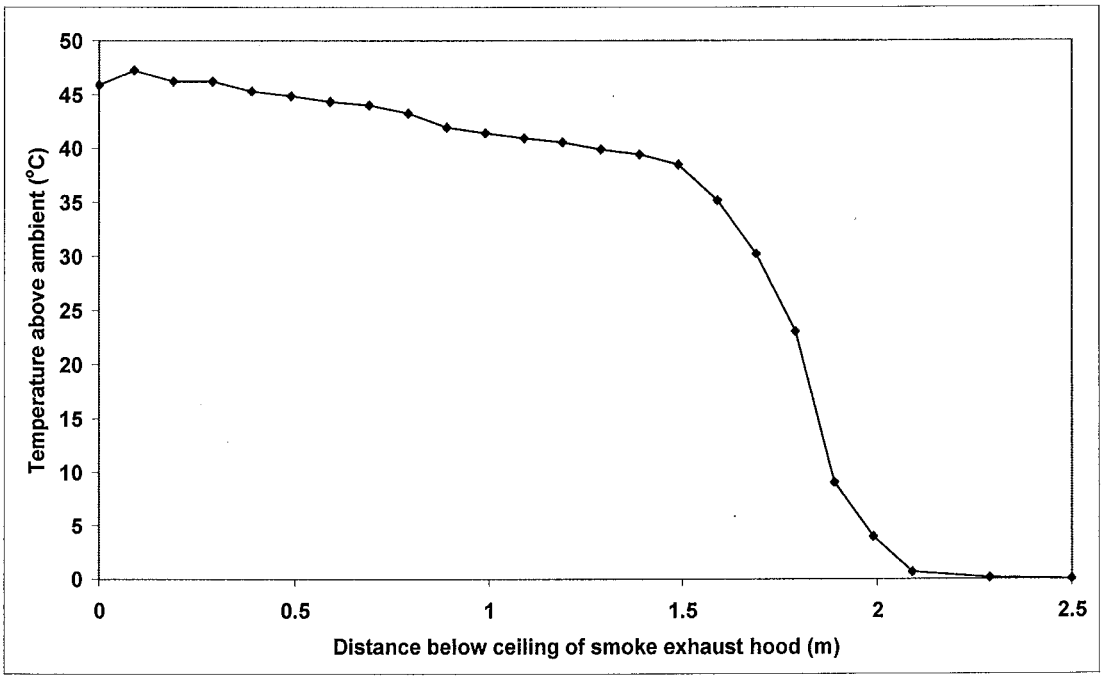

Figure F50: Temperature profile in smoke exhaust hood for Test 59

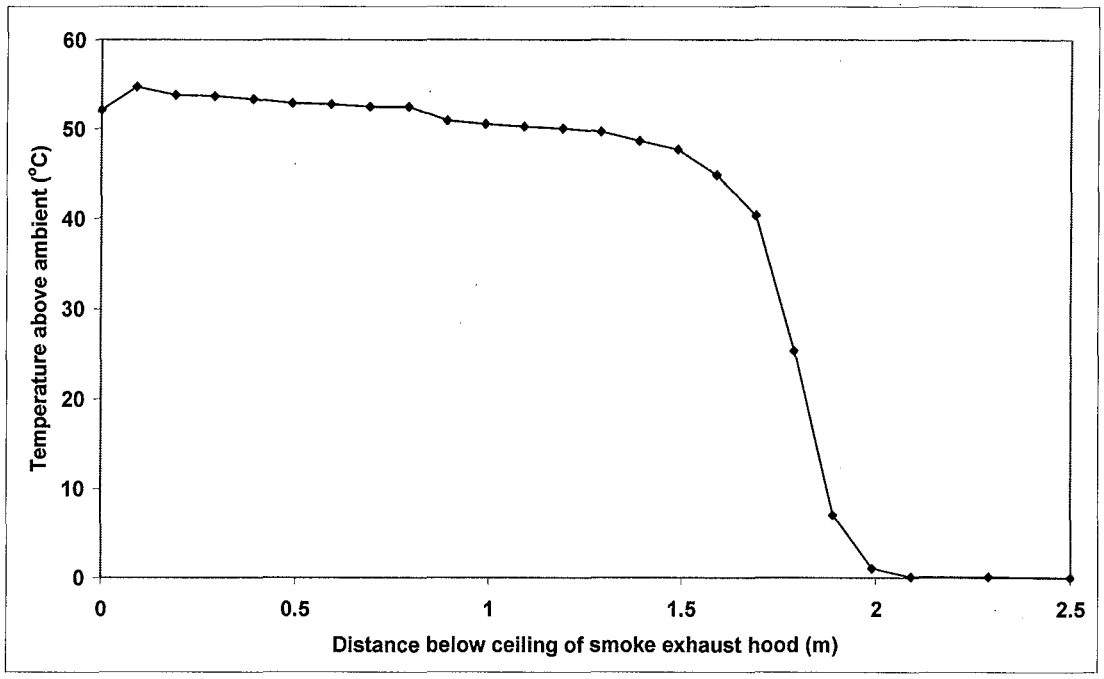

Figure F51: Temperature profile in smoke exhaust hood for Test 60

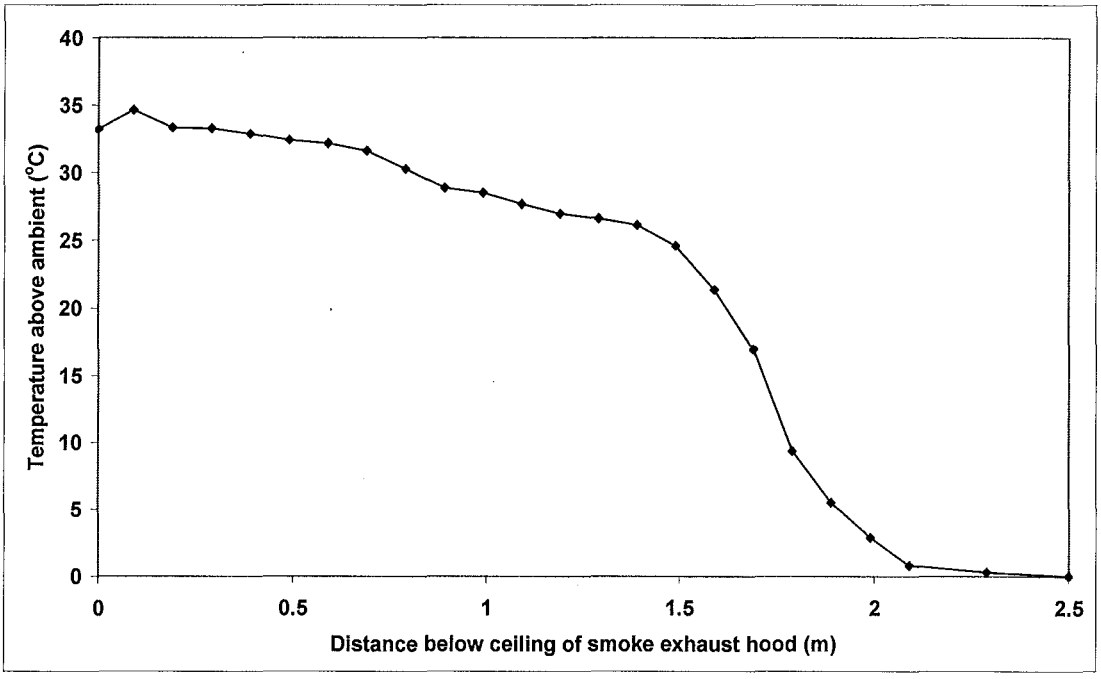

Figure F52: Temperature profile in smoke exhaust hood for Test 61

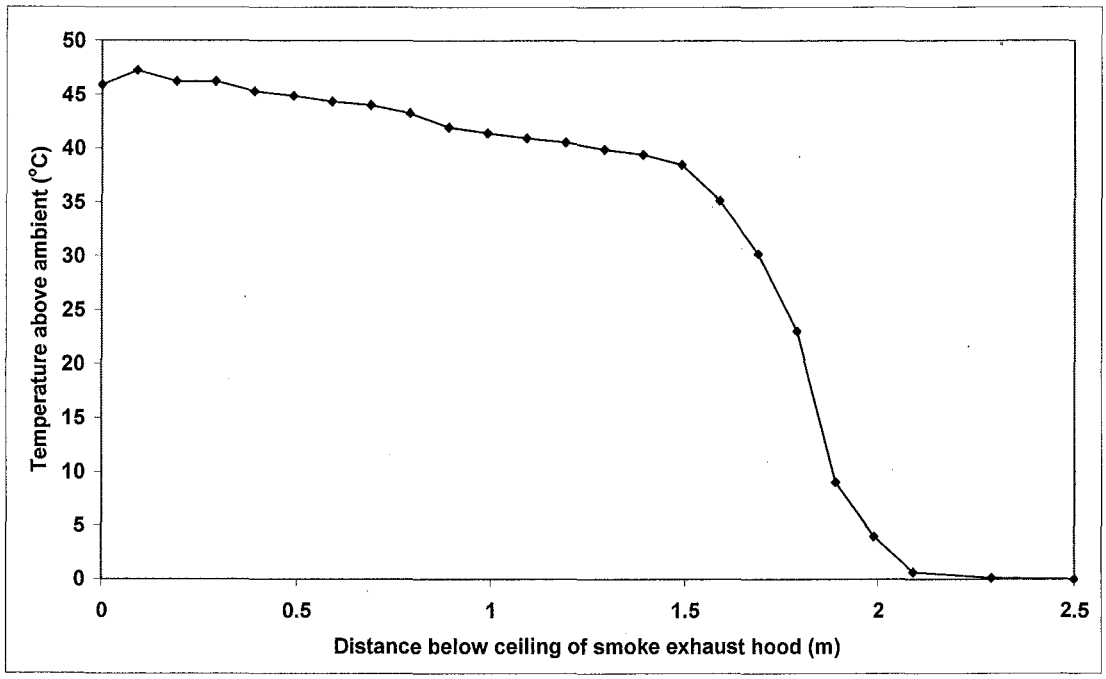

Figure F53: Temperature profile in smoke exhaust hood for Test 62

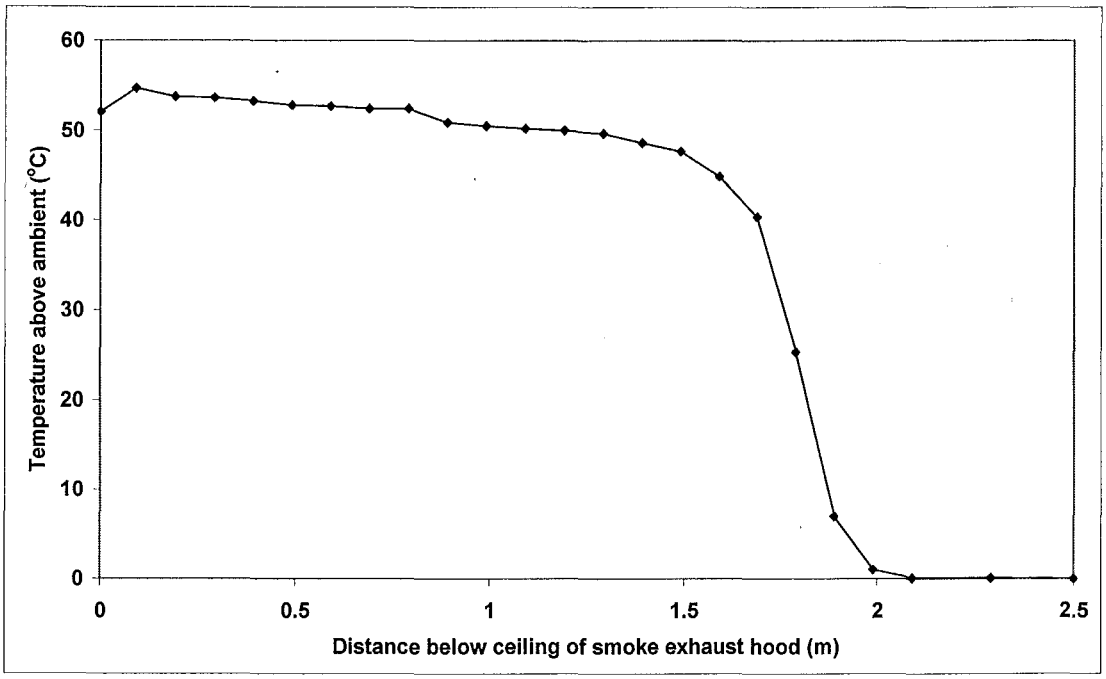

Figure F54: Temperature profile in smoke exhaust hood for Test 63

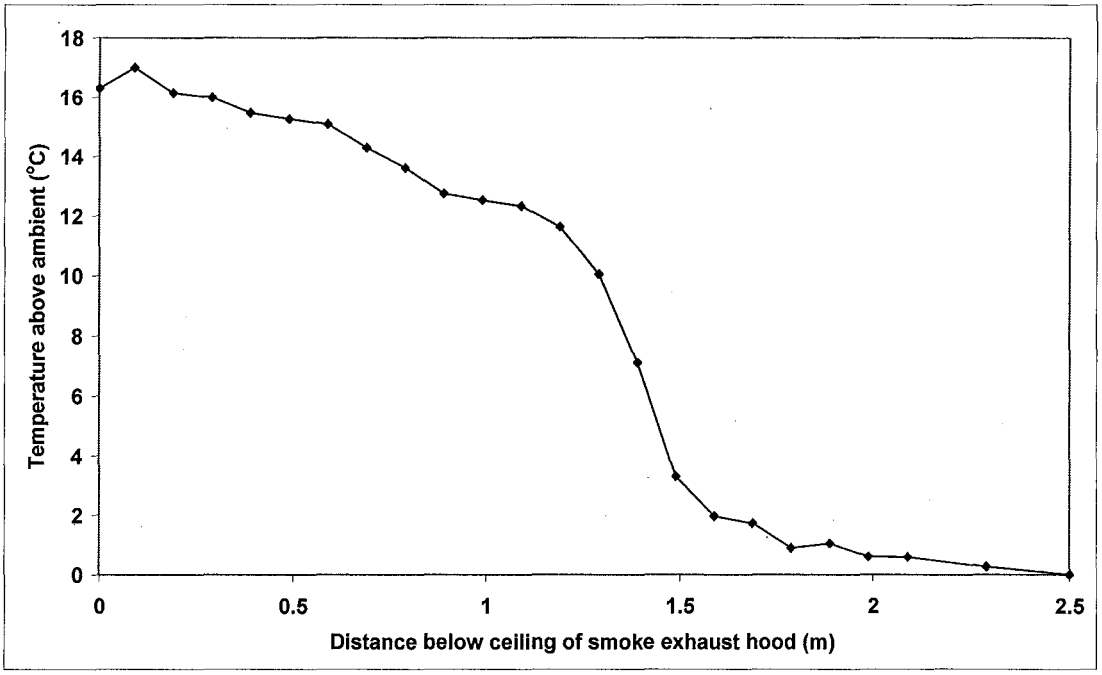

Figure F55: Temperature profile in smoke exhaust hood for Test 64

APPENDIX G FDS TEMPERATURE PROFILES (SIMULATIONS 1 TO 25)

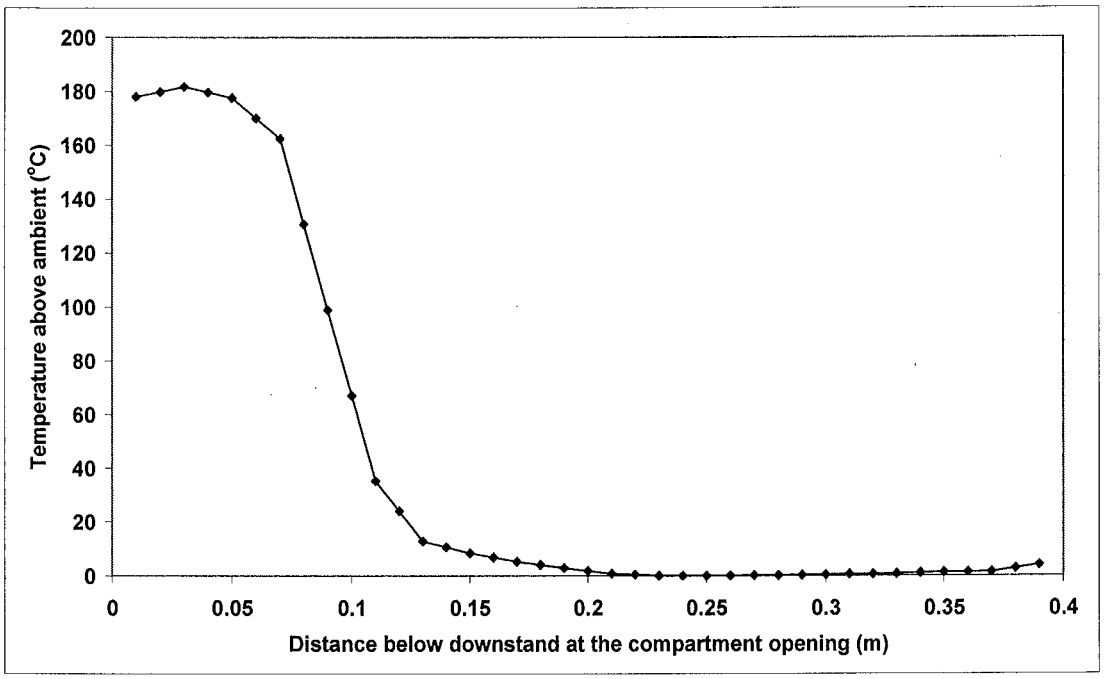

Figure G1: Temperature profile at the compartment opening for Simulation 1

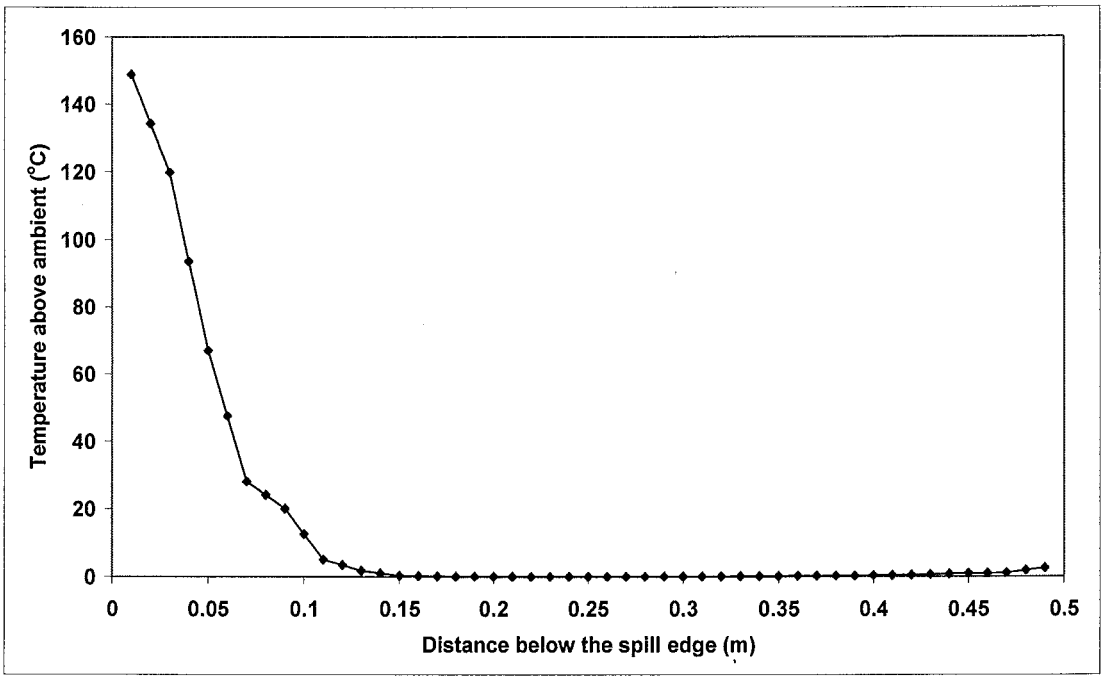

Figure G2: Temperature profile at the spill edge for Simulation 1

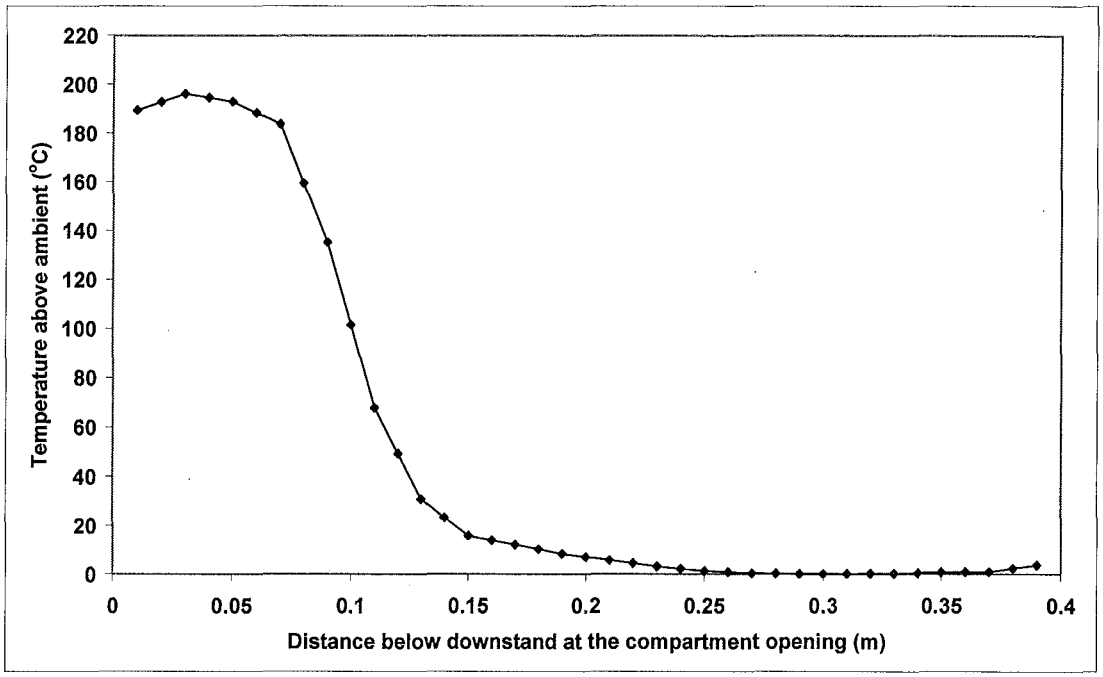

Figure G3: Temperature profile at the compartment opening for Simulation 2

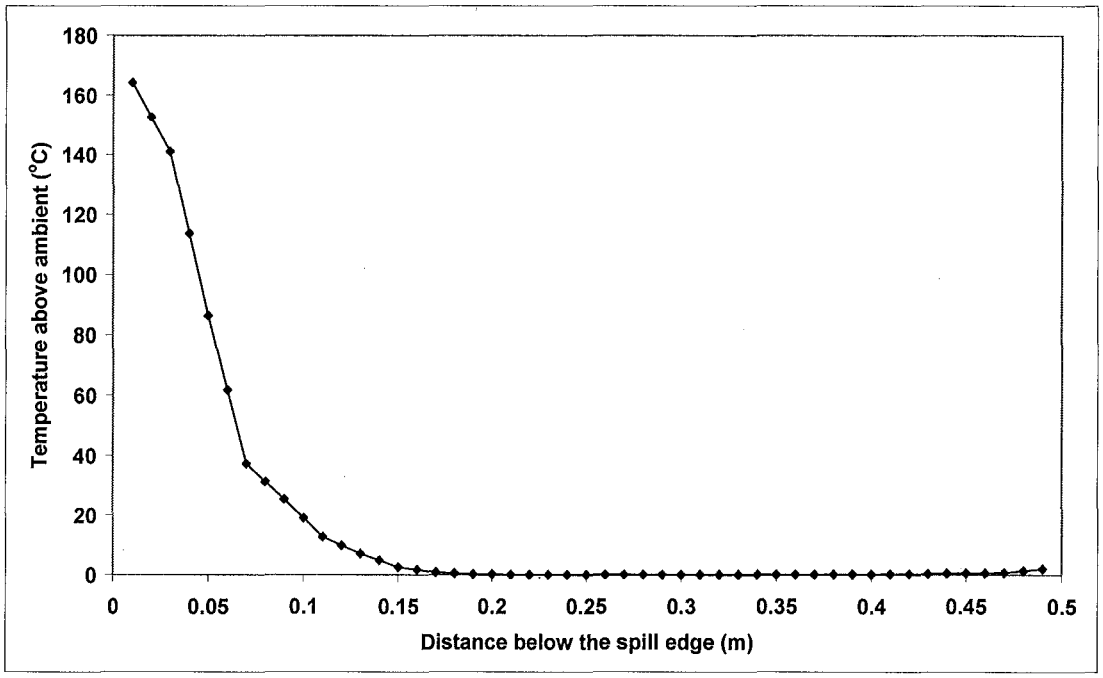

Figure G4: Temperature profile at the spill edge for Simulation 2

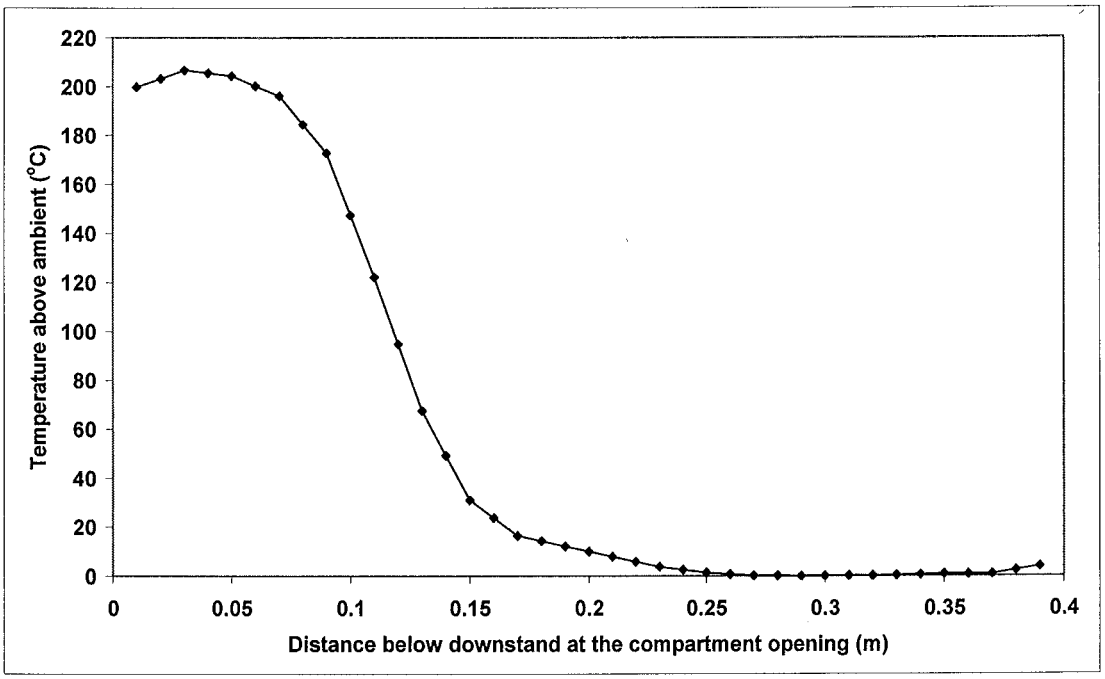

Figure G5: Temperature profile at the compartment opening for Simulation 3

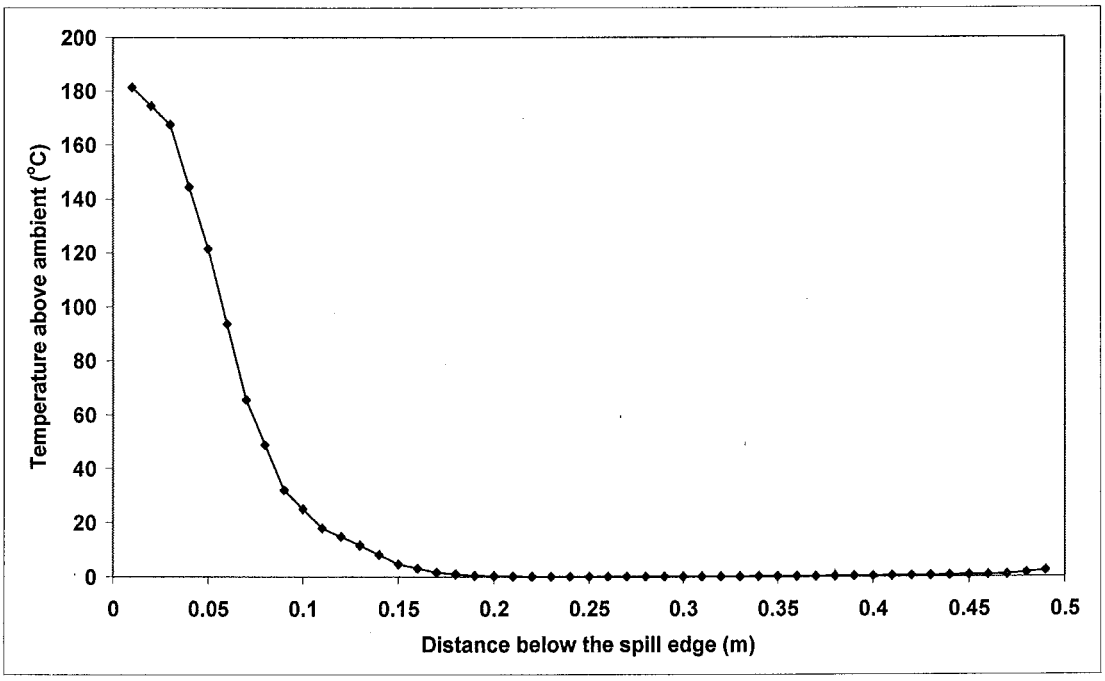

Figure G6: Temperature profile at the spill edge for Simulation 3

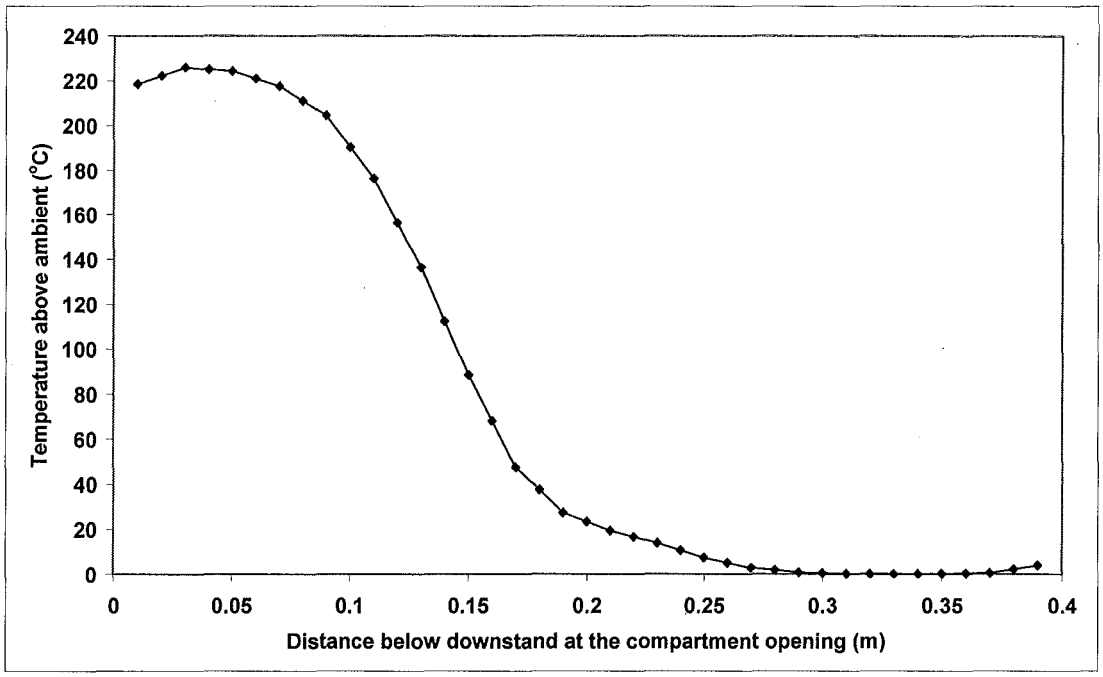

Figure G7: Temperature profile at the compartment opening for Simulation 4

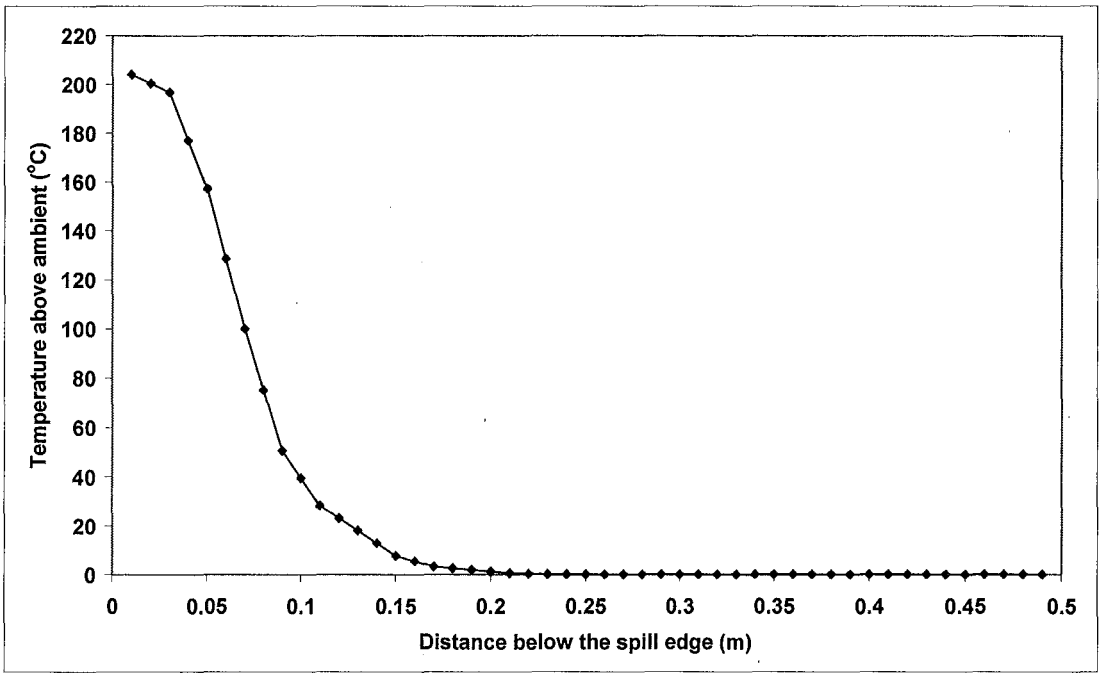

Figure G8: Temperature profile at the spill edge for Simulation 4

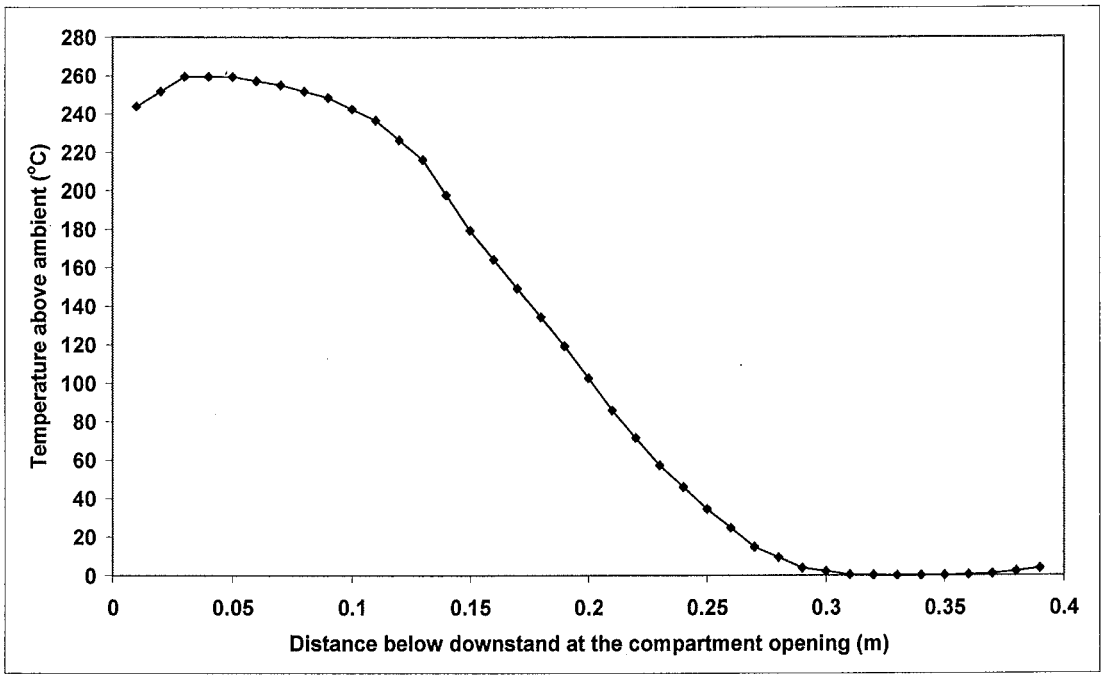

Figure G9: Temperature profile at the compartment opening for Simulation 5

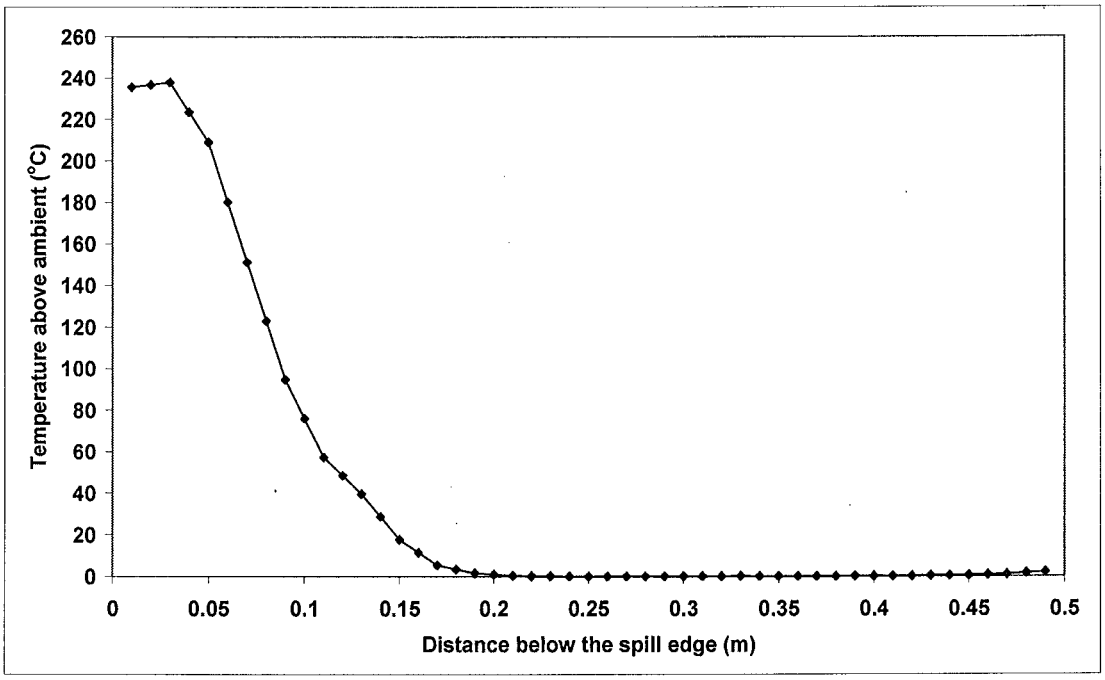

Figure G10: Temperature profile at the spill edge for Simulation 5

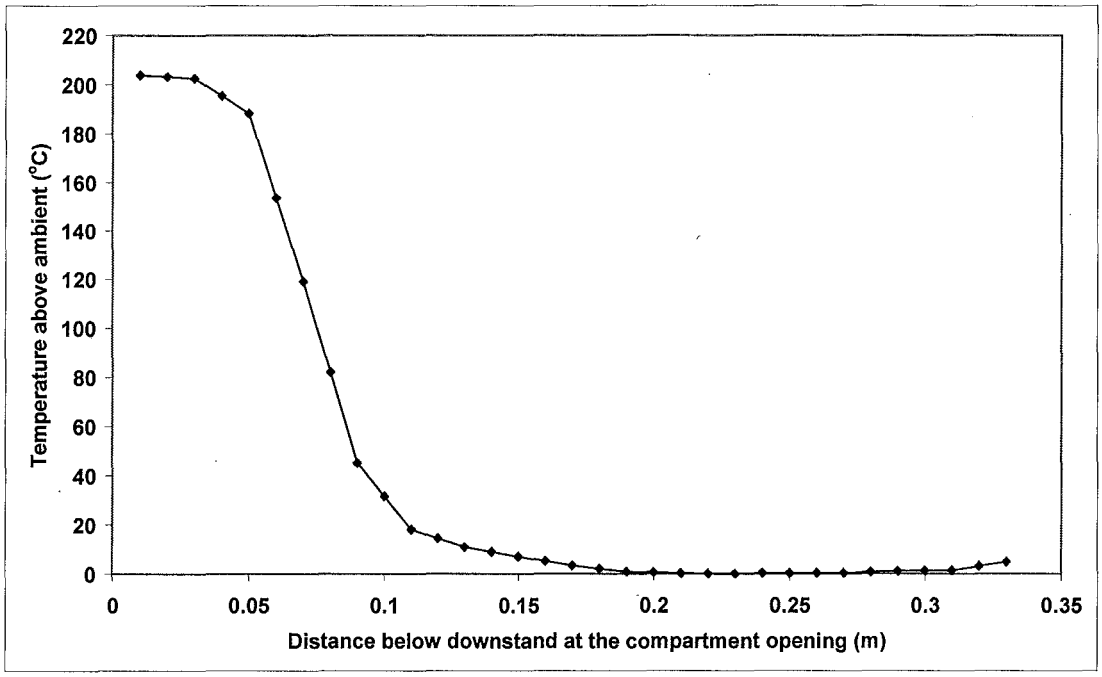

Figure G11: Temperature profile at the compartment opening for Simulation 6

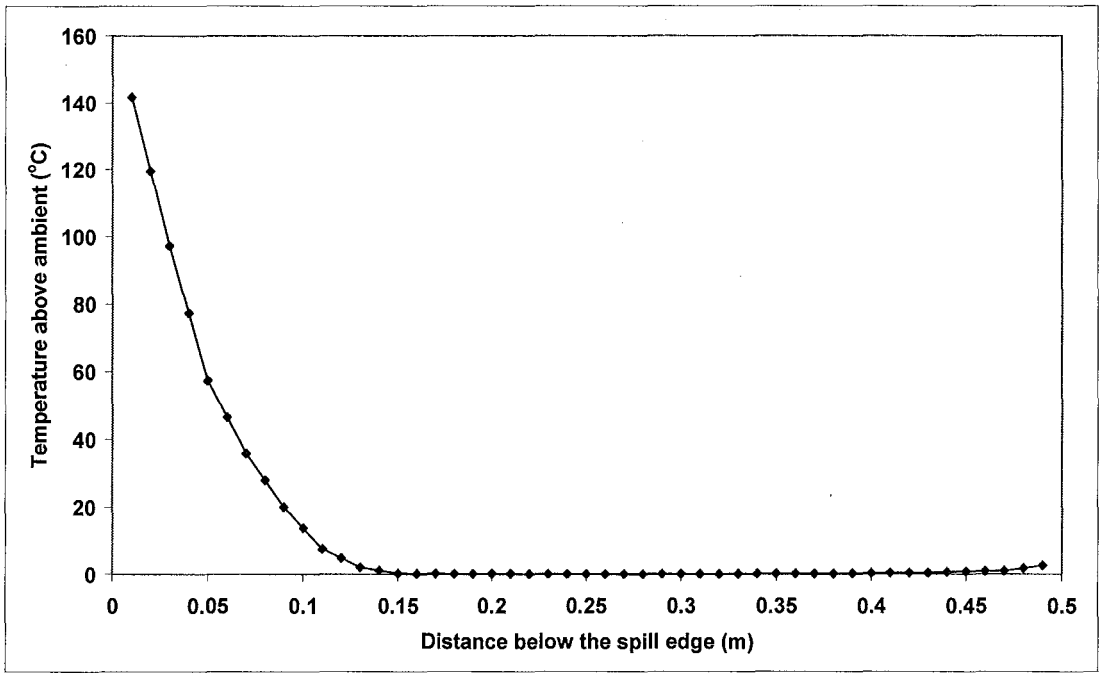

Figure G12: Temperature profile at the spill edge for Simulation 6

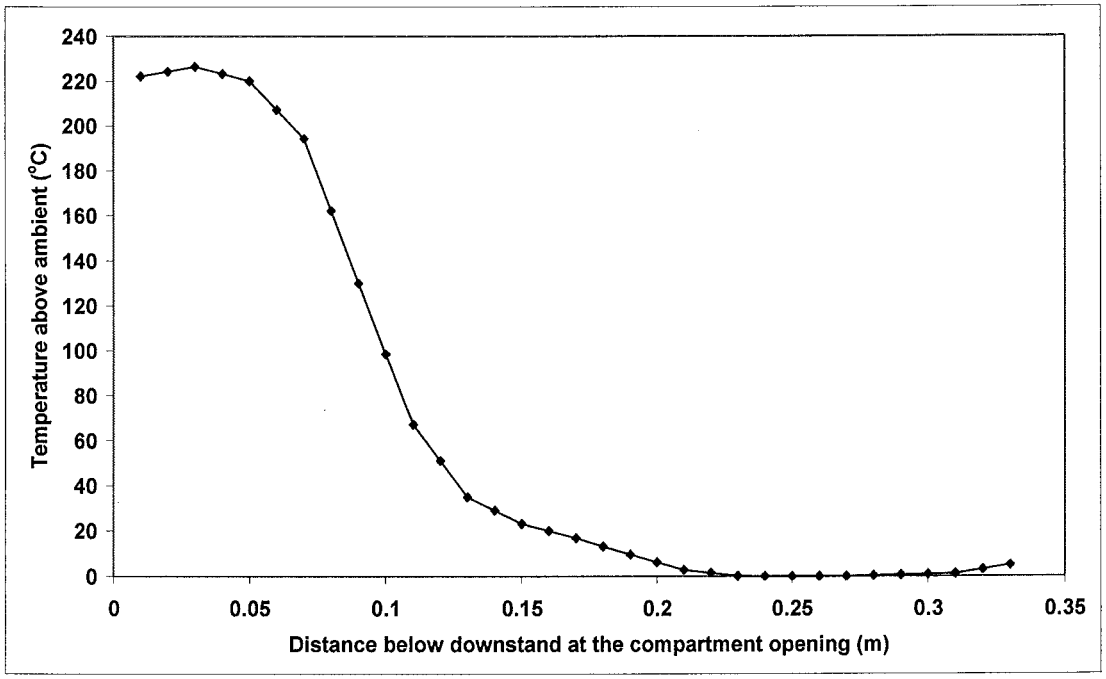

Figure G13: Temperature profile at the compartment opening for Simulation 7

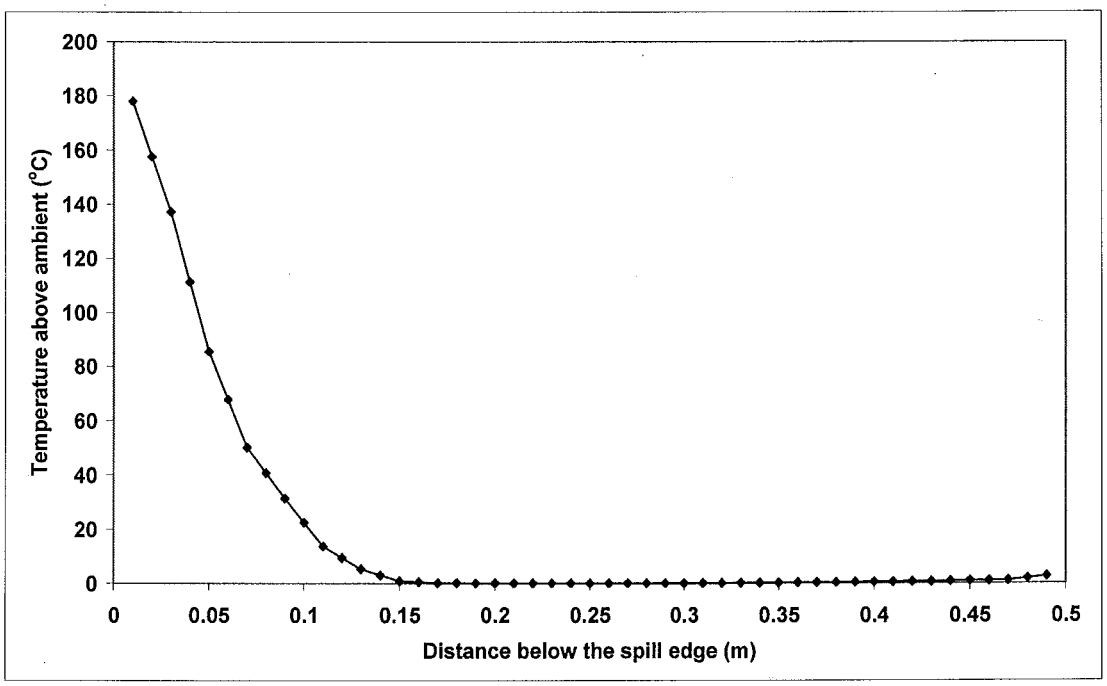

Figure G14: Temperature profile at the spill edge for Simulation 7

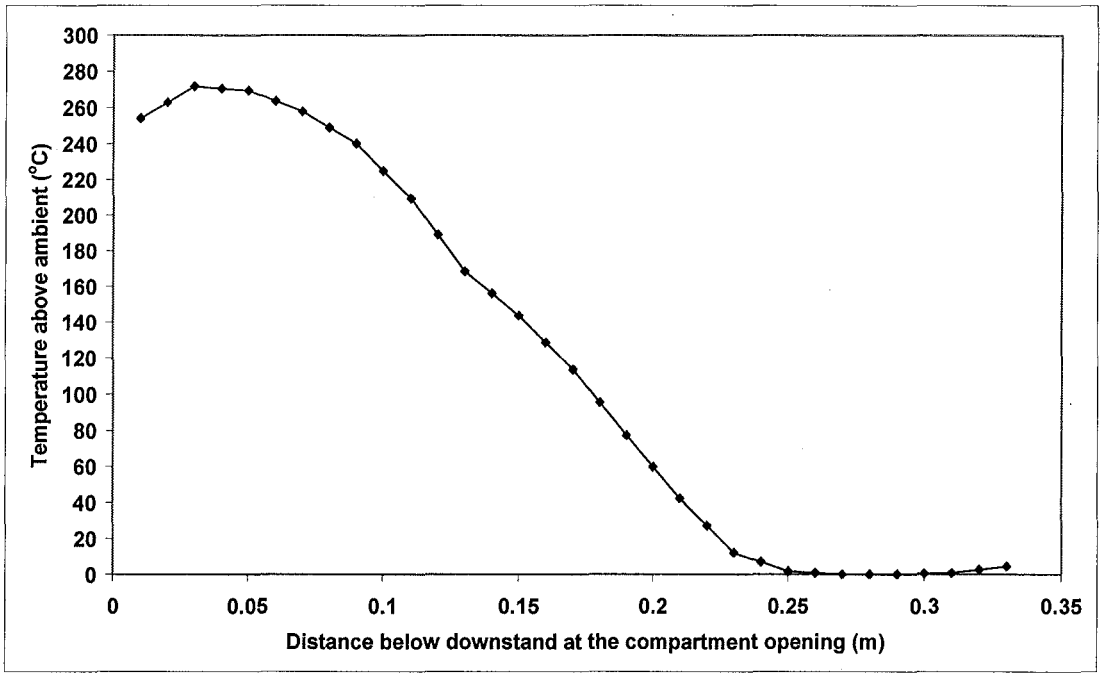

Figure G15: Temperature profile at the compartment opening for Simulation 8

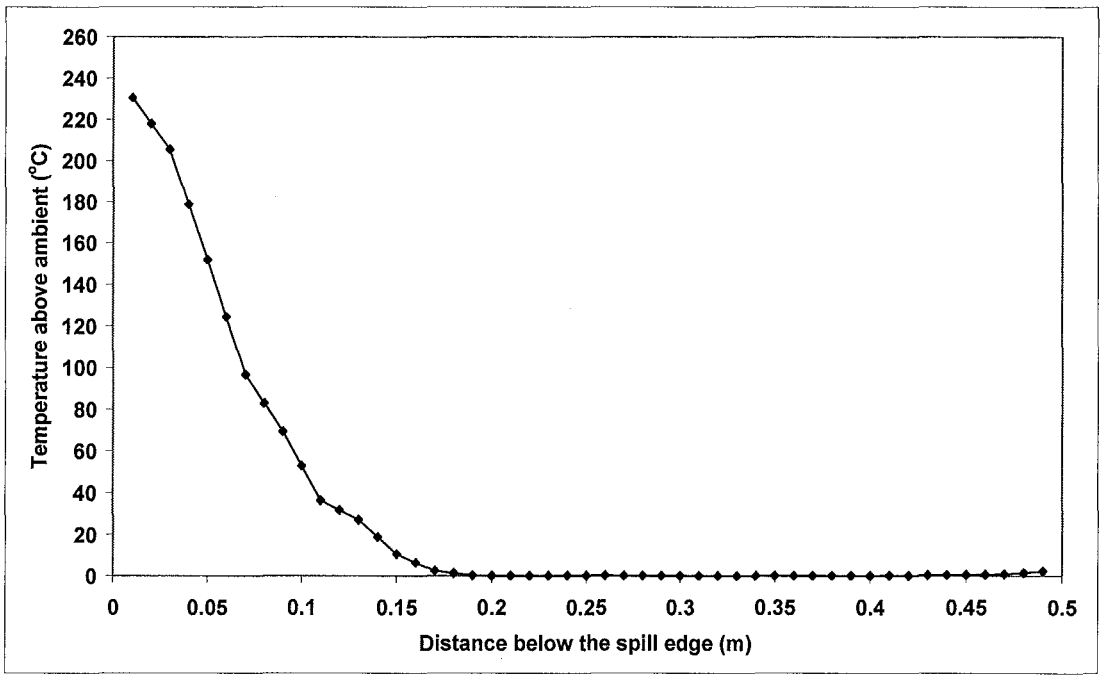

Figure G16: Temperature profile at the spill edge for Simulation 8

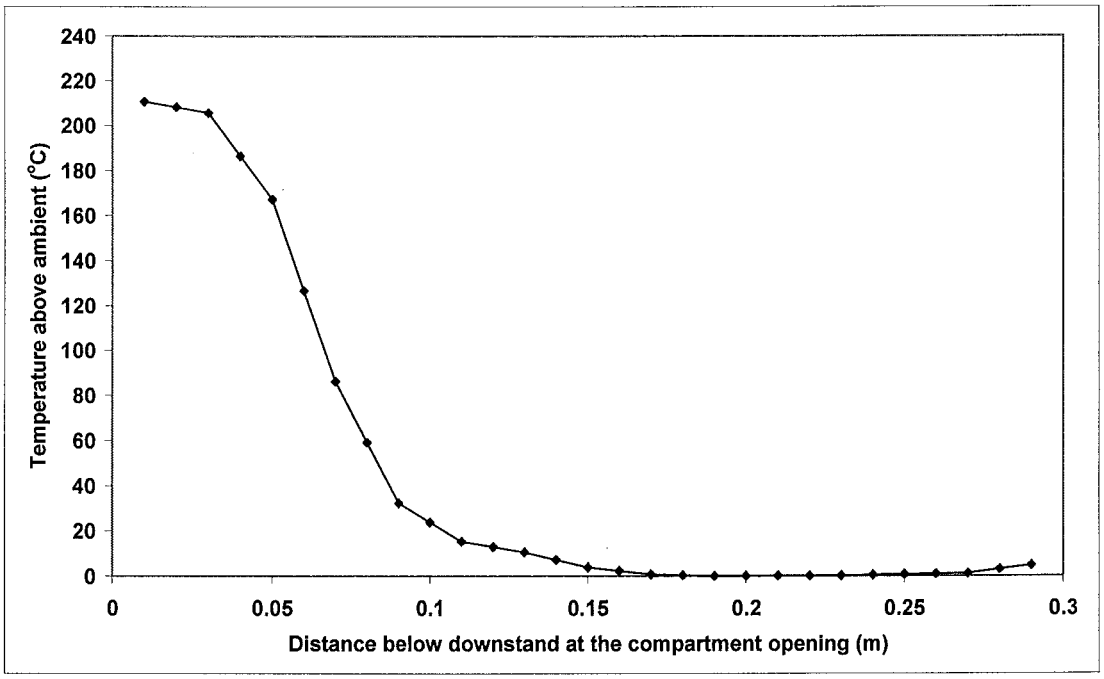

Figure G17: Temperature profile at the compartment opening for Simulation 9

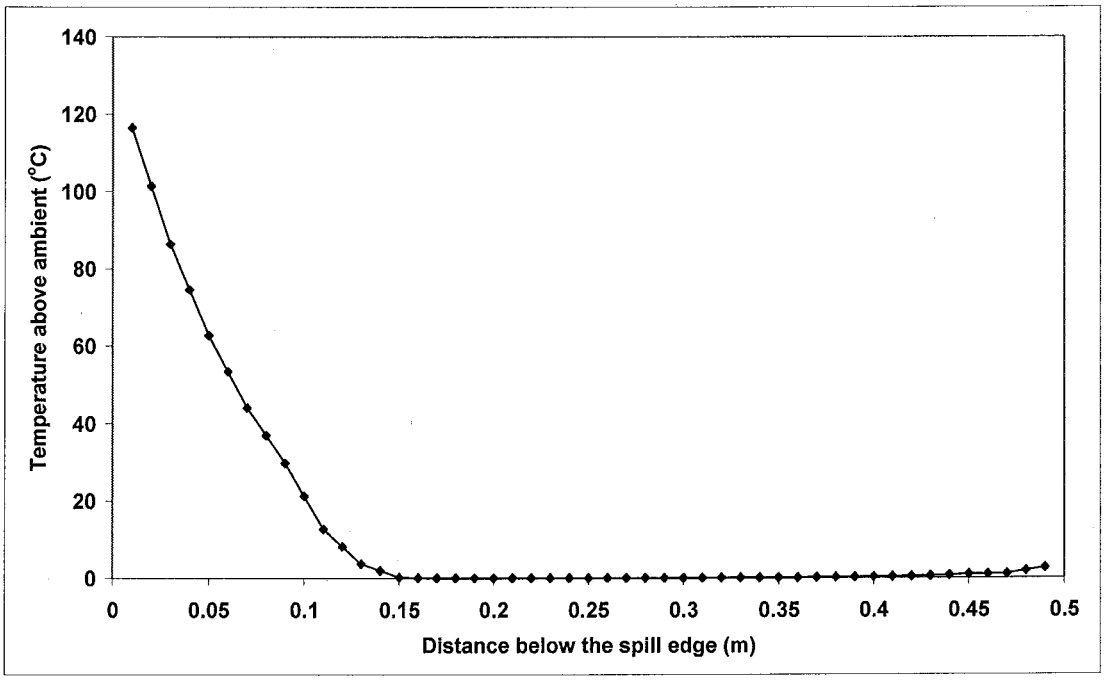

Figure G18: Temperature profile at the spill edge for Simulation 9

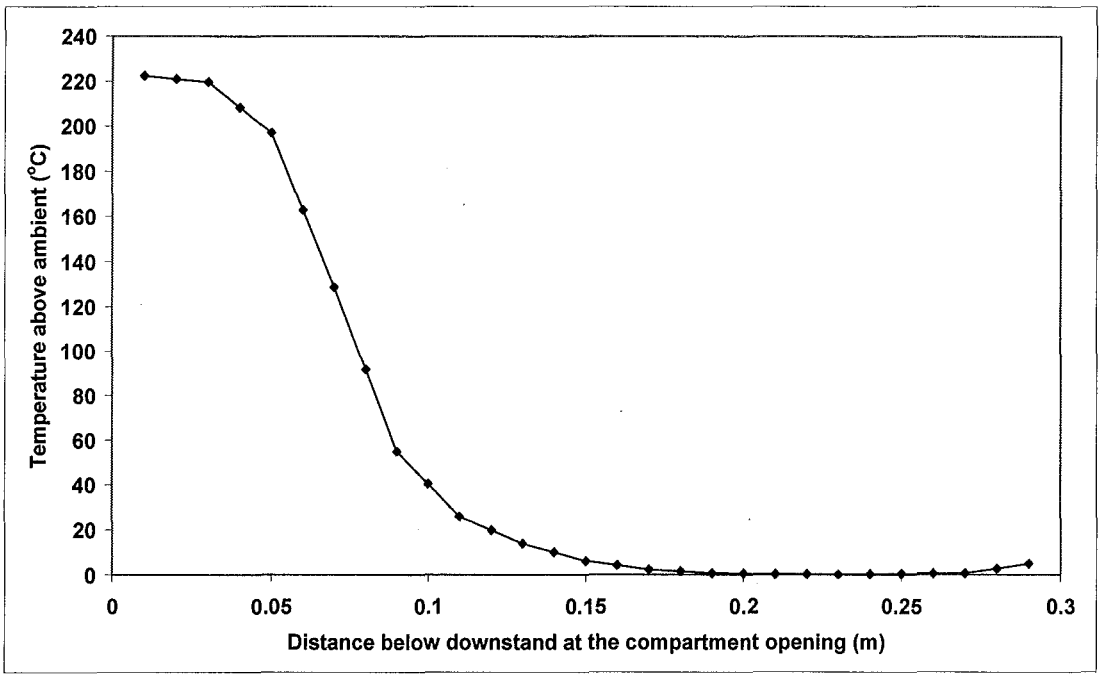

Figure G19: Temperature profile at the compartment opening for Simulation 10

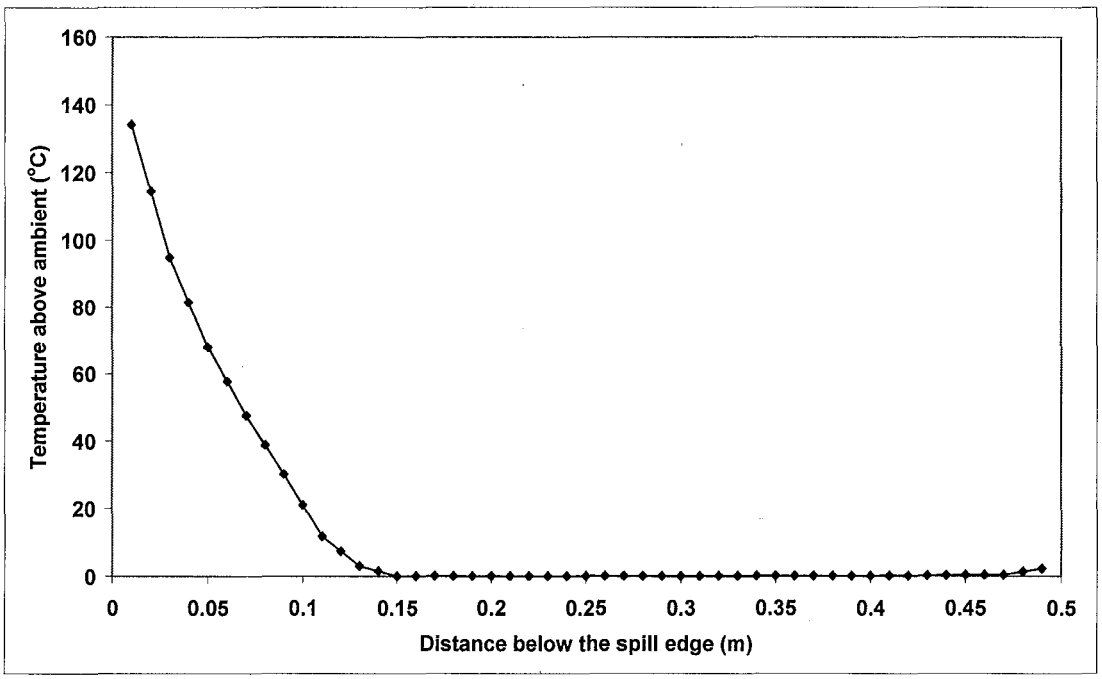

Figure G20: Temperature profile at the spill edge for Simulation 10

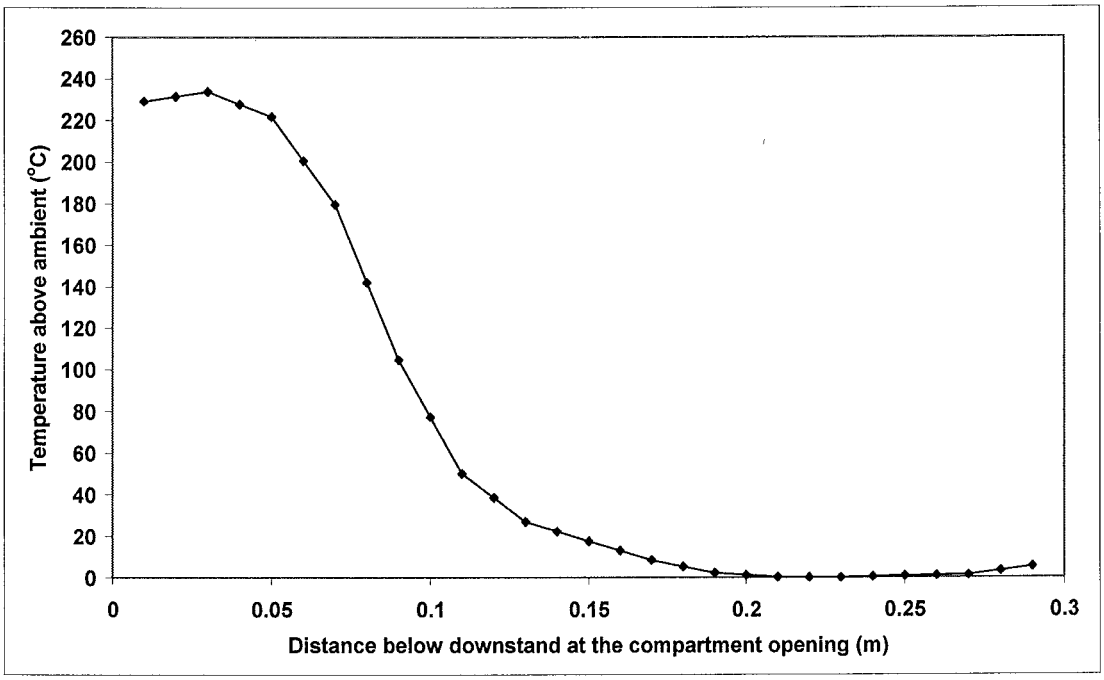

Figure G21: Temperature profile at the compartment opening for Simulation 11

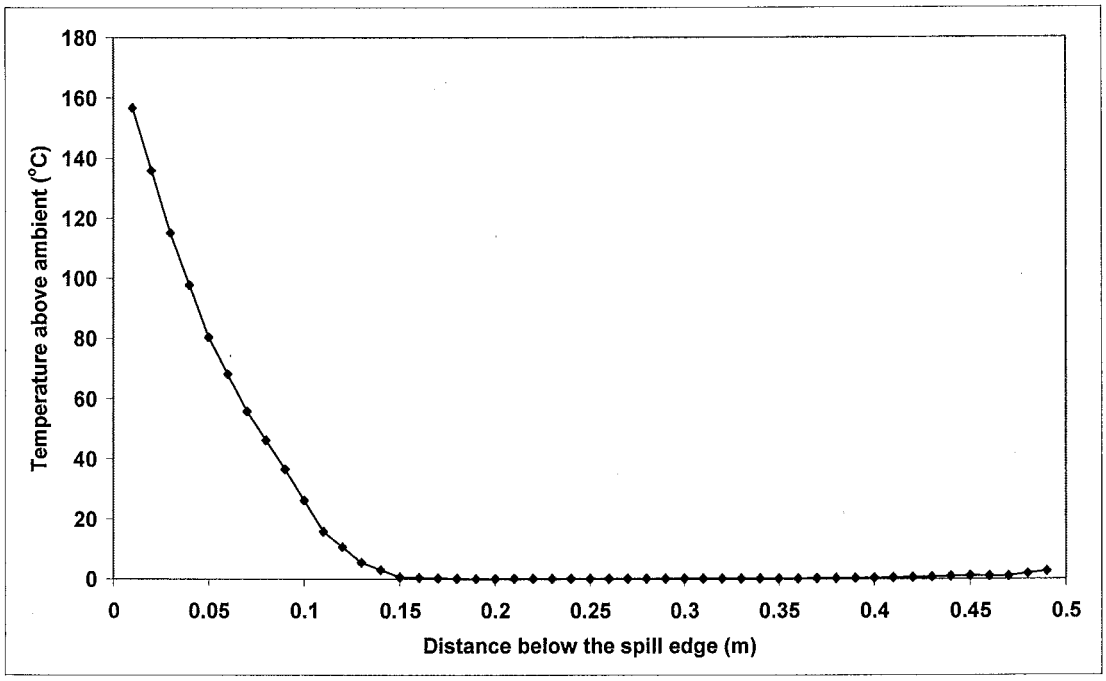

Figure G22: Temperature profile at the spill edge for Simulation 11

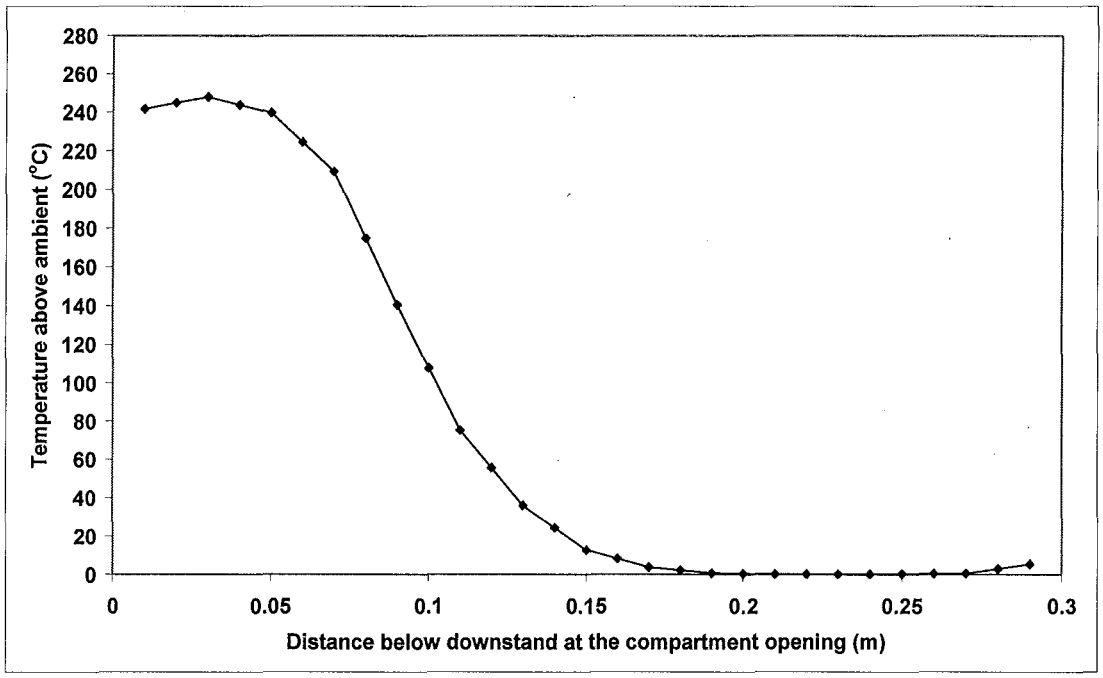

Figure G23: Temperature profile at the compartment opening for Simulation 12

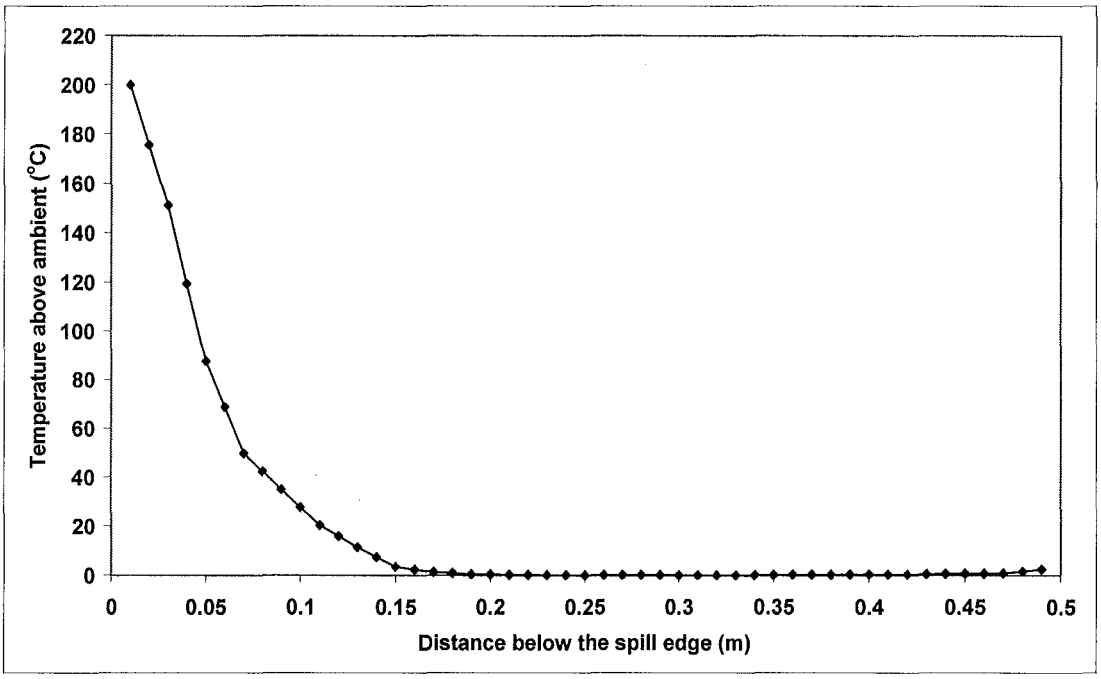

Figure G24: Temperature profile at the spill edge for Simulation 12

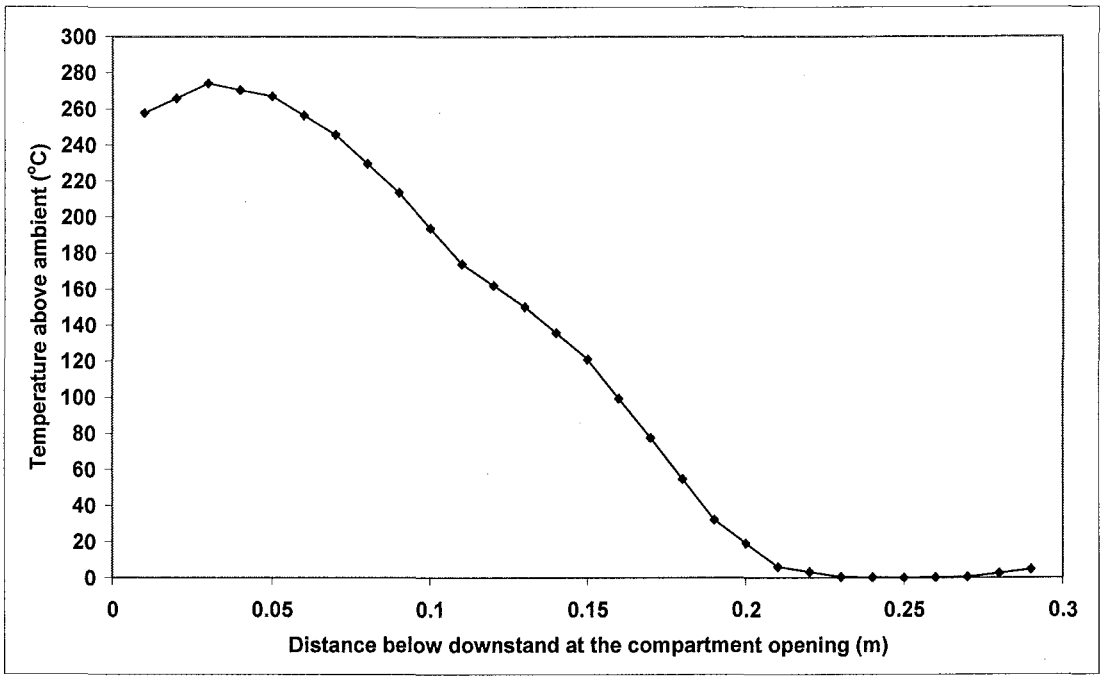

Figure G25: Temperature profile at the compartment opening for Simulation 13

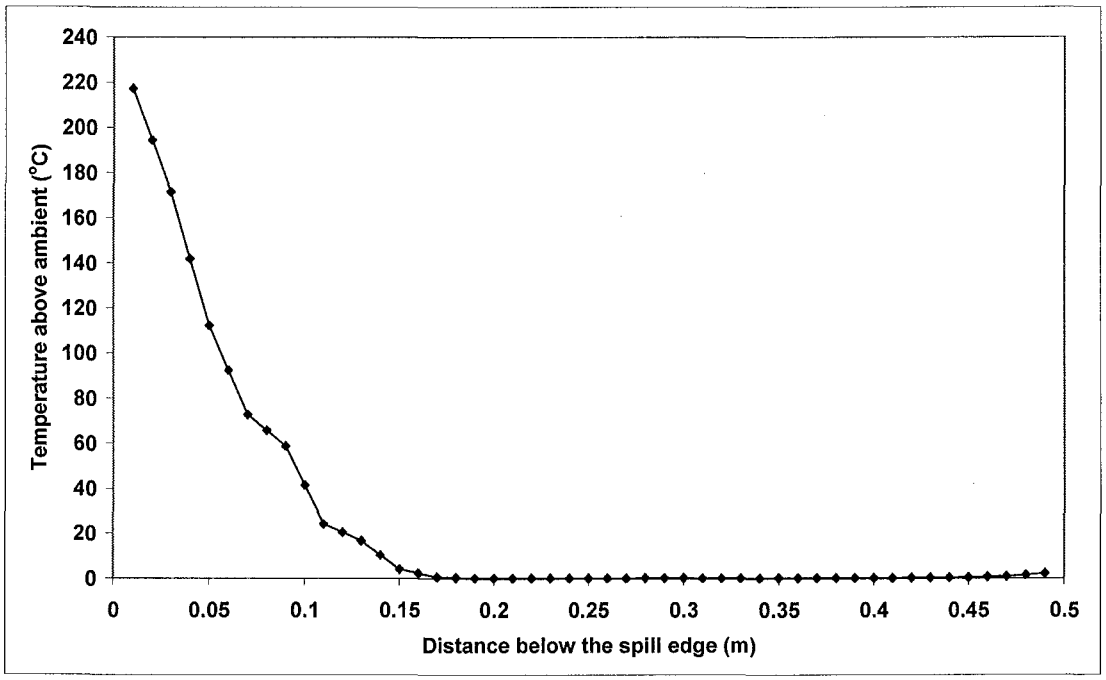

Figure G26: Temperature profile at the spill edge for Simulation 13

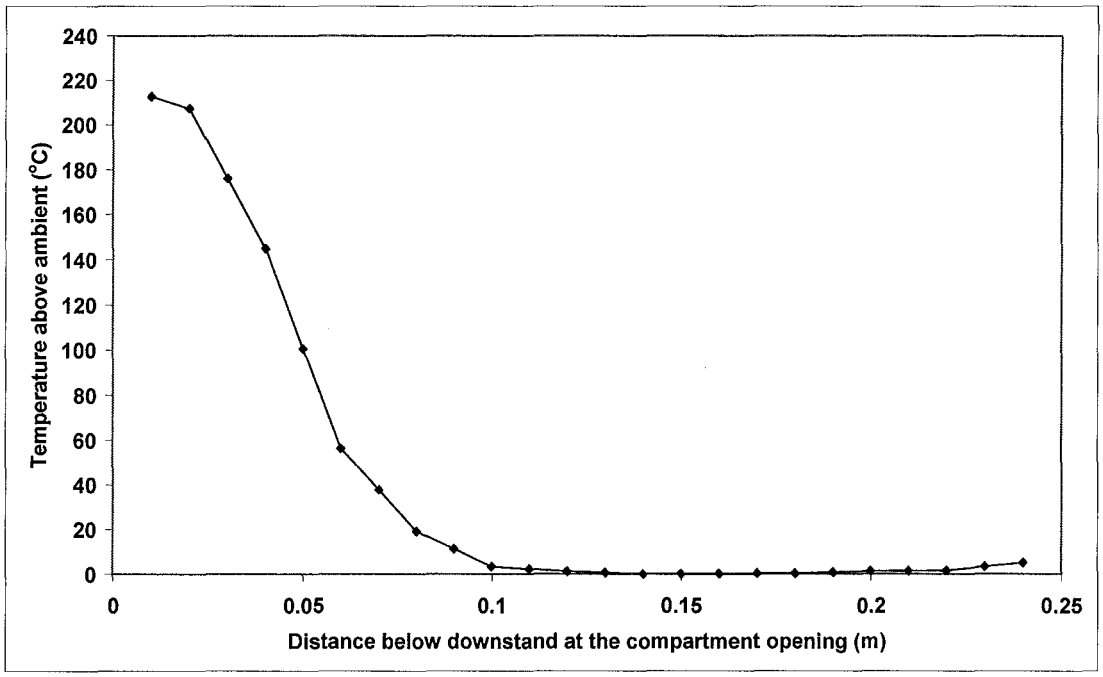

Figure G27: Temperature profile at the compartment opening for Simulation 14

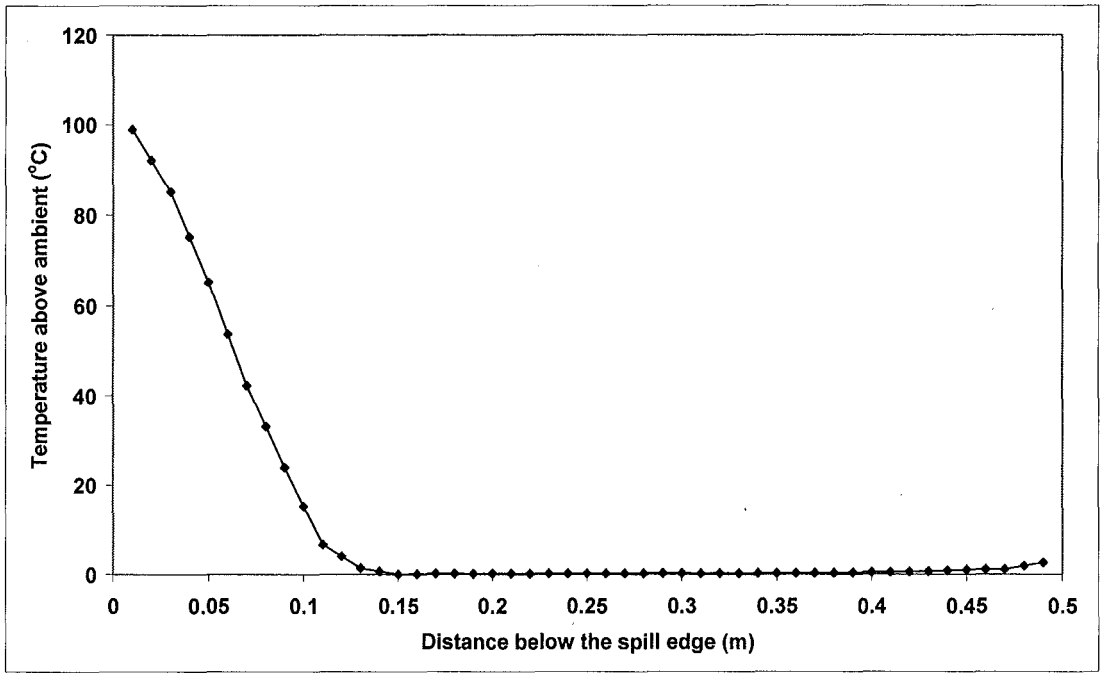

Figure G28: Temperature profile at the spill edge for Simulation 14

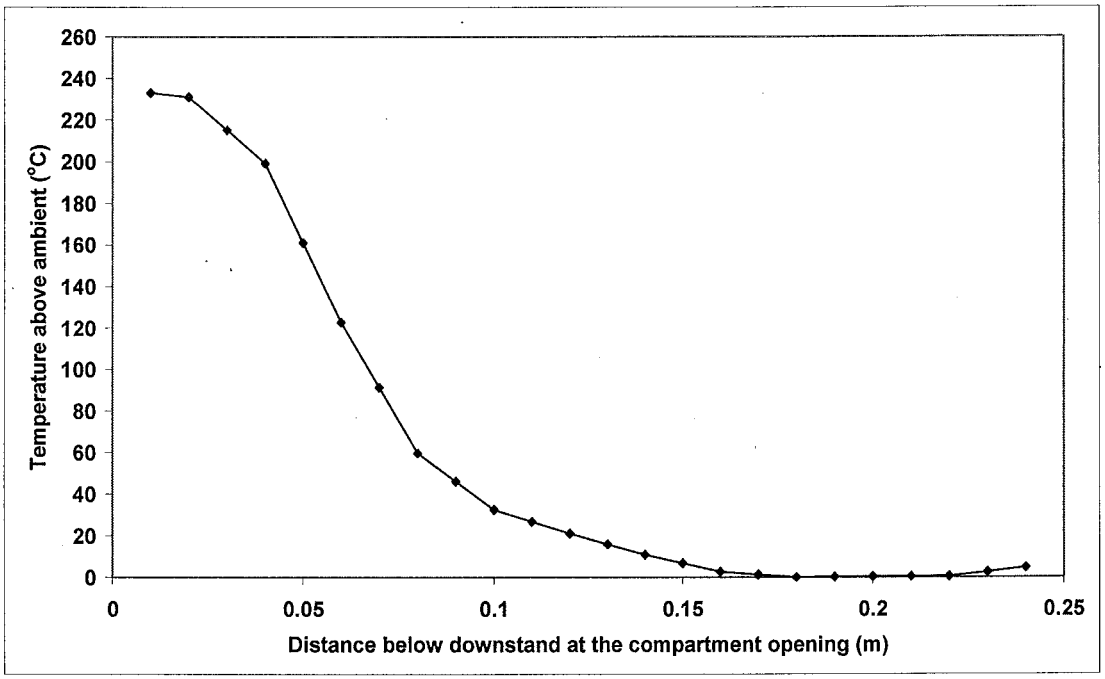

Figure G29: Temperature profile at the compartment opening for Simulation 15

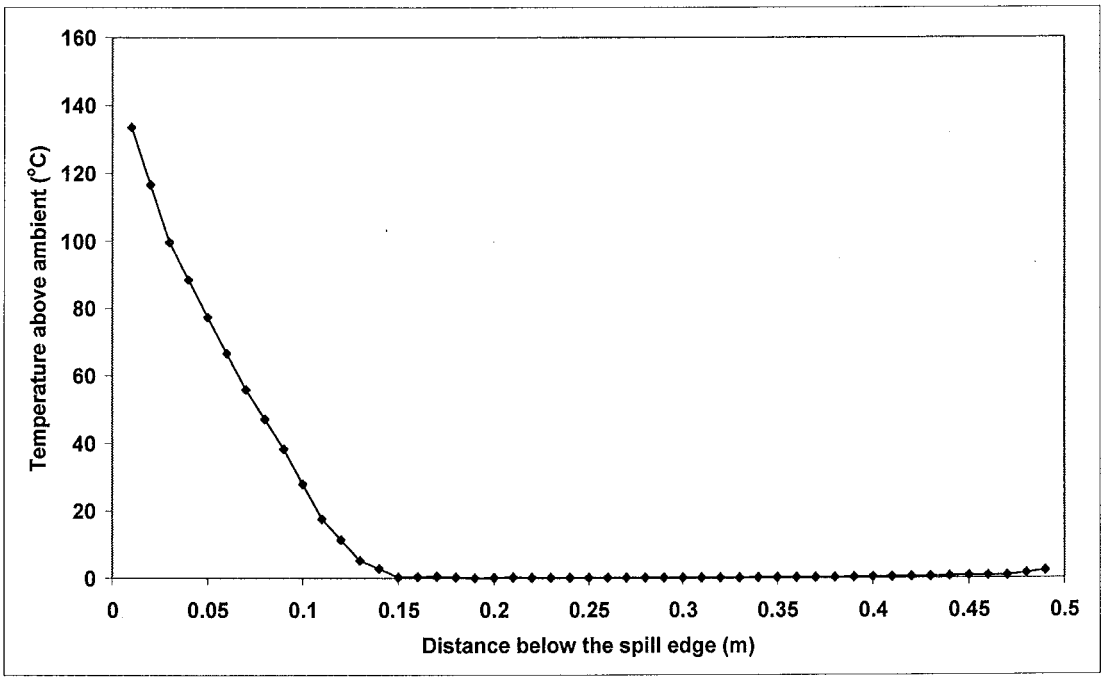

Figure G30: Temperature profile at the spill edge for Simulation 15

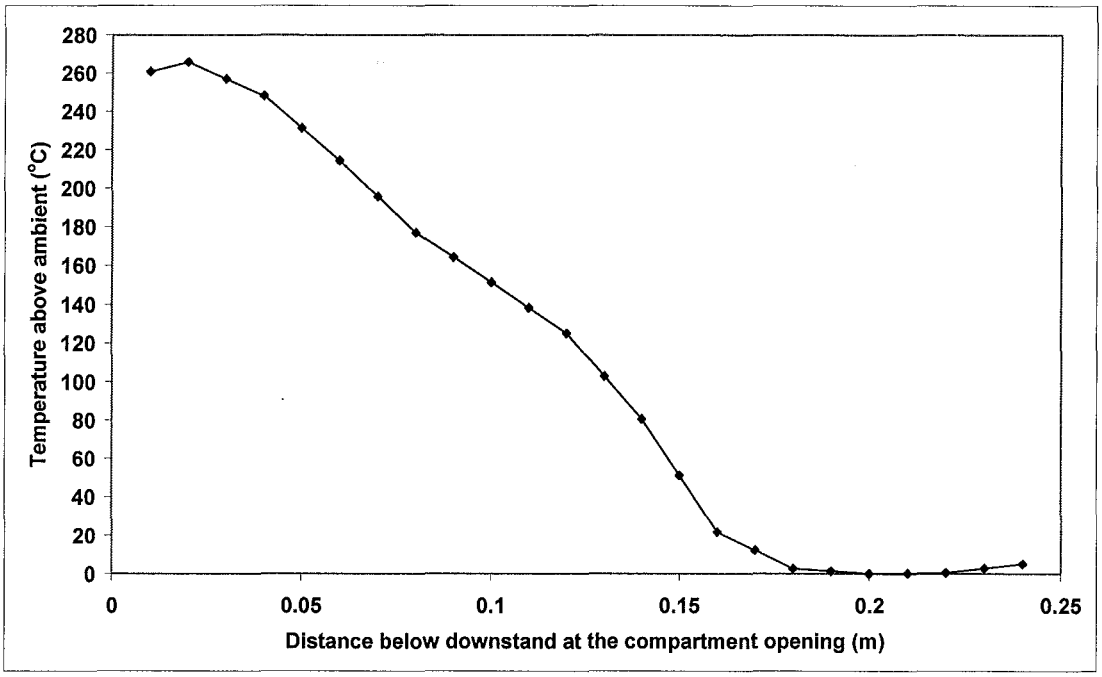

Figure G31: Temperature profile at the compartment opening for Simulation 16

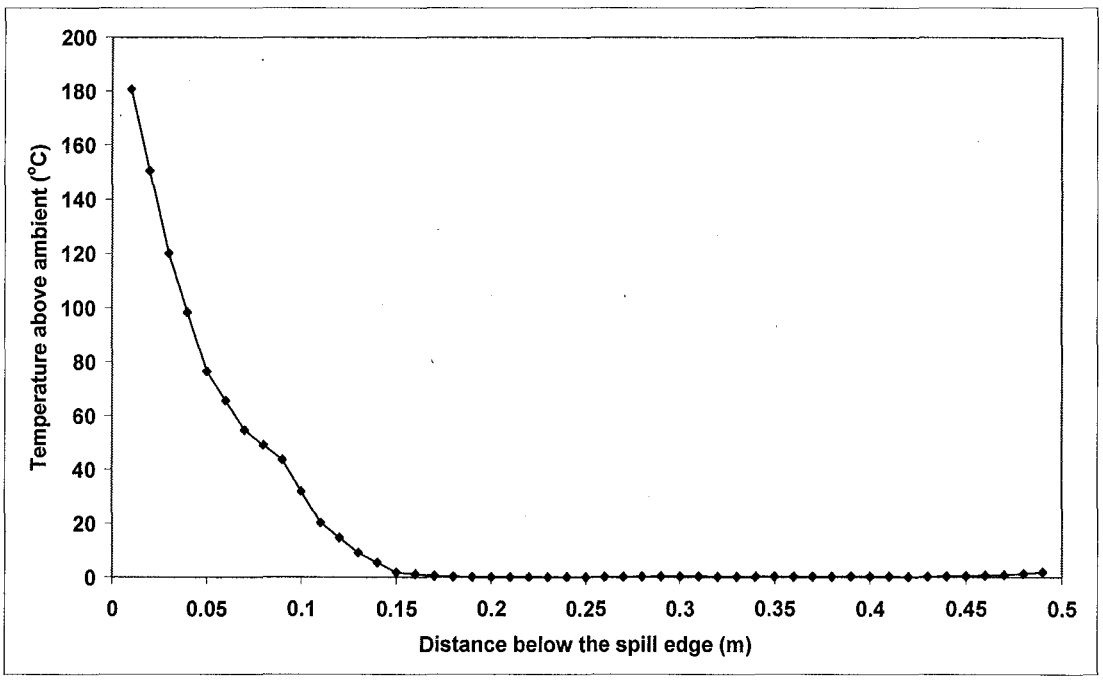

Figure G32: Temperature profile at the spill edge for Simulation 16

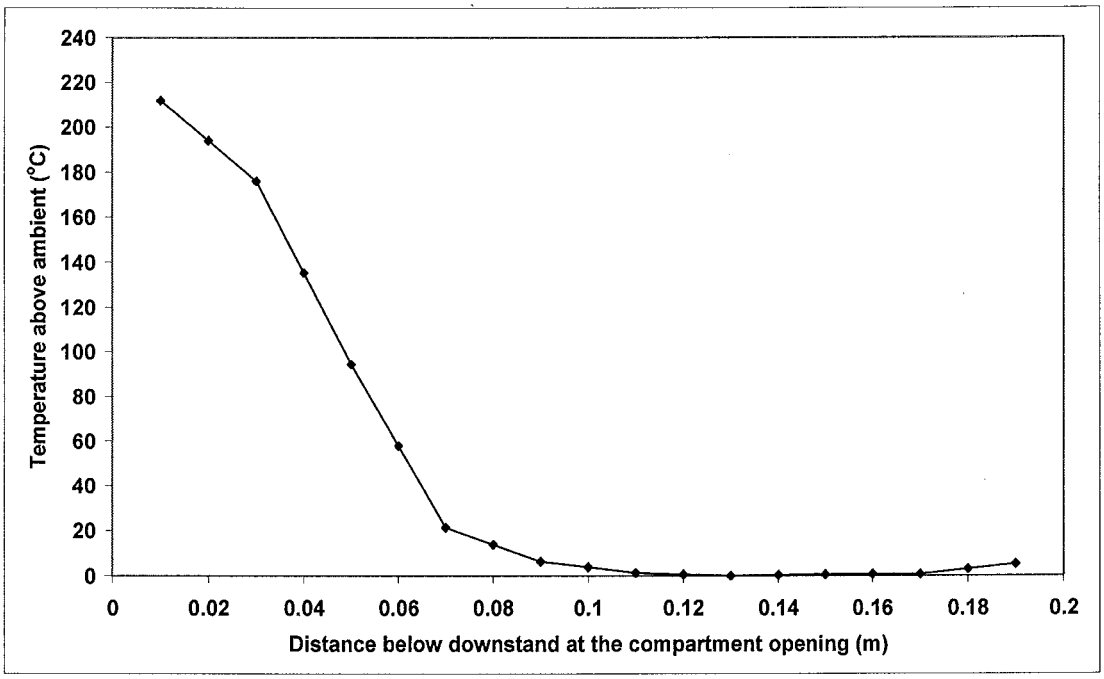

Figure G33: Temperature profile at the compartment opening for Simulation 17

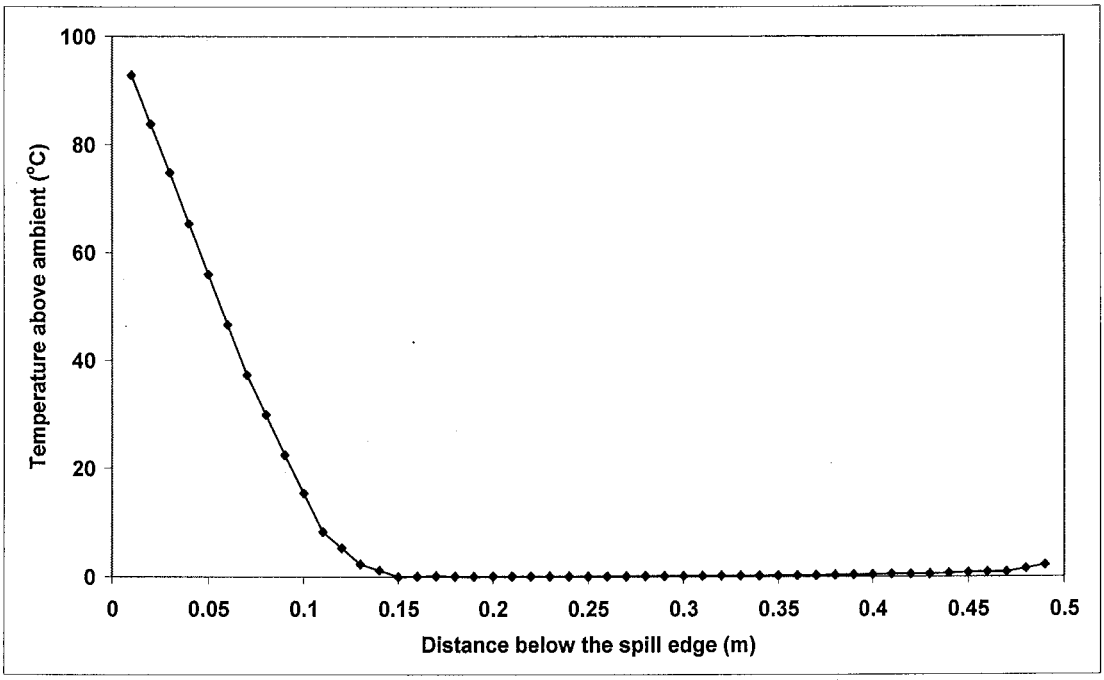

Figure G34: Temperature profile at the spill edge for Simulation 17

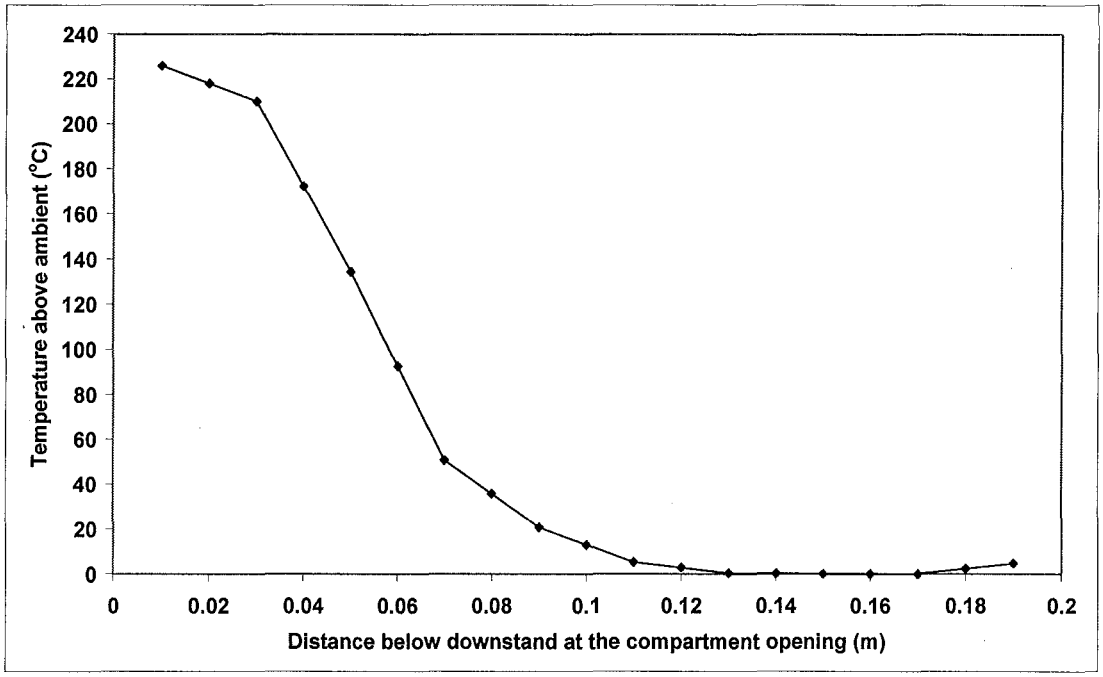

Figure G35: Temperature profile at the compartment opening for Simulation 18

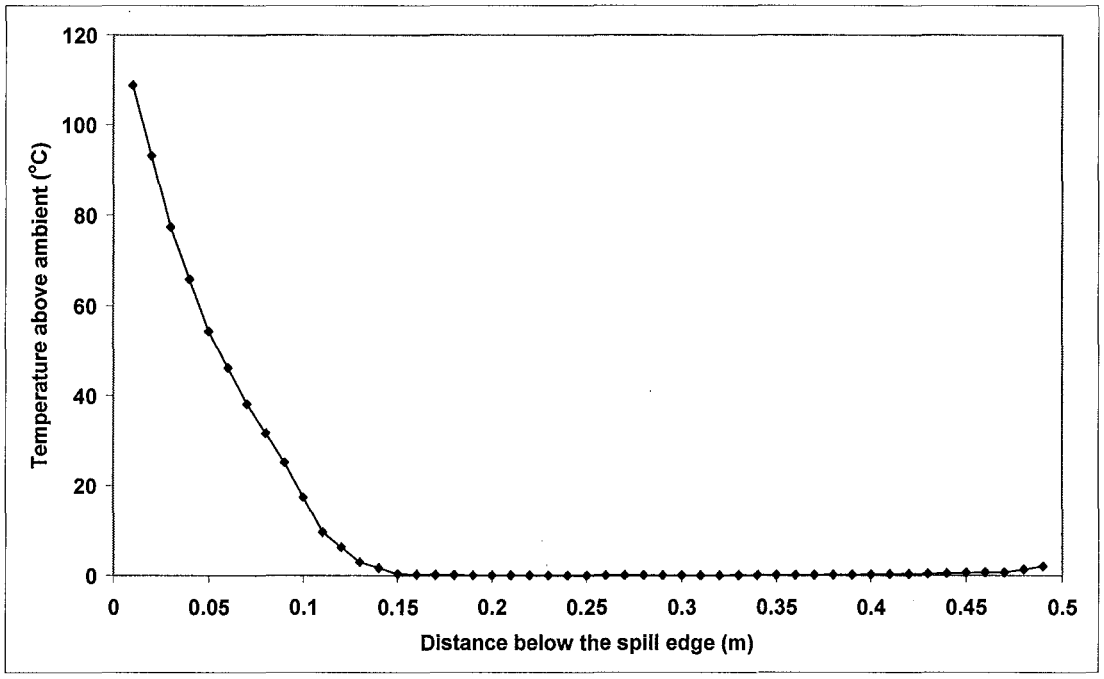

Figure G36: Temperature profile at the spill edge for Simulation 18

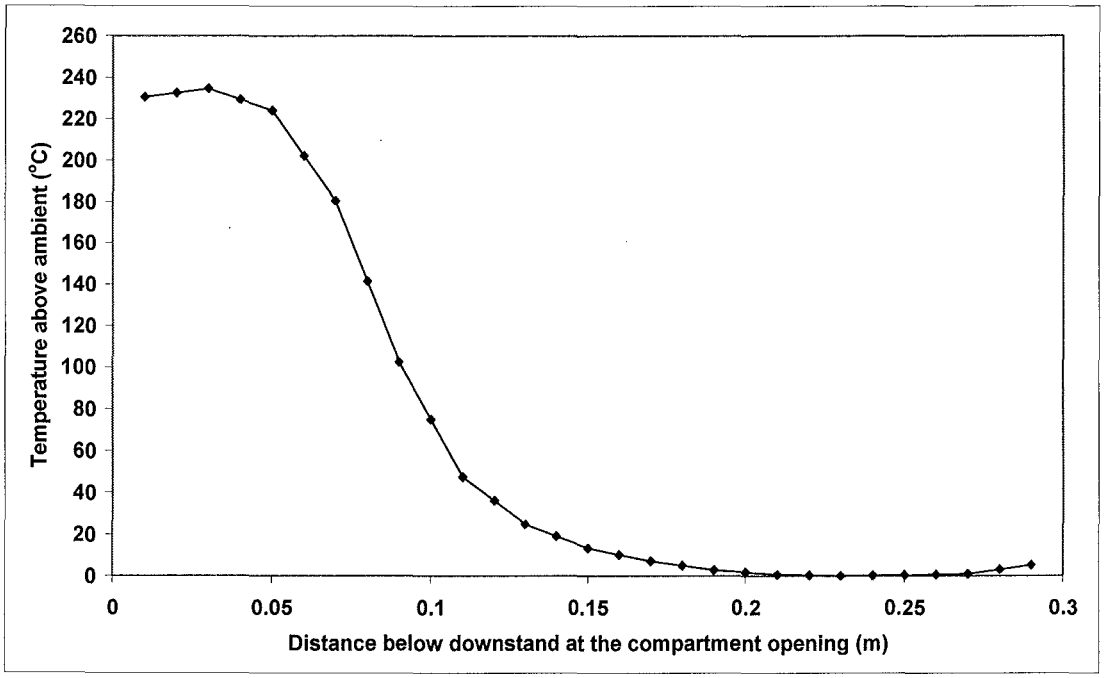

Figure G37: Temperature profile at the compartment opening for Simulation 19

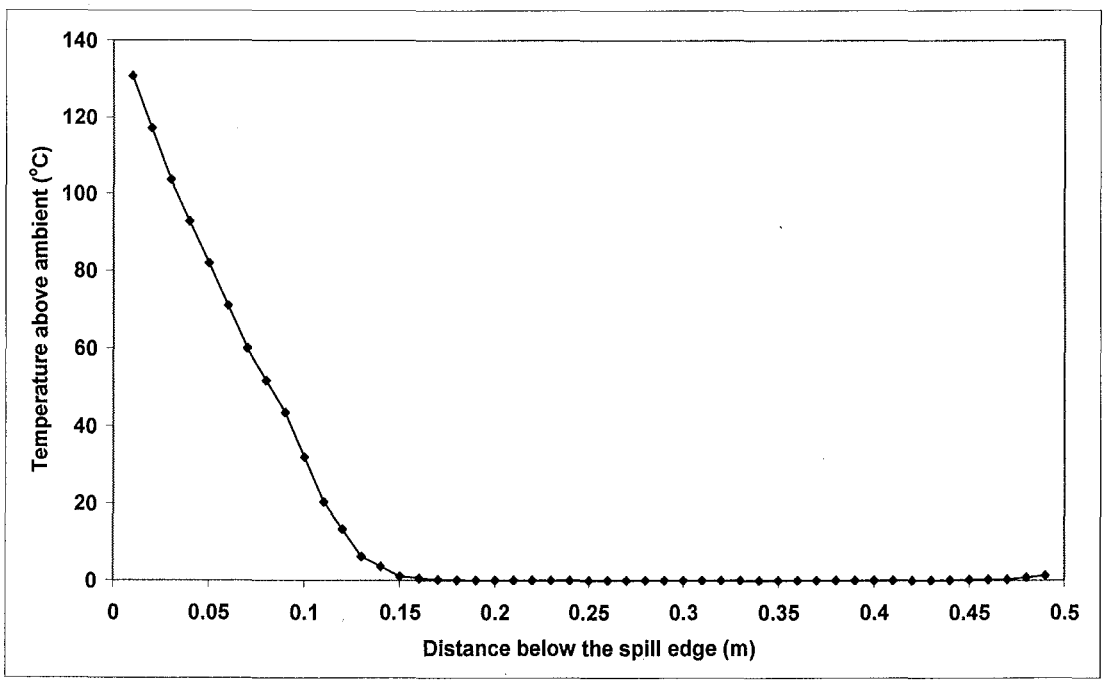

Figure G38: Temperature profile at the spill edge for Simulation 19

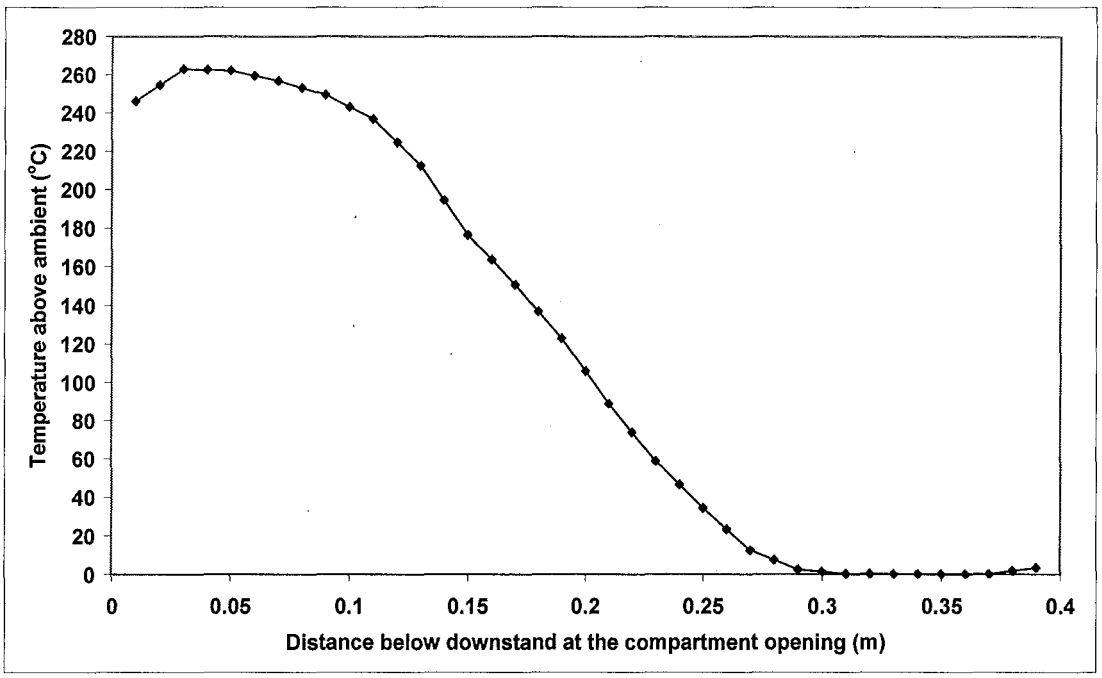

Figure G39: Temperature profile at the compartment opening for Simulation 20

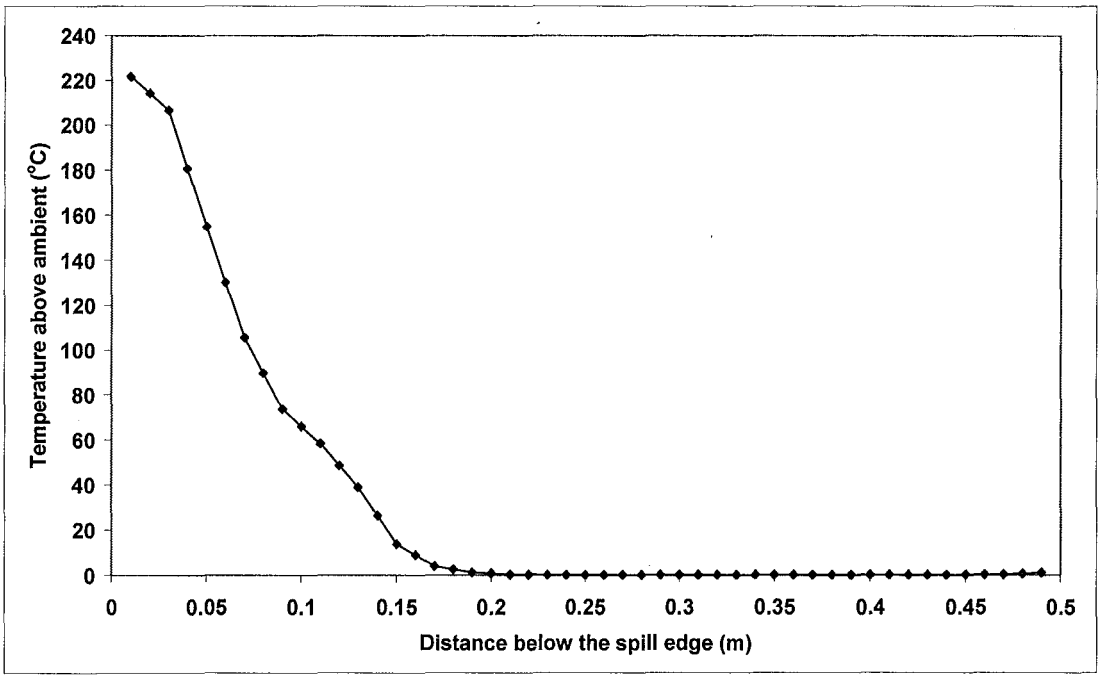

Figure G40: Temperature profile at the spill edge for Simulation 20

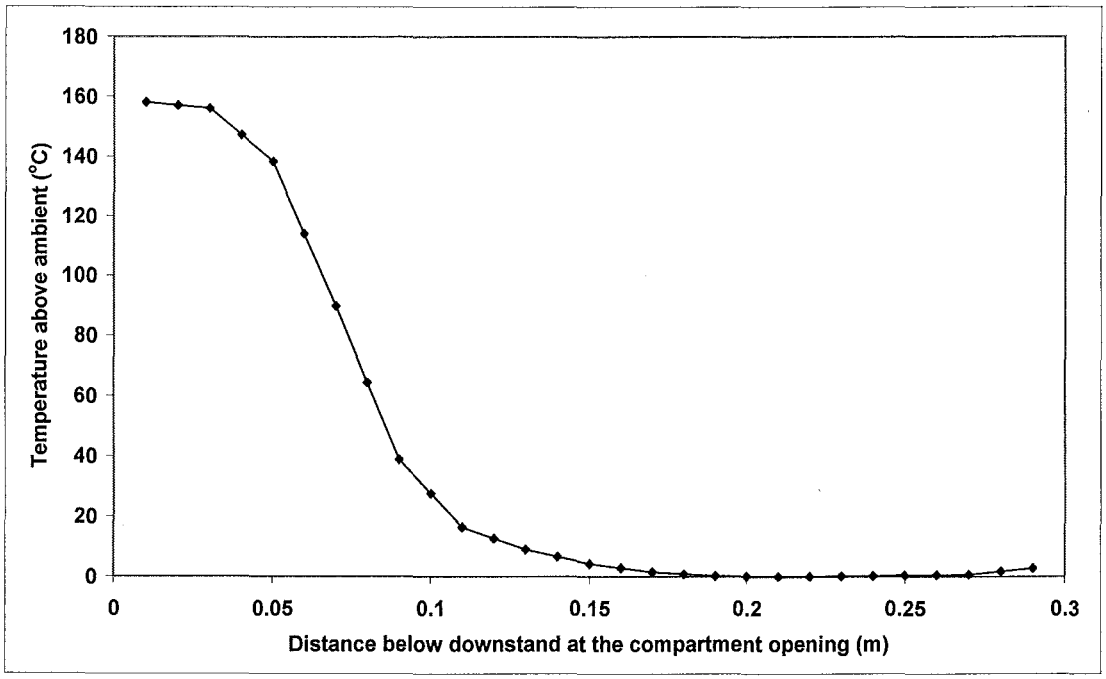

Figure G41: Temperature profile at the compartment opening for Simulation 21

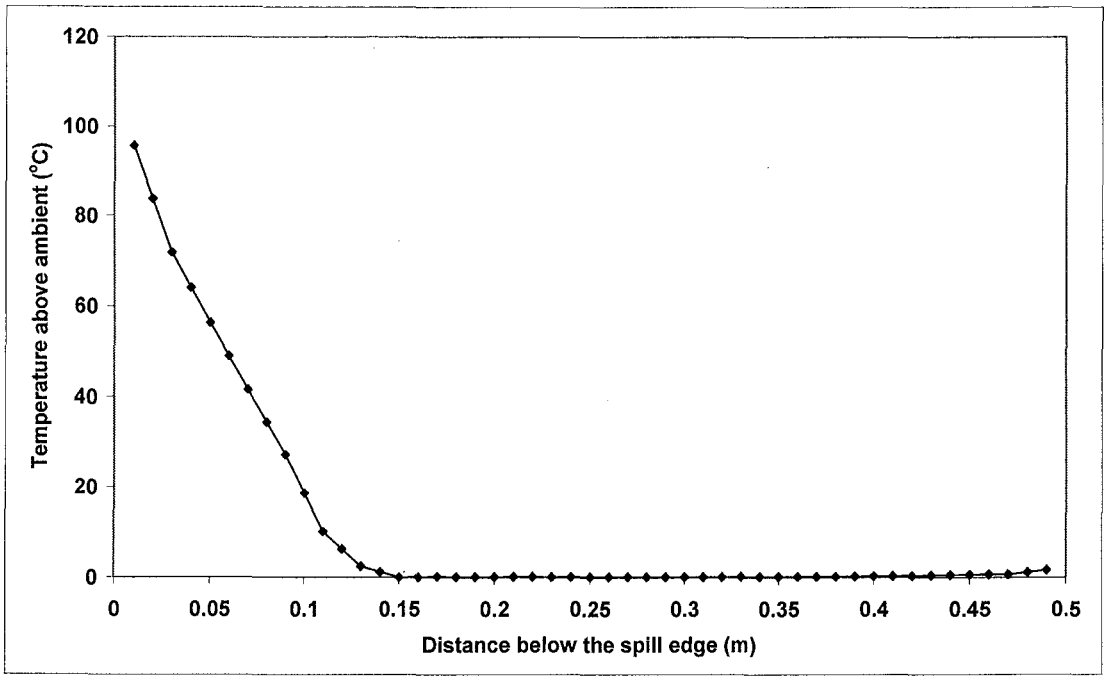

Figure G42: Temperature profile at the spill edge for Simulation 21

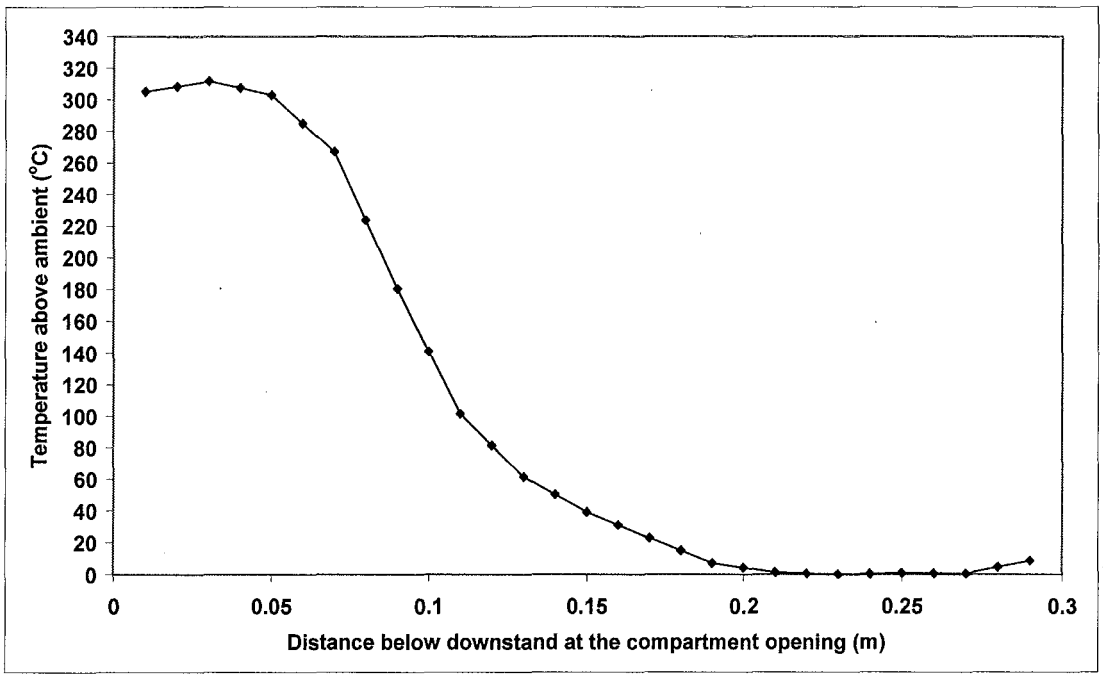

Figure G43: Temperature profile at the compartment opening for Simulation 22

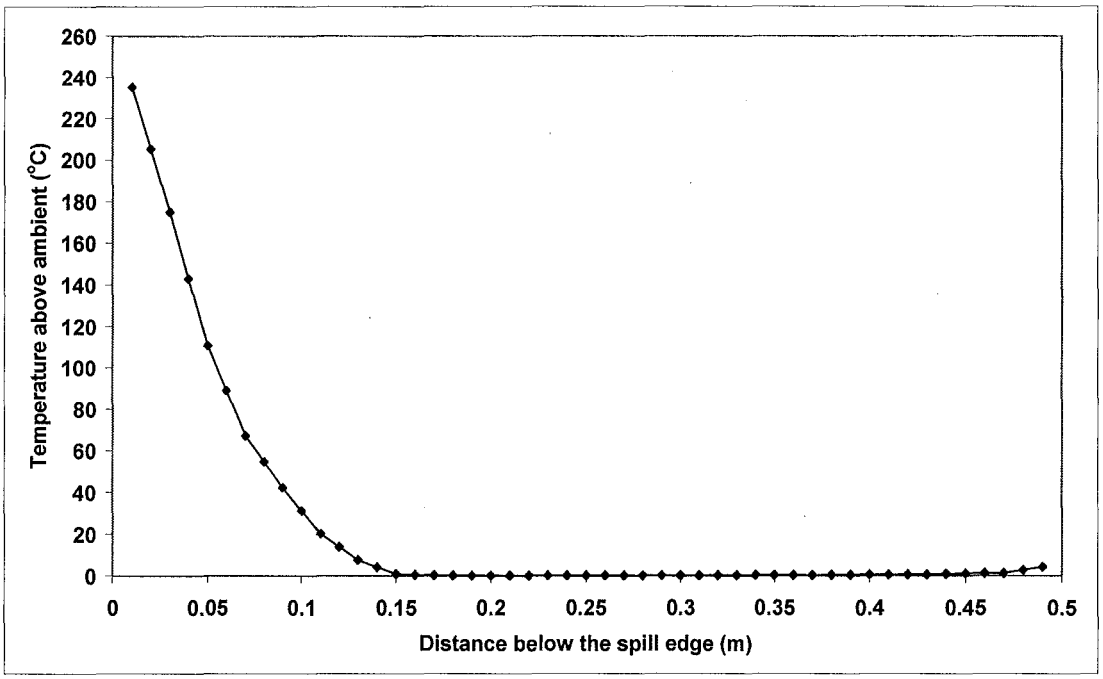

Figure G44: Temperature profile at the spill edge for Simulation 22

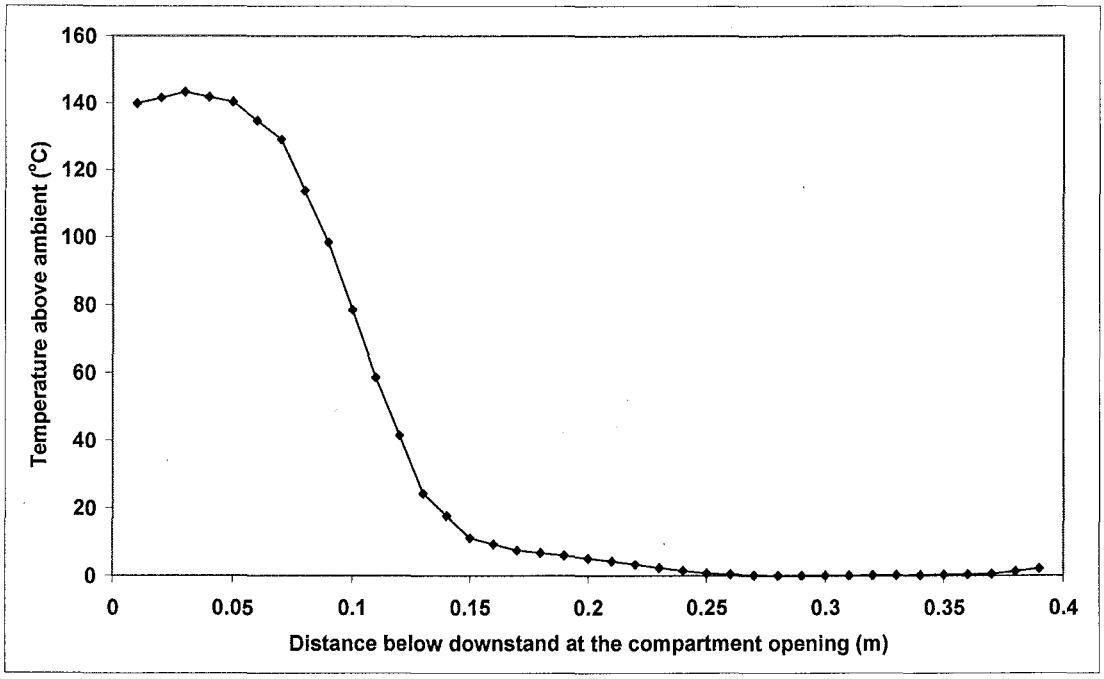

Figure G45: Temperature profile at the compartment opening for Simulation 23

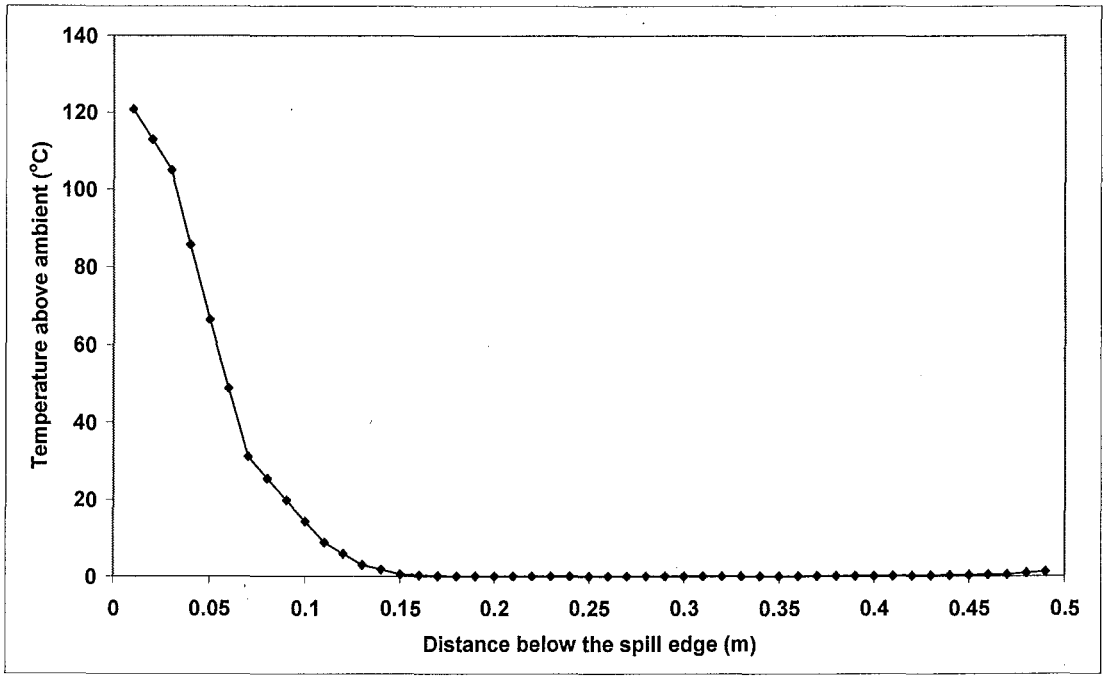

Figure G46: Temperature profile at the spill edge for Simulation 23

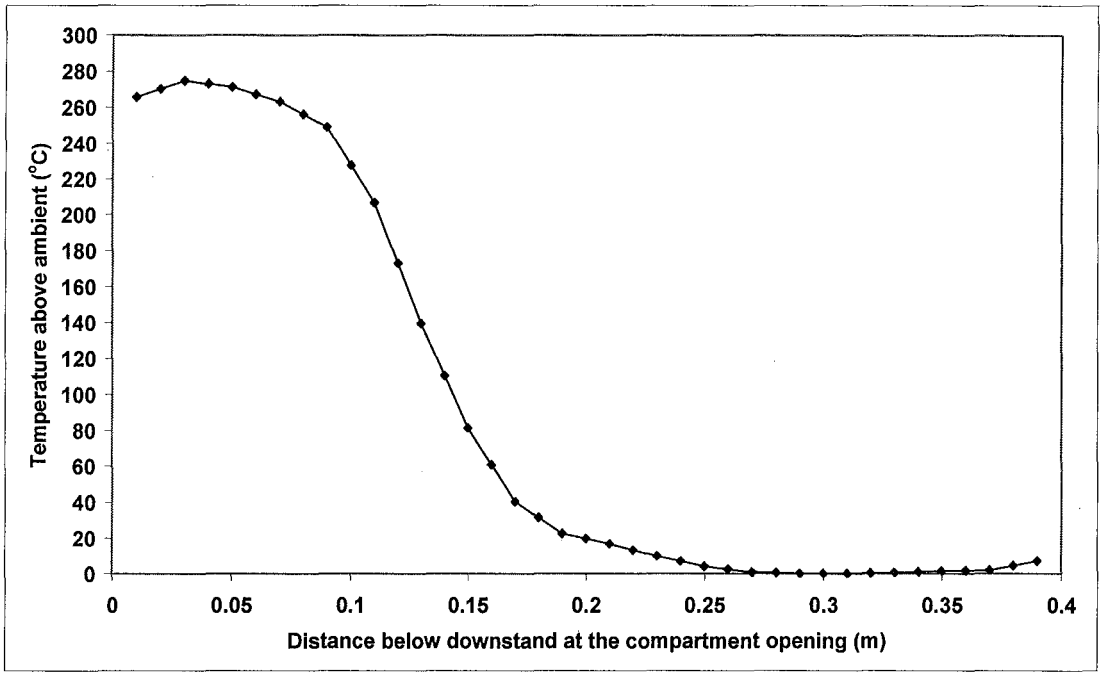

Figure G47: Temperature profile at the compartment opening for Simulation 24

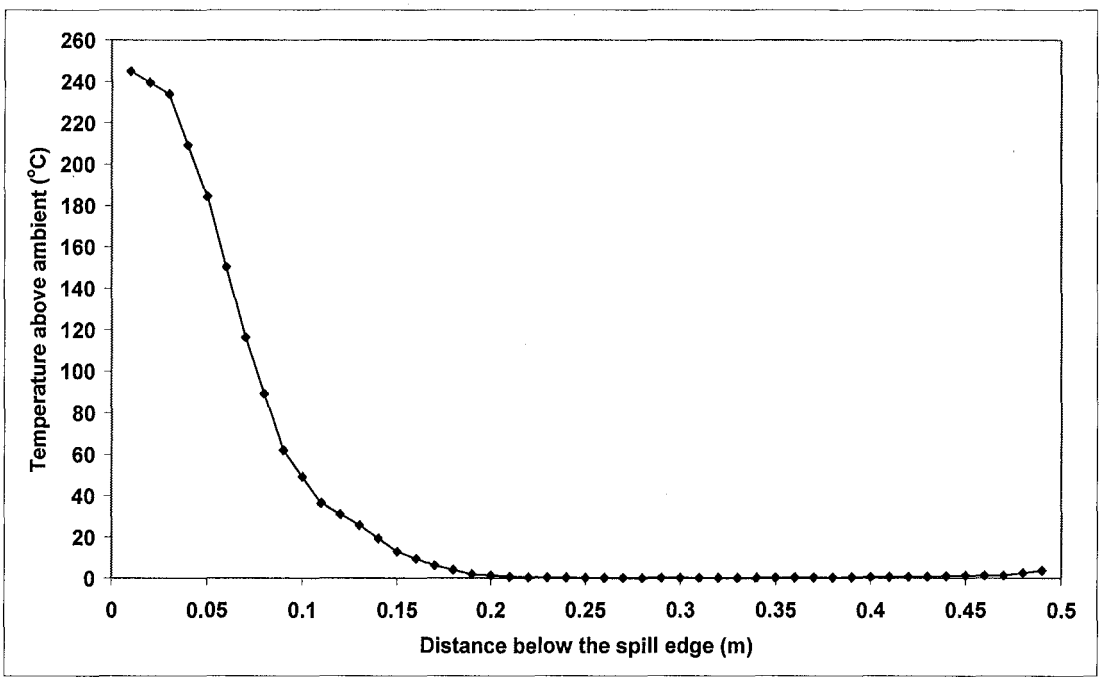

Figure G48: Temperature profile at the spill edge for Simulation 24

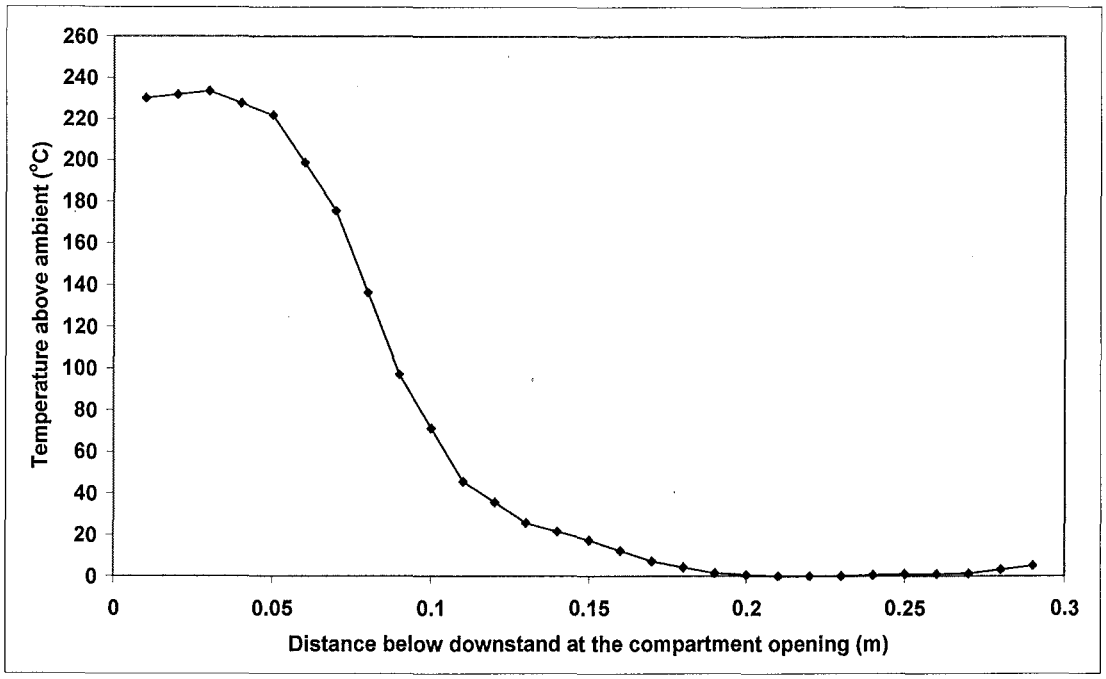

Figure G49: Temperature profile at the compartment opening for Simulation 25

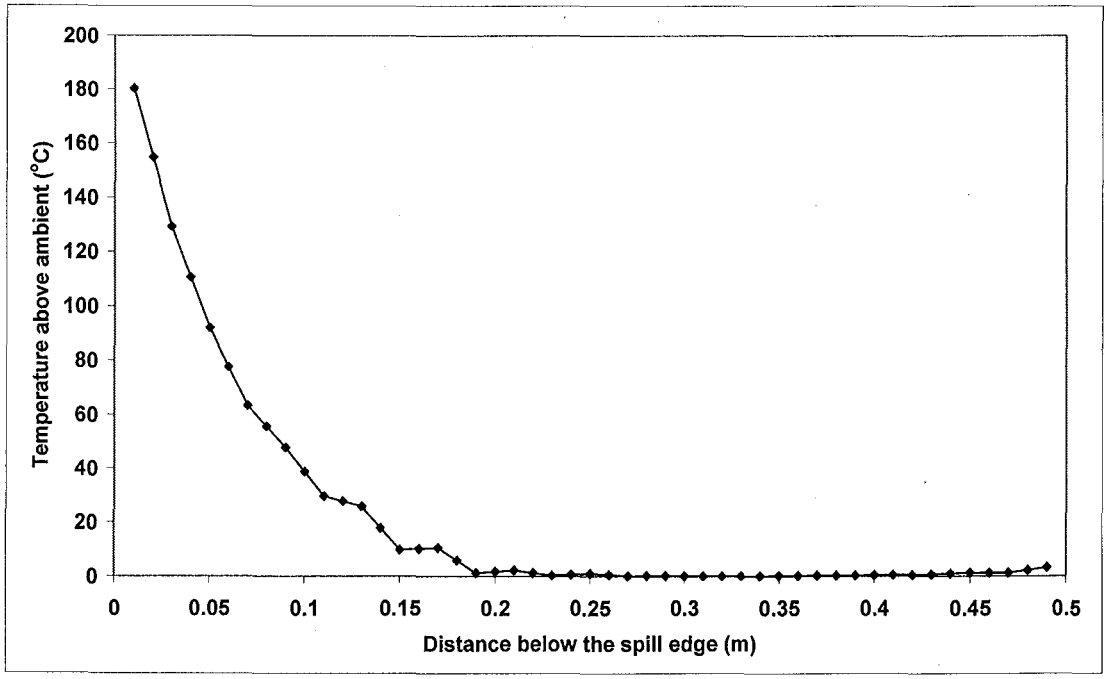

Figure G50: Temperature profile at the spill edge for Simulation 25

Appendix G

APPENDIX H FDS VELOCITY PROFILES (SIMULATIONS 1 TO 25)

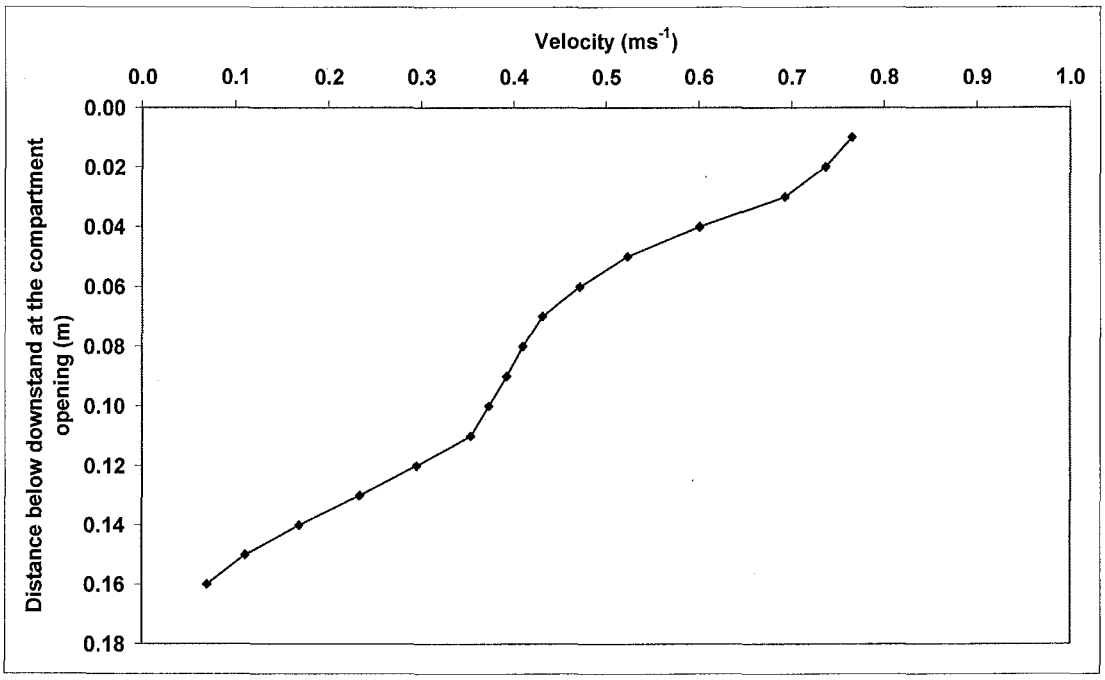

Figure H1: **Velocity profile at the compartment opening for Simulation 1**

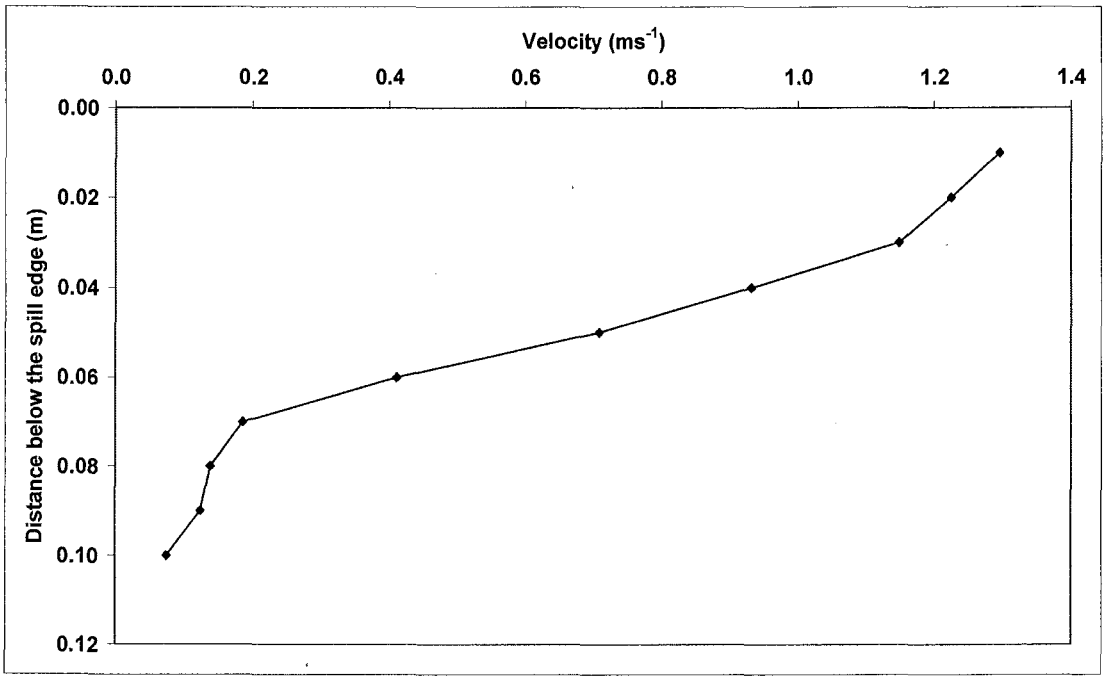

Figure H2: **Velocity profile at the spill edge for Simulation 1**

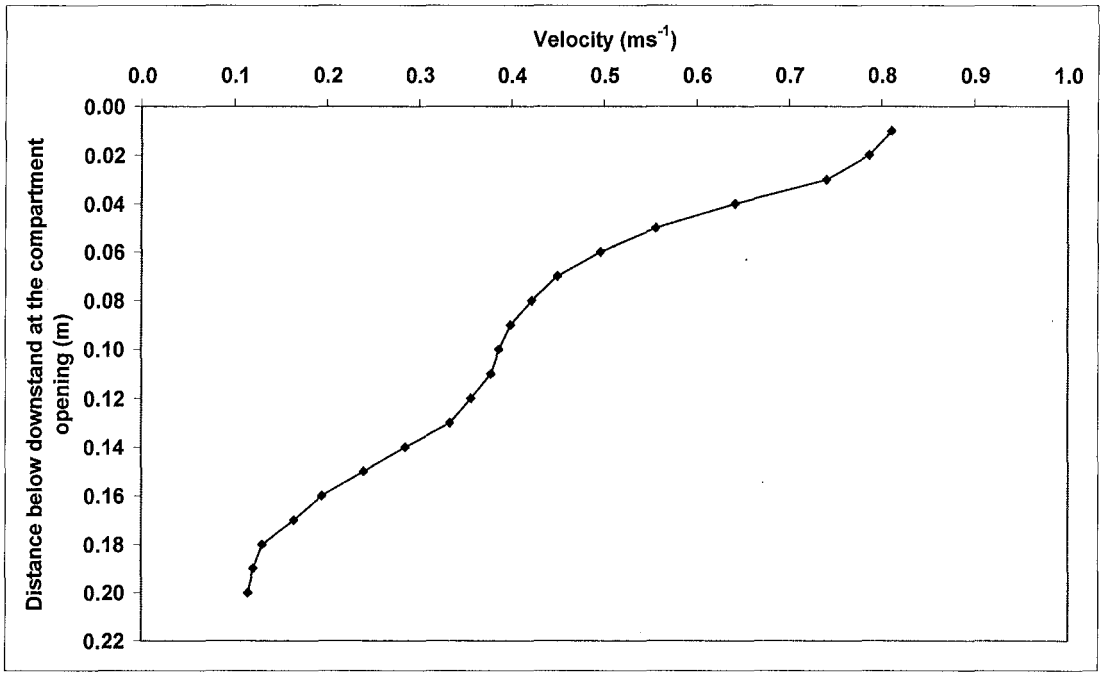

Figure H3: Velocity profile at the compartment opening for Simulation 2

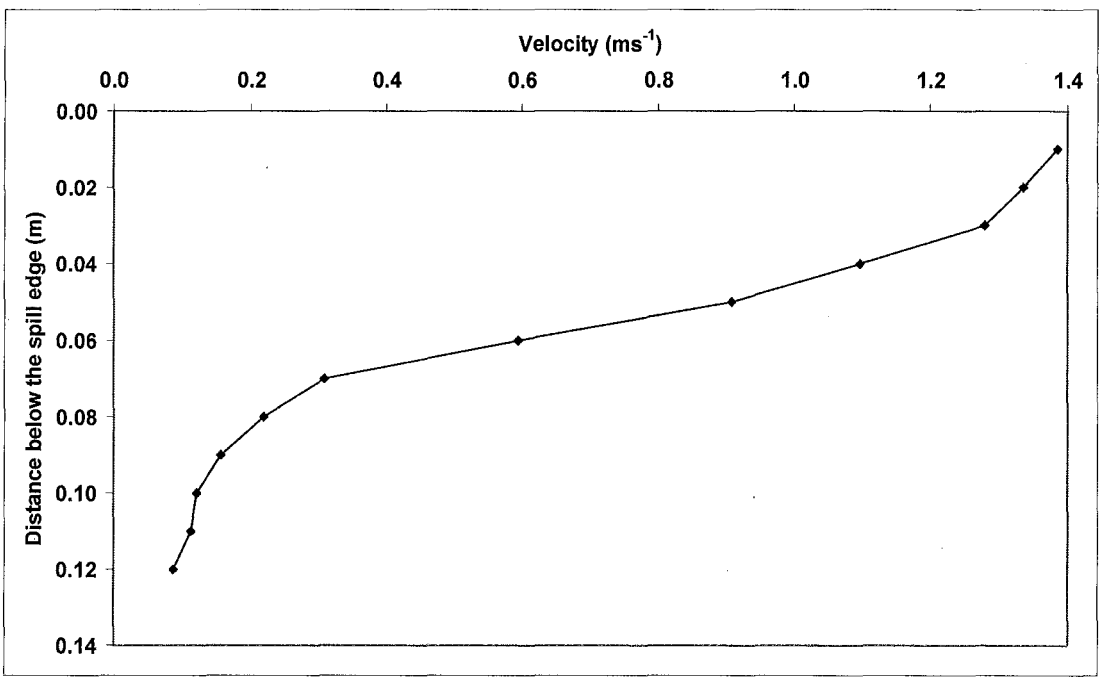

Figure H4: Velocity profile at the spill edge for Simulation 2

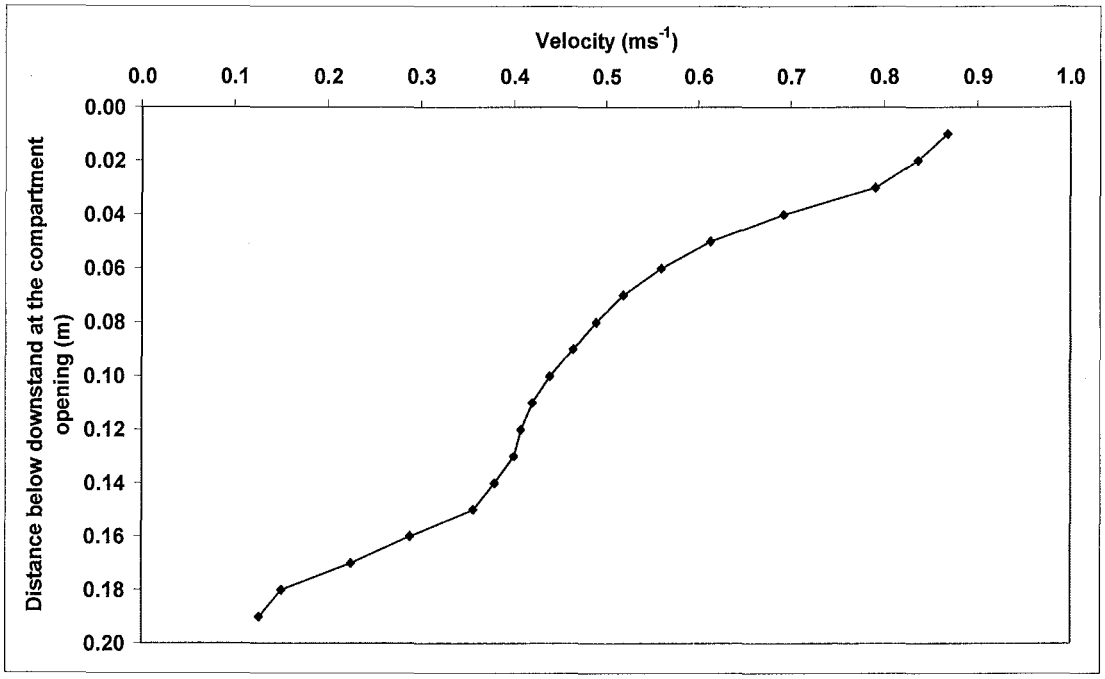

Figure H5: Velocity profile at the compartment opening for Simulation 3

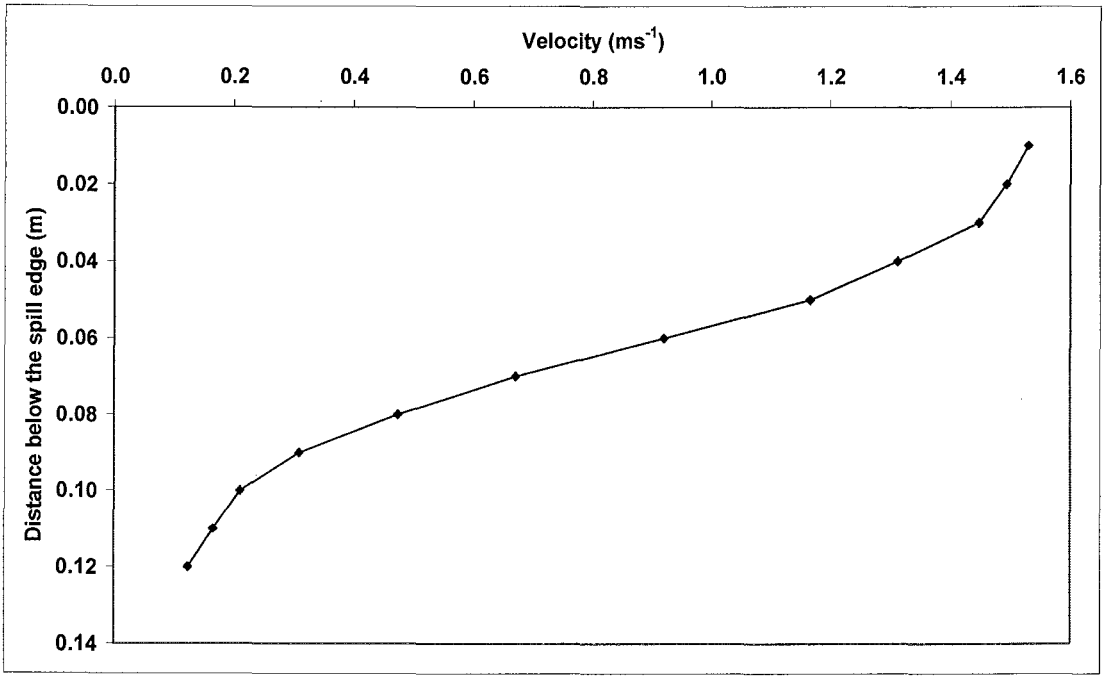

Figure H6: Velocity profile at the spill edge for Simulation 3

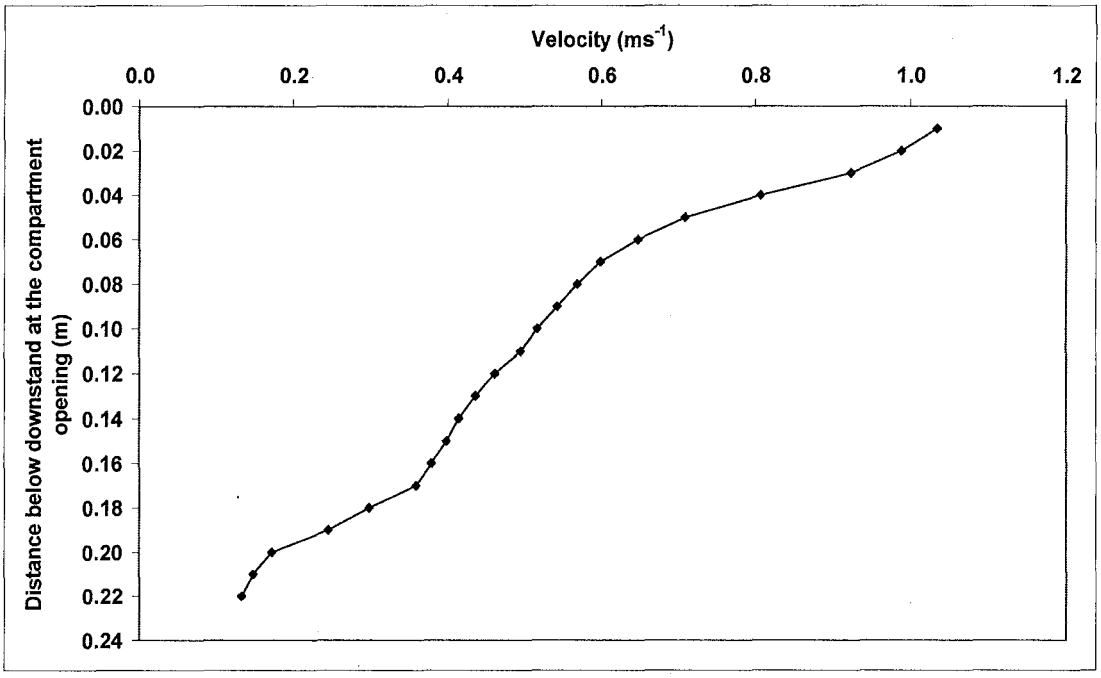

Figure H7: Velocity profile at the compartment opening for Simulation 4

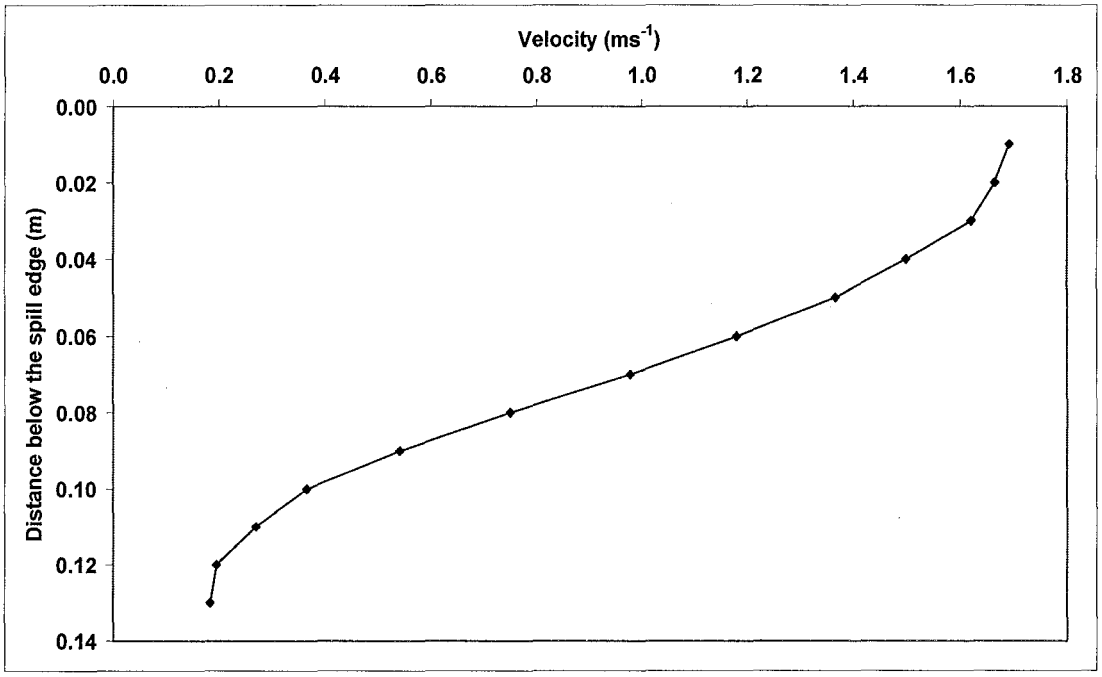

Figure H8: Velocity profile at the spill edge for Simulation 4

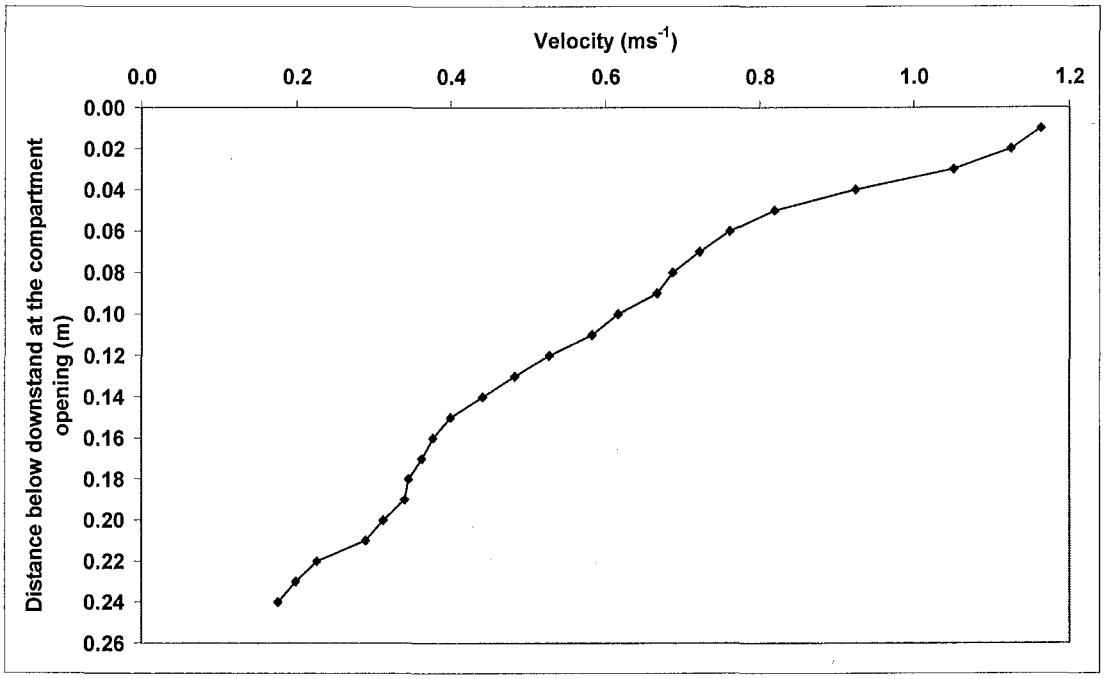

Figure H9: **Velocity profile at the compartment opening for Simulation 5**

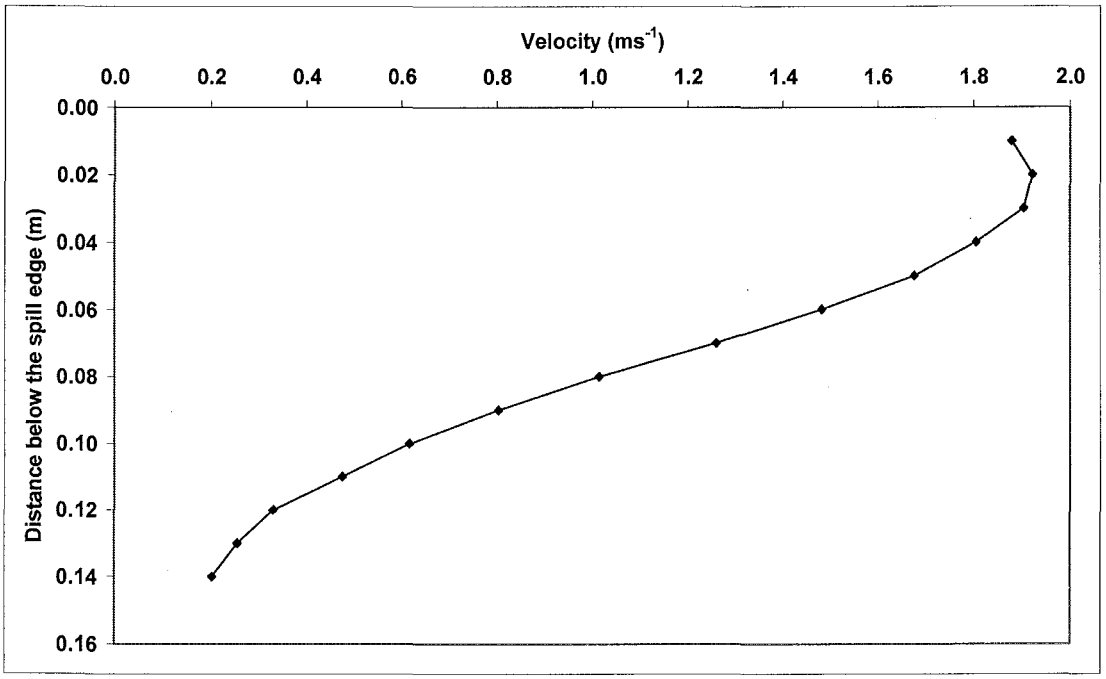

Figure H10: **Velocity profile at the spill edge for Simulation 5**

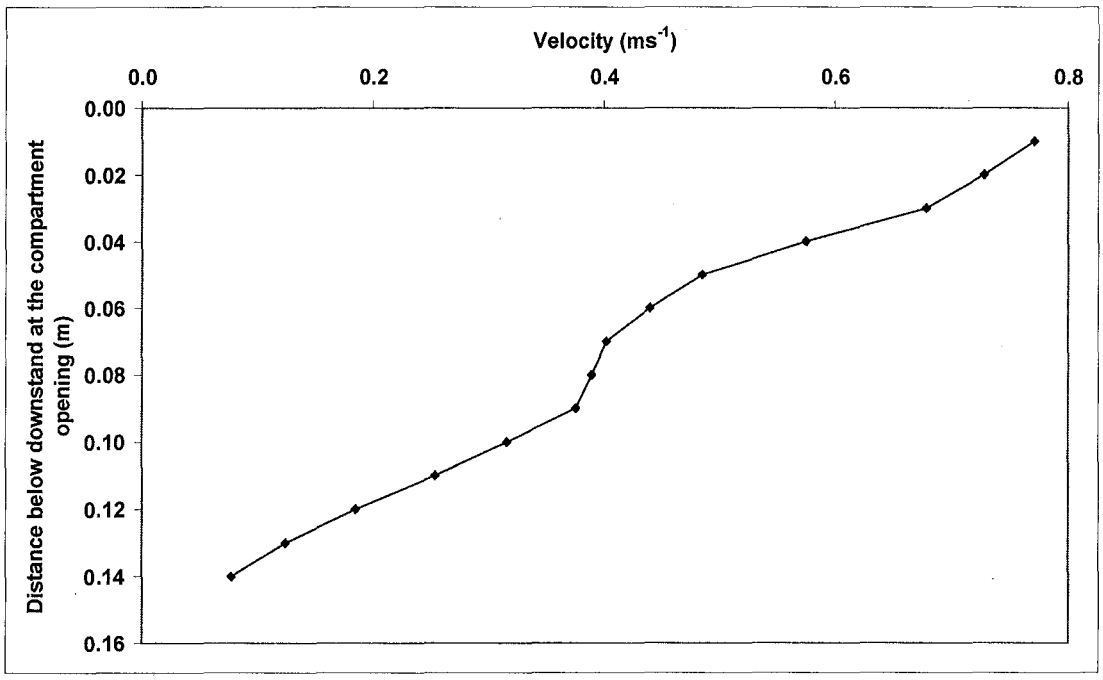

Figure H11: Velocity profile at the compartment opening for Simulation 6

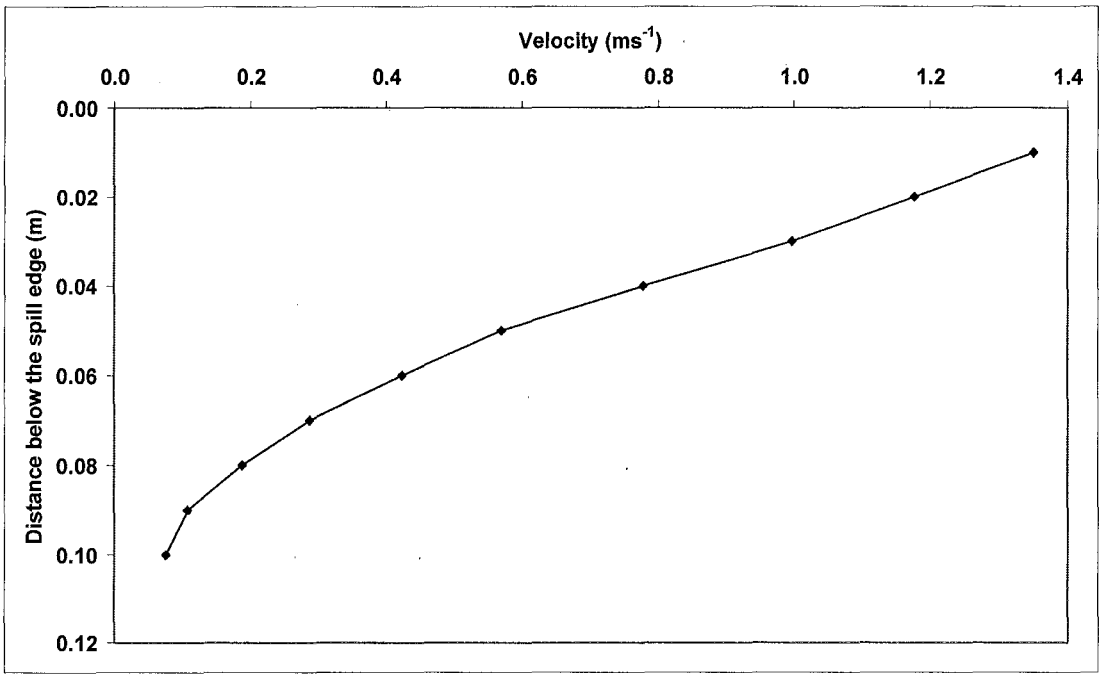

Figure H12: Velocity profile at the spill edge for Simulation 6

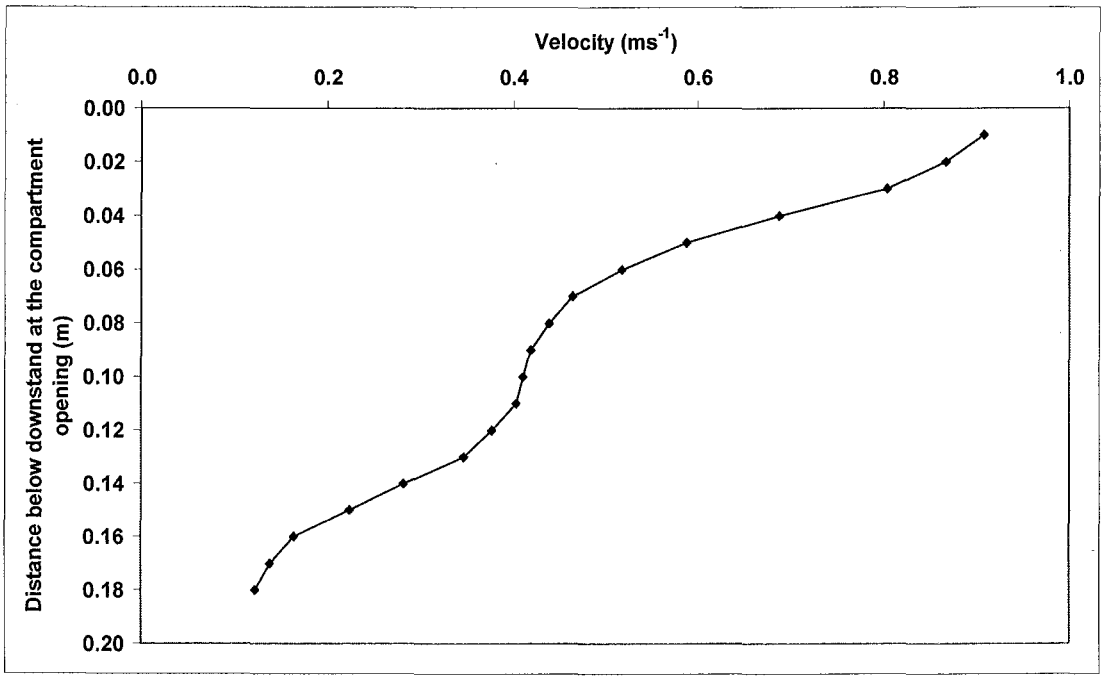

Figure H13: Velocity profile at the compartment opening for Simulation 7

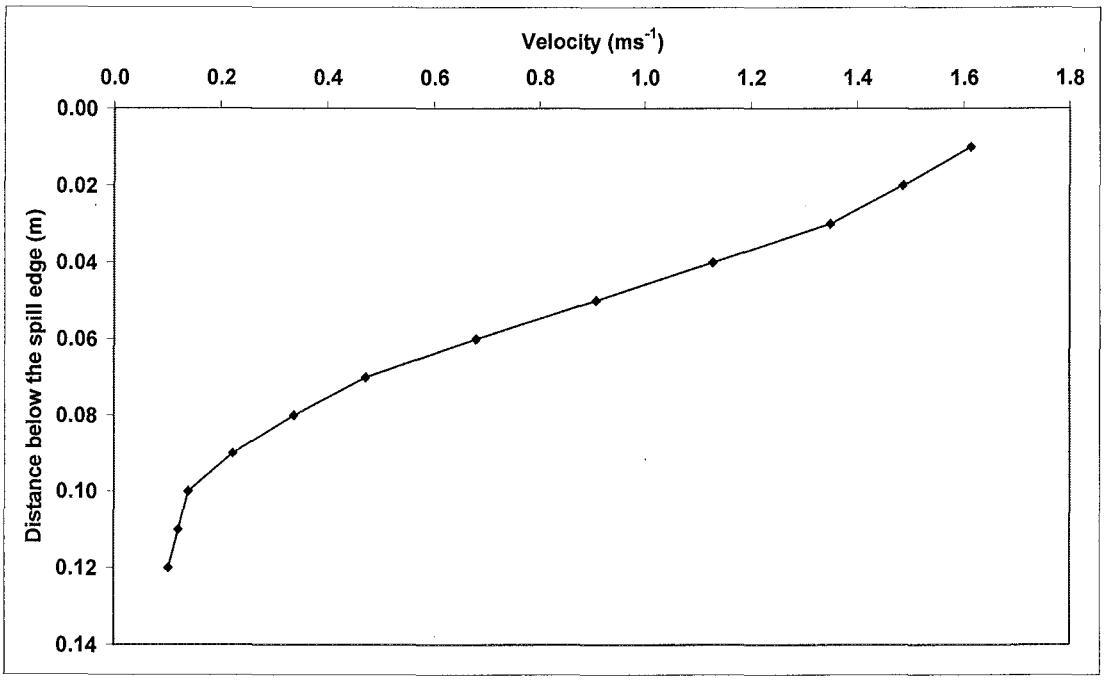

Figure H14: Velocity profile at the spill edge for Simulation 7

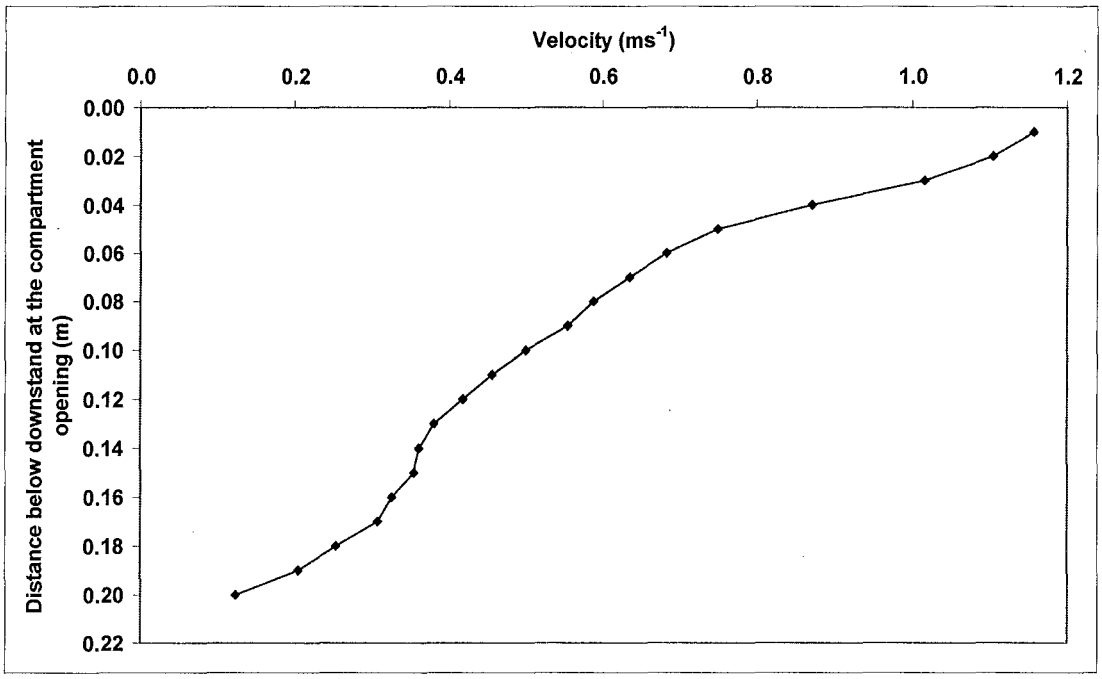

Figure H15: Velocity profile at the compartment opening for Simulation 8

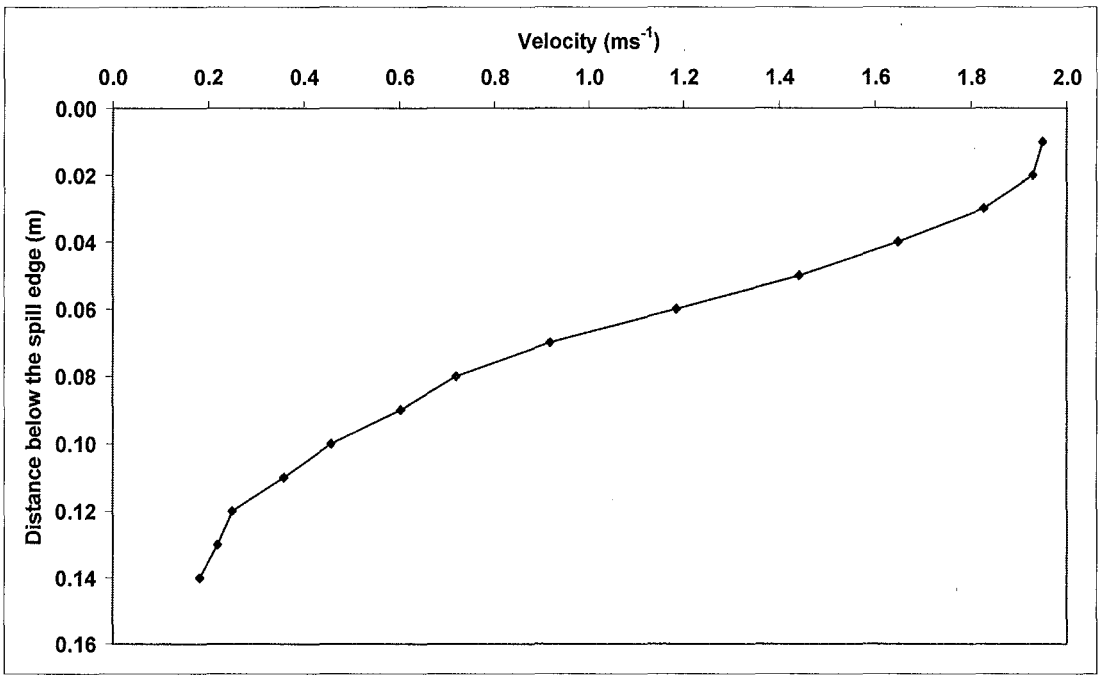

Figure H16: Velocity profile at the spill edge for Simulation 8

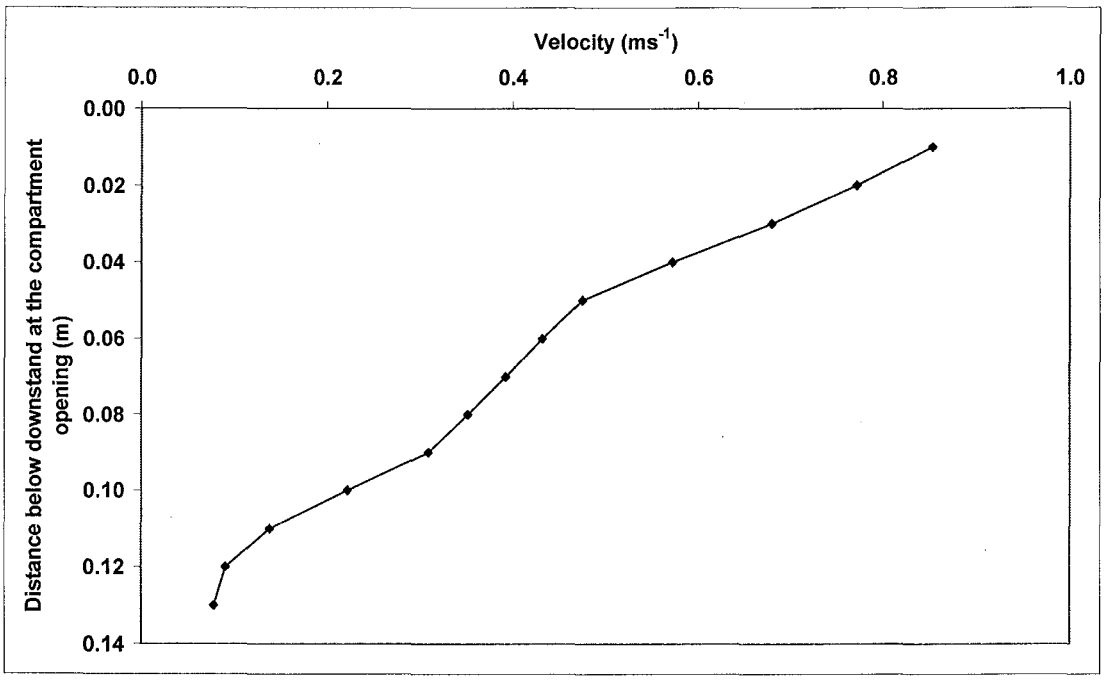

Figure H17: Velocity profile at the compartment opening for Simulation 9

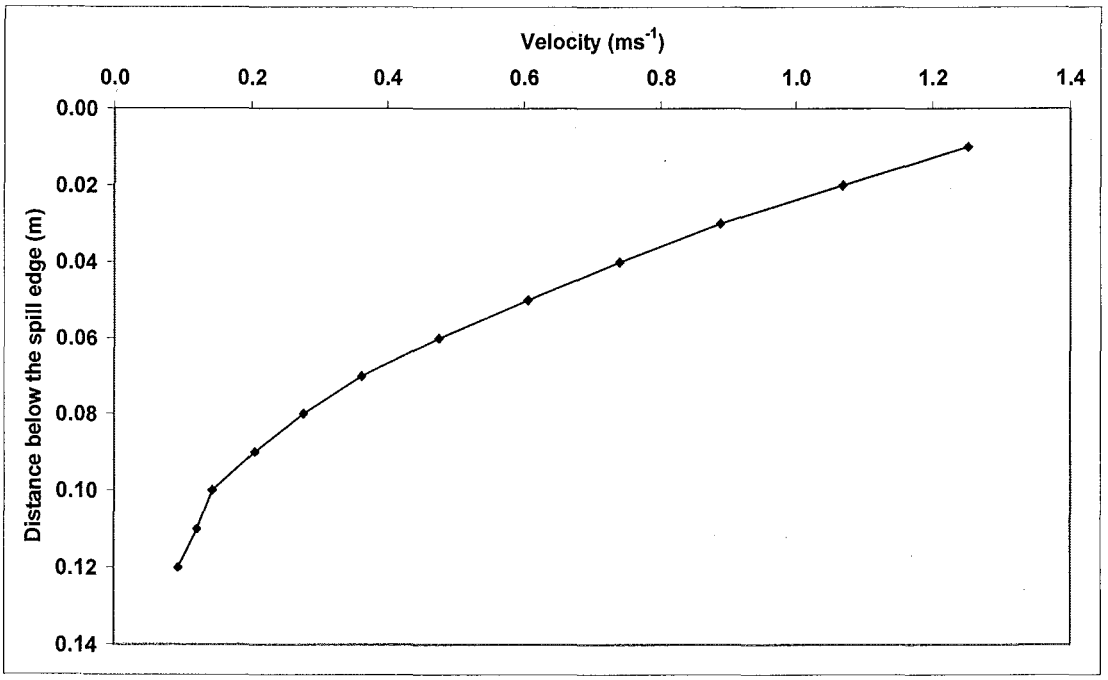

Figure H18: Velocity profile at the spill edge for Simulation 9

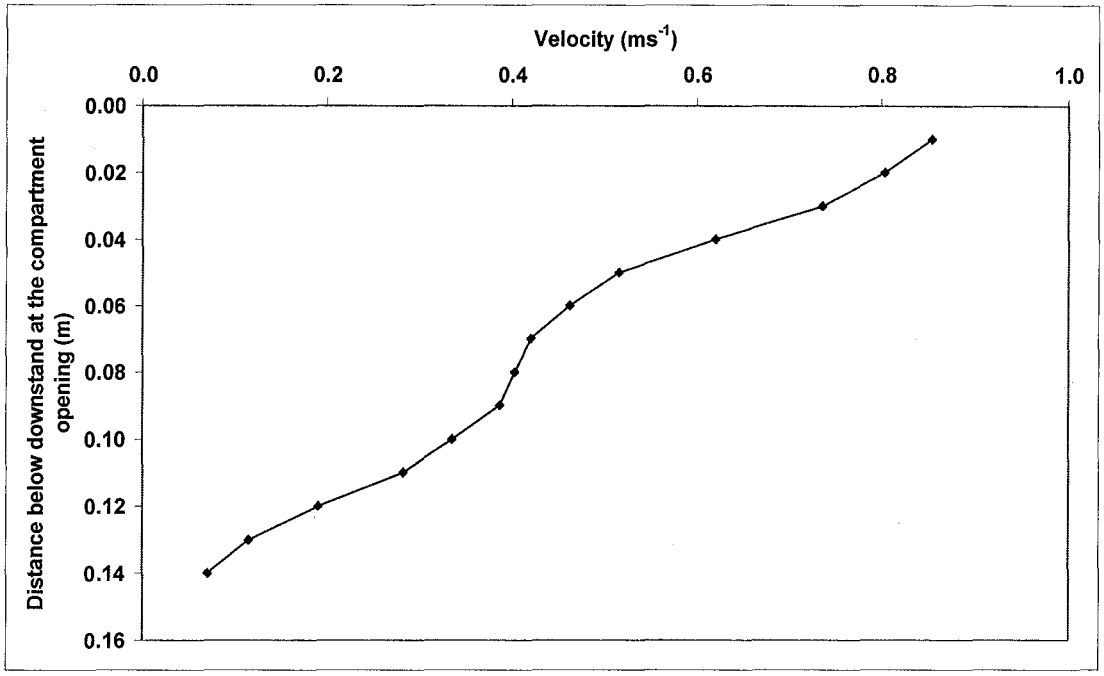

Figure H19: Velocity profile at the compartment opening for Simulation 10

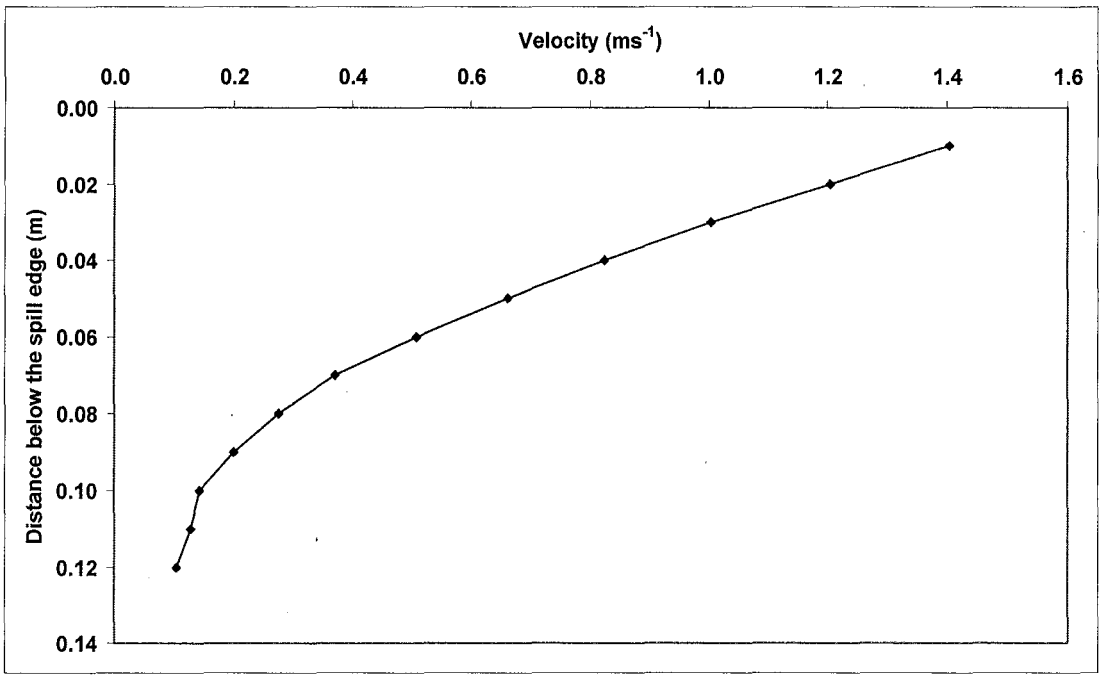

Figure H20: Velocity profile at the spill edge for Simulation 10

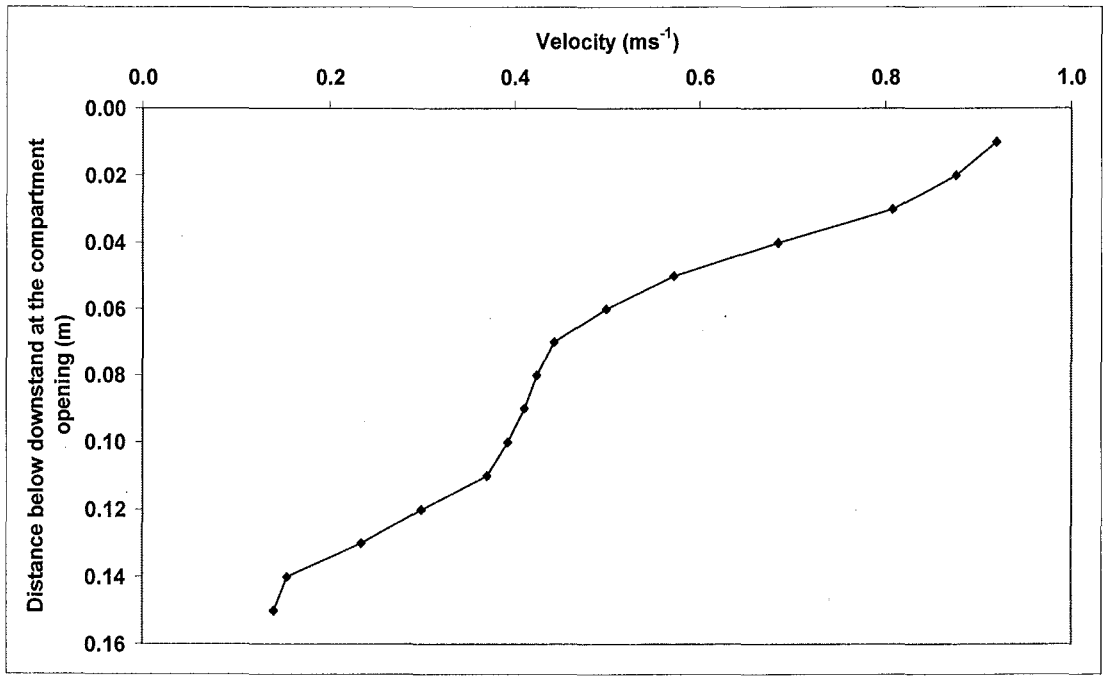

Figure H21: Velocity profile at the compartment opening for Simulation 11

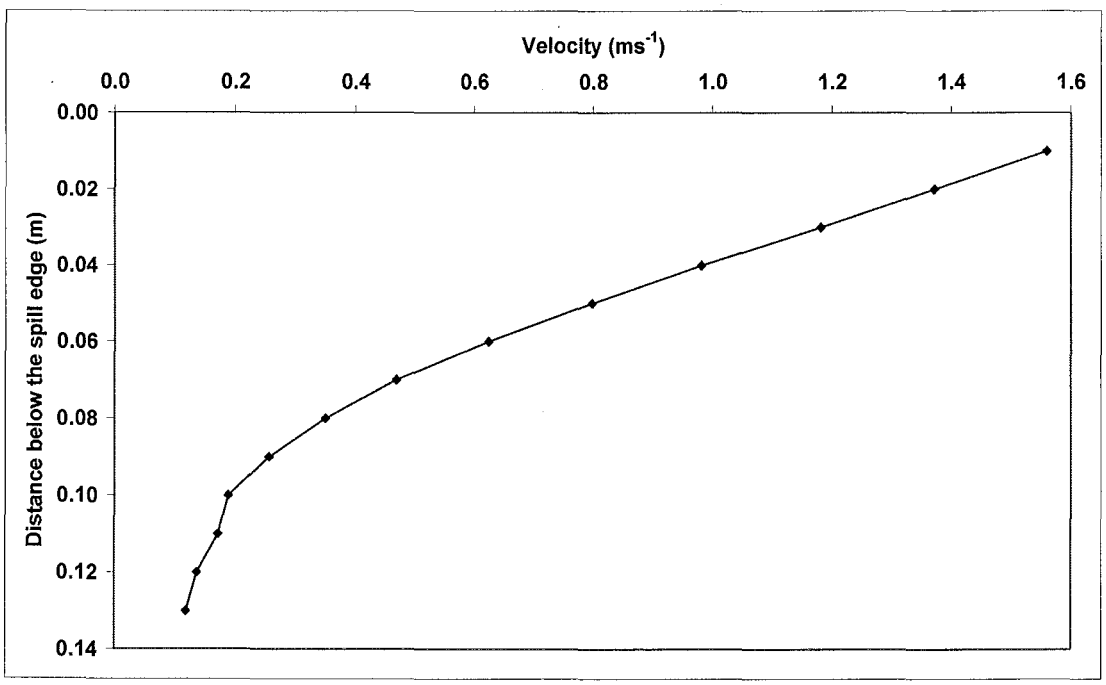

Figure H22: Velocity profile at the spill edge for Simulation 11

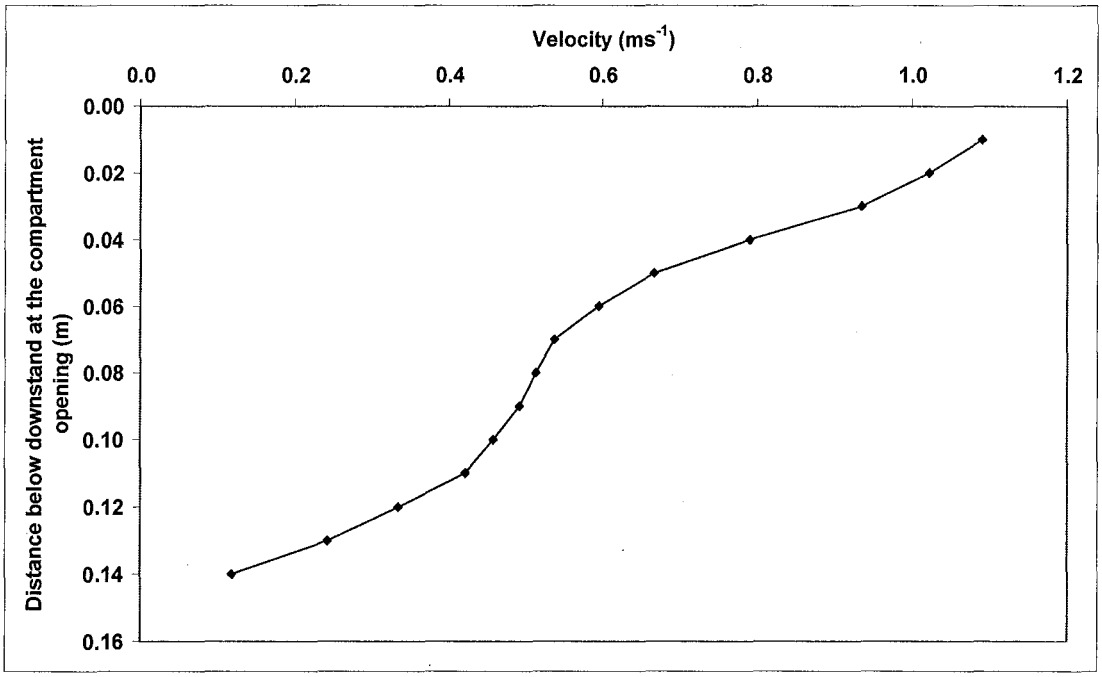

Figure H23: Velocity profile at the compartment opening for Simulation 12

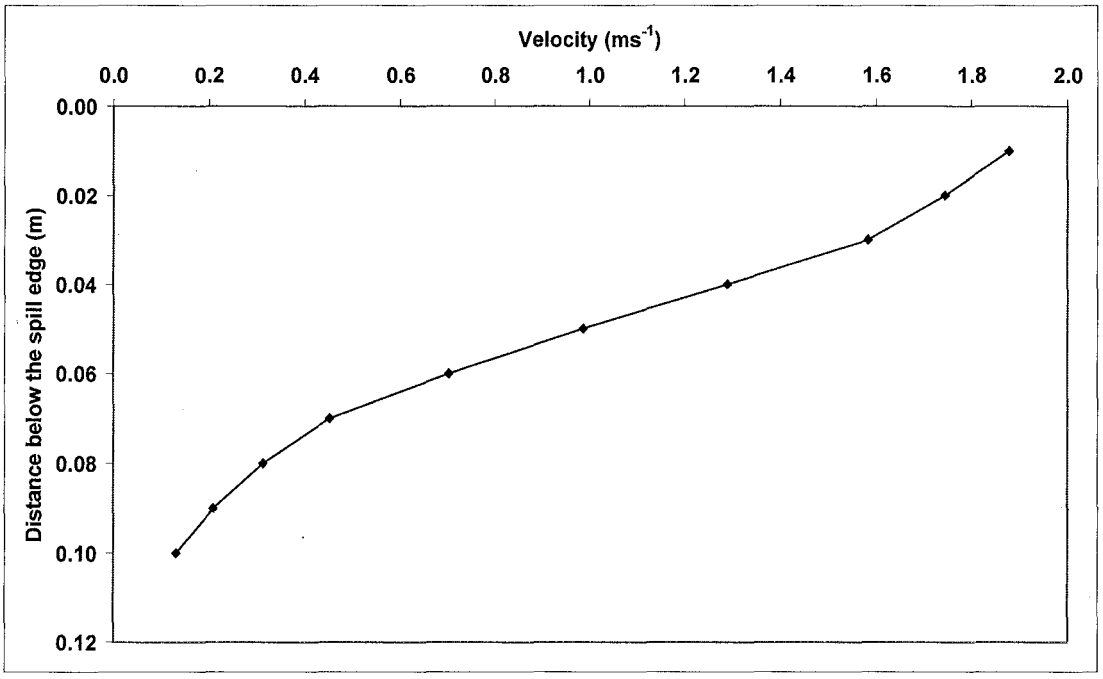

Figure H24: Velocity profile at the spill edge for Simulation 12

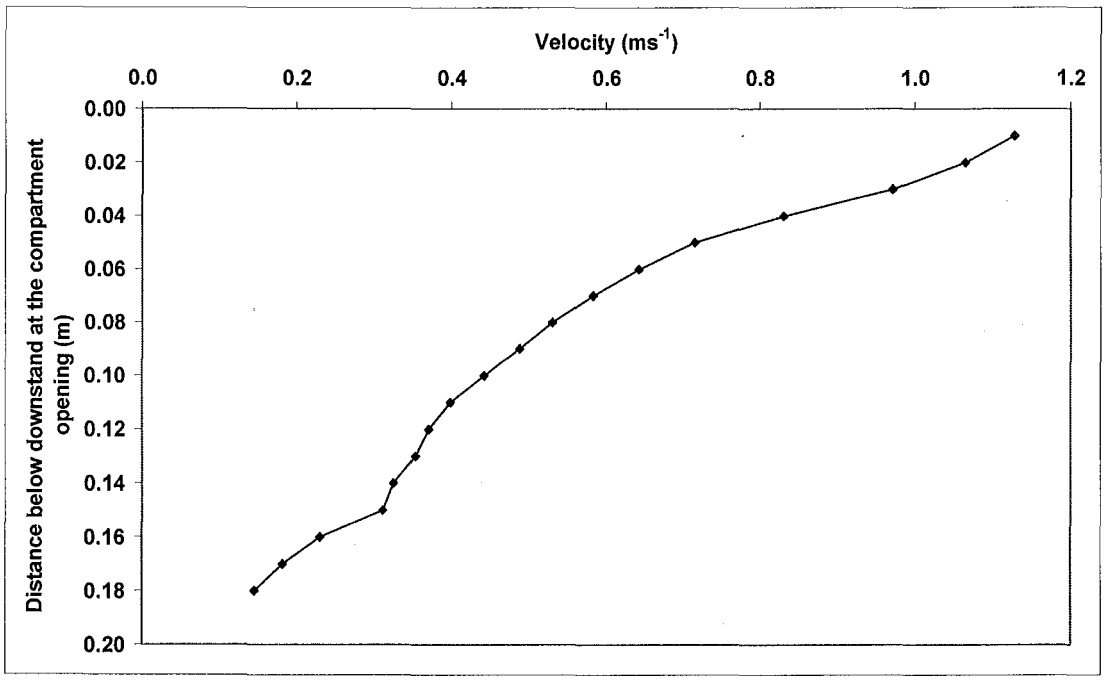

Figure H25: Velocity profile at the compartment opening for Simulation 13

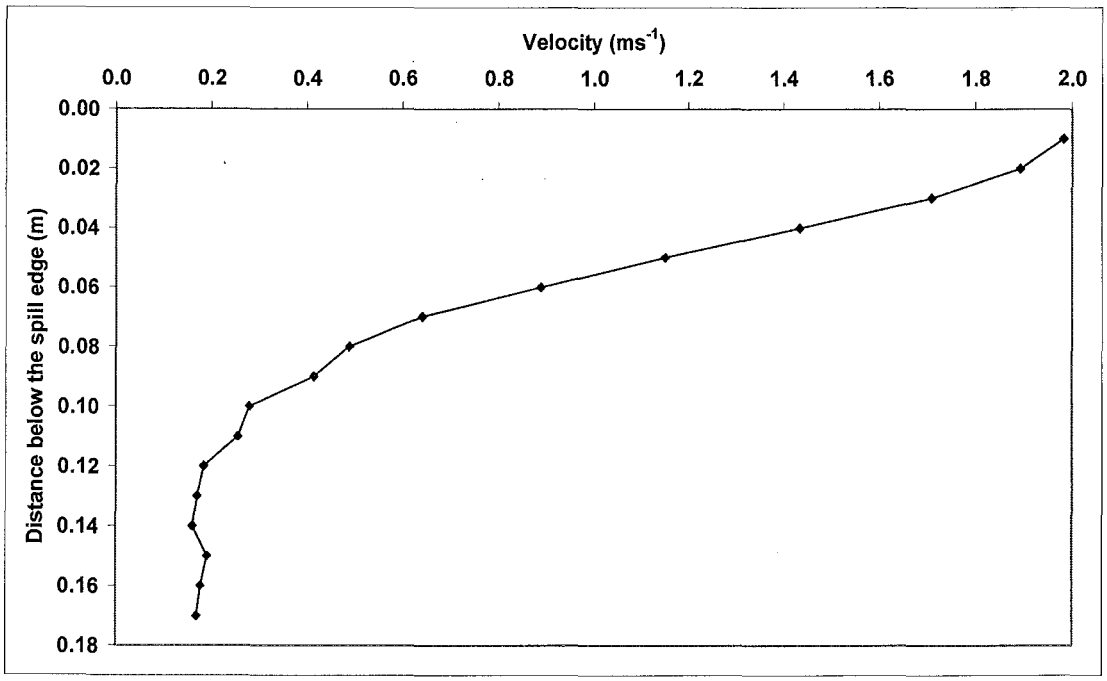

Figure H26: Velocity profile at the spill edge for Simulation 13

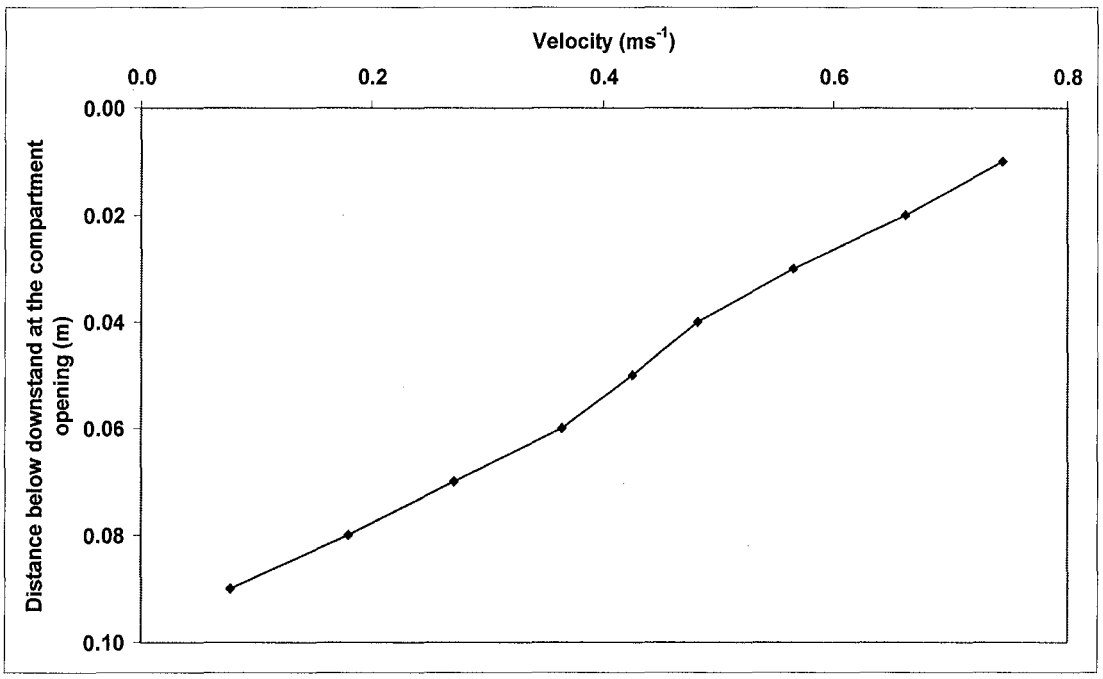

Figure H27: Velocity profile at the compartment opening for Simulation 14

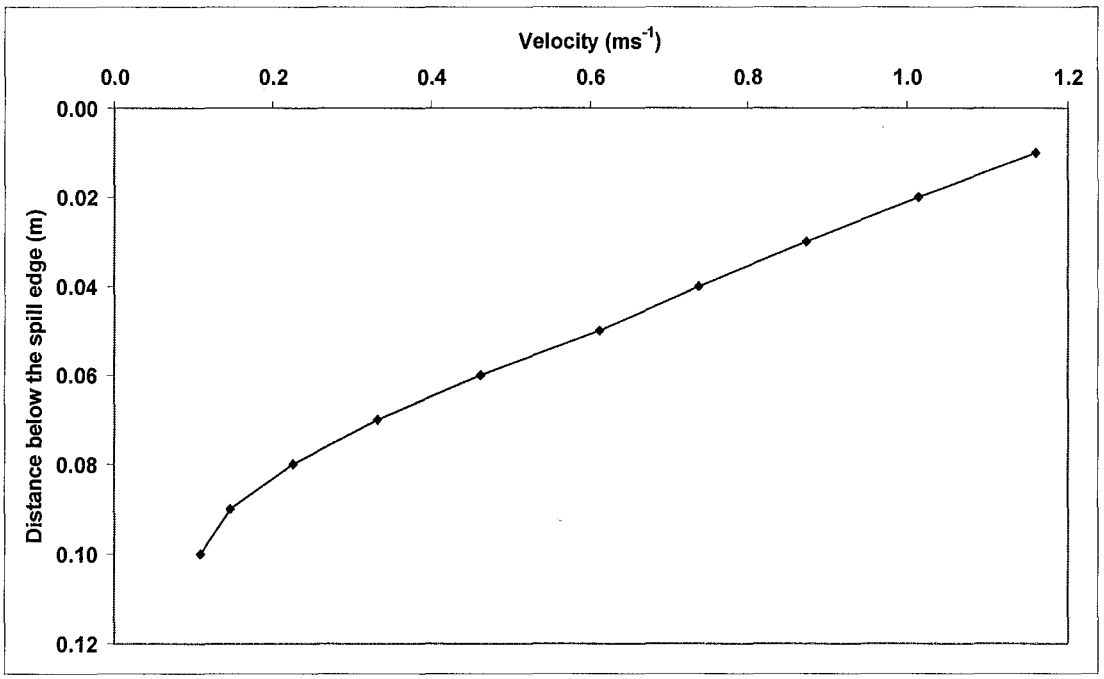

Figure H28: Velocity profile at the spill edge for Simulation 14

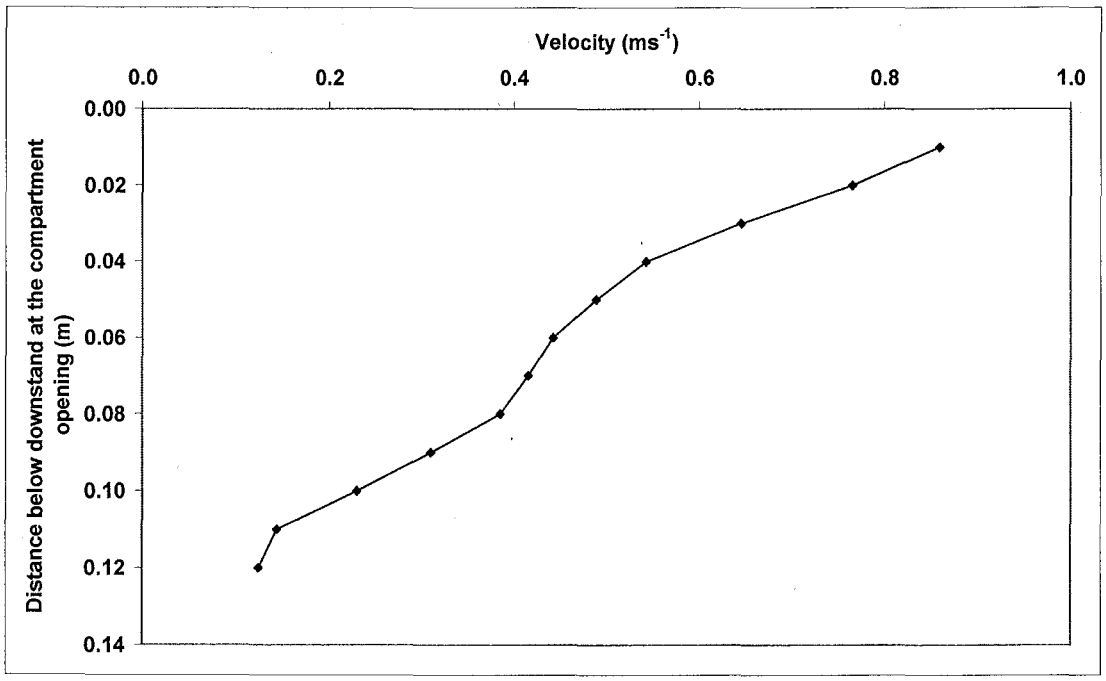

Figure H29: Velocity profile at the compartment opening for Simulation 15

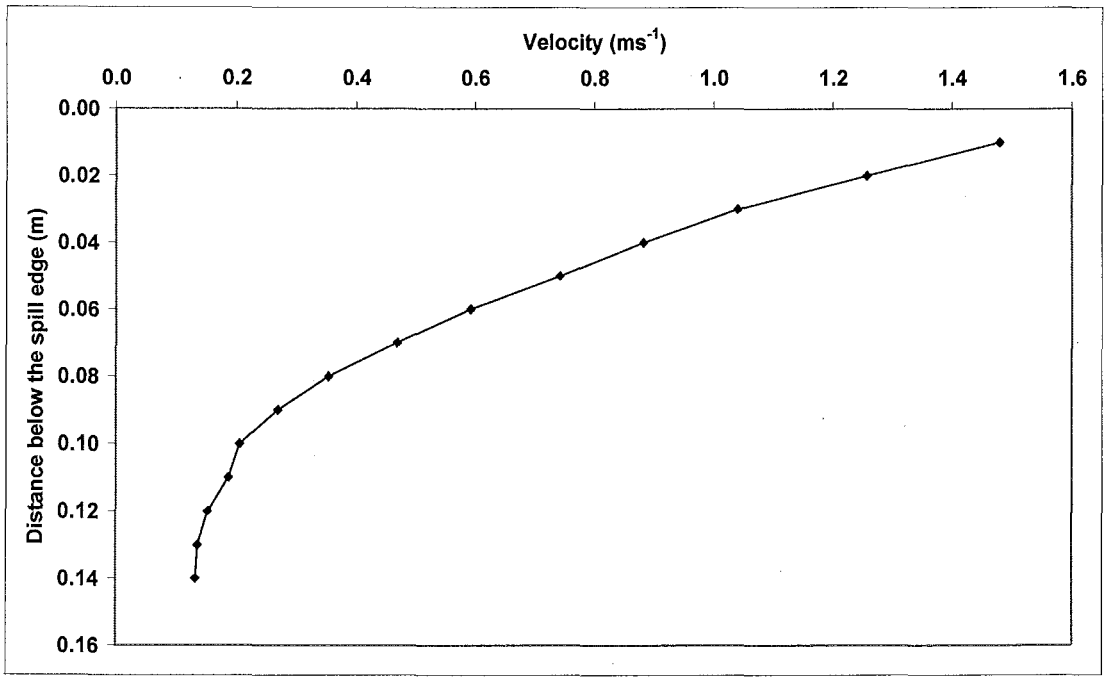

Figure H30: Velocity profile at the spill edge for Simulation 15

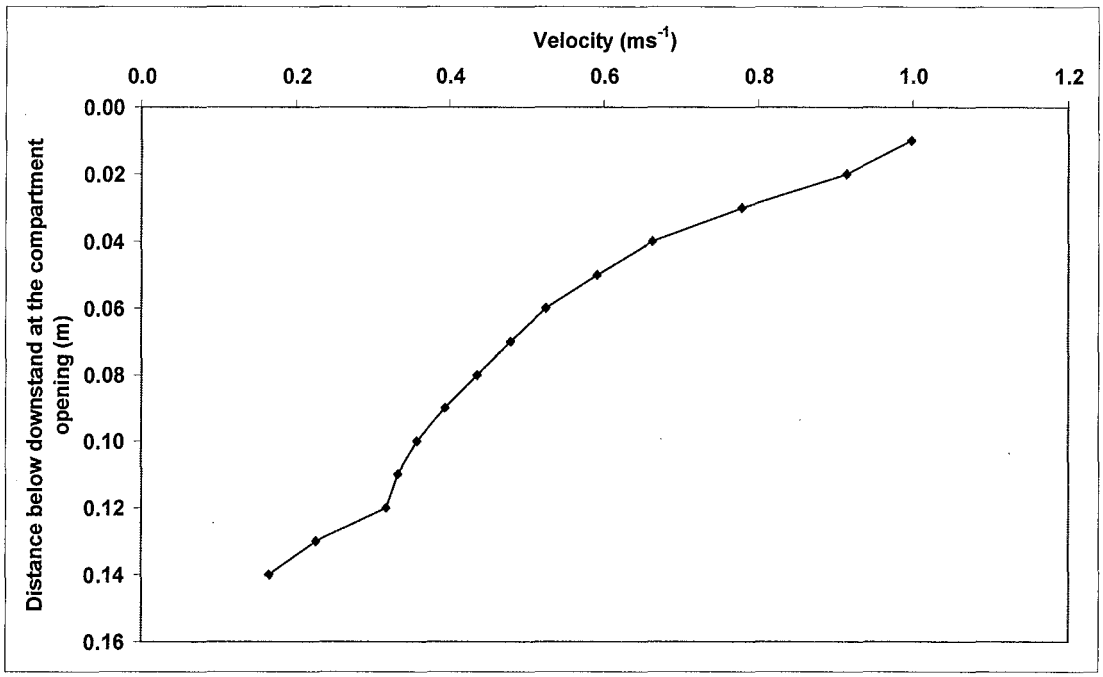

Figure H31: Velocity profile at the compartment opening for Simulation 16

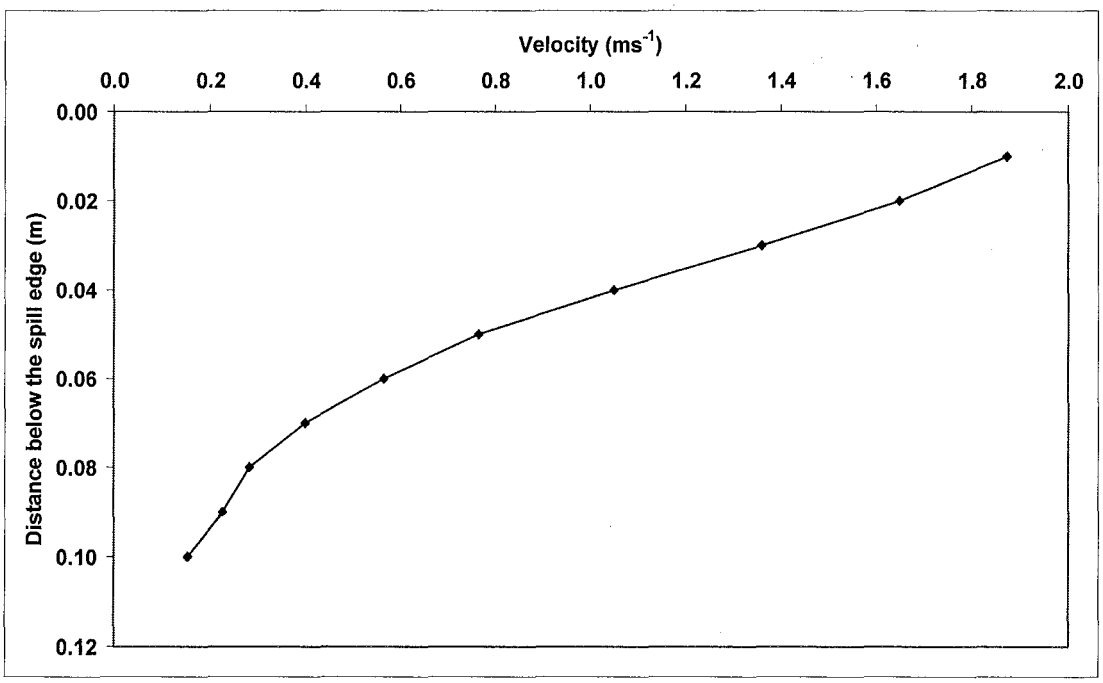

Figure H32: Velocity profile at the spill edge for Simulation 16

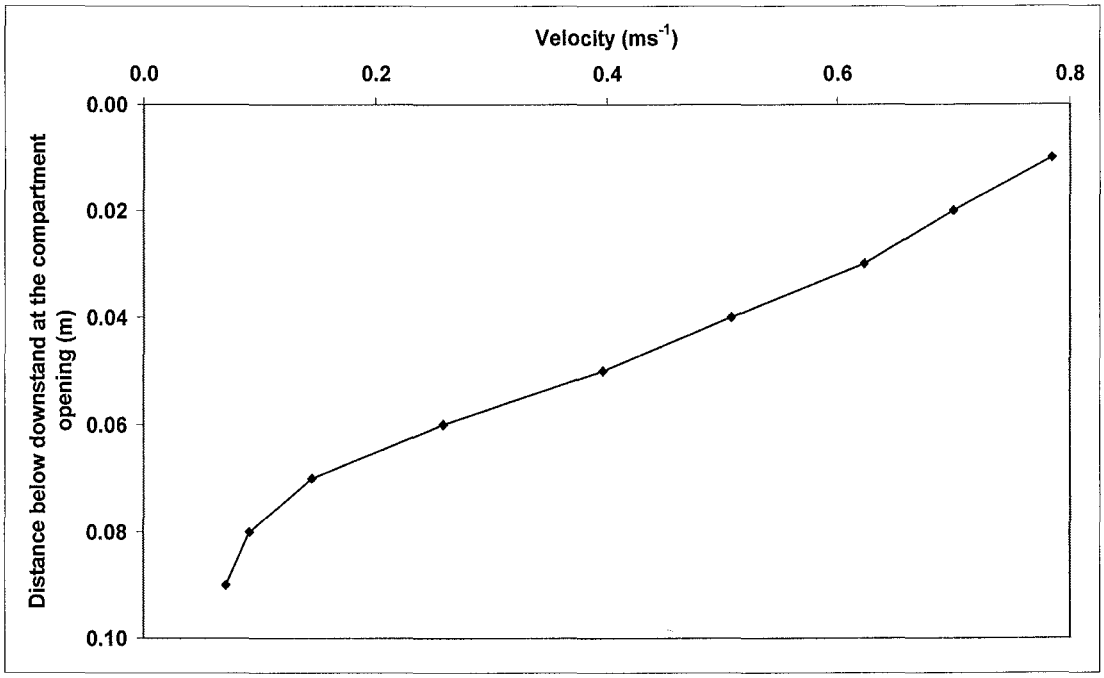

Figure H33: Velocity profile at the compartment opening for Simulation 17

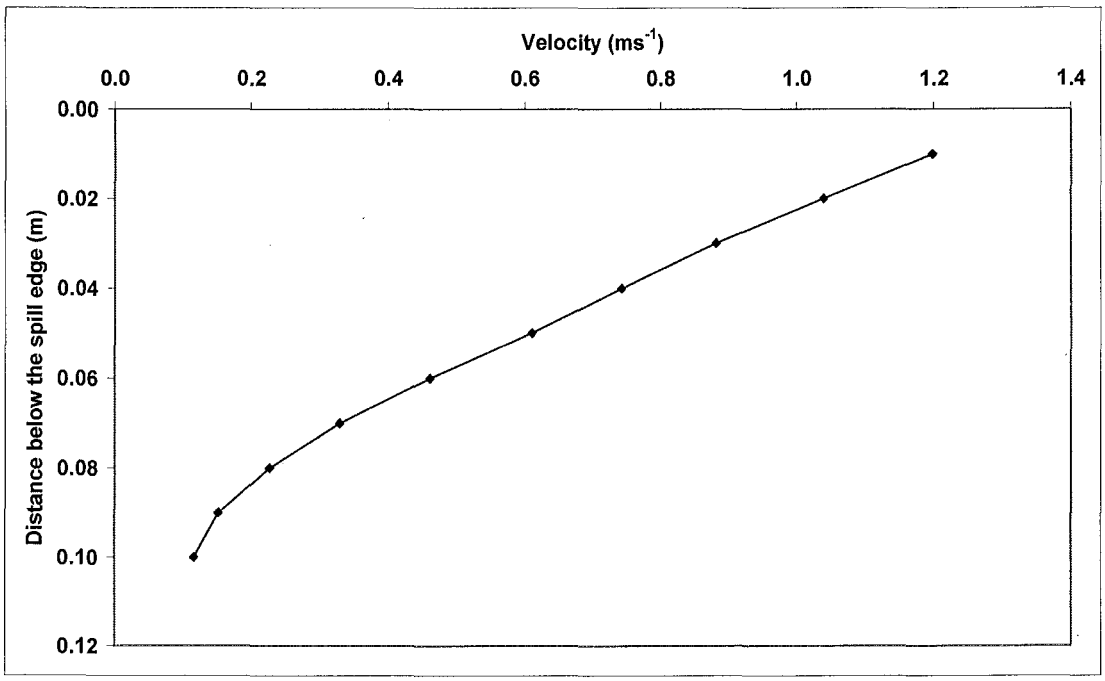

Figure H34: Velocity profile at the spill edge for Simulation 17

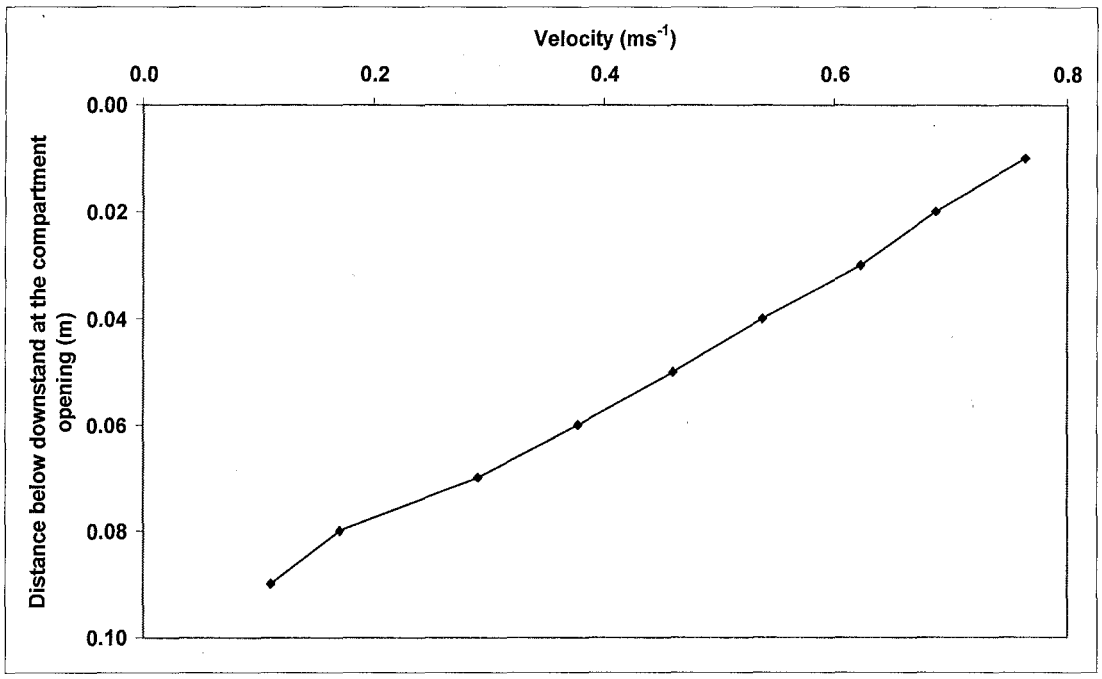

Figure H35: Velocity profile at the compartment opening for Simulation 18

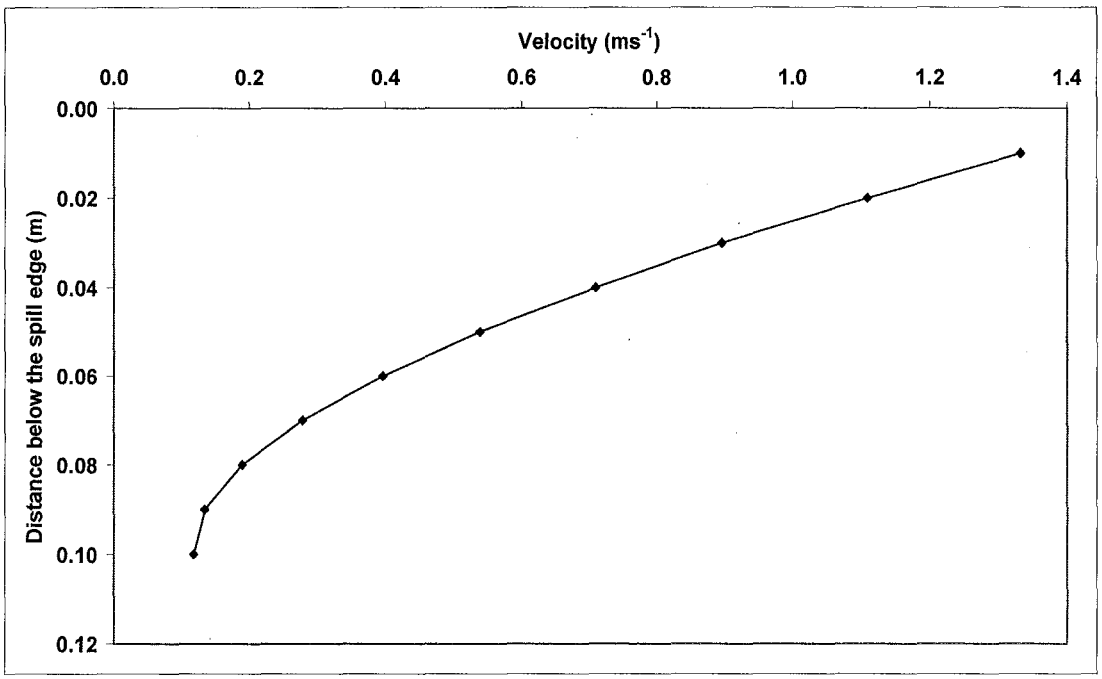

Figure H36: Velocity profile at the spill edge for Simulation 18

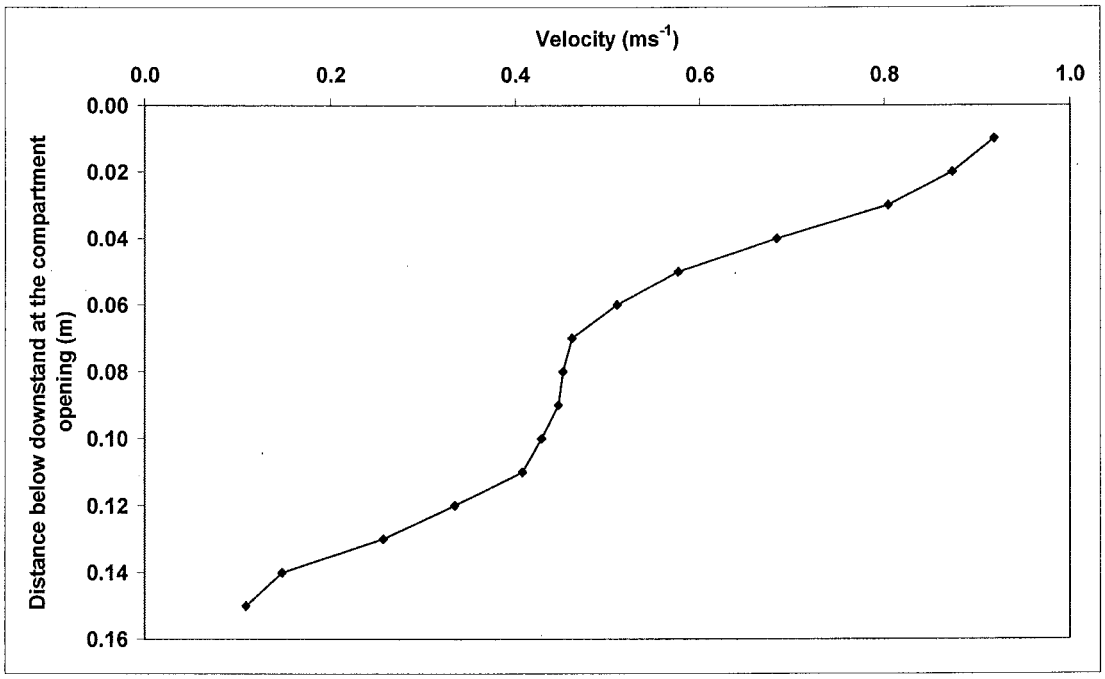

Figure H37: Velocity profile at the compartment opening for Simulation 19

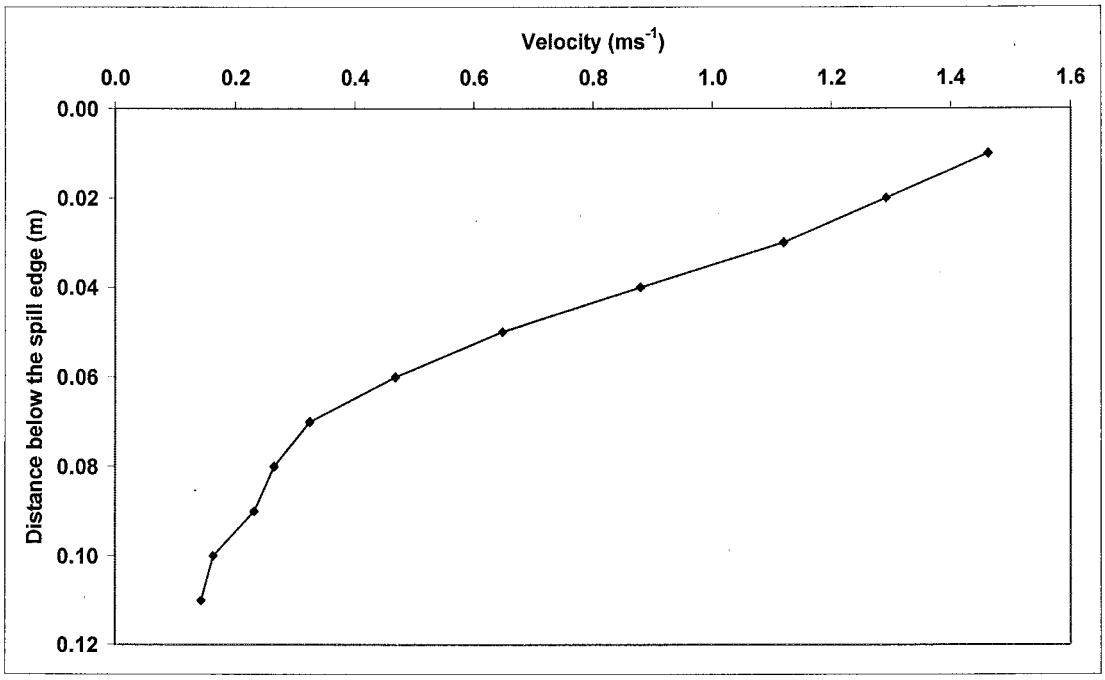

Figure H38: Velocity profile at the spill edge for Simulation 19

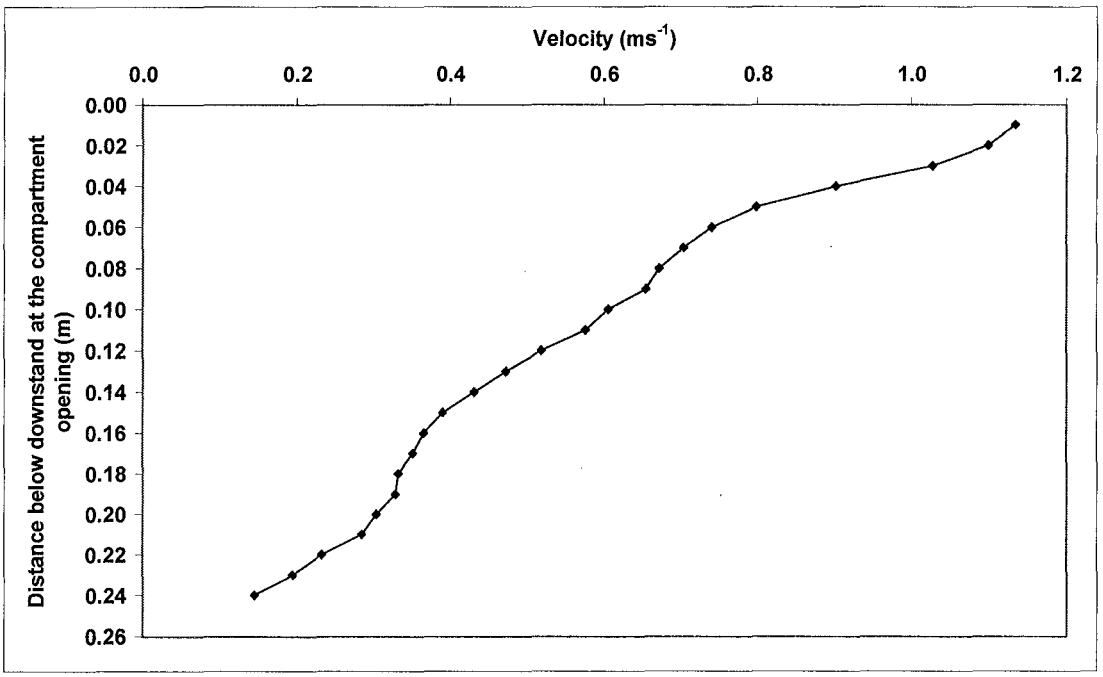

Figure H39: Velocity profile at the compartment opening for Simulation 20

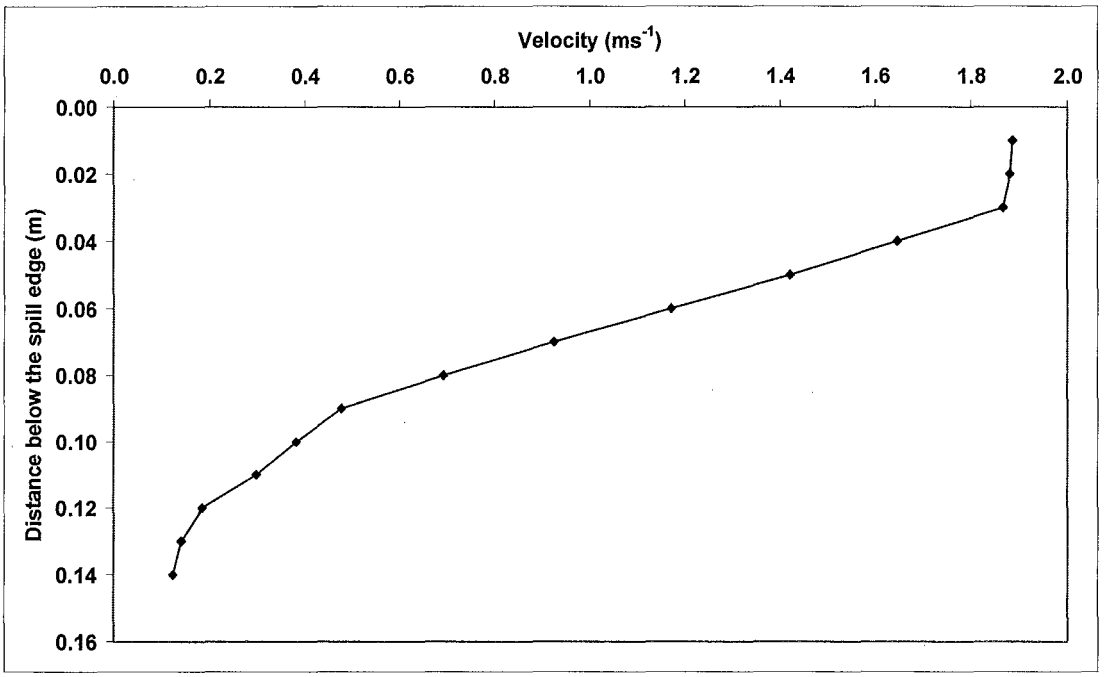

Figure H40: Velocity profile at the spill edge for Simulation 20

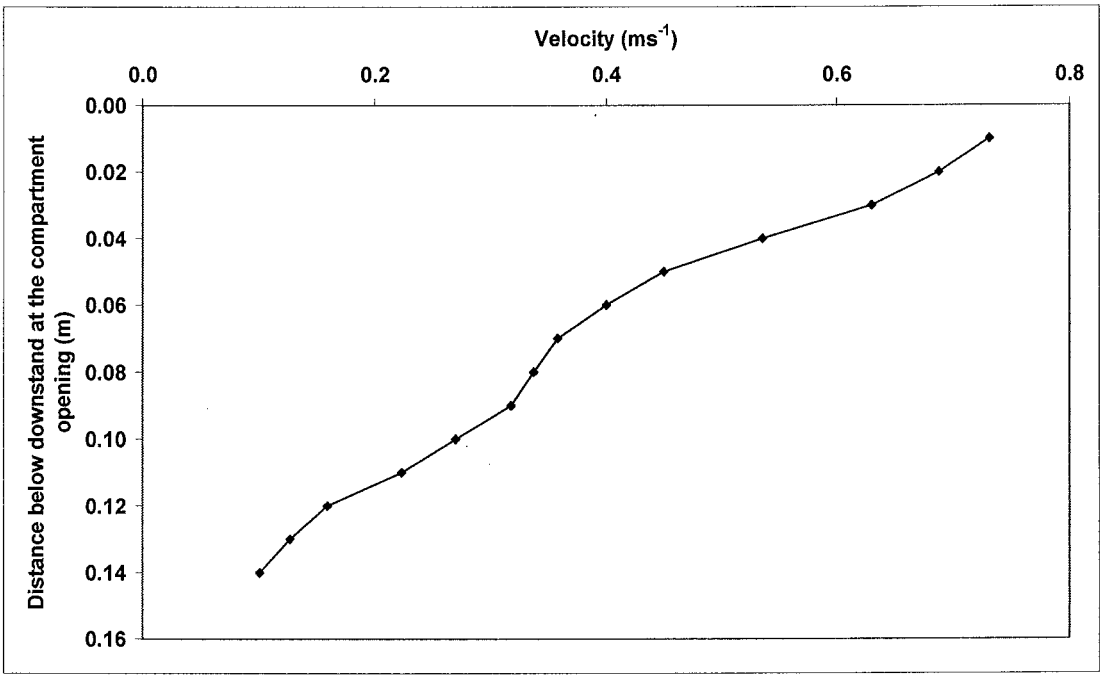

Figure H41: Velocity profile at the compartment opening for Simulation 21

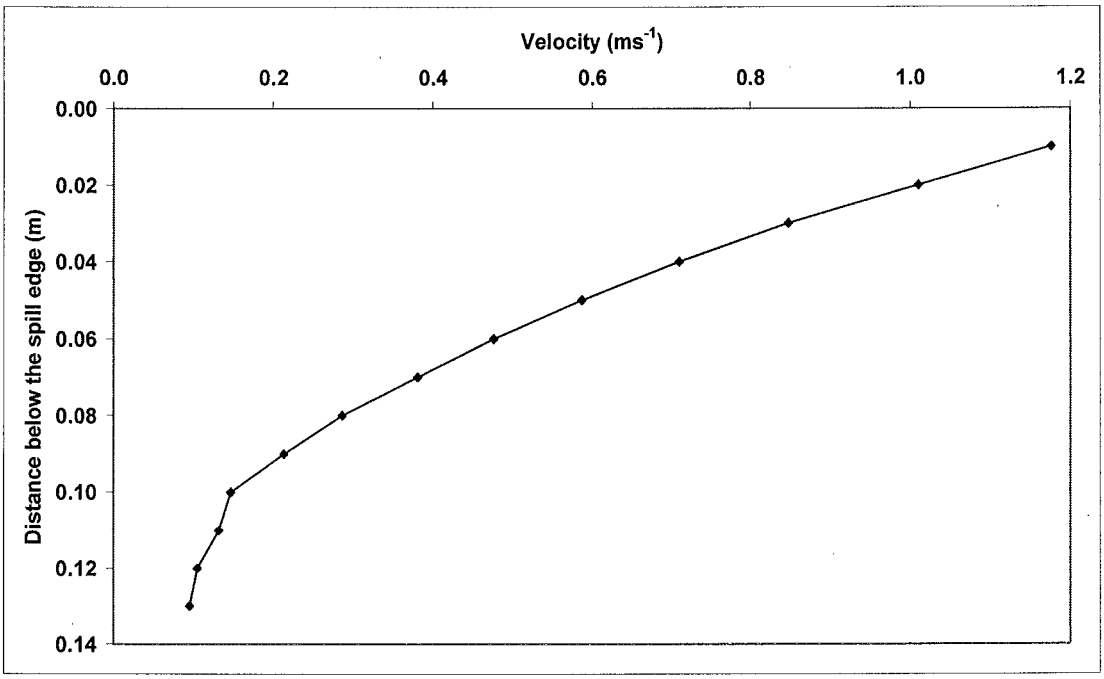

Figure H42: Velocity profile at the spill edge for Simulation 21

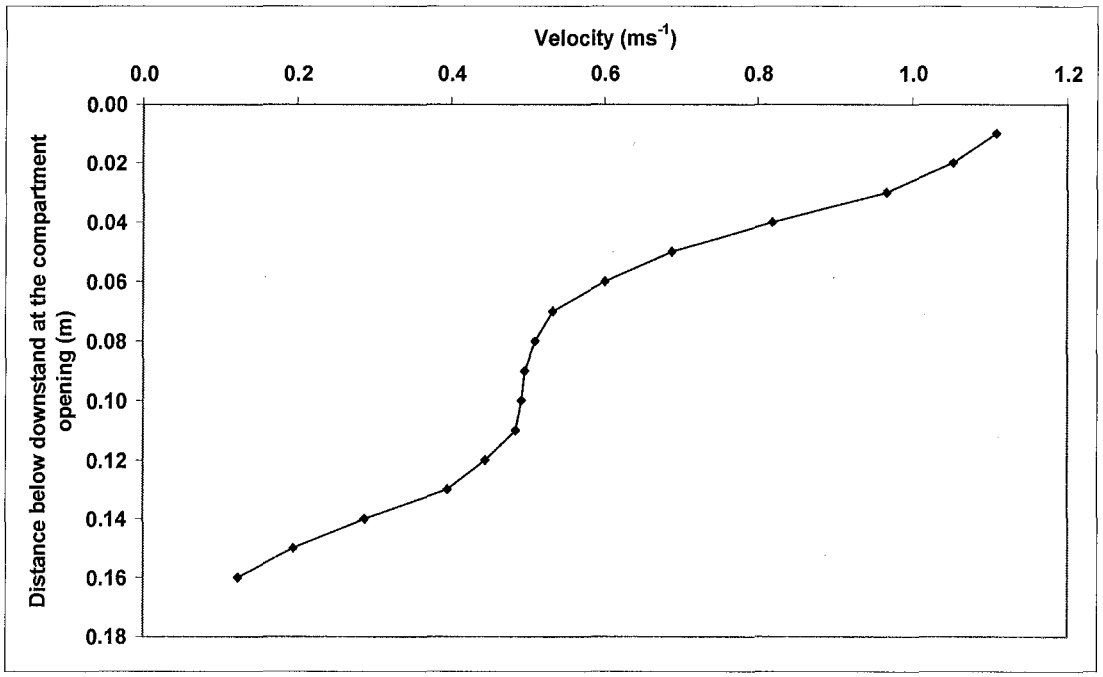

Figure H43: Velocity profile at the compartment opening for Simulation 22

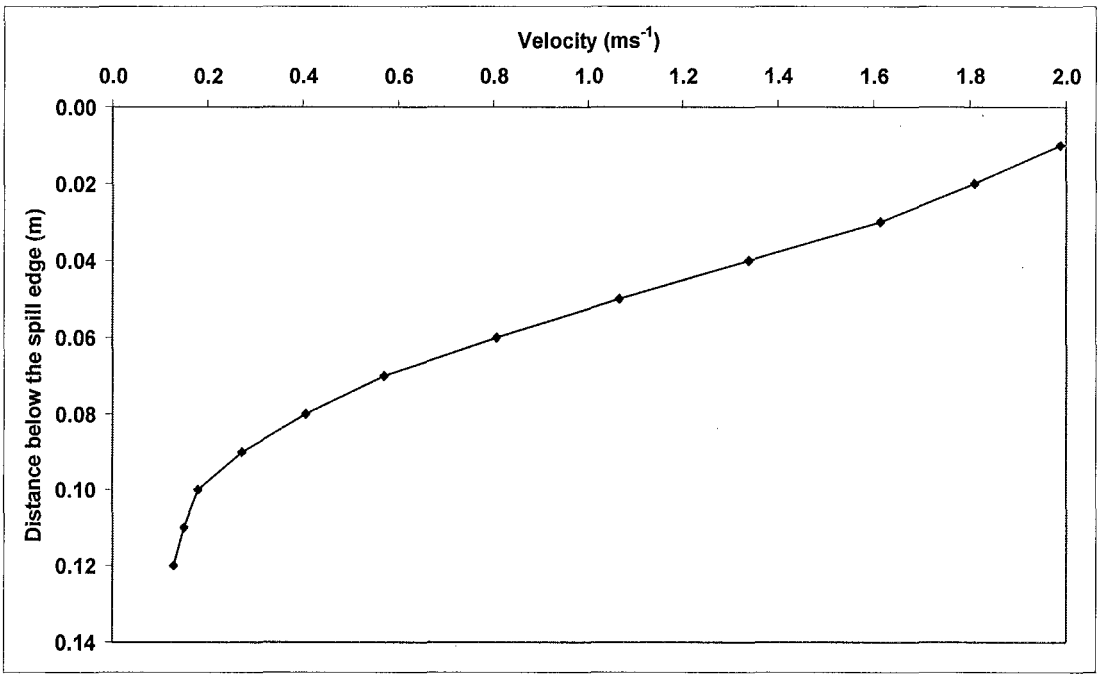

Figure H44: Velocity profile at the spill edge for Simulation 22

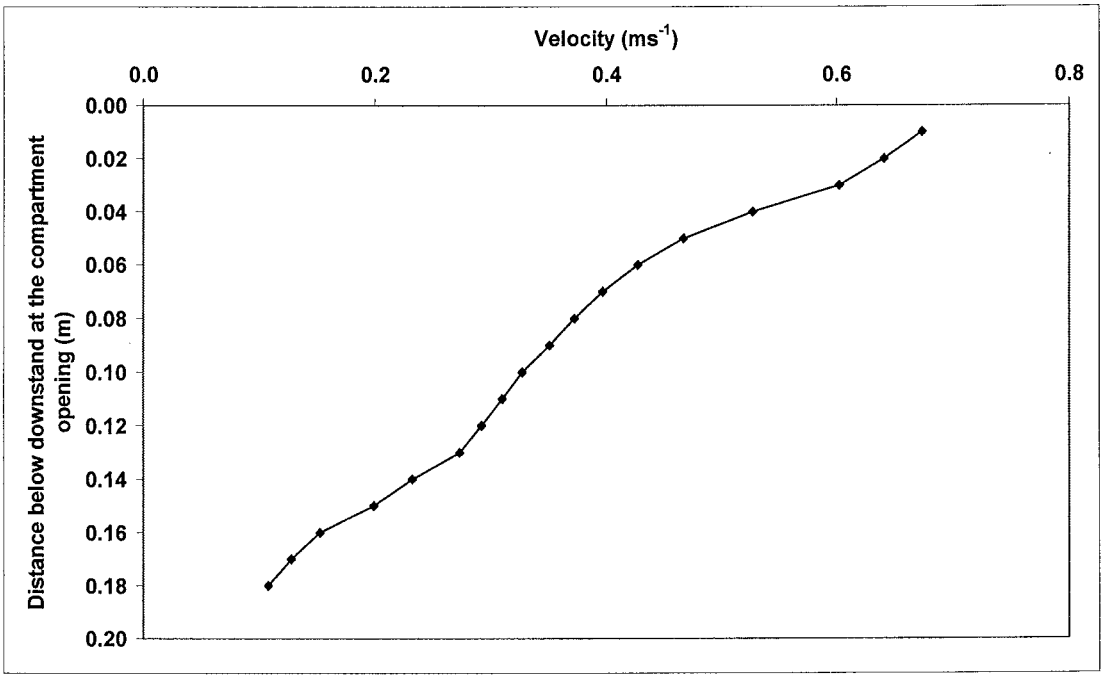

Figure H45: Velocity profile at the compartment opening for Simulation 23

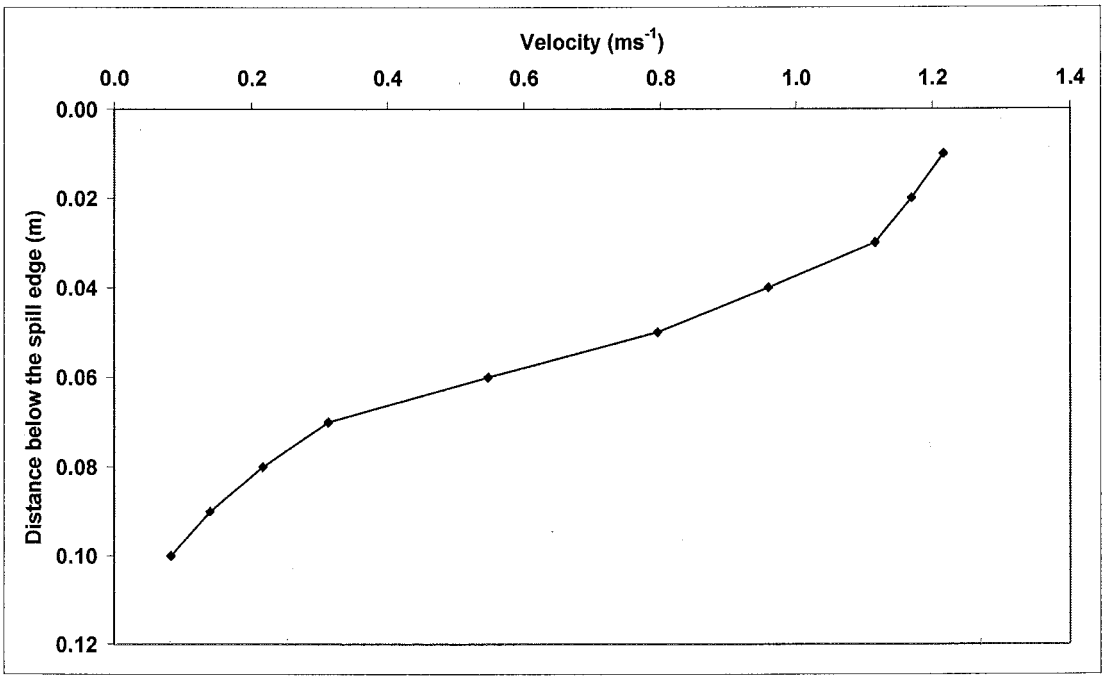

Figure H46: Velocity profile at the spill edge for Simulation 23

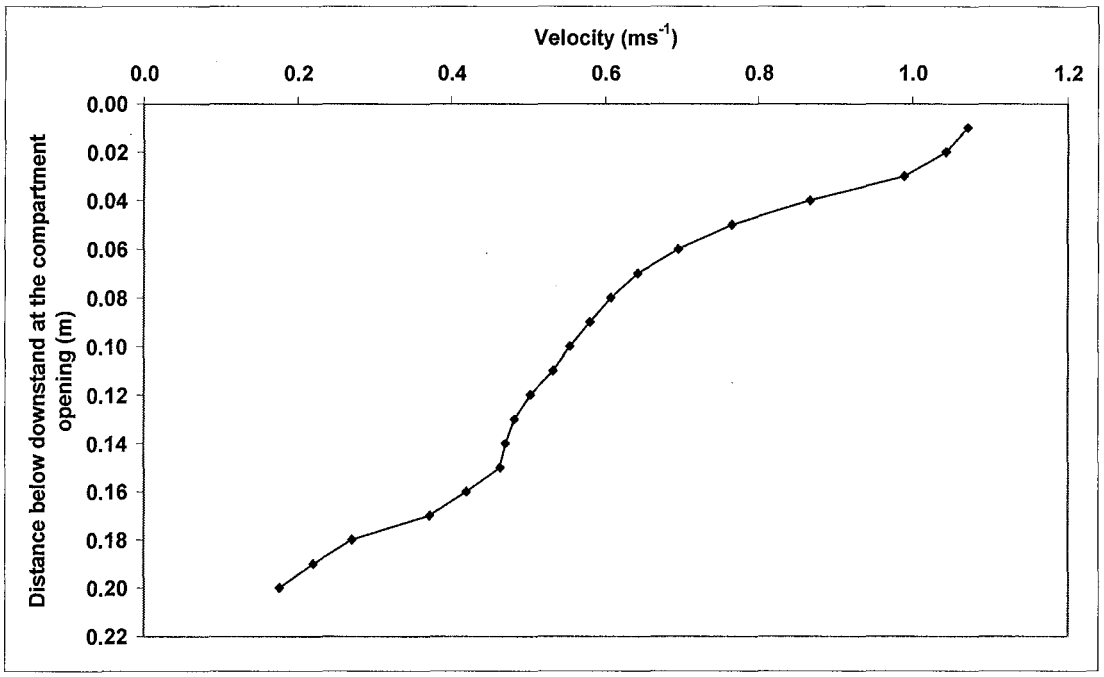

Figure H47: Velocity profile at the compartment opening for Simulation 24

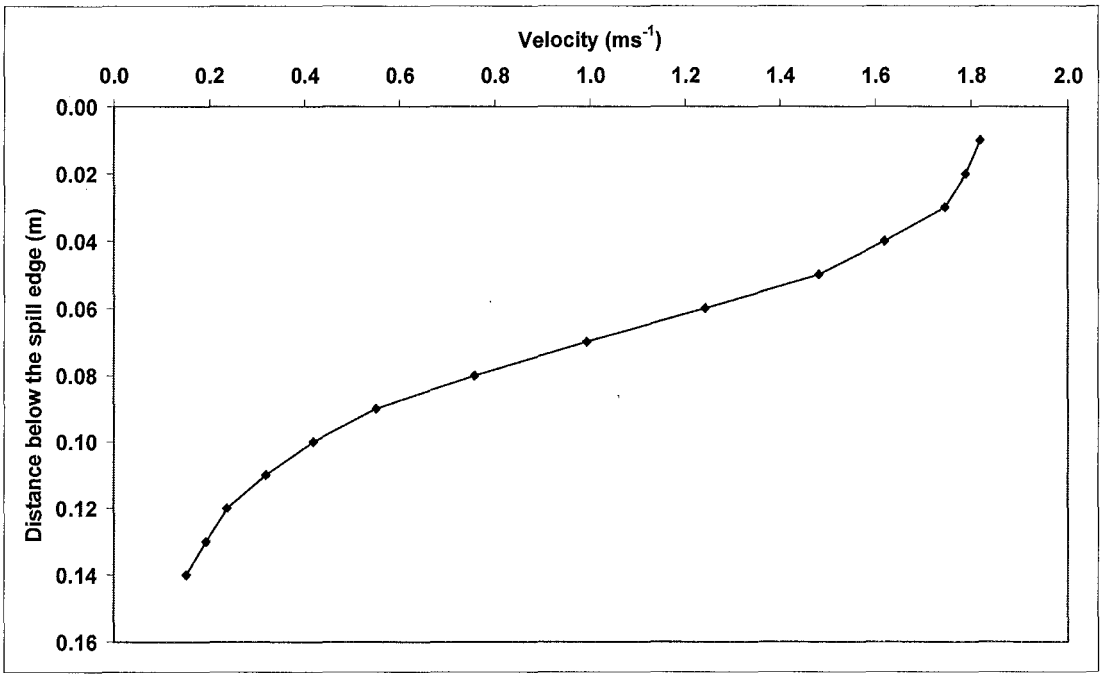

Figure H48: Velocity profile at the spill edge for Simulation 24

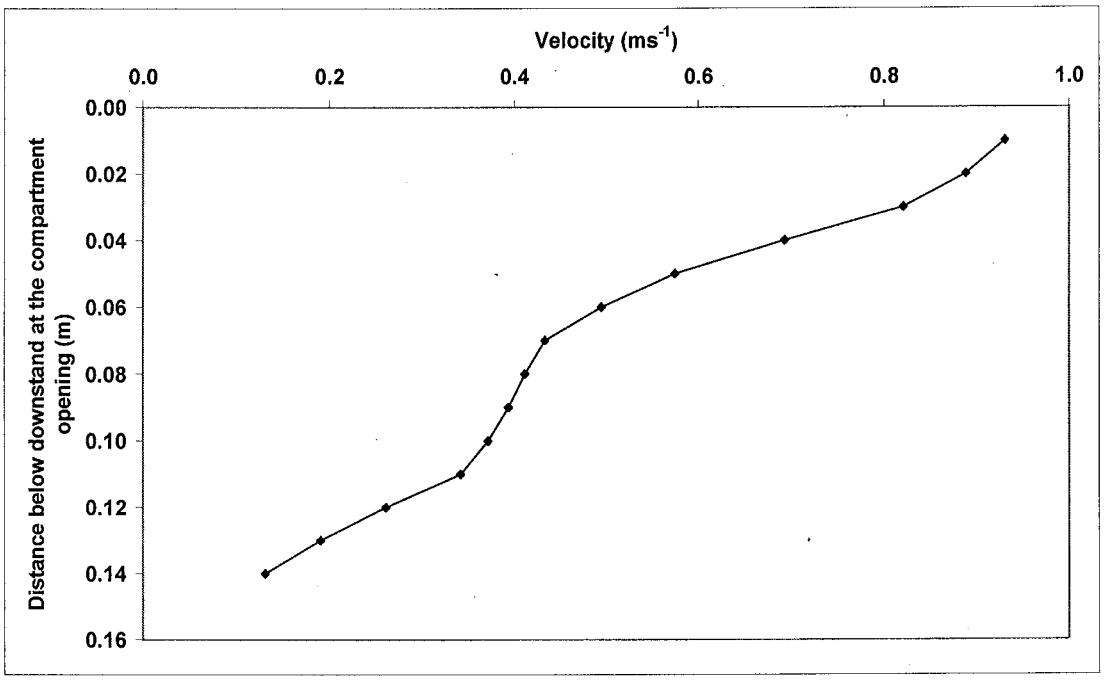

Figure H49: Velocity profile at the compartment opening for Simulation 25

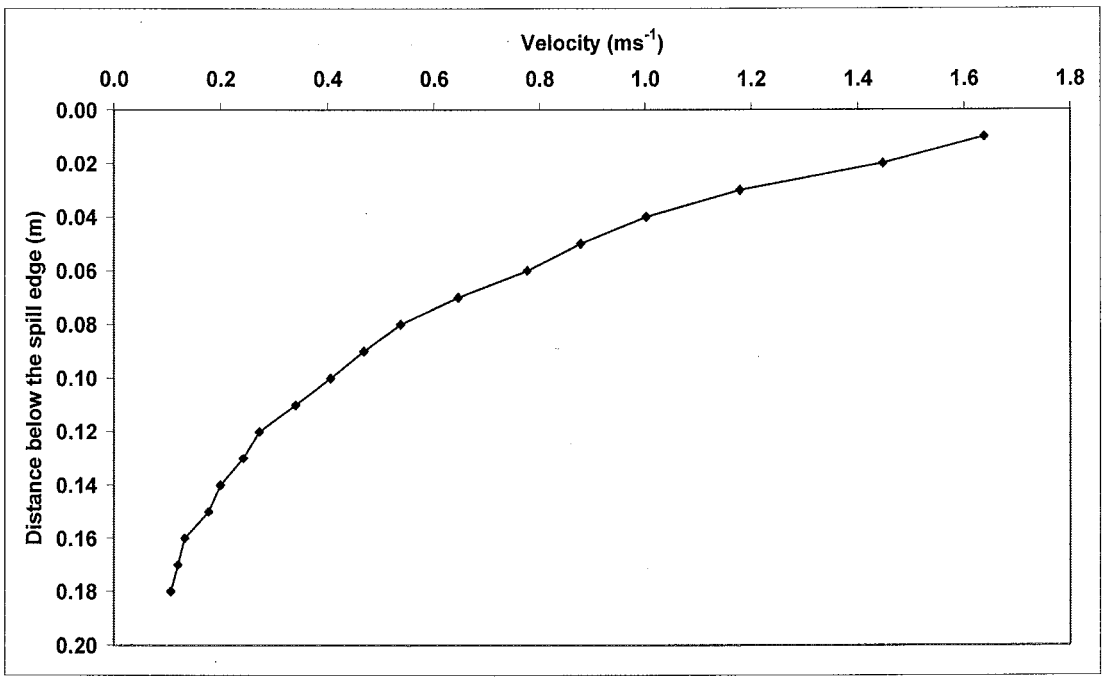

Figure H50: Velocity profile at the spill edge for Simulation 25

Appendix H

APPENDIX I EXPERIMENTAL TEMPERATURE PROFILES (TESTS 65 TO 68)

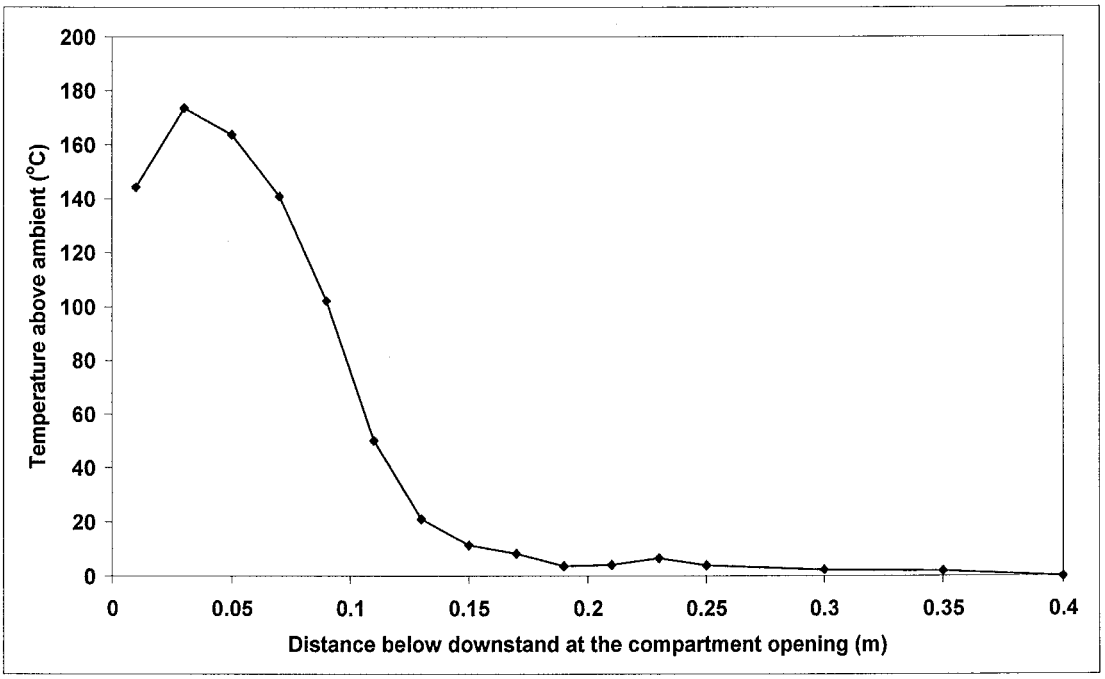

Figure I1: Temperature profile at the compartment opening for Test 65

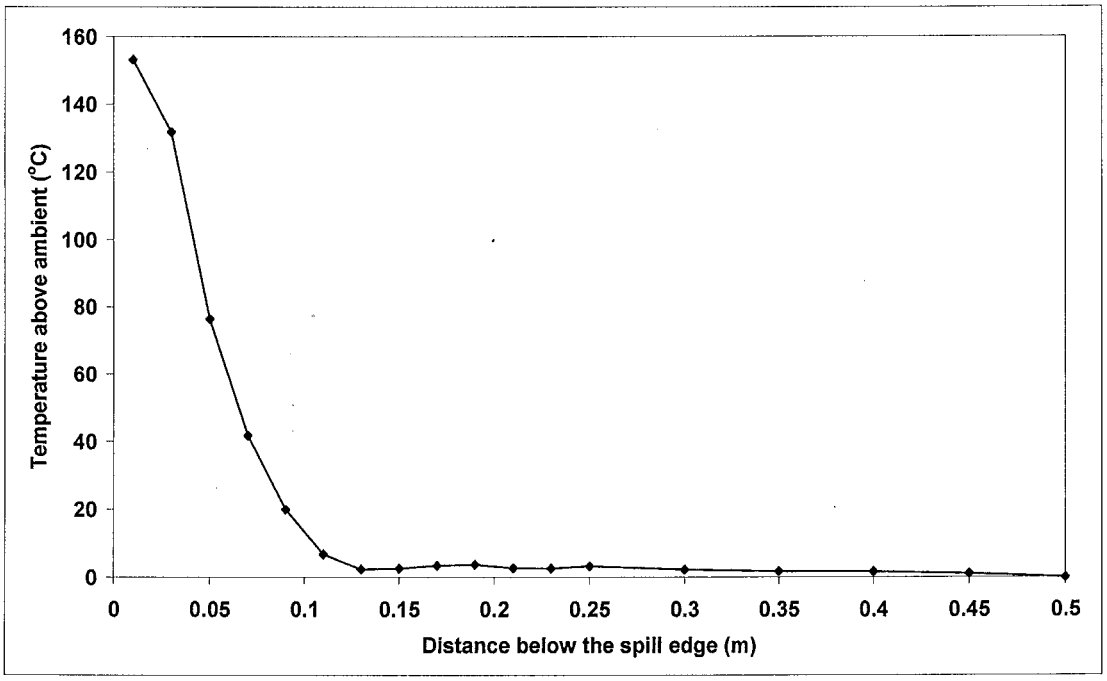

Figure I2: Temperature profile at the spill edge for Test 65

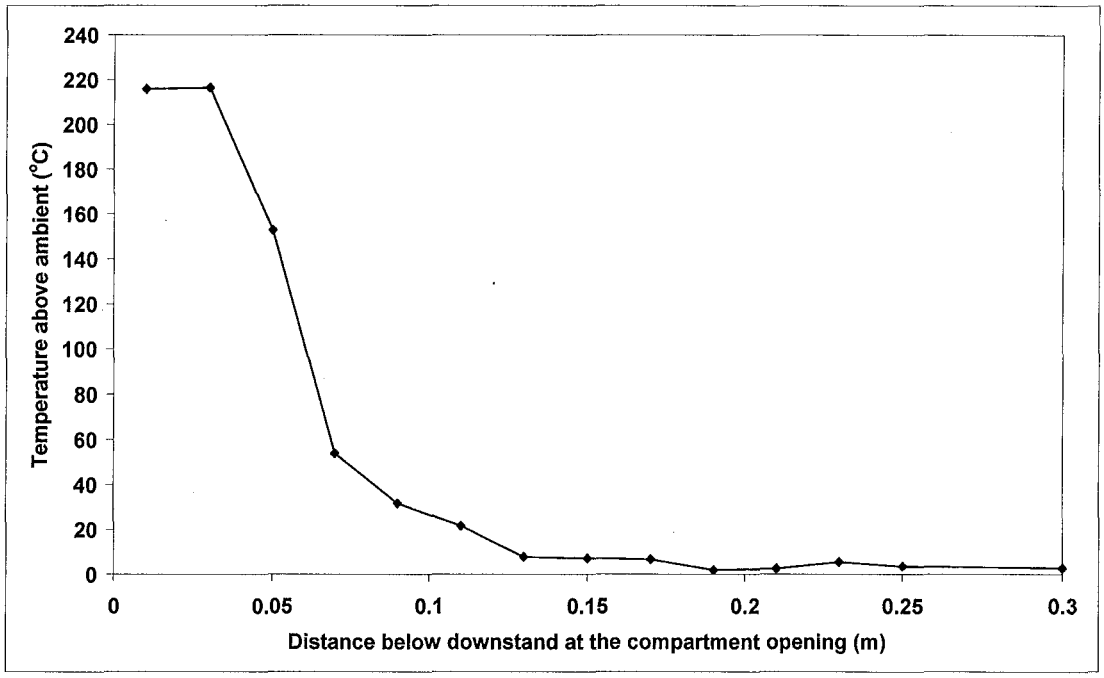

Figure I3: Temperature profile at the compartment opening for Test 66

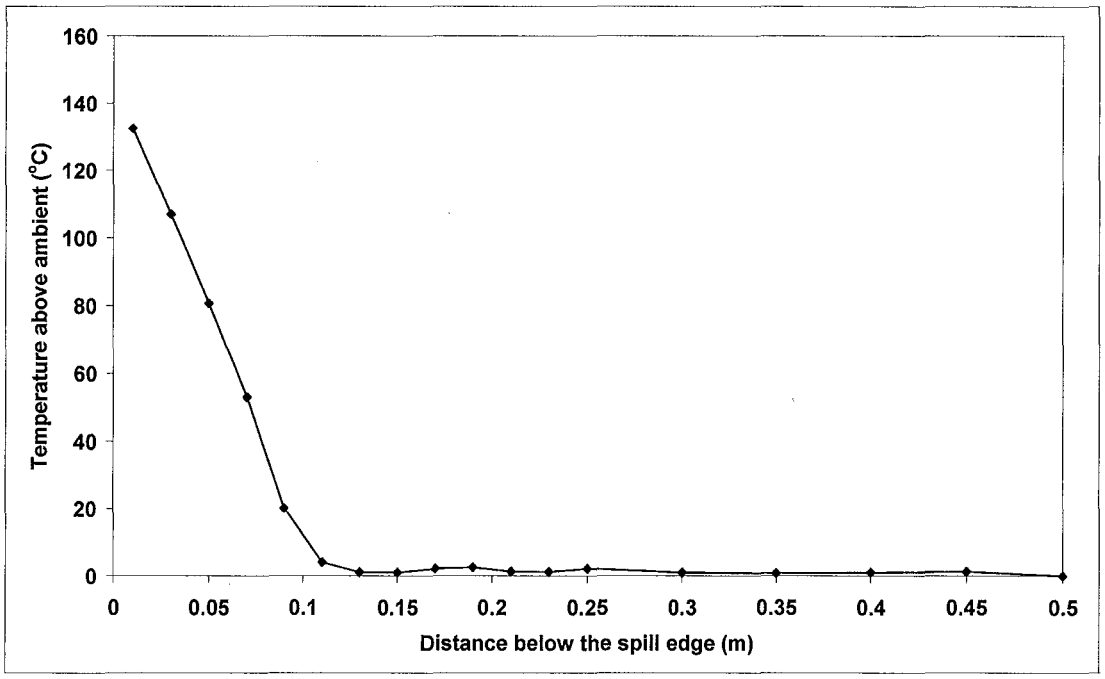

Figure I4: Temperature profile at the spill edge for Test 66

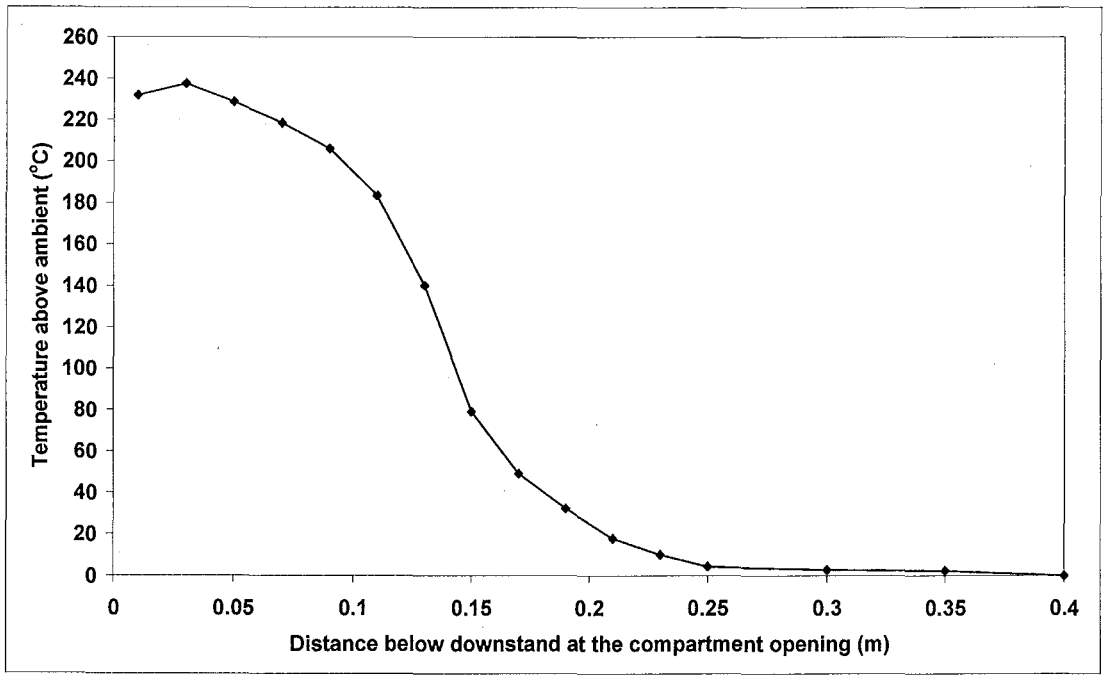

Figure I5: **Temperature profile at the compartment opening for Test 67**

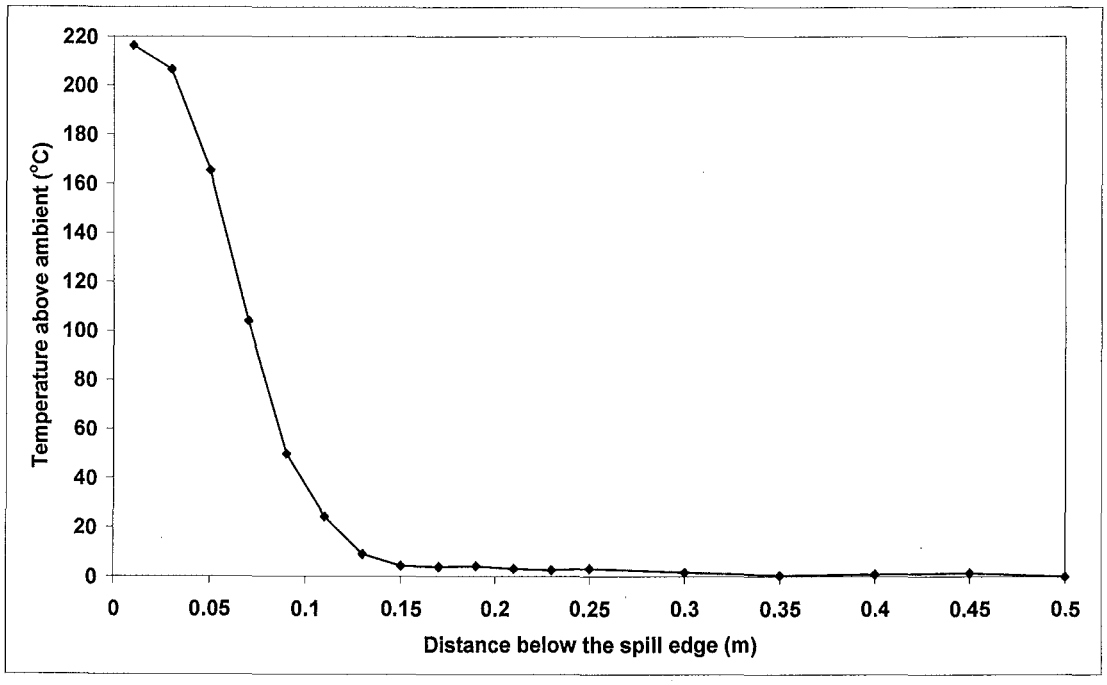

Figure I6: **Temperature profile at the spill edge for Test 67**

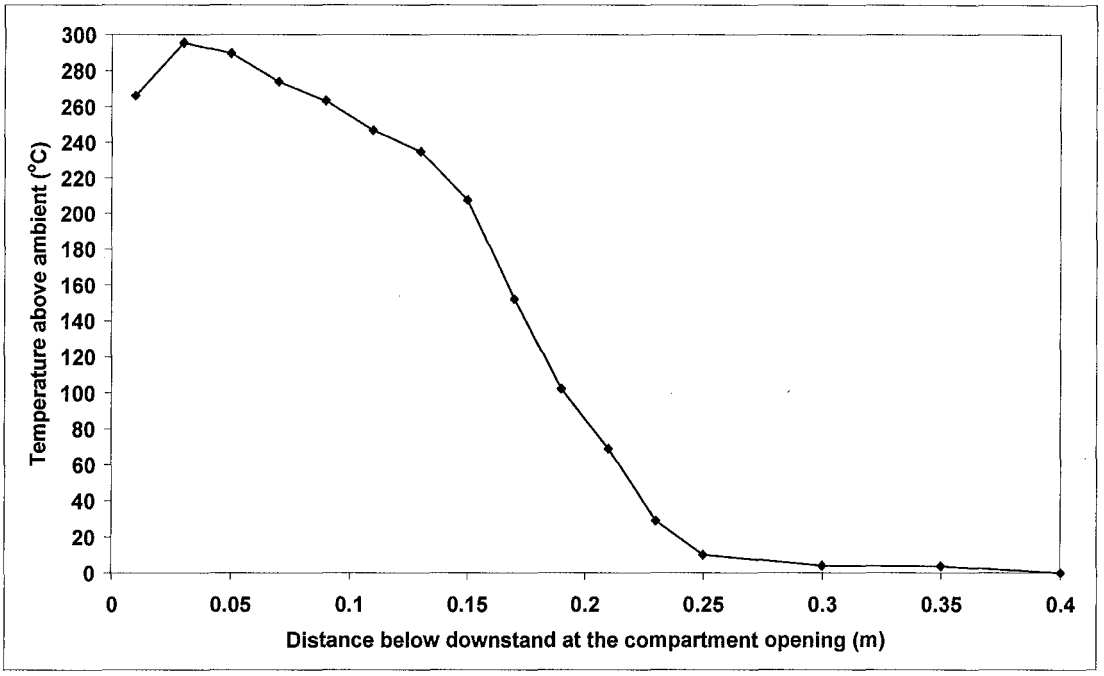

Figure I7: Temperature profile at the compartment opening for Test 68

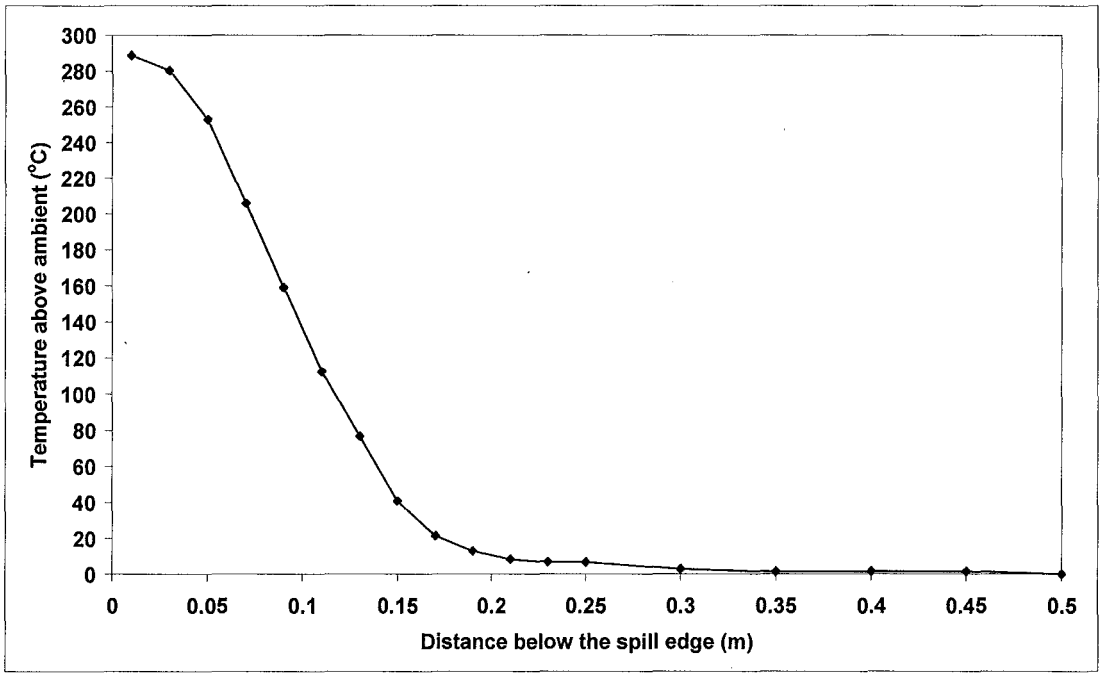

Figure I8: Temperature profile at the spill edge for Test 68

APPENDIX J EXPERIMENTAL VELOCITY PROFILES (TESTS 65 TO 68)

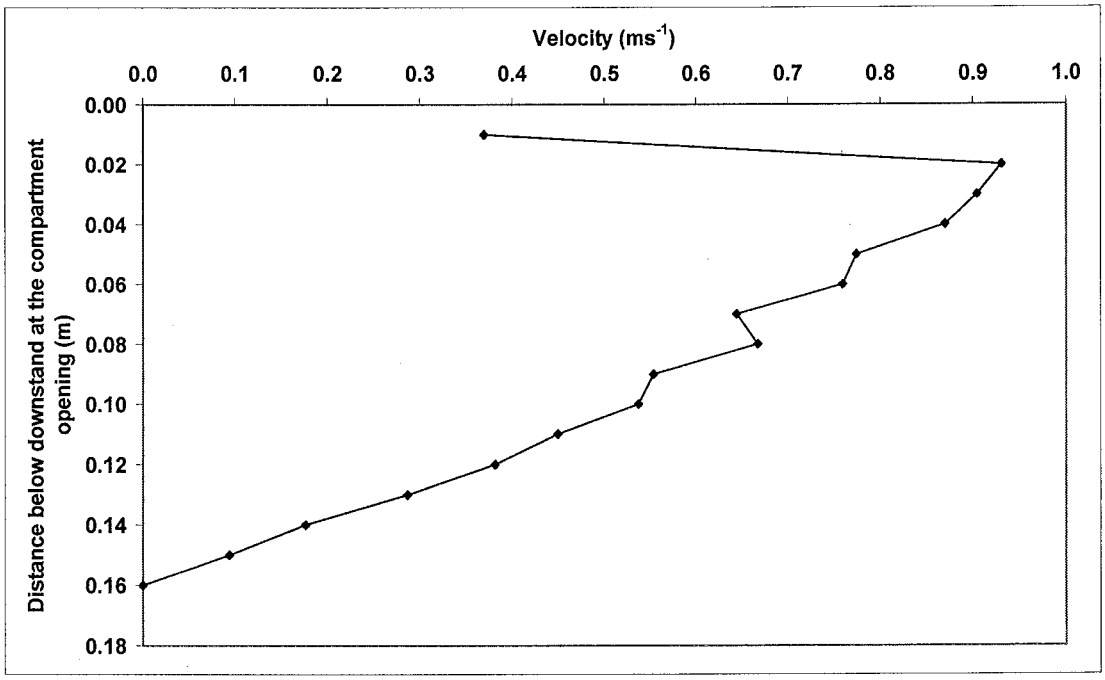

Figure J1: Velocity profile at the compartment opening for Test 65

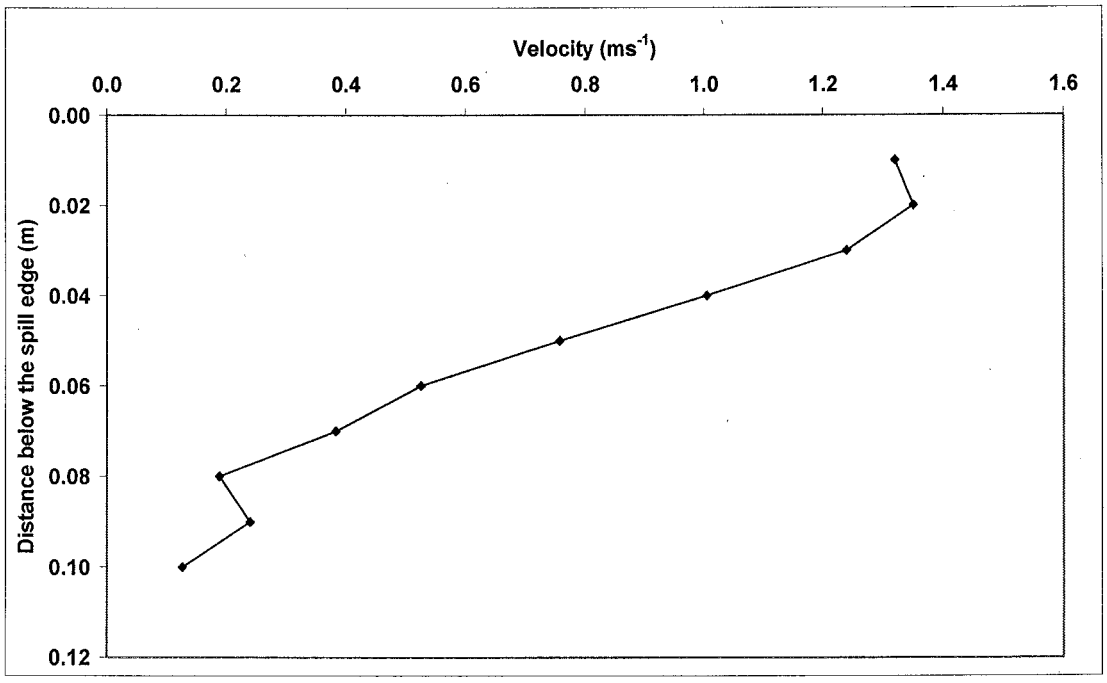

Figure J2: Velocity profile at the spill edge for Test 65

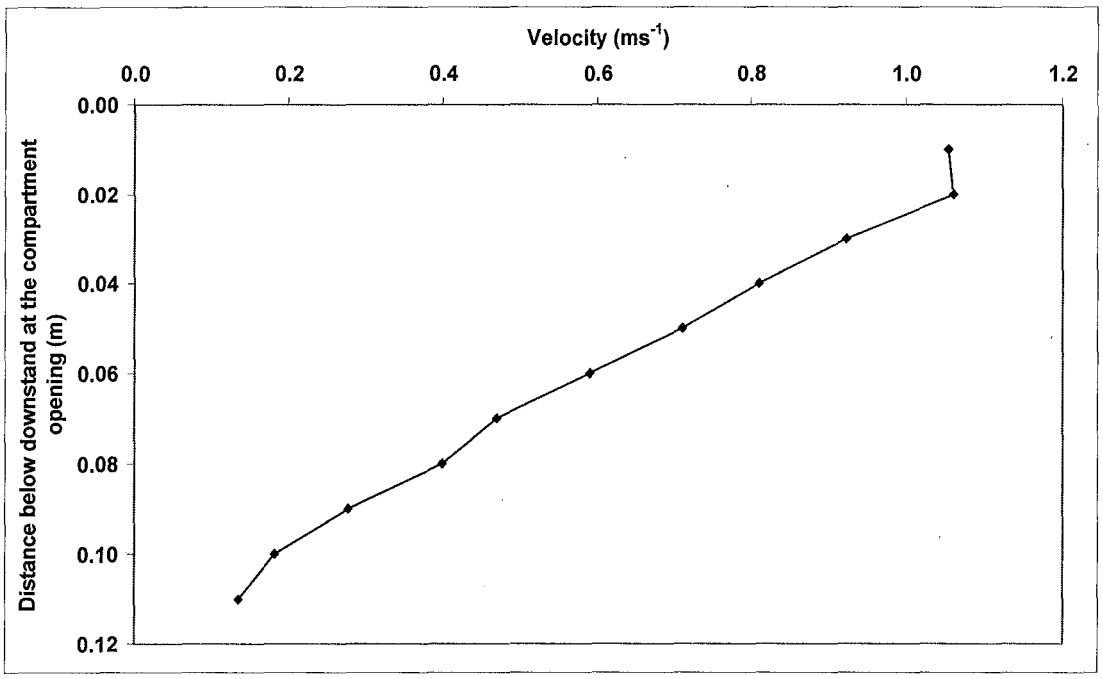

Figure J3: **Velocity profile at the compartment opening for Test 66**

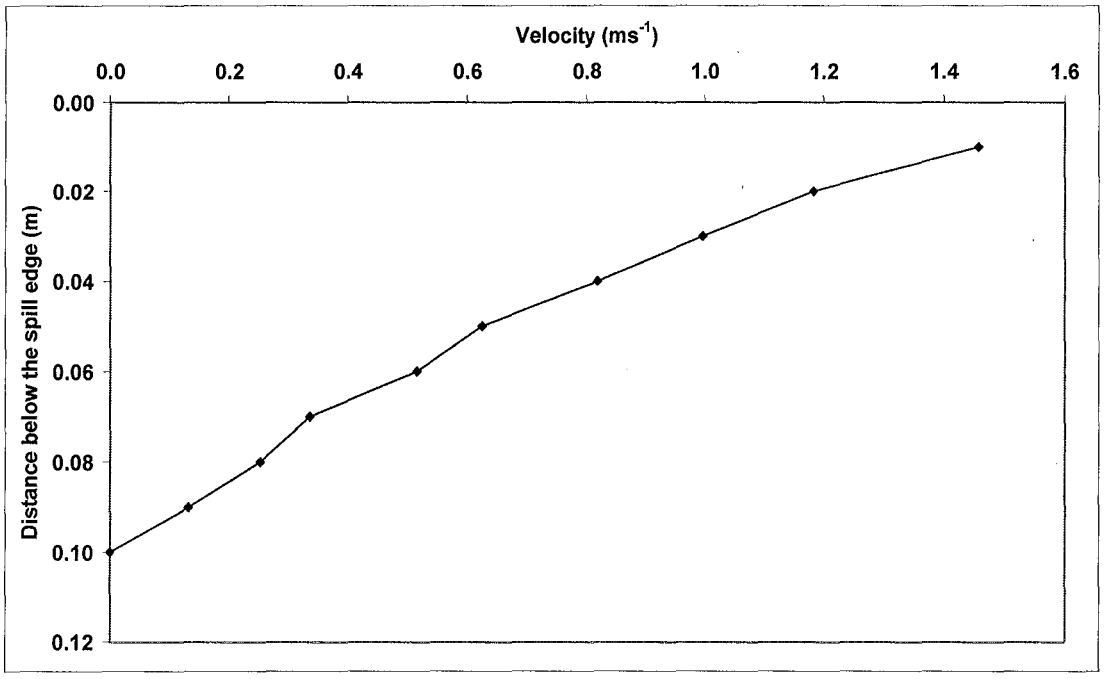

Figure J4: **Velocity profile at the spill edge for Test 66**

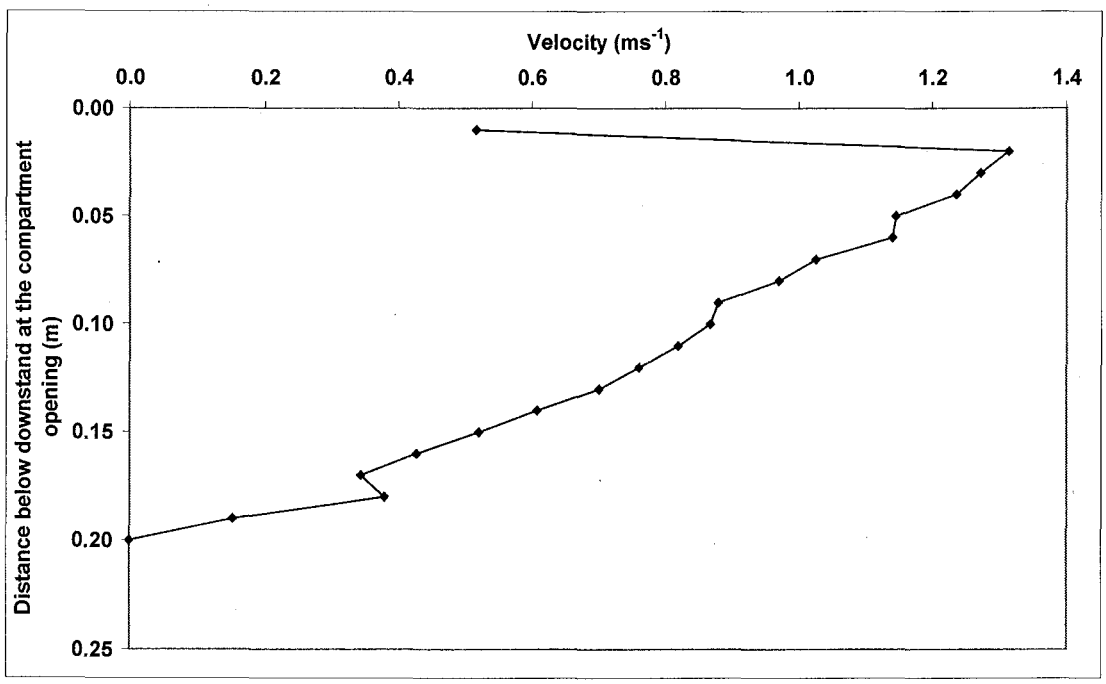

Figure J5: **Velocity profile at the compartment opening for Test 67**

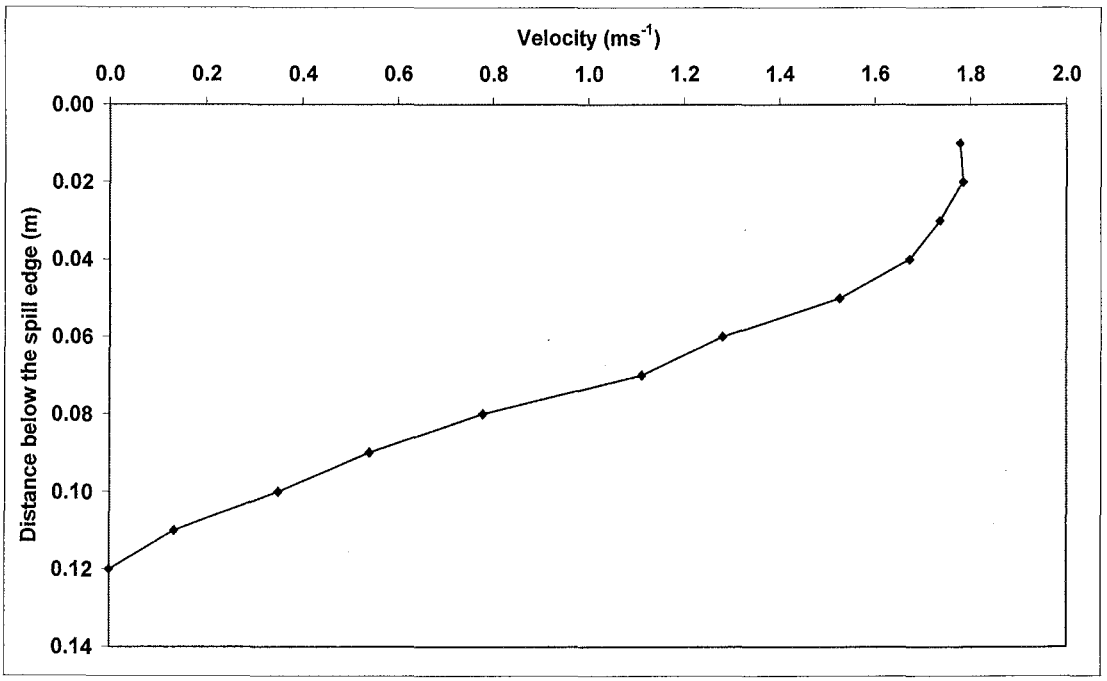

Figure J6: **Velocity profile at the spill edge for Test 67**

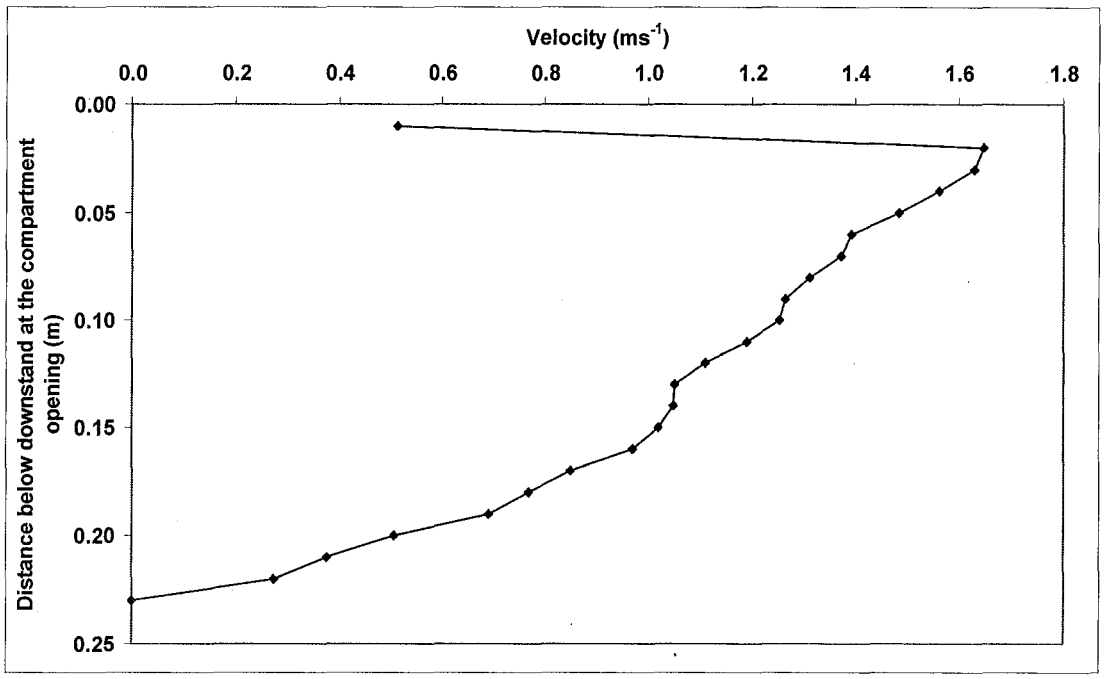

Figure J7: **Velocity profile at the compartment opening for Test 68**

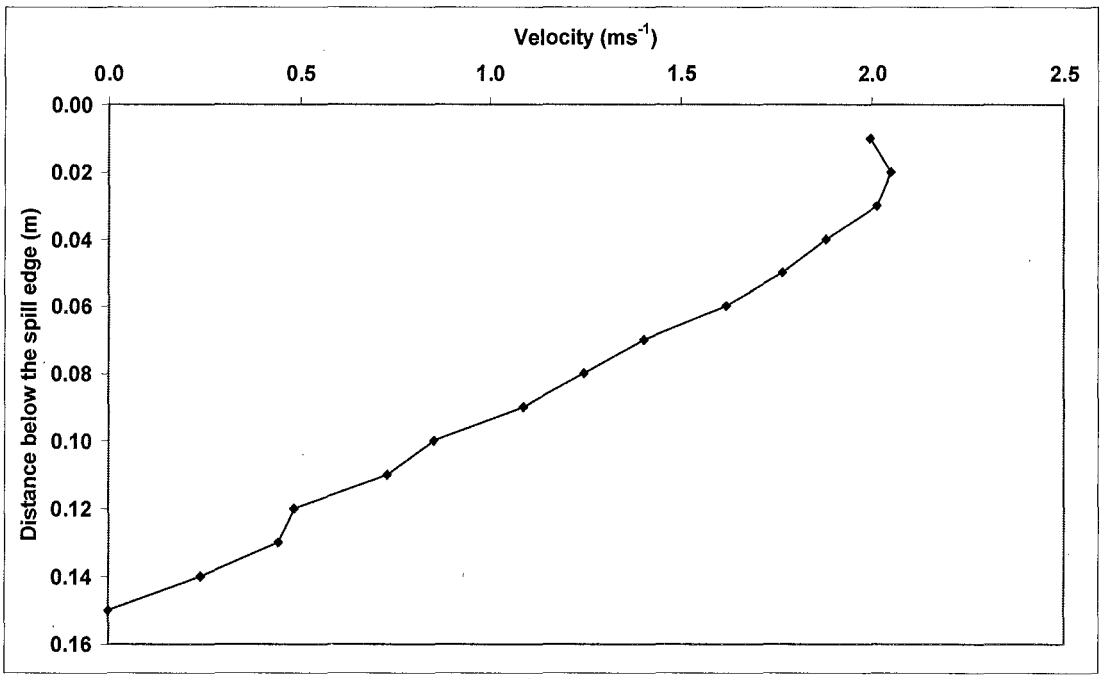

Figure J8: **Velocity profile at the spill edge for Test 68**

APPENDIX K COMPARISON OF EXPERIMENTAL AND FDS TEMPERATURE PROFILES (TESTS 65 TO 68, SIMULATIONS 1, 4, 5 AND 9)

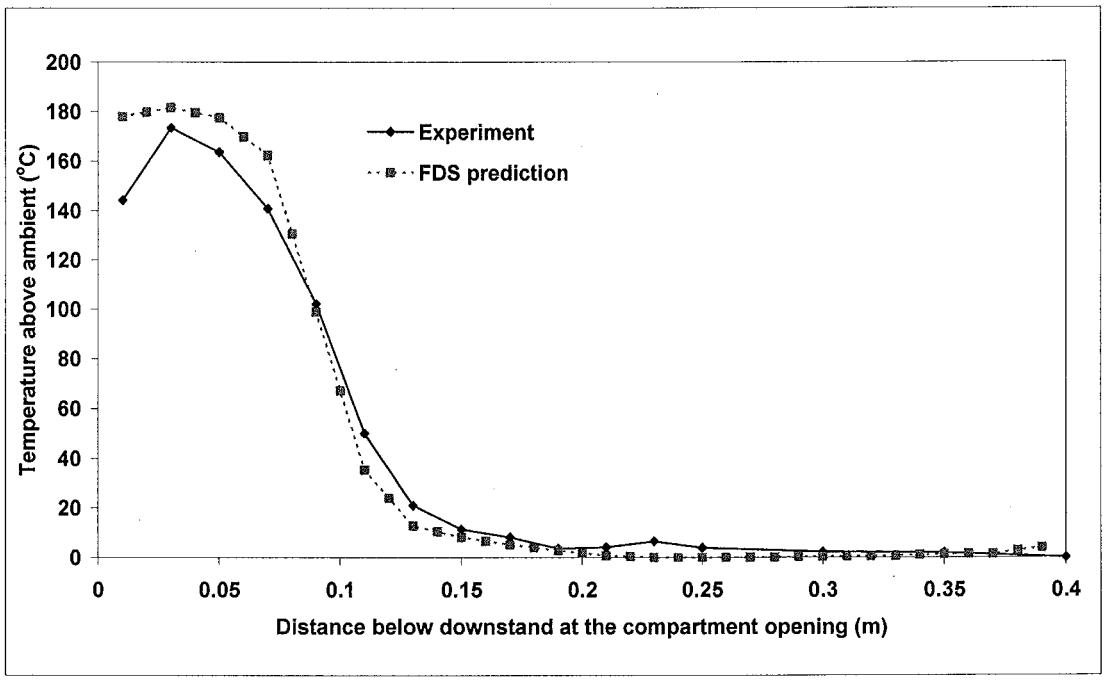

Figure K1: Comparison of temperature at the compartment opening (Test 65, Simulation 1)

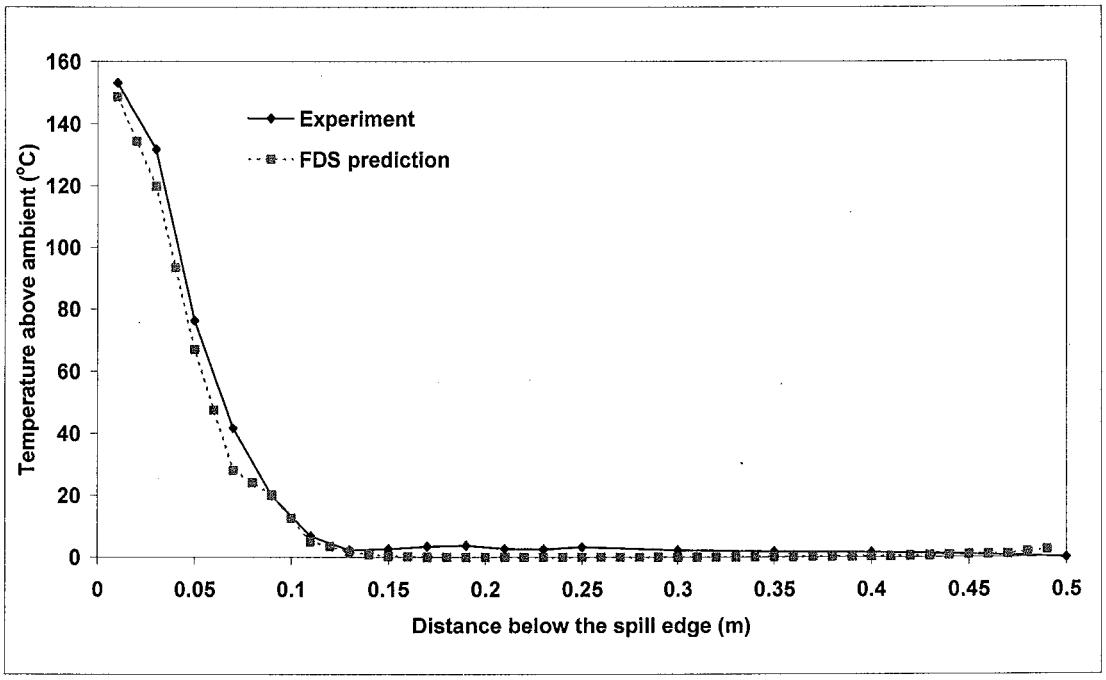

Figure K2: Comparison of temperature at the spill edge (Test 65, Simulation 1)

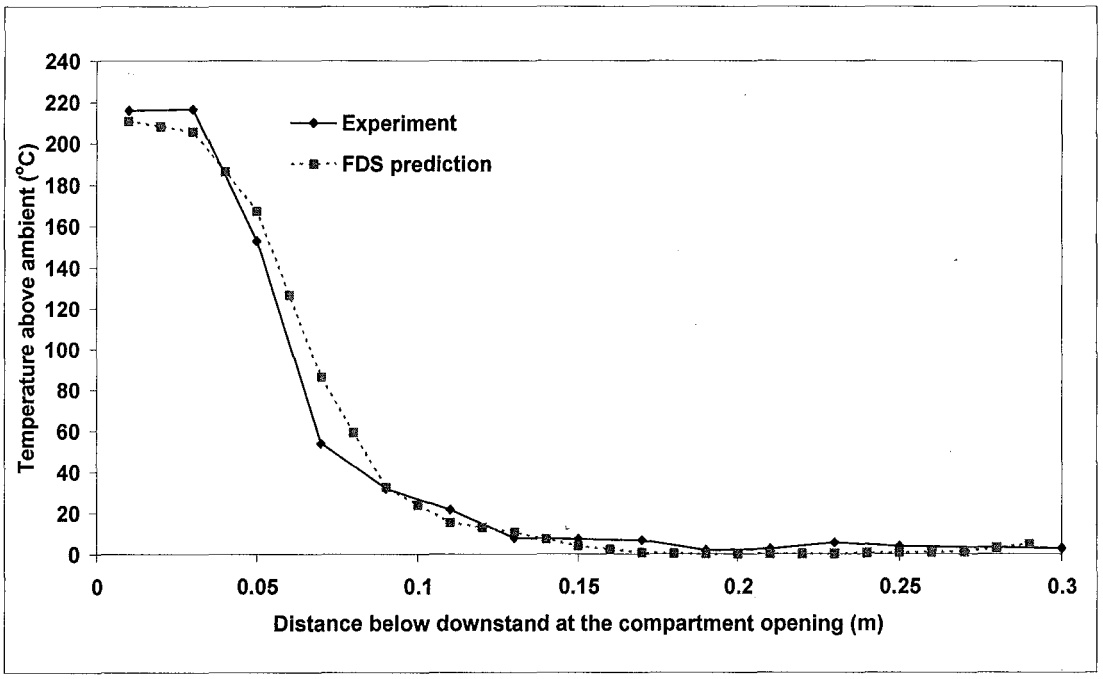

Figure K3: Comparison of temperature at the compartment opening (Test 66, Simulation 9)

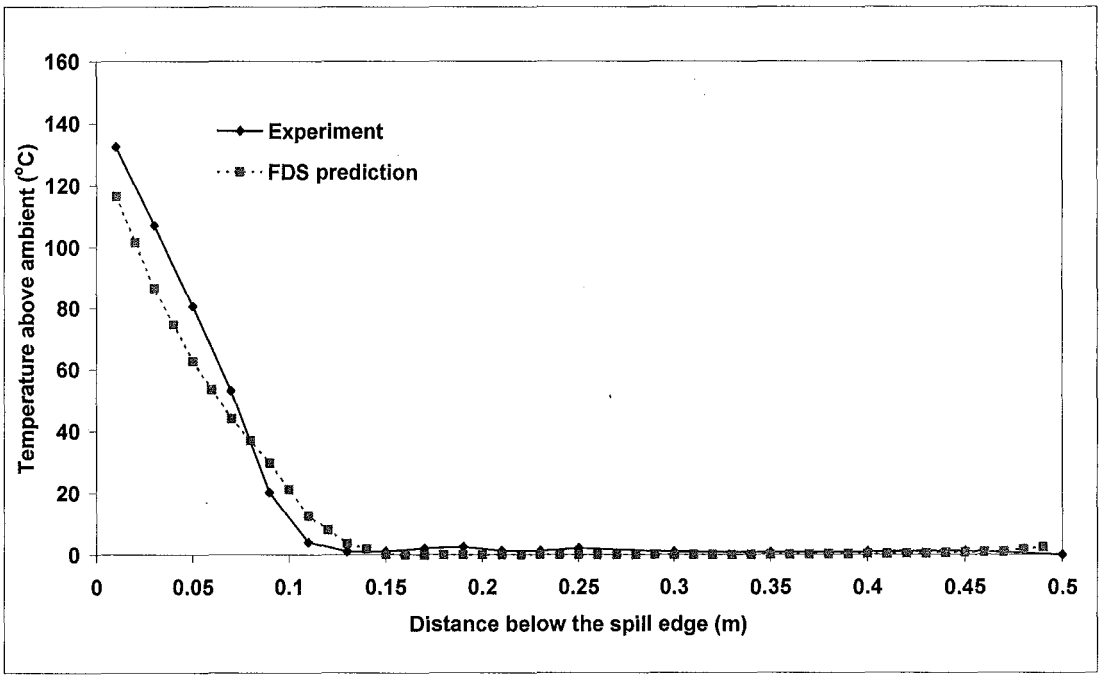

Figure K4: Comparison of temperature at the spill edge (Test 66, Simulation 9)

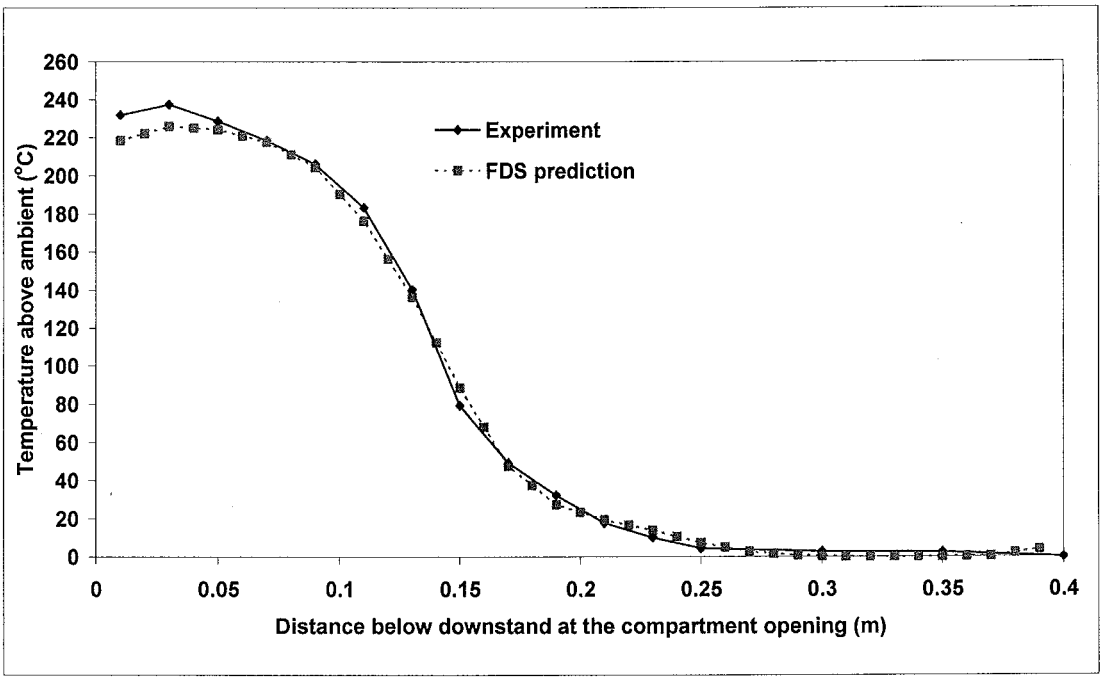

Figure K5: **Comparison of temperature at the compartment opening (Test 67, Simulation 4)**

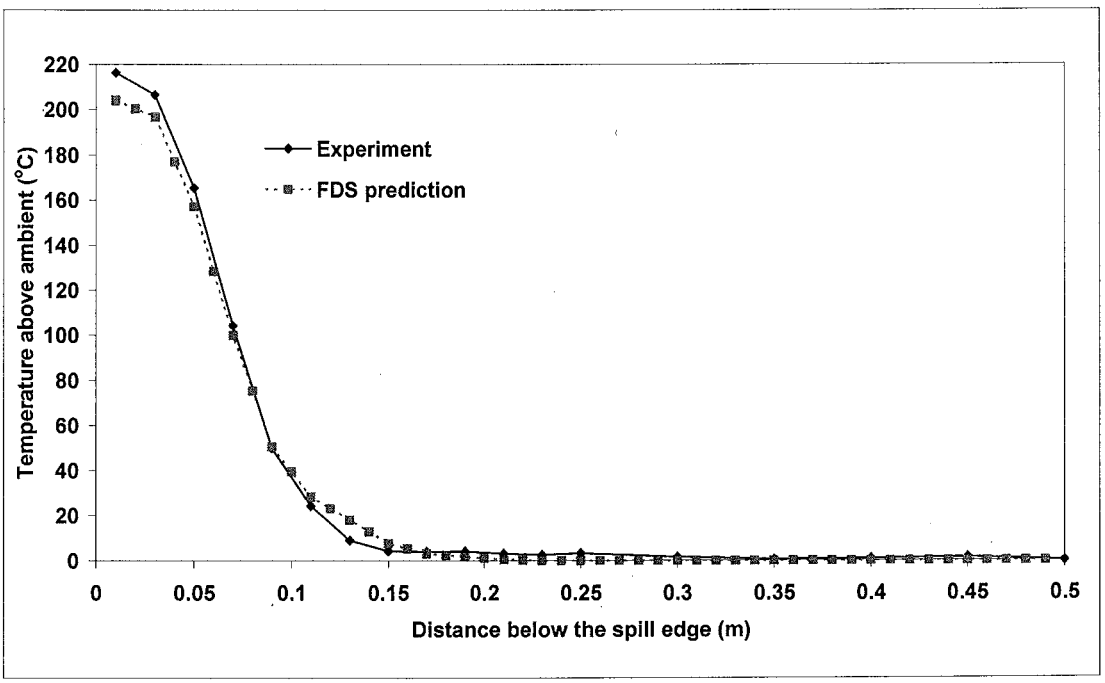

Figure K6: **Comparison of temperature at the spill edge (Test 67, Simulation 4)**

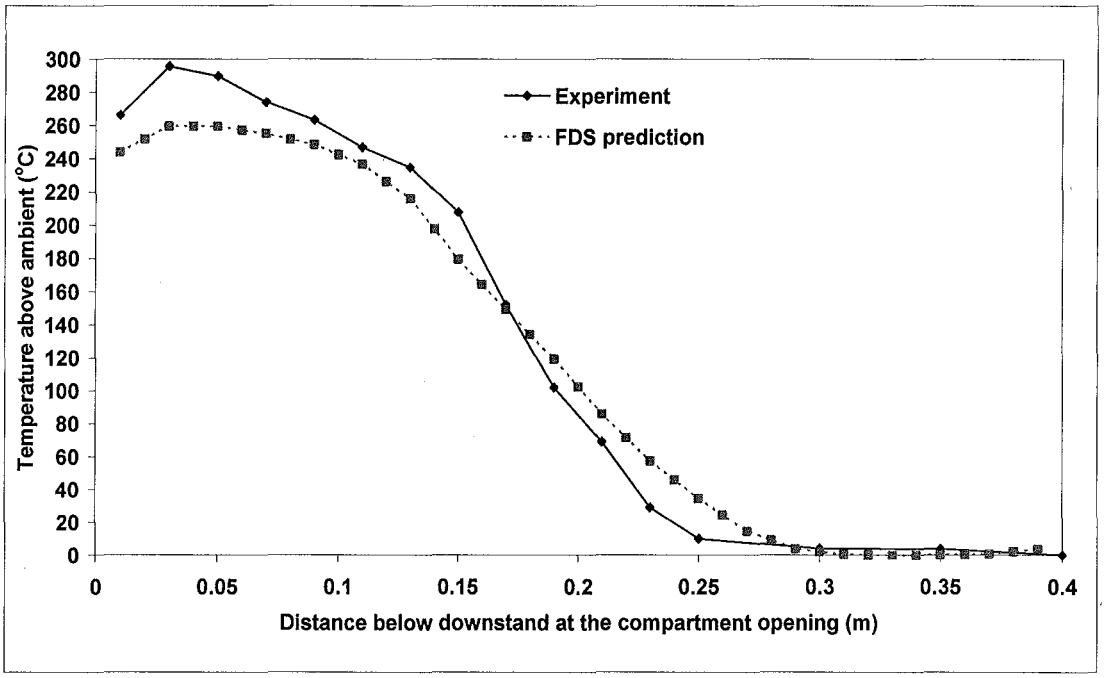

Figure K7: Comparison of temperature at the compartment opening (Test 68, Simulation 5)

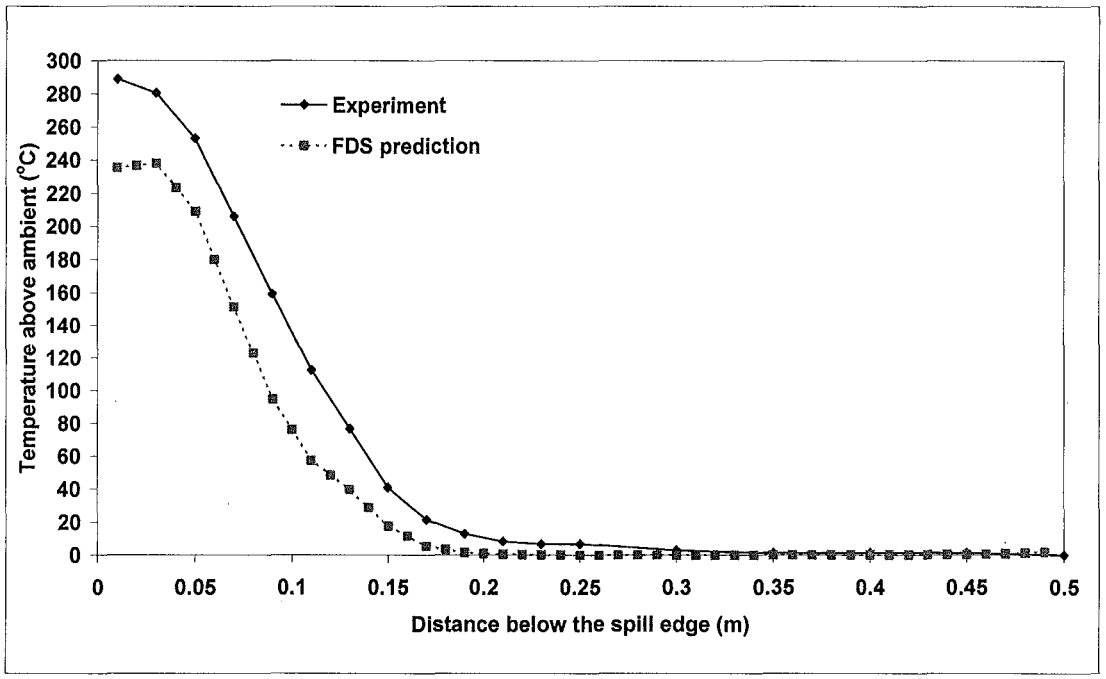

Figure K8: Comparison of temperature at the spill edge (Test 68, Simulation 5)

APPENDIX L COMPARISON OF EXPERIMENTAL AND FDS VELOCITY PROFILES (TESTS 65 TO 68, SIMULATIONS 1, 4, 5 AND 9)

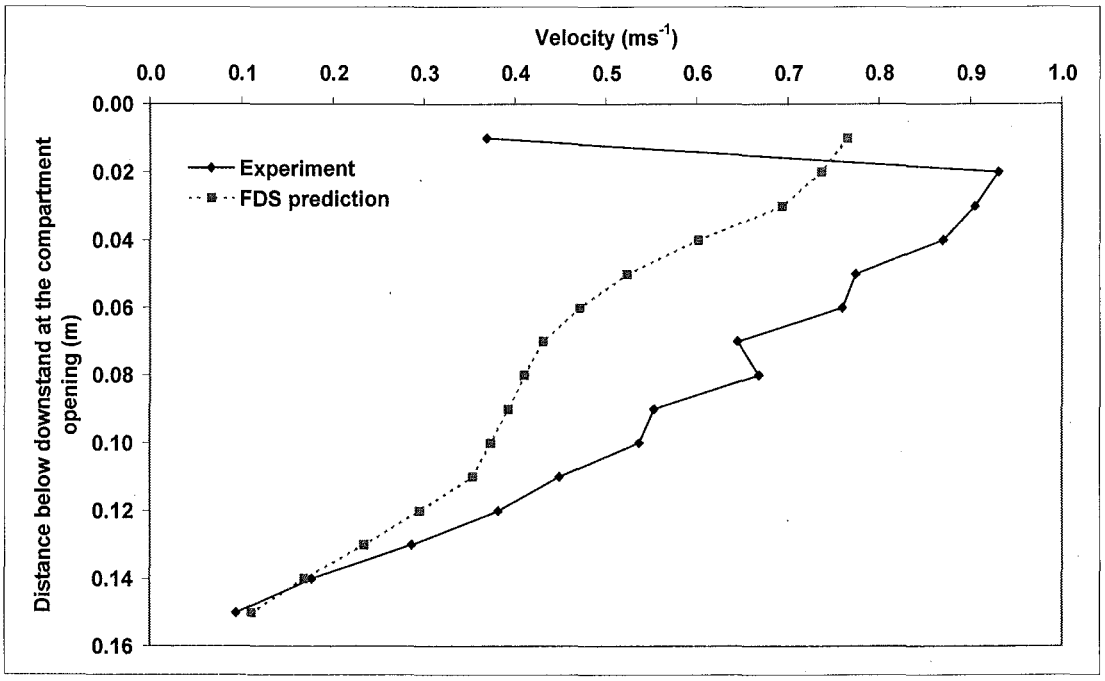

Figure L1: Comparison of velocity at the compartment opening (Test 65, Simulation 1)

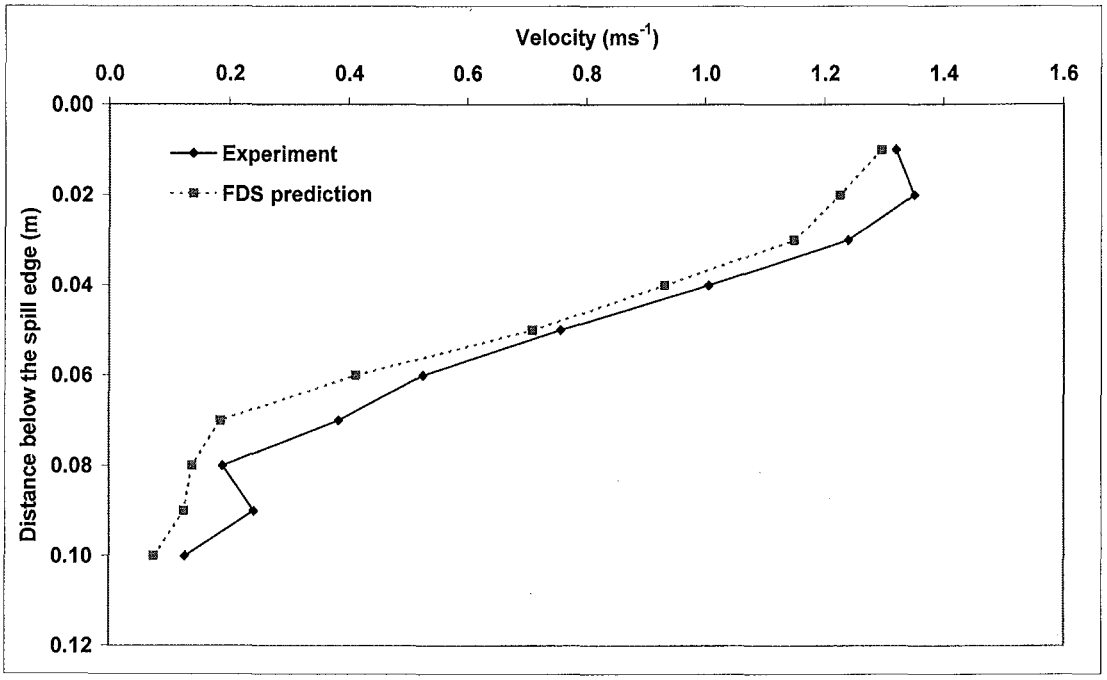

Figure L2: Comparison of velocity at the spill edge (Test 65, Simulation 1)

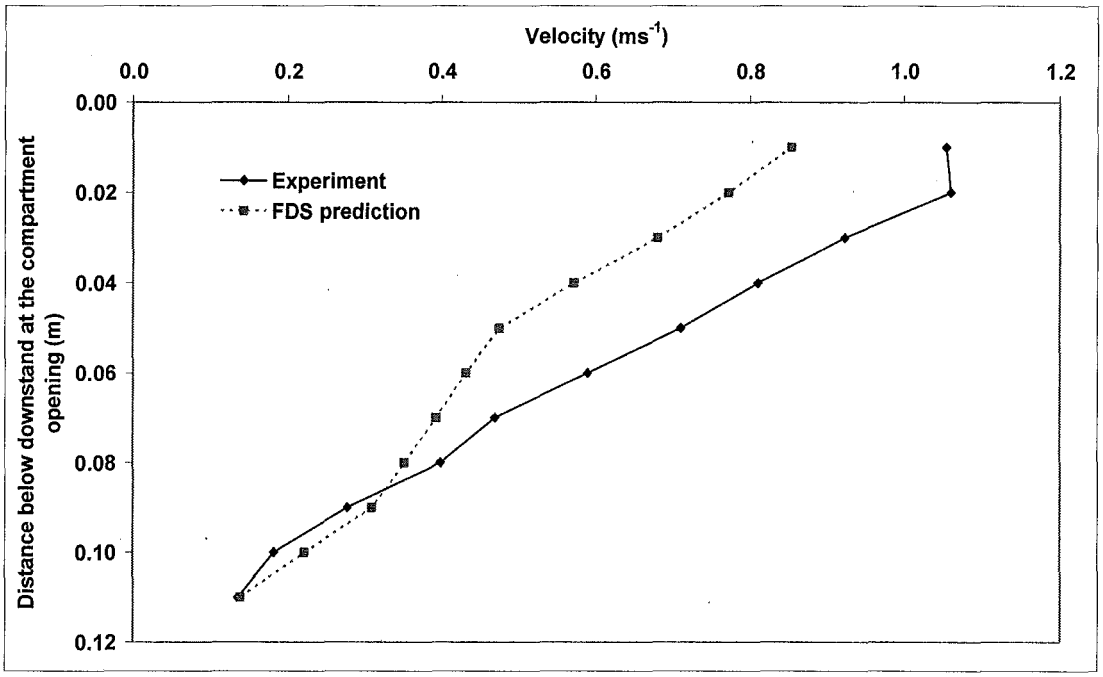

Figure L3: Comparison of velocity at the compartment opening (Test 66, Simulation 9)

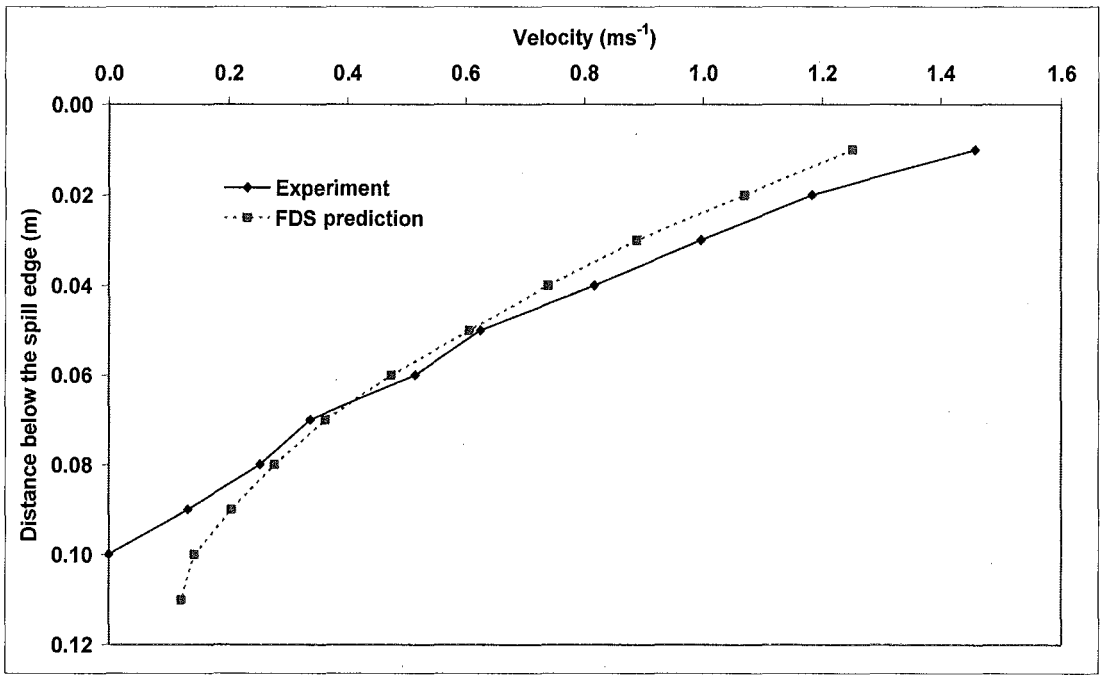

Figure L4: Comparison of velocity at the spill edge (Test 66, Simulation 9)

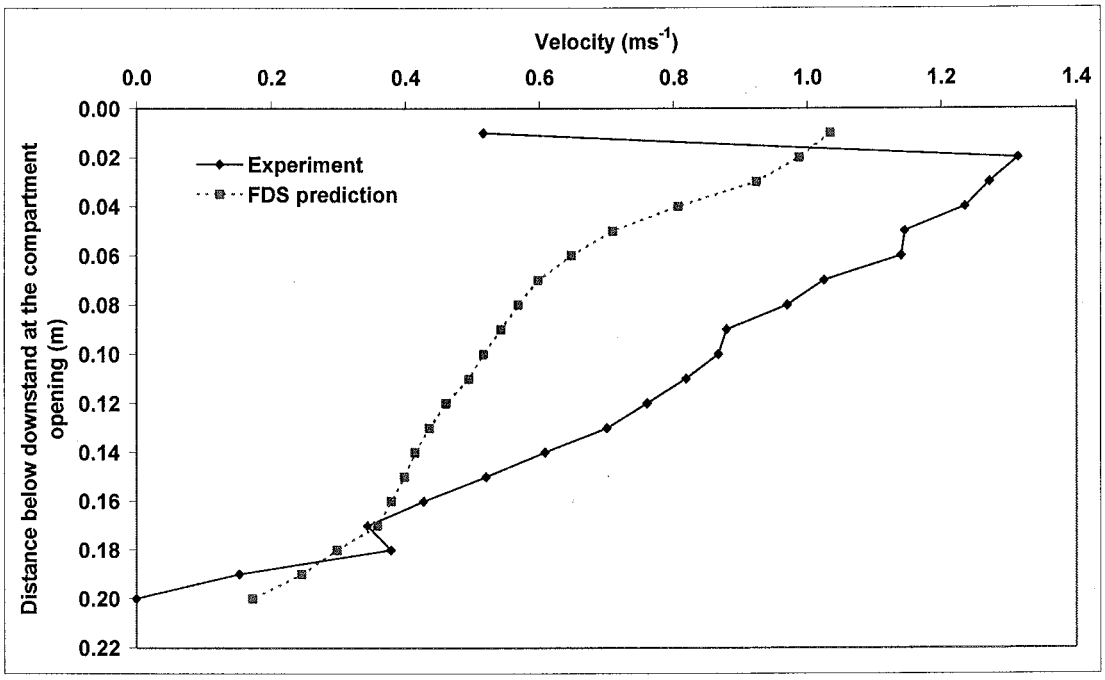

Figure L5: **Comparison of velocity at the compartment opening (Test 67, Simulation 4)**

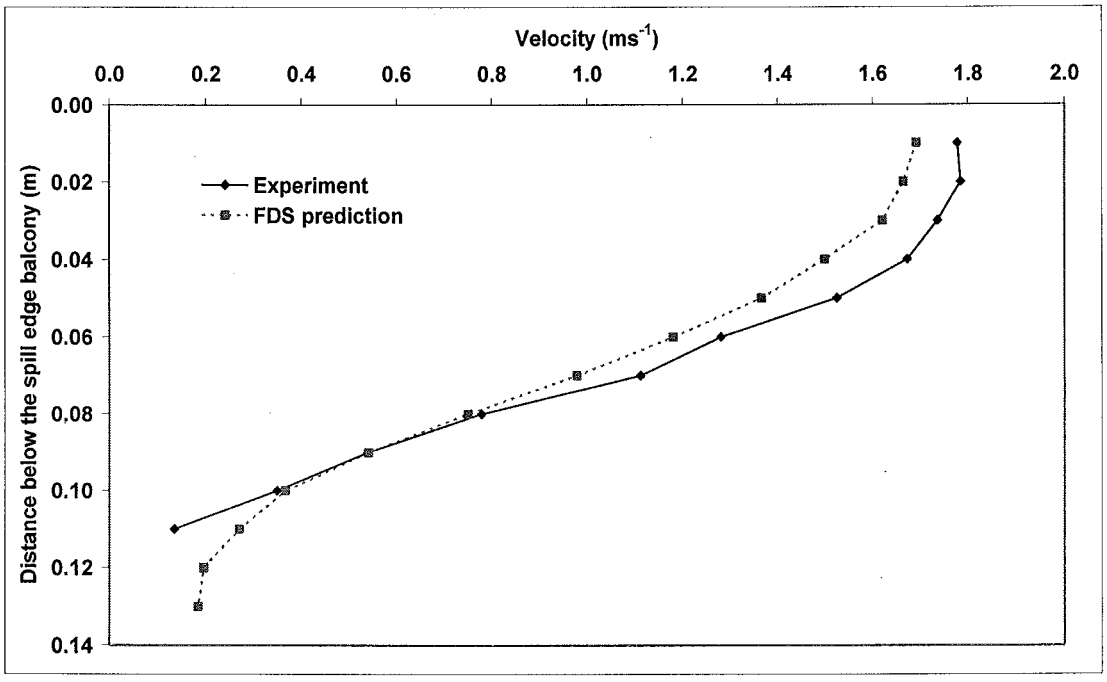

Figure L6: **Comparison of velocity at the spill edge (Test 67, Simulation 4)**

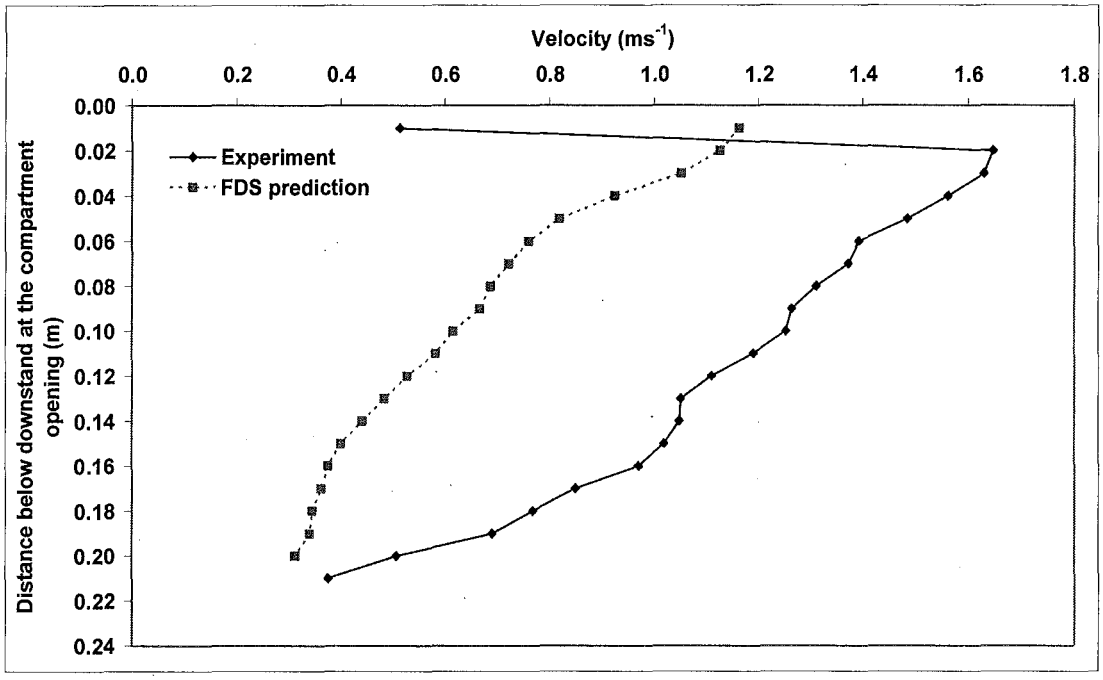

Figure L7: Comparison of velocity at the compartment opening (Test 68, Simulation 5)

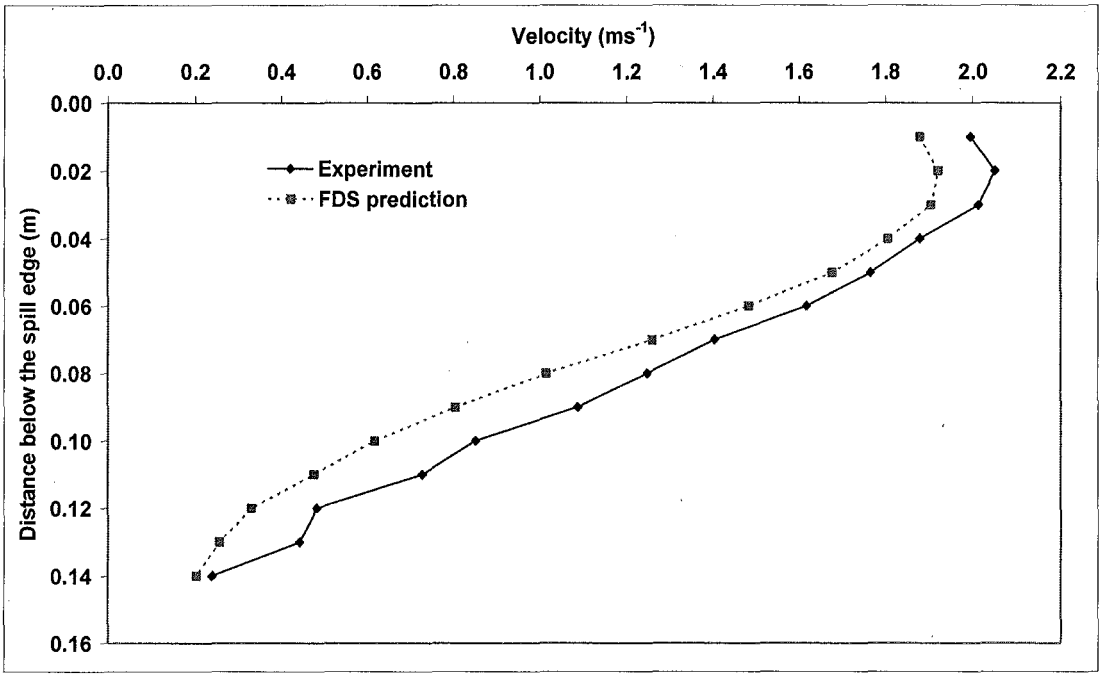

Figure L8: Comparison of velocity at the spill edge (Test 68, Simulation 5)